

2



WRDC-TR-89-4044
Volume I

CONFERENCE ON AEROSPACE TRANSPARENT MATERIALS AND ENCLOSURES
VOLUME I - SESSIONS I-V

S. A. Marolo
Materials Engineering Branch
Systems Support Division

April 1989

Conference Report for Period 16-20 January 1989

Approved for Public Release; Distribution Unlimited

DTIC
ELECTE
JUL 24 1989
S B D

MATERIALS LABORATORY
WRIGHT RESEARCH AND DEVELOPMENT CENTER
AIR FORCE SYSTEMS COMMAND
WRIGHT-PATTERSON AIR FORCE BASE, OHIO 45433-6533

89 7 24 032

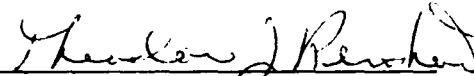
AD-A210 488


NOTICE

When Government drawings, specifications, or other data are used for any purpose other than in connection with a definitely related Government procurement operation, the United States Government thereby incurs no responsibility nor any obligation whatsoever; and the fact that the government may have formulated, furnished, or in any way supplied the said drawings, specifications, or other data, is not to be regarded by implication or otherwise as in any manner licensing the holder or any other person or corporation, or conveying any rights or permission to manufacture use, or sell any patented invention that may in any way be related thereto.


This report has been reviewed by the Office of Public Affairs (ASD/PA) and is releasable to the National Technical Information Service (NTIS). At NTIS, it will be available to the general public, including foreign nations.

This technical report has been reviewed and is approved for publication.


THEODORE J. REINHART, Chief
Materials Engineering Branch
Systems Support Division
Materials Laboratory


RALPH J. SPEELMAN, Chief
Aircrew Protection Branch
Vehicle Subsystems Division
Flight Dynamics Laboratory

FOR THE COMMANDER


MR. WARREN JOHNSON, Chief
System Support Division
Materials Laboratory

If your address has changed, if you wish to be removed from our mailing list, or if the addressee is no longer employed by your organization please notify WRDC/FIVR, W-PAFB, OH 45433-6533 to help us maintain a current mailing list.

Copies of this report should not be returned unless return is required by security considerations, contractual obligations, or notice on a specific document.

UNCLASSIFIED

SECURITY CLASSIFICATION OF THIS PAGE

REPORT DOCUMENTATION PAGE

Form Approved
OMB No. 0704-0188

1a. REPORT SECURITY CLASSIFICATION UNCLASSIFIED			1b. RESTRICTIVE MARKINGS		
2a. SECURITY CLASSIFICATION AUTHORITY			3. DISTRIBUTION / AVAILABILITY OF REPORT Approved for public release; distribution unlimited.		
2b. DECLASSIFICATION / DOWNGRADING SCHEDULE					
4. PERFORMING ORGANIZATION REPORT NUMBER(S) WRDC-TR-89-4044, Vol I			5. MONITORING ORGANIZATION REPORT NUMBER(S)		
6a. NAME OF PERFORMING ORGANIZATION Materials Laboratory		6b. OFFICE SYMBOL (if applicable) (WRDC/MLSE)		7a. NAME OF MONITORING ORGANIZATION	
6c. ADDRESS (City, State, and ZIP Code) Materials Laboratory (WRDC/MLSE) Wright Research and Development Center, AFSC Wright-Patterson AFB, OH 45433			7b. ADDRESS (City, State, and ZIP Code)		
8a. NAME OF FUNDING / SPONSORING ORGANIZATION Flight Dynamics Laboratory		8b. OFFICE SYMBOL (if applicable) WRDC/FIVR		9. PROCUREMENT INSTRUMENT IDENTIFICATION NUMBER F33615-84-C-3404	
8c. ADDRESS (City, State, and ZIP Code) Flight Dynamics Laboratory (WRDC/FIVR) Wright Research and Development Center, AFSC Wright-Patterson AFB OH 45433			10. SOURCE OF FUNDING NUMBERS		
			PROGRAM ELEMENT NO. 64212F/62102F	PROJECT NO. 1926	TASK NO. 01
			WORK UNIT ACCESSION NO. 12		
11. TITLE (Include Security Classification) CONFERENCE ON AEROSPACE TRANSPARENT MATERIALS AND ENCLOSURES Volume I - Sessions I-V					
12. PERSONAL AUTHOR(S) Compiled by Samuel A. Marolo					
13a. TYPE OF REPORT Final		13b. TIME COVERED FROM 16JAN89 TO 20JAN89		14. DATE OF REPORT (Year, Month, Day) April 1989	
15. PAGE COUNT 773					
16. SUPPLEMENTARY NOTATION					
17. COSATI CODES			18. SUBJECT TERMS (Continue on reverse if necessary and identify by block number)		
FIELD	GROUP	SUB-GROUP	Polycarbonate, Acrylic, Interlayers, Windshields, Canopies, Coatings, Transparent Materials, Environmental Resistance, Optical Requirements, Computed Design, Design Criteria, Cost of Ownership Reduction, Transparency Refurbishment, Frameless		
19. ABSTRACT (Continue on reverse if necessary and identify by block number) Transparency, New Transparent Materials. The purpose of this report is to make available the technical papers presented at the Fifteenth Conference on Aerospace Transparent Materials and Enclosures. Seventy-two technical papers are presented in nine sessions that address transparent material for enclosures, coatings for transparencies, transparency design; bird impact resistance; human factor and optics; operational problems; design criteria on transparent plastics, glasses and elastomers; aircraft-structural integration of windshields and canopies; computed design; testing techniques; and cost of ownership reduction. The papers contained herein have been reproduced directly from the original manuscripts.					
20. DISTRIBUTION / AVAILABILITY OF ABSTRACT <input checked="" type="checkbox"/> UNCLASSIFIED/UNLIMITED <input type="checkbox"/> SAME AS RPT. <input type="checkbox"/> DTIC USERS			21. ABSTRACT SECURITY CLASSIFICATION Unclassified		
22a. NAME OF RESPONSIBLE INDIVIDUAL Theodore J. Reinhart			22b. TELEPHONE (Include Area Code) 513-255-3691		22c. OFFICE SYMBOL WRDC/MLSE

The report was submitted by the author in March 1989.

Publication of this report does not constitute Air Force approval of the findings or conclusions presented. It is published only for the exchange and stimulation of ideas.



Accession For	
NTIS GRA&I	<input checked="" type="checkbox"/>
DTIC TAB	<input type="checkbox"/>
Unannounced	<input type="checkbox"/>
Justification	
By	
Distribution/	
Availability Codes	
Dist	Avail and/or Special
A-1	

TABLE OF CONTENTS

<u>SESSION I: SYSTEMS OVERVIEW - PART A</u>	<u>Page No.</u>
V-22 OSPREY WINDSHIELD DEVELOPMENT AND VISIBILITY ASSESSMENT Sherman D. Stewart, PPG Industries; Vincent P. Gallagher, Boeing Helicopters; and Neal E. Mason, Boeing Helicopters	2
ADVANCED CONCEPTS IN TRANSPARENCY SYSTEM DESIGN/DEVELOPMENT G. C. Stone, Ph.D., General Dynamics Fort Worth Division	28
<u>SESSION I: SYSTEMS OVERVIEW - PART B</u>	
THE DEVELOPMENT OF LARGE COMPOSITE HELICOPTER WINDSHIELDS R. S. Bruce and R. W. Wright, Triplex Aircraft and Special Products Ltd.	57
THE FLOW OF TECHNOLOGY BETWEEN AIRCRAFT AND AUTOMOTIVE Glenn E. Freeman, PPG Industries	87
<u>SESSION II: EMERGING CAPABILITIES - PART A</u>	
NEW AND UNIQUE PROCESS FOR RESURFACING AIRCRAFT CABIN WINDOWS R. Dorey and E. Mountford, EMI-MEC Ltd. and M. Stedman, National Physical Laboratory	104
BIRD IMPACT RESISTANT WINDSHIELD AFT ARCH DESIGN METHODOLOGY G. J. Stenger, M. P. Bouchard, and D. R. Bowman, University of Dayton	122
OPERATIONAL OVERVIEW OF THE "ROBOTIC CANOPY POLISHING SYSTEM" Douglas L. Michalsky, Southwest Research Institute and Halver V. Ross, OO-ALC/MANEP, Hill Air Force Base	153
EVALUATION OF COMPOSITE MATERIALS FOR BIRD IMPACT RESISTANT TRANSPARENCY SYSTEMS G. J. Stenger, University of Dayton, and W. R. Pinnell, AFWAL/FDER, Wright-Patterson Air Force Base	164
REPAIR AND RESTORATION OF COMBAT DAMAGE TRANSPARENCIES G. Renieri and D. Kovensky, McDonnell Aircraft Company (paper was withdrawn)	191
<u>SESSION II: EMERGING CAPABILITIES - PART B</u>	
HIGH PERFORMANCE POLYCARBONATE TRANSPARENCY COATING J. E. Miller, Sherwin-Williams Company, and J. E. Kochanowski, G.E. Plastics	193
F-4 WINDSCREEN - AN ALL COMPOSITE FRAME Scott A. Speelman, Texstar, Inc.	206

VERSATILE APPLICATIONS OF POLYURETHANES IN AIRCRAFT TRANSPARENCIES Dr. William Lewis and Dr. Janet Andrechak, Swedlow, Inc.	212
T-38 COMPOSITE BIRD-IMPACT-RESISTANT-WINDSHIELD FRAME S. J. Cieslak and F. N. Smith, Alcoa Technical Center	227
NEW LOW VOLTAGE HEATING ELEMENT DESIGN FOR AIRCRAFT TRANSPARENCIES Charles R. Graham, PPG Industries	240
<u>SESSION III: UNDERSTANDING CURRENT MATERIALS - PART A</u>	
WEATHERING OF PLAIN AND COATED POLYCARBONATE: A COLLABORATIVE STUDY CARRIED OUT BY TECHNICAL PANEL PTP3 OF THE TECHNICAL COOPERATION PROGRAM Peter Burchill, National Research Laboratory, and W. B. Moniz, Naval Research Laboratory	248
MODES OF IMPACT FAILURE Dr. Gerald L. Robbins, Mobay Corporation	264
SILICONE INTERLAYER ADHESION CHARACTERISTICS Dr. Cliff Juengst, Don LeMasters, and Hai-Tao Wang, Swedlow, Inc.	290
TRANSPARENT CONDUCTIVE COATINGS Dr. Harold Gurev and Dr. Mohammad Nisar, Swedlow, Inc.	312
ACRYLIC AIRCRAFT GLAZING MATERIALS PERFORMANCE OF PMMA WITH LOW WATER ABSORPTION G. G. Schreyer, Rohm GmbH and F. J. Hewitt, CYRO Industries	331
<u>SESSION III: UNDERSTANDING CURRENT MATERIALS - PART B</u>	
THE RAIN EROSION OF SOME AS-CAST AND PRESSED/STRETCHED ACRYLIC MATERIALS N. S. Corney, E. M. Minter, and P. Tattershall, Royal Aircraft Establishment	345
EFFECTS OF SOLVENTS ON CRAZE INITIATION AND CRACK PROPAGATION IN TRANSPARENT POLYMERS Janice J. Vanselow, Alex J. Hsieh, and Jennie H. Brown, U.S. Army Materials Technology, and John I. Stevens, U. S. Army Chemical Research, Development and Engineering Center	360
ACRYLIC MATERIALS FOR AIRCRAFT TRANSPARENCIES: STRUCTURE AND EFFECTS OF ENVIRONMENT AND AGE ON CRAZE RESISTANCE P. J. Burchill, R. H. Stacewicz, G. Mathys, and R. G. Davidson, Materials Research Laboratory	370
THE CAUSE AND EFFECT OF STRUCTURAL DEGRADATION OF IN-SERVICE AGED F-111 ADBIRT WINDSHIELD TRANSPARENCIES Daniel R. Bowman and Blaine S. West, University of Dayton	387

ACRYLIC WINDOW CRAZING Klaus Ewald, Lufthansa German Airlines	434
<u>SESSION IV: NEW MATERIALS AND PROCESSES - PART A</u>	
TRANSPARENT COMPOSITE Raymond J. Skubic, McDonnell Aircraft Company	476
THE EFFECT OF ION BEAM PROCESSING ON TRANSPARENT PLASTICS I. H. Loh, P. H. Lu, R. A. Moody, P. Sioshansi, Spire Corporation, and T. J. Reinhart, AFWAL/MLSE, Wright-Patterson Air Force Base	497
FRAMELESS AIRCRAFT TRANSPARENCY TECHNOLOGY DEVELOPMENT William R. Pinnell, AFWAL/FDER, Wright-Patterson Air Force Base	507
DIRECT FORMING PROCESSES FOR AIRCRAFT TRANSPARENCIES D. B. Fuller, Loral Defense Systems-Arizona	522
ULTRAVIOLET-CURED PROTECTIVE COATING SYSTEMS FOR AEROSPACE TRANSPARENT PLASTICS Alexander Z. Bimanand and J. A. Raffo, Sierracin/Sylmar Corporation	555
<u>SESSION IV: NEW MATERIALS AND PROCESSES - PART B</u>	
GAC-590 AN ADVANCED TRANSPARENCY MATERIAL J. Uram, Jr., Loral Defense Systems and S. Sandlin, Swedlow, Inc.	582
FLUOROACRYLATE POLYMERS FOR WATER RESISTANT TRANSPARENCIES R. L. Soulen and J. R. Griffith, Naval Research Laboratory	605
NEW TRANSPARENCY MATERIALS Stephen E. Bales, Dow Chemical Company	621
A VACUUM COATER FOR THE APPLICATION OF ITO TO PLASTIC CANOPIES Paul E. Schumacher, Sierracin/A.P.G.	639
<u>SESSION V: TESTING TECHNOLOGY - PART A</u>	
AIRCRAFT TRANSPARENT MATERIALS CHARACTERIZATION Richard A. Smith, AFWAL/FDER and Blaine S. West, University of Dayton	660
AIRCRAFT TRANSPARENCY LIFE CYCLE DURABILITY FACILITY Russ Urzi, AFWAL/FDER and Capt. John Anselmo, AFWAL/FDST	678
AN EXPERIMENTAL EVALUATION OF THE AIR CANNON TECHNIQUE FOR USE IN IMPACT RESISTANCE SCREENING OF POLYCARBONATE Lt. Paul J. Kolodziejski, AFWAL/FDER and Michael P. Bouchard, University of Dayton	702
METHODS FOR THE DETERMINATION OF THE DEGRADATION OF POLYCARBONATE Lance Teten, Texstar, Inc.	714

SESSION V: TESTING TECHNOLOGY - PART B

EVALUATION OF THE AIRCRAFT TRANSPARENCY DURABILITY TEST METHODOLOGY	727
K. I. Clayton, University of Dayton and Malcolm Kelley, AFWAL/FDER	
SCREENING TESTS FOR HARDENED TRANSPARENCY MATERIALS	737
Ken Clayton, University of Dayton	
VIDEO THERMOGRAPHY, A TRANSPARENT(CY) APPLICATION	742
Don Chapin, Sierracin/Sylmar Corp.	

SESSION VI: BIRDSTRIKE HAZARD - PART A

DEVELOPMENT OF A BIRD PROOF WINDSHIELD FOR THE B-2 BOMBER	762
J. B. Hoffman, Northrop Corporation (paper was withdrawn)	
ESTIMATING THE BIRDSTRIKE RISK TO THE SPACE SHUTTLE ORBITER	763
Maj. Jeffrey J. Short, AFWAL/FDER	
BIRDSTRIKES TO UK CIVIL AIRCRAFT WINDSHIELDS	775
John Thorpe, UK Civil Aviation Authority	
DEVELOPMENT OF A CALCULATION MODEL FOR WINDSHIELD BIRDSTRIKE DESIGN	797
Rolph Wegmann and Lars Sjöström, Saab Aircraft Division	

SESSION VI: BIRDSTRIKE HAZARD - PART B

A-7 IMPROVED TRANSPARENCY DEVELOPMENT PROGRAM	821
D. Dversdall, AFWAL/FDER, Gregory J. Stenger, University of Dayton, and S. Hargis, AFWAL/FDER	
BIRD STRIKES TO U.S. AIR FORCE AIRCRAFT 1987	834
Capt Russell P. DeFusco, Capt Robert L. Dogan and Maj Ronald L. Merritt, Bird Aircraft Strike Hazard (BASH) Team	
DEFINITION AND REDUCTION OF THE F-18 WINDSHIELD BIRDSTRIKE HAZARD	845
G. J. Stenger, University of Dayton and J. L. Terry, Flight Dynamics Laboratory	

SESSION VII: UNDERSTANDING CURRENT SYSTEMS - PART A

MANAGEMENT OF TRANSPARENCY RELATED COSTS IN AIR FORCE AIRCRAFT: A PARETO APPROACH	875
Paul S. Lee and Japheth Nkonge, North Carolina A & T University, Nisar Shaikh, University of Nebraska-Lincoln, and Arnold H. Mayer and Michael Gran, Air Force Wright Aeronautical Laboratories	
MANAGEMENT OF TRANSPARENCY RELATED COSTS IN ELECTROSTATIC DISCHARGE DAMAGE TO F-16 CANOPY SOLAR COATINGS	898
B. G. Hinds and H. DeCamp, Sierracin/Sylmar Corporation	

T-38 FLIGHT SERVICE AND LABORATORY TESTING OF PPG 5300 OUTBOARD LINER James W. Myers, PPG Industries, Inc.	917
IMPROVED OPTICAL INTERLAYER ADHESIVES BOOST PERFORMANCE OF VISION SYSTEMS Madhu "Dolly" Baile, Kent R. Larson and David G. Coble, Dow Corning Corporation	936
TRANSPARENCY SYSTEM MISHAPS Malcolm E. Kelley, AFWAL/FDER	943
<u>SESSION VII: UNDERSTANDING CURRENT SYSTEMS - PART B</u>	
TRANSPARENCY SEALANTS Malcolm E. Kelley, AFWAL/FDER	952
RESIDUAL STRESSES IN F-16 AIRCRAFT M. G. Gran, Flight Dynamics Laboratory	976
B-1B EXTENDED LIFE WINDSHIELD PROGRAM Capt Steve Kolbow, AFWAL/FDER and Capt Paul Berry, OC-ALC/MMBRE	998
IN-SERVICE CRACKING OF F-16 WINDSHIELD/CANOPIES B. G. Hinds and J. A. Raffo, Sierracin/Sylmar Corporation	1013
AN ANALYSIS OF FLIGHT AND WINDSHIELD FAILURES IN F111 AIRCRAFT P. J. Burchill and R. H. Stacewicz, Materials Research Laboratory	1033
<u>SESSION VIII: OPTICS - PART A</u>	
VISION THROUGH AIRCRAFT TRANSPARENCIES H. Lee Task, Ph.D., Human Engineering Division, AAMRL	1046
MEASURES OF DISTORTION: ARE THEY RELEVANT? William N. Kama, Human Engineering Division, AAMRL	1072
RECENT ADVANCES IN OPTICAL MEASUREMENTS OF TRANSPARENCIES Capt Harold S. Merkel, AAMRL/HEF	1094
TRANSPARENCY OPTICAL PERFORMANCE PREDICTION John W. Fielman and Dr. John S. Loomis, University of Dayton	1105
<u>SESSION VIII: OPTICS - PART B</u>	
THE SWITCHABLE TRANSPARENCY - WHAT WILL IT BE? Charles B. Greenberg, PPG Industries, Inc.	1124
GRUMMAN/FAA LIGHTNING STUDY: A POTENTIAL COUNTERMEASURE FOR LIGHTNING INDUCED FLASHBLINDNESS OF AIRCREW MEMBERS H. D. Kivlighn, Jr., Grumman Corporation (paper was withdrawn)	1135
A NEW APPROACH TO LASER FILTERS John A. Brown and William A. Thornton, John Brown Associates	1136

LARGE-AREA OPTICAL FILTER FABRICATION BY PLASMA POLYMERIZATION Roy F. Wielonski, Battelle	1144
<u>SESSION IX - COMPUTER AIDED ANALYSIS - PART A</u>	
HIGH PERFORMANCE TRANSPARENCY DESIGN F. F. Abdi, G. L. Savoni, G. Clark, Rockwell International, and R. A. Smith, Flight Dynamics Laboratory	1159
EXPLICIT FINITE ELEMENT TECHNIQUES FOR TRANSPARENCY IMPACT ANALYSIS R. A. Brockman and T. W. Held, University of Dayton	1173
FINITE ELEMENT ANALYSIS OF THE B-1B AIRCRAFT WINDSHIELD SYSTEM Michael P. Bouchard and William R. Braisted, University of Dayton	1195
AIRCRAFT WINDSHIELD DESIGN WITH LARGE STRUCTURAL ANALYSIS CODES Arnold H. Mayer and Richard A. Smith, Flight Dynamics Laboratory	1231
MAGNA ANALYSIS OF BIRD IMPACT ON AN F-4 SINGLE PIECE WINDSHIELD USING SHEAR CORRECTION AND ON AN F-4 FORWARD CANOPY Michael G. Gran, Flight Dynamics Laboratory	1256
<u>SESSION IX - COMPUTER AIDED ANALYSIS - PART B</u>	
ASSESSMENT OF BIRD IMPACT PROTECTION PROVIDED BY THE SPACE SHUTTLE ORBITER WINDSHIELD SYSTEM USING THE MAGNA COMPUTER PROGRAM Robert E. McCarty and Richard A. Smith, Flight Dynamics Laboratory	1327
RESPONSE OF TRANSPARENCIES TO INTENSE THERMAL RADIATION Robert G. Oeding, PDA Engineering	1360
ANALYTIC ASSESSMENT OF BIRD IMPACT RESISTANT T-46A AIRCRAFT WINDSHIELD SYSTEM DESIGNS USING MAGNA (MATERIALLY AND GEOMETRICALLY NONLINEAR ANALYSIS) Robert E. McCarty, Air Force Wright Aeronautical Laboratories and Paul Landry, Lockheed Aeronautical Systems Company	1378
HYPERSONIC THERMAL ANALYSIS FOR AIRCRAFT TRANSPARENCIES Bret L. Boman, McDonnell Aircraft Company and Charles A. Babish III, Flight Dynamics Laboratory	1425
NONLINEAR DYNAMIC FINITE ELEMENT ANALYSIS FOR THE BIRD IMPACT RESPONSE OF A PREPROTOTYPE T-38 AIRCRAFT WINDSHIELD SYSTEM R. E. McCarty, D. E. Trudan and Lt A. D. Davis, Flight Dynamics Laboratory	1447
AUTHOR INDEX	1486

SESSION I

SYSTEMS OVERVIEW (PART A)

Chairman: D. S. Riddle
Grumman Aerospace Corp.
Bethpage, New York

Co-Chairman: W. L. Early
General Dynamics Corporation
Fort Worth, Texas

Coordinator: J. Hansen
Grumman Aerospace Corp.
Bethpage, New York

V-22 OSPREY WINDSHIELD DEVELOPMENT AND VISIBILITY ASSESSMENT

Sherman D. Stewart
PPG Industries

Vincent P. Gallagher
Boeing Helicopters

Neal E. Mason
Boeing Helicopters

Paper Title: V-22 Osprey Windshield Development and Visibility Assessment

Authors:

Sherman D. Stewart
PPG Industries, Inc.
Technology Development Aircraft Products
1719 Highway 72E
Huntsville, AL 35811

Vincent P. Gallagher M/S P30-18
Boeing Helicopters
Human Factors Engineering
P.O. Box 16858
Philadelphia, PA 19142

Neal E. Mason M/S P23-59
Boeing Helicopters
Crew Systems Design
P.O. Box 16858
Philadelphia, PA 19142

ABSTRACT

The V-22 Osprey Tilt Rotor aircraft, employs advanced state of the art technology in all its transparencies. The large curved windshield is electrically heated and bird strike protected. Protection from a number of identified threats is integrated into each laminate.

This paper provides a detailed description of the evolution of the current V-22 windshield design through eight design alternatives. During design development, the design was changed alternatively from a laminate of one ply of Herculite II glass and two plies of polycarbonate to a laminate of two piles of Herculite II glass and a single ply of polycarbonate and then returned to original concept.

To verify visual acceptability, a comprehensive test plan was developed which included three phases: bench test, ground test, and airborne tests. Evaluations reported upon include: Spectroradiometric transmittance evaluation of preliminary windshield concepts; Spectroradiometric transmittance evaluation of the V-22 cross section and two other aircraft windshields when observers used night vision goggles during ground tests; Subjective evaluation of night time airborne operational effectiveness utilizing night vision goggles in the A-6E aircraft in flight.

Copywrite by Boeing Company and PPG Industries.

INTRODUCTION

The V-22 Osprey was designed to meet a variety of threats (Fig. 1). The large curved windshield has a single curvature. During the preliminary conceptual stage, threat protection requirements were quite extensive, requiring the most advanced techniques under development at that time. When all processes were included in one transparency it soon became apparent that the resultant reduced light transmission might be unacceptable, particularly when the use of night vision goggles was required (Fig. 2).

After a number of basic light transmittance tests, threat protection requirements were reduced to obtain acceptable light transmission. A comprehensive test program was devised to determine visual acceptability under operational conditions.

Operational Requirements of the Aircraft

The design requirements imposed upon the aircraft included virtually every protection then available. These were P-static, radar cross section, electromagnetic pulse, nuclear flash and overpressure, high power microwave, laser, anti-ice, birdstrike, hail, and prop rotor ice. The basic dilemma at this stage was insufficient surfaces for coating deposition.

Another operational requirement for this windshield was the use of ANVIS (AN/AVS-6) or CATS EYE night vision goggles by the flight crew. The facilitation of light transmission within the specific bandwidths of sensitivity of the Image Intensifier tubes was necessary.

In addition, the flight envelope of this tilt-rotor aircraft calls for a ceiling of 24,000 ft., 300 kt, 4.0 g and 2.0 psi differential pressure when operating in aircraft mode.

DESIGN ALTERNATIVES

The original design proposal (Fig. 3) consisted of an aluminum outboard retainer and an inboard composite Z section extending beyond the edge of the unit for outboard grounding and mounting of the window. The window was potted into the retainer and Z section using conductible fillers and structural adhesives. To provide protection from a 4 lb. bird at 275 kts and a 47 degree impact angle two plies of .250 polycarbonate were proposed. Other requirements of the window that had to be incorporated in the design were antistatic protection, anti ice protection, microwave protection, EMP protection, some laser protection and abrasion protection for the inboard surface.

NOTE: The principal designers of the innovative V-22 windshield were Peter Bain of Boeing Helicopters (since retired) and Sherman Stewart of PPG, Industries.



Figure 1. V-22 Osprey Tiltrotor

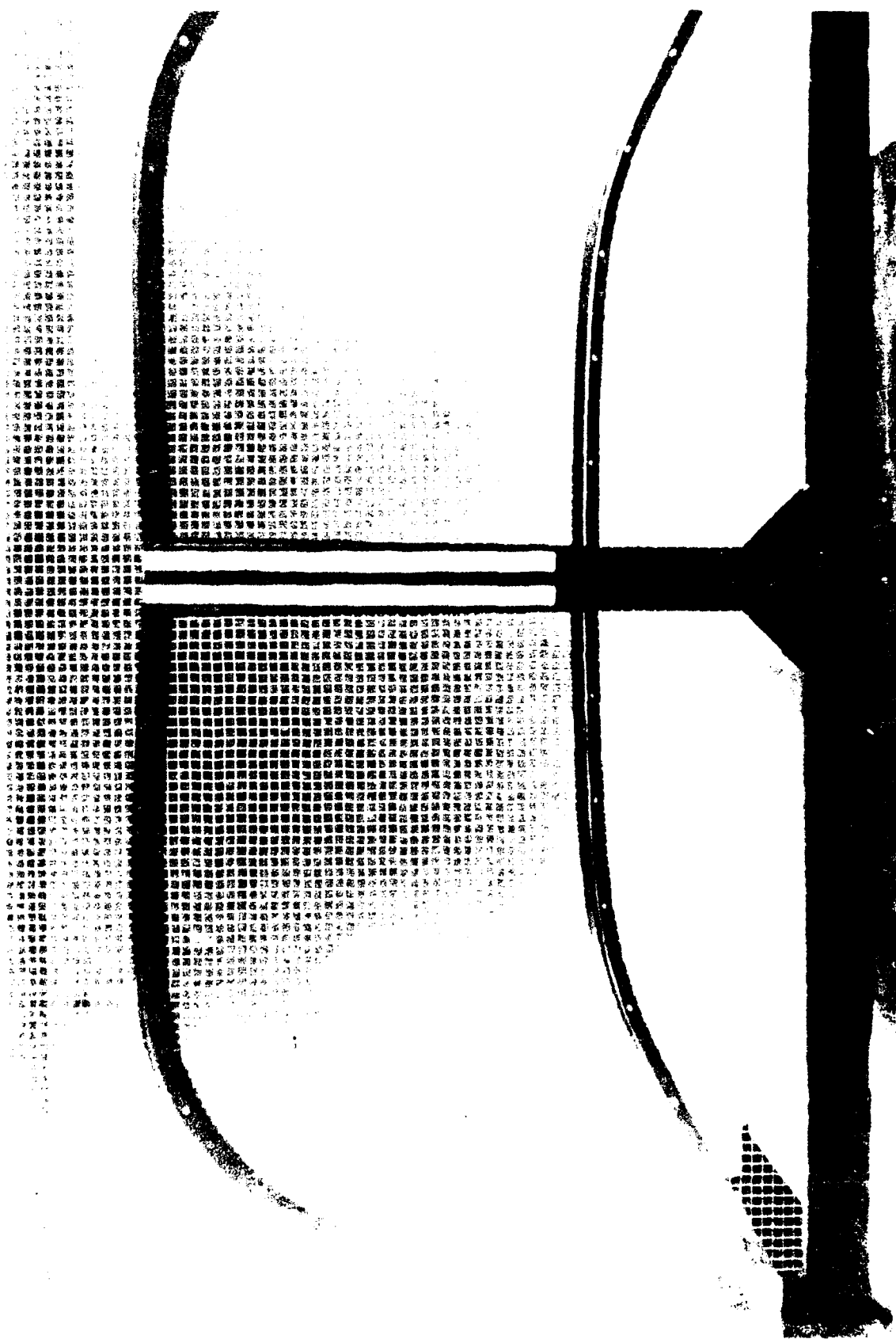


Figure 2. Windshields in Distortion Inspection Fixture

V-22 MAIN WINDSHIELD

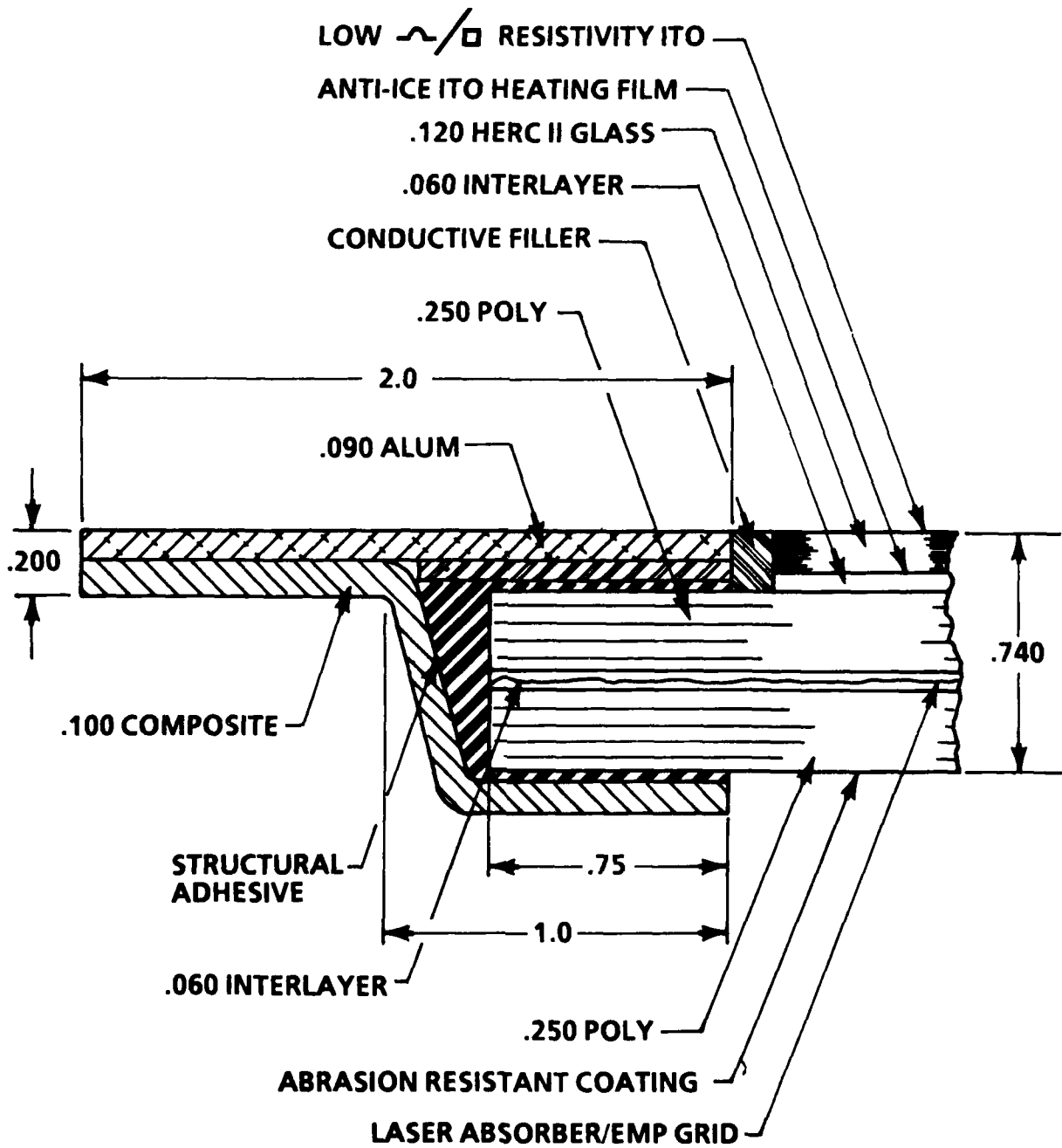


Figure 3. Original Design Proposal

The "A" revision (Fig. 4) to the design changed the edge grounding requirements and removed the Z section for mounting. The attachment system changed to a bolt through the polycarbonate to provide more daylight opening and the grounding was moved to the inboard mounting surface. An antistatic protection was added and the laser protection was deleted. All other requirements remained the same.

The "B" revision (Fig. 5) to the design changed the cross section of the window to two plies of glass and one ply of polycarbonate to segregate all of the films on to different glass surfaces. To protect the outer ply a fiberglass Z strap has been added. All grounding is still on the inboard mounting surface. All other requirements remain the same.

The "C" revision (Fig. 6) to the design only changed the monolithic polycarbonate design to two plies of polycarbonate to provide some additional failsafe.

The "D" revision (Fig. 7) to the design returned to the single glass ply with three independent films applied to it. These provide heating, antistatic, and microwave protection. The grid was moved between the plies of polycarbonate to get it away from the heating film. The grounding system was again moved to the outboard surface. The structural plies were reversed to get the grid as far outboard as possible.

The "E" revision (Fig. 8) to the design is the same basic structural design as "D" with the grid removed. Two reasons for the removal of the grid were the necessity to increase the light transmission and the removal of some of the threat requirements.

The "F" revision (Fig. 9) to the design has been changed to agree with the framing dimensions of the aircraft. The grounding system has been moved to the inboard mounting surface again.

The final Full Scale Development (FSD) design (Fig. 10) maintained the basic structural design (F Revision) of the window with only a reduction in the outboard interlayer thickness. The edge configuration of the window was altered to change the grounding of the outboard surface from a stainless strap to the use of a grounding system covered with a fiberglass strap for environmental protection.

The Full Scale Development aircraft windshield design consists of these features:

- Birdstrike, 3 lbs at 275 kt without penetration
- Design Pressure, 2.9 psi ultimate
- Hard Coating, inner surface
- P-static, over complete outer surface
- HPM, coating in intimate contact with conductive frame
- Anti-Ice, three zones
- Spall resistant

V-22 MAIN WINDSHIELD

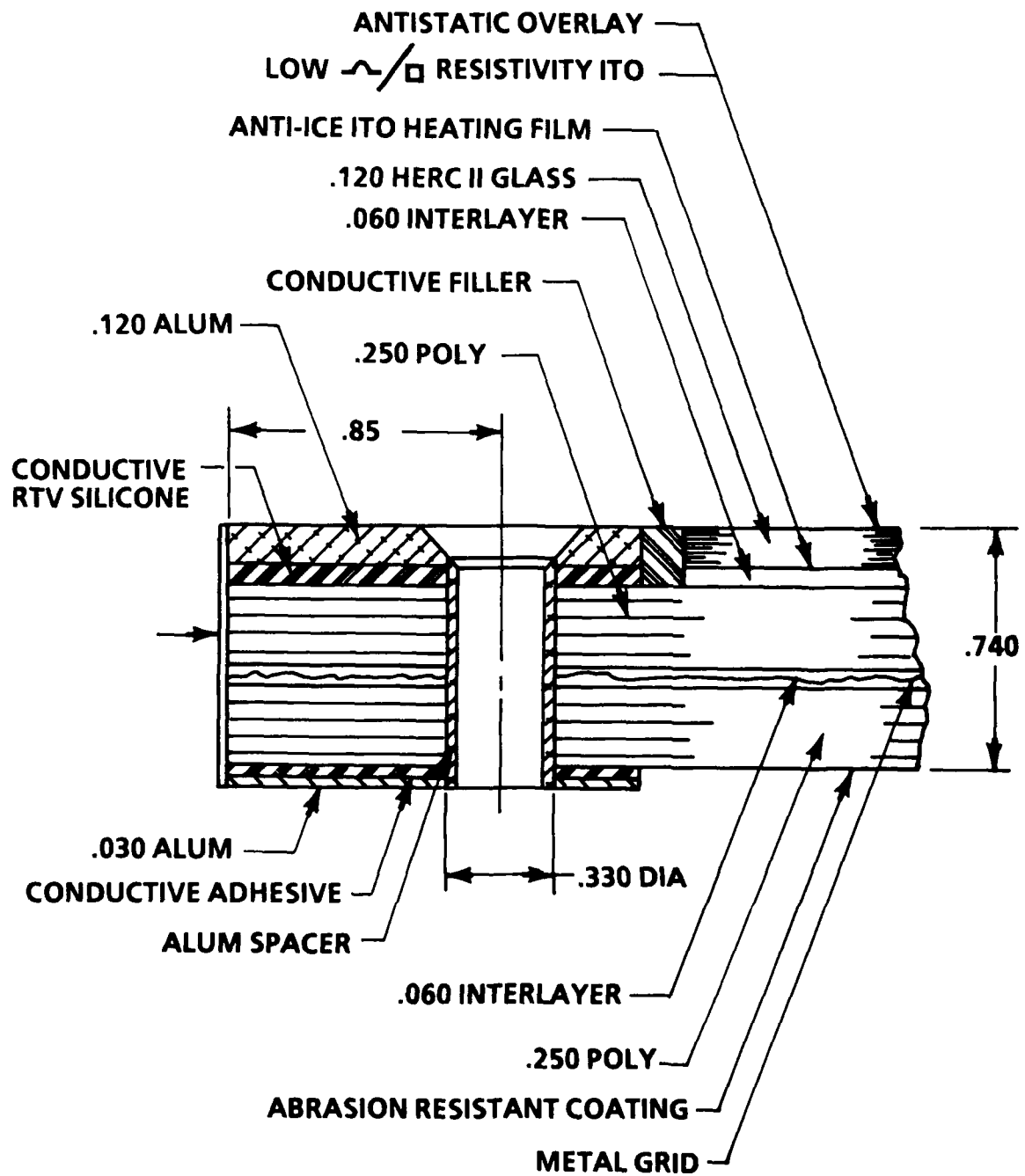


Figure 4. Design Revision A

V-22 MAIN WINDSHIELD

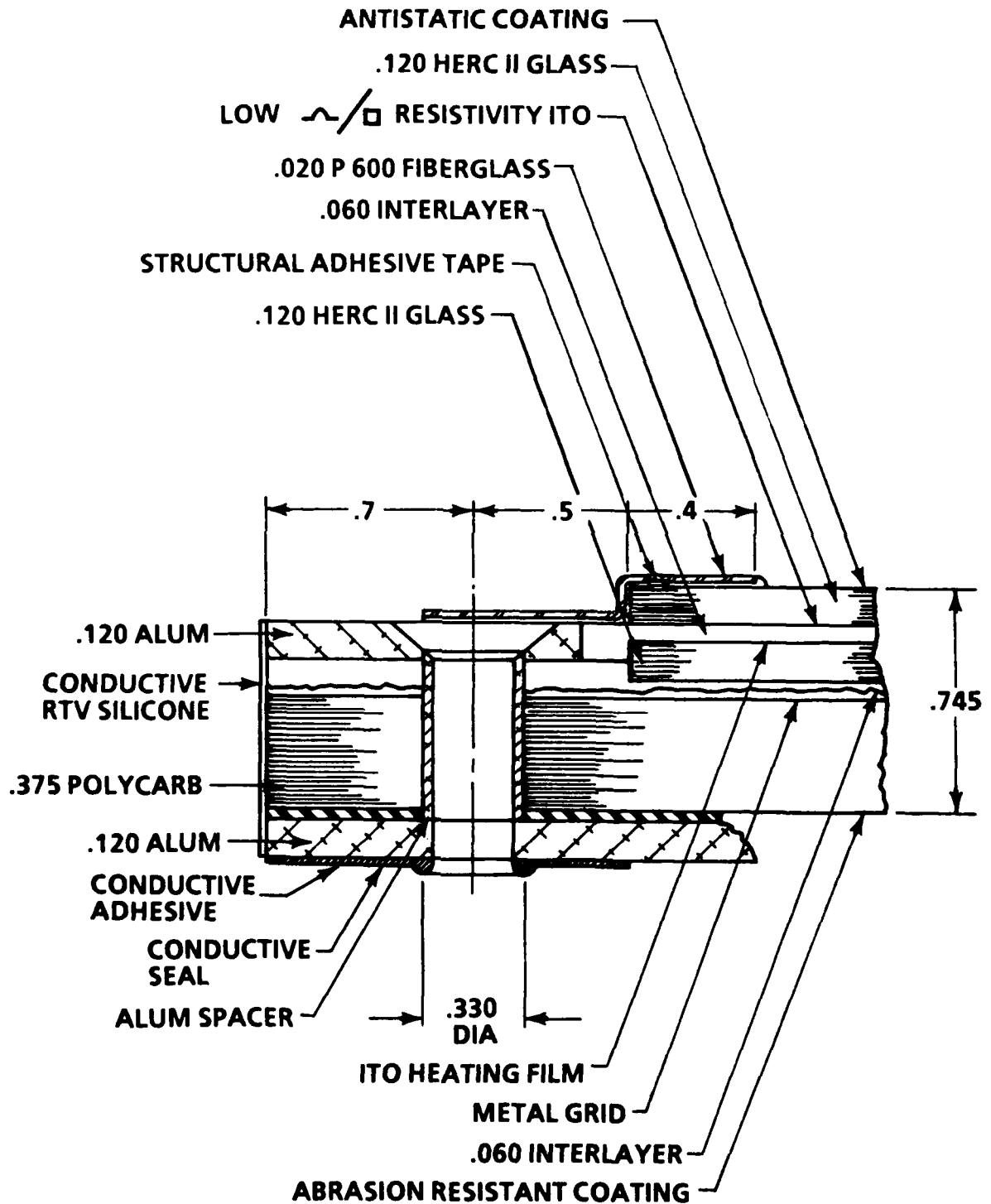


Figure 5. Design Revision B

V-22 MAIN WINDSHIELD

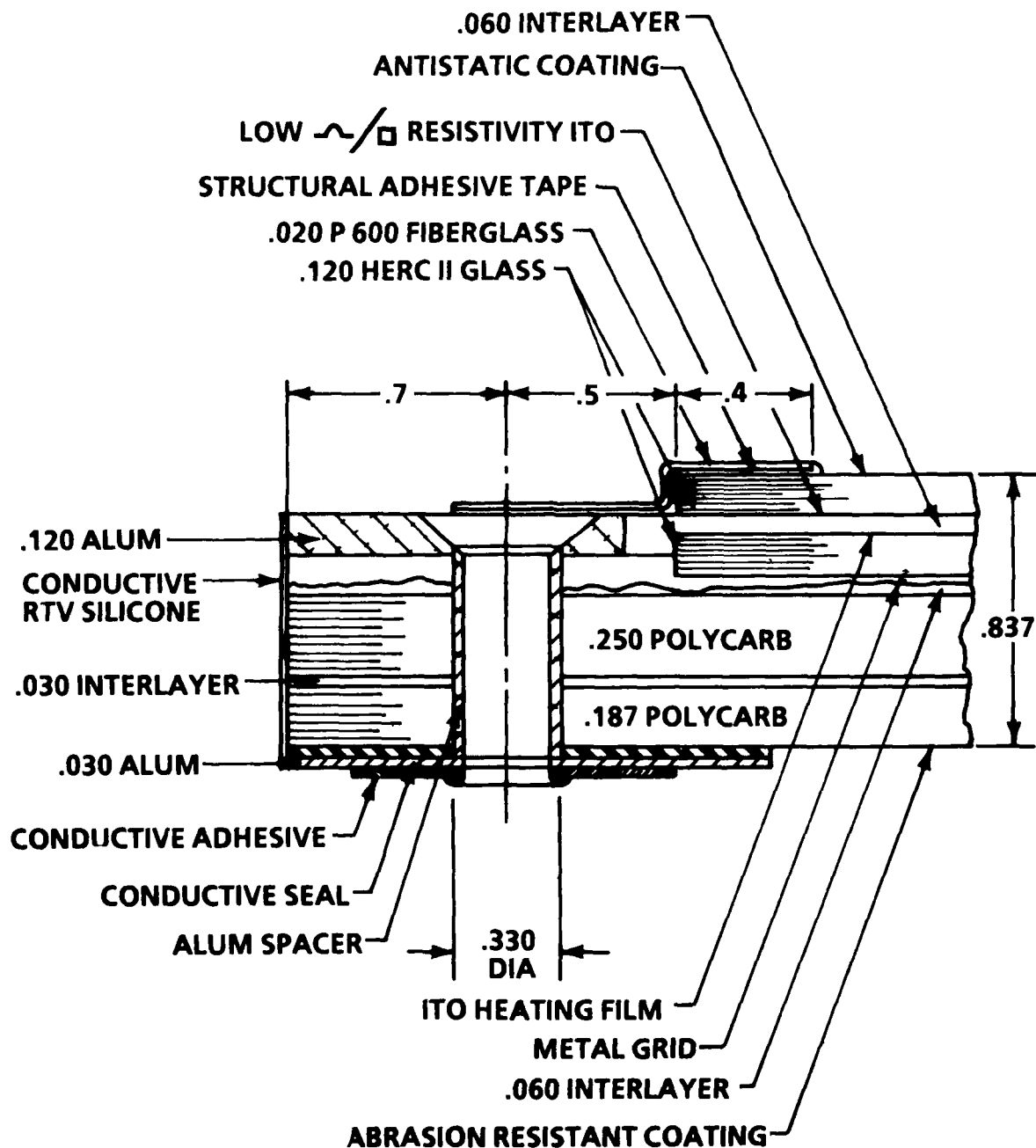
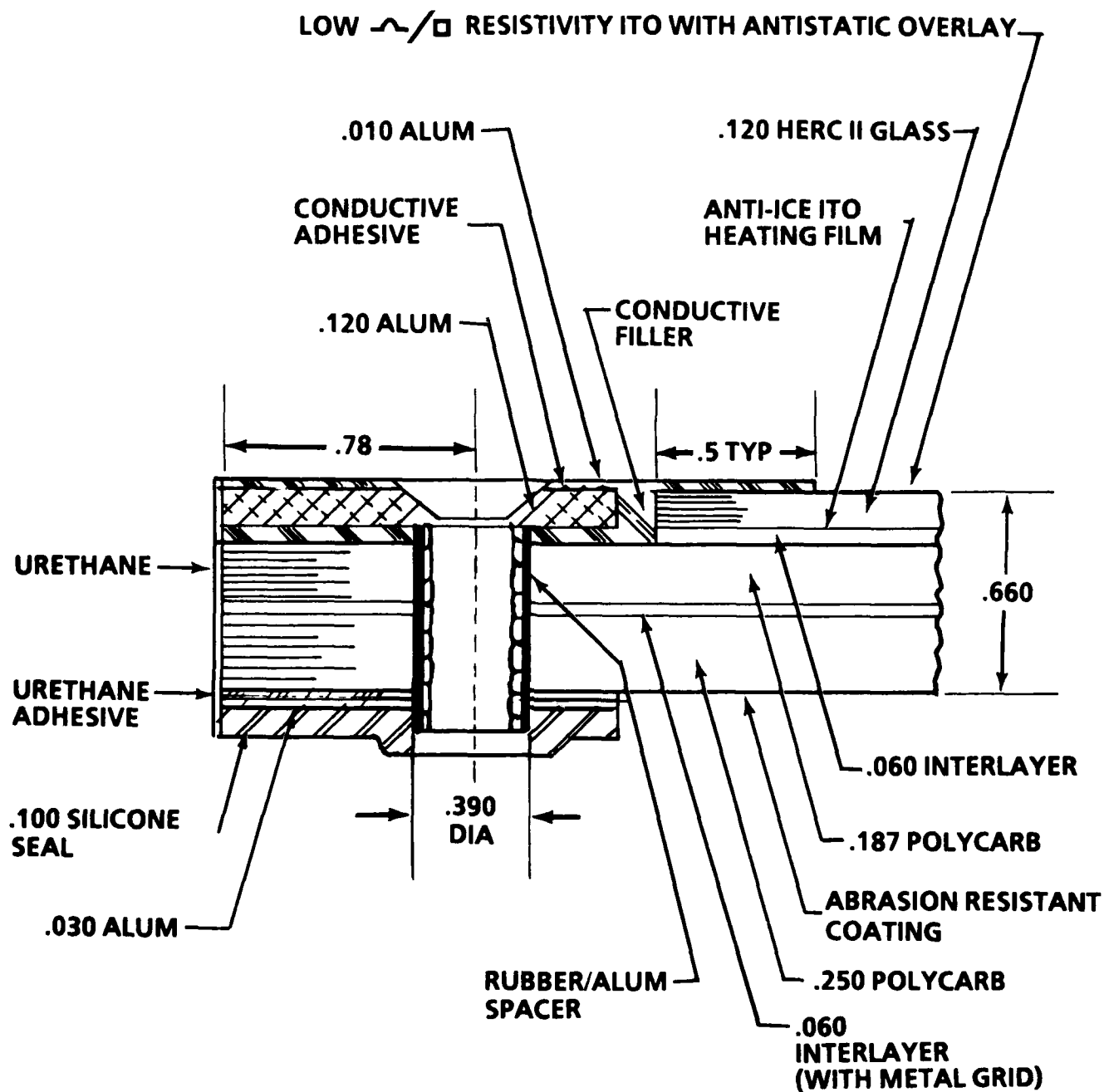
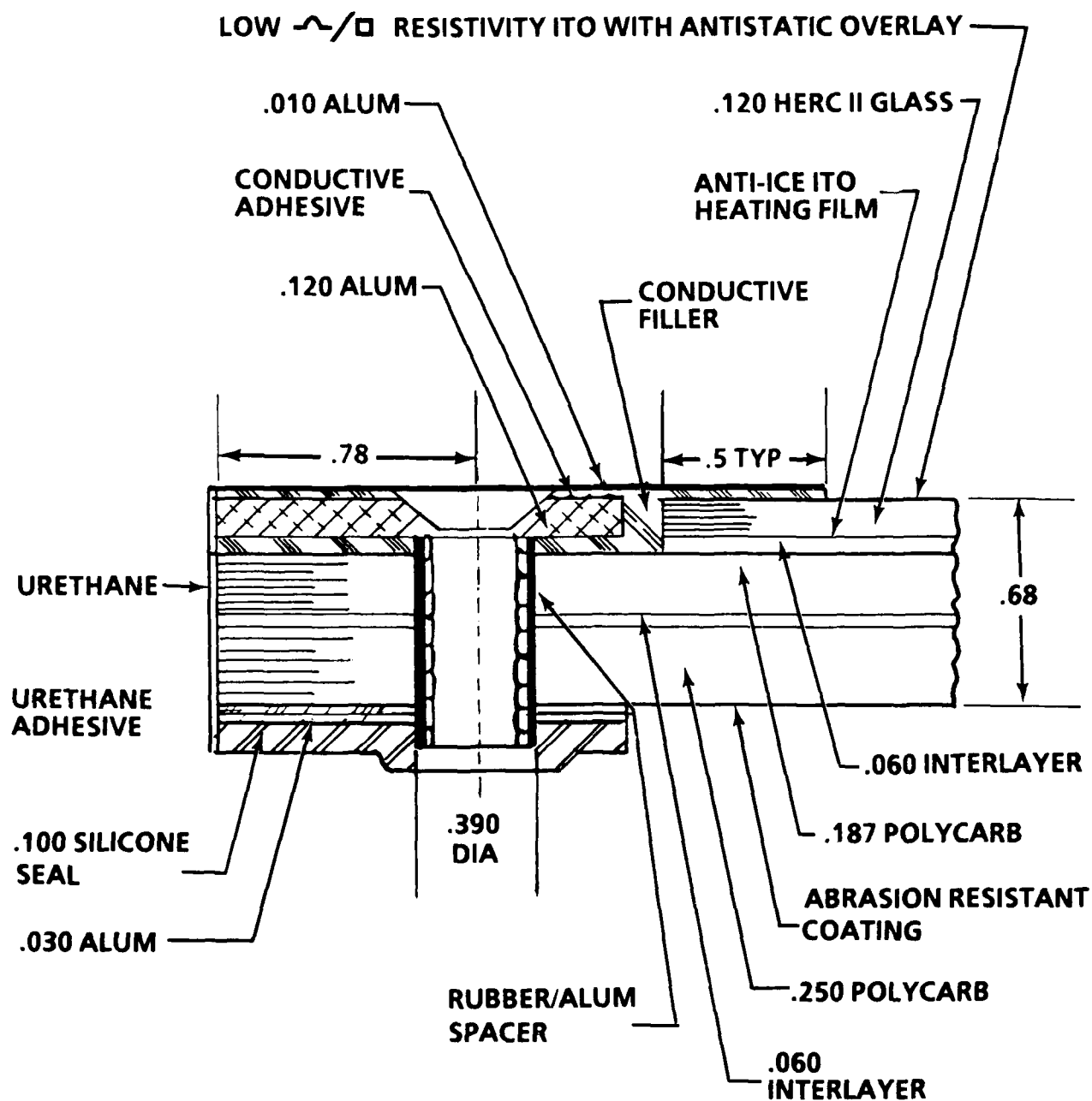


Figure 6. Design Revision C



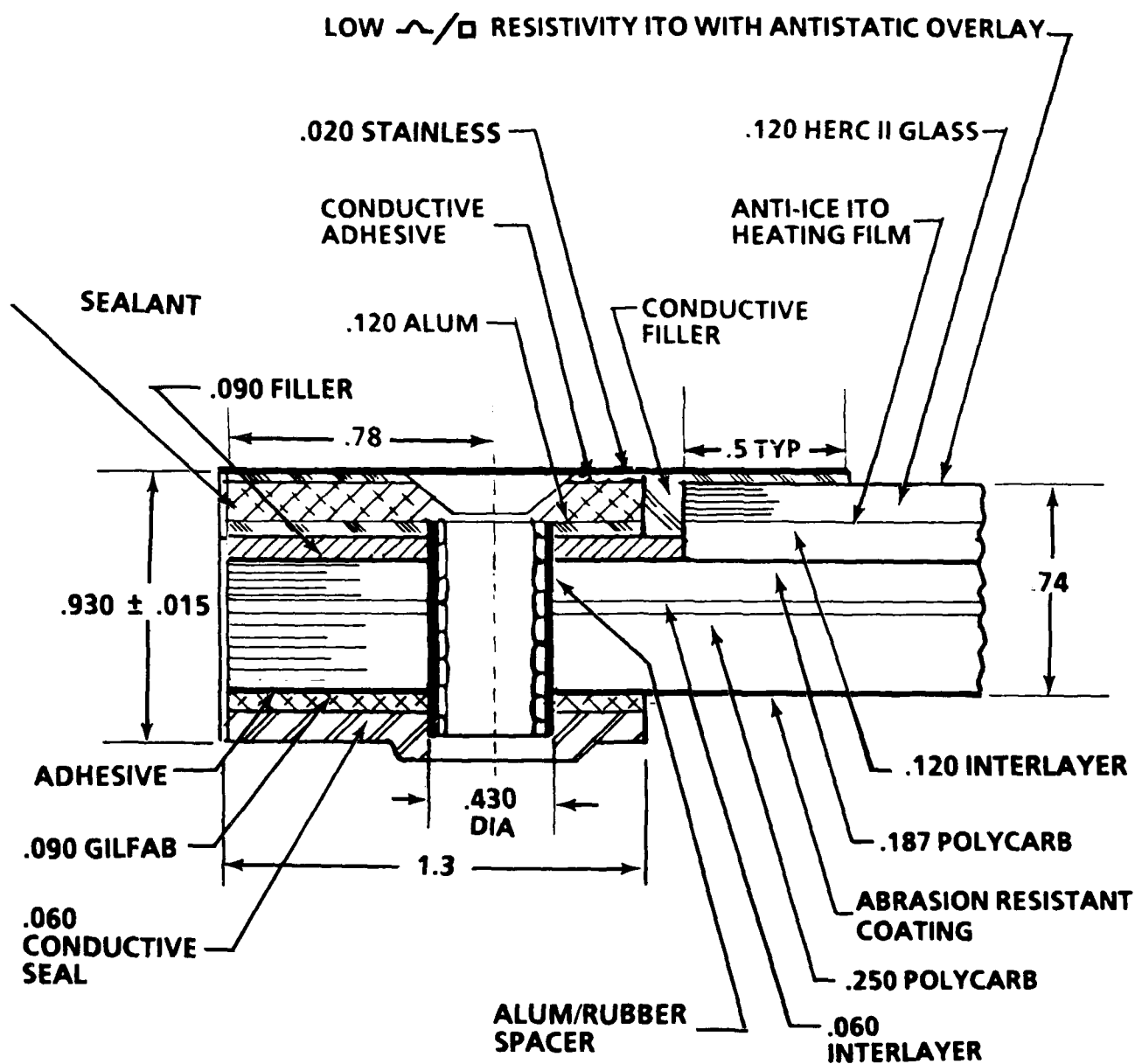
V-22 MAIN WINDSHIELD

Figure 7. Design Revision D



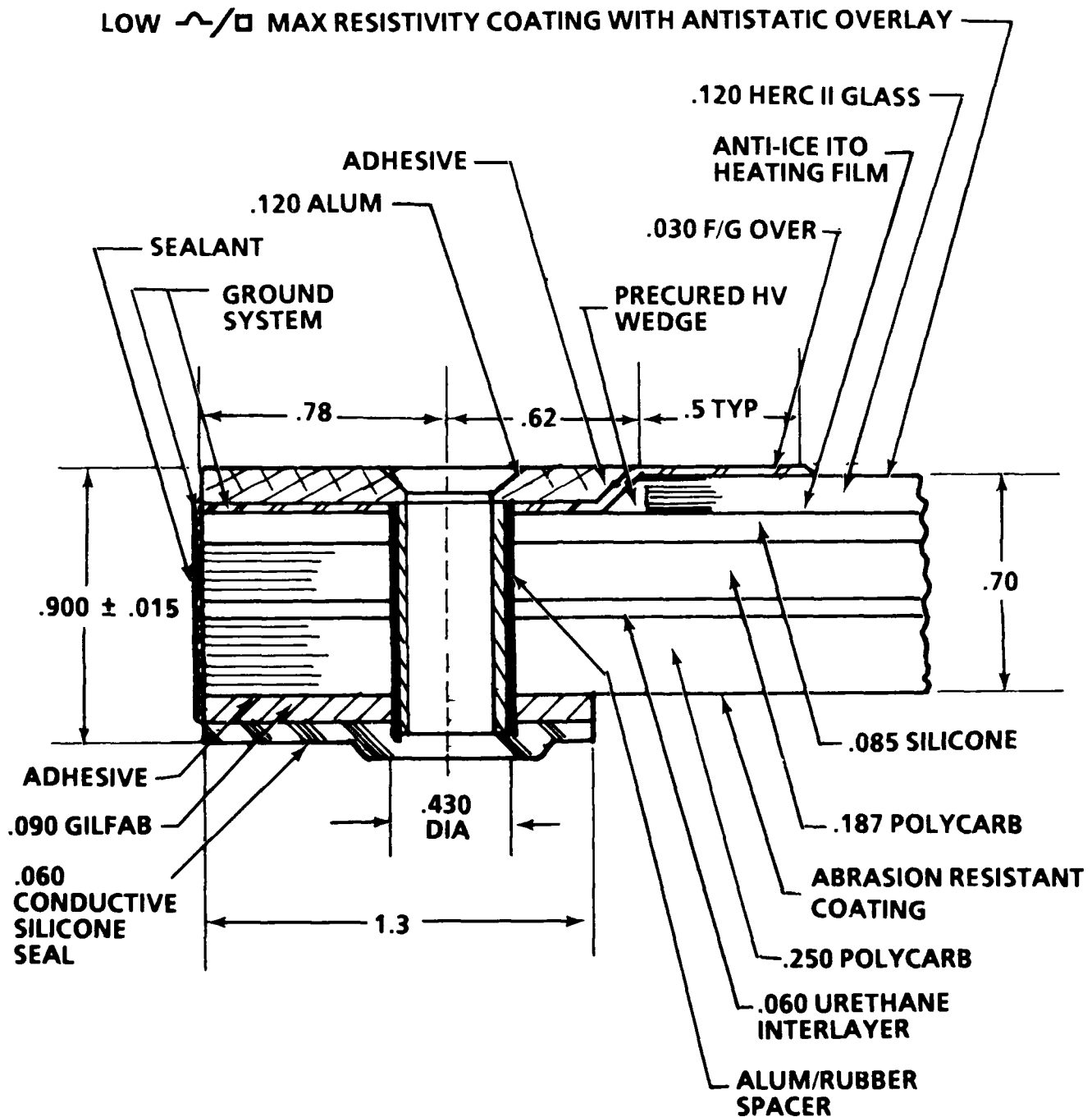
V-22 MAIN WINDSHIELD

Figure 8. Design Revision E



V-22 MAIN WINDSHIELD

Figure 9. Design Revision F



V-22 MAIN WINDSHIELD

Figure 10. Final Design (FSD)

VISION TESTING AND PHOTOMETRY

The concern throughout the design process was that of providing adequate visibility. This was defined as the integral of the photopic (daylight levels) response curve of the human eye and the integral of the area of sensitivity of the NVIS (Night Vision Imaging System) (Ref. 1). The level of light transmittance under the photopic and the NVIS curves was evaluated using a classic method for estimation of loss of contrast sensitivity experienced by observers through a medium of less than perfect transmittance (Ref. 2). The unavailability of a visibility model to use as an acceptance criterion directed attention toward the use of empirical measures, in particular an airborne test to provide the final determination. Special concern was expressed by USMC Brig. Gen. Harold W. Blot, Jr. (V-22 PMO) and a test program was set in place.

Test Plan

The test plan was devised to be broad scoped to overcome some limitations of relying upon airborne evaluations alone. This was achieved by using a three phase study consisting of bench test, ground based test of resolution and an airborne test of operational acceptability. The bench test consisted of measurement of the spectroradiometric transmittance of the V-22 cross section, an A-6E REALNIGHT program windshield and an A-6E production windshield. The Ground Based resolution test involved a subjective appraisal by pilots using ANVIS and CATS EYE Night Vision Goggles while viewing a 3-Bar Target (Ref. 3) with windshield samples interposed. The airborne test was designed to evaluate the A-6E REALNIGHT program Acrylic windshield already mounted in the aircraft and the V-22 windshield cross section in a specially designed mounting.

Prototype Tests

Early-on, optical transmission tests were conducted on a 12-inch square test specimen provided by the vendor. The specimen was divided into quadrants. Each quadrant had different optical characteristics depending upon its construction. The characteristic design differences of each quadrant follows:

<u>QUAD #</u>	<u>CHARACTERISTICS EVALUATED</u>
1	One ITO coating (HPM)
2	Two ITO coatings (HPM and Heating)
3	One ITO coating with EPM Grid
4	Two ITO coatings with EMP Grid

Spectral and photopic transmissions of the above test specimen was studied using a broad spectrum light source. Ultimately, the quadrant with two ITO coatings was selected for full scale development. The quadrants with the EMP grids were rejected based on a 10% lower photopic transmission and objections of Boeing test pilots who felt that the EMP grid was visually distracting under certain lighting conditions.

Aircraft Selection

The selection of the aircraft for the airborne test took several turns as we first looked toward using available Boeing Chinooks. The requirement for high speed, long view testing conditions led toward accepting the U.S. Navy offer of the use of an A-6E REALNIGHT program aircraft based at Naval Air Test Center, Patuxent River, Maryland.

Test Specimen

A windshield was fabricated by PPG Industries which duplicated the V-22 cross section but was dimensioned and contoured to fit the A-6E. It was mounted on the right-hand side in front of the bomber/navigator seat (B/N) (Fig. 11).

Test Flight Operational Limitations

The following envelope restrictions were placed on the aircraft due to the uncertain structural integrity of the windshield/canopy structure:

- Airspeed not to exceed 290 KIAS
- Minimize operations in areas of high bird concentration, since windshield birdstrike testing was not conducted.
- Avoid altitudes less than 250 ft. AGL
- The low-level route shall contain benign terrain reducing the need to pull up during low-level flight.

Night Vision Goggles

Two types of NVGs were used, two AN/AVS-6(v)2 (one pair was modified to a 665nm minus blue cutoff, while the other pair was unmodified to a 625nm minus blue cut off) and CATS EYE (MK3C). The modified AN/AVS-6(v)2 (665nm cutoff) are proposed for use in the V-22.

Bench Test Results

Spectroradiometric transmission measurements using a continuous broad band source (Fig. 12 and Table 1) were performed on the V-22, the A-6E REALNIGHT program and the A-6E production windshields. Although the A-6E production windshield was not evaluated during airborne tests, bench and groundtest were conducted on the windshield because of the familiarity of our test pilot evaluators with this windshield.

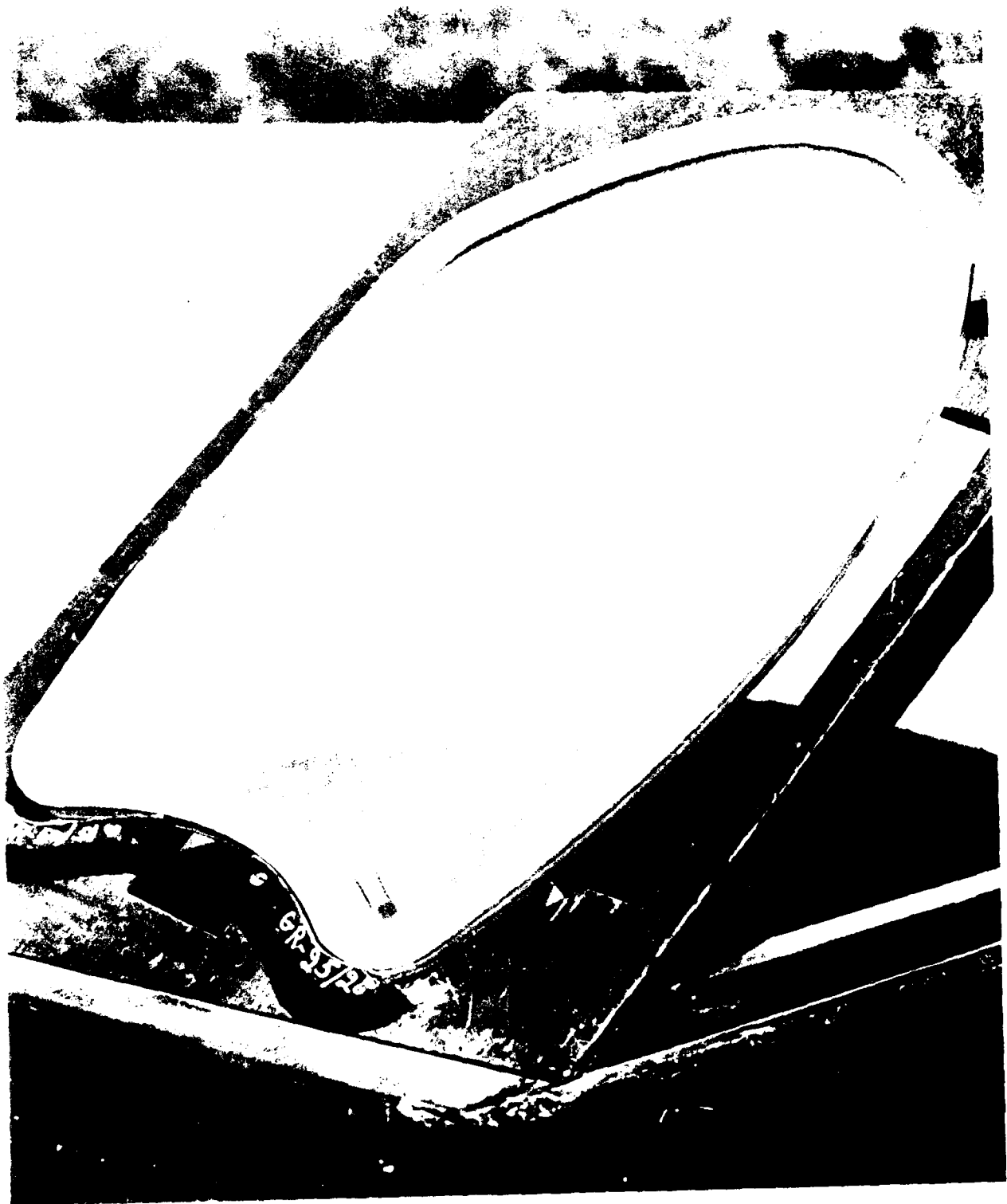


Figure 11. V-22 Cross Section Used in A-6E Aircraft Airborne Test

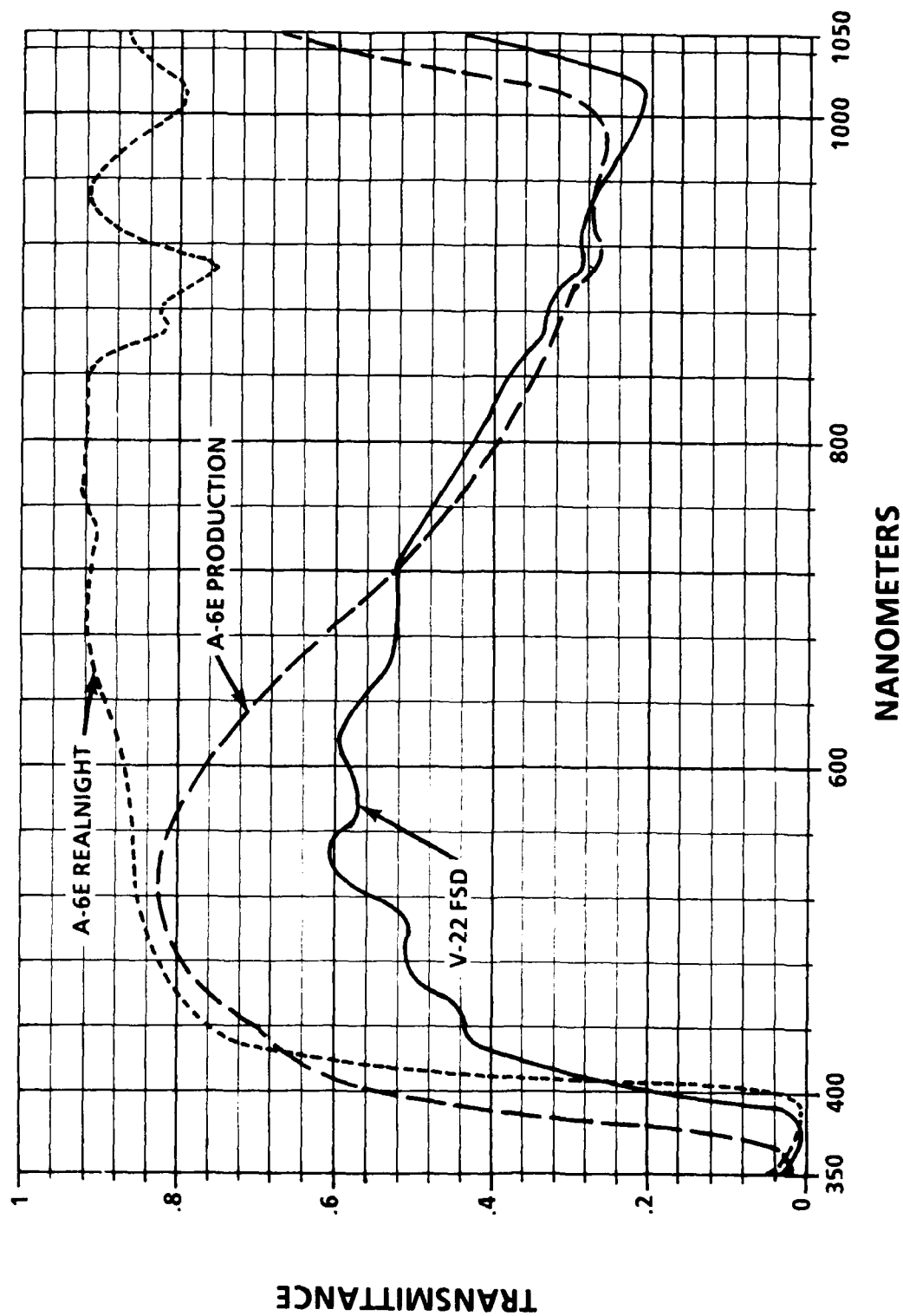


Figure 12. Relative Spectroradiometric Transmittance for 3 Windshields

TABLE 1
TEST WINDSHIELD LIGHT TRANSMISSION*

<u>Photopic Transmission</u>		<u>NVIS Transmission**</u>
V-22	65.4%	54.0%
A-6E REALNIGHT	86.7%	90.5%
A-6E Production	79.4%	46.4%

**Relative NVIS Transmission Calculations:

$$\text{Relative NVIS Transmission} = \frac{\int_{930}^{450} G(\lambda) N(\lambda) d\lambda}{\int_{930}^{450} G(\lambda) d\lambda}$$

$G(\lambda)$ = Relative Spectral Response of Class B NVIS
 $N(\lambda)$ = Spectral Transmission of Windscreen
 $d\lambda$ = 5nm

Ground Based Subjective Test Of Resolution

A test of resolution was set up using Night Vision Goggles in a darkened tunnel at the Naval Air Test Center at Patuxent River, MD.

Two different night vision devices were used, ANVIS and CATS EYE (both of which use Generation III intensifier tube technology). The CATS EYE uses a 665nm minus blue filter and the ANVIS employ a 625nm minus blue filter.

Two test subjects were used in the test, both were A-6E pilots, 40 and 31 years of age. Prior to the evaluation both subjects were tested for Snellen visual acuity. The test indicated that both subjects had 20/20 vision. Both pilots were experienced with the NVG's. Throughout the evaluation the subjects were not told which windshield they were evaluating.

The target employed was a Large Scale 3-Bar Resolution Target (Ref. 3).

Each subject viewed the 3-Bar Target with and without windshield specimens interposed. They were asked to state the level of resolution provided under each condition.

* All transmission measurements were conducted using Boeing Helicopter's Lighting Lab equipment, specifically a Photo Research 1980B spectroradiometer and a EG&G GAMMA Scientific C-11 spectroradiometer system (Fig. 13).

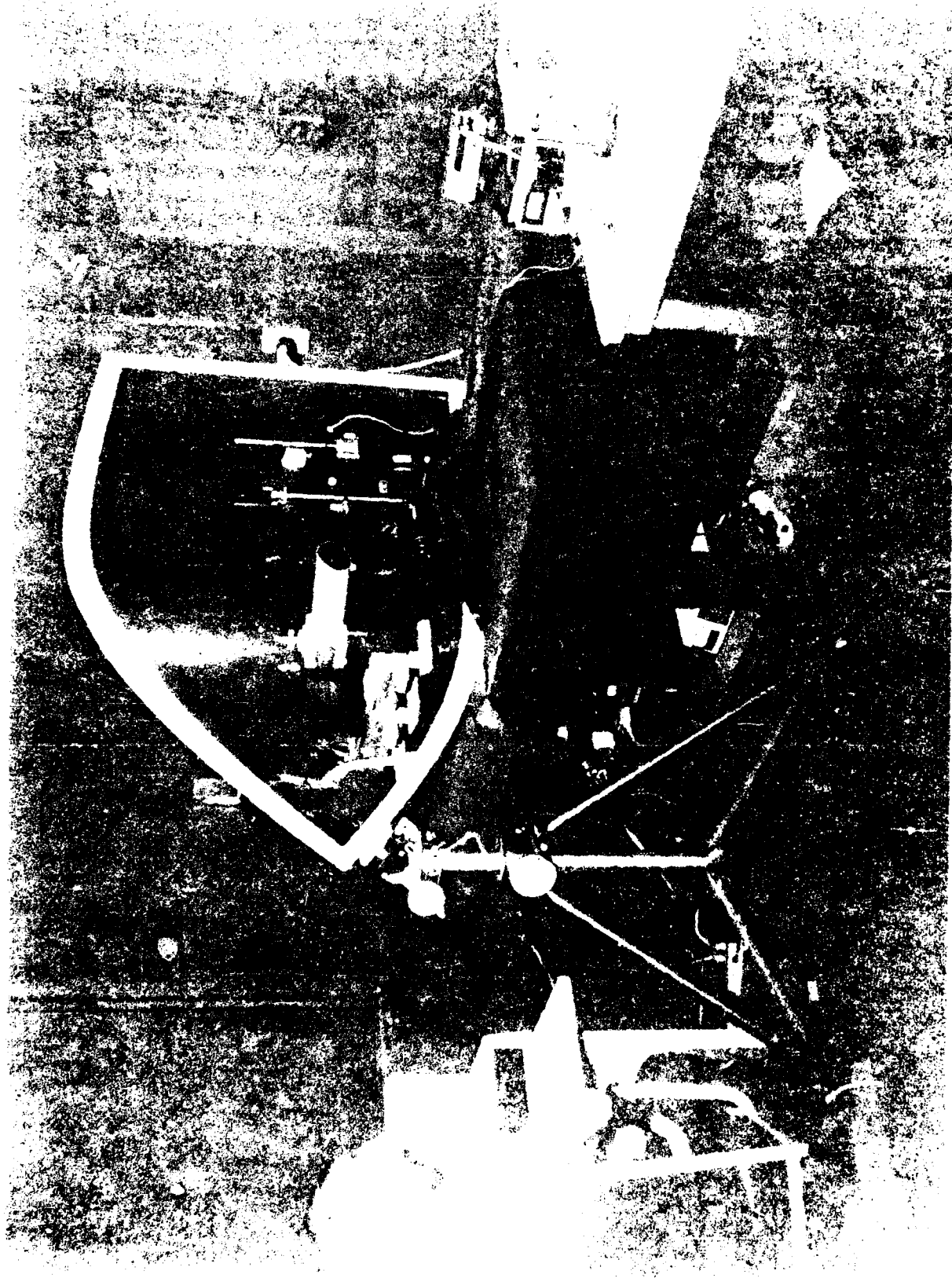


Figure 13. Photometry Lab Setup at Boeing Helicopters

The results of these evaluations (Fig. 14) indicated that in all cases, the V-22 windshield had a higher or an equal resolution when compared to the A-6E production windshield. The pilots' evaluation of resolution placed the REALNIGHT program windshield above the V-22. These findings are consistent with the photometric data.

TABLE 2
COMPARISON OF NIGHT VISION GOGGLES RESOLUTION
FOR THREE WINDSHIELD AND TWO GOGGLE TYPES
(Units are Lines per Millimeter)

	<u>ANVIS</u>	<u>CATS EYE</u>
No Windshield	.037	.02
A-6E REALNIGHT	.035	.021
V-22 FSD	.034	.018
A-6E Production	.033	.018

Although these data are from a very limited sample, the better performance using ANVIS is quite consistent. These data show the same rank ordering as the photometric data.

Results Of Airborne Test

Airborne tests using the V-22 windshield in an A-6E REALNIGHT aircraft were conducted at Naval Air Test Center, Patuxent River, MD under the flight envelope restrictions described earlier. Four test flights were planned.

The first two flights were conducted on Sunday evening, March 27, 1988 under excellent night flying conditions (unlimited ceiling, clear, 7 miles visibility and low relative humidity) with illumination from a half moon almost directly overhead. The March 27th flights were scheduled under half moon conditions in order to allow the pilots and the B/N to familiarize themselves with the terrain of the selected route and to identify any problems in structure or visibility with the V-22 windshield.

The second pair of flights were conducted early on Tuesday morning March 29th under similar weather conditions except that the illumination was from a slightly greater than half moon setting (30 degrees from the horizon) on the first flight and with only star light illumination (near worst case for NVG's) during the second flight.

The following are comparative evaluations between the A-6E REALNIGHT and the V-22 windscreens as stated by the pilots (Ref. 4).

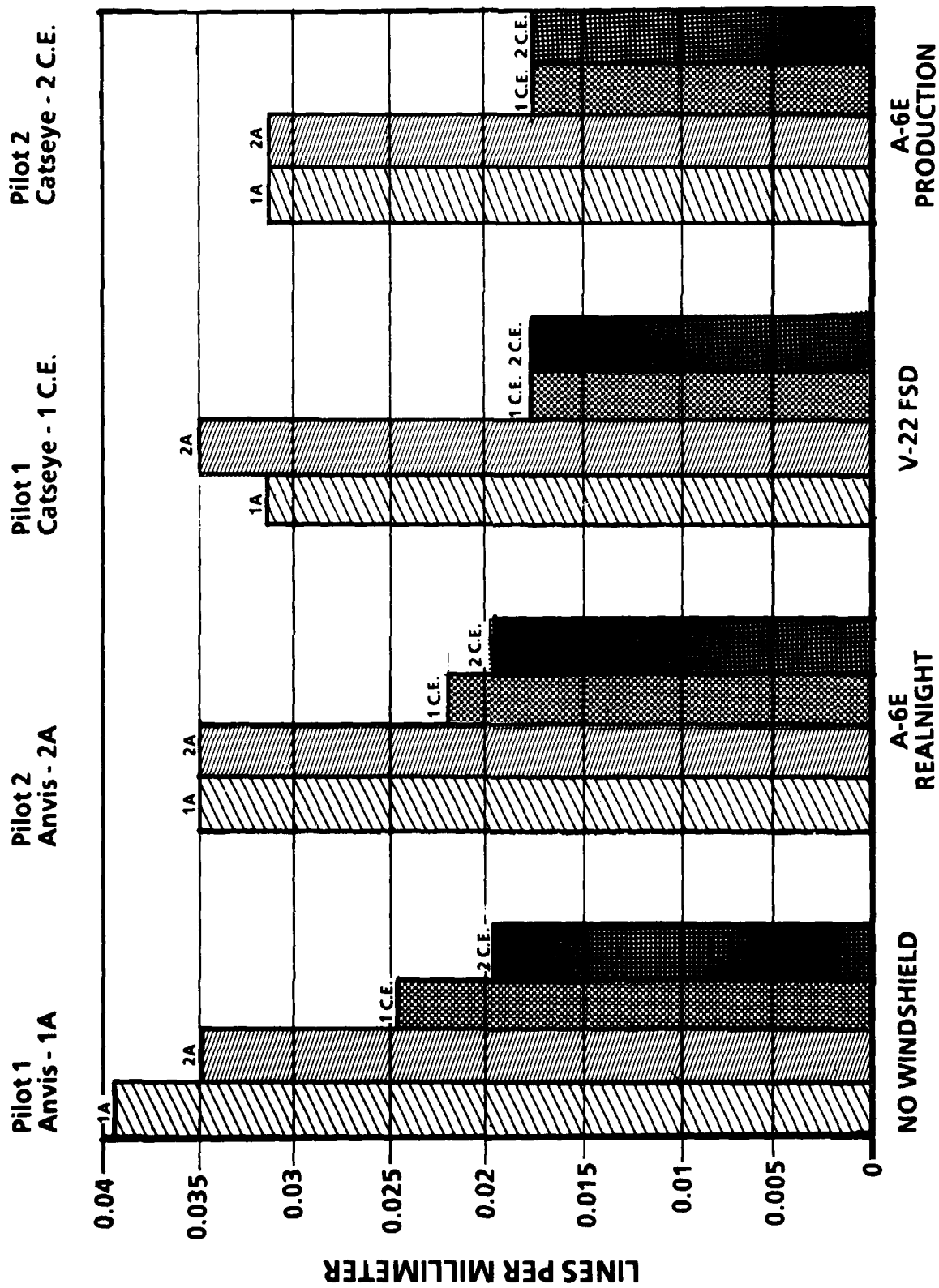


Figure 14. Subjective Appraisal of Resolution (3 Windshields)

"With bright moonlight overhead - The environment appeared slightly darker through the V-22 windscreen, and contrast was better through the REALNIGHT windscreen. Objects such as lakes, towers and roads were detected at approximately 2 miles through the REALNIGHT windscreen and 1 mile through the V-22 windscreen. A ridge line that projected above the horizon at a distance of 25 miles could be seen more distinctly through the REALNIGHT windscreen. Land/water contrast was slightly better through the REALNIGHT windscreen."

"Under mean starlight - Land/water contrast, detail, and brightness were slightly better through the V-22 windscreen. There was sharper definition of terrain and cultural features through the V-22 windscreen in haze."

"Within the scope of the test the V-22 windscreen as installed in the A-6E was satisfactory for low altitude flight with NVG's over benign terrain."

SUMMARY AND CONCLUSIONS

These test results indicate that the V-22 Osprey FSD windshield adequately satisfies the visibility requirements for operation during day and night operations. The photopic transmittance and high level of optical quality insures excellent resolution for general navigation purposes and target detection/recognition. The transmittance in the sensitivity bandwidth of the Night Vision Goggles (i.e., ANVIS and CATS EYES) has been shown by pilot evaluations during airborne tests to be satisfactory for the night mission objectives simulated during the airborne testing.

REFERENCES

1. MIL-L-85762A; Lighting, Aircraft, Interior, Night Vision Imaging System (NVIS) Compatible.
2. IES Lighting Handbook, Reference Volume, Chapter 3, IES, N.Y.C., 1984.
3. Naval Surface Weapons Center, "Instruction Manual for use of Large Scale Resolution Test Objects," Official NAVAIR Report (Report No. NOLTR-72-18).
4. Pickering, T. and Emmerich, S., "V-22 Windscreen Test in the A-6E for Night Vision Goggle Compatibility," NATC, Report No. RW-32R-88.

Visibility Test Plan

- **BENCH TESTS**
- **GROUND BASED TESTS WITH GOGGLES**
- **AIRBORNE TESTS WITH GOGGLES**

Vision Testing

- **PROTOTYPE TESTS**
- **AIRCRAFT SELECTION**
- **TEST SPECIMEN**
- **NIGHT VISION GOGGLES**

Test Results

- **SPECTRAL TRANSMISSION**
- **SUBJECTIVE RESOLUTION EVALUATION**
- **AIRBORNE EVALUATIONS**

ADVANCED CONCEPTS IN TRANSPARENCY SYSTEM
DESIGN/DEVELOPMENT

G. C. Stone, Ph.D.

General Dynamics
Fort Worth Division

ADVANCED CONCEPTS IN TRANSPARENCY SYSTEM DESIGN/DEVELOPMENT

G. C. Stone, PhD

Escape Systems Design

General Dynamics Fort Worth Division

Fort Worth, Texas 76116, U.S.A.

Abstract

Advanced transparency concepts at General Dynamics Fort Worth are rooted in a broad background and experience with transparency development spanning three major airplane programs and 30 years. Transparency design development began at General Dynamics Fort Worth Division in the mid-1950s with the flat and slightly curved multipaneled windshield system for the B-58 supersonic bomber and is highlighted by three technology advancements: (1) the multipaneled system for the F-111 series that contained highly curved chemically tempered, twin-ground glass, (2) the first military aircraft one-piece bubble canopy for the YF-16 prototype, and (3) the laminated combination of polycarbonate and cast acrylic separated by a polyurethane interlayer for the F-16 production aircraft. Ongoing activities have included F-16 worldwide multiversion production support; support of F-16 derivatives development; sputter and evaporative coating developments; bird-strike hardening analyses using the ABAQUS and MAGNA finite-element codes with energy absorbing bowframe, and wave limiting HUD development and high-temperature aerodynamic heating analyses using the STAPAT finite-element code.

Our concerns for the future center in four areas: (1) new requirements, (2) new materials, (3) new forming/shaping techniques, and (4) working with/"incentivizing" suppliers.

Future thrusts include chemical cracking analyses of polycarbonate and cast acrylic in the F-16 canopy; ballistics research and testing; bird strike testing/qualifying the F-16 transparency system to a 4-pound, 500-knot condition; laser hardness testing in a newly constructed General Dynamics laser laboratory; photochromics research for nuclear flash hardening and special material and forming technique development - all aimed at designing, building, and testing the most advanced transparency system for the next-generation tactical fighter aircraft operating in circa 1995.

Gathering of the Clan

In the trichairmen letter of invitation, the fifteenth conference on Aerospace Transparent Materials and Enclosures was referred to as a "gathering of the clan." What an interesting clan it is with government agencies, industry, and academia represented by so many talented, experienced, and innovative people.

Triad Operation

Historically, from an operational perspective, these various government agencies, companies, and academic institutions have fashioned themselves into a loose triad, as depicted in Figure 1. At the top of the triad are the sponsoring government agencies or government customers, the System Project Offices (SPOs) for the Air Force Fleet (F-16, F-15, B-1, ATF, etc.), the Air Force Wright Aeronautical Laboratories (AFWAL) (primarily the Flight Dynamics Laboratory and the Materials Laboratory), Ogden Air Logistics Center (OO-ALC), and a newcomer - the Producibility, Reliability, Availability, and Maintainability (PRAM) Office. PRAM has the charter to invest in existing technology to apply to a given airplane program to reduce life-cycle cost. The second part of the triad is the group of prime contractors (General Dynamics, Lockheed, McDonnell Douglas, Northrup, Rockwell International, Grumman, etc.). The third part of the triad is the supplier community, which is a varied combination of companies, academic institutions, research institutions, and consultants. This combination can best be characterized by three categories: the "shapers" or transparency builders (Sierracin, Texstar, PPG, Loral, Swedlow, Perkins, etc.), the "processors" or those who go from dust to sheets of material (Dow Chemical, GE, Celanese, Rhom and Haas, etc.), and the "speciality houses" (UDRI, Battelle Memorial Institute, Southwest Research Institute, and a host of consultants).

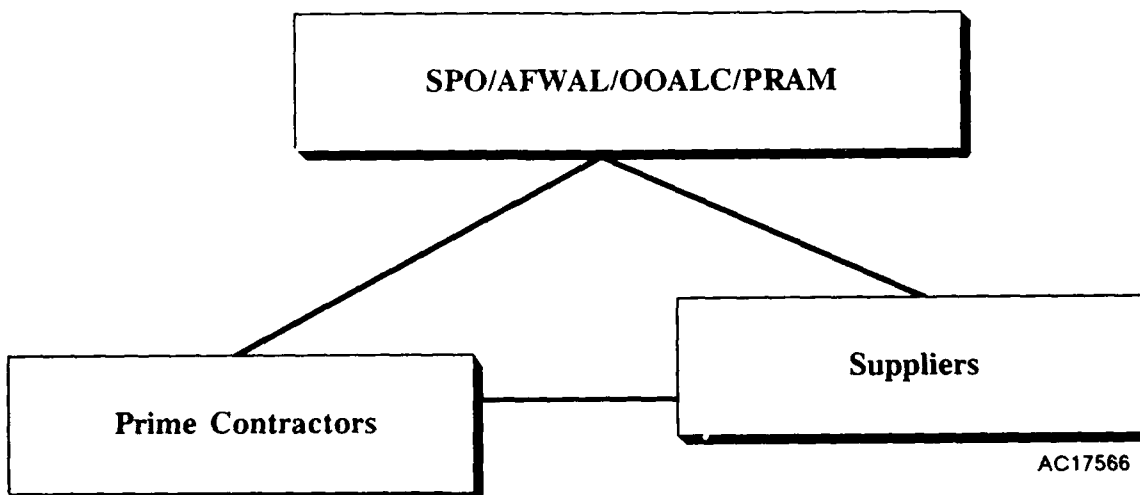


Figure 1 Transparency System Triad

As stated earlier, this is a loose triad. Not every company, institution, or agency fits neatly into the triad at all times during every program. Roles do change and the triad can operate in different and in what appears to be strange ways. The traditional way the triad works is for the SPOs to award major airplane contracts to prime contractors who in turn award subcontracts to the suppliers. For special developmental support, the prime contractors may go directly to the suppliers and award special

(usually small) contracts with internal research and development funding. During the traditional operation of the triad, the prime contractor designs a canopy assembly, subcontracts to a supplier to build and deliver the transparency, and then assembles the transparency into a canopy, installs the canopy on the airplane, and delivers the airplane to the Air Force customer. During this process, the prime contractor continues to improve the canopy system through engineering change proposal (ECP) activities approved by the respective SPO on a contractor-furnished equipment (CFE) basis. During this process, AFWAL and now PRAM serve as advisors on approval of the "improvements" and OO-ALC provides the depot and spares role.

The triad can operate in the opposite direction if, after several years of airplane production, the SPO ascertains and the prime contractor agrees that it is cheaper for the Government to purchase the transparency from the supplier and deliver it to the prime contractor on a Government-furnished equipment (GFE) basis. When this decision is made by the SPO, AFWAL becomes more directly involved in the transparency improvement process and tends to award transparency improvement contracts directly to the suppliers with the prime contractor assuming the advisory role. Therefore, the CFE/GFE decision of the SPO can serve as an important driver in the direction of the flow of investment in transparency improvement activities. Operations of the triad and their influence on transparency system development will be pointed out throughout this paper.

Transparencies Mature

General Dynamics Fort Worth Division has been an active and effective member of the transparency system triad for almost 50 years as a prime contractor. Although windshields were installed on B-24, B-32, and B-36 bombers, it was not until the supersonic B-58 bomber program that transparency systems were designed and developed at General Dynamics.

The B-58 transparency system (Figure 2) was a multipaneled windshield featuring two 1/4-inch-thick glass sheets in each panel. The glass panels were provided by Libby Owens Ford (LOF). The glass sheets were laminated with Silastic "K" bonding material to form a total panel thickness of 1/2 inch. Of the six panels this system was composed of, the aft two panels were slightly curved and the other four panels were straight. The B-58 transparency system was designed to the following requirements: (1) temperature (Mach 2.4), (2) pressure, (3) rain/hail/ice, and (4) optical quality.

Bird Strike Testing Emerges

During the later stages of this program, General Dynamics performed the first bird-strike testing using a B-58 forward fuselage fashioned into a sled that was originally used for ejection seat testing. Ejection seat sled testing was being performed during the summer of 1959 at Hurricane Mesa, Utah. The test engineer on site was asked to plan and conduct an "adapted" bird-strike test on the sled windshield. This bird-strike test was probably one of the most realistic tests ever performed. The test, as shown in Figure 3, consisted of a dead bird (which turned out to be a duck because of unavailability of chickens in the area) suspended in a sack between two poles across the track. The bird was then impacted by the sled at over 400 knots. Our first bird-strike setup differed considerably from the present setup of mounting the transparency system to a stationary fixture and firing the bird at the transparency.

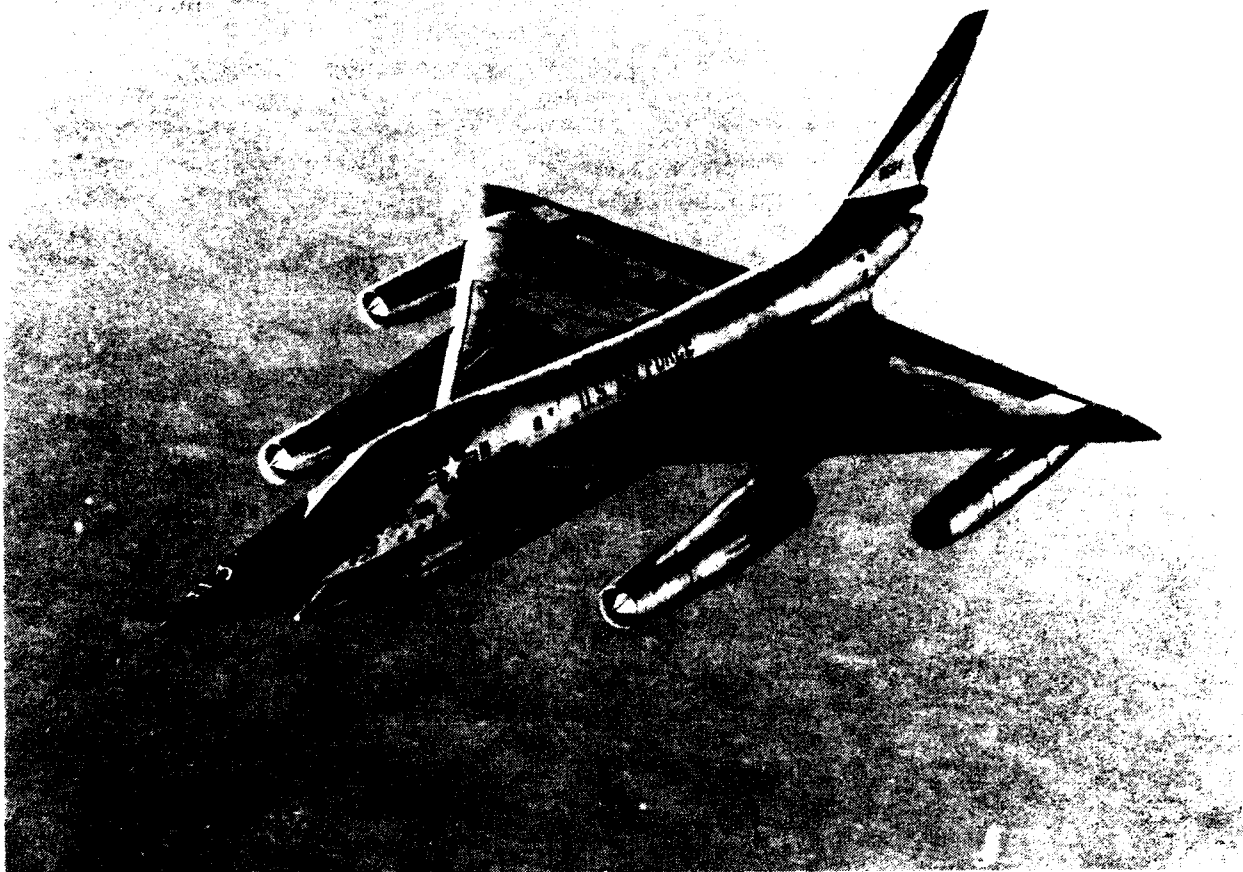


Figure 2 B-58 Transparency System

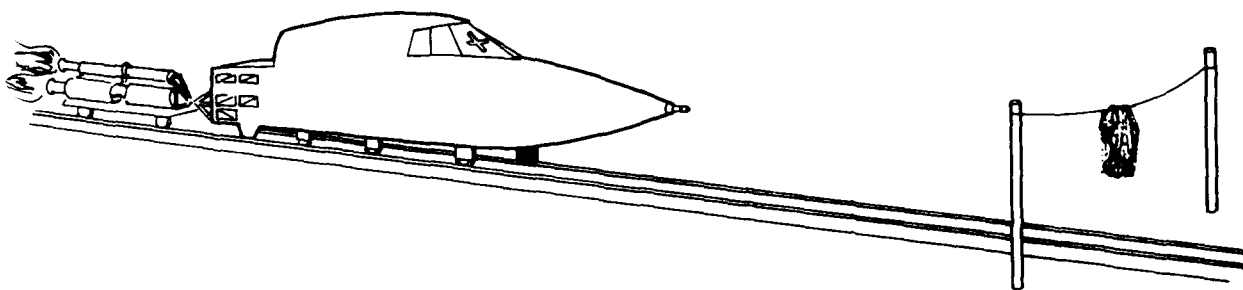


Figure 3 GDFW's First Bird-Strike Test

Results were considered unofficial and details were not well documented. But transparency system failure did occur. From a positive viewpoint, this first bird-strike test provided a glimpse of the challenges that lay ahead in the field of bird proofing. For the near future, however, the idea of bird proofing would lie dormant.

The transparency system triad operated in the traditional way throughout the B-58 program. General Dynamics' transparency design development effort gathered momentum during the early 1960s with the curved multipaneled system designed for the F-111 series aircraft shown in Figure 4. The F-111 Program began in 1962 with McDonnell Aircraft Co. handling fabrication, development, and certification of the transparency system as a part of a crew module subcontract to General Dynamics. This is another example of how the transparency system triad can operate: one prime contractor subcontracting to another prime contractor.



Figure 4 F-111 Transparency System

First Technological Advancement

However, after roughly two years, by mutual agreement between both companies, transparency system fabrication, development, and certification tasks were transferred back to General Dynamics. By this time, McDonnell had launched a three-version transparency program consisting of monolithic stretched acrylic and a laminate fea-

turing stretched acrylic as the structural material covered by cast acrylic as a protective outer ply. Both of these versions were furnished by Swedlow. The third version was chemically tempered glass furnished by PPG.

The F-111 transparency system was designed to the following requirements: (1) temperature (370°F), (2) pressure (greater than 20 psi), (3) rain/ice/sunshine, (4) abrasion/solvents, and (5) optical quality.

The third version, featuring glass by PPG, was the beginning of the first technology advancement in transparency systems.

Because of temperature and optical quality difficulties with the first two acrylic versions, General Dynamics began to look seriously at the PPG glass version. After a concerted effort with PPG and experimenting with many grinding technique variations, a glass version was chosen over the two earlier plastic versions. PPG finally had to go to Pisa, Italy, to find someone who could accomplish the precision grinding required. These *curved, chemically tempered, twin-ground glass panel systems* became the *first technology advancement* in transparency panel systems.

Customer Approval Necessary

An important constraint that every major air framer works within is that no prime contractor can put any item or feature on an airplane during production without customer approval (in this case, the F-111 SPO). By 1964, General Dynamics was two years into the F-111 program and five years past that first unofficial B-58 bird-strike test. And with the F-111, General Dynamics had, for the first time, an airplane with its new terrain following system (TFR) – flying frequently "on the deck" (500 feet or lower) at speeds up to Mach 1.2 for extended periods – ripe conditions for finding a bird. Therefore, General Dynamics began a quest for customer approval to seek new bird-hardening methods. This quest lasted seven years and included a new bird-hardened full-scale test transparency designed by General Dynamics and built by a supplier (Goodyear, now Loral). The new bird-hardened panel was a laminate consisting of (1) polycarbonate structural plies, (2) an outer protective acrylic ply fused to the polycarbonate for grinding and forming ease, and (3) instrumentation for ground testing. Fusing acrylic to the polycarbonate would later prove to be ineffective and would require some sort of crack arrestor (such as an interlayer) to separate these two laminated materials.

Bird-Proofing Development Begins

Finally, in 1971, the F-111 SPO announced that they would commit budget for bird-proof development. However, the F-111 SPO also placed the F-111 transparency system on GFE status, which reversed the operation of the transparency system triad with AFWAL's Flight Dynamics Laboratory performing bird-proof development. Bird-proof development of the F-111 transparency system was accomplished with direct support from PPG through the Bird Impact Resistant Transparency and Advanced Bird Impact Resistant Transparency (BIRT/ADBIRT) Programs. This activity included evolving from the 0.32-inch thick chemically tempered, twin-ground glass version to an 0.9-inch thick multiple polycarbonate/cast acrylic version certified to a 4-pound, 500-knot bird-strike condition at the critical corner and to 600 knots at other locations. F-111 transparency system improvement has continued from that point and is ongoing.

First One-Piece Bubble Transparency

General Dynamics' transparency system design development effort evolved to a higher level of sophistication with the F-16 series aircraft during the early 1970s. This family of aircraft began with the YF-16 prototype, which first flew in 1973. The YF-16 featured the first *one-piece bubble transparency* for U.S. military aircraft, which was the *second technology advancement* in transparency system development. The YF-16 prototype is shown in Figure 5. This one-piece bubble transparency, which consisted of 3/8-inch thick coated monolythic polycarbonate material, did not just happen. Rather, like the chemically tempered, twin-ground glass concept of the F-111, the one-piece bubble concept was the result of a concerted effort on the part of Sierracin who took General Dynamics' new innovative design and, with a shared investment, did successfully build it.

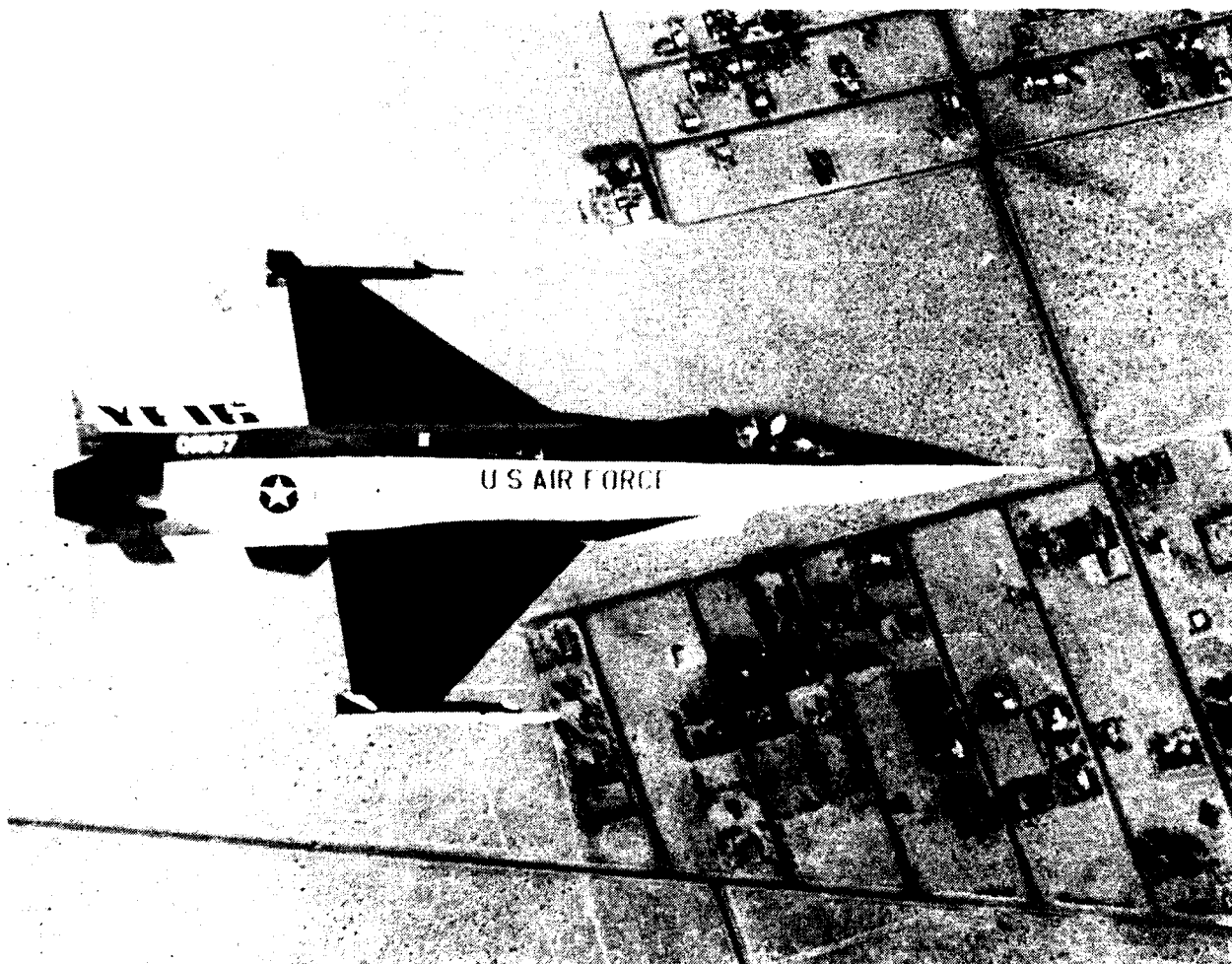


Figure 5 YF-16 Prototype One-Piece Bubble Transparency

In early 1975, after winning the YF 16/17 prototype fly-off competition, General Dynamics was awarded a full-scale development (FSD) contract for six single-place and two two-place F-16 aircraft. General Dynamics revised their design for slight airplane size scale-up and transparency thickness increase for bird-hardening. By this time, the transparency subcontract competition had expanded to two candidate suppliers and General Dynamics proceeded into the FSD phase of the program. The F-16A FSD

transparency system (Figure 6) consisted of 0.5-inch thick monolithic polycarbonate and employed Texstar's C254C1 protective coating. In addition to other requirements, this transparency system was designed to a 4-pound, 300-knot bird-strike condition.



Figure 6 F-16A (FSD) Transparency System

The next year (1976), General Dynamics was awarded the F-16 production contract. Transparency thickness was increased again as the specifications were crystalized and transparency system certification was initiated. The first multiyear buy for transparencies was consummated on a CFE basis and would extend to 1980. The transparency system triad was again operating in the traditional way.

General Dynamics then transitioned from FSD to full production of the F-16A/B series. This first F-16 production version (Figure 7), which was provided by Texstar, consisted of 3/4-inch thick monolithic polycarbonate with Texstar's C254C1 coating. This system was certified to the F-16 bird-strike specification of 4 pounds, 350 knots and has been successfully tested to 4 pounds, 400+ knots with less than 2 1/4-inch deflection over the pilot's head. In addition to bird strike, this system was certified to (1) temperature (265°F), (2) pressure ($\Delta P = 12.45$ psi), (3) rain/ice/fungus/sunshine, (4) abrasion/solvents, (5) optics, and (6) maintainability/interchangeability.



Figure 7 F-16A Transparency System

Laminates Emerge

During the first multiyear buy (1976-1980), a third supplier joined the group and was involved in fabrication, development, and certification of F-16 transparencies with a fourth supplier (PPG) competing for the monolithic business when they had the opportunity. This group of suppliers, working independently, achieved the capability to efficiently and economically *form laminated sheets of different transparency materials into complex shapes*, such as the F-16 bubble. From this breakthrough, the *third technology advancement* in transparencies was achieved, i.e., the laminated combination of polycarbonate/cast acrylic separated by a polyurethane or silicon interlayer. Within a short period, this version began to emerge as an F-16 transparency concept.

Between 1980 and 1981, General Dynamics' customer (F-16 SPO) placed the F-16 transparencies on GFE status and once again reversed the operation of the transparency system triad (Figure 1). With the GFE decision, the F-16 SPO assumed the fabrication, development, and certification role for the F-16 transparencies and competed the work to the group of three suppliers. In October 1981, the first GFE SPO production buy was awarded to Sierracin and Goodyear who would produce a 3/4-inch thick laminated polycarbonate/cast acrylic version. The second SPO production buy followed in October 1984 and was awarded to Texstar and Sierracin. In August of the following year (1985),

Goodyear announced that they were discontinuing their F-16 transparency business, which left Sierracin and Texstar as the F-16 transparency suppliers for the third and current SPO production buy awarded in October 1987. The next F-16 transparency buy will be awarded in October 1990 and will be the first OO-ALC combined production and spares buy.

At present, three types of F-16 transparencies are in service (Figure 8). The most prevalent type is Type I (the later version), which is the polycarbonate/cast acrylic laminate with one polycarbonate structural ply covered by one acrylic outer play built by Sierracin and Texstar. Roughly 2000 units are in service worldwide. Type II is the monolythic coated polycarbonate structural ply built by Sierracin for the F-16 prototypes with roughly 800 units in service built by Texstar. Type III is an elaborate polycarbonate/cast acrylic laminate composed of two polycarbonate structural plys covered by both outer and inner acrylic plys built by Goodyear.

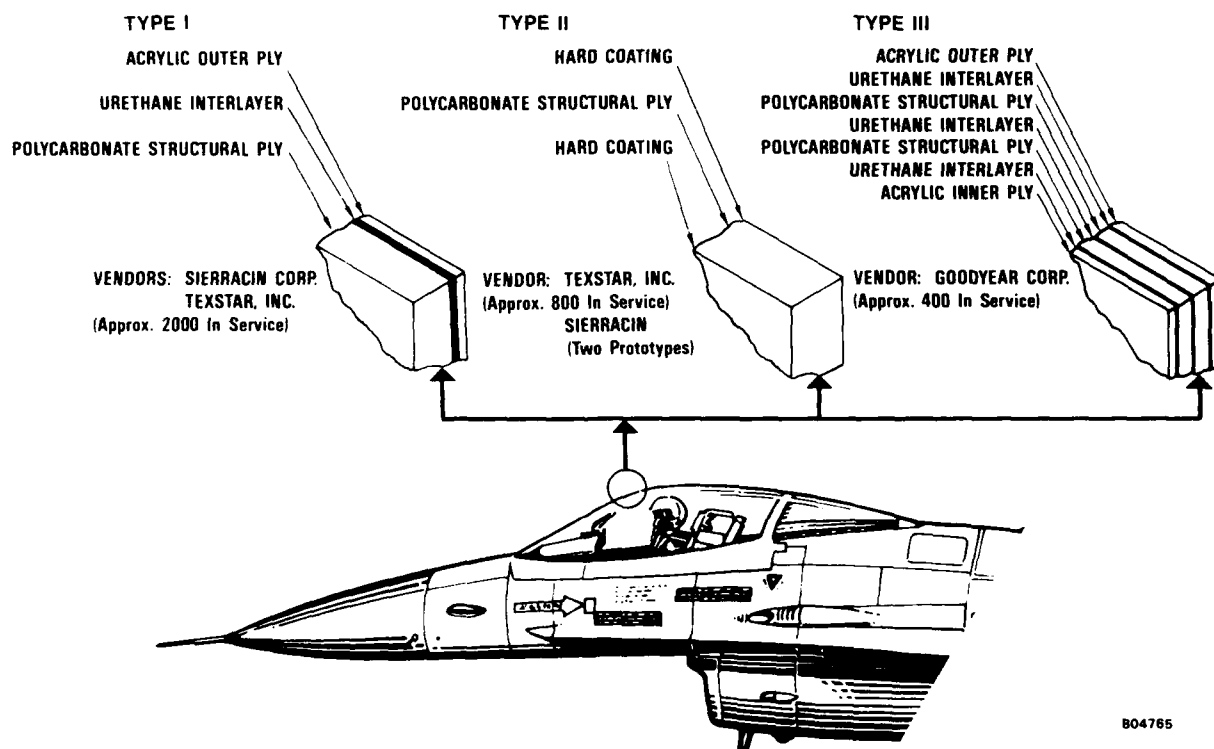


Figure 8 F-16 Transparency Types In Service

Throughout the 1980s, AFWAL's Flight Dynamics Laboratory has been quite active with F-16 transparency improvement for GFE conditions. But unlike the GFE days of the F-111 Transparency Program, General Dynamics has had a more active role in F-16 transparency improvement efforts than the traditional advisor. A certain portion of this increased role can be attributed to the development of different versions of the F-16, such as the Advanced Fighter Technology Integrator (AFTI) and F-16XL prototype but more significantly to changes in the F-16 mission. Also, transparency system design has expanded to the point that transparency-to-frame integration, canopy-to-fuselage integration, and canopy-to-cockpit integration have all become essential parts of the transparency design. The prime contractor must be involved with these three types of integration, especially the last two. These three types of integration are becoming even

more sophisticated with each succeeding airplane program. As a result and as will be pointed out later in this paper, General Dynamics participation in F-16 transparency improvement efforts is expanding.

F-16 Ongoing Support Activities

At present, General Dynamics is participating in a wide variety of F-16 transparency improvement activities. Transparency design and development will continue to support F-16 derivatives with new, faster, lower altitude missions that significantly increase bird-strike risk. Typical F-16 transparency improvement activities are (1) qualification testing of F-16 transparencies with indium tin oxide (ITO) coating applied, (2) pilot instrument training vision restriction development (VRD) technology, (3) new, fast, low-altitude mission bird-strike risk studies, and (4) acrylic star-burst cracking prevention.

ITO, as a replacement candidate for the existing F-16 transparency solar coating, was developed under Air Force sponsorship (F-16 SPO Industrial Technology Modernization Program). The subject qualification testing that uses ITO coating applied to Sierracin transparencies is 90 percent complete. A very positive result of these tests is that the ITO coating is satisfying environmental requirements that are more severe than those called for by the F-16 canopy specification.

The VRD program involved designing and developing a purple colored sheet into the forward section of an F-16B/D two-place canopy and coordinating it with an amber colored visor sheet mounted on the pilot's helmet. The intended result is zero visibility through the transparency for a student pilot with his helmet visor in place.

This zero visibility condition simulates an adverse weather situation through which the student must fly using instruments only, while an instructor pilot in the rear seat has sufficient visibility to avoid other aircraft or safety threat situations. Although a test transparency has been built by Texstar and indicates satisfactory results, VRD has not been accepted yet by the Air Force because of reduced visibility through the purple sheet during night flight with the helmet visor not in place. However, the design and development exercise challenged General Dynamics to cover new ground to coordinate cockpit lighting conditions as well as pilot functions and design the transparency with active supplier (Texstar) participation to a band-pass filter concept.

The fast, low-altitude mission bird-strike studies consist of probability analyses to assess possible increase in bird-strike risk to the newer versions of the F-16.

Methods for conducting bird-impact risk analyses is shown in Figure 9. This methodology consists of

- o Estimating bird densities in atmospheric layers
 - Using reported strikes on the F-16 canopy from 1982 to 1986
 - Using bird altitude strike hazard (BASH) data furnished by the Air Force
 - Using volume swept by the F-16 during 1982 through 1986 with a mission profile/mix method
- o Forecasting the volume the canopy will sweep per layer with a projection mission profile mix method

- o Forecasting canopy damaging strikes by
 - Sweeping the volume and bird density to determine expected number of strikes
 - Using velocity and bird weight to determine expected number of damaging strikes.

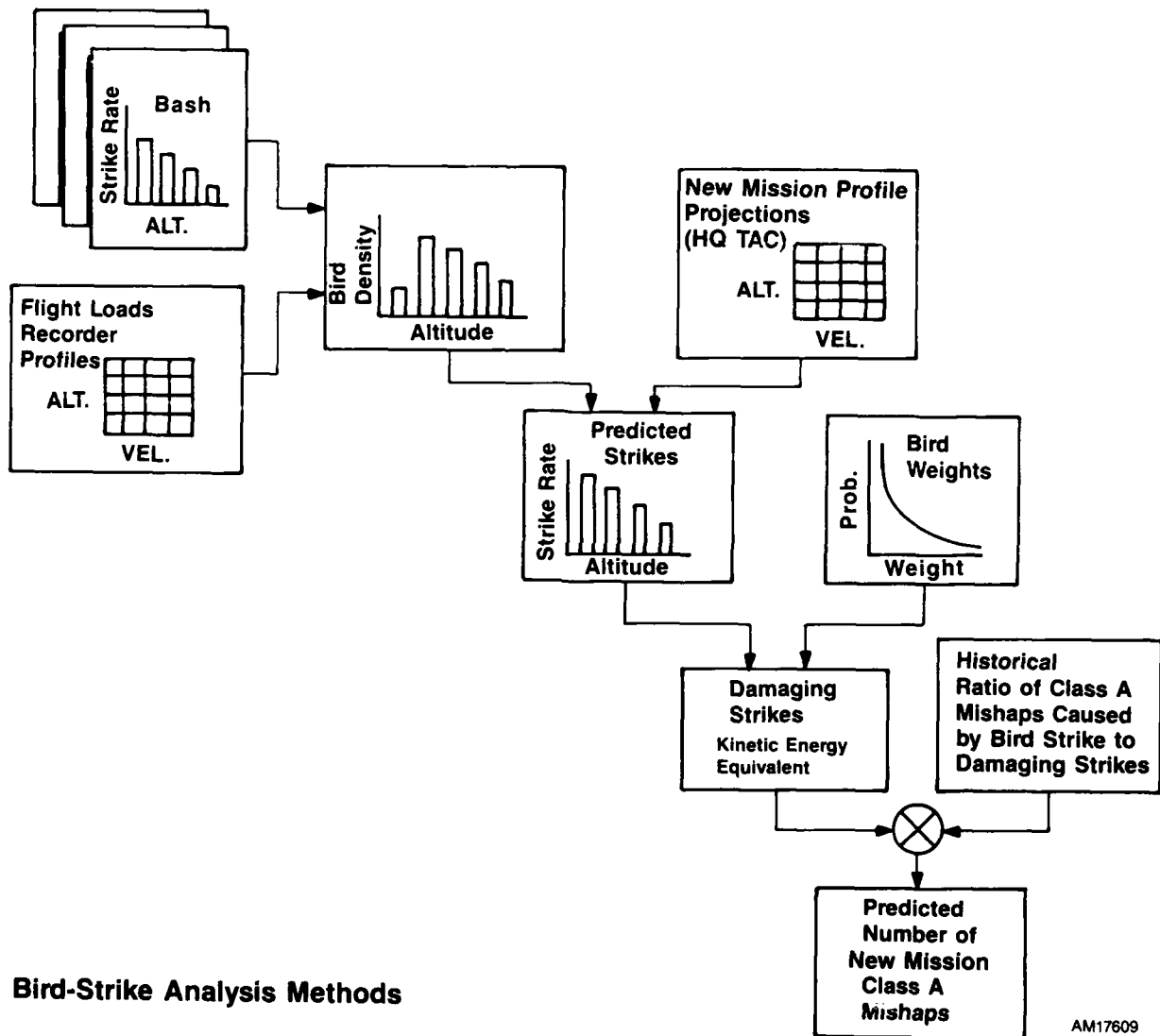


Figure 9 Methodology for Conducting Bird-Impact Risk Analysis

A damaging bird strike in this analysis is defined as one that generates kinetic energy equal to or greater than that called for by the F-16 canopy specification (4 pound bird at 350 knots). Figure 10 depicts a plot of damaging strike rate (damaging strikes per million flight hours per square foot of canopy sweep area) versus canopy toughness velocity rating (knots). The lower curve in this figure represents the predicted number of damaging bird strikes for the existing F-16 canopy with its existing bird-strike hardness for a given canopy toughness velocity rating. For example, the predicted

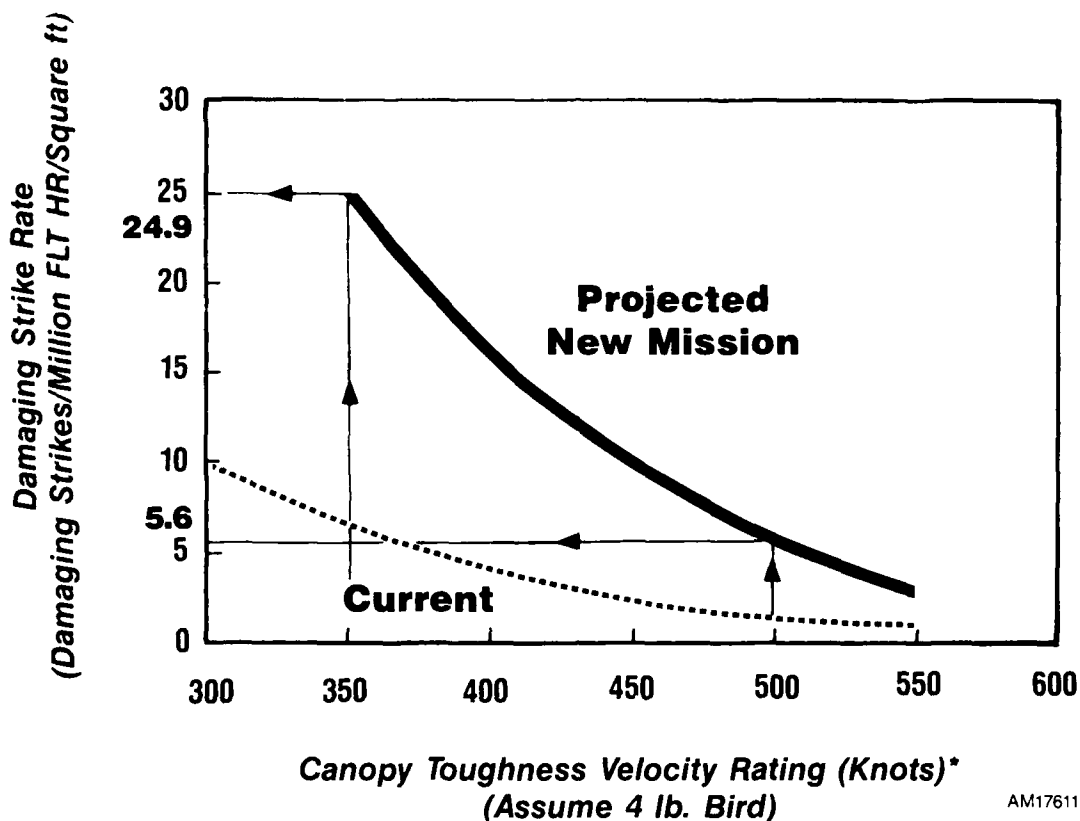


Figure 10 Damaging Strike Rate Versus Canopy Toughness Velocity (Knots)

number of damaging bird strikes for the existing F-16 canopy, which is qualified to a canopy toughness velocity rating of 350 knots, is 5.6. The upper curve represents the projected number of damaging bird strikes to be generated by the new mission. If no bird hardening is added design-wise to the existing F-16 canopy, then the number of projected damaging bird strikes to be generated by the new mission is 24.9 or roughly five times that of existing F-16 missions presently flown. Conversely, if sufficient hardness to qualify the F-16 canopy to a toughness velocity rating of 500 knots is designed into the F-16 canopy, then the projected number of damaging bird strikes would be 5.6 or the same as that of the F-16 during 1982 through 1986 with a mission profile/mix method, original canopy at a toughness velocity of 350 knots. Final phase of this bird-impact analysis is to predict (Figure 9) the percentage of damaging bird strikes that will result in Class A mishaps (loss of aircraft). This is accomplished by using historical F-16 flight data relating Class A mishaps to damaging bird strikes.

Recently, we have been trying to prevent a new type of cracking in the outer acrylic ply of F-16 transparencies, which we call the star-burst pattern. A nontraceable material (probably high-speed rain) pits the outer acrylic surface during flight. Then cleaning chemicals (particularly isopropal alcohol) collect in the pits and mix with any residual moisture and break the surface molecular lattice structure and creating tiny star-burst cracks. These tiny cracks are shown in Figure 11, on the forward surface of an F-16 transparency. Star-burst cracks eventually propagate throughout the acrylic ply and cause transparency rejection. A supplier is seeking a solution to this problem by looking for a material/coating combination as a substitute for the outer acrylic ply that is less susceptible to pitting and cracking.

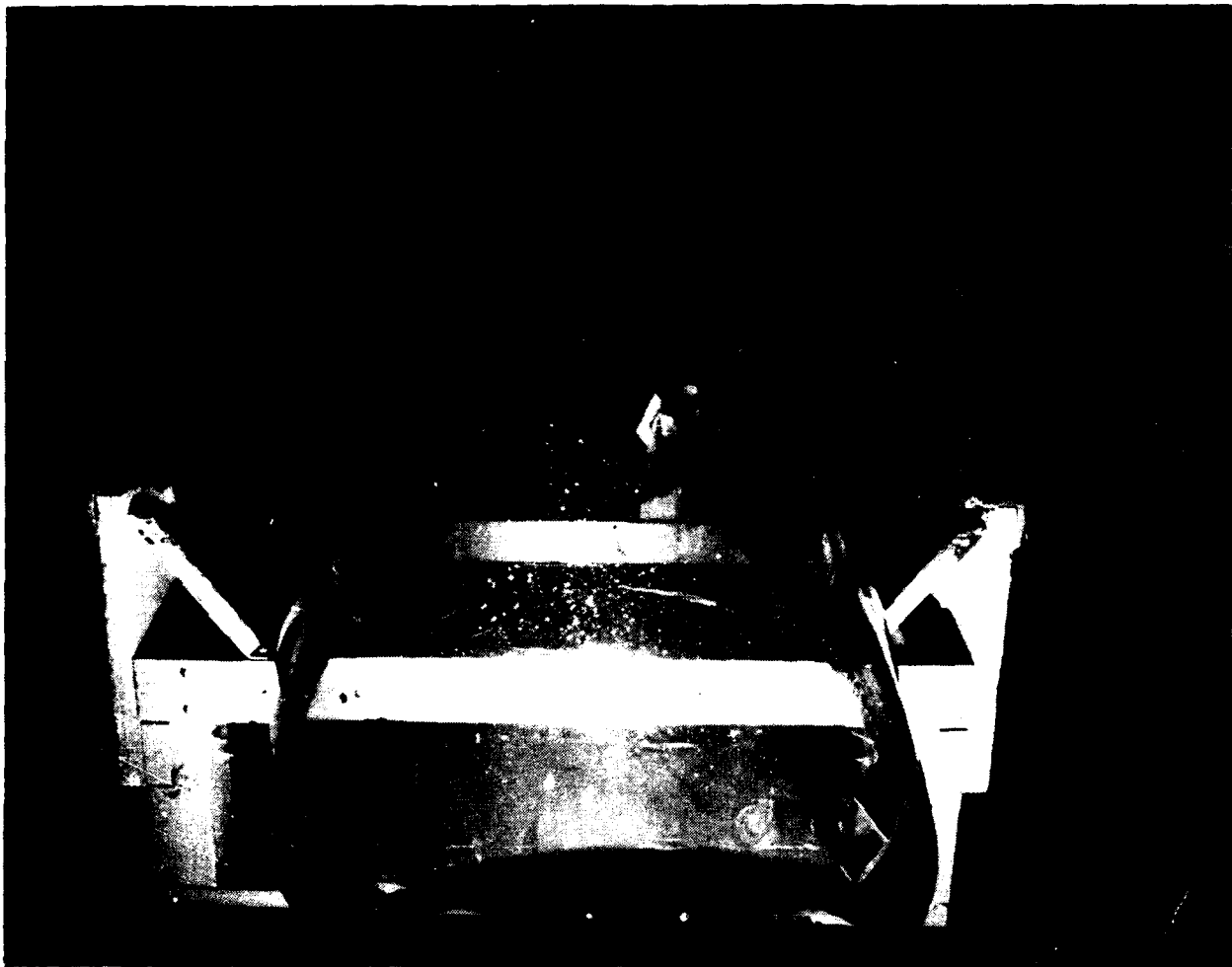


Figure 11 F-16 Transparency With Star-Burst Cracks in Outer Acrylic Ply

This is a brief account of General Dynamics' background and experience with transparency design and development highlighted by three technology advancements as used in ongoing F-16 transparency improvement activities.

Future Thrusts

General Dynamics' transparency design and development concerns for the future center around

- o New materials
- o New requirements
- o New forming and shaping techniques
- o Working with/incentivizing suppliers.

MITS

These areas of concern are sharply focused by our role as prime contractor for the Mission Integrated Transparency System (MITS) Program. MITS is a contracted research and development (CRAD) program sponsored by the Aircrew Protection Branch (FDER) and the Structural Dynamics Branch (FDBA) of the AFWAL Flight Dynamics Laboratory. The MITS AFWAL Program Manager is James L. Terry and the General Dynamics Program Manager is Dr. Gordon Stone.

At contract award, September 1988, we estimated that MITS will cost \$7.7 million and will take five years to complete. Influence and pressures are already at work to increase both these numbers before this broadly scoped program is finished.

The overall MITS objective is to use a generic approach to design, fabricate, and experimentally demonstrate MITS for advanced tactical fighter aircraft that will operate in the 1995 - 2000 time period.

Benefits of MITS

MITS benefits are

- o Transparency system design methodology applicable to advanced aircraft and the existing Air Force fleet
- o Full-scale ground tested generic canopy units
- o Possible canopy retrofit candidates for the Advanced Tactical Fighter (ATF) and the Air Force Fleet (F-16, T-38, T-37, A-10, B-1, F-15, T-46, X-29, and F-111).

The MITS emphasis on a generic canopy of the future is illustrated in Figure 12. Due to its broad scope, the MITS Program will be discussed by the author in detail later during this conference.

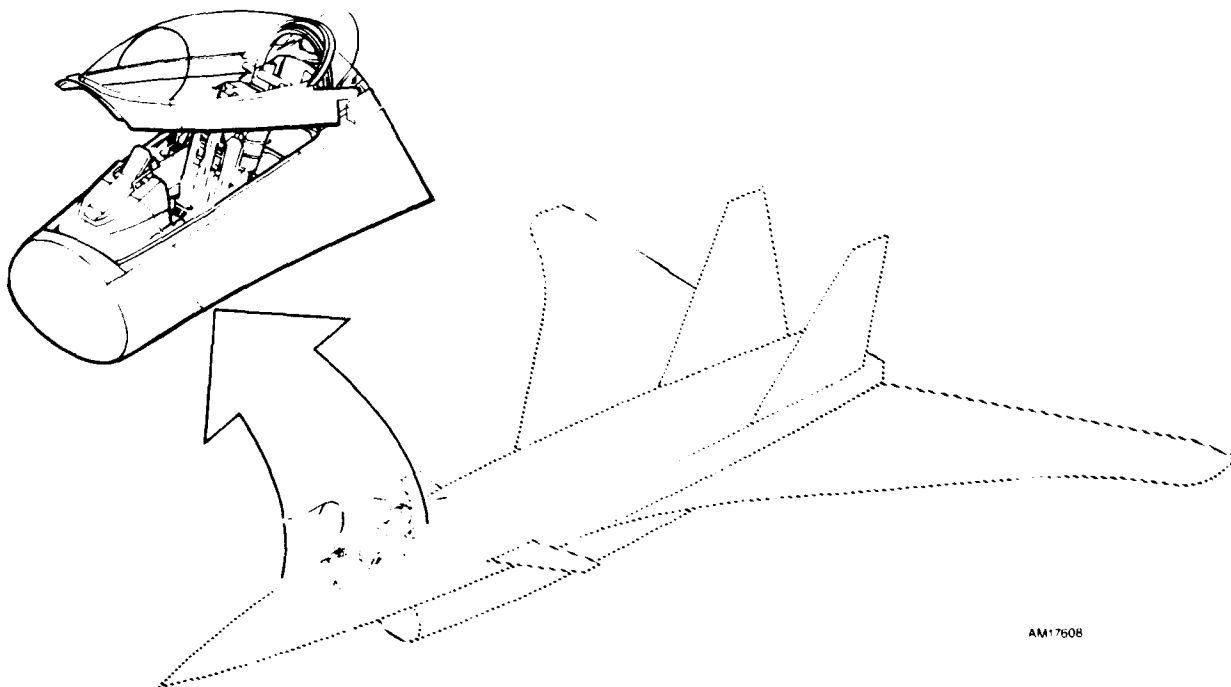


Figure 12 MITS: Canopy of the Future

Along with the MITS Program, important companion programs will provide technologies to be evaluated and applied by MITS. These companion programs and their relationship to MITS are shown in Figure 13. Of the five companion programs, External Optics II (EO II) is probably the most interrelated program with MITS. The EO II objective is to harden transparency materials to laser attack. This program is sponsored by AFWAL's Materials Laboratory (MLPJ) with Mr. Tom Page as the AFWAL program manager. Prime contractor is Loral with Mr. Bill Willers serving as Loral's program director. Loral has employed Swedlow as a major subcontractor to provide coating technologies. Loral has also chosen General Dynamics as a subcontractor to provide laser testing. In an unusual arrangement, the author of this article (Dr. Gordon Stone) will act as a sub-tier subcontractor and provide related requirements evaluation and prioritization. The EO II program intent is illustrated in Figure 14.

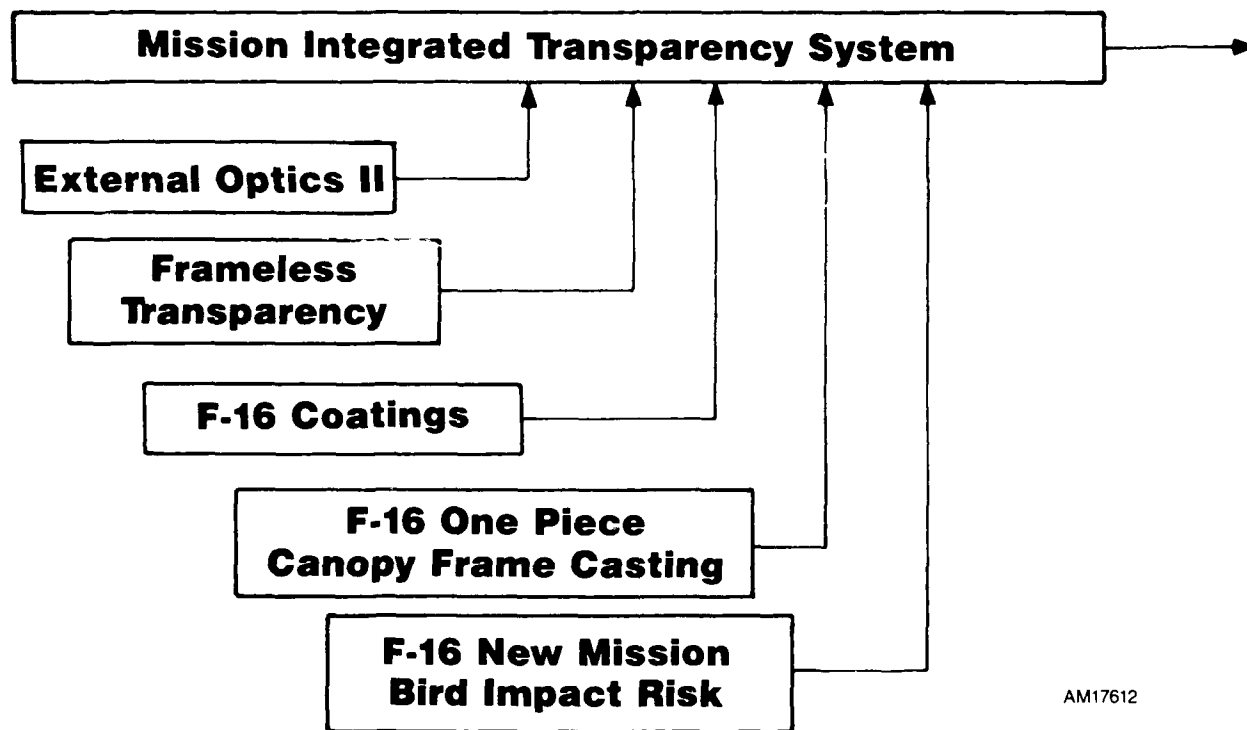


Figure 13 Companion Programs and Their Relationship to MITS

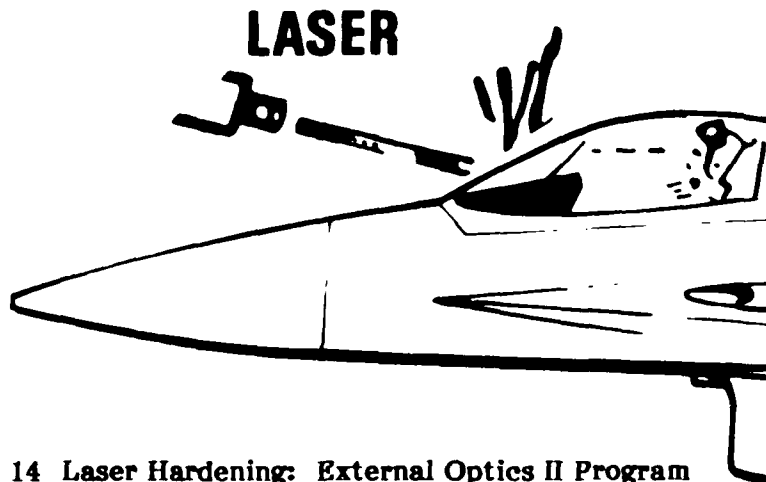


Figure 14 Laser Hardening: External Optics II Program

External Optics II

If we refer back to the transparency systems triad, EO II is an interesting example of an extended reverse operation of the triad (i.e., AFWAL to supplier as prime contractor; prime contractor as both subcontractor and subtier contractor).

Conversely, because of this close coordination between AFWAL and Loral, we plan for EO II serve as the initial stages of the laser hardening portion of the MITS program. Although the EO II Program will not progress past the coupon/subscale specimen stage, all coupon/subscale specimen designs, material combinations, coatings, etc., will be coordinated as parts of workable MITS generic transparency designs. EO II technology will then be integrated into the MITS Program.

General Dynamics laser testing during the EO II Program will be performed in a new high-energy laser laboratory at the Fort Worth Division and operated by Mr. Jack Hagameyer, principal investigator. Some laboratory features are shown in Figure 15.

A more detailed presentation of the EO II Program will be provided later by Mr. John Uram of Loral, chief engineer for EO II.

Frameless Transparency

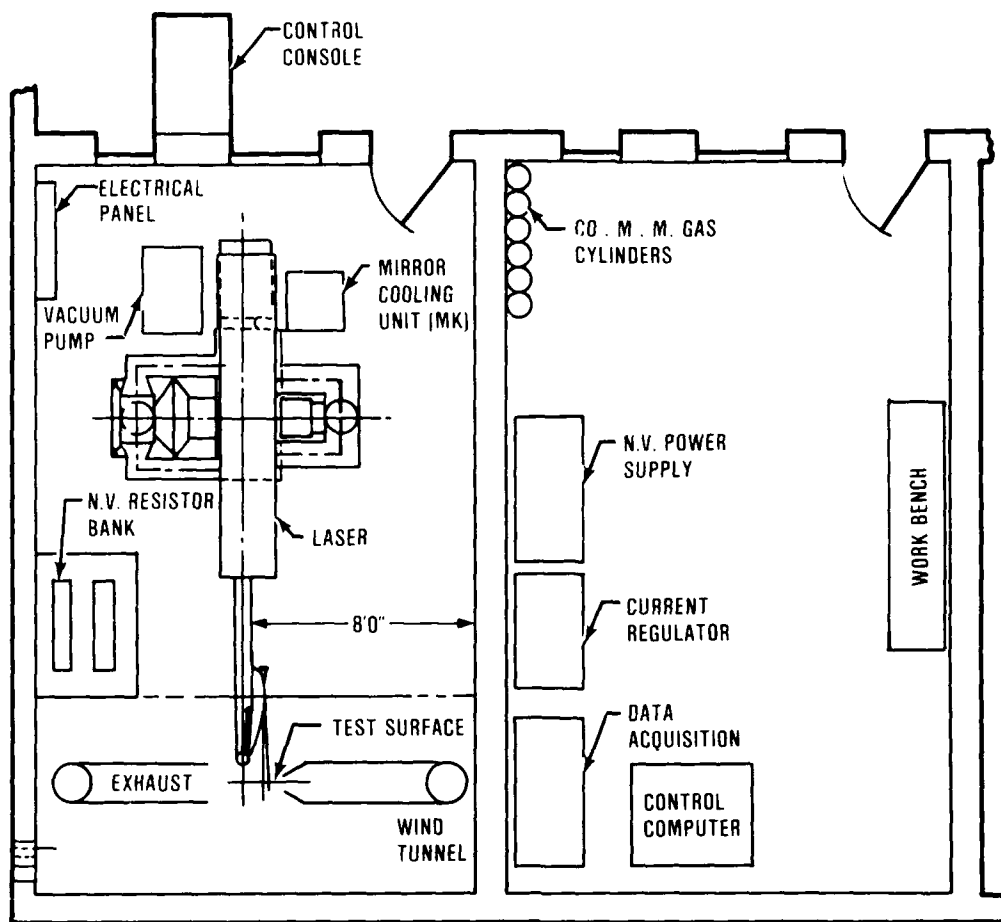
Closely associated with the MITS program is the Frameless Transparency Program. As with MITS, this program is sponsored by the Aircrew Protection Branch of AFWAL's Flight Dynamics Laboratory. The frameless transparency AFWAL program manager is Mr. Bob Pinnell; we anticipate General Dynamics will be the single-sourced contractor. Our program objective is to develop the capability to mold transparencies to their final shape integral with the canopy frame section, in lieu of costly bending and shaping of multiple transparency sheets into laminates with attachment holes drilled later. Our frameless transparency concept is depicted in Figure 16.

Principal investigator of the Frameless Transparency Program for General Dynamics will be Mr. Jim Peoples, Chief of the Systems Materials group. This program will be monitored closely by MITS personnel because MITS could be a major recipient of frameless technology, such as (1) edge attachment, side rail, latching, sealing concepts, (2) transparency configurations (whether windshield, bowframe or one-piece, monolithic or laminated), and (3) new moldable materials.

The Frameless Transparency Program will be presented later in much more detail by Mr. Bob Pinnell, AFWAL Program Manager.

Coating Research

During the last three years, General Dynamics has pursued candidate coatings, coverings, and surface protection materials for the polycarbonate and acrylic materials the F-16 transparency is made of (Ref. Figure 13). The previously described star-burst cracking of the cast acrylic ply of the F-16 transparencies is an example of the susceptibility of acrylic to cracking. Polycarbonate has the tendency to rapidly lose its structure strength when flawed. Therefore, it is obvious that both materials require surface protection. General Dynamics has contracted Battelle Memorial Institute for coatings development and research in the past and we continue to seek CRAD funding from Government sponsors, such as AFWAL, PRAM, etc. If no CRAD funding can be found, General Dynamics plans to conduct a limited F-16 coatings program in parallel with the frameless transparency program with our Internal Research and Development (IR&D) funding.



B98916A

HIGH ENERGY LASER SPECIFICATIONS

TYPE: Multimode. CW. Carbon Dioxide. Axial Flow

WAVELENGTH: 10.6 Micrometers

OUTPUT POWER: 10.000 Watts Minimum

PRIMARY BEAM DIAMETER: 4.0 Inches

FOCUSED BEAM DIAMETER: 0.4 Inches Minimum

BEAM PROFILE: Flat Top

BEAM SPATIAL QUALITY: $\pm 5\%$ Over 80% of Diameter

BEAM TEMPORAL QUALITY: $\pm 33\%$ Over Entire Diameter

SHOT-TO-SHOT REPEATABILITY: $\pm 5\%$ of Output Energy

Figure 15 GD/FW's High-Energy Laser Laboratory

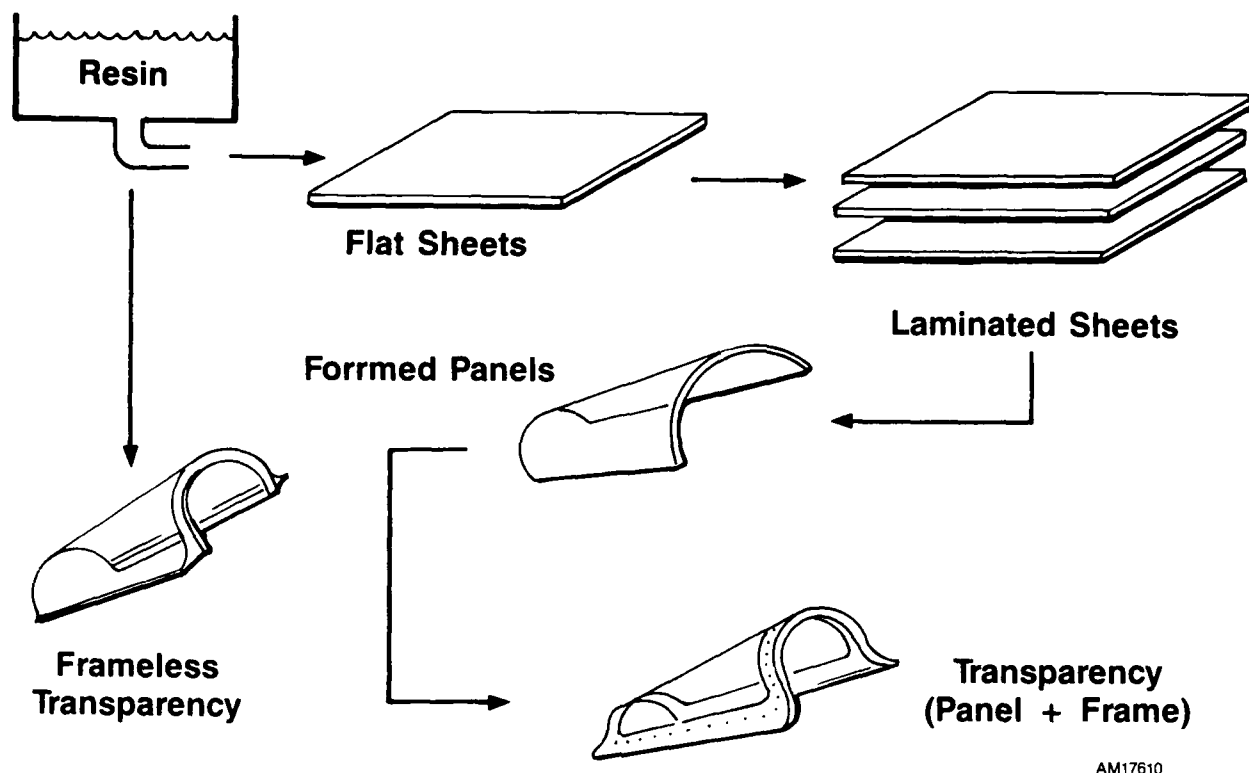


Figure 16 Frameless Transparency Concept

MITS will also monitor this program since a significant portion of MITS will involve accessing, applying, and testing various material and coating combinations. If AFWAL is also pursuing F-16 coatings development, General Dynamics will advise, participate with, or provide hardware to AFWAL.

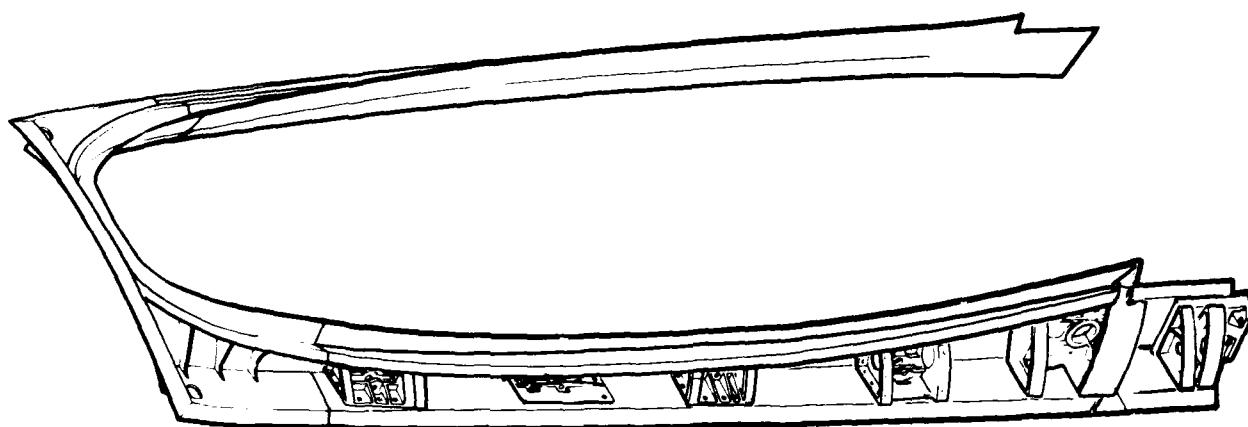
One-Piece Frame Casting

Another program to be conducted by General Dynamics and to be monitored by MITS is a One-Piece F-16 Canopy Frame Casting concept. The existing F-16 canopy frame is shown in Figure 17. As you can see, the existing F-16 canopy frame consists of a forward nose casting attached to side rails built of sheetmetal and small individual castings and forgings and difficult to maintain location tolerances, which are expensive to build and cause difficulty in maintaining location tolerances.

This new one-piece canopy frame would be designed to satisfy interchangeability and could be integrated with a semi-frameless molded transparency from the aforementioned Frameless Transparency Program. Also, this new one-piece frame would be compatible with a 4-pound, 500-knot bird hardening level. From a MITS standpoint, this program represents another set edge attachment, side rail, latching, and sealing concepts.

New Mission and CAS Impact Studies

Finally, the F-16 New Mission Bird Impact Studies (Ref. Figure 13) are listed as a companion program since they can be directly integrated into the MITS program as a part of bird strike structural analyses (described later in this paper). The F-16 New Mission Bird Impact Risk Analysis was described earlier (Ref. Figures 10 and 11).



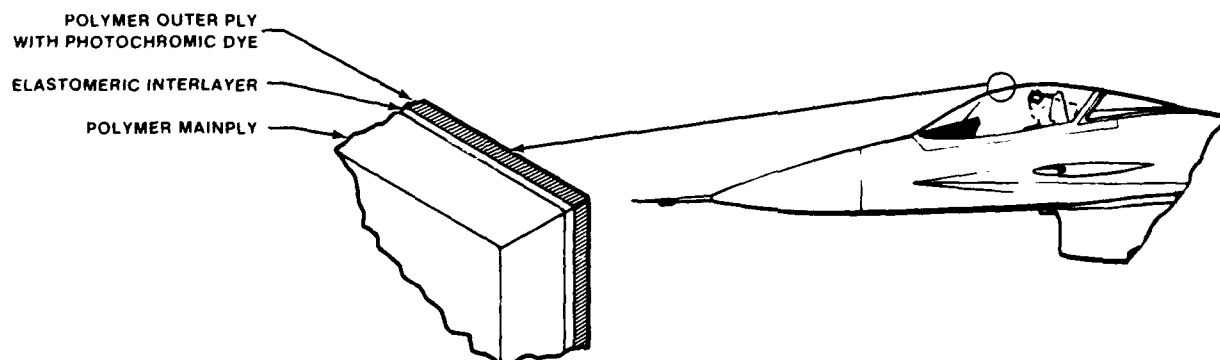
AM17613

Figure 17 Existing F-16 Canopy Frame

In addition to the companion programs, General Dynamics is performing and sponsoring technology development related to the F-16 transparency system with IRAD funding, including (1) analysis of chemically-induced cracking of polycarbonate by gas chromatography and mass spectrometry with Texstar, (2) ballistics research including extensive testing of rejected F-16 transparencies by Southwest Research Institute, and (3) nuclear flash hardening of the F-16 transparency using a photochromic sheet integrated into the laminate. The photochromic dye in the sheet is triggered by the ultraviolet light generated during the initial stage of the blast to turn dark enough, quickly enough to shield the pilot's eyes from the flash. This concept is illustrated by Figure 18.

The darkened state of the photochromic dye continues after the flash longer than is desirable, which will require additional research to improve its "turn-back-to-clear" characteristic.

DESIGN CONCEPT



898917

Figure 18 F-16 Transparency Nuclear Flash Hardening With Photochromic Dye

Technology Integration

To support MITS and the companion programs, General Dynamics will attempt to design features into a generic canopy that are driven by 30 different transparencies system requirements. The requirements are summarized in Figure 19.

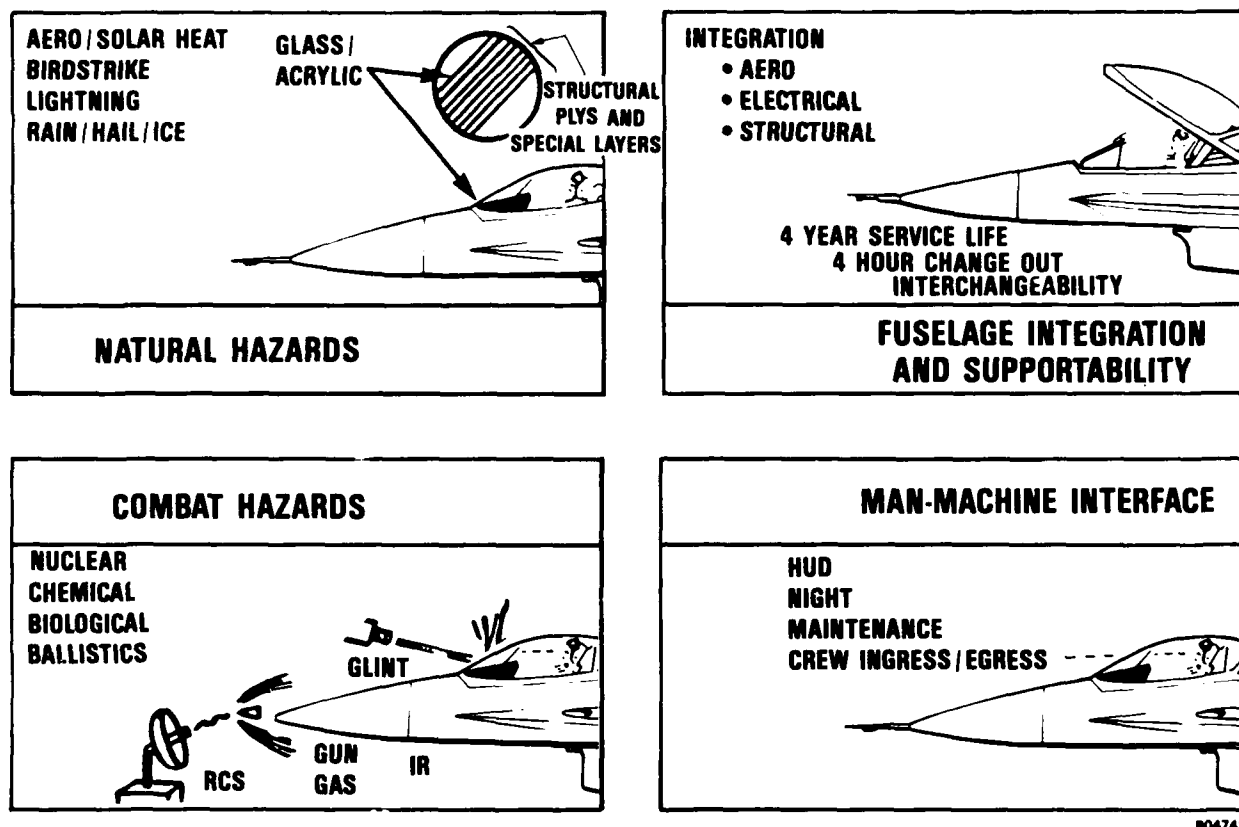


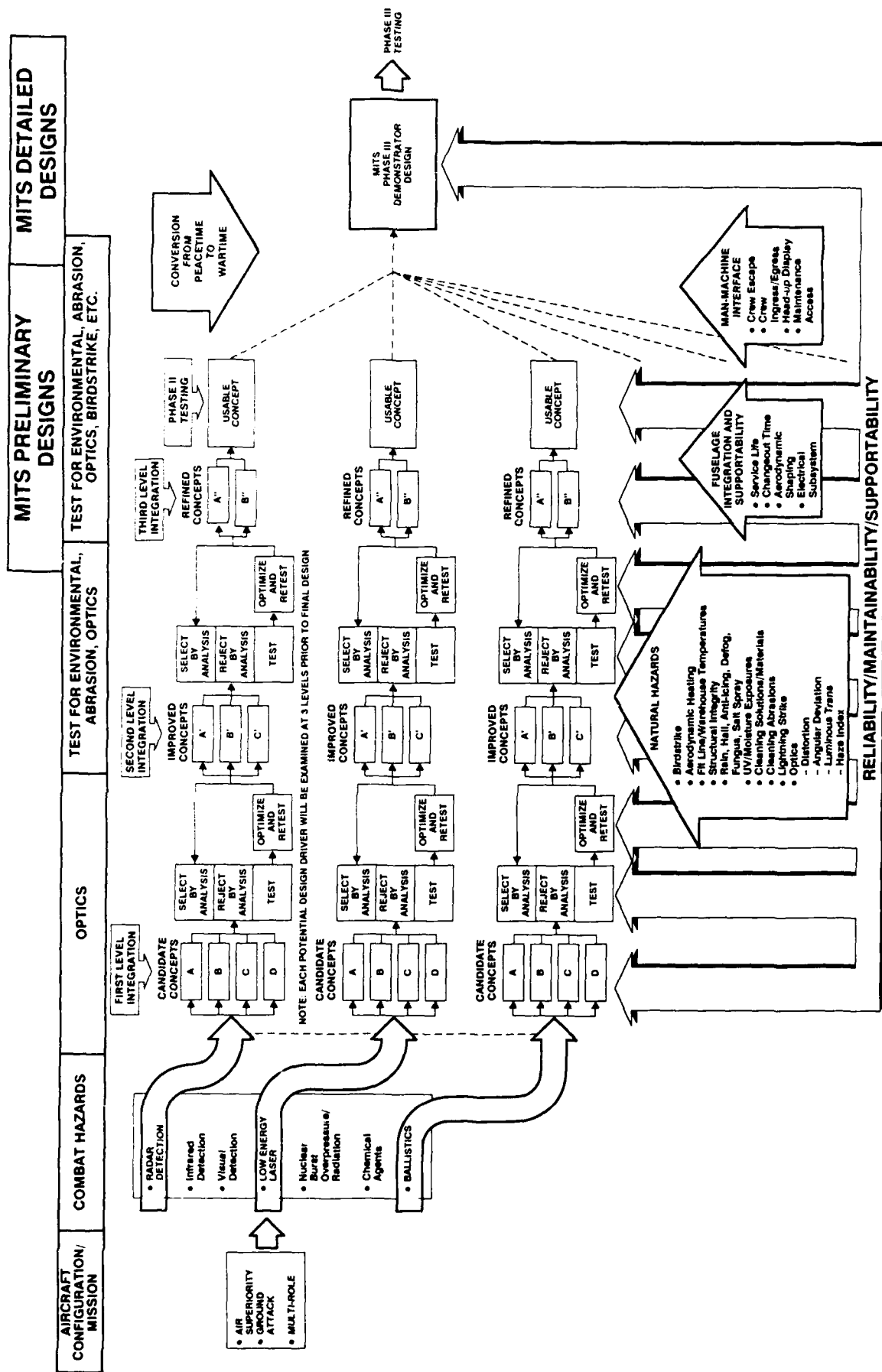
Figure 19 MITS Requirements

To gain a perspective of the challenge this generic design poses, the B-58 transparency system was designed to meet four requirements, the F-111 transparency system was designed initially to satisfy five requirements with a sixth (bird strike) added later, and the F-16 transparency system was designed to seven requirements.

In order to integrate all of the technologies required to satisfy the vast array of requirements summarized earlier, General Dynamics will utilize an iterative concept selection process. This process (Figure 20) begins with candidate concepts and traverses through a series of select-by-analysis, test, optimize findings, and retest cycles until a usable concept can be integrated with other technologies.

Finite-Element Procedures

The MITS generic approach requires generation of three full canopy designs and 90 options. Designs and design options generated will reside on IBM CATIA/CADAM data bases. MITS designs and design options will be analyzed to assess their capability to satisfy the aforementioned design, performance, and supportability requirements. Among these analysis techniques are four finite-element computerized procedures that will utilize the CADAM/CATIA data bases for generation of their structural models.



Two of these procedures are for bird strike simulation. The older one is the Materially and Geometrically Nonlinear Analysis (MAGNA) (developed and owned by the University Dayton Research Institute) used extensively by the MITS AFWAL sponsors. Once the canopy toughness velocity is established from the bird impact risk analysis (Ref. Figure 11), this value along with other key data are fed into MAGNA for a bird strike structural analysis. In addition to MAGNA, General Dynamics has purchased and established with great success a newer code called ABAQUS and uses this code extensively for bird strike analysis on a number of airplane projects. Typical bird-strike results from MAGNA and ABAQUS modeling are shown in Figure 21.

Detailed structural sizing of both the transparency and canopy frame for internal pressure loads will utilize a finite-element variation of ABAQUS called ADS/ABAQUS. ADS/ABAQUS will be used broadly for analyzing edge attachment, side rail, and latching concepts.

The fourth finite-element code, used for aerodynamic heating analysis is called STAPAT. This code is also used extensively by the MITS AFWAL sponsors. Typical STAPAT procedure results show surface temperature variation on transparency (Figure 22).

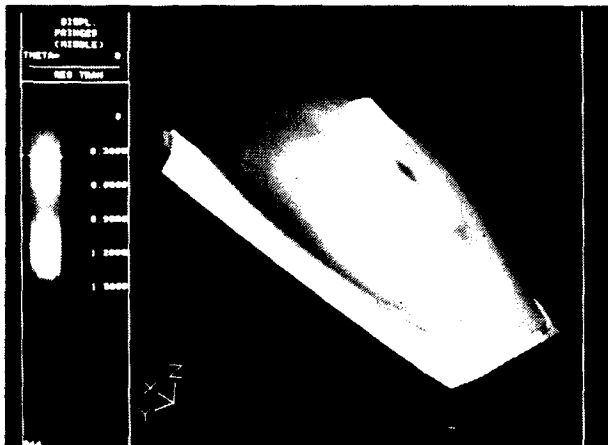


**Figure 21 ABAQUS Bird-Strike
Analysis of F-16 Canopy for
a 4-lb Bird @ 350 Knots**

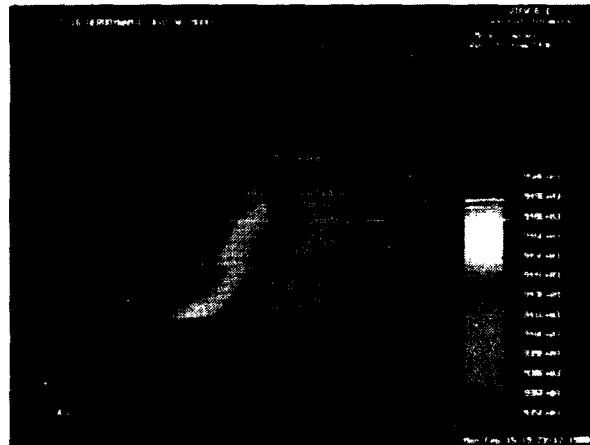


**Figure 22 STAPAT Temperature
Variation on Transparency
Outer Surface**

In addition to the finite-element codes used for structural and thermal analyses, a smaller, yet valuable computer code, will also be used. This code, which can be operated on smaller capacity computers, provides optics prediction for various shapes, material combinations, coatings, liners, and interlayers in the MITS designs. This optics prediction code is based on Snell's law and generates image distortion data from a ray-trace concept. The ray-trace concept is depicted in Figure 23.

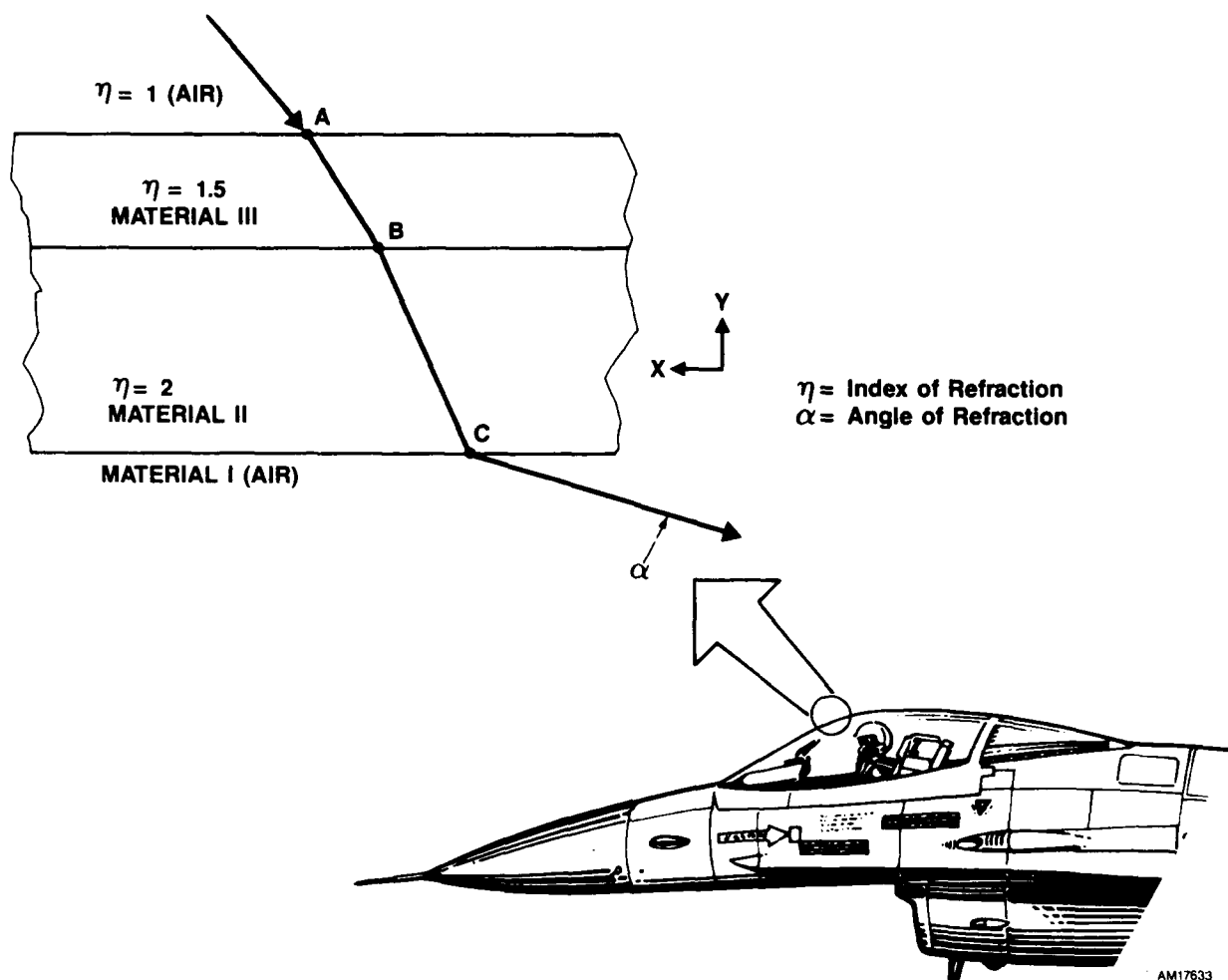


Figure 23 Optics Prediction Computer Ray-Trace Technique

Computerized Network

In order to accommodate all of the anticipated MITS generic transparency designs and design options and the various finite-element analysis techniques, a computerized network is being devised (Figure 24).

The cockpit/canopy transparency designs will be resident on the IBM CATIA/CADAM data bases. Data based geometry can be transferred to other computers at General Dynamics by using the IGES translator to transform the data in CATIA/CADAM from machine binary to ASCII code that can be transported through the hyperchannel to the VAX cluster. Once on the VAX, the ASCII data base can be read by another translator, ISYS, to be converted to a GIFTS data base for preprocessing, or it can be moved to the Silicon Graphics IRIS workstation through Ethernet to be converted into a PATRAN data base.

Whichever preprocessor is used, the steps are the same. The geometry data is used in the definition of the elements and nodes for the finite-element model. Material

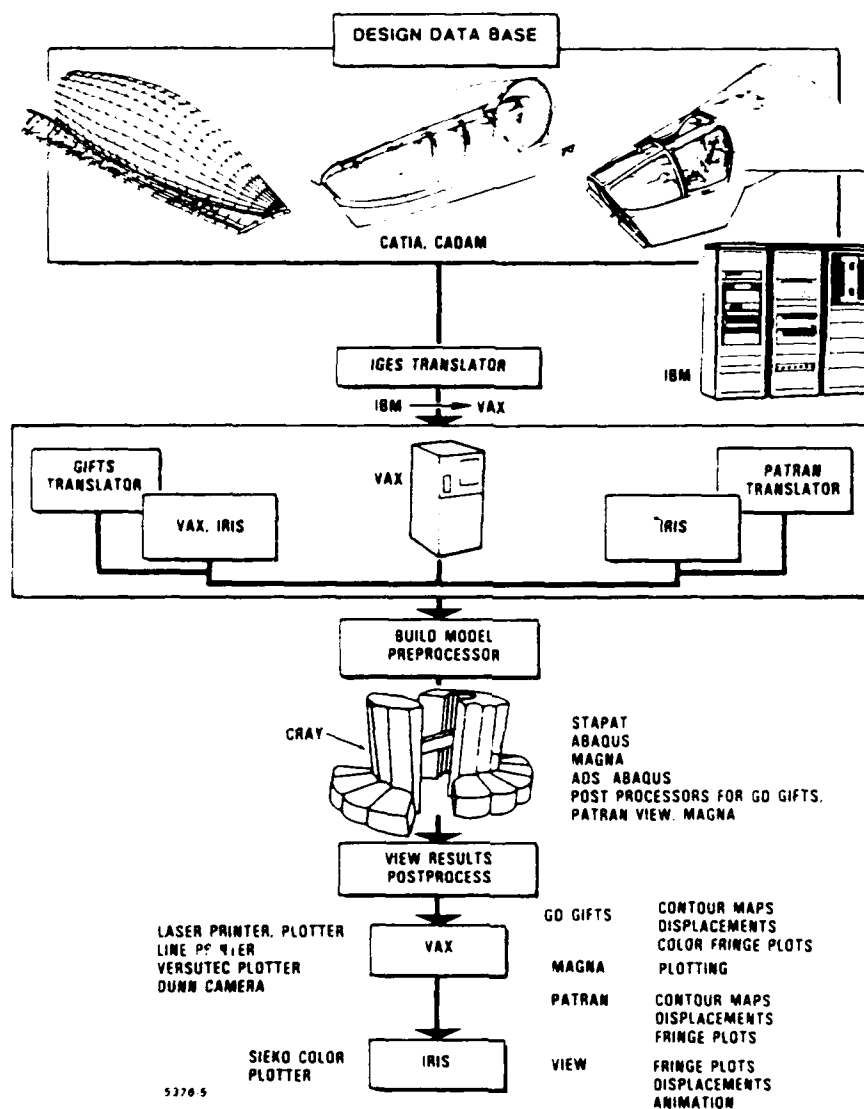


Figure 24 MITS Computer Design of Structural Analysis Network

properties, loads, and boundary conditions are added to complete the preprocessing stage. In the case of PATRAN, the completed model must be moved back to the VAX through the Ethernet and the analysis job (NASTRAN, ABAQUS, MAGNA, STAPAT, etc.) submitted to the CRAY XMP for execution.

Analysis results are postprocessed on the CRAY from binary files and moved to the VAX as ASCII files to be read by the various postprocessing programs. PATRAN, GIFTS, and VIEW can all make contour plots, deflected shape plots, and color fringe maps of the analyses. Animation of bird-strike analyses can be achieved with GIFTS in conjunction with the RAMTEK color monitor and the Dunn camera link. The Dunn camera can shoot pictures on 8 by 10 and 4 by 5 Polaroids or view graph formats, and 35mm slides. VIEW can perform real-time animation of analysis results on the IRIS that can then be downloaded to commercial format VCR tape.

Key to Future Advancements

Thus far, a running account of General Dynamics' involvement in the progression of transparency design and development has revolved around three technology advancements. When and where will the next technology advancements occur?

The key to these next advancements lies in the linkage of two major concerns not yet discussed - working with and incentivizing suppliers to develop new materials.

The ideal way to make new advanced transparency system programs, such as MITS, EO II, and Frameless Transparency, achieve resounding success is to have a supplier come up with an all-purpose, quantum-leap material that

- o Is strong enough to handle high temperatures and bird strikes
- o Can shield against laser, nuclear, chemical, and ballistics threats
- o Is impervious to rain, hail, ice, fungus, ultraviolet ray, and lightning
- o Can be readily formed to any transparency shape ranging from wrap-around windshield to one-piece bubble
- o Retains optical quality
- o Is economical to produce.

However, the track record of the transparency system triad indicates that this will not happen anytime soon. Therefore, the triad works with what is available, which is (1) acrylic in "as cast" form as an outer ply or stretched to form a structural ply but susceptible to natural hazards, (2) polycarbonate as a structural ply but prone to rapidly lose its structural strength if flawed, (3) glass that must be treated delicately, (4) interlayer made from silicone and polyurethane, and (5) multipurpose coatings. Transparencies can be constructed from these materials in monolithic, partially laminated, or fully laminated forms (Figure 25).

Fortunately, new materials and improved versions of existing materials, such as Loral's GAC 590, Dow Chemical's AEC, PPG's 5300 liner, Swedlow's 351 acrylic, and Celenese's Durell are emerging and are finding limited application. However, none of these materials are in the category of the ideal, all-purpose material.

We have not ruled out the possibility that some revelation of a new material or ideas for new materials may occur during this conference or in the near future. If not, then the challenges facing government and industry are clear cut and formidable as they quest to design, fabricate, ground test, and flight certify the next-generation transparency systems that must shield against combat and natural hazards, retain acceptable optical quality, meet supportability demands, and preserve the man-machine interface.

ACRYLIC

- As Cast
- Stretched

POLYCARBONATE

GLASS

INTERPLAYERS

- Silicone
- Polyurethane

MULTIPURPOSE COATINGS

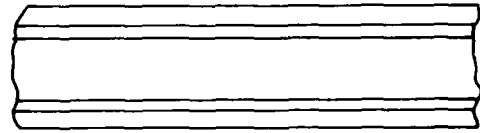
**TRANSPARENCY
CONSTRUCTION**



**MONOLITHIC
PROTECTIVE COATING**



PARTIAL LAMINATED



FULL LAMINATED

**Figure 25 Available Transparency Materials and
Basic Transparency Construction**

804749

SESSION I

SYSTEMS OVERVIEW (PART B)

Chairman: W. L. Early
General Dynamics Corporation
Fort Worth, Texas

Co-Chairman: D. S. Riddle
Grumman Aerospace Corp.
Bethpage, New York

Coordinator: J. Hansen
Grumman Aerospace Corp.
Bethpage, New York

THE DEVELOPMENT OF LARGE COMPOSITE HELICOPTER WINDSHIELDS

R. S. Bruce
R. W. Wright

Triplex Aircraft and
Special Products Ltd.

THE DEVELOPMENT OF LARGE
COMPOSITE HELICOPTER WINDSHIELDS

by

R.S. Bruce
R.W. Wright

TRIPLEX AIRCRAFT AND SPECIAL PRODUCTS LIMITED

THE DEVELOPMENT OF LARGE COMPOSITE HELICOPTER WINDSHIELDS (Figure 1)

1. INTRODUCTION

The purpose of this paper is to examine trends in windshield development, particularly in helicopter transparency requirements. Although intended to be a general examination, special attention is given to the EH101 helicopter, now undergoing flight development by European Helicopter Industries Ltd., (EHI). EHI is a company jointly owned by Westland Helicopters in England, and Agusta Helicopters in Italy. The EH101 is a large transport vehicle, in the 30/35,000 lb. (13/16,000 kg.) size range. (Figure 2)

Before discussing detailed design concepts, let us summarise the key operational considerations.

2. GLAZING CONSIDERATIONS

The modern transport helicopter is now reliably operating in some of the wildest areas of the world, such as the oil fields of the North Sea. The latest developments in electronic flight aids have made single pilot operation possible in all weathers, emphasising the need for full de-icing and bird impact resistant capabilities.

Inevitably, the list of design aims (Figure 3) is formidable and several requirements directly conflict with others.

Examining these in turn:-

2.1. Maximum Vision Area

Maximum vision area would be high on the list of a pilot's operational needs. Looking at the approximate areas of the windshields on several current helicopters, (e.g. S.76, Al09, Jet Ranger), the movement towards bigger vision areas is evident.

In the case of the EH101, with over 16 square feet per windshield, this is one of the largest windshields currently envisaged for helicopters.

To provide minimal obstruction from pillars, the trend towards large curves is also apparent. (Figure 4)

2.2. Maximum Heated Area

A large windshield loses its advantage in adverse weather conditions if only a small vision area can be de-iced or de-fogged. As larger and larger windshields are designed, the available power is often a restraint and some compromise is necessary.

In the case of the EH101, a total power limit of around 4 kw per windshield and a required power dissipation of 2.4 watts/in² (37.5 watts/dm²) dictated a heated area covering about 75% of the total windshield area.

2.3. Bird Impact Resistance

Until recently, the bird impact requirements for helicopters were minimal or non-existent. For transport helicopters, both military and civil, airworthiness regulations have now been enforced to include bird impact resistance. Typically this would call for a 4 lb. (1.8 kg) bird impact resistance, at the aircraft's cruise speed.

2.4. Hail Impact Resistance

As with the introduction of bird impact requirements, the threat from large hailstones is also to be evaluated. Although the forward speeds are likely to be much less than those of fixed wing aircraft, the impact of 1 inch (25.4 mm) diameter hailstones is still a significant threat at cruise speeds.

2.5. Resistance to Stone and Grit Bombardment

This has long been a major problem with helicopters, brought about by the rotors' downwash effectively imprisoning a hovering helicopter in its own recirculating dust storm. The airflow can uplift small stones of up to 1/4 inch (6 mm) and as these descend through the rotor disc, they are 'batted' by the rotor blades onto the windshields. Impact speeds several times higher than forward cruise speeds are experienced. The choice and strength of the transparency's face ply is critical against this threat.

2.6. Abrasion Resistance

Linked with the previous criterion, the need for abrasion resistance, particularly on helicopters using windshield wipers is fundamental. Glass face plies or plastic materials incorporating good abrasion resistant coatings are essential.

2.7. Minimal Spalling in the Event of Breakage

With all of the previously mentioned impact considerations, the risk of spalling (i.e. the shedding of particles from the rear of the windshield) should be absolutely minimal, or preferably, non-existent. Any spalling not only presents the risk of injury to the crew, but could also cause possibly critical damage elsewhere.

2.8. Residual Vision in the Event of Breakage

Whether breakage is due to hail or stone impact, thermal stress cracking, or electro-conductive coating failure, it is imperative that adequate residual vision remains to allow safe completion of the mission.

2.9. Aerodynamic Loading

The pressure or suction loading across the front of a typical helicopter is extremely complex. It will change according to the vehicle's forward, vertical and lateral speeds, the rotor disc angle, the attitude and the nearness to the ground. As a broad guide line, most windshields could experience pressure/suction within an envelope of up to about $\pm 1 \text{ lb/in}^2$ ($\pm 65 \text{ mb}$). With the larger windshields, the total load that this represents is appreciable, both in terms of the edge attachments and the overall bending strength of the laminate.

Occasionally, as in the case of ship-based naval helicopters, the firing of nearby weaponry can impose short-pulse over-pressures, possibly in the range of 1 to 2 lb./in^2 (65 to 130 mb).

2.10. Temperature Extremes

Operating in climates ranging from equatorial to arctic, most helicopters in this class have to be 'all-weather'. As such, operational temperatures of approximately -40°F to $+120^\circ\text{F}$ (-40°C to $+50^\circ\text{C}$) must be catered for, together with the ability to survive elevated ground temperatures of perhaps $+195^\circ\text{F}$ (90°C).

2.11. Minimum Weight

Always a subject of crucial importance, but never more so than in a helicopter where weight savings relate exactly to potential payload.

2.12. Composite Airframes and Adhesively Glazed Transparencies

Load carrying transparencies, acting as an integral part of the airframe structure have long been sought by designers. In some fixed wing aircraft this concept has been achieved, with bolted attachments.

With the development of composite plastics, particularly for helicopters, primary structures are now being manufactured, embodying reinforcements such as Kevlar, glass, carbon or boron fibres. A typical frame structure may be seen in Figures 5 and 6. However, with these structural materials, conventional bolted attachments become more difficult and the concept of adhesively bonded glazings becomes doubly attractive.

The possibility of applying this philosophy to unpressurised helicopters offers numerous advantages, including the following:-

- uniform stress distribution under bird impact or pressure loadings, thus avoiding localised stress concentrations,
- no requirement to install anchorages or fasteners into composite pillars or sills,
- no weakening holes in the structure,
- no external cappings or retainer strips,
- flush fitting,
- instant integral water-proof sealing,
- minimum pillar width.

2.13. Ease of Replacement

Whether of conventional bolted installation or adhesively glazed, windshields must be readily replaced in the shortest possible time. This is especially the case, not only in the civil market where down-time drastically affects revenue earnings, but also in the military sphere, particularly in times of hostility.

2.14. Special Modern Day Military Threats

Security reasons prevent much discussion on this subject other than mentioning that all of the above requirements may be further complicated by the need to incorporate protection

against other 'special' threats. These could include special coatings, screens, etc. to reflect, absorb or otherwise deal with various levels and forms of energy.

3. SOLUTIONS

Although this discussion primarily addresses the EH101's windshields, the development of the associated canopy rooflights is also discussed, since many of the requirements and design solutions are related.

With all of these design considerations, it is often a problem to reconcile the conflicting requirements. As size and curvature are generally fixed by the airframe constructor, the start point for establishing a design is usually the bird impact requirement, in this case a 4 lb. (1.8 kg.) bird at a speed of 160 knots (295 km/hr).

Broadly, the design sequence followed the order detailed hereunder, resulting in novel solutions, which have been patented.

3.1. Windshields

3.1.1. Choice of Facing Ply

For the best abrasion resistant properties, glass was selected as the preferred material. The known small particle and hail impact performance of the 0.120 inch (3 mm) thickness chosen adequately met these impact requirements. A further key feature, favouring glass for the outer ply, was the considered superior reliability of an ITO (Triplex HYVIZ) heating coating when applied to this substrate, as opposed to plastics.

Furthermore, the subsequent application of any external electro-conductive coatings, for whatever need, would be better facilitated.

Considerable discussion and evaluation has been and is still being undertaken into the relative merits of thermal versus chemical toughening. Both methods have their respective advantages, both can provide adequate strength for this application, and both can demonstrate excellent residual vision after breakage. (Figure 7)

During the past two years, for EH101 and other programmes, Triplex have designed, installed and developed to a full production capability major new thermal and chemical toughening facilities able to handle the size, shape, strength and quality required.

The need for precision shape control and high optical quality became deciding factors in material selection. The current choice of material for EH101 is chemically toughened glass and production items currently use Triplex's "CHEMPLEX" material as standard. This glass has a Modulus of Rupture (MOR) of about 36,250 lb/in² (250 MPa). All Qualification and Flight Testing has satisfactorily endorsed this selection.

CHEMPLEX has also been developed for other applications and can now be supplied in a range of thicknesses from 0.06" to 0.75" (1.5 mm to 19 mm) or above, with MOR's and toughening penetration (case depth) to suit.

3.1.2. Construction Iterations (Figure 8)

Several approaches were made to optimise the structural design. The various iterations were:-

- An 'All-Glass' solution.

Ruled out predominantly for weight and severe spalling reasons.

- Glass faced stretched acrylic.

A reasonable prospect, but a considerable thickness of stretched acrylic, of the order of 3/8 inch (9 mm), would be required. A further complication concerns the eventual adhesive edge bonding principle, described later. In this process, the maximum service temperature of 195°F (90°C) leaves a very narrow 'operational gate' in which to carry out a thermal bond process, before the stretched acrylic's reversion temperature would be reached.

- Glass faced polycarbonate

From previous Bird Impact test results with polycarbonate, a thickness of about 0.2 inch (5 mm) was thought to be necessary. However, during development tests using the Triplex Bird Gun, the polycarbonate thickness needed, allowing face ply breakage, was even thinner and hence considerably less than the required stretched acrylic thickness.

A fundamental problem was very evident with this asymmetric design, namely geometric instability with temperature changes.

Free standing, the laminate changed its curvature dramatically with change of ambient temperature due to the radical difference in expansion coefficients of glass and polycarbonate. Since the system has to survive temperatures ranging from -40°F to +195°F (-40°C to +90°C) and also allow fitment in service conditions ranging from +40°F to +90°F (+4°C to +32°C) it was necessary to change the design to a more symmetrical one, in which the differential expansion and contraction stresses would be balanced and consequently maintain windshield shape.

There was also concern, since proved to be well founded, that the use of relatively thick polycarbonate to carry virtually all of the bird impact load, could result in an unacceptably short service life due to the natural ageing of polycarbonate and resulting loss of impact strength.

- Glass/Polycarbonate/Glass/ASP

Tests were carried out on a variety of designs employing a second stabilising glass to provide a 'balanced' design and to carry some of the bird impact load. A relatively high strength glass was chosen for this second, or inner, ply and the design was optimised using a 0.080 inch (2 m) CHEMPLEX glass with an M.O.R. of 43,500 lb./in². (300 MPa). CHEMPLEX proved to be very suitable

for this application since it is possible to "tailor" its strength to meet a given requirement. For perfect symmetry, the laminate would theoretically need to be glass/polycarbonate/glass, but this would have resulted in glass spall from the rear surface under bird impact. This problem was overcome by the addition of Triplex's Anti-Spall Protection material (ASP). ASP, a Triplex patented product, is itself a combination of a very thin polycarbonate with a scratch resistant coating of Self Healing Urethane (SHU). The resulting design, as shown in Figure 9 has a weight of 3.79 lb./ft² (18.5 kg/m²).

Using this construction, we were able to meet the bird impact and stringent thermal stability requirements for the windshield whilst virtually matching the weight of the previous asymmetric design. Patent applications with respect to this design have been filed.

The use of a composite design, using both glass and two thin polycarbonate layers to resist the bird impact load was particularly of value as the effect of natural ageing of the polycarbonate material is significantly reduced. Windshields that have been installed and in service for two years have recently been bird impact tested with no apparent performance deterioration.

The Triplex SHU material has also been developed for other applications and is in service on aircraft, railroad and security products. The very latest developments have produced versions suitable as exterior liners in demanding military applications.

3.1.3. Adhesive Glazing Principles

Having provided a basically temperature stable windshield, development then addressed the problem of refining the edge attachment method. Basic requirements demanded a rapid replacement under an ambient temperature range of +40°F to +90°F (+4°C to +32°C). This posed one of the most stringent objectives which is being met by providing a peripheral band of adhesive material laminated to the inside of the

windshield. The band itself consisted of a subtle combination of both thermoset and thermoplastic layers containing an internal electrical heating element, (Figure 10). Permanent terminations on the windshield lead to the element itself and to integral thermal sensors to control the interface temperatures during bonding. The element's location is biased towards the rearmost face (i.e. towards the bonding surface) of the peripheral band. Prior to installation, a thin layer of thermoset material is applied to the airframe to take up any slight irregularities between it and the transparency. With the transparency in position, the embedded heating element is energised which cures the thermoset interface and the bond to the composite airframe structure is complete.

For removal of the windshield, the integral edge element is re-energised which melts a thin layer of a thermo-plastic material adjacent to the originally applied thermo-set adhesive and the windshield can then be simply pushed out, leaving only a thin residue on the structure. The surface is cleaned back and the process repeated with a replacement transparency.

Laminated samples, bonded in this manner, have undergone cyclic testing between -75°F to $+195^{\circ}\text{F}$ (-60°C to $+90^{\circ}\text{C}$) including exposure to high humidity and after many cycles, the bond remains intact. The entire design and procedure is the subject of a patent application.

Bird Impact tests, on full scale windshields, bonded by this process, were entirely satisfactory, with the bond remaining sound, even when the location of the impact point was adjacent to an edge, (Figure 11 and 12).

3.1.4. Attachment/Installation Fixtures

To guarantee the accurate location of the windshield prior to making the bond and to provide a means of exerting a clamping pressure, a special jig was

evolved. This consists of a very stiff base, having a concave inner surface to match the aircraft and windshields' external profile.

The installation jig, for which a patent has been sought, provides a peripheral load in the area to be bonded by means of an inflatable ring, located around the edge of the installation jig (Figure 13).

The resulting loads applied to the installation jig are reacted back to the airframe itself via four slave bolts, one in each corner, at specially engineered structural 'hard points' (Figure 6). Once bonding has been completed, the jig is removed and four floating bolts fitted at the hard-points to provide a full 'fail-safe' emergency attachment to cover the unlikely event of the adhesive failure. A complete installation kit comprises the jig and the necessary pneumatic controls to govern the air pressures in the inflatable ring. Means are also provided to monitor the bond interface temperature and modulate the power supply to the adhesive system heating elements.

Full scale trials have demonstrated that a windshield change can be completed in around 4 hours.

3.2. Canopy Rooflights

The Canopy Rooflights of the EH101 are also novel in that they employ thin polycarbonate to resist the 160 knot (295 km/hr) bird test and this has to be protected from UV degradation and abrasion on both its inner and outer surfaces.

For the outer ply of this double curved canopy, cross-linked, UV stabilised, acrylic was selected as having acceptable scratch and small particle impact resistant properties, together with adequate weathering performance.

For solar control purposes and to minimise the adverse stroboscopic effects of the rotor blades, the polycarbonate ply incorporates a neutral grey body tint. This lowers the overall light transmission to approximately 50%.

To protect the inner surface of the polycarbonate from scratching and abrasion, a layer of Triplex Self Healing Urethane (SHU) was applied to this surface, well able to tolerate most forms of in-service mal-treatment, (Figure 14).

The canopy roof-light is also adhesively glazed and has a similar bonding band around its periphery for installation to the composite airframe structure in the manner already described for the windshields, (Figures 15 and 16).

4. CONCLUSIONS

After considerable experimental effort, we believe at this stage that we have met all of the design requirements, the most stringent being the development of the bird impact resistance capability and the evolution of a truly bonded transparency system.

The suitability of these principles for future composite structural helicopters of any class or size has been demonstrated both by test and by the EH101 prototype aircraft now flying in Italy and the U.K. (Figure 17).

In addition, important "spin-off" developments have been achieved, particularly in chemical toughening of glass, urethane liners, and a greater understanding of the use of polycarbonate with respect of natural ageing and loss of impact strengths.

THE DEVELOPMENT OF LARGE
COMPOSITE HELICOPTER WINDSHIELDS

by

R.S. Bruce
R.W. Wright

TRIPLEX AIRCRAFT AND SPECIAL PRODUCTS LIMITED

Figure 1.



Figure 2.

GLAZING CONSIDERATIONS FOR LARGE TRANSPORT HELICOPTERS

- . MAXIMUM VISION AREA.
- . MAXIMUM HEATED AREA (DE-ICE/DE-FOG).
- . BIRD IMPACT RESISTANCE.
- . HAIL IMPACT RESISTANCE.
- . STONE AND GRIT BOMBARDMENT.
- . ABRASION RESISTANCE.
- . MINIMUM SPALLING.
- . RESIDUAL VISION.
- . AERODYNAMIC LOADING.
- . TEMPERATURE EXTREMES.
- . MINIMUM WEIGHT.
- . COMPOSITE AIRFRAMES AND ADHESIVELY GLAZED TRANSPARENCIES.
- . EASE OF REPLACEMENT.
- . SPECIAL MODERN-DAY MILITARY THREATS.

Figure 3.



Figure 4.

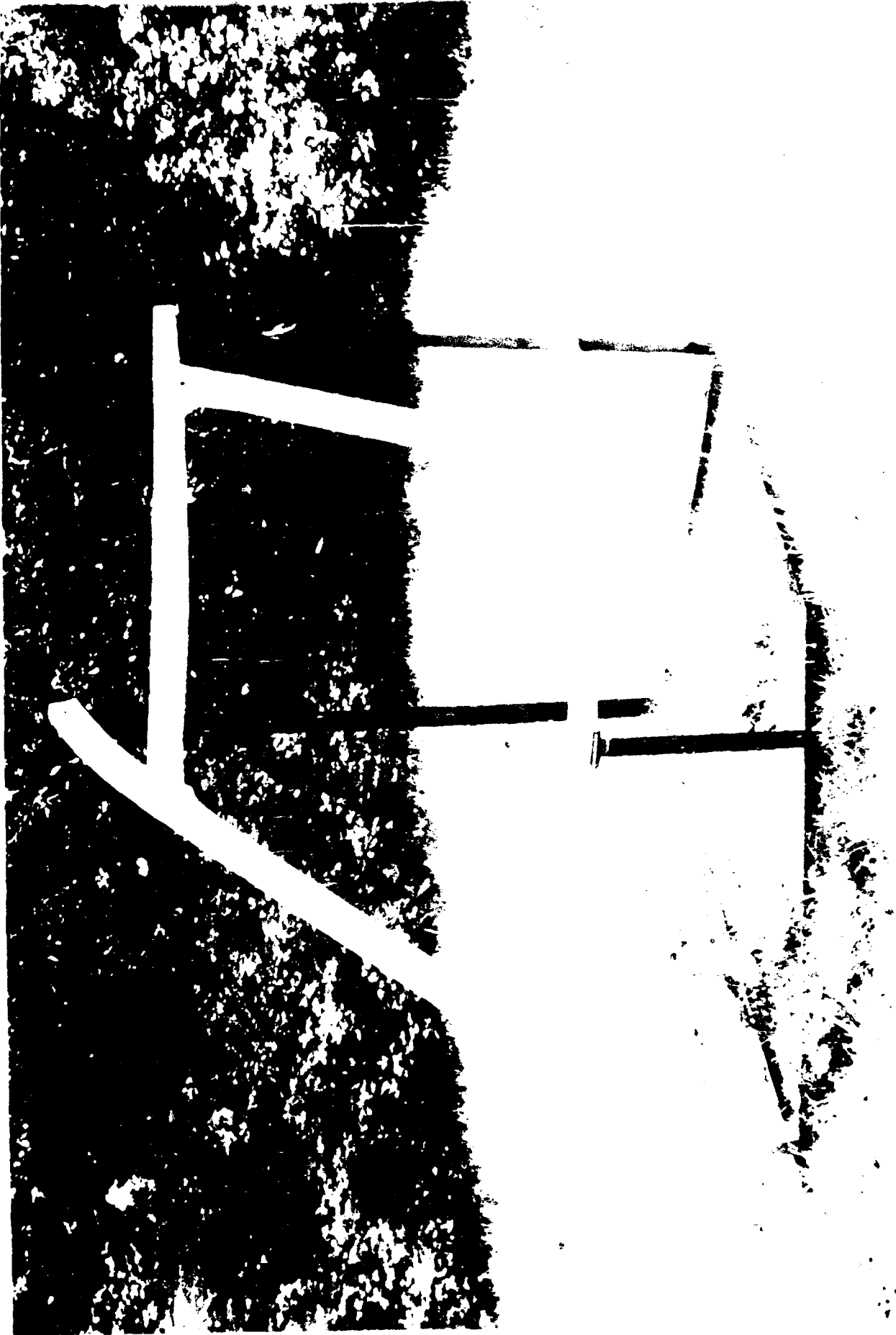


Figure 5.

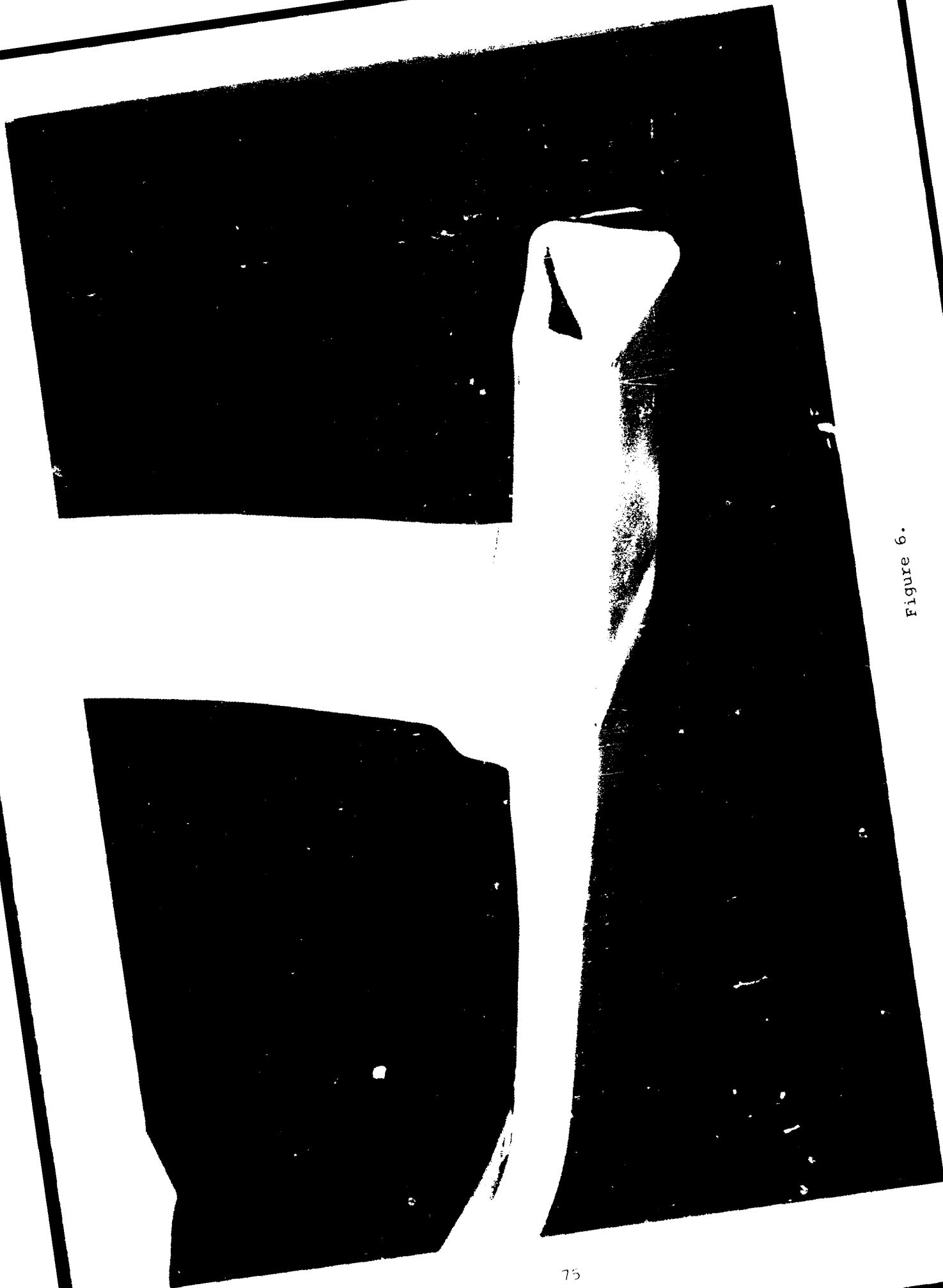


Figure 6.



Figure 7.

EHIOI WINDSHIELD DESIGN ITERATIONS

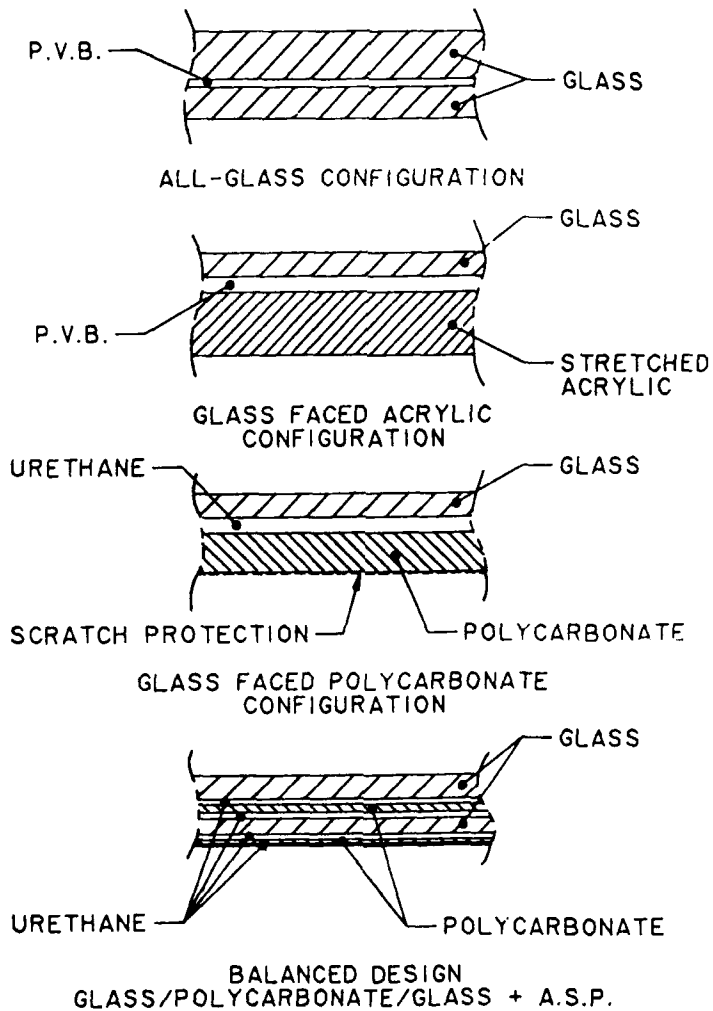
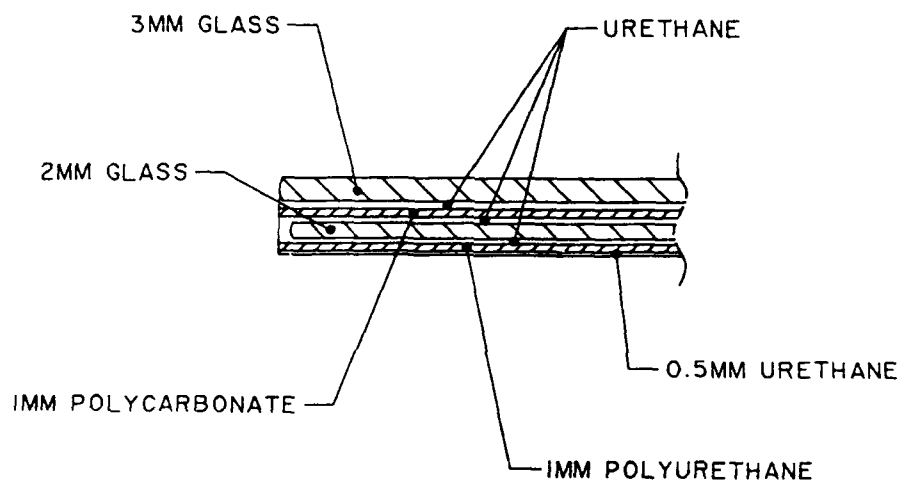


Figure 8.

EHIOI WINDSHIELD DEFINITIVE DESIGN



EDGE SECTION

Figure 9.

EHIOI WINDSHIELD DEFINITIVE DESIGN
(WITH EDGE BONDING)

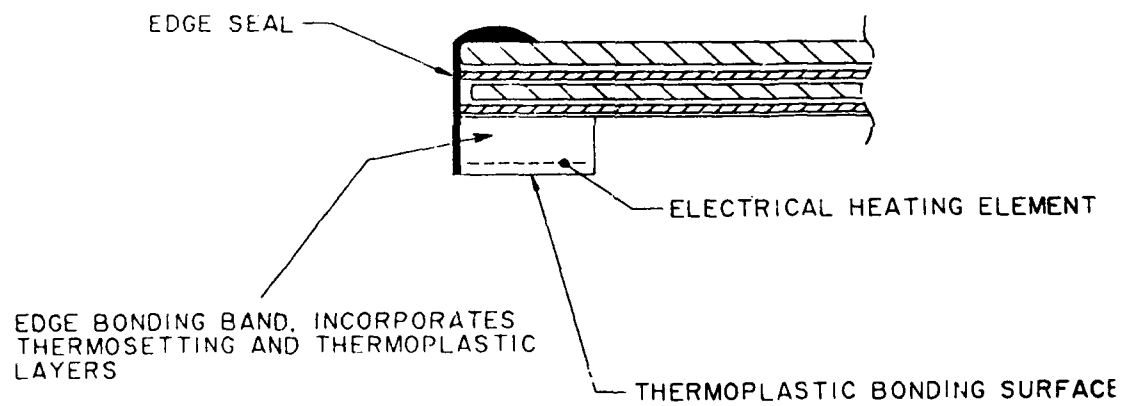


Figure 10.



Figure 11.

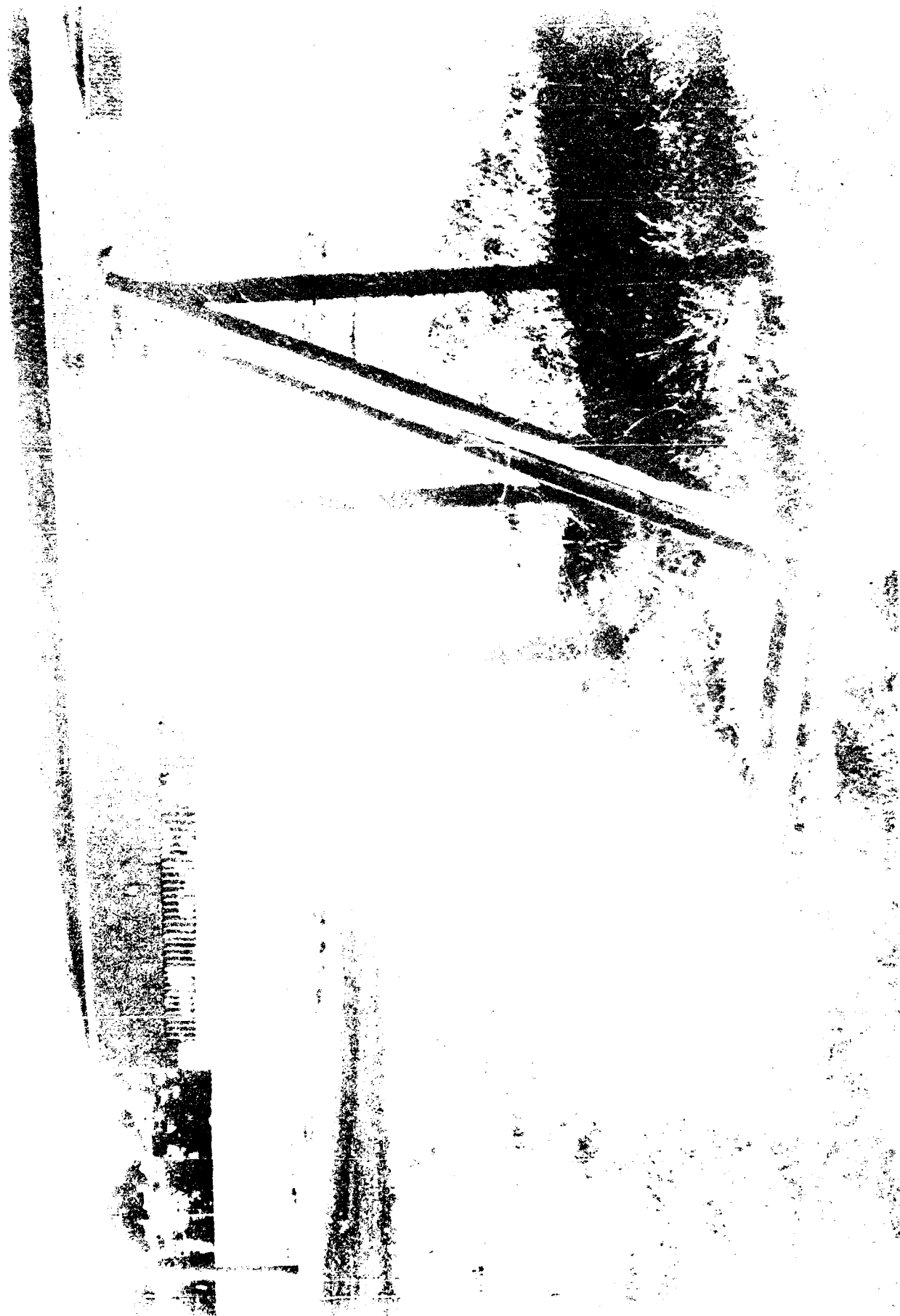


Figure 12.

EHIOI WINDSHIELD INSTALLATION FIXTURE

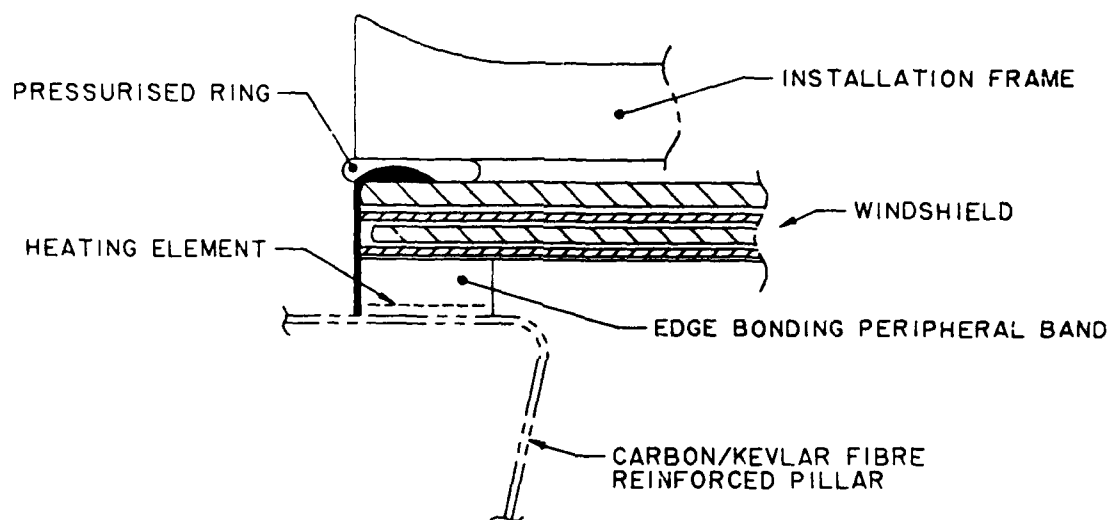
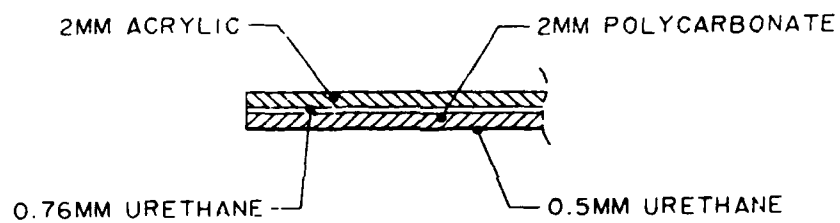


Figure 13.

EHIOI CANOPY ROOFLIGHT DEFINITIVE DESIGN



EDGE SECTION

Figure 14.

EHIOI WINDSHIELD AND CANOPY ROOFLIGHT
INSTALLED

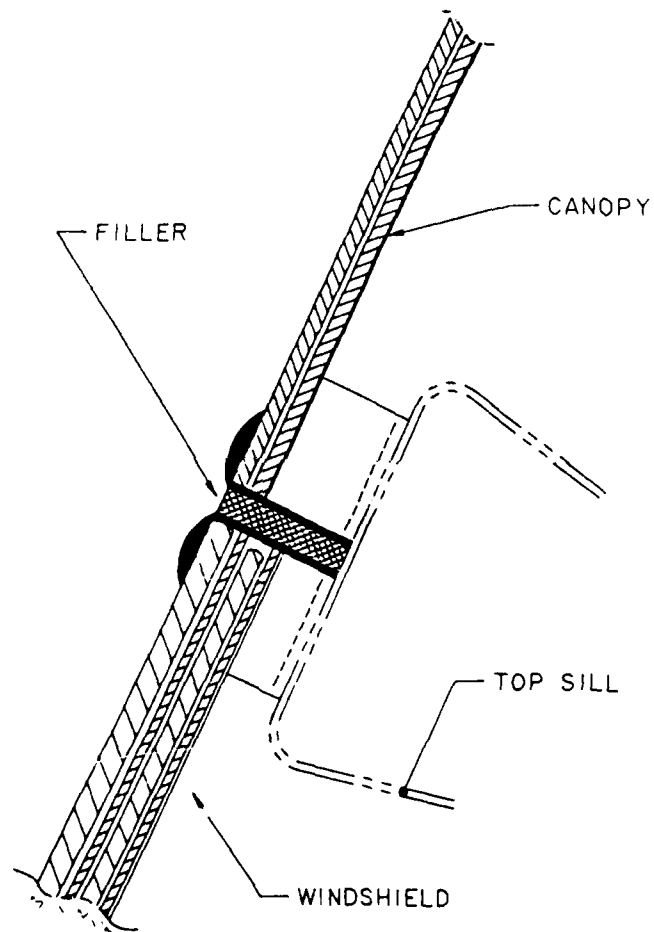


Figure 15.

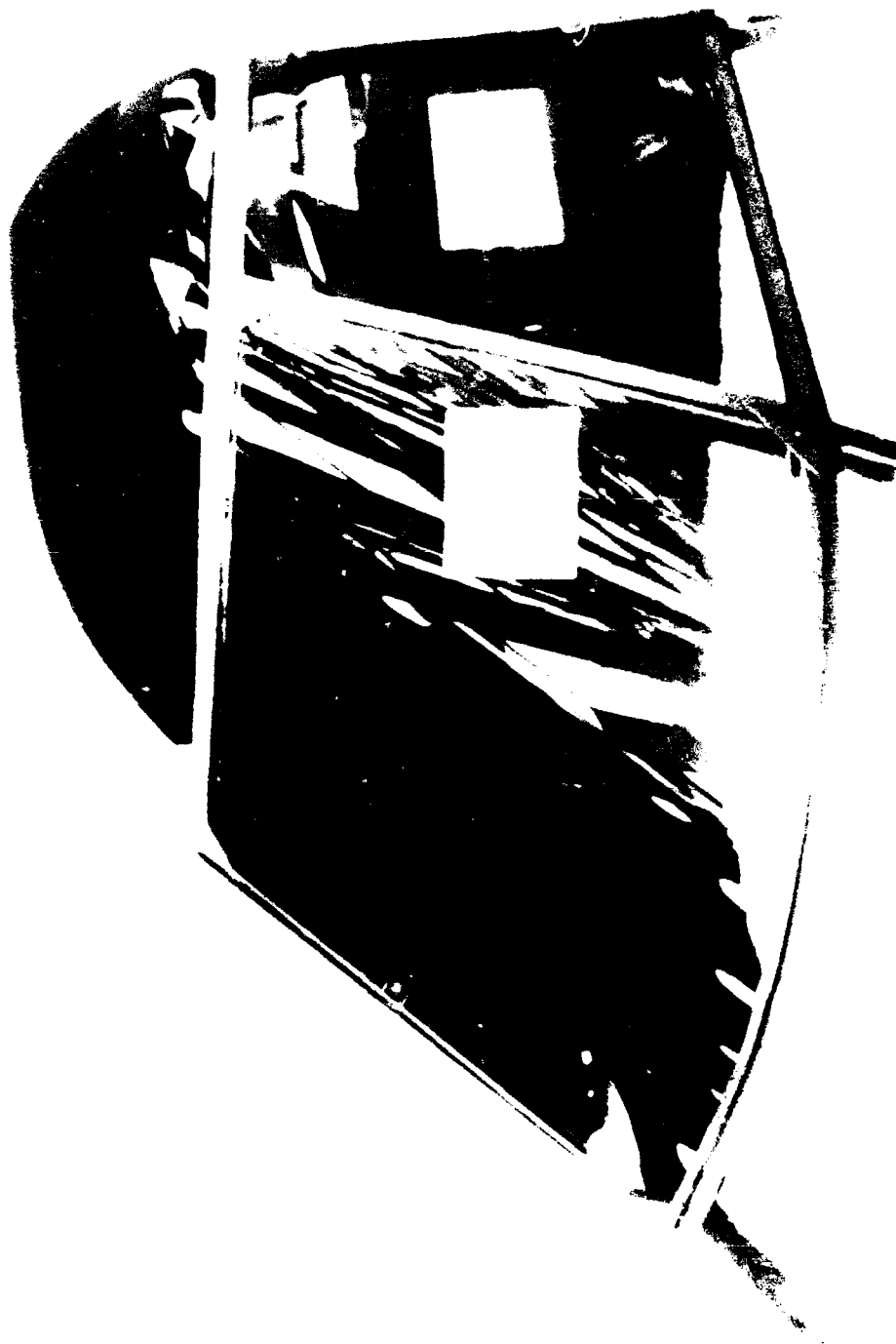


Figure 16.



Figure 17.

THE FLOW OF TECHNOLOGY BETWEEN AIRCRAFT AND AUTOMOTIVE

Glenn E. Freeman
PPG Industries

THE FLOW OF TECHNOLOGY BETWEEN AIRCRAFT AND AUTOMOTIVE

Glenn E. Freeman

PPG Industries, Inc.
P.O. Box 11472
Pittsburgh, PA 15238

ABSTRACT

The interchange of technology between aircraft and automotive has afforded new products for both applications. Improved performance, safety, and economy are dictating that the transparencies in cars do more than just act as a barrier to the elements. Aerodynamic considerations are bringing about larger transparencies with complex bends and flush glazing via encapsulation that results in improved fuel economy. New multilayered metallic coatings have made electrically de-icing windshields practical along with coatings designed to reflect the infrared energy from the sun thereby reducing the solar heat load in the automobile's interior. Head-up-displays, once used for target acquisition on military aircraft, are now projecting information to the driver's field of view, allowing the driver to monitor operational data without taking his eyes off the road.

© 1989 PPG INDUSTRIES, INC.

1.0 Introduction

Glass has been used in automobiles since the turn of the century. The first application was a flat piece of annealed glass whose primary purpose was to protect the driver against air flow, insects and rain. This ordinary piece of glass was subject to impact breakage and was a danger to occupants in an accident. By the 1930s laminated safety glass was developed using polyvinyl-butylal interlayers. The 1950s brought about safety glazing laws which made the use of laminated glass in windshields compulsory. Tempered safety glass was developed for sidelights and rear windows. Further glass developments beyond this were rather slow to progress until the 1980s. Fueled by the energy crisis and the increasing amount of glass used in automobiles, weight reduction, aerodynamic flushness, passenger comfort from solar radiation, and safety are setting the stage for a new era of automotive glazing advancements.

A large amount of the technology has been used in aerospace applications before, although some advancements are being developed for automotive applications and could be used in aircraft transparency design. One such development is multilayer MSVD coatings for solar control. The large volumes associated with the automotive market and the need for a relatively lower priced windshield has driven the development of very sophisticated coating equipment capable of producing high quality multilayer vacuum deposited metallic coatings. This paper will describe some of these recent product innovations in an attempt to give the aircraft transparency designers an opportunity for new materials and processes.

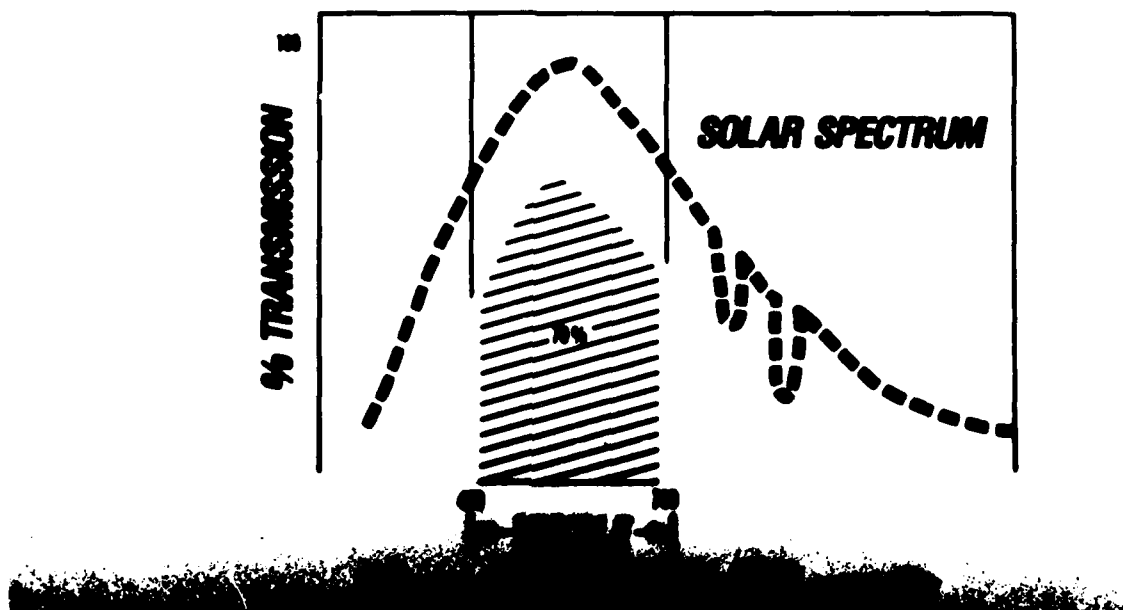
2.0 Solar Heat Load Reduction

Approximately 30% of today's surface area is transparent glazing. This amounts to an average of 35 square feet. Aerodynamic styling is dictating that the forward facing windshields and rear windows be raked back at lower installation angles, as low as 24° from horizontal. This increases the solar heat load (greenhouse effect) in the passenger compartment. Fuel efficiency concerns and downsizing of the engines places limitations on the amount of power available for air conditioning loads. In addition the Environmental Protection Agency is limiting production of Freon due to damage to the ozone layer. There is no refrigerant available that is as efficient as Freon. This dilemma created an opportunity for a low emissivity coating that would reflect the sun's shortwave infrared energy and transmit sufficient light to meet the Federal specification of 70% minimum light transmission. Energy from the sun ranges from 0.3 microns in the ultraviolet range to 2.1 microns in the solar infrared end. Of the total energy emitted by the sun, about 3% is ultraviolet, 44% is visible, and 53% shortwave infrared. A plot of the solar spectrum is shown in Figure 1. An optimized transparency would not transmit any UV or infrared energy and only 70% of the visible.

FIGURE 1

SOLAR & IDEAL ENERGY TRANSMISSION

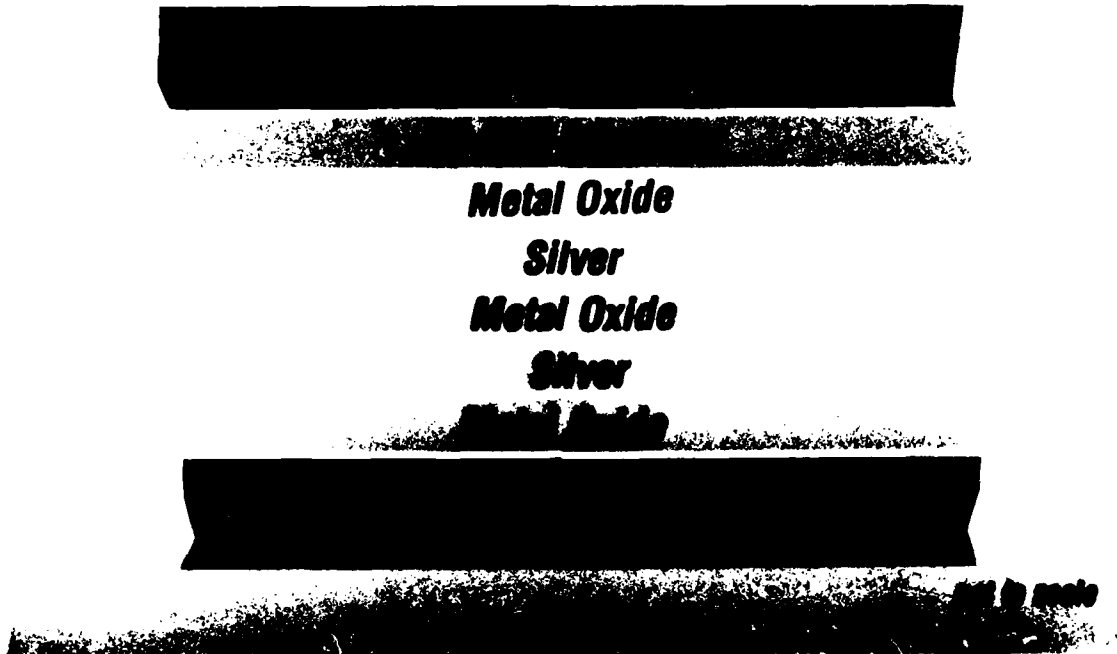
Solar and Ideal Energy Transmission vs. Wavelength



Currently, automobiles use a green tinted SOLEX[®] glass which absorbs the infrared energy and relies on convective heat transfer to dissipate the energy. Another approach is to apply coatings to the glass to reflect the infrared energy. The coating consists of two metallic silver layers sandwiched between various metal oxide layers as shown in Figure 2.

FIGURE 2

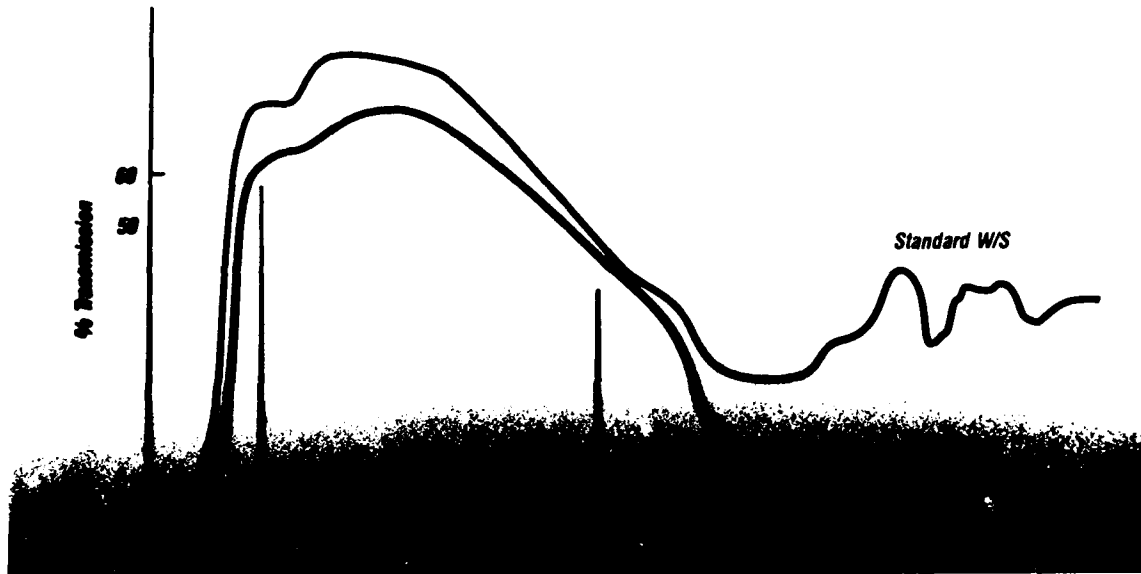
HEAT-LOAD REDUCTION CROSS SECTION



The silver is a very effective infrared reflector while the oxide layers serve to antireflect the silver and provide durability and adhesion to the glass substrate. Although the coatings are durable enough to withstand handling and washing without damage, they must be protected from the environment by laminating or protective overcoats. The coating is conductive with a surface resistivity of 4 ohms per square, has a neutral color, and a surface reflectance of 8% which is the same as uncoated glass. A coated windshield transmits 38% of the total solar energy compared to 52% for a standard tinted glass windshield, a reduction of 26%. This comparison of total solar energy transmitted is shown in Figure 3.

FIGURE 3

TRANSMISSION OF COATED VS TINTED GLASS WINDSHIELD



In-car tests over the past two summers in Phoenix, Arizona have shown that the new solar control glazing reduced interior temperatures by 20°F compared to standard SOLEX glazing after a one hour soak test at 100°F ambient. Studies have shown that heat load by solar radiation accounts for 70% of the entire air conditioning heat load under the air recirculation mode. These same studies further indicate that a reduction of air conditioning heat load from solar radiation on the order of about 700 watts corresponds to a reduction of air temperature in the passenger compartment of about 12 degrees.

As in aircraft, the amount of electronics being used in automobiles has raised concerns with engineers about electromagnetic interference. Low resistivity coatings such as these have been shown to be effective barriers against EMI and in radar attenuation.

3.0 De-ice/De-fog Windshields

While de-ice and de-fog windshields are a necessary operational function in aircraft transparencies, they are becoming popular as a convenience item in automobiles. Aircraft windshields use a pyrolitic tin oxide coating, or a vacuum sputtered indium-tin oxide coating, applied to the inner surface of the outboard glass ply. The tin oxide coatings are very durable but have resistivity limitations of 40-50 ohms per square minimum. For the automotive use, resistivities as low as 4 ohms per square with high light transmission and low reflectance were required for the automotive applications. A typical automotive windshield has a heated area of 1600 square inches with an aspect ratio of 2 to 1. The bus to bus distance is around 36 inches and available voltages from the automotive electrical system is less than 100 volts. As in aircraft a fired on silver ceramic bus bar provides electrical interface to the coating. The coating is similar in construction to the solar control coating. By controlling the thickness of the silver layer the sheet resistivity of the coating can be made as low as 4 ohms per square and still meet minimum light transmission requirements of 70%. A typical cross section of an automotive heated windshield is shown in Figure 4.

FIGURE 4

HEATED WINDSHIELD CROSS SECTION



Metal Oxide

Silver

Metal Oxide



not to scale

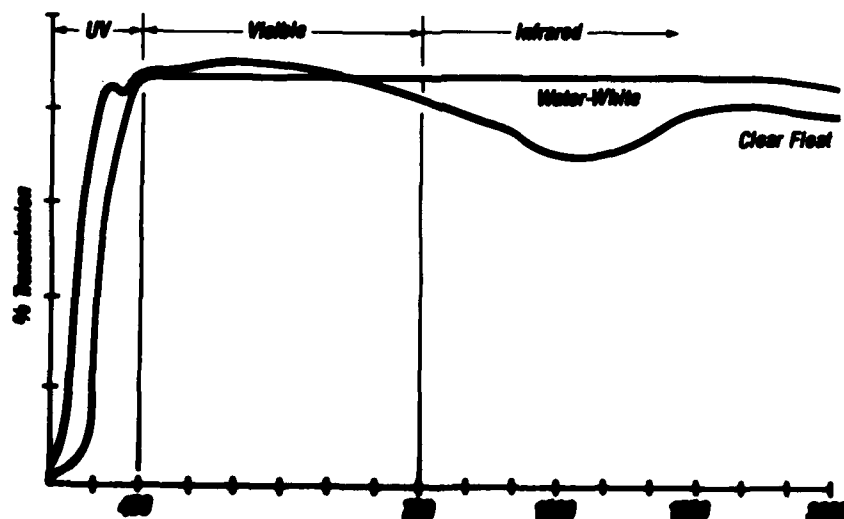
The windshield is powered at 78 volts and has a density of one watt per square inch. This is sufficient to melt one tenth inch thick ice in under three minutes in a 0°F ambient.

4.0 Glass Compositions

Recently, a water white glass was produced to enhance night vision systems on certain aircraft. As shown in Figure 5, this glass has high transmission in the infrared spectrum, transmitting 90% of the total infrared energy compared to 73% for conventional clear glass of an equivalent thickness.

FIGURE 5

TRANSMISSION WATER-WHITE VS CLEAR GLASS

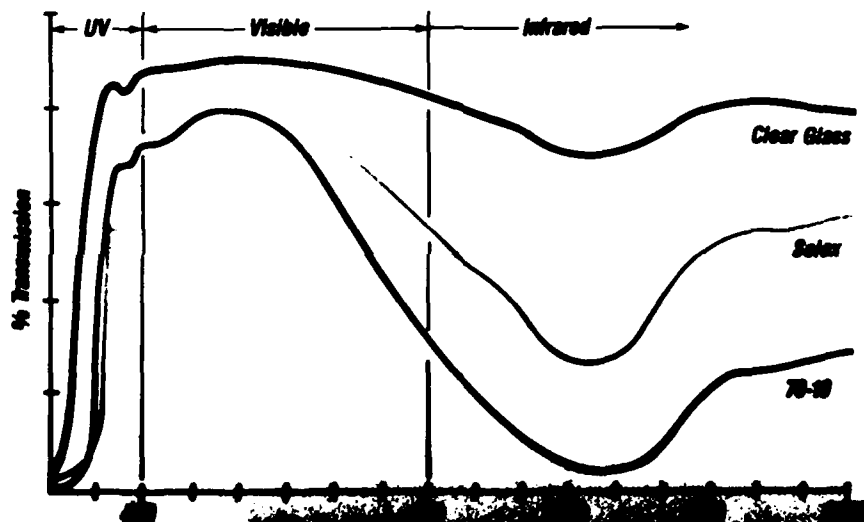


Night vision systems may be another area of technology transfer to automotive designs of the future.

Another new composition being developed is a more effective heat absorbing glass. This is a neutral blue color and the advantage over coatings is the durability of glass for monolithic glazing in side windows. Figure 6 shows the comparison of various windshield glass types. The new composition transmits 11% of the total solar infrared energy compared to 32% for standard tinted automotive SOLEX glass and 73% for conventional clear float.

FIGURE 6

TRANSMISSION OF HEAT ABSORBING GLASS VS CLEAR

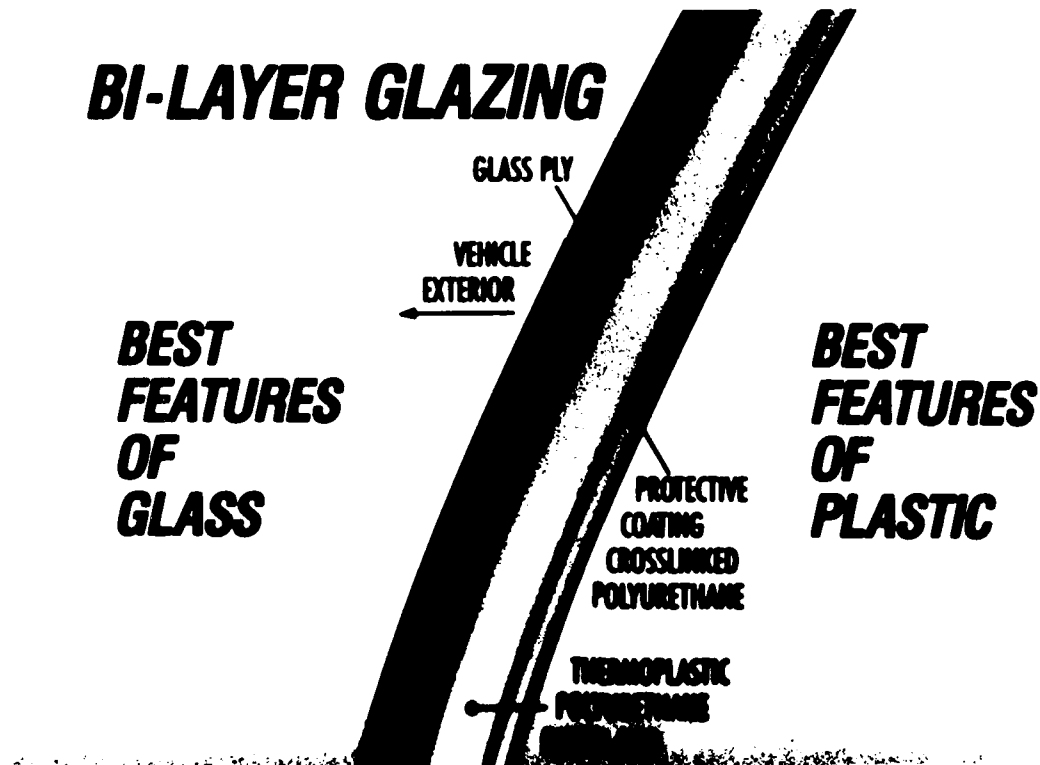


Another glass type being developed will allow stronger thermally tempered glass. Preliminary test results show an increase in MOR of approximately 20% over conventional soda lime glass of the same thickness. Again this type of glass could have applications in aircraft to provide more efficient light weight designs.

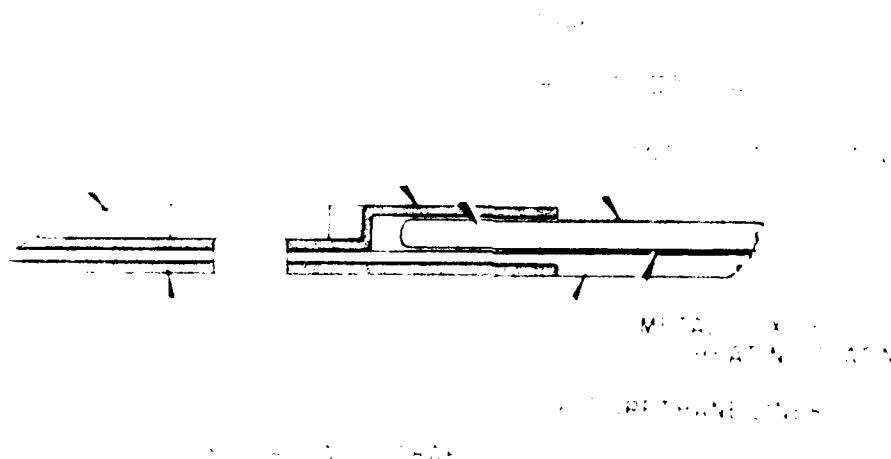
5.0 Bi-layer Transparencies

A two-layer glass/plastic automotive windshield was designed several years ago to reduce lacerations and injury suffered during a head-on collision. To accomplish this, a high strength sheet urethane interlayer material was developed by PPG's Chemical Division. Although this material has been used in automotive products, it has seen wide use in aircraft products. The urethane interlayer material has proven to be effective in eliminating cold chipping and delamination of conventional glass laminates. It also has superior strength and impact resistance over a wider temperature range than standard PVB interlayers. The Agusta A129 helicopter has bi-layer windshields currently in service.

FIGURE 7



4. HELIUM-TER BILAYER WINDSHIELD



Head-up-displays ("HUD") have been used in aircraft applications for many years. A typical HUD utilizes a separate reflector screen to combine the informational data on the real world screen as viewed through the transparency. In aircraft the information is conformal with the real world and is used for target acquisition and landings in inclement weather. In the automobile the HUD is considered a safety device allowing the driver to monitor operational data and warning signals without taking his eyes off the road, as shown in Figure 9. Also for styling and durability reasons the combiner has been integrated into the windshield. Another difference is where the image is collimated to infinity for the aircraft application, the automotive application is focused approximately 10 feet in front of the drivers eye, and below the primary viewing area. It was determined that this distance minimized eye refocusing while creating a boundary for the front of the automobile, and allows the driver to concentrate on the traffic in front of him.

FIGURE 9



PPG's Automotive HUD program has included development of an integrated holographic combiner windshield along with fabrication of a prototype drivable system by Flight Dynamics, Inc. As shown in Figure 10, the image display is a transmissive liquid crystal display illuminated with a quartz lamp. A four element relay lens collimates the light, with the last element being an asphere to correct for the curvature of the windshield. The reflective hologram is a di-chromated gelatin exposed to reflect in selected wavelengths. The hologram is fabricated on a flexible substrate with the gelatin layer being laminated inside the windshield. The advantages of using a holographic windshield is an increase in absolute display brightness which results in improved display contrast ratio. A standard glass windshield reflects 24% at 69° incident angle. The holographic element has a reflectivity of 20% at angle. When the hologram characteristics are added to the glass surface reflections, the total holographic windshields reflectivity is approximately 45%, or an increase of 50% over a standard windshield.

FIGURE 10

AUTOMOTIVE HEAD-UP DISPLAY SYSTEM BLOCK DIAGRAM

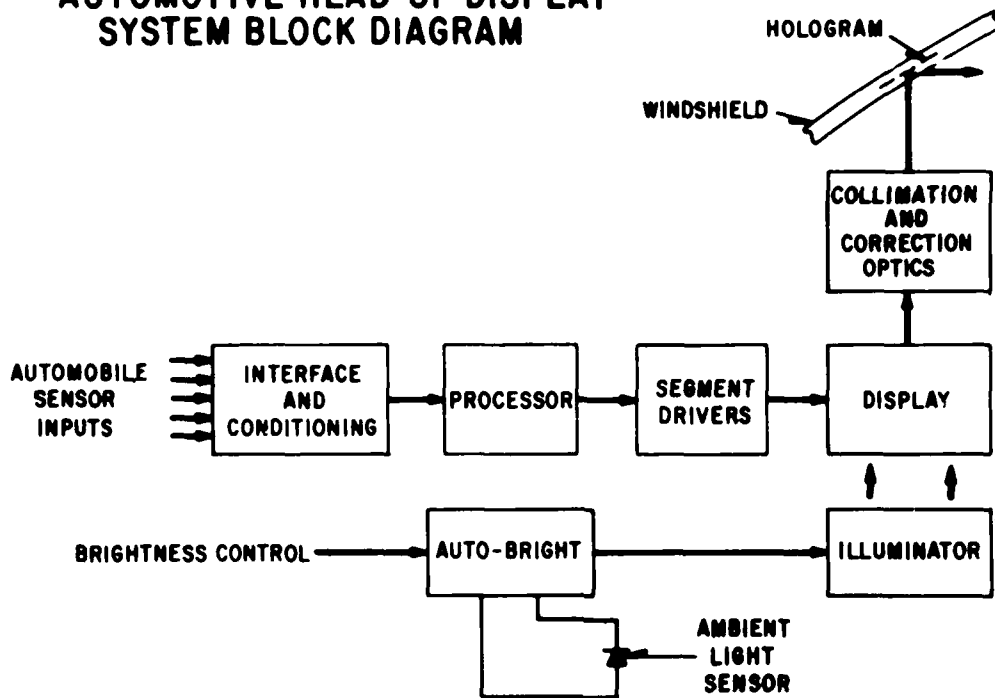
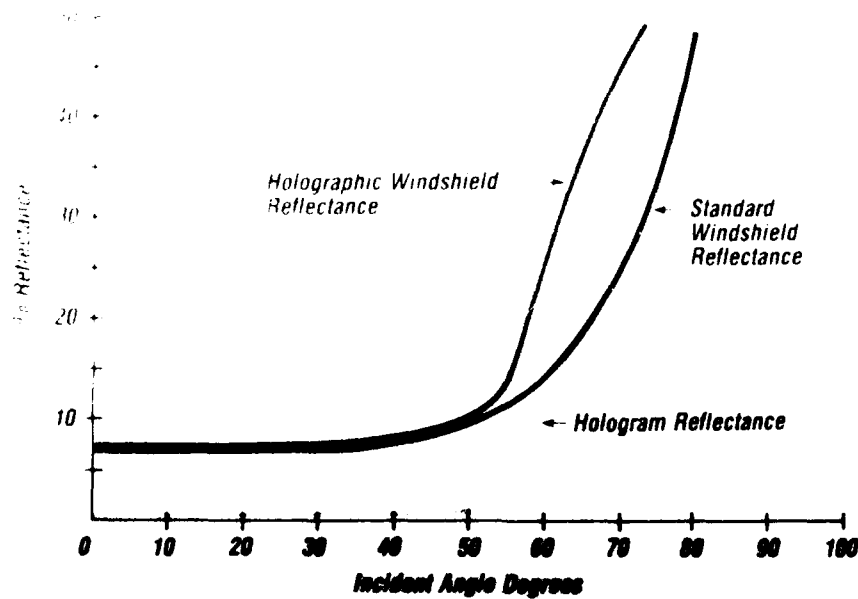


FIGURE 11

REFLECTANCE VS ANGLE

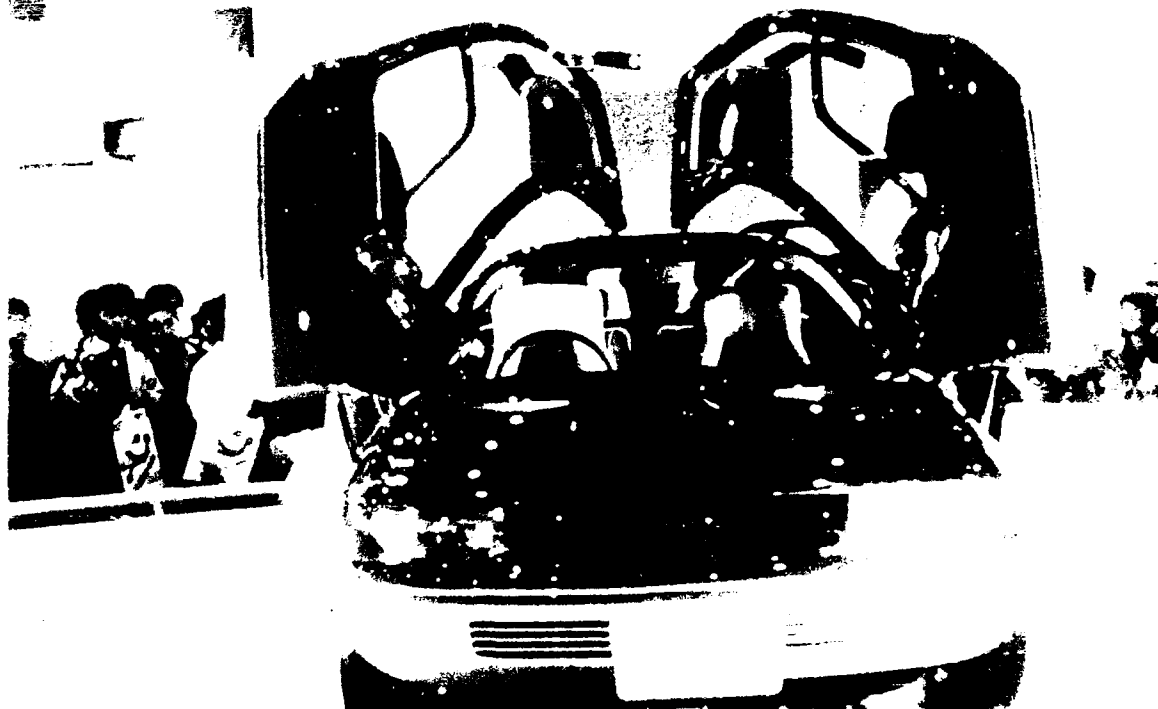


I believe that head-up-displays will be integrated with other developing technologies such as navigational systems and on-board radar. This will make it possible to project direction cues or warning signals of impending collisions or obstructions ahead.

7.0 Complex Shapes

The use of glass is on the increase with styling dictating that the parts be bent into shapes that wrap around the body, have an S shape and a spherical curvature.

FIGURE 12



Flush glazing along with lower installation angles have helped achieve drag coefficients of 0.30 or lower on several models. Bending equipment to produce such large complex shapes with acceptable optics and costs is a continuing development effort at PPG. Abrasive jet cutting of openable windows out of larger glass areas is a concept that provides a way to achieve closer tolerances on mating parts without the need of additional

framing members. Some of the futuristic designs will incorporate aircraft-type canopies that will be made from chemically strengthened glass. These large parts will be formed in one piece using male and female molds along with pressure to form the compound curves. The various transparencies will then be cut from the curved glass bubble. This technique would allow for all the parts to match creating a smooth exterior skin, Figure 14.

FIGURE 13

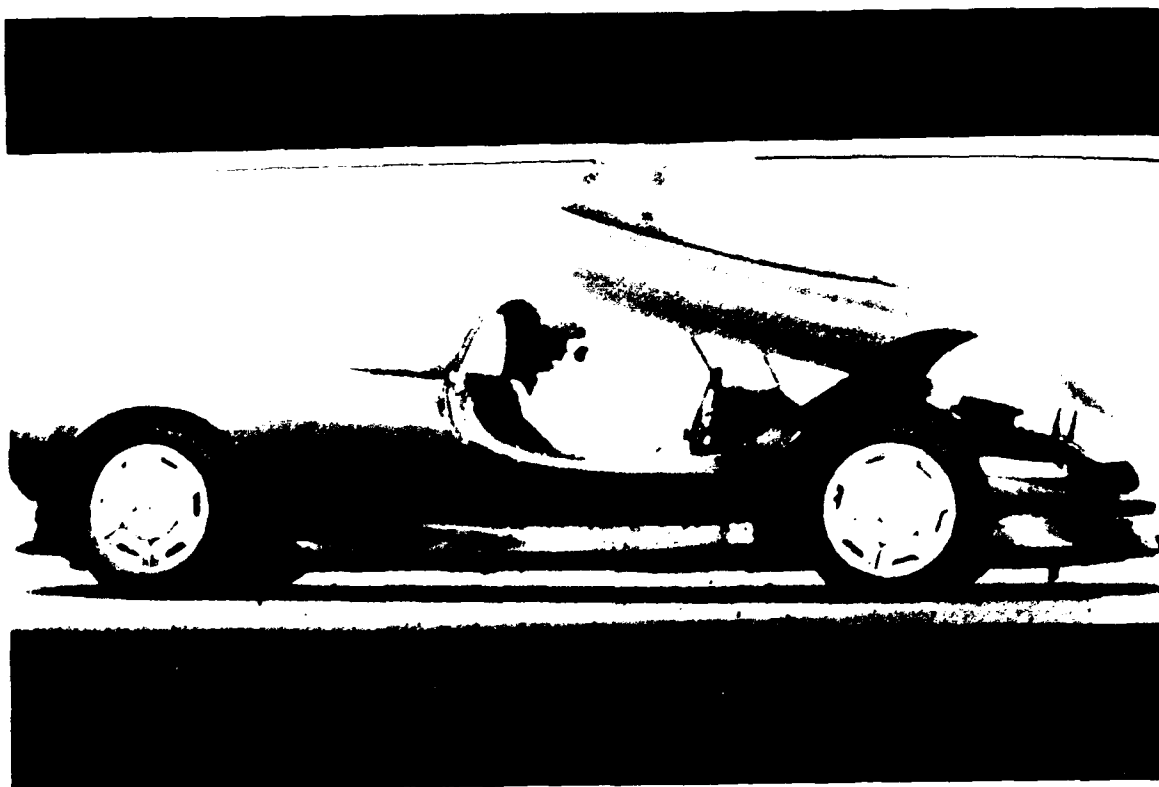
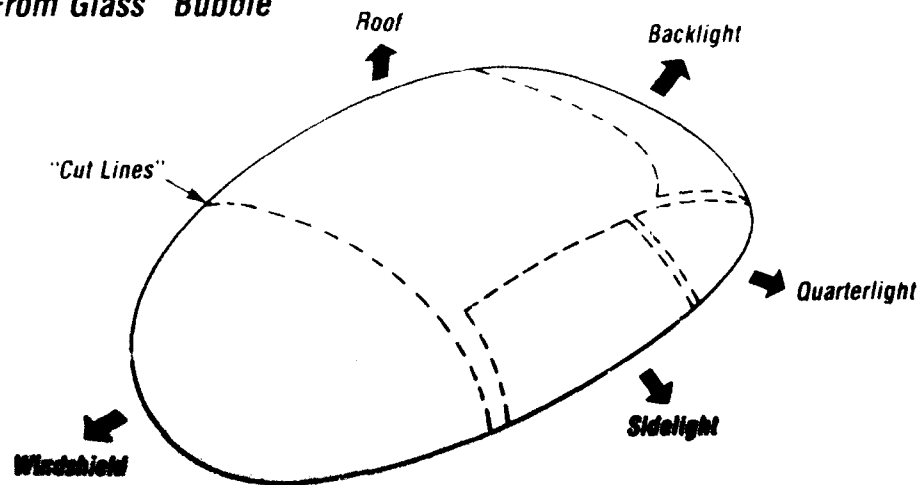


FIGURE 14

PPG **COMPLEX AERODYNAMIC SHAPES**

*Forming of Matching Entire Car Sets By Cut Down
From Glass "Bubble"*



SESSION II

EMERGING CAPABILITIES (PART A)

Chairman: R. E. Colclough
Flight Dynamics Laboratory
Wright-Patterson AFB, Ohio

Co-Chairman: G. J. Stenger
University of Dayton
Dayton, Ohio

Coordinator: C. Szczepan
San Antonio Air Logistics
Center
Kelly AFB, Texas

NEW AND UNIQUE PROCESS FOR RESURFACING AIRCRAFT CABIN WINDOWS

R. Dorey
E. Mountford

EMI-MEC Ltd.

M. Stedman

National Physical Laboratory

NEW AND UNIQUE PROCESS for RESURFACING AIRCRAFT CABIN WINDOWS

R. DOREY, E. MOUNTFORD C.Eng, M.I.Prod.E. M. STEDMAN Ph.D.DIC CPhys
FInstP*

The paper addresses the limitations of traditional methods of resurfacing cabin windows and briefly describes experiments which led to the development of a new method of achieving an improved optical finish at a very fast and economical production rate.

The EMI-MEC AWP-1 is described in detail followed by the presentation of comparative measurements of surface finish and visual distortion of cabin windows produced on the AWP-1 and by traditional grinding and polishing methods.

* R Dorey and E Mountford are part of the development team at EMI-MEC Ltd and Dr M. Steadman is with the division of Mechanical and Optical Metrology at the National Physical Laboratory, Teddington, England.

1. INTRODUCTION

Conventional methods of resurfacing aircraft cabin windows have been considered unsatisfactory for some time.

Those who have attended previous conferences will recall the presentations that have been made by Mr. K. Evald* of Lufthansa German Airlines, who has researched the subject of Window Crazing more than anyone else in the industry.

His findings have shown conclusively that the use of polishing compounds has a detrimental effect on windows and gives rise to many of the initial scratches and embedded particles which contribute to in flight crazing. This premature crazing dramatically reduces in-service life.

However, this is only one aspect of the problem, grinding and polishing also leave the window with an undulating surface, thus making it difficult to determine the area of minimum thickness. A critical consideration when the window is close to the allowable minimum.

Furthermore these are slow, labour intensive and expensive processes taking up unnecessary floor space which could be more profitably employed.

2. DEVELOPMENTS

Fine diamond machining appears to offer significant potential advantages. Development has thus far been concentrated upon diamond milling with some encouraging results. However, it has several serious inherent shortcomings.

*K Evald, Acrylic Window Crazing, presented at the meeting of ASTM subcommittee F7.08 October 1986. Hyannis, Cape Cod, Massachusetts

Firstly, with high speed rotating tools it is not possible to accommodate sufficiently rigid tool-holders with the necessary means of precise adjustment, it is also difficult to keep the assembly accurately balanced. All these parameters are important in the achievement of a fine surface finish.

Secondly, with a revolving tool it is virtually impossible to prevent momentary coolant starvation at the diamond tool cutting edge. The resulting heat build up can produce areas of opacity. Acrylic with its very low melting point of 90 degrees celsius is particularly susceptible to heat damage.

Thirdly, the process is one where the tools are cutting intermittantly thus introducing the possibility of shock patterns on the surface of the window as the tool commences to cut. This intermittant cutting also has a deleterious effect on the life of the diamond cutting tool.

Fourthly, the debris removed during the cutting process is flung in all directions making it extremely difficult to collect satisfactorily. This can become a problem in the production situation.

3. THE EMI-MEC SOLUTION

Consideration of the limitations of the milling process led EMI-MEC to study alternative possibilities. Turning, that is the rotation of the window against stationary traversing tools seemed to offer the best theoretical solution as it positively addresses the majority of the shortcomings inherent in the milling process.

Initial experiments with the window rotating, using stationary diamond tools set into rigid and steplessly adjustable pre-set tool blocks with copious coolant flow to each tool and debris collected by a vacuum exhaust immediately above the tools, proved the process to be viable. It was also extremely fast since the total distance travelled by the tools is only from edge to centre, half that required in the milling process

Subsequent developments to support the process with a satisfactorily stiff and accurate machine to achieve the very fine finishes necessary have confirmed the many benefits inherent in this unique EMI-MEC system.

The EMI-MEC MODEL AWP-1 RESURFACING MACHINE removes a controlled thickness of material from the window, to a finish which in many cases will require no subsequent polishing. The machine, which is largely automatic, requires little operator skill or knowledge and completes the task in a fraction of the time taken using old conventional grinding and polishing techniques.

Continuing Research and Development has refined the process to the point where the outside surface of a typical 747 window is machined in one and one half minutes. Allowing for loading this can result in the reprocessing of approximately 30 surfaces per hour.

The process has additional benefits. The thickness of the window across the whole of its surface will be uniform within plus or minus 0.025mm after machining. More importantly, the amount of material removed can be controlled in increments of 0.001mm to remove the absolute minimum of material. The number of times resurfacing can be carried out is therefore increased, prolonging the service life of the window considerably.

The process is clean, quiet and free from odours or any other contamination. The highly efficient debris extraction unit is however, somewhat noisy and is best sited remote from the machine and could serve several machines if required.

Theoretically the "achilles heel" of the process is the known propensity for turning to produce a small pip in the centre of a surface as the cutting speed reduces to zero. In practice this has not proved a problem with the AWP-1 window resurfacing machine. Provided the diamond tool is accurately adjusted to be within 0.001mm of the centre height, the centre section of the window will have a finish indistinguishable from any other area. The machine is, of course, provided with the means by which this adjustment can be made quickly, precisely and easily verifiable.

4. MACHINE SPECIFICATION

The AWP machine, see figure 1, has been designed specifically for window resurfacing using the latest techniques available for the production of ultra high precision flat surfaces with optical surface textures better than 40 Angstroms (Peak to Valley). This is equivalent to 0.4 Micro-inches Ra.

4.1. MACHINE BASE

To achieve the adequate rigidity and stiffness the machine base is constructed of reconstituted granite and epoxy resin as is frequently used for bases of high precision measuring machines.

The purpose designed structure possesses stiffness and damping characteristics that are six times better than a similar cast iron structure.

The base is mounted on three vibration-absorbing mountings to isolate it from any external sources of vibration.

The main machine base has a small footprint of only 2 metres square. in addition there are three smaller floor standing units, situated to the rear of the machine namely :--

- c) A refrigeration unit for cooling the spindle.
- b) A vacuum pump and resevoir for the window chuck feature.
- c) A vacuum debris extraction unit.

This ancillary equipment occupies an area of one and one half square metres and can be placed remote from the machine if necessary to suit site restrictions.

4.2. SPINDLE

The headstock spindle is an ultra high precision air bearing spindle with independent front water cooled air thrust bearings. It has the

capacity to swing a fixture of 600 mm diameter and is built to achieve accuracies as follows:

ROTATIONAL ROUNDNESS 7 MAXIMUM AXIAL ERROR: - 0.12 microns

MAXIMUM SPINDLE LOAD: Axial -- -- 500 Kgs.

SPINDLE STIFFNESS:-- Axial 45,312 Kgs/ mm. Deflection

4.3. VACUUM SYSTEM

The spindle supports a vacuum chuck for mounting the windows. Vacuum is provided by a pump which is powered by compressed air at 5.5 bar. Operating pressure is monitored to ensure positive safety, the slightest drop in pressure shuts the machine down in three seconds.

4.4. SPINDLE DRIVE

The spindle is driven by a direct mounted AC motor with special windings to give high torque for starting and low power during running to minimize the effects of 60 cycle ripple from the main electrical supply. Starting is achieved by electronic "soft-start" and DC injection braking is employed for rapid stopping.

The spindle and drive are water cooled for thermal stability, the water being pumped through a chiller unit to control the temperature.

4.5. MAIN SLIDE

The main slideway is carried on vee and flat slideways, precision ground and replicated to achieve high accuracy with anti stick-slip properties. They are automatically lubricated.

The slide is hydro-pneumatically actuated with steplessly variable feed rates. Maximum travel is 457 mm.

4.6. TOOL CONTROL

The tool holder incorporates three diamond tools, for progressive roughing and finishing and is capable of forward feed and retraction. The diamond tools have been the subject of considerable development and their geometry plays a significant role in the achievement of the superb finish. You will understand if I decline to share with you the details of the precise shape.

All tools have steplessly variable centre height adjustment and an optical setting fixture is provided to facilitate the rapid and accurate achievement of centre height.

To automatically cater for the variable thickness of windows, a contact probe is provided to sense the position of the surface of the window. Electronic feedback from the probe in conjunction with the pre-set depth of cut ensures the tools are correctly positioned.

The entire process is controlled by a micro-processor and the depth of cut required is entered through a key-pad.

4.7. CUTTING COOLANT

The tools and the window are constantly sprayed with a special chemical mist coolant during cutting. This fluid is already being used in the refurbishment of acrylic aircraft windows. The coolant is switched on and off automatically during the machining process.

4.8. SWarf EXTRACTION

A cyclone vacuum swarf-extraction unit is supplied to be installed remote from the machine and is connected by a 100 mm diameter hose. This unit collects the cutting process debris into easily accessible disposable plastic bags.

4.9. GUARDING

The machine is totally enclosed to ensure operator safety and to contain swarf and coolant spray. The front access sliding doors are electrically interlocked to prevent access by the operator during the machining process.

4.10. PAINTING

The machine is finished throughout in white to present a clean appearance.

5. OPERATING PROCEDURE

Various alternatives can be specified via the micro-processor control these being for:-

- a) One cut only across the front face.
- b) A second cut across front face. This option may be required in the event of an insufficient depth of cut being called up to eliminate all scratches or to reach the low spots in an out of flat window.
- c) Cut across the back face.

The amount of material necessary to remove crazing will vary from window to window and is a matter of operator decision based upon experience. The required ammount is entered on the data entry key pad on the front face of the micro-processor in microns. This will accept values in the range of 1 to 500 (500 equals 0.020 inch).

The operator loads the window on to the vacuum chuck with sufficient force to overcome the natural curve of the window and initiates vacuum to grip the part. Every new window profile requires an individual vacuum fixture and centralising template.

The guard is slid closed and cycle start buttons pressed; this energises a guard safety interlock and initiates the automatic cycle.

The toolslide traverses in fast motion to position the probe approximately in the centre of the non-rotating window. The probe moves forward to sense the position of the window surface, and on contact conveys the information to the control.

The probe is retracted and the slide returned in fast motion to the start machining position. During this operation the spindle is brought to full operating speed and the tools moved to the correct position with respect to the window surface to remove the desired amount of material.

Feed traverse of the cutting tools is initiated and continues until the third (finish finishing) tool reaches the centre of the window. Here it is automatically retracted away from the part, the spindle stops and the operator opens the access doors to remove the window.

With a spindle speed of 3,000 rpm and a feed of 0.002 inches per revolution, the machining time for a typical Boeing window of 380 mm x 280 mm would be one and one half minutes per side, resulting in a floor to floor time of approximately two minutes.

6. SURFACE METROLOGY OF RESURFACED ACRYLIC WINDOWS

Surface profiles of samples of diamond-turned and of conventionally polished windows were measured at the National Physical Laboratory using a Rank Taylor Hobson Form Talysurf machine. In order to display waviness, the best-fit circle was subtracted from each profile, to remove its primary curvature, and the data processed to remove features of width less than cut-off lengths of 0.8 and 2.5 mm. Figure 2 shows a comparison of typical results for a 2.5 mm cut-off, in which the waviness of the polished surface is seen to be much greater than that of the diamond-turned surface.

To quantify these observations a series of profiles was recorded, and the waviness parameter W_{Ra} (which is defined analogously to roughness R_a) was estimated by averaging results from 6 independent runs at each combination of sample and cut-off length. The results are given in figure 3.

The effect of waviness on visual distortion can be predicted by considering the angular deviation caused to a ray of light by the wedging created by local slope errors. The angular discrimination of the normal human eye is about 1 minute of arc. Taking the refractive index of acrylic as 1.5, one can show that a beam of light normal to a window would be deviated by 1 arcmin if the surfaces were wedged by about 2 arcmin. Consider a sinusoidal profile of amplitude A and wavelength W on one face of an otherwise perfect window. A maximum local slope error of 2 arcmin can be shown to occur for an A/W ratio of 0.000093. For a given wavelength, values for amplitude and Ra (noting that $Ra=2A/$ for a sine wave) can then be calculated. Thus, for wavelengths of 0.8 and 2.5 mm one can derive Ra thresholds for visual distortion of 0.05 and 0.15 μm respectively. Referring to Figure 3 one predicts, on this basis, that the polished windows will exhibit visible waviness distortion, whilst the diamond-turned ones will be free of it. Computation shows that when the window is viewed at 45 degrees incidence, the Ra thresholds are reduced to 0.03 and 0.09 μm (for $W = 0.8$ and 1.5 mm) , so that the diamond-turned windows will still be free of visual distortion.

7. VISUAL TEST

Samples of windows produced on the AWP-1 and those produced by conventional polishing techniques were subjected to a test similar to that defined by Lockheed. A gridboard of half inch grid spacing was photographed through the windows with the window and grid board being positioned 60 inches and 180 inches respectively from the camera.

Figures 4 and 5 show the results with the window perpendicular to the line of sight. As can be seen the grid viewed through the polished window is distorted, whereas, when viewed through the diamond turned window there is no perceptible distortion.

These tests support the theoretical conclusion reached from the surface topography measurements and graphically demonstrate the superiority of windows produced on the AWP-1.

8. SUMMARY

It has been demonstrated that windows produced by diamond turning on the EMI-MEC machine exhibit a surface finish whose waviness is an order of magnitude less than a polished surface.

More importantly the windows so produced are optically clear and distortion free as perceived by the human eye.

It is therefore possible to resurface cabin windows without the use of polishing compounds which are perceived to be a cause of premature crazing in service. Alternatively, if polishing is deemed necessary for cosmetic or other reasons then the time required is minimal when starting from such a near perfect surface.

The spin off benefits of this particular machine are most attractive from an investment viewpoint, and are listed in Figure 6. However, the potential secondary benefits of much longer service intervals for cabin windows may be an overwhelming consideration in favour of the adoption of this process by airline operators.

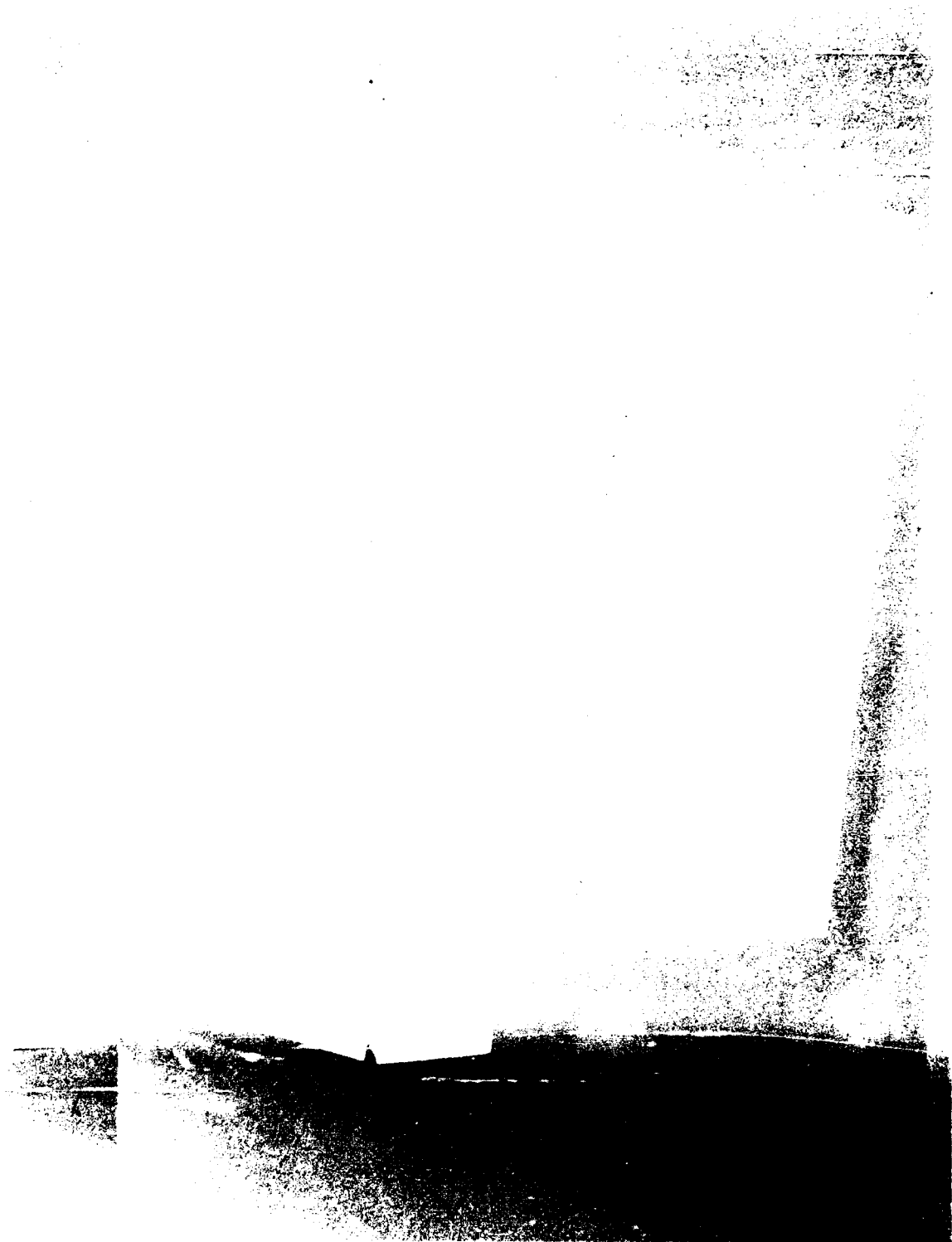
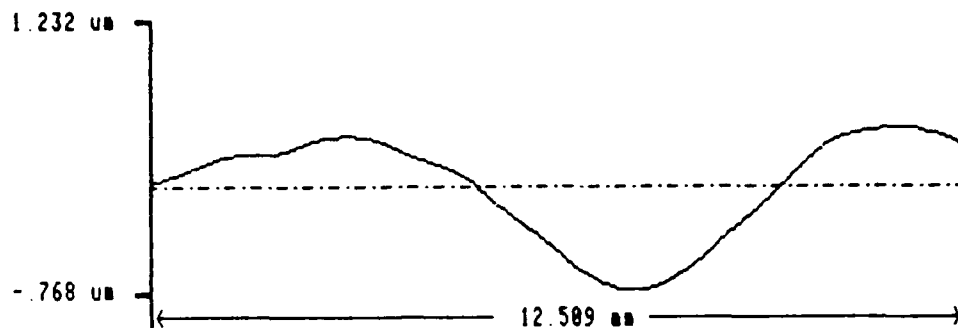


Figure 1. EMI-MEC AWP-1

F1 - Analysis
 F2 - Graph
 F3 - Dump
 F4 - Expand
 F5 - Exclude
 F6 - Z_Range *

Mode	Cut Off	Filter	Reference	Ignore
WAVINESS	2.50 mm	ISO	CONVEX	0 %
EMI-MEC Sample: Rectangle Run: 25				



Peak To Valley = 1.218 um
 Z_Range = 2.000 um

TIME: 15: 9
 DATE: 6-DEC-88

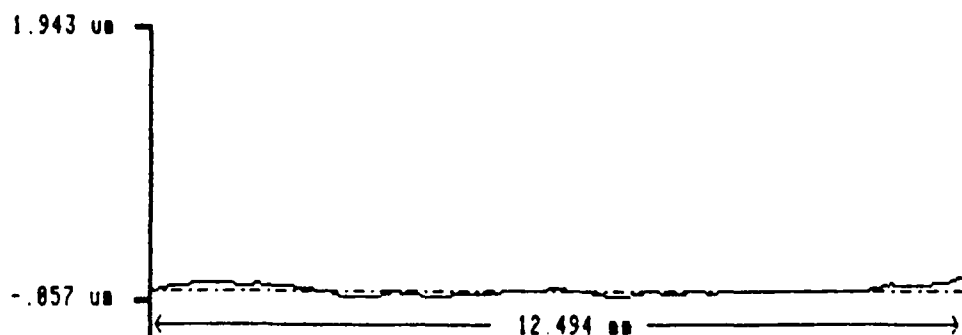
-1-

Taylor-Hobson

(A) POLISHED SURFACE

F1 - Analysis
 F2 - Graph
 F3 - Dump
 F4 - Expand
 F5 - Exclude
 F6 - Z_Range *

Mode	Cut Off	Filter	Reference	Ignore
WAVINESS	2.50 mm	ISO	CONVEX	0 %
EMI-MEC Sample: 6 Run: 26				



Peak To Valley = .152 um
 Z_Range = 2.000 um

TIME: 15:13
 DATE: 6-DEC-88

-1-

Taylor-Hobson

(B) DIAMOND TURNED SURFACE

FIG 2 WAVINESS PROFILES WITH CUT-OFF LENGTH 2.5mm

	CUT-OFF LENGTH	
	0.8 mm	2.5 mm
DIAMOND-TURNED SURFACE	0.024 μm	0.026 μm
POLISHED SURFACE	0.087 μm	0.349 μm

FIG 3. VALUES OF WAVINESS (WR_a)

Figure 4. Grid Viewed Through a Polished Window

Figure 5. Grid Viewed Through a Diamond Turned Window

FEATURE

BENEFIT

WINDOW SURFACES ARE REPROCESSED IN ONE
SIMPLE OPERATION BY A SINGLE OPERATOR.

UP TO 30 SURFACES
PER HOUR CAN BE
MACHINED.

FLOOR SPACE REQUIREMENT REDUCED TO
6 SQUARE YARDS.

REDUCTION IN
OVERHEAD COST.

THE MINIMAL MATERIAL NEED ONLY BE REMOVED
TO ELIMINATE SURFACE DEFECTS.

MORE REFURBISHMENTS
POSSIBLE PER WINDOW.

ELIMINATES THE USE OF POLISHING COMPOUNDS.

EXTENDS THE ONSET
OF CRAZING.

FIG 6. BENEFITS OF THE EMI-MEC AWP-1 PROCESS.

BIRD IMPACT RESISTANT WINDSHIELD AFT ARCH DESIGN METHODOLOGY

G. J. Stegner
M. P. Bouchard
D. R. Bowman

University of Dayton

BIRD IMPACT RESISTANT WINDSHIELD AFT ARCH DESIGN METHODOLOGY

G. J. Stenger, M. P. Bouchard, and D. R. Bowman
University of Dayton Research Institute
Dayton, Ohio 45469

ABSTRACT

Aft arch design is critical to the performance of bird impact resistant transparency (BIRT) systems. BIRT windshield system design consists of two primary tasks that are performed interactively: first, the transparency cross-section must be selected, and second, the transparency support structure must be designed. A transparency material system, or a number of candidate systems, is selected to meet bird impact performance, optics, service life, and weight requirements. Transparency thickness is selected based on bird impact resistance requirements (assuming BIRT requirements are more critical than other mission related requirements). Parametric equations and birdstrike test results, normalized to the impact angle and taking into account windshield and support structure geometry and edge condition, are used to predict the bird impact capability.

The material system for the aft arch is dependent on geometric, manufacturing, cost, weight, and mission related requirements. Currently, high strength metals such as titanium and several varieties of nonmagnetic stainless steel, as well as advanced composite materials, are being used in new BIRT windshield systems. The aft arch cross-section properties must be designed to match transparency structural response. Lightweight BIRTs require that the aft arch flex with the transparency yet be stiff enough to prevent excessive deflection. In addition, the strength of the arch must be tailored to the windshield strength to prevent catastrophic failure of the system.

This paper discusses an aft arch design methodology which incorporates empirical design curves, manual calculations, and finite element analysis (using the nonlinear finite element program MAGNA). Successful demonstration of the methodology on the A-7 single piece BIRT (with composite aft arch) is also presented.

DISCUSSION OF WINDSHIELD SYSTEM DESIGN PHILOSOPHY

Military aircraft of today and the future are flying faster and lower, utilizing advanced guidance systems. Transparency systems must be designed to perform in this demanding environment. Bird impacts pose a significant threat to high performance aircraft, and are only one of many design challenges facing the transparency designer. This paper

discusses a design methodology which can be used to design the transparency system support structure to optimize the bird impact resistance capability of the transparency.

Successful aft arch design requires knowledge and understanding of all the transparency system components, and their interaction with and effect on the total system. The method described in this paper can be used in the design of both metal and composite windshield support structure. The total transparency system design process is outlined in Figure 1 and described in this paper.

High performance aircraft transparency systems must be designed to meet many different, specific, and sometimes conflicting requirements and goals. Numerous technologies must be integrated to develop a light weight, affordable transparency system which meets the pilot requirements for optics, visibility, and protection from the environment, as well as user requirements for maintainability, interchangeability, and durability, and vendor requirements for producibility. In general, the final design is a compromise between the various design requirements and goals.

The critical first step in generating a transparency design is to have a clear definition of the guidelines and constraints which govern a specific design, and a clear definition of the requirements and goals which must be met and considered in a specific design. The transparency must have very good optics and structural integrity, must be light weight, and must provide protection from natural and mission-related thermal, birdstrike, and combat threats. Built-in features such as anti-ice heating elements and metallic coatings are also important considerations in the transparency cross-section design. The methodology for determining cross-section configuration and thickness for bird impact resistance is based on the use of design curve and actual full scale birdstrike test data points as indicated in Figures 2-5 (Reference 1). The UDRI, in conjunction with the transparency manufacturers, has developed a methodology² for evaluating candidate transparency configurations on the basis of cost (initial and life cycle), weight, producibility, durability, interchangeability, maintainability, optics, visibility, and birdstrike resistance. Understanding of the problem, experience, and engineering judgement are also important factors in final cross-section definition.

UDRI holds the philosophy that the most efficient energy absorbing structure is a design that enables the transparency and the aft arch to respond dynamically as an integral structural unit. The proper design of the mechanisms to transfer load from the transparency to the aft arch is critical to achieving this. Failure to give proper attention to the details of the

transparency edge treatment can result in catastrophic failure for an otherwise well designed structural system. For a bolted edge design³ these details include bolthole edge distance, fastener strength and ductility, fastener size and spacing, bushing design, structural ply continuity, bearing strip requirement, and retaining strip geometry, stiffness, and bearing strength. In a near optimum design, the shear strength of the bolt should equal the bearing strength in the transparency, and the bolts should be spaced to minimize tensile failure of the transparency and/or shear tearout. If the windshield is bonded to or sandwiched by the support structure, the edge member design must be considered as well as the strength and toughness of the adhesive/sealant. If the windshield will be sealed in a channel, the channel flange length must be designed to prevent the transparency from pulling out of the channel during birdstrike. Also, the adhesive/sealant must be sufficiently flexible to allow movement due to expansion and contraction of the transparency.

AFT ARCH FRAME DESIGN

An aft arch design is developed after selecting a candidate transparency cross-section for evaluation. The performance of the transparency, especially during birdstrike, is highly dependent on the structural characteristics of the aft arch. In the system design approach, the aft arch is matched to the selected transparency, providing a desired level of bird impact resistance while maximizing visibility and minimizing weight. The system must be designed from an energy standpoint, using both strength and stiffness to define the structural requirements, to absorb and transmit the impact loads.

The approach used by UDRI is to design an aft windshield arch to strain as equally as possible at as many points along the arch as possible (absorbing and distributing as much energy as possible) at a load level just below that required to cause failure of the transparency.

There are three basic steps to aft arch design: geometric envelope definition, material selection, and cross-section design. The aft arch design envelope should maximize visibility, it should not interfere with existing structure, and it must be compatible with instrumentation requirements. The forward edge of the transparency bearing surface should be radiused to minimize stress concentration in the transparency as the transparency is deflected.

The best cross-section geometry for an aft arch is one with a high shape factor; that is, one which absorbs the greatest amount of plastic strain energy prior to failure and minimizes the possibility of a catastrophic failure. A problem with these sections is high weight; typically they are not as structurally

efficient as thin open sections. Generally, a problem with thin open sections is that they tend to buckle which substantially reduces the energy absorbed. The best aft arch cross-section geometries are stable sections (those which are thick enough to prevent buckling) with high shape factors and which meet the weight and visibility requirements.

After a transparency cross-section is selected, a design "not to exceed" arch strength can be calculated. This strength will be based on the peak load that the transparency can transmit into the arch. Designing the arch to yield prior to failure of the transparency prevents catastrophic failure of the system. The centerline cross-section for candidate arch materials is defined to meet the strength and functional requirements. At this point, several alternate materials and arch configurations can be evaluated in terms of including visibility, formability, nonmagnetic, producibility, cost, corrosion, and weight requirements. Current high performance system material choices include austenitic stainless steel, titanium, and advanced hybrid composites. It is important that the aft arch material be inherently tough. For metals this requires a reasonable elongation (greater than 10%) to failure (usable plastic region), and for composites an energy absorbing failure⁴ mode (eliminate catastrophic failure) and good secondary load carrying capability after first ply failure. Low elongation metals and composites which have a brittle failure mode should be avoided.

The details of the arch can now be determined. A nonlinear static analysis has been used to determine how the arch should be tapered from the centerline to the sill. The arch is tapered to equalize, as best as possible, the stresses in the arch. Transparency mounting flanges on the arch, if any, should be sized to yield prior to failure of the transparency.

The arch-to-sill attachment fittings are important to the overall performance of the system. These fittings should be designed to minimize the load generated at the arch-to-fuselage interface. The moment applied by the arch about the longitudinal axis of the sill can be reduced by orders of magnitude by reducing the stiffness (about the longitudinal axis of the sill) of the arch-to-sill connection.

Finally, the details of the arch design, some of which have been described above, are extremely important to the performance of a transparency, and many times are the difference between a successful and an unsuccessful transparency system. The use of this design philosophy/methodology is illustrated below by its application to the design of an aft arch for the A-7 wraparound windshield.

A-7 AFT ARCH DESIGN

The A-7 windshield system was redesigned from a three-panel system having a critical birdstrike capability of 160 knots when impacted by a four-pound bird to a single-panel wraparound system having a birdstrike capability of 480 knots when impacted by a four-pound bird (see Figure 6). This section describes the design of the new aft arch, which is a hybrid composite consisting of Kevlar-49, S-2 glass, and epoxy. Note that the calculations given below reflect the current procedure used by UDRI in composite arch design, and are somewhat different than those originally used in designing the A-7 aft arch.

INITIAL CROSS-SECTION SELECTION

The initial cross-section is selected by using a prediction of the maximum birdstrike load and designing an arch that will withstand that load. The peak normal load on the windshield is determined from the momentum equation

$$P_n \Delta t = mV_n \quad (1)$$

where P is the normal component of the peak load on the arch, Δt is the time duration of the impact, m is the bird mass, and V_n is the normal component of the velocity, where

$$V_n = V \sin \theta \quad (2)$$

see Figure 7. The time of impact is assumed to equal the "squash up time" of the bird,

$$\Delta t = \frac{L_b}{V} \quad (3)$$

where L_b is the effective length of the bird. Finally, a constant K is introduced to adjust for the fact that only a percentage of the energy (and thus the peak load) introduced into the windshield is transmitted to the aft arch. The remainder of the energy is absorbed by the windshield and other support structure. Thus

$$P_n = \frac{KmV^2 \sin \theta}{L_b} \quad (4)$$

or, for V in knots, substitute $V_{fps} = 1.69 V_{kts}$, giving

$$P_n = \frac{Km(1.69)^2 V^2 kts \sin \theta}{L_b} \quad (5)$$

This peak normal load can be resolved into two components, an in-plane component (radial to the arch), P_r , and an out-of-plane component (normal to the arch), P_o .

$$P_r = P_n \cos(\theta - \phi) \quad (6)$$

$$P_o = P_n \sin(\theta - \phi) \quad (7)$$

ϕ is defined in Figure 7. The maximum stress in the aft arch may be expressed by the classic bending stress equation,

$$\sigma = \frac{Mc}{I} \quad (8)$$

where I is the moment of inertia and C is the distance to the outermost fiber. M , the maximum moment, depends on the end fixity of the arch. For a circular arch with pinned ends (most aft arches can be assumed to be circular), the maximum moment for a point load applied at the center is

$$M = \frac{PD}{11} \quad (9)$$

where P is the peak load and D is the arch diameter. The final equation for the maximum in-plane stress in the arch is

$$\sigma_r = \left[\frac{Km(1.69)^2 V^2 kts \sin \theta \cos(\theta - \phi)}{L_b} \right] \left[\frac{D}{11} \right] \left[\frac{C}{11} \right] \quad (10)$$

To estimate the value of K , the percentage of peak load reaching the aft arch, the T-38 composite reinforcement data was used. The K value for one system does not apply to another system unless the two are of similar geometry, arch material, arch-to-sill fixity, and windshield shape and construction. The T-38 composite successfully defeated a four pound bird at 400 knots. The angle of incidence $\theta = 27.5^\circ$, and $\phi = 27.9^\circ$. The arch diameter is approximately 30.7 inches. The in-plane moment of inertia, $I = 0.22 \text{ in}^4$, and the distance to the outermost fiber $C = 0.6 \text{ in}$. At 400 knots, the T-38 composite reinforcement was experiencing some outer ply failure. This would correspond to a maximum in-plane stress of 110,000 psi. Although the T-38 arch-to-sill connection was not a pinned joint, the stiffness was much less than a true fixed end condition; therefore it was modeled as a pinned end condition.

Inputting these values into Equation 10,

$$110,000 = K \left[\frac{4}{32.2} \right] \frac{(1.69^2 (400)^2 \sin(27.5) \cos(27.5-27.9))}{1} \left[\frac{30.7}{11} \right] \frac{0.6}{0.2225}$$

and solving for the unknown, $K=0.558$.

The peak radial load on the arch for the T-38 can be estimated by combining Equations 5 and 6,

$$P_r = \frac{Km(1.69)^2 V^2_{kts} \sin\theta \cos(\theta-\phi)}{L_b} \quad (11)$$

$$P_r = \frac{0.558 \left[\frac{4}{32.2} \right] (1.69^2 (400)^2 \sin 27.5 \cos(27.5-27.9))}{1}$$

$$P_r = 14,600\# \text{ for the T-38}$$

Assuming a similar composite system is used for the A-7, with a pinned end condition and a 480-knot design goal, the K value for the T-38 can be used for the A-7. Additional A-7 data: $\theta=30$, $\phi=23$, and $D=32$.

The peak radial load on the aft arch for the A-7, from Equation 11,

$$P_r = \frac{0.558 \left[\frac{4}{32.2} \right] (1.69^2 (480)^2 \sin 30 \cos(30-23))}{1}$$

$$P_r = 22,600\#$$

Equation 10 can be used to determine required cross-section properties for an A-7 composite arch.

$$110,000 = (0.558) \left[\frac{4}{32.2} \right] (1.69)^2 \sin 30^\circ \cos(30^\circ-23^\circ) \left[\frac{32}{11} \right] \frac{C}{I}$$

and solving for the minimum required section modulus

$$S_{min} = \frac{I}{C} \quad (12)$$

$$S_{min} = 0.599$$

Therefore, a cross-section with a section modulus of about 0.6 would be used as a starting point for the finite element analysis.

The ratio I/C is not sufficient for determining the initial geometry of the cross-section (that is, specific values for I and C are not known). Another equation involving the unknown I is needed. Bending stiffness (EI) is selected based on experience, where E is the effective tensile modulus of elasticity for the material. In this composite laminate, a nominal value of $E = 7 \times 10^6$ psi was assumed based on three-point beam bending tests of similar laminates.⁴ As shown in Table 1, the bending stiffnesses for similar wraparound windshield systems is in the vicinity of 4×10^6 lb-in². A bending stiffness of 3×10^6 psi was used for the initial A-7 arch cross-section design (chosen before all of the information in Table 1 was available). At this point the section modulus equation and the bending modulus equation were together sufficient to define initial values for I and c :

$$I = 0.42 \text{ in}^4$$

$$C = 0.76 \text{ in.}$$

It should be noted that the value for bending stiffness relies on previous experience with similar windshield systems. Departures in the windshield system geometry or in the aft arch material system could substantially alter the design bending stiffness and invalidate the use of Table 1 and the beam test moduli.⁴

With the initial values for I and c determined, the next step was to design an arch cross-section which would match these values and also match the geometry design envelope (in this case, retain the same pilot field of vision around the aft arch as on the existing aircraft). Figure 8 shows that the wedge-shaped forward edge of the recommended section provided increased field of view for the pilot, thus meeting the requirements imposed by the geometry design envelope. The forward tip was rounded to relieve stress concentration when the windshield deflects down onto the arch during bird impact. The cross-section dimensions provided the necessary values of I and c . The lay-up consisted of uniaxial tape oriented parallel to the arch perimeter to provide the necessary bending stiffness and strength, and inner and outer wraps of ± 45 weave to provide the necessary shear strength to prevent catastrophic delamination.

With the arch geometry and gross material properties thus defined, finite element evaluation of the initial design was then conducted.

MAGNA FINITE ELEMENT ANALYSIS OF THE A-7 ARCH DESIGN

The MAGNA⁴ finite element analysis program was used to review the A-7 arch design. The analyses provided a good

qualitative evaluation of the arch and provided insight on ways to improve the design. The following criteria were used to evaluate the performance of the design:

1. Absorbed Energy - Maximize the absorbed energy;
2. Arch Deflection - Maximum deflection should not be so great as to allow the bird to enter the cockpit, yet not be so small that only minimal energy is absorbed by the arch;
3. Strength - The failure load of the arch should be less than that of the windshield to prevent catastrophic shear failure of the windshield at the arch/windshield interface;
4. Failure Location - It is desirable to have initial failure of a composite occur at the center of the arch, followed by failure at the two high stress points approximately half-way between the centerline and sill. Failure of the side points first could result in catastrophic collapse of the arch. Note that for metal arches the criterion used is simultaneous yielding of a broad region of the arch, which ensures good energy absorption and load dissipation. Failure locations are controlled by tapering the arch using the FEA as a design tool; and
5. Sill Reactions - the reactive load imposed by the arch on the sill must be controlled so that damage to the fuselage is limited to an acceptable level (or completely eliminated).

The A-7 finite element model, shown in Figure 9, consisted of a series of three-node beam elements, a single truss element, appropriate boundary conditions, and loads. The beam elements provided for independent entry of the tensile and shear moduli (E and G) and allowed for large displacements. The model did not distinguish between plies and ply orientations, but instead modeled the arch as a homogeneous continuum. An equivalent value of shear modulus was used which ensured that the shear stiffness of the gross laminate model matched that of the actual arch. The locations of the nodes relative to the centroid of the arch cross-section were chosen to ensure that twisting as well as bending of the arch occurred (that is, the loads were applied at the forward edge of the arch). The truss element at the sill provided a means of modeling the torsional stiffness on the sill connection about the axis of the sill. The tensile modulus could be varied to vary the torsional stiffness. This approach was used because MAGNA does not provide a torsional spring element. Symmetry boundary conditions were applied at the center so that only half of the arch needed to be modeled. The entire arch was constrained to prevent out-of-plane translation as a simplified model of the actual out-of-plane restraint provided by the transparency. The base of the arch and the free

end of the sill support were pinned to prevent translation. The applied loads consisted of a series of equal-magnitude vertical nodal loads applied from 0 to 3.75 inches away from the centerline, which approximately matches the width of the bird footprint resulting from bird impact along the centerline 6 to 10 inches forward of the aft arch.

An eigenvalue analysis was first performed to check the model. Nonlinear static analysis was then performed to evaluate the arch design. The loads were applied incrementally until the ultimate stress for the gross laminate was reached. Geometric nonlinearities (large deflections) were expected. Material nonlinearities (plasticity) did not occur since the arch stress-strain curve was assumed to be linear up to the ultimate point.

From the MAGNA output listing, several sets of data were plotted. Figure 10 is a plot of applied load versus centerline displacement. Note that curves for several different designs are plotted. A summary of the designs appears in Table 2. The curves terminate at the ultimate load. the relationship between the load and displacement is nonlinear and indicates that the arch stiffness (slope of the curve) is "softening" with increasing load. From the curves it can be seen that designs 1, 3, and 4 met the strength criterion (arch failure at a load less than that of the windshield failure load of 22,600 lbs) and design 4 also minimized the centerline displacement (centerline deflection of 1.5 inches).

The energy absorbed by the arch was computed as the area under the load-displacement curve. Figure 11 presents plots of energy versus applied load for the various designs.

Figures 12 and 13 present plots of the distribution of axial stresses at the outer and inner fibers along the length of the arch for the load at which initial arch failure occurred. It is apparent that there were two high stress regions, one at the centerline and the other approximately half-way between the centerline and the sill. As mentioned previously, good design practice dictates that failure of the composite arch should initiate at the centerline, not at the sides. From the plots it can be seen that all designs but model 1 meet this criterion.

Using the MAGNA reaction output and simple statics, the loads (compressive, shear, and moment) at the sill were computed (see Figure 14). Table 2 summarizes the results. It was determined that the high moment loads for designs 2, 4, 5, and 6 may cause unacceptable damage to the fuselage. As a result, it was recommended that the connection between the arch and sill provide little torsional stiffness about the axis of the sill. This recommendation led to the development of a clevis connection, shown in Figure 15, which minimized torsional loads on the sill.

As a result of the MAGNA analyses, design number 3 of Table 2 was initially recommended for the A-7 aft arch. After the initial design was developed, LTV generated an envelope for the arch. This initial design was then modified by narrowing the width and increasing the thickness to stay within the bounds of the design envelope. The final arch design is shown in Figure 16. Birdstrike testing of the windshield/arch/clevis system demonstrated the design to be capable of defeating an impact by a four pound bird at 480 knots at a point 9.5 inches from the aft arch along the windshield centerline.⁶

SUMMARY

A methodology for the design of aft arches to support bird-impact-resistant wraparound windshield systems typical of high-performance fighter aircraft has been presented. The methodology was successfully demonstrated for the A-7 wraparound windshield with a hybrid composite aft arch. The methodology blends manual calculation, testing, and finite element analysis to achieve an acceptable design. The methodology is not a "cook book" approach and should be augmented by comparison with known birdstrike test performance data at all stages of the design process.

An earlier version of this approach was used by UDRI to successfully design the T-38 arch support structure. Because of similarities between the A-7 and the T-38, and because of limitations on time and resources, it was judged unnecessary to perform a full nonlinear dynamic birdstrike analysis to further verify/refine the A-7 design. However, in instances where differences to existing systems are significant, a full nonlinear dynamic analysis should be used to support the design process. It is recommended that the procedures described here be exercised to provide a good preliminary design. This will ensure that iterations/refinements to the design are being made relative to a good starting point and will maximize the likelihood for success while minimizing the cost of computer resources.

REFERENCES

1. J. H. Lawrence, Jr., Guidelines for the Design of Aircraft Windshield/Canopy Systems, AFWAL-TR-80-3003, February 1980.
2. Gregory J. Stenger, Blaine S. West, Richard A. Nash, and J. Patrick Ryan, Definition and Reduction of the F/RF-4 Windshield Birdstrike Hazard, AFWAL-TR-84-3003, May 1984.
3. David J. Peery, Aircraft Structures. Chapter 12. McGraw-Hill, New York, 1950.

4. Gregory J. Stenger, Composite Windshield Arch Reinforcement, Phase II: Hybrid Composite Material Evaluation, UDR-TR-84-144, December 1984.
5. R. A. Brockman, A Finite Element Program for the Materially and Geometrically Nonlinear Analysis of Three-Dimensional Structures Subjected to Static and Transient Loading, AFWAL-TR-80-3152, January 1981.
6. Data Package, "A-7 Birdstrike Test," Volume I of IV, Project CH63VJ, Arnold Engineering Development Center.

TABLE 1
TYPICAL BENDING STIFFNESSES FOR ARCHES

Arch	Capability (kts)	Bending Stiffness (EI) at Centerline (lb-in ²)	Deflection During Birdstrike (in)
F-4 Titanium	500	4.16x10 ⁶	
T-38	400	2.19x10 ⁶	3-4
F-111 Titanium ADBIRT Reinforcement	490	4.48x10 ⁶ *	1-2
F-111 UDRI 4130 Steel Arch	470	4.46x10 ⁶ *	1-2

*Not a wraparound system--stiffness reported directly behind impact point.

TABLE 2
SUMMARIZED RESULTS OF NONLINEAR STATIC FINITE ELEMENT ANALYSIS

Model	Arch Geometry		End Condition	Failure		Side Load	Moment Ft-Lbs	Deflection		Energy In Lbs
	C _L	End		Load Lbs	Load Lbs			In	In	
1	1.4"	tapering to 3/4"	Pinned	18,600	3280		0	1.9		17,700
2	1.4"	tapering to 3/4"	Fixed through link	23,100	6410		2540	1.5		17,300
3	1.4"	tapering to 1"	Pinned	21,900	4490		0	1.6		17,500
4	1.4"	tapering to 1"	Pinned with link/ torsional spring	22,600	5040		520	1.5		17,000
5	1.4"	tapering to 1"	Fixed through link	26,700	8000		3340	1.3		17,400
6	1.4"	tapering to 1"	Fixed	25,700	7420		1570	1.4		18,000

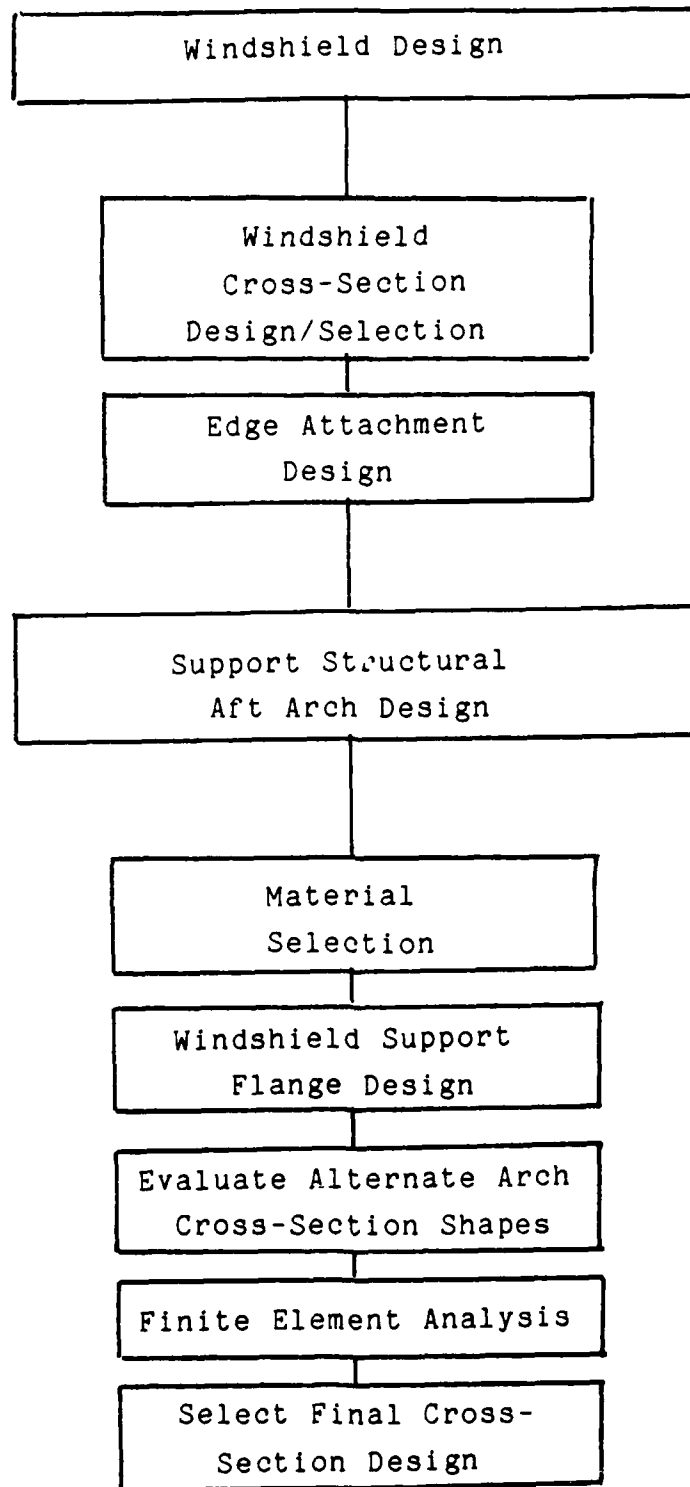


Figure 1. Transparency System Design Flow Chart.

Normalized Impact Capability Curve (Four Pound Bird Impacts)

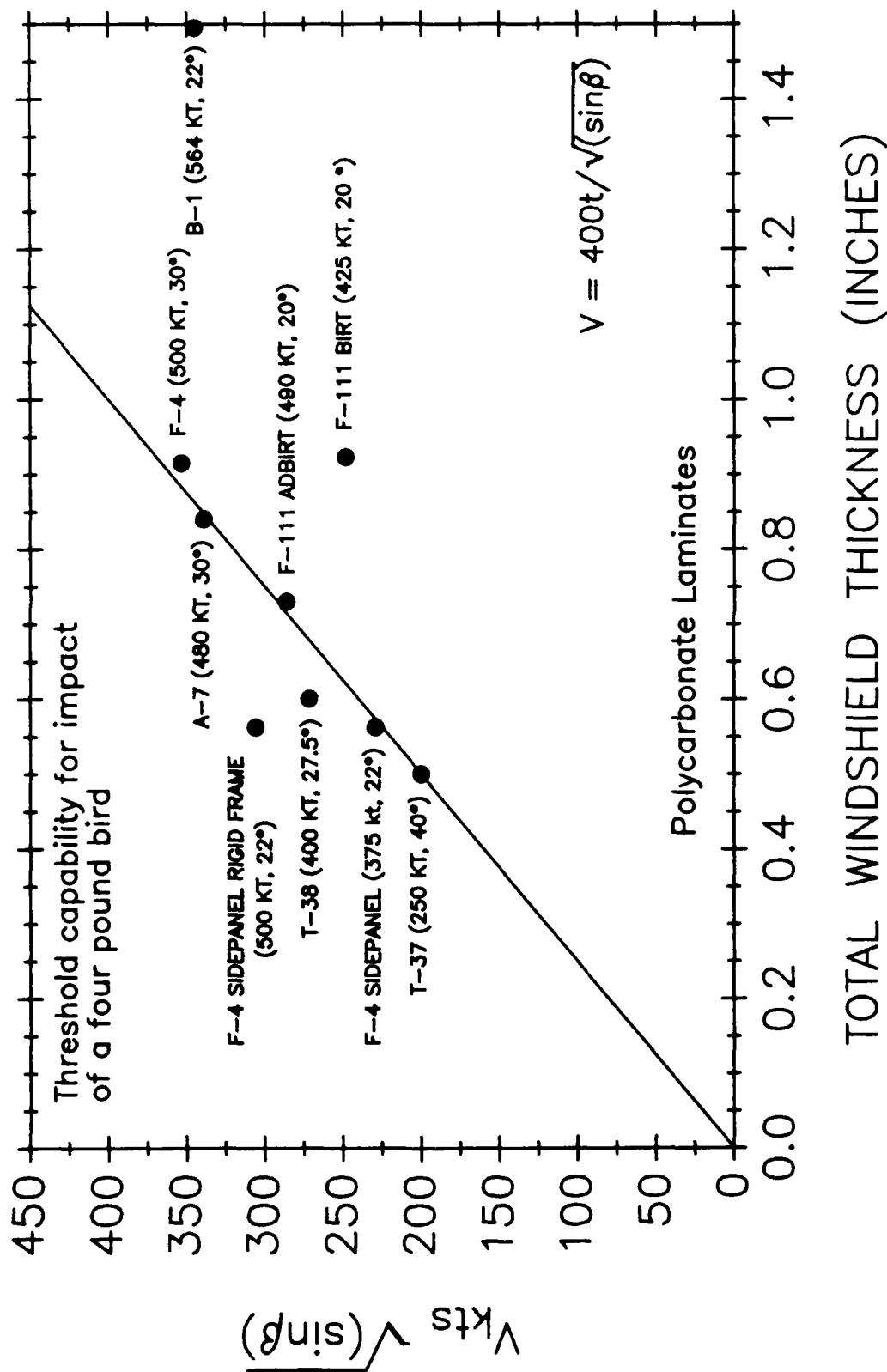


Figure 2. Normalized Acrylic Birdstrike Data.

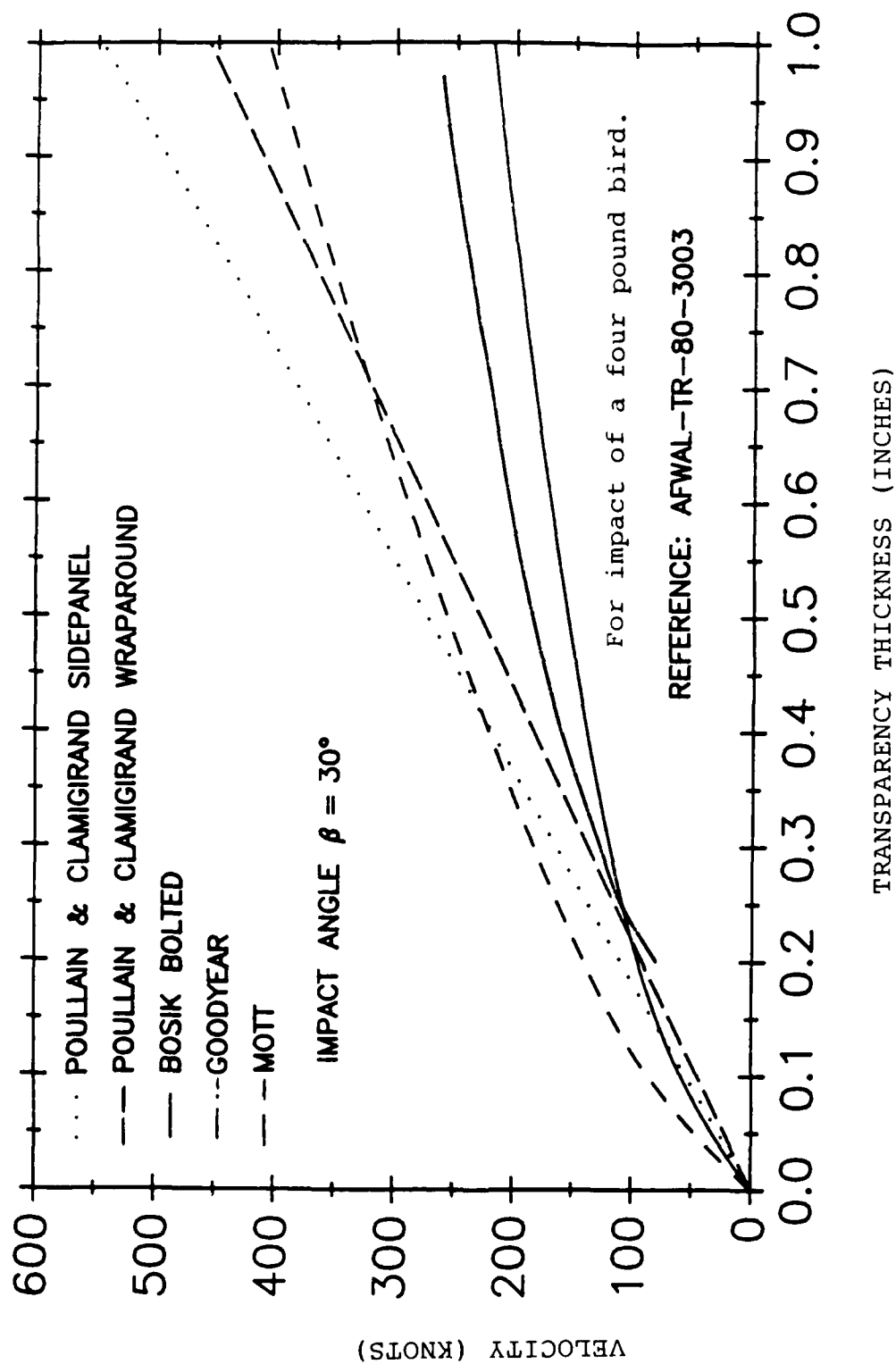


Figure 3. Empirical/Theoretical Impact Capability Curves for Monolithic Stretched Acrylic.

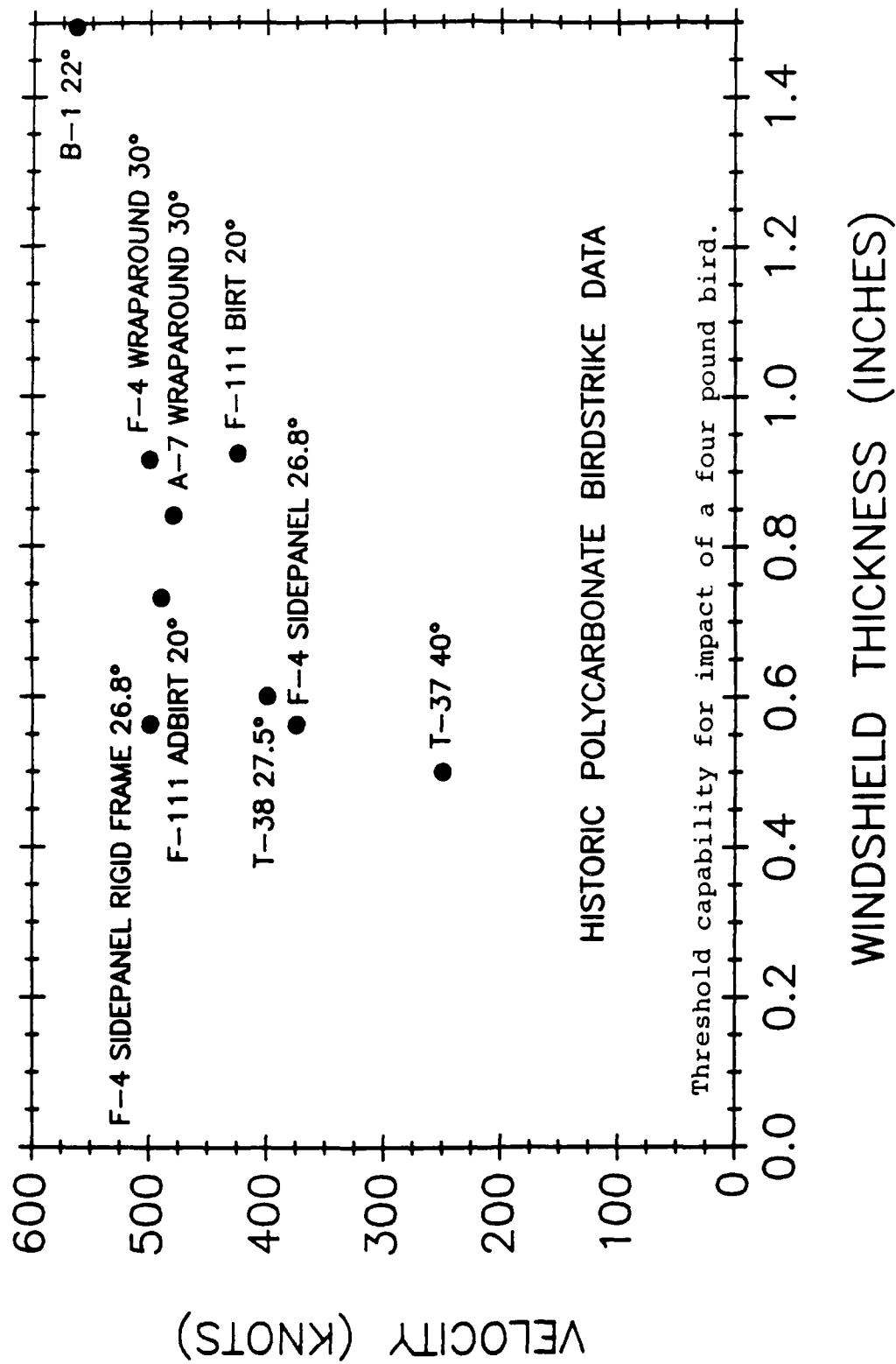


Figure 4. Polycarbonate Birdstrike Data.

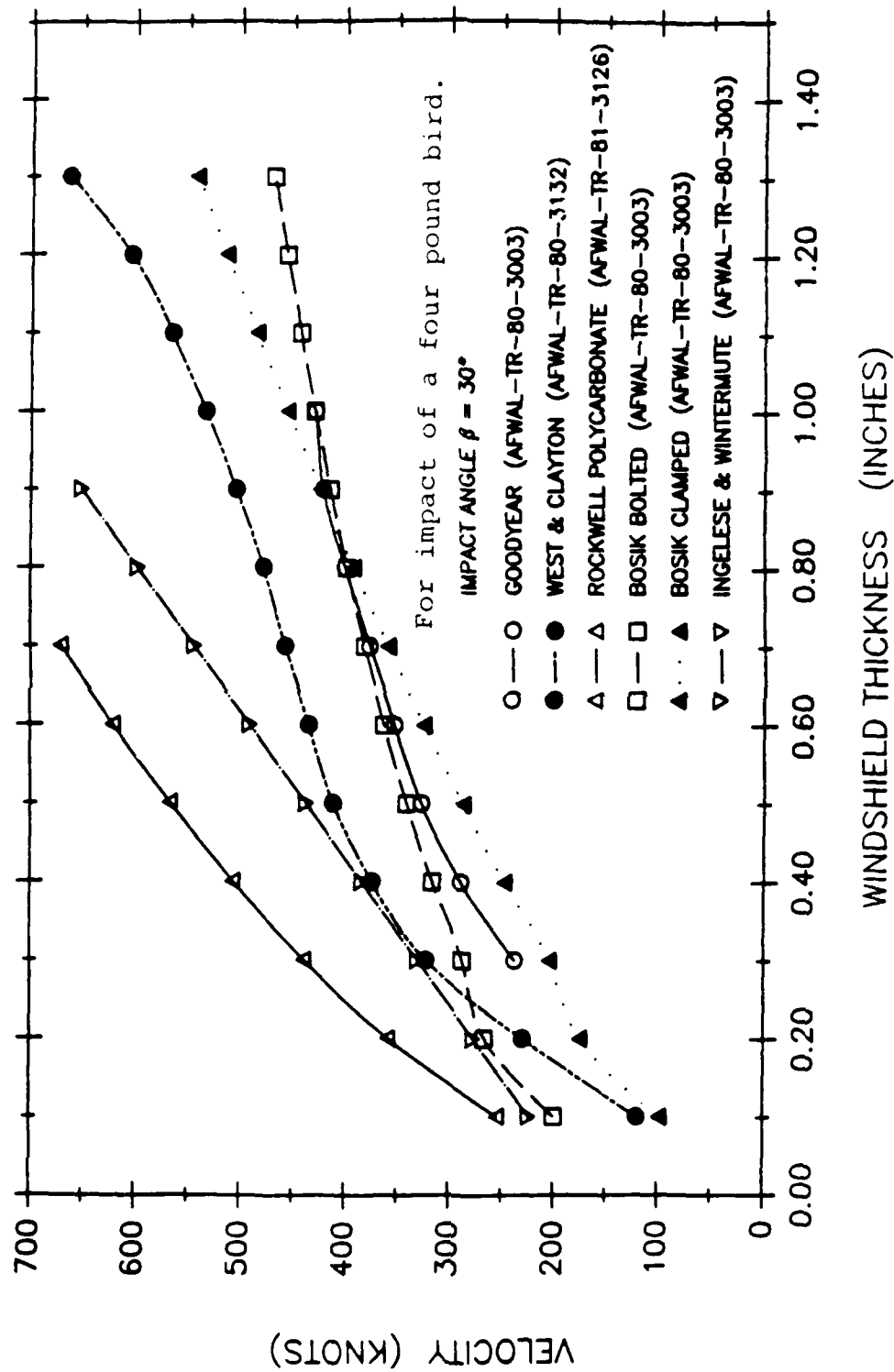
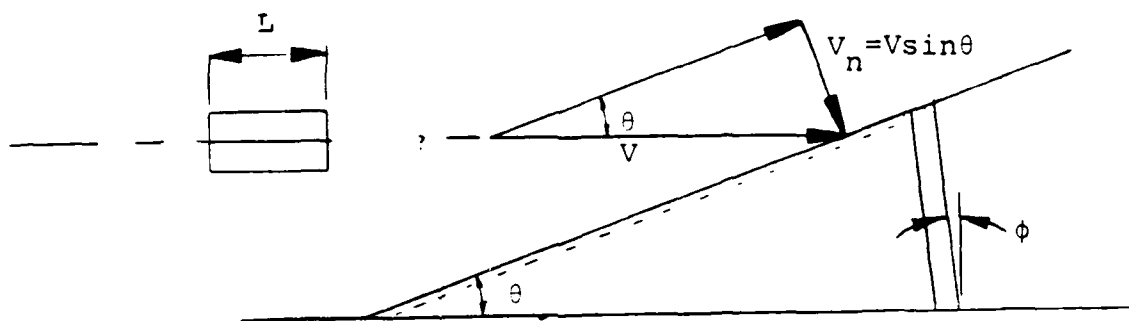


Figure 5. Empirical/Theoretical Polycarbonate Laminate Impact Capability Curves.



Figure 6. Comparison of Three-Piece and Single-Piece Windshield Systems for the A-7 Aircraft.



NOTE: L_b , the effective length of the bird, is assumed to be equal to 12 inches.

L , the bird length, does not equal L_b .

Figure 7. Bird Impact Angle of Incidence and Velocity Vectors.

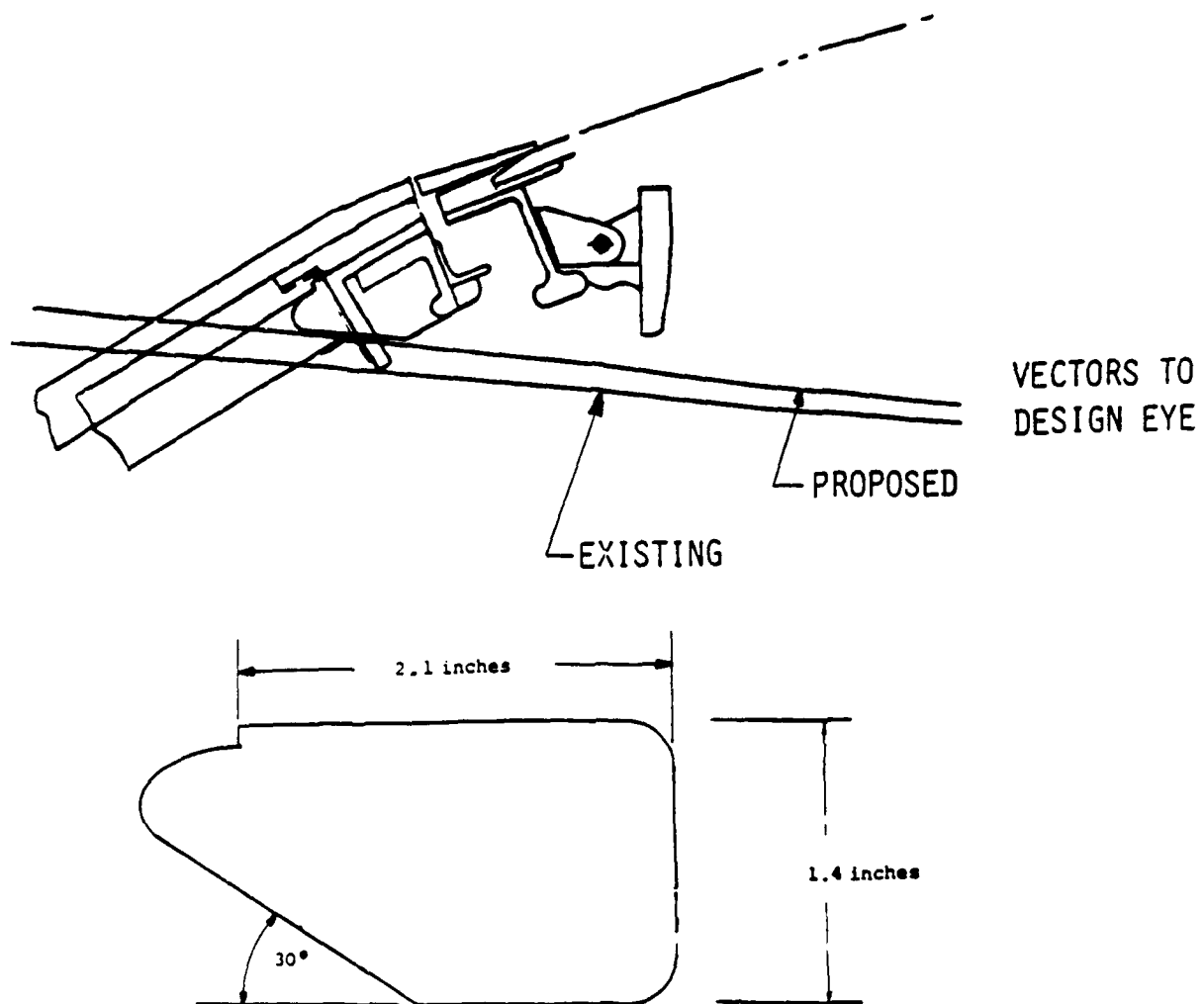
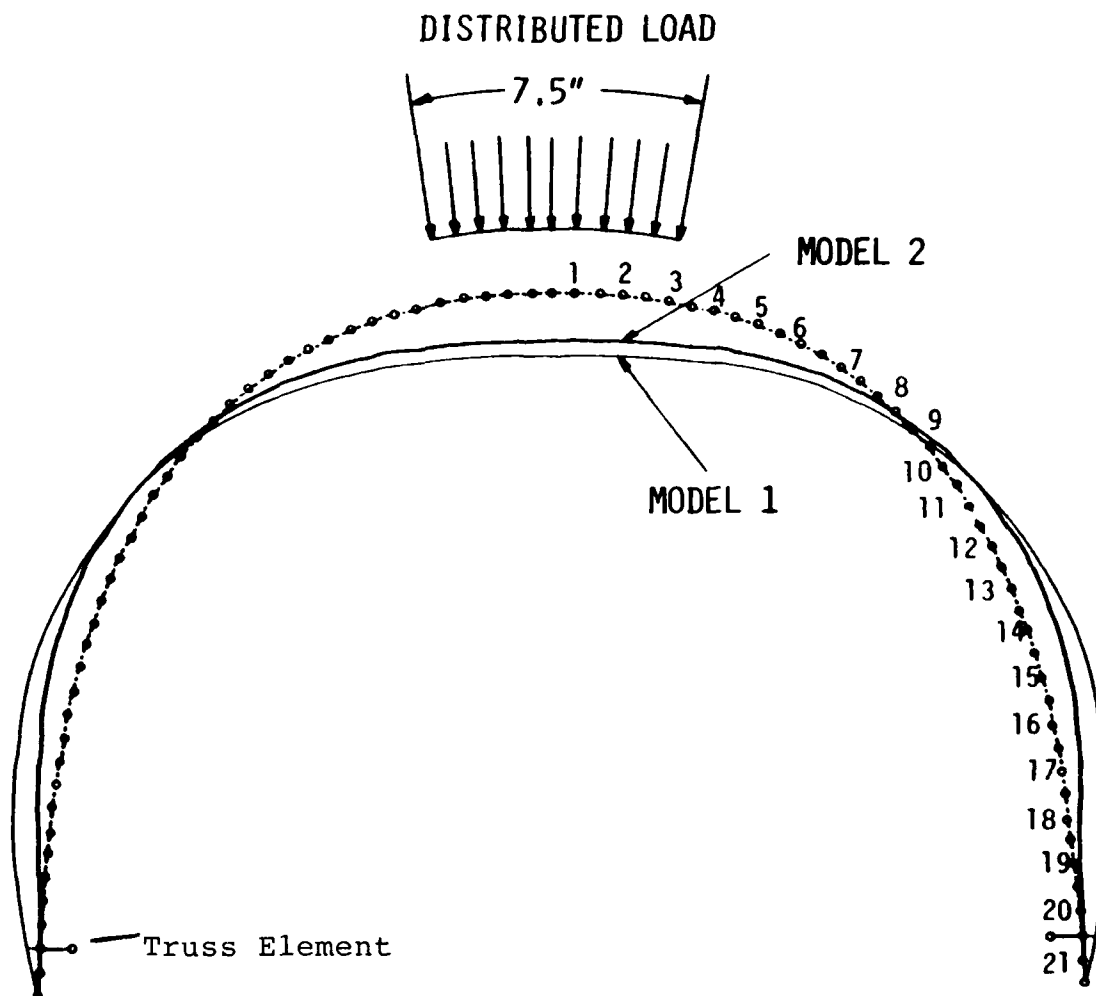


Figure 8. Initial Composite A-7 Arch Cross-Section.



Note: Due to symmetry, only one-half of the arch was actually modeled.

Figure 9. Aft Arch Finite Element Model Showing Deflected Shapes.

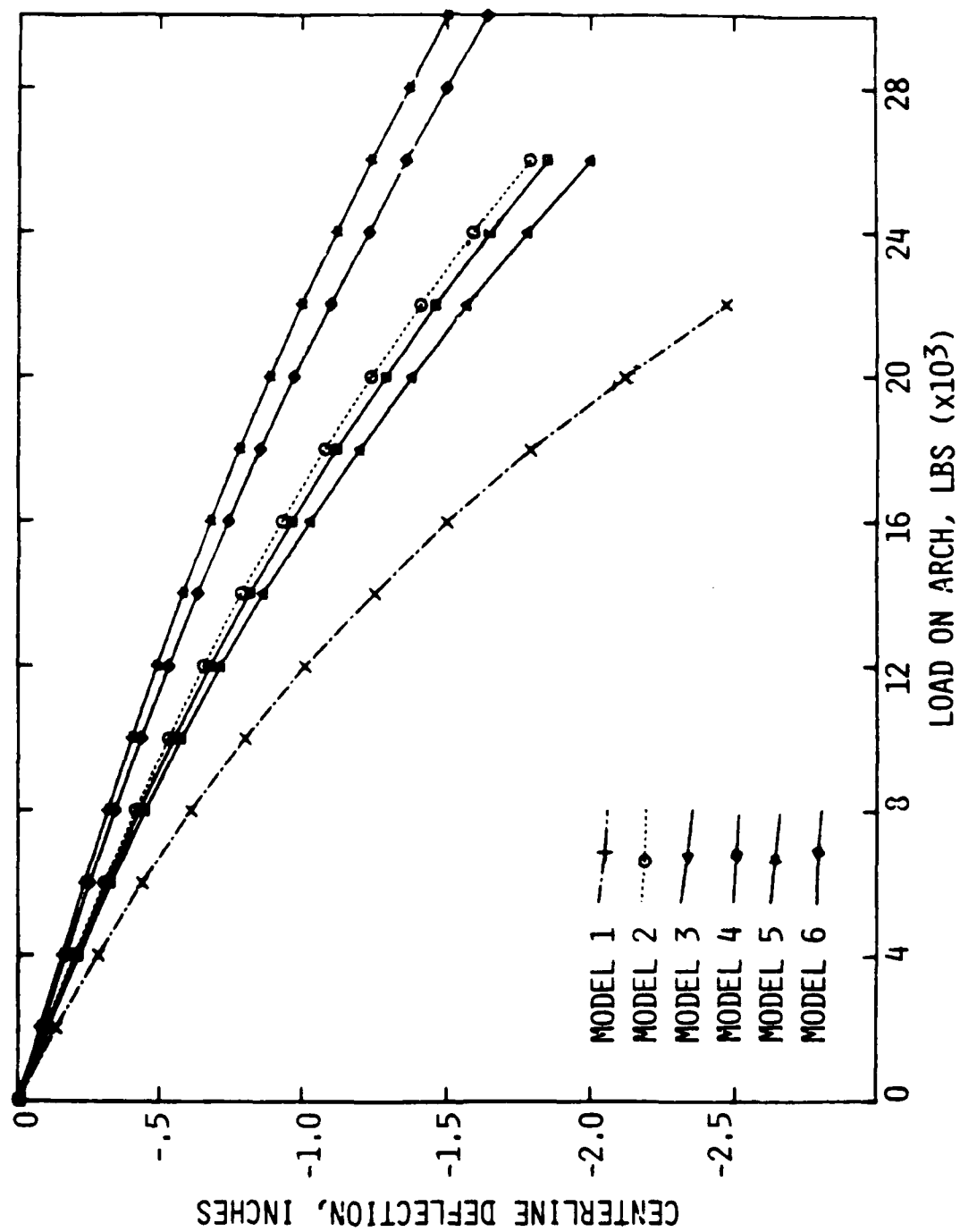


Figure 10. Results of Nonlinear Static Analysis: Centerline Deflection vs. Applied Load.

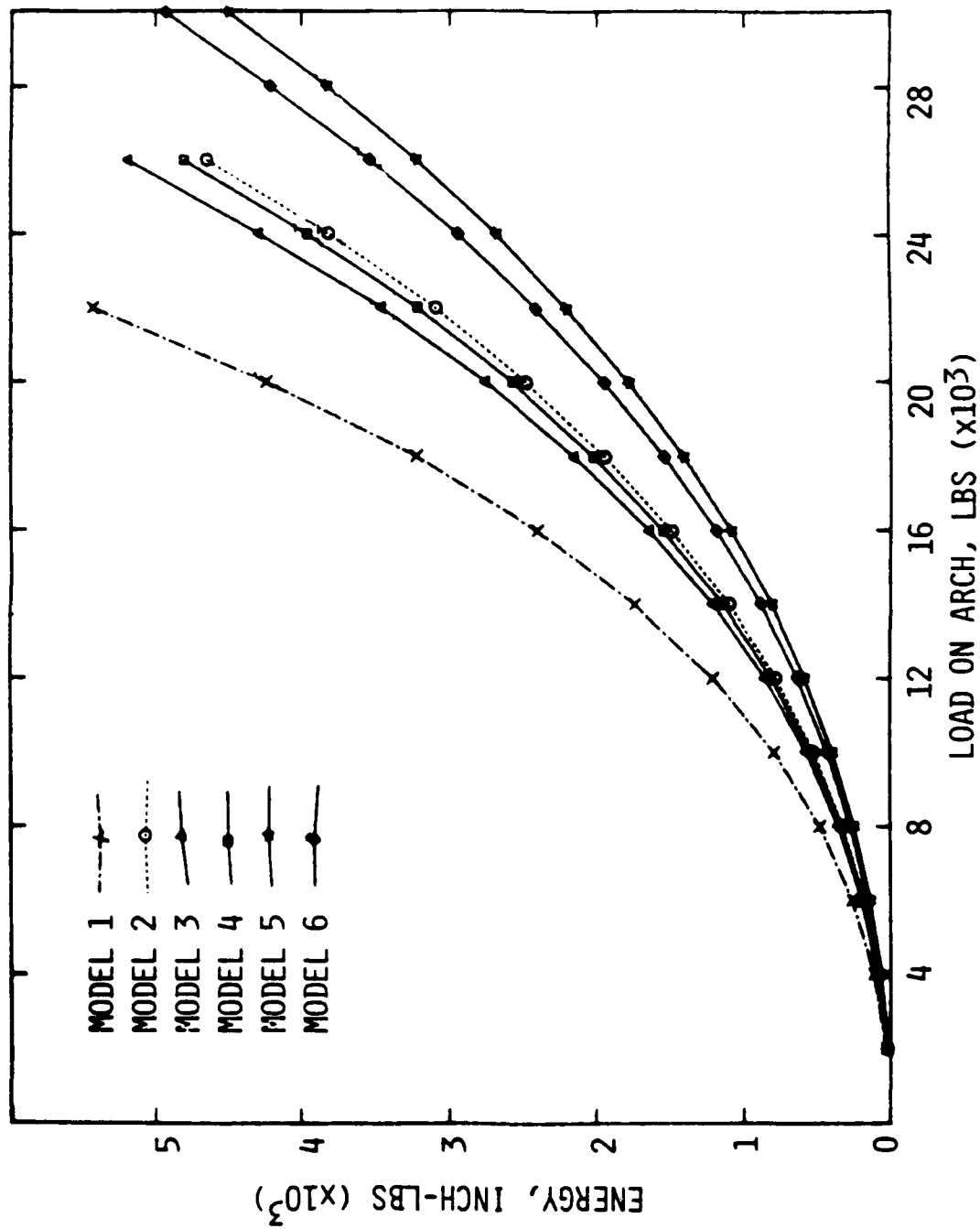


Figure 11. Results of Nonlinear Static Analysis: Energy vs. Applied Load.

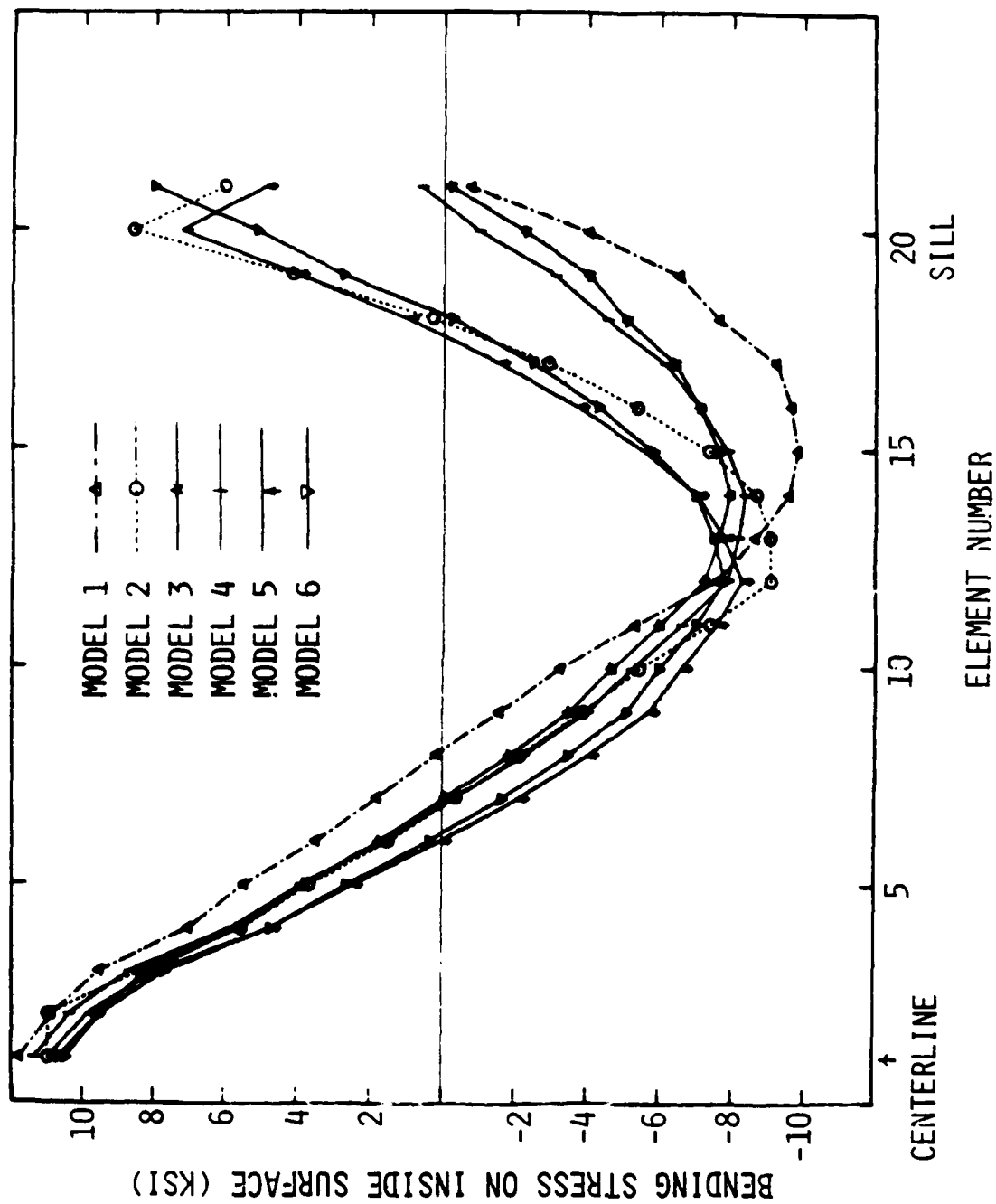


Figure 12. Results of Nonlinear Static Analysis: Bending Stress in Inside Fibers of Arch.

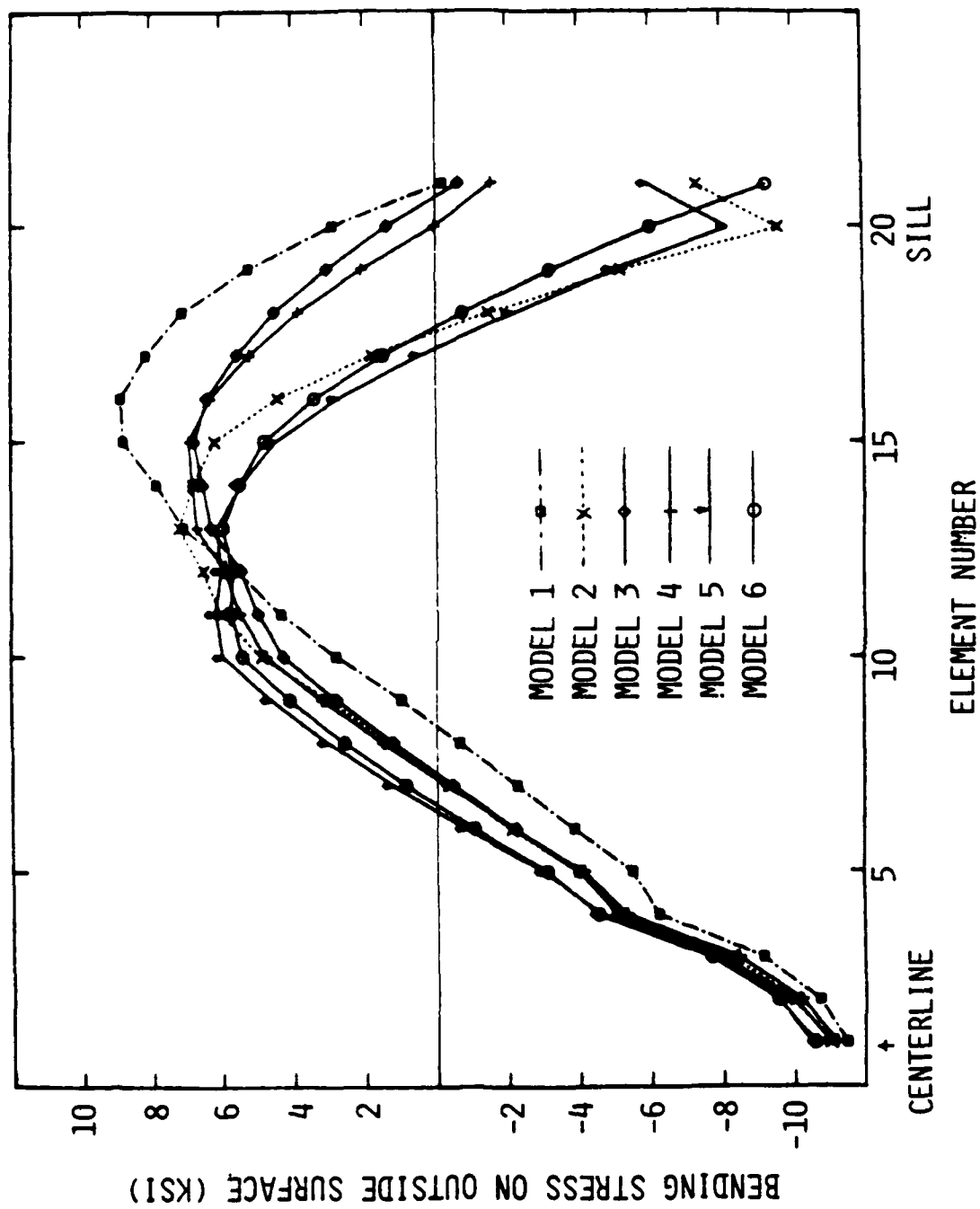


Figure 13. Results of Nonlinear Static Analysis: Bending Stress in Outside Fibers of Arch.

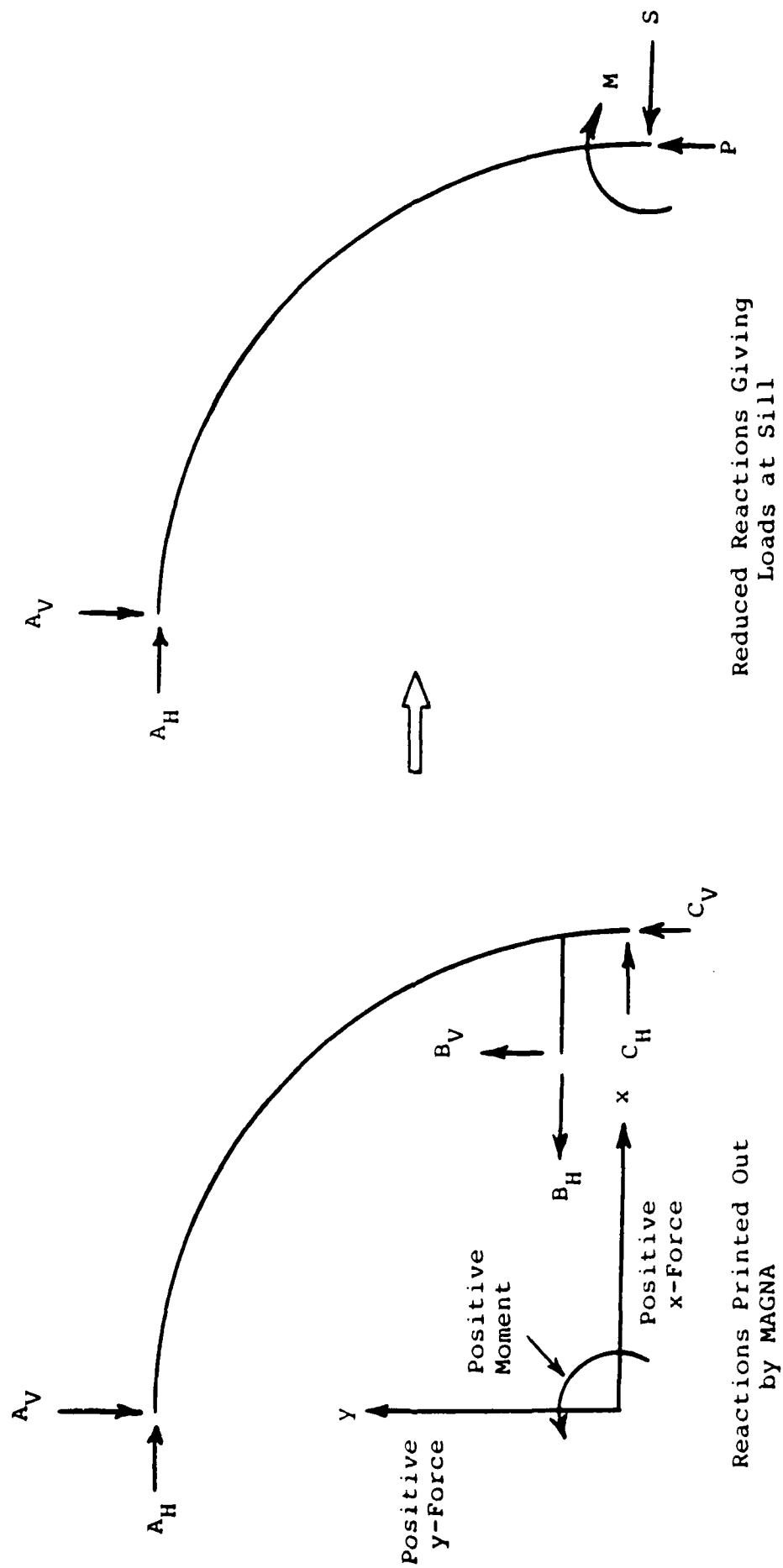


Figure 14. Reduction in Sill Loads from MAGNA Results.

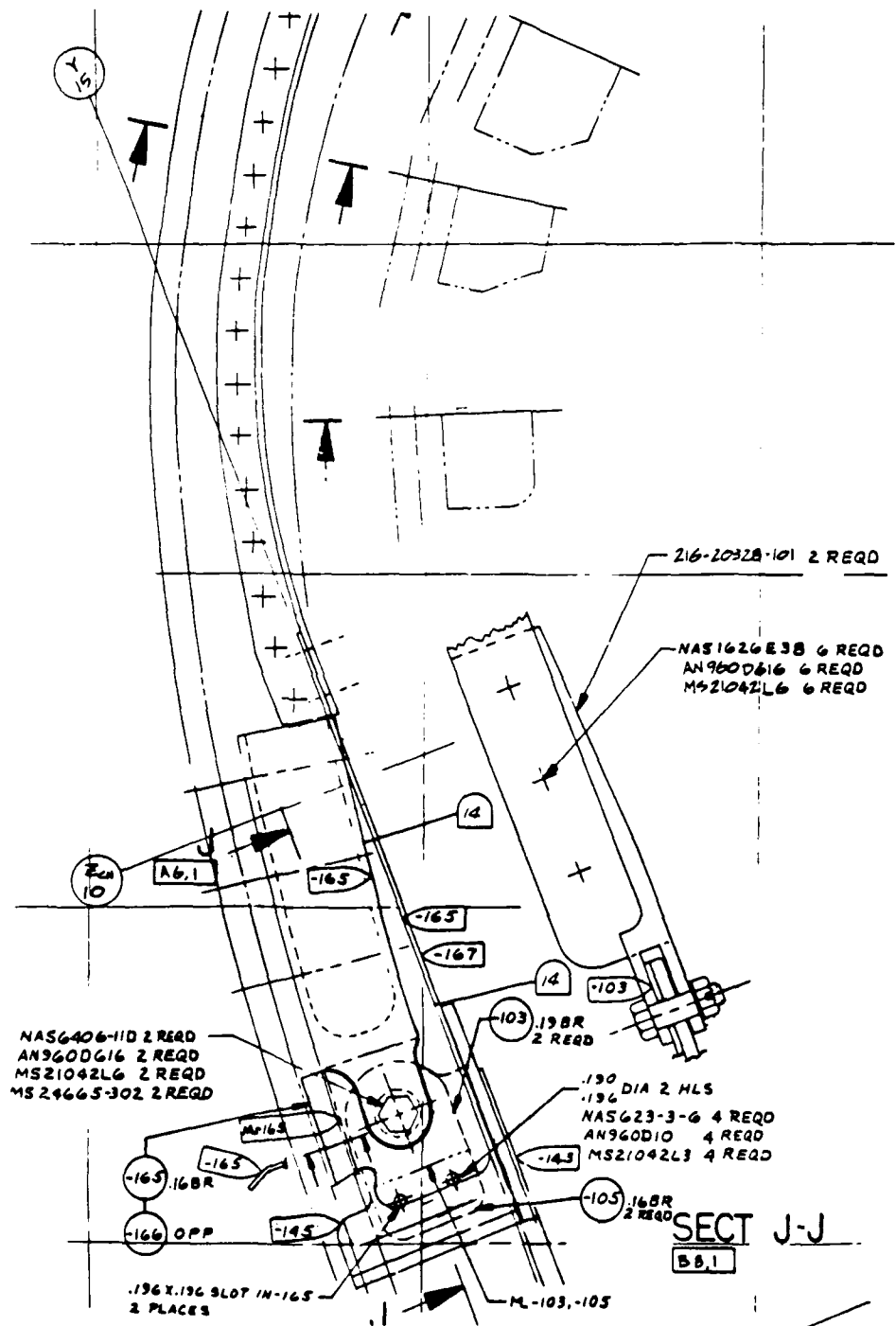
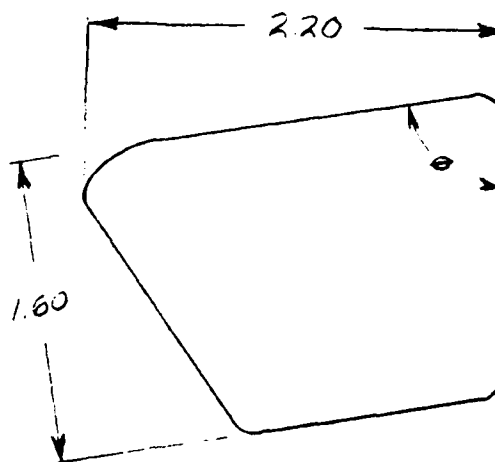


Figure 15. Clevis.



Note: Modified to meet LTV design envelop-

Figure 16. Final Cross-Section Dimensions at Arch Centerline.

OPERATIONAL OVERVIEW OF THE "ROBOTIC CANOPY POLISHING SYSTEM"

Douglas L. Michalsky

Southwest Research Institute

Halver V. Ross

OO-ALC/MANEP

Hill Air Force Base

OPERATIONAL OVERVIEW OF THE "ROBOTIC CANOPY POLISHING SYSTEM"

Douglas L. Michalsky, Sr. Research Engineer
Southwest Research Institute

Halver V. Ross, P.E., Industrial Engineer
00-ALC/MANEP, Hill Air Force Base

ABSTRACT

Replacement of scratch-damaged aircraft canopy transparencies is very expensive. Many damaged transparencies can be restored by careful polishing of the surface to remove flawed areas. Canopy polishing is currently done at Hill Air Force Base, other Air Force and naval bases, and by private industry. Manual polishing methods clearly predominate at the government facilities and in industry. Canopy polishing is a time-consuming process, requiring skilled labor, and is not always successful. Southwest Research Institute has recently demonstrated the feasibility of using industrial robots to restore aircraft canopy transparencies and has completed fabrication of "The Robotic Canopy Polishing System" (RCPS) which is installed and operational at Hill AFB. The RCPS uses two robots for polishing individual aircraft canopies simultaneously, each robot sharing inspection services of a third robot for monitoring progress of the polishing. The inspections are performed using machine vision techniques. This paper presents an overview of the RCPS development work and describes early operational experience obtained at Hill AFB.

INTRODUCTION

Aircraft canopy transparencies are subjected to harsh environments, leaving them scratched, pitted, and crazed. This damage adversely affects the vision of the pilot and weakens the canopy structure. Replacing the canopy is expensive¹. A less costly alternative to replacement is to rework the transparency by polishing to improve optical characteristics and to relieve stress in areas prone to cracking. This work has been done manually at Hill Air Force Base (AFB), other Air Force and naval bases, and by private industry. The work is labor intensive and not always successful. Also, canopy polishing is truly an art, requiring years of experience to develop the "knack" for performing acceptable rework. Southwest Research Institute (SwRI) has demonstrated the feasibility of robotic polishing of aircraft transparencies for Hill AFB under contract F42650-86-C-3276. Restoration of the aircraft transparencies has shown to be a good use of robotic technology as the rework will be cost-effective, the quality of rework is good and very repeatable, and the best qualities of man and machine are utilized effectively to perform the rework. SwRI has recently (September 1988) completed fabrication of a full Robotic Canopy Polishing System (RCPS) and installed the system at Hill. A description of the RCPS development effort follows.

DISCUSSION

BACKGROUND

Currently at Hill AFB, canopies are brought into a work area where a human expert inspects the transparencies visually. Some canopies are obvious rejects to the inspector, but others require a very close inspection to identify flaws that exceed a critical depth into the plastic or to locate stress crazing. Canopies that fail inspection require the costly replacement of the transparencies. Canopies passing the inspection are manually sanded and polished to correct the flaws. Sanding in the vicinity of a flaw has to be done expertly to avoid improper removal of transparency material that would introduce unacceptable optical distortion or remove excessive material and to avoid overheating of the plastic which weakens and discolors it.

Hill AFB sponsored a Phase 1 effort in February, 1986 aimed at demonstrating the technical and economic feasibility of developing an automatic canopy polishing system. This work was motivated by the facts that the number of canopy polishing experts is small, some key Hill canopy polishing personnel have recently retired, and successful polishing of canopies yields dramatic savings over the alternative of transparency replacement. In our research to ascertain feasibility of robotic transparency rework, we learned that manual methods predominate throughout the Air Force, the Navy, and private industry. We are aware² that investigations were conducted in General Dynamics Industrial Technology Modernization (ITM) programs to develop robotic primary finishing of transparencies (removal of flaws about 0.001 in. deep or less), but we believe that the RCPS work is the first organized attempt to automatically repair major transparency defects (flaws to about 0.010 in. in depth).

Following a successful feasibility demonstration in the Phase 1 effort in June, 1987, SwRI was awarded a Phase 2 project to build a fully integrated prototype Robotic Canopy Polishing System that was installed at Hill AFB in August, 1988.

APPROACH TO THE PROBLEM

The fundamental problems to be addressed in the RCPS development were:

- 1) automated location and characterization of canopy flaws, and
- 2) the automated removal of these flaws by a polishing procedure.

Use of a human operator in the rework process was to be considered in maintaining cost-effectiveness of the RCPS.

Canopy Transparency Inspection

Optical and machine vision techniques were evaluated for performing the following inspection functions:

- 1) locating transparency flaws in a camera field-of-view,
- 2) determining the inside/outside location of the flaws,
- 3) determining the severity of the flaws (depth, width, and length).

(Machine vision is a technology which uses a computer and special electronic hardware to obtain images, usually from a video camera, to enhance the images, and to provide understanding and quantitative data about the objects in the image.) As might be expected, determining flaw depth on a plastic surface is a very difficult problem. Various techniques, in addition to machine vision, were tried in this work as well as in other efforts³⁴. Location of flaws in a camera field-of-view, determining whether a flaw is on the inside or outside surface, and determination of width and length of the flaws was done with machine vision, but determining flaw depth accurately and quickly continues to be an unsolved problem. The human can perform necessary inspection in a small portion of the total rework cycle time; therefore, due to his superior performance, in this case, inspection of the canopies to judge their fitness for rework remains a human function for the RCPS. However, a significant degree of machine vision is used in the RCPS to reduce the time required by the human operator, namely:

- 1) registering human inspector markings on a canopy to determine the 3-dimensional flaw location for robotic polishing,
- 2) determination of gross flaw severity (indicated by its reflectance) for use in selecting an initial polishing schedule, and
- 3) determining when the flaw is eliminated to minimize the amount of transparency material that is removed.

Canopy Transparency Polishing

Through consultation with industry experts and manual testing of polishing techniques, an approach to the polishing problem was devised. A robot end effector (tooling on the robot wrist) was developed that uses a pneumatic random-orbital polishing tool. Foam-backed adhesive sanding discs of a variety of grit sizes are used as the polishing media. The sanding discs are attached to polishing pads and the pads are attached to the polishing tool. The pad is designed to maintain as even a pressure distribution across the pad surface as possible during polishing. Allowance has been made to channel liquids through the polishing pad to provide cooling and cleaning mechanisms. A slurry of very fine (0.3 micron aluminum oxide) abrasive and water is used with a buffing pad for final polishing steps. The general polishing schedule used consists of "grinding" with 30 micron paper to remove the flaw and contour the flawed area for minimum distortion, and "refinishing" the surface using 15 micron paper, followed by 9 micron paper, and, finally, primary finishing using the abrasive slurry with a special polishing paper.

To identify the best motions of the polishing tool for grinding to remove the bulk of the plastic material around a flaw, mathematical simulations were performed using various polishing pad pressure profiles and various polishing

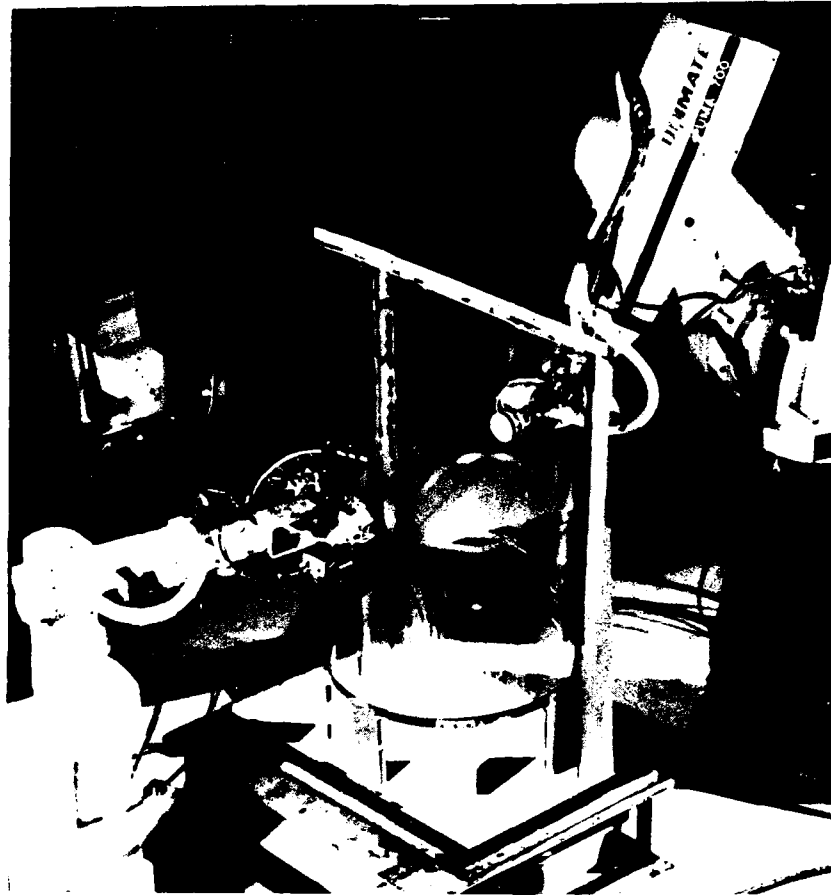
motions. Maximizing rework speed and minimizing resultant canopy distortion were major considerations in choosing a process (the grinding step, as opposed to the polishing step, largely establishes the optical distortion that will inevitably remain after rework). Grinding motions investigated include concentric circular patterns, "rose petal" patterns, "rose petal" patterns avoiding concentration of time spent at the center of the pattern, and "zig-zag" patterns, which would appear to imitate some human polisher motions. A numerical integration of material removed was performed on a computer for each grinding pattern, assuming a given pad shape and pad pressure distribution profile. Promising patterns and combinations of patterns were then actually implemented with a robot and pad. In general, the appearance of the transparency surface after the grinding was as expected from the simulation. Note, however, that a good method for "viewing" the infinitesimal surface perturbations resulting from the grinding did not avail itself in the course of this work. The distortion resulting from the rework was, in practice, judged by viewing the reworked area against a gridboard, at angles that would maximize the appearance of distortion to a pilot. Also, a bright point source of light was shone through the transparency under evaluation, which would project a distortion pattern on a screen behind the transparency. These distortion viewing techniques were adequate for judging relative improvements in the grinding rework. In the end, the best grinding performance was obtained by using concentric circular motions about the flaw area, with slight random excursions from the circular robot paths. The randomness in the motions distinctly improved the appearance of the reworked areas to human inspectors.

Primary finishing, or the "final polish", of a transparency was accomplished by making an overlapping longitudinal raster scan motion over the transparency surface. The polishing pad was made as large as possible to cover the area most rapidly, but the size of the pad had to be small enough to reach into corners of the transparency and to be effective around the transparency edges close to the canopy frame. The amount of overlap was optimized to promote uniform coverage over the surface while minimizing the time to polish the entire surface. The polishing motion had to be verified for both inside and outside canopy surfaces, as the concave vs. convex shapes affect polishing performance. In general, canopy surfaces needing rework are covered with many fine scratches, so that 2 to 3 of the polishing passes are needed per canopy side.

Robotic Canopy Polishing System - Description

Figure 1 shows the robotic work cell that was used to demonstrate feasibility of the RCPS in the Phase 1 effort. It is included here to show the relative positions of robots and the work piece. Note that this Phase 1 task made use of SwRI laboratory equipment to demonstrate concepts, and purchase of expensive robots and other equipment was avoided to minimize cost of the initial effort. Figure 2 shows the actual deliverable RCPS hardware at an SwRI laboratory before shipment to Hill AFB. Figure 3 shows the basic Hill AFB floor plan for the RCPS. The RCPS uses a Masscomp MC5450 minicomputer (with a UNIX/C software environment) as the cell control computer for orchestrating the events in the polishing work cell. The RCPS work cell contains three Westinghouse/Unimation PUMA 761 robots. One robot serves as the

SOUTHWEST RESEARCH INSTITUTE

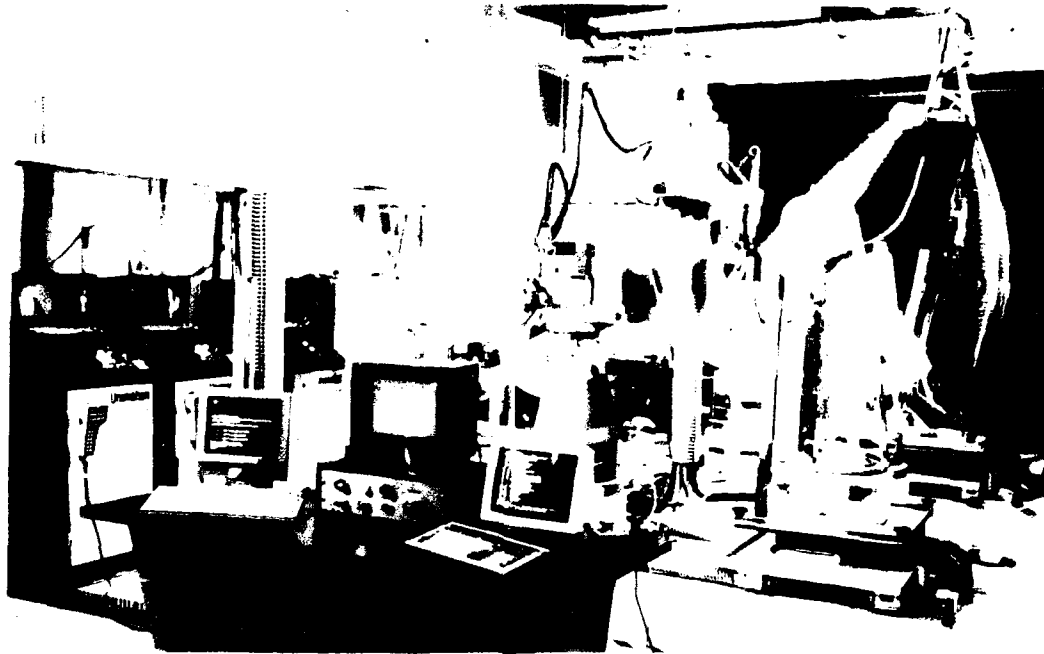


ROBOTIC CANOPY POLISHING SYSTEM

PHASE I DEVELOPMENT FOR HILL AFB

Figure 1. RCPS Feasibility Demonstration Hardware.

SOUTHWEST RESEARCH INSTITUTE



ROBOTIC CANOPY POLISHING SYSTEM
PHASE II DEVELOPMENT FOR HILL AFB

Figure 2. The Deliverable RCPS at an SwRI Laboratory.

"Inspection Robot" and holds a machine vision camera and lighting for use in identifying flaw location, for estimating initial severity of flaws, and for the "in-process inspection" to determine when a flaw is removed. The location and severity of flaws are entered into a database in the cell control computer by input from the machine vision system (an International Robomation/Intelligence IRI-D256). The other two robots are referred to as "Polishing Robots" and these share the inspection services of the single Inspection Robot. The two Polishing Robots work independently of each other, simultaneously, on different canopies. Working from Inspection Robot information, the cell control computer directs a Polishing Robot to a flaw location and then downloads polishing contour information to the Polishing Robot's controller. This information guides the Polishing Robot through the motions optimum for removing the canopy flaw. The Polishing Robot controller also monitors position feedback from its end effector to maintain proper polishing action.

A computer model for each canopy type is stored in the cell control computer. The Polishing Robot coordinate information needed to generate the polishing motions and to maintain the polishing tool normal to the canopy surface is derived from the canopy models. Sufficient adaptability and compliance are built into the Polishing Robot end effector and polishing routines to accommodate the canopy-to-canopy part variation from the computer model.

Cost Justification of the RCPS

At the project "Feasibility Acceptance Test", polishing of various type flaws on several canopies was done to simulate rework of a typical canopy. Careful timing of inspection and polishing events was kept. The test data indicated that the throughput of the RCPS should be about four times that of a human polisher. Also, the project "Life Cycle Cost Document", updated with actual Feasibility Acceptance Test data, indicates that, if a canopy workload is supplied that is commensurate with the potential throughput of the RCPS, the system payback period should be slightly more than four years. A side benefit of the system is that a record of flaw locations and severities will be automatically kept for each reworked canopy which may prove useful to canopy manufacturers in improving their products.

INITIAL PRODUCTION RESULTS

Training of RCPS maintenance and operation personnel was completed in September 1988. Production personnel have since exercised the RCPS to gain a working familiarity with the system. In the process, they have conducted further experimentation with new sandpaper types and have used the flexibility in the RCPS control program to tailor the system for maximum usefulness in their work environment. Several F-4 and F-16A acrylic transparencies have already been successfully reworked. This includes two F-4 canopies that had been condemned due to their overall poor condition. Multiple polishing passes restored these canopies to usable condition, negating the need for installation of new transparencies. Also, Hill AFB is investigating other canopy workloads which include the A-10 transparency. Though the RCPS is a fairly complex machine, the Operators at Hill AFB have mastered the basic operation in a very short time. No serious problems have

been encountered in the early operation of the RCPS hardware and software. However, the harsh, high vibration environment for the Polishing End Effectors have caused a few parts on the End Effectors (the slide mechanism and a pad change gasket) to wear prematurely. Minor modifications have been made to the End Effectors that promise to greatly increase the MTBF for them.

FUTURE TECHNOLOGY NEEDS

The following are potential research programs related to the RCPS technology for future consideration:

- 1) automating techniques for quantifying canopy optical distortion,
- 2) automated repair of other types of transparencies,
- 3) automated polishing of aircraft canopies in-place on the aircraft,
- 4) automated polishing of polycarbonate materials, which is still only marginally successful with manual polishing, and,
- 5) automated removal of canopy transparency coatings for rework of the underlying material, and re-application of coatings.

POTENTIAL RELATED APPLICATIONS

The architecture of the RCPS is flexible in that it contains programmable robots, multiple-axis positioners, and room for expansion of process control, such as end effector force feedback or additional machine vision feedback. A key feature of the RCPS is its ability to acquire sparse part surface coordinates and to generate a computer model of the part using interpolation methods to define the total part surface. Therefore, additional canopy types or other parts can be added to the system. The flexibility of the RCPS should be considered where other applications of this technology might benefit. The RCPS can be thought of, in more general terms, as a surface finishing work cell, such as might be used for grinding or sanding parts. Also, the polishing tool of the RCPS could be replaced with other tools to perform functions such as hole drilling or painting. Realization of such work cells could be done at a fraction of the cost of the RCPS due to savings in development costs.

References:

- 1 Poehlmann, Harold, "A Requiem for the Aircraft Canopy", Maintenance Magazine, Jul/Sep 1986.
- 2 Grabits, George A., "Polishing Aerospace Transparencies", RI/SME Technical Paper No. MS86-203, proceedings of the "Robotic Solutions in Aerospace Manufacturing" Conference, March 3-5, 1986, Orlando, Fla.
- 3 Teller, et. al., "Development of Non-Destructive Inspection Procedures and Equipment for F-5 Canopy Acrylic Panels", Southwest Research Institute, San Antonio, Tx., USAF Contract No. F41608-78-G-0010 Final Report, June, 1978.
- 4 Michalsky, et. al., "Automated (Robot) Canopy Polishing System" Final Report, Southwest Research Institute, San Antonio, Tx., USAF Contract No. F42650-86-C-3276, June 18, 1987.

EVALUATION OF COMPOSITE MATERIALS FOR BIRD IMPACT RESISTANT
TRANSPARENCY SYSTEMS

G. J. Stenger

University of Dayton

W. R. Pinnell

AFWAL/FDER

Wright-Patterson AFB

EVALUATION OF COMPOSITE MATERIALS FOR BIRD IMPACT RESISTANT TRANSPARENCY SYSTEMS

G. J. Stenger
University of Dayton

W. R. Pinnell
Air Force Wright Aeronautical Laboratories

The University of Dayton Research Institute (UDRI) was contracted by PPG Industries, Inc. to evaluate the feasibility of designing a cost effective composite arch reinforcement for the T-38 student windshield frame. A composite reinforcement for this arch had been pursued as an attractive alternative to a metal reinforcement because of its low weight, high strength, formability, low cost, and nonmagnetic properties.

The reinforcement was to be designed to provide four pound-400 knot birdstrike capability with a PPG transparency. As a result of the feasibility study (Reference 1), UDRI recommended that additional data was needed to better characterize the material properties and failure modes of thick composite materials loaded at high strain rates. A comprehensive beam test program, summarized in this paper, was recommended to evaluate the properties and characteristics of hybrid composite materials. these materials consisted of various combinations of graphite, glass, and Kevlar fibers in an epoxy matrix.

A 4130 steel tube arch reinforcement was demonstrated by PPG Industries to withstand a four pound-400 knot birdstrike. the steel tube was evaluated as part of this study. This data was used as input when establishing the arch reinforcement design requirements.

Objective and Scope

The objective of this beam test program was to screen various hybrid composite configurations to determine which laminate design best meets the stiffness/strength/toughness design requirements needed to withstand a birdstrike event. the data generated in this program was used as input into the design of a windshield arch reinforcement for the T-38 forward windshield to enhance the birdstrike resistance capability of the system.

The effort involved fabricating nominal 1-inch and 1/2-inch thick composite beam specimens from various combinations of

graphite, Kevlar, and glass fibers in an epoxy matrix. Three and four point loaded beam tests were conducted on the specimens at displacement rates which varied from 70 in/min to 30,000 in./min. This test method was chosen because the loading mode and strain rates could simulate to some degree the arch loading during an actual birdstrike event. The results of these tests included a load displacement curve, energy under the curve, flexure modulus, outer fiber stress at peak load, and failure mode. The tests were conducted in the UDRI Structural Testing Laboratory using MTS electrohydraulic closed loop test equipment.

Failure Characteristics of Composite Materials

The fracture of hybrid composite materials is generally characterized by a multimode failure which may include variations of brittle fracture, cleavage fracture, fiber debonding and pullout, and delamination. Graphite fiber-reinforced composites exhibit a brittle cleavage type of fracture which absorbs little energy. The glass and Kevlar fibers in the graphite composite increase the impact resistance by absorbing the strain energy released by the failed graphite fibers, thereby preventing the propagation of an unstable crack (Reference 2). The principal failure mode of Kevlar fiber-reinforced panels is tensile strain in the fiber, fiber debonding, and ensuing fiber pullout (Reference 3). It has been shown that the energy absorbed by debonding is two orders of magnitude higher than the energy absorbed in the cleavage (Reference 4). The principal failure mode of glass fiber-reinforced composites is delamination (Reference 2). This failure mode is an excellent crack stopper, which increases the impact resistance.

Test Materials

The test materials, listed in Table 1, were purchased from Ferro Corporation in the prepreg form. An epoxy resin system, CE-321R, was used in all test materials. This was a modified structural epoxy resin system formulated for general purpose applications up to 200°F with good moisture resistance. The system is flame retardant and has excellent hot/wet strength. The CE-321R can be "snap cured" in approximately 3 minutes at 350°F or autoclave cured for 20 minutes at 250°F under 70 psi. The 250°F cure temperature was chosen to minimize residual stresses when cocuring a composite reinforcement on a cast magnesium windshield frame.

Test Matrix

The test matrix consisted of a total of 29 different specimen configurations. Table 2 summarizes material combinations to be evaluated; for example, Specimen Type I, material D, is a combination of 80% graphite and 20% S-glass

fibers in an epoxy matrix with the laminate having four plies of graphite alternating with one ply of glass.

Two different specimen thicknesses were evaluated: nominal 1-inch thick fabricated from 176 plies (24 plies of fabric and 152 plies of tape) and nominal 1/2-inch thick fabricated from 90 plies (10 plies of fabric and 80 plies of tape). These thicknesses were believed to be representative of the thickness of a composite windshield arch reinforcement.

The beam specimen configurations were chosen so as to evaluate a broad range of materials and to establish a database in which strength and toughness of the materials could be compared. The hybrid materials were designed to maximize the amount of interply delamination, preventing catastrophic failure. Generally, the higher modulus fibers were placed near the outside surfaces of the beam to maximize the stiffness, and after initial failure of the specimen the lower modulus fibers would provide secondary strength. The surface plies of each specimen were fabric because previous testing of a composite arch indicated that fabric surface plies were needed for overall surface durability.

Test Specimen Fabrication

Test specimens were fabricated in the UDRI Nonmetallic Laboratory. Two replicates of each specimen were made by laying up plates about twice as wide as the final specimen. The specimens were sawed out of the plates after the material had been cured. The following paragraphs outline the procedure used in fabricating the composite beams.

Plies for the Type I specimens were cut to 18.5 inches long by 5 inches wide, plies for Type II specimens were cut to 12.5 inches long by 4 inches wide; both stacked in groups of about eleven plies. Each of these groups were placed under a vacuum bag and debulked overnight at room temperature under full vacuum (minimum of 20 in. mercury). The groups of plies were stacked as required to achieve the proper sequence. Square aluminum bars, 1-inch by 1-inch, were used as mold sides. Figure 1 shows the 18.5"xx5" plates vacuum-bagged and ready for curing.

A 1/4-inch thick aluminum caul plate was used on top of each plate (no surface bleed). Plates were cured at 250°F for two hours under full vacuum and 50 psi pressure. After curing, the 1-inch thick plates were sawed lengthwise forming two 2-inch-wide specimens. Plates containing Kevlar were bandsawed, all others were sawed with a diamond wheel.

Structural Test Procedure

Figure 2 shows the UDRI Structural Test Laboratory, specifically the test setup for the high rate (30,000 in/min), three point loaded beam tests conducted on the Type II specimens. Four point loaded beam tests were also conducted on both the Type I and Type II specimens. The four point loaded beam test method was chosen for two reasons: first, the loading span could be adjusted to control the ratio of shear stress to bending stress, thereby creating a test representative of the actual loading in a windshield arch. Second, four point loading minimizes the concentrated load and reduces the possibility of a compressive failure under the loading nose.

A total of four test series were conducted in this program. The first series was conducted on the baseline steel tubing and the Type I, Number 1 specimens. The second series was conducted on the Type I, Number 2 specimens which had been modified by drilling and bolting the beams along the centerline. The third series of tests was conducted on the Type II, Number 1 specimens at a loading rate of 875 in/min with the four point loading. The fourth test series was conducted on the Type II, Number 2 specimens with three point high rate (30,000 in/min) loading. In the first test series conducted (Type I, Number 1), the overall span was 14 inches with a loading span of 1.25 inches. A loading rate of 70 in/min was used in these tests.

The series two tests were conducted using Type I specimens with 5/16" grade 8 bolts located as shown in Figure 3. These bolted specimens were incorporated in the test matrix for two reasons: first, to evaluate the stress concentration resulting from the drilled hole, and second, to evaluate changes in the failure mode which result from the bolts. The effects of the drilled holes, especially in the hybrids, were unknown and required some evaluation to determine the design allowance required in an actual reinforcement. Because the majority of the failure modes involved delamination, it was important to determine if bolts (as in the actual arch reinforcement) through the specimen would permit delamination or completely change the failure mode by preventing or minimizing delamination. The loading rate used in these tests was 500 in/min. Figure 4 shows the test setup.

The third series of tests was conducted to evaluate the effects of beam thickness as well as evaluating additional material configurations. A comparison between this test series and the first test series can be made to determine how the material properties or failure mode changes with material thickness. A loading rate of 875 in/min was used in this test series.

The fourth test series was conducted to determine the effect of very high strain rate on both the failure mode and material properties. This data was compared with the third series test data to determine the effects of very high strain rates. Three point loading was used in this test series to minimize the weight (maximize the rate) of the actuator. A loading rate of 30,000 in/min (no feedback control) was used in this test series. The high rate necessitated acceleration of the load nose up to speed prior to loading the specimen. Because specimens tended to bounce off the actuator during the initial impact, a 1/4-inch pad of E.A.R. C1002-12 damping material was added between specimen and loading nose to minimize this bounce. This damping material had a hardness of Shore A 72-75. Figure 5 shows the test setup prior to testing.

Test Results

A total of 62 three- and four-point loaded beam tests were conducted by UDRI to determine the strength and toughness of the various hybrid composite materials and to establish a database for comparison with the steel tube. Initial tests were conducted with four point loading on 1.0x1.5x.080-inch 4130 rectangular steel tube specimens ($S_y = 94,750$ psi). This size steel tube had been successfully demonstrated as a windshield arch reinforcement providing four pound-400 knot birdstrike protection, and was included in the tests to provide a basis for comparison of the composite materials. The test results for the steel tubing and the Type I, Number 1 specimens has been summarized in Table 3.

The load-displacement curve for the steel tube is shown in Figure 6. Note that the load increases with displacement linearly until onset of yielding, followed by the peak load, after which the load decreases with increasing displacement. Steel is good for impact applications because of the large amount of energy absorbed and the low peak load.

The Type I, Number 1 materials had a lower elastic modulus than the steel tube and demonstrated much higher peak load carrying capability than did the steel tube. Figure 7 shows the typical failed specimens. The graphite/epoxy composite (panel A1) failed catastrophically in a brittle, cleavage type mode with very little delamination. The Kevlar/epoxy composite (panel B1) failed by delamination and fiber yielding as evident by the permanent deformation. The glass/epoxy composite (panel C1) failed primarily in delamination with some ply cleavage directly under the loading nose. The failures demonstrated by each of these materials was representative of how each material behaved in the hybrid composite. For example, the addition of glass fiber plies to a graphite matrix increases the number of interply delaminations during failure, preventing a catastrophic

cleavage type failure. The results of this first series of tests indicated that a Kevlar/glass/epoxy hybrid (panel K1) or a glass/graphite/epoxy hybrid (panel L1) may have the most desirable characteristics: the greatest amount of energy absorbed with the lowest peak load.

The row of bolts in each Type I, Number 2 specimen did significantly affect the failure mode, peak load, and energy (see Table 4). The ratio of energy to peak load increased for every material; most significantly in the Kevlar where the ratio increased about 60% over the unbolted specimens. The graphite specimen showed almost no change in this ratio. The increase in the ratio of energy to peak load was primarily a result of the changed failure mode. The bolts tend to minimize catastrophic delamination of the material and increase both the compression and tensile ply failures.

The third test series was conducted on the Type II, Number 1 specimens. The results of these tests have been summarized in Table 5. The failure modes were similar to the Type I, Number 1 specimens. Figure 8 shows specimens A1, B1, and C1 after testing. Figure 9 shows specimens L1, F1, and O1 after testing. Material O1 exhibited the most desirable characteristics: low peak load and high energy absorption (Reference 1). The secondary peak load was over 60% of the primary peak load as shown on the load displacement curve in Figure 10.

The results of the tests conducted on the Type II, Number 2 specimens are summarized in Table 6. Figure 11 shows tested specimens A2, B2, and C2. The failure modes of both specimens A2 and B2 changed from the series three tests. Specimen A2 did not fail catastrophically and exhibited much more delamination. Specimen B2 demonstrated much more outside ply failure with only local delamination. This change in failure mode is attributed to the increased strain rate. The failure mode of the hybrid materials did not seem to change as drastically. Figure 12 shows specimens L2, F2, and O2. The main difference in results between these specimens and the L1, F1, and O1 specimens was the difference in displacement at peak load, due in part to the damping material. The peak load carrying capability of the materials containing graphite increased significantly as a result of the increased strain rate; however, the ratio of the energy to the peak load remained about the same for all hybrid materials.

Discussion of Results

The test results demonstrated the feasibility of tailoring hybrid composite materials to meet specific requirements for strength and toughness. As expected, none of the materials tested demonstrated the yield characteristics of a

ductile steel. However, many of the hybrid composite materials failed in a progressive, energy absorbing, non-catastrophic failure mode.

The combination of Kevlar and fiberglass fibers in an epoxy matrix provided the most desirable characteristics for application to birdstrike. The load displacement curve for specimen type II Material O (50% Kevlar-49, 50% S-glass fibers), Figure 10, shows the desirable characteristics of a composite designed to absorb energy. The load carrying capability of the material is relatively high after the initial failure, and total failure occurs only after very large displacements. Material configuration Type O was chosen for the T-38 composite windshield arch reinforcement because of the relatively low peak load and relatively high secondary load carrying capability. The failure mode of this material was among the most efficient of the materials tested; the outside plies failed in tension, the inside plies failed in compression, and there was extensive delamination.

The following observations were made concerning the test results. The thickness of the composite materials did not affect the toughness (energy/peak load) or failure mode of the materials even though there was some variation in specific material properties. The bolted test specimens showed that the bolts do minimize delamination and that the holes resulted in significant stress concentrations and a subsequent compressive failure mode. However, there appeared to be no reduction in toughness.

Conclusions and Recommendations

Significant differences in the performance of various hybrid composite materials to impact loading have been documented in this paper. Variations in the stacking sequence and material combinations can have significant effects on the behavior of the composite under impact, and depending on the design requirements, hybrid composites can be tailored to specific needs. In general, hybrid composites should be considered a viable alternative to metals in applications where a controlled failure is desired.

In these tests, a hybrid composite containing half Kevlar-49 and half S-glass fibers in an epoxy matrix (specimen Type II Material O) demonstrated the most desirable characteristics for absorbing energy, minimizing peak load, and preventing catastrophic failure. This material has been successfully demonstrated on the T-38, A-7, and F-4 windshield aft arches to increase the birdstrike capability.

Future work in this area should include the following:

o Evaluate additional material combinations and stacking sequences, including combinations of Kevlar-49, Kevlar-29, and glass.

o Evaluate the effects of different resin systems on the toughness and failure modes of hybrid composites.

o Conduct additional high strain rate testing to better document the effects of strain rate on the material properties.

References

1. Stenger, Gregory J., Composite Windshield Arch Reinforcement Phase I: Feasibility Study, UDR-TR-84-22,d University of Dayton Research Institute, Dayton, Ohio, March 1984.
2. Phillips, L. N., "The Development and Uses of Glass/Carbon Hybrids," Royal Aircraft Establishment, Farnborough, U.K.
3. Wardle, M. W. and Edward W. Tokarsky, "Drop Weight Impact Testing of Laminates Reinforced with Kevlar Aramid Fibers, E-Glass, and Graphite," Composites Technology Review, Vol. 5, No. 5, Spring 1983, pp. 4-10.
4. Mullin, J. V. and V. F. Mazzio, "Basic Failure Mechanisms in Advanced Composites, Final Report," NASA Contract NASW-2093, April 1971.
5. Peterson, R. E., "Design Factors for Stress Concentration," Machine Design, Vol. 23, No. 3, March 1951, p. 161.

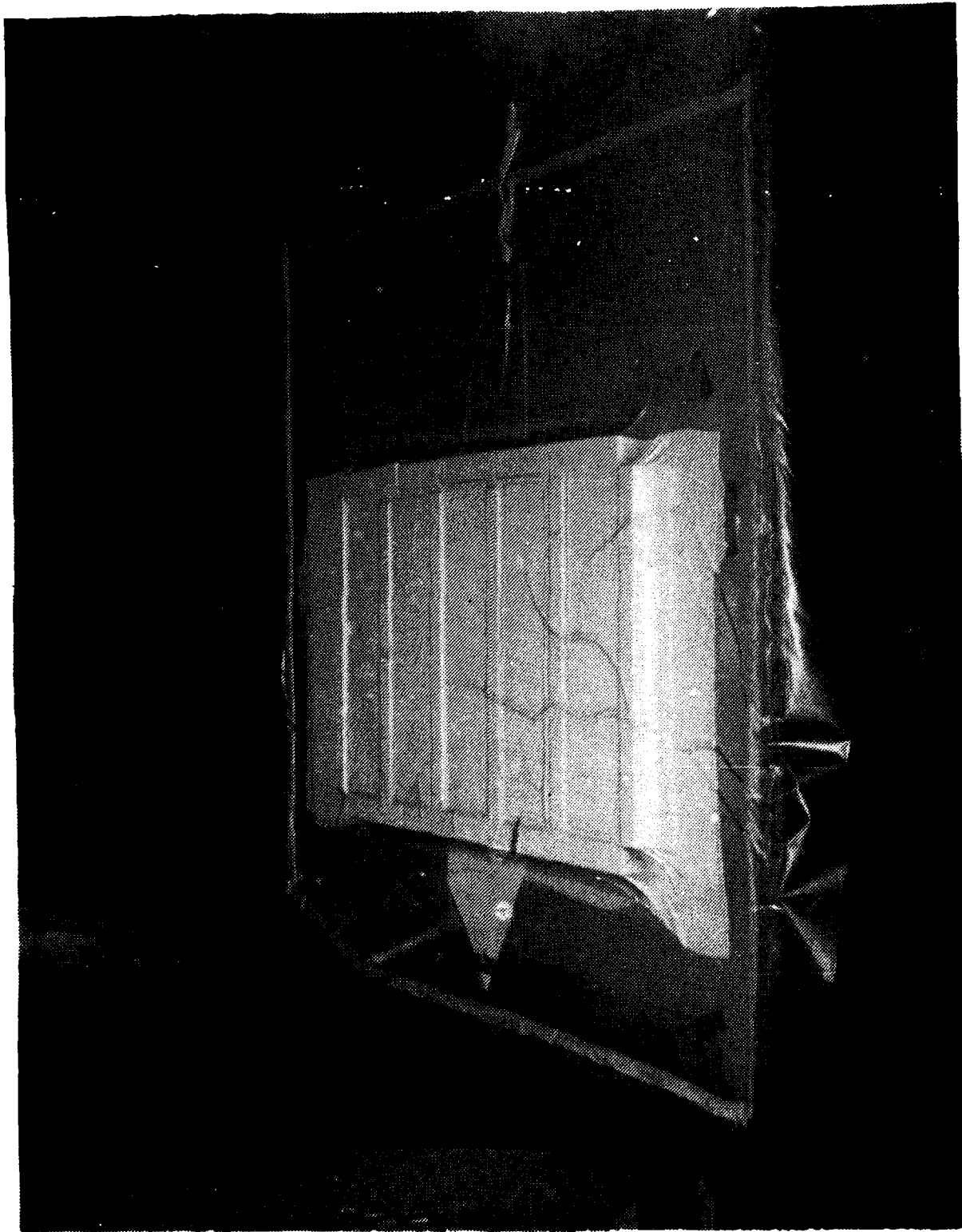


Figure 1. Type I Specimens Ready to be Cured in Autoclave.

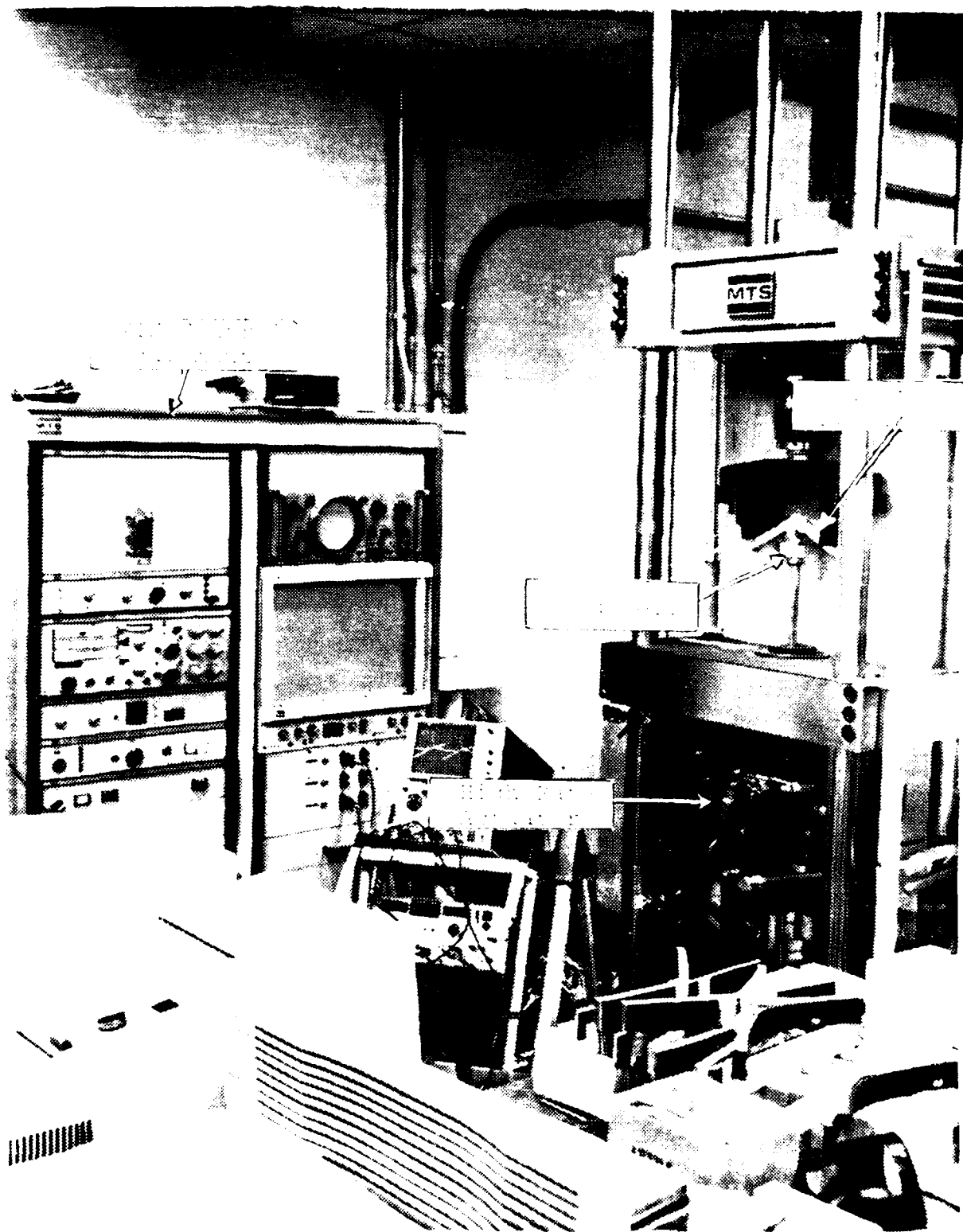


Figure 2. Structural Test Laboratory.

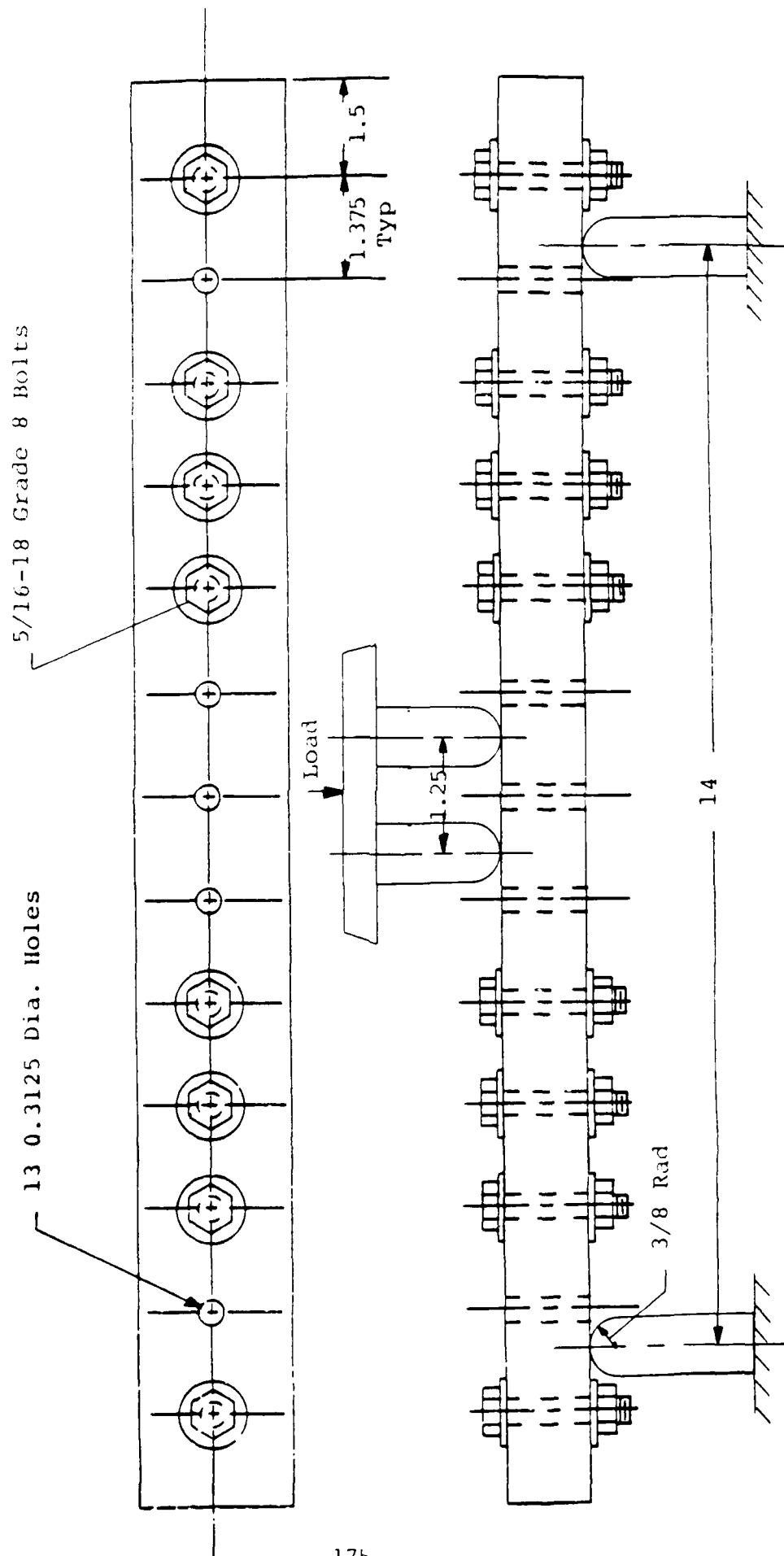


Figure 3. Hole and Bolt Locations in Type I Number 2 Specimens.

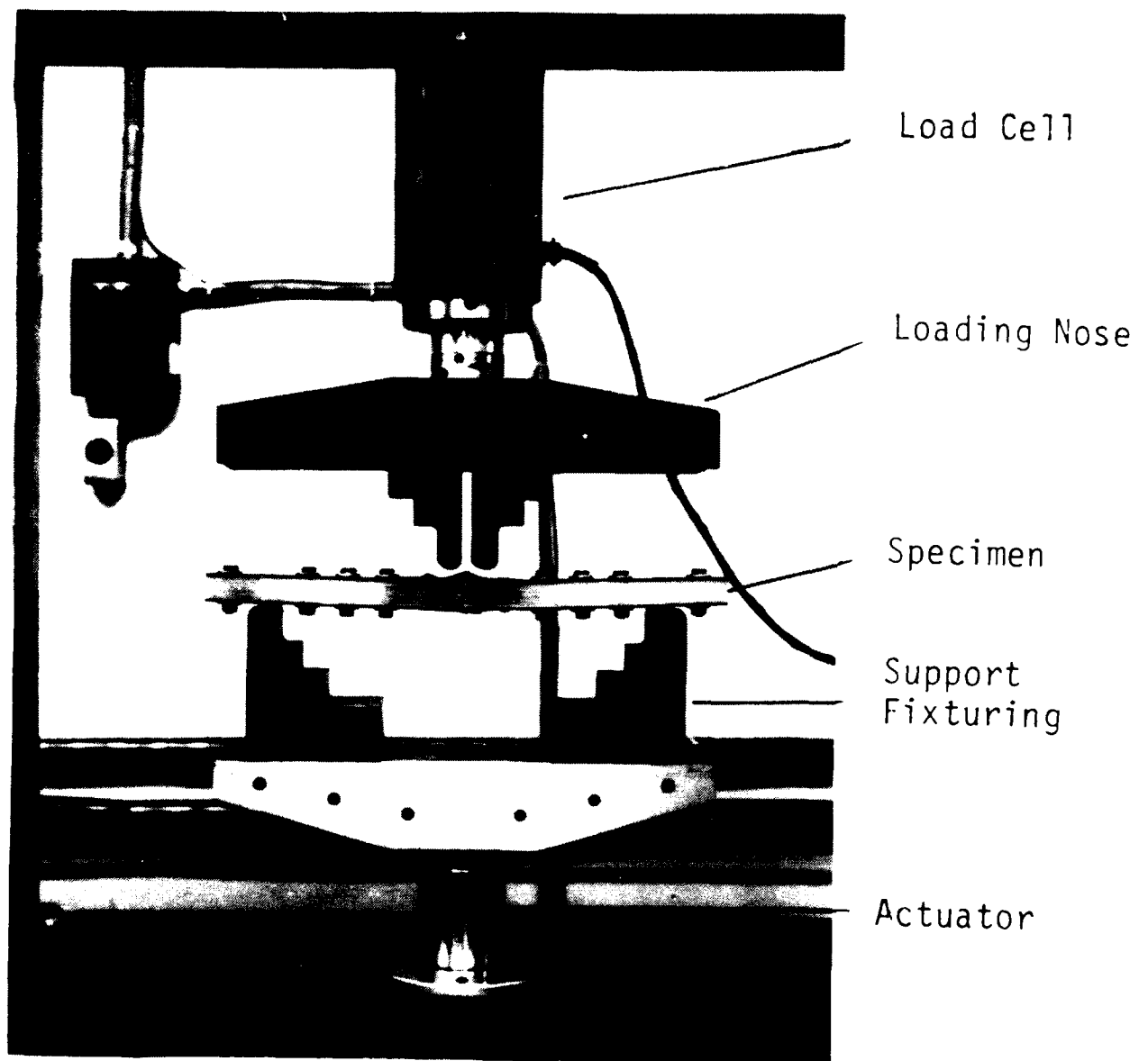


Figure 4. Test Setup of Type I Number 2 Specimen.

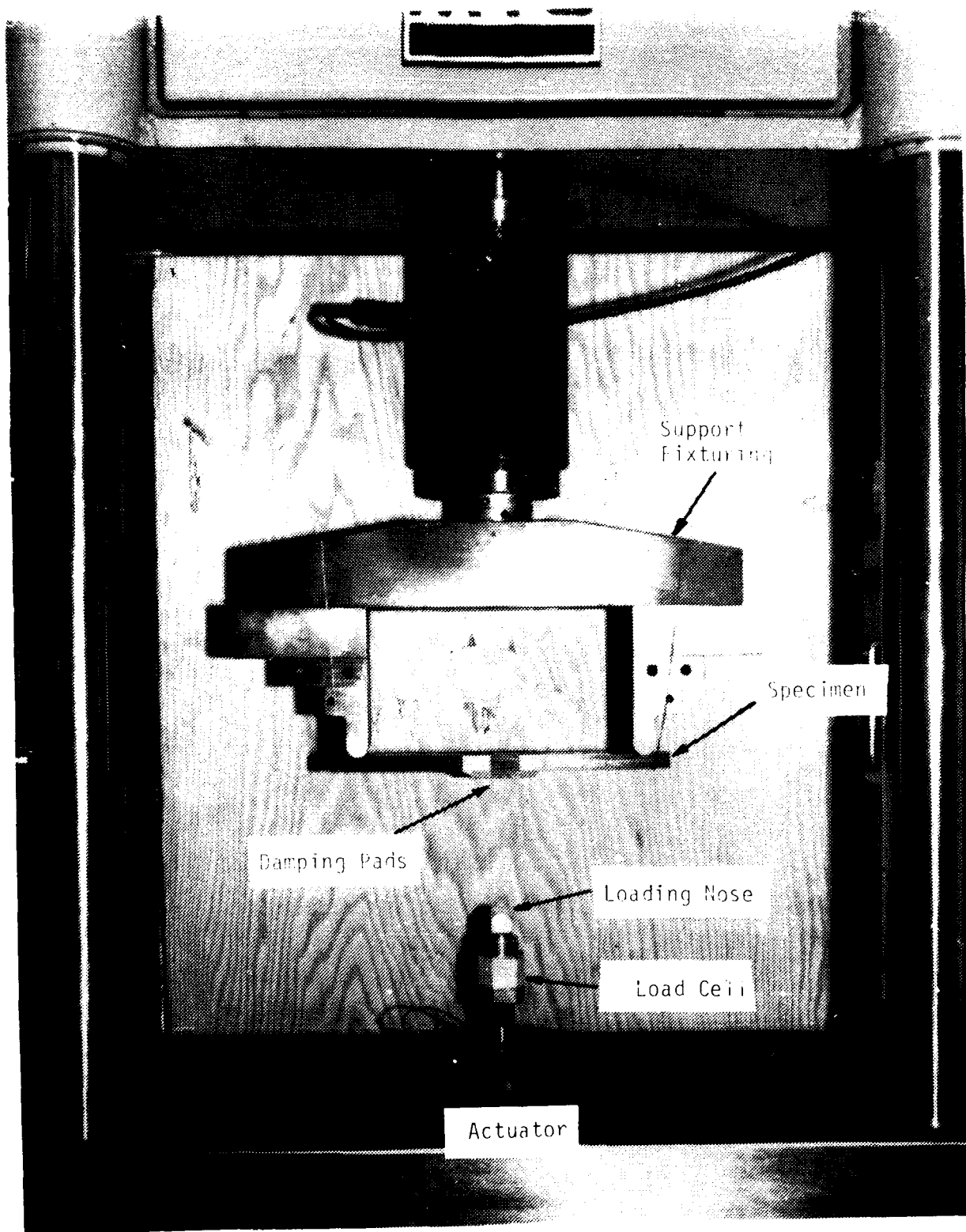


Figure 5. Test Setup of Series 4 High Rate (30,000 in/min) Tests on the Type II Number 2 Specimens.

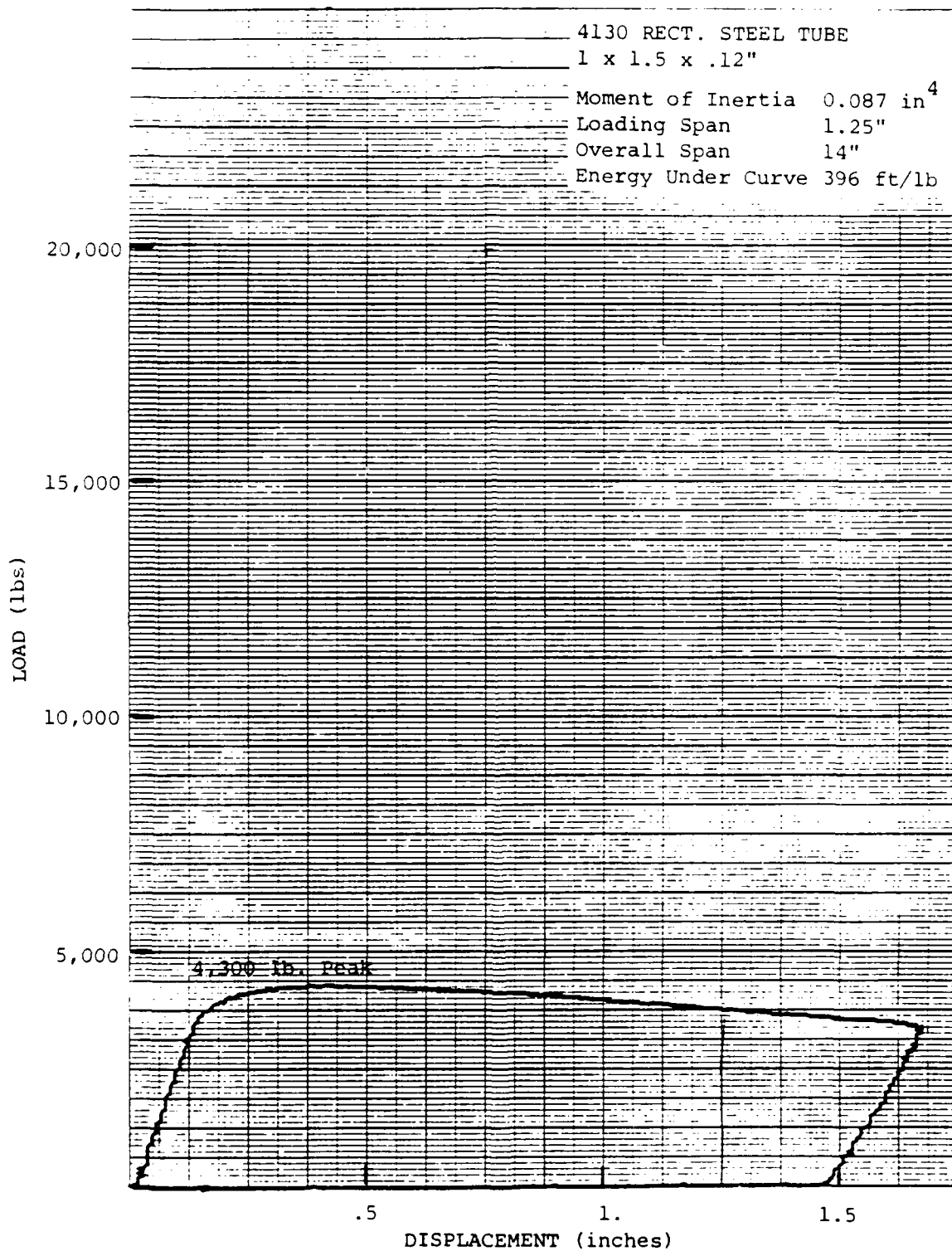


Figure 6. Load-Displacement Curve for Steel Tube.

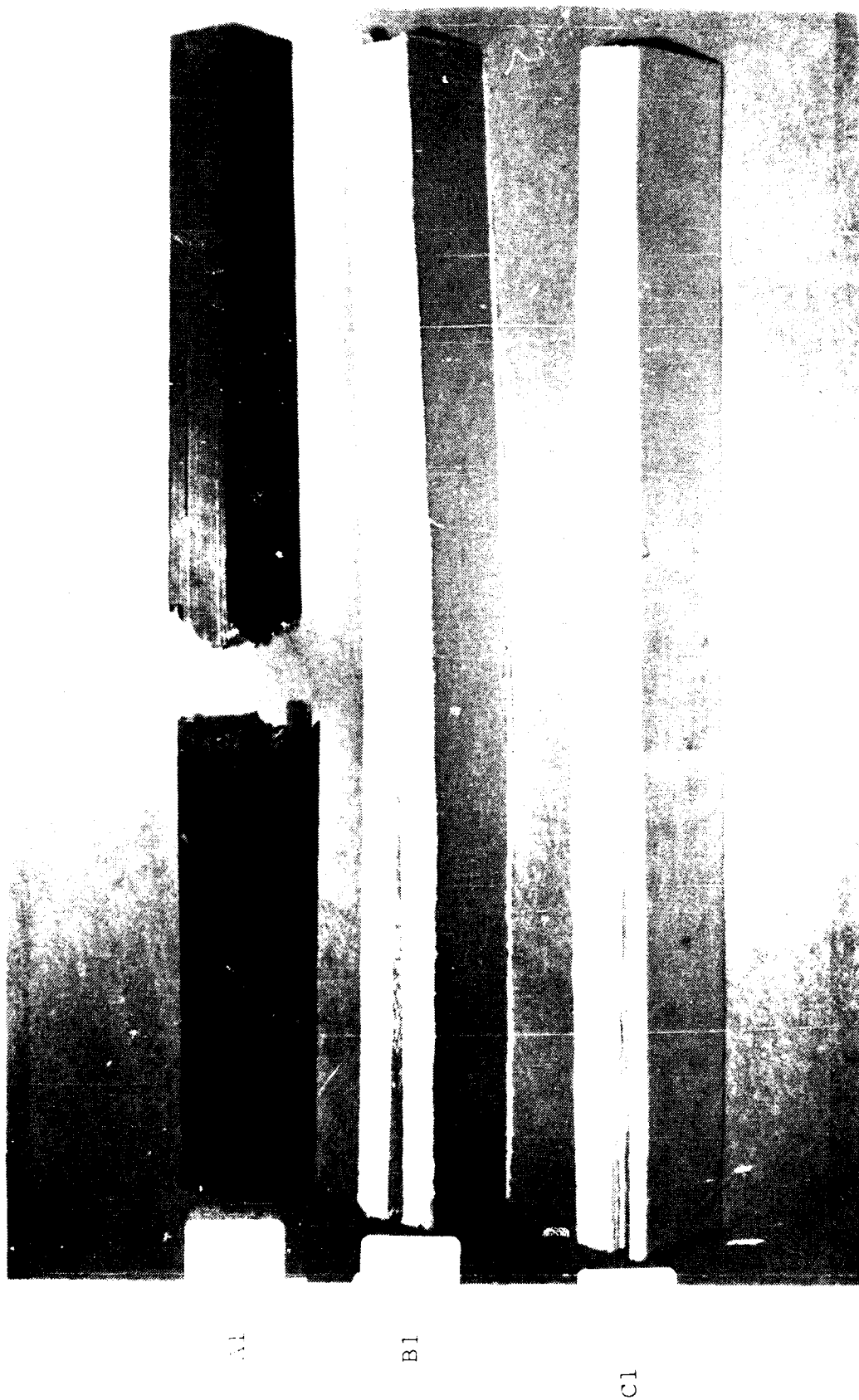


Figure 7. Type I Specimens A1, B1, and C1 After Testing.



Figure 8. Type II Specimens A1, B1, and C1 After Testing.

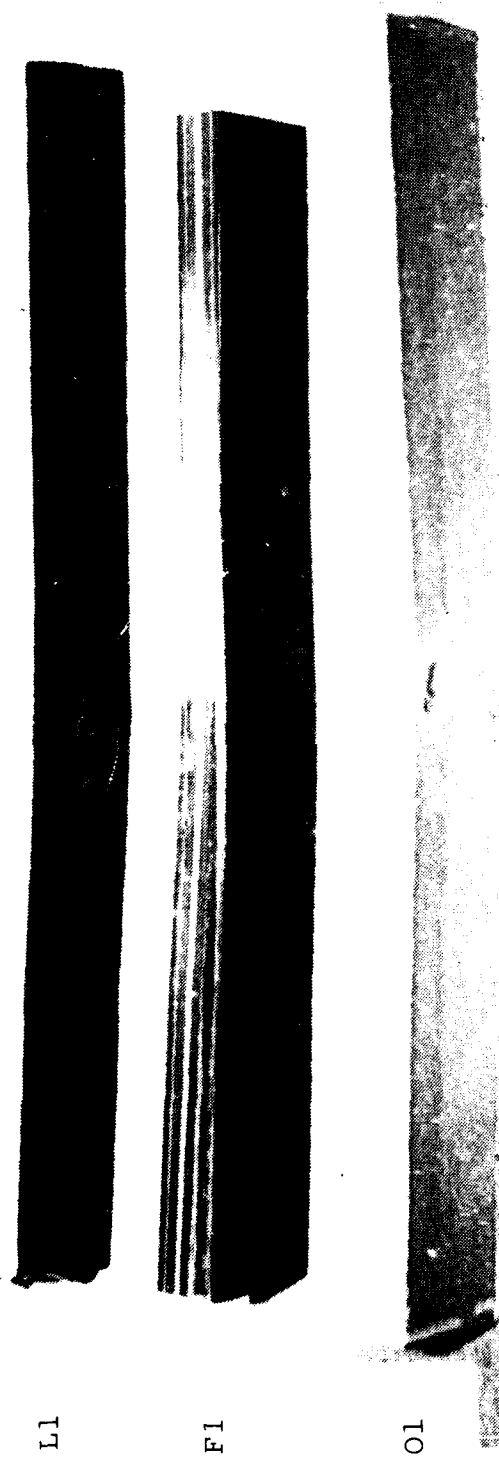


Figure 9. Type II Specimens L1, F1, and O1 After Testing.

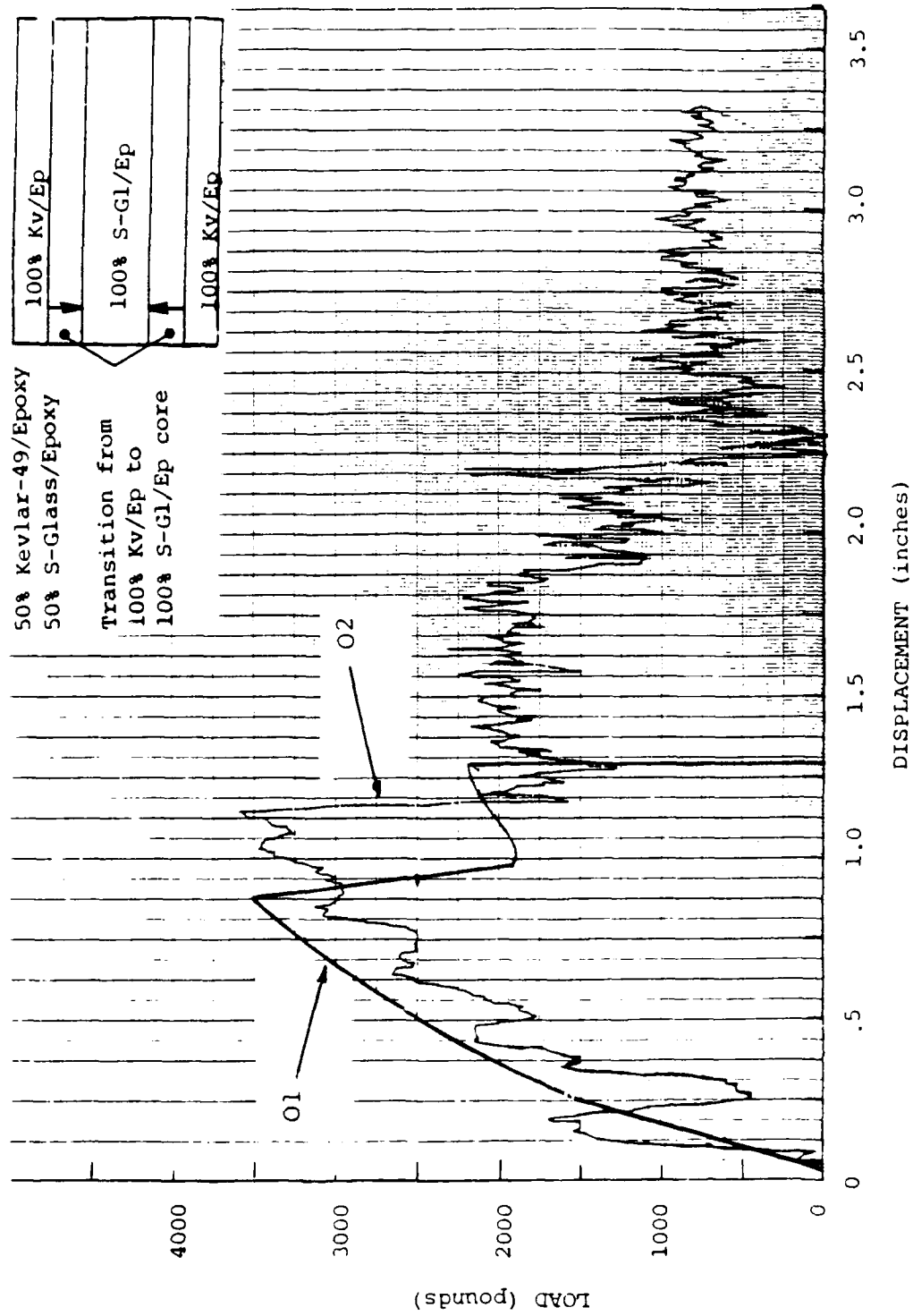


Figure 10. Load-Displacement Curve for Type II Material O Specimens.



Figure 11. Type II Specimens A2, B2, and C2 After Testing.



Figure 12. Type II Specimens L2, F2, and O2 After Testing.

TABLE 1
HYBRID COMPOSITE BEAM MATERIALS

Graphite/Epoxy Prepreg

- 0° - Tape, 12" wide Celion 6K/CE-321R Epoxy,
45% resin content, 5.5 mil/ply nominal
cured thickness
- +45°- Fabric, 42" wide Celion 3K70P Fabric/CE-321R
Epoxy, 45% resin content

S-Glass/Epoxy Prepreg

- 0° - Tape, 12" wide S-2 glass/CE-321R Epoxy,
7 mil/ply nominal cured thickness
- +45°- Fabric, 50" wide S-2 Glass Fabric, type
6781/CE-321R epoxy, 40±3% resin content

Kevlar-49/Ep

- 0° - Tape, 12" wide Kevlar-49/CE-321R Epoxy,
5.5 mil/ply nominal cured thickness
- +45°- Fabric, 50" wide Kevlar-49 Fabric,
Type 285/CE-321R Epoxy, 50±4% resin content

TABLE 2

HYBRID COMPOSITE MATERIALS TO BE EVALUATED

TYPE I Specimen Size 1.0x2.0x18 inches
 Four point loaded
 Span 4 inches
 Loading Span 1.25 in
 Tested with and without 5/16-18 bolts

MATERIAL	% FIBER COMPOSITION*	LAMINATE CONFIGURATION
A AS/Ep	100	
B Kev-49/Ep	100	
C S-Glass/Ep	100	
D AS/Ep//S-G/Ep	80/20	4/1 (4 plies AS alt. 1 ply S-G)
E AS/Ep//S-G/Ep	40/10//50	4/1//Laminated Glass Core
F AS/Ep//S-G/Ep	70/30	14/6 (14 plies AS alt. 6 plies S-G)
G AS/Ep//S-G/Ep	50/50	Alternating every 2 plies
H AS/Ep//S-G/Ep	50/50	Alternating every 10 plies
I AS/Ep//Kev-49/Ep	80/20	4/1 (4 plies AS alt. 1 ply Kev)
J AS/Ep//Kev-49/Ep	50/50	Alternating every 2 plies
K Kev-49/Ep//S-G/Ep	25/25//50	2/2//Glass Core
L AS/Ep//S-G/Ep	30/70	6/14 (6 plies AS alt. 14 plies S-G)

Type II Specimen Size 0.5x1.5x12 inches

Four point loaded:

Loading rate 875 in/min

Span 10 inches

Loading span 0.25 in

Three point loaded:

Loading rate 30,000 in/min

Span 10 inches

MATERIAL	% FIBER COMPOSITION*	LAMINATE CONFIGURATION
A AS/Ep	100	
B Kev-49/Ep	100	
C S-Glass/Ep	100	
D AS/Ep//S-G/Ep	80/20	4/1 (4 plies AS alt. 1 ply S-G)
E AS/Ep//S-G/Ep	70/30	14/6 (14 plies AS alt. 6 plies S-G)
F AS/Ep//S-G/Ep	50/50	Alternating every 2 plies
G AS/Ep//S-G/Ep	50/50	Alternating every 10 plies
H AS/Ep//S-G/Ep	30/70	6 plies AS alt. 14 plies S-G
I AS/Ep//S-G/Ep	40/10//50	4/1//Glass Core
J AS/Ep//S-G/Ep	50/50	Transition to Glass Core
K AS/Ep//Kev-49/Ep	80/20	4/1 (4 plies AS alt. 1 ply Kev)
L AS/Ep//Kev-49/Ep	50/50	Alternating every 2 plies
M AS/Ep//Kev-49/Ep	30/70	6/14 (6 plies AS alt. 14 plies Kev)
N AS/Ep//Kev-49/Ep	50/50	Transition to Kev-49 Core
O Kev-49/Ep//S-G/Ep	50/50	Transition to Glass Core
P Kev-49/Ep//S-G/Ep	70/30	7/3 (7 plies Kev alt. 3 plies S-G)
Q Kev-49/Ep//S-G/Ep	30/70	3/7 (3 plies Kev alt. 7 plies S-G)

* 80% tape oriented [0], 20% fabric oriented [+45], all specimens.

AS - graphite

Kev - Kevlar-49

S-G - S-Glass

Ep - Epoxy

TABLE 3
TEST RESULTS FOR FOUR POINT LOADED BEAM SPECIMENS

Specimen	Width (in)	Thickness (in)	Moment of Inertia (in ⁴)	Loading Span (in)	Overall Span (in)	Peak Load (lbs)	Displace- ment at Peak Load (in)	Energy (ft-lbs)	Flexure Modulus (psi x 10 ⁶)	Outer Fiber Stress at Peak Load (psi)	Energy Peak Load (ft)
Steel Tube	1.5	1.	.087	1.25	14	4300	.375	39.	34.0	157540.	.0921
Steel Tube	1.5	1.	.087	1.375	12	5250	.313	48.3	34.1	160290.	.0920
Steel Tube	1.5	1.	.087	3.	12	6125	.375	569	32.6	158400.	.0923
Steel Tube	1.5	1.	.087	3.	12	5875	.375	555	31.4	151940.	.0940
Type I											
Panel A1	1.921	1.271	.3287	1.25	14	20300	.500	620	14.1	250200.	.0305
Panel B1	2.017	1.300	.3693	1.25	14	14080	.550	653	9.68	157980.	.0464
Panel C1	2.277	1.063	.2279	3.	12	20625	.720	1042	7.86	216450.	.0505
Panel D1	2.088	1.234	.3270	1.25	14	19780	.525	784	14.1	237930.	.0396
Panel E1	1.952	1.113	.2243	1.25	14	15170	.488	648	15.6	239940.	.0427
Panel F1	2.127	1.208	.3125	1.25	14	19300	.475	807	14.9	237810.	.0418
Panel G1	1.987	1.162	.2587	1.25	14	16730	.550	721	13.7	238510.	.0431
Panel H1	2.074	1.092	.2251	1.25	14	17875	.438	678	23.1	276400.	.0379
Panel I1	1.975	1.250	.3215	1.25	14	17680	.425	667	14.8	219110.	.0377
Panel J1	2.00	1.245	.3216	1.25	14	17230	.450	805	14.1	212610.	.0467
Panel K1	1.945	1.125	.2308	1.25	14	14580	.950	751	7.75	226530.	.0516
Panel L1	2.130	1.037	.1979	1.25	14	13230	.563	732	13.9	220980.	.0553

Loading Rate 70 in/min

TABLE 4
TEST RESULTS FOR FOUR POINT LOADED BEAM SPECIMENS

SPECIMEN	WIDTH (IN)	THICKNESS (IN)	MOMENT OF INERTIA (IN**4)	LOADING SPAN (IN)	OVERALL SPAN (IN)	PEAK LOAD (LBS)	DISPLACE- MENT AT PEAK LOAD (IN)	ENERGY (FT-LBS)	FLEXURE MODULUS (MPSI)	OUTER FIBER STRESS AT PEAK LOAD (KSI)	ENERGY PEAK LOAD (FT)
TYPE 1*											
A2	1.949	1.282	.342	1.250	14.	16650.	.369	519.	14.74	199.	.031
B2	1.950	1.140	.241	1.250	14.	10900.	.369	801.	13.72	165.	.074
C2	2.160	1.057	.213	1.250	14.	13250.	.975	779.	7.15	210.	.059
D2	2.005	1.152	.255	1.250	14.	13475.	.413	593.	14.29	174.	.050
E2	2.068	1.087	.221	1.250	14.	11125.	.375	561	14.98	174.	.050
F2	1.992	1.217	.299	1.250	14.	13575.	.381	599.	13.30	176.	.044
G2	2.112	1.114	.243	1.250	14.	11325.	.406	593.	12.80	165.	.052
H2	2.180	1.091	.231	1.250	14.	13450.	.475	663.	13.73	203.	.049
I2	1.980	1.260	.330	1.250	14.	15850.	.375	629.	14.31	193.	.040
J2	1.960	1.270	.335	1.250	14.	13125.	.375	711.	11.69	159.	.054
K2	1.950	1.140	.241	1.250	14.	8675.	.600	517.	6.71	131.	.060
L2	2.017	1.064	.202	1.250	14.	8525.	.488	503.	9.65	143.	.059

Loading Rate 500 in/min

* Bolted every 1-3/8" with 5/16-18 Grade 8 bolts.

TABLE 5
TEST RESULTS FOR FOUR POINT LOADED BEAM SPECIMENS

SPECIMEN	WIDTH (IN)	THICKNESS (IN)	MOMENT OF INERTIA (IN ⁴)	LOADING SPAN (IN)	OVERALL SPAN (IN)	PEAK LOAD (LBS)	DISPLACE- MENT AT PEAK LOAD (IN)	ENERGY (FT-LBS)	FLEXURE MODULUS (MPSI)	OUTER FIBER STRESS AT PEAK LOAD (KSI)	ENERGY PEAK LOAD (FT)
TYPE II											
A1	1.590	.590	.027	.250	10.	6000.0*	.400	131.0	22.92	317.	.022
B1	1.510	.670	.038	.250	8.	4650.0	.300	260.4	8.71	153.	.056
C1	1.650	.450	.013	.250	8.	4590.0	.725	205.5	10.75	319.	.045
D1	1.610	.570	.025	.250	10.	5000.0	.406	193.6	20.61	280.	.039
E1	1.660	.560	.024	.250	10.	4950.0	.413	201.9	20.52	278.	.041
F1	1.600	.490	.016	.250	10.	4100.0	.575	165.1	18.90	312.	.040
G1	1.570	.530	.019	.250	10.	3950.0	.475	202.6	17.76	262.	.051
H1	1.590	.460	.013	.250	10.	3225.0	.663	171.0	15.69	280.	.053
I1	1.590	.480	.015	.250	10.	1700.0	.938	94.3	5.14	136.	.055
J1	1.600	.450	.012	.250	10.	3475.0	.450	164.6	26.43	314.	.047
K1	1.540	.550	.021	.250	10.	4450.0	.413	185.0	20.99	279.	.042
L1	1.540	.560	.023	.250	10.	4225.0	.438	180.6	17.80	256.	.043
M1	1.580	.670	.040	.250	10.	4700.0	.438	201.0	11.27	194.	.043
N1	1.570	.620	.031	.250	10.	4950.0	.388	177.6	17.02	240.	.036
O1	1.510	.560	.022	.250	10.	3500.0	.863	217.3	7.63	216.	.062
P1	1.510	.590	.026	.250	10.	3950.0	.738	218.8	8.61	220.	.055
Q1	1.510	.540	.020	.250	10.	3800.0	.950	210.4	8.40	252.	.055

Loading Rate 875 in/min

* Estimated

TABLE 6
TEST RESULTS FOR FOUR POINT LOADED BEAM SPECIMENS

SPECIMEN	WIDTH (IN)	THICKNESS (IN)	MOMENT OF INERTIA (IN**4)	LOADING SPAN (IN)	OVERALL SPAN (IN)	PEAK LOAD (LBS)	DISPLACE- MENT AT PEAK LOAD (IN)	ENERGY (FT-LBS)	FLEXURE MODULUS (MPSI)	OUTER FIBER STRESS AT PEAK LOAD (KSI)	ENERGY PEAK LOAD (FT)
A2	1.600	.470	.014	.250	10.	6900.	.863	327.	24.04	571.	.047
B2	1.510	.670	.038	.250	10.	4700.	.938	332.	5.51	203.	.071
C2	1.610	.580	.026	.250	10.	4575.	2.013	192.	3.61	247.	.042
D2	1.640	.570	.025	.250	10.	6400.	.913	285.	11.53	351.	.045
E2	1.570	.560	.023	.250	10.	5650.	.738	118.	13.87	336.	.021
F2	1.570	.460	.013	.250	10.	3750.	1.213	168.	10.10	330.	.045
G2	1.630	.470	.014	.250	10.	4575.	.925	235.	14.59	372.	.051
H2	1.630	.450	.012	.250	10.	5050.	.775	150.	21.89	448.	.030
I2	1.550	.490	.015	.250	10.	2300.	1.275	157.	4.94	181.	.068
J2	1.570	.520	.018	.250	10.	6500.	.850	310.	17.29	448.	.048
K2	1.560	.550	.022	.250	10.	6300.	.963	317.	12.59	390.	.050
L2	1.580	.610	.030	.250	10.	5900.	.738	247.	11.13	294.	.042
M2	1.560	.650	.036	.250	10.	4325.	.613	200.	8.23	192.	.046
N2	1.520	.610	.029	.250	10.	7050.	.825	319.	12.36	365.	.045
O2	1.520	.560	.022	.250	10.	3537.	1.275	213.	5.19	217.	.060
P2	1.500	.600	.027	.250	10.	4250.	.950	285.	6.89	230.	.067
Q2	1.530	.590	.026	.250	10.	3800.	.963	271.	6.27	209.	.071

Loading Rate 30,000 in/min

REPAIR AND RESTORATION OF COMBAT DAMAGE TRANSPARENCIES

G. Renieri
D. Kovensky

McDonnell Aircraft Company

PAPER WAS WITHDRAWN

SESSION II

EMERGING CAPABILITIES (PART B)

Chairman: G. J. Stenger
University of Dayton
Dayton, Ohio

Co-Chairman: R. E. Colclough
Flight Dynamics Laboratory
Wright-Patterson AFB, Ohio

Coordinator: C. Szczepan
San Antonio Air Logistics
Center
Kelly AFB, Texas

HIGH PERFORMANCE POLYCARBONATE TRANSPARENCY COATING

J. E. Miller

Sherwin-Williams Company

J. E. Kochanowski

G.E. Plastics

HIGH PERFORMANCE POLYCARBONATE TRANSPARENCY COATING

J. E. Miller, Sherwin-Williams Company and
J. E. Kochanowski, G.E. Plastics

ABSTRACT: Coated polycarbonate became the material of choice for the automotive headlamp materials early in this decade. This material allowed for design freedom not before realized, as follows a dramatic reduction in headlamp breakage due to road gravel impact. The early acrylic lacquer coatings provided the requisite performance with respect to ultraviolet ray absorption to protect the polycarbonate from degradation in the engineering performance and yellowing. It was soon realized, however, that this coating technology would not be suitable for maintaining photometrics over time due to the fact that road dust impinging on the headlamp surfaces at high speed caused the deterioration of the coating surface, which resulted in haze and a slight loss in light transmission values. Therefore, a new generation of coatings based on a two coat silicone hardcoat system was developed. This system has demonstrated a high degree of commercial acceptability in headlamp applications and has passed greater than three years Florida and Arizona exposure. This coating technology found its way into other polycarbonate applications such as glazing where cosmetic as well as quantitative haze and transmission standards were important. This generation of products showed a tendency for a micro-cracking to develop in the coating, which had no effect on performance other than a cosmetic defect viewable only at shallow angles from the surface with transmitted light. Since the current commercial system appeared to be potentially unsuitable for glazing applications in the automotive and other application areas, an advanced silicone coating system was developed to maintain all the desirable properties of the current commercial product while minimizing the micro-cracking effect. This system has been commercialized in the automotive industry and shows several-fold improvement in micro-crack resistance compared to the current product based on accelerated and artificial weathering testing. Thus, it has the potential for applications in aircraft transparencies.

INTRODUCTION

The purpose of this paper is to show how aerodynamic automotive lighting technology might be applied to transparencies. The driving force for the change from glass to polycarbonate as automotive headlamp material was the opportunity to reduce the replacement of headlamps due to stone damage. In 1979, 28 million headlamps burned out, 10.8 million were replaced due to stone damage and 10.7 million due to accidents in passenger cars. In addition, 2.4 million lenses were replaced in trucks and motorcycles for a total of 13.2 million headlamps replaced in 1979 due to stone damage. Plastic headlamps made from polycarbonate are approximately 100 times more resistant to breakage from flying objects

such as stones when compared to glass. Considering all aspects, including the costs of the bulb and labor costs, there was a potential savings of over 800 million dollars in replacement costs occurring to the motor- ing public if polycarbonate composite headlamps were used to replace seal beam systems.¹ This would include cost savings of burn-outs as well since the composite systems would use a replaceable bulb. In addition, due to design flexibility, it was possible to design polycar- bonate aerodynamic headlamps such that as much as a half mile per gallon could be saved on some cars, thus reinforcing the cost savings signifi- cance of this approach. While the initial costs of a composite polycar- bonate headlamp system would be \$25 greater per vehicle than a conven- tional dual lamp glass seal beam system, the cost benefit ratio clearly favored molded polycarbonate headlamps lenses.

DISCUSSION

Since automotive headlamps are regulated by the Department of Trans- portations' Federal Motor Vehicle Safety Standard 108 (the Standard for Lamps, Reflective Devices and Associated Equipment for Passengers, Multi- purpose Passenger Vehicles, Truck, Buses, Trailers and Motorcycles) it was necessary to address the specific requirements for both original and replacement lamps, reflective devices and associated equipment necessary for signaling and for safe operation of motor vehicles during darkness and other conditions of reduced visibility. Under the standard, head- lamps are divided into two categories; sealed beam headlamps and replac- able (or composite) lamps. There are separate/different sets of perfor- mance requirements that have been established for each type of headlamp. Because the seal beam headlamps are regarded as disposable items whether glass or plastic, the material requirements are not very severe. Tradi- tionally, the lense had been made of glass or polycarbonate and the reflector made of metal, glass or plastic which is metallized for reflec- tivity. Federal Motor Vehicle Safety Standard 108 requires that the plastic lense material meet the requirements of SAEJ576 (Society of Auto- motive Engineers) the recommended practice for plastic materials for use in optical parts such as lenses and reflectors of motor vehicle lighting devices. This recommended practice sets material performance standards after three years of weathering at 45° South facing in Florida and Arizona. At the conclusion of the tests the samples must not show physi- cal changes that would affect performance such as color bleeding, delami- nation, hazing or cracking. Additionally, the luminous transmittance of the exposed samples must not have changed more than 25%, the chromaticity coordinants must conform to the requirements of SAEJ578D and the haze must not be greater than 30%. Unlike seal beam lights, replacable bulb or composite headlamps are considered to be a permanent part of a car and, hence, they're required to meet much more stringent performance standards. In the composite system, reflectors are constructed of thermoplastic or thermoset materials and our lenses are formed of glass or polycarbonate. The majority of the material requirements refer to

After the thermocycling, the lense of the same headlamp is sprayed uniformly with a mixture of dust and water until the photometric output at the test point H-V is 25% of the original output. The lamp is then conditioned for one hour at 95°F and then soaked for an additional hour with the highest wattage filament energized, allowing the ambient temperature to rise from 95°F. After this test the lamp is checked for warpage and photometric behaviour, the assembled must also undergo humidity tests at 100°F and 90% +/- 10% relative humidity. The test consist of 20 consecutive six-hour test cycles; in each cycle the highest wattage filament is energized for one hour and then de-energized for five hours. After the last cycle the lamp is soaked for one hour at 73°F and 30% +/- 10% relative humidity for one hour. The headlamp is then examined and checked for photometrics within ten minutes. The headlamp must not have any delamination, moisture fogging or condensation visible and it must pass photometric testing.

Seal beam plastic headlamps described earlier were considered a disposable item and as such did not have the requirement to meet the abrasion resistance tests described, which is required for the aerodynamic/composite headlamps which are the subject of this paper. These latter composite/aerodynamic polycarbonate headlamps are required to meet the quadruple aught steel wool test described and following are some correlations to actual haze changes in the automotive headlamps as a function of various tests and actual road conditions.

Through an evaluation of various artificial abrasion test methods, e.g., falling sand, taber abrader, hard brush, block and grit, brush and grit and steel wool, only the steel wool test provided repeatability of results. An evaluation of field return lamps showed that haze and transmission losses were proportional to mileage accumulated.² By plotting haze and transmission values vs. mileage the resultant haze and transmission values at 100,000 miles were projected to 38.8% and 86.95% respectively. (Figure 1)² The haze appears to be not only the most sensitive laboratory measure of abrasion, but is also more closely analogous to the glare produced by a light dispersion from a headlamp. For reference, a measured haze of more than 5% is required to be noticeable to the normal human eye. Using the photometric results of artificially abraded lenses and the recorded haze values on the same lenses, it was possible to correlate these results to the field return samples and estimate the mileage at which a plastic lense lamp would no longer meet the SAEJ579 glare requirements. This mileage was estimated at 44,000 miles. Six cycles of abrasion on the steel wool abrasion machine was demonstrated to provide the equivalent haze as revealed on the field return lamps at 44,000 miles. Eleven cycles of abrasion using the steel wool test simulates the abrasion can be expected at 100,000 miles of vehicle operation. (Figure 2)²

In order to meet the tests and standards involving lenses, it was necessary to develop a coating system which would allow the polycarbonate to be resistant to UV yellowing, scratches and abrasions

and attack by common automotive fluids. This system is known as LHP/LHC 100 and is composed of a primer and a silicone hardcoat applied to Lexan polycarbonate. These coatings can be applied from solution by dip, spray or flow coating, followed by an air and a thermo-drying to obtain the optimum coating performance. The LHP100 Primer is applied at .02 to .03 mils film thickness, while the silicone hardcoat LHC100 is applied at .18 to .26 mils. The product features of this system are ultraviolet resistance, abrasion and mar resistance, scratch resistance, clarity, good flow-out, no haze increase, solvent and chemical resistance. This leads to the benefits of weatherable coated parts, durable coated parts and optical quality parts. Typical performance properties of this system on polycarbonate are a delta haze of 2 to 8% after 500 cycles of taber abrasion with a 500 gram load using CS10F wheels. Also, this system allows for water immersion of greater than 250 hours at 65° C and greater than 2,000 hours QUV using QFS40 lamps, which is the same spectrum, but lower intensity than the 313 lamps. The QUV cycle used is 8 hours UV at 70°C and 4 hours dark, condensity humidity at 50°C. In addition, the yellowness index after 1500 hours QUV is less than 1 as measured per ASTM1925 yellowness index.

The specific chemical resistance and solvent resistance data for this system is as follows: using a saturated cotton ball with 30 minutes exposure to ethylene glycol antifreeze, heavy duty brake fluid (glycol based), heavy duty brake fluid (silicone-type, diesel fuel, gasoline, 10W-30 motor oil, paste auto polish, transmission fluid (type A), windshield washer fluid and heavy duty detergent; showing no blistering, peeling or loss of adhesion in any of these exposures.

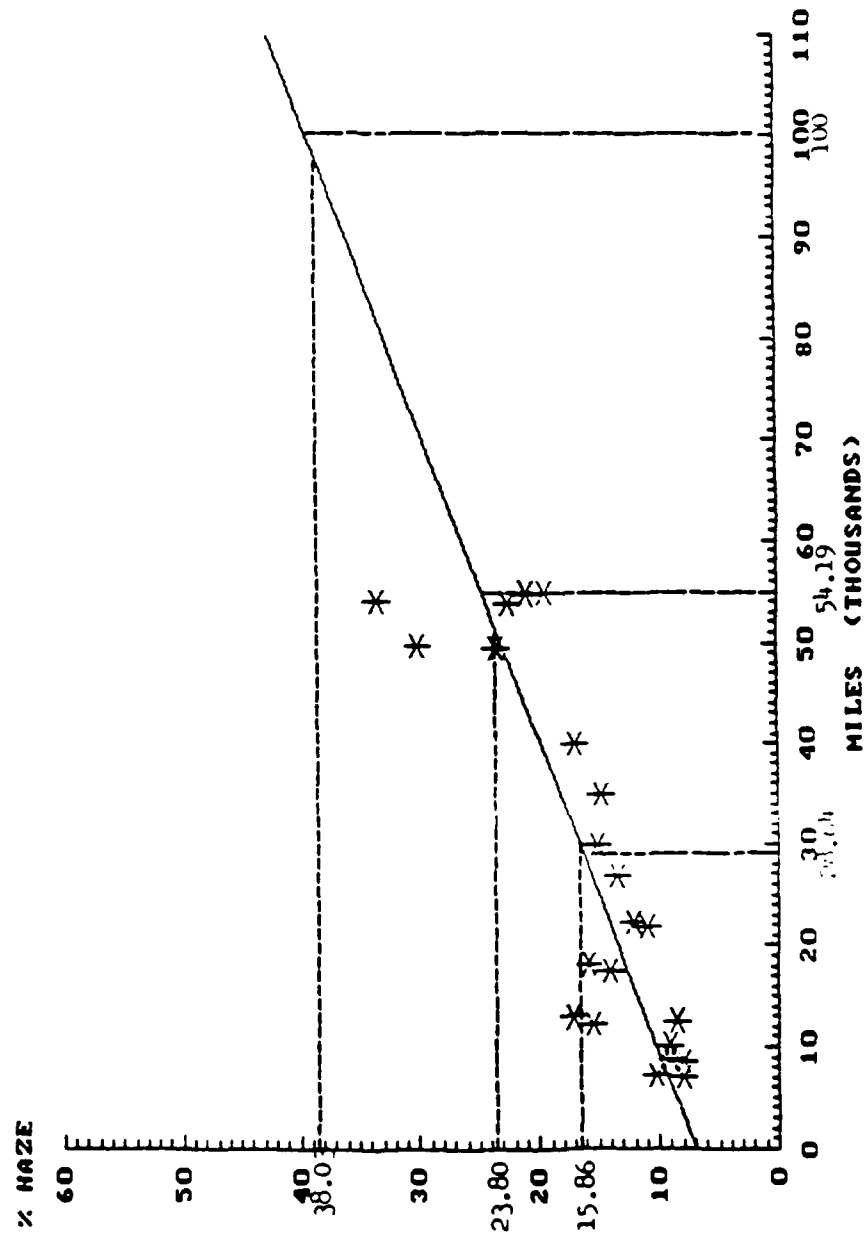
This system has been used since 1984 and was first commercialized on the Ford's Mark VII composite headlamps.³ This system has proved to be a commercial success and has spread to many other passenger cars in the United States with the volume of headlamps well into the millions. While this technology was obviously extremely successful, a cosmetic issue developed in both accelerated and real-world testing. Micro-cracking is an optical cosmetic defect which occurs as a function of weathering; it is visible only at shallow viewing angles. (See photographs of 90° and 20° viewing angle.) Micro-cracking has no effect on physical properties, such as chemical resistance of the film, and as such is of aesthetic concern only. This affect occurs at between nine and fourteen months Florida weathering with the LHP/LHC coating system, which is composed of an acrylic primer and a silicone resin hardcoat. In consideration of this aesthetic problem, a second generation silicone hardcoat was made available, and is designated AS4000. This product has micro-crack resistance in excess of 24 months in Florida weathering and maintains all the desirable properties of the original silicone hardcoat system. These data and information regarding the maintenance of taber abrasion resistance with weathering are shown in tables 1 and 2.

Application of the silicone hardcoat systems to polycarbonate follows the procedure indicated.

1. If parts are above 1450 psi stress level, they are annealed for 30 minutes at 266°F per 100 mils. (Stress can be tested with solvent immersion.) These parts then are cooled down and then put through a cleaning procedure of either detergent water, rinsed with deionized water and subsequently a freon final rinse or ultrasonic freon is used; both are followed with ionized air blow-offs. Coatings are then applied in a Class 100 clean room after being filtered through a 3-5 micron prefilter and a 1/2 micron final filter. The application environment is 70°F and below 50% relative humidity. The coatings are applied by spray, dip or flow and the primer is applied between .02 and .03 mils. The hardcoat is applied at between .18 and .26 mils and is measured for thickness non-destructively using a beta backscatter device. Primer is applied and flashed for 20 minutes and subsequently baked for 20 minutes at 125 +/- 5 C. The part is then cooled and the hardcoat applied. Subsequent to a 10-15 minutes flash, this is also baked at 130°C +/- 5 C in either an electric or indirect gas-fired oven. It is necessary to store the hardcoat at 40°F or less, while the primer can be indefinitely stored at room temperature. Acrylic substrates can be treated in a similar manner, excepting for the bake schedule which must be lowered in temperature to 185°F and the bake extended, in the case of the primer, to 1 hour, and in the case of the hardcoat up to 8 hours at these temperatures. This silicone hardcoat system has been evaluated on a preliminary basis on both polycarbonate and acrylic, and appears to have application in areas of aircraft transparencies. It is felt that this automotive lighting and glazing technology can be transferred to the aircraft industry.

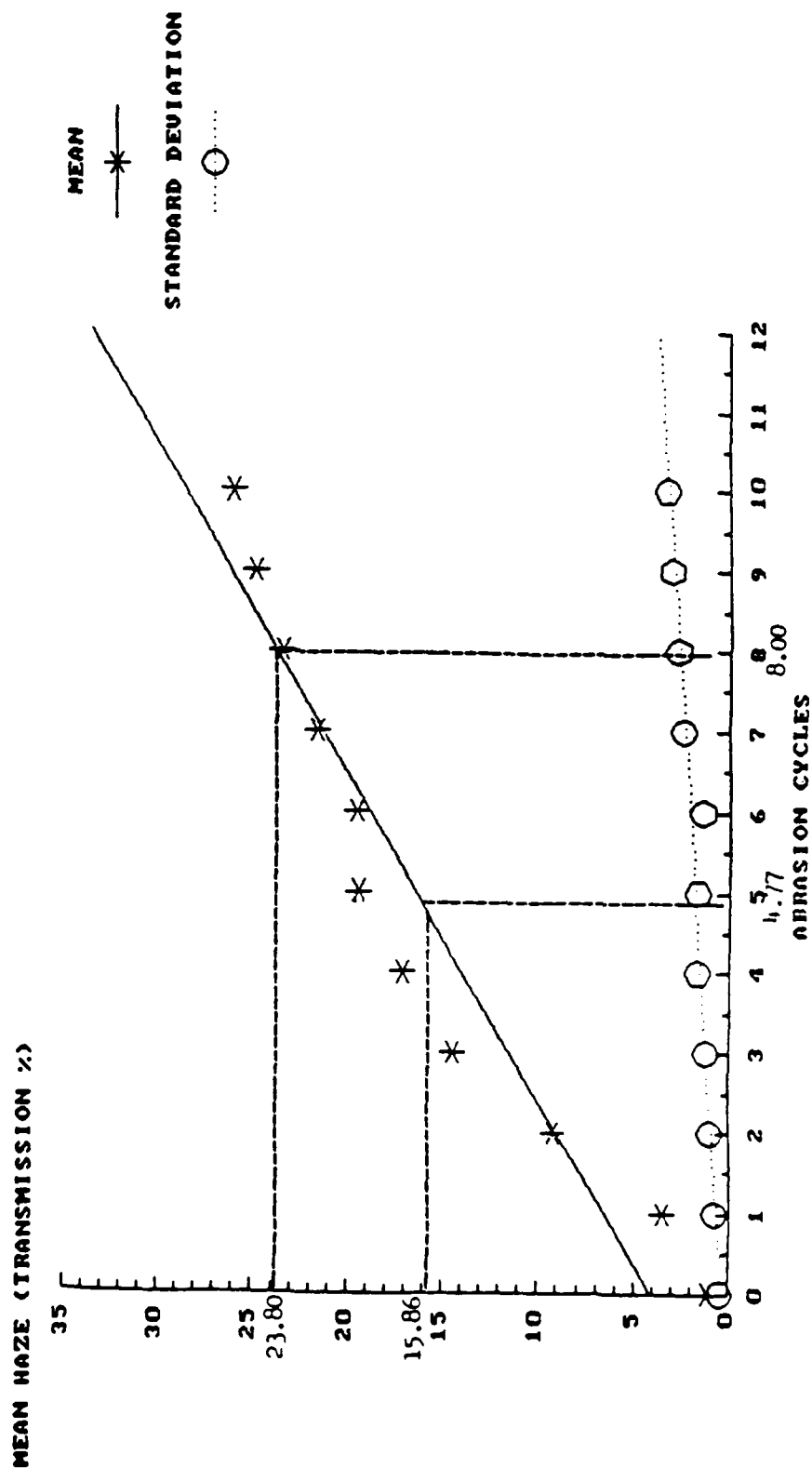
Concerning future work, we expect a new silicone hardcoat system to be available at some point, which will have even greater resistance to micro-cracking as a function of weathering and, in addition, have even better weathering than the LHP/LHC standard system which is in excess of three years in Florida and Arizona. Finally, some activity using UV curable systems is already underway; with respect to acrylics and polycarbonate systems, and are expected to be available also in the future.

FIG 1.
HAZE VS MILEAGE
100,000 MILE PROJECTION



FORD MOTOR COMPANY

FIG 2.
 MEAN TRANSMISSION HAZE VS. ABRASION
 CYCLES ON LENS TEST PLAQUES



SAMPLES #1-25
 CONTROL PLAQUES

90 DEGREE



20 DEGREE



TABLE 1

Plant Scale Samples

	<u>LHP100/LHC100</u>	<u>AS4000</u>
QUV (hours) microcracking adhesion delamination	500-1000 2000 -	> 3500 3000 3500
Xenon Arc (hours)	> 3000	> 3000
EMMA-NTM (Langleys) (MJ/m^2) microcracking adhesion	200,000 600,000	1,000,000 (11115) > 1,000,000 (>11115)
Florida (months) microcracking adhesion	9-14 > 36	24+ 24+
Arizona (months) microcracking adhesion	9-14 > 36	18 24+

● AS-4000 SHOWS SIGNIFICANT IMPROVEMENTS OVER LHC100

TABLE 2

AS-4000 PLANT SCALE SAMPLES

TRANSMISSION, COLOR, HAZE MEASUREMENTS VS WEATHERING AND TABER ABRASION

EXPOSURE	THICKNESS (IN)	% T	YI	% H	% H 500 CYCLES TABER
UNEXPOSED	1/16	92.4	.5	1.1	6.5
	1/8	91.6	1.2	2.1	3.7
	1/4	87.8	1.0	2.0	4.1
6 MO FLORIDA	1/16	93.3	.5	.6	NA
	1/8	91.7	.2	.5	NA
	1/4	89.2	-1.2	.8	NA
12 MO FLORIDA	1/16	93.6	.7	.8	3.4
	1/8	91.9	.5	1.0	3.0
	1/4	89.2	-1.0	1.0	2.9
18 MO FLORIDA	1/16	93.7	1.0	.7	4.0
	1/8	91.6	1.1	1.0	3.1
	1/4	89.4	-.3	1.2	4.8
24 MO FLORIDA	1/16	93.6	.8	.5	4.6
	1/8	90.8	1.2	1.6	6.4
	1/4	89.2	-1.0	1.8	6.0
1 MM LANGLEYS ENNA-NTN	1/16	91.3	1.5	7.1	NA
	1/8	91.2	1.6	5.9	NA
	1/4	89.4	.7	4.9	NA
6 MO ARIZONA	1/16	93.0	.6	.6	NA
	1/8	92.2	.1	.5	NA
	1/4	89.3	-1.2	.9	NA
12 MO ARIZONA	1/16	93.8	.5	.5	NA
	1/8	92.5	.2	.9	NA
	1/4	89.6	-1.4	1.0	NA
18 MO ARIZONA	1/16	93.8	1.0	.9	4.5
	1/8	92.2	.6	1.3	2.8
	1/4	89.7	-.9	1.3	NA
24 MO ARIZONA	1/16	93.6	1.0	1.3	4.8
	1/8	92.0	.6	1.9	4.7
	1/4	89.6	-.6	1.5	7.2

REFERENCES

- (1) Ford Motor Co. - The Aerodynamic Composite Headlamp -
August 1982 - AAMVC
- (2) Erion, J. - Development of a Minimum Level of
Acceptable Performance for the Abrasion Resistance
of Plastic Headlamp Lenses
August 1982 - SAE Lighting Committee
- (3) Kochanowski, J. and West, M. - Advancements in
Thermoplastic Automotive Forward Lighting -
1986 - ANTEC

F-4 WINDSCREEN - AN ALL COMPOSITE FRAME

Scott A. Speelman

Texstar, Inc.

F-4 Windscreen - An All Composite Frame

Scott A. Speelman
Texstar, Inc.

The F-4 fighter aircraft, which began service with the Air Force in the early 60's, is now expected to remain in service well beyond the year 2000. As well as extending the service life of the aircraft, the combat role of the aircraft is being extended to include low altitude missions. With the addition of these low altitude missions, the threat of a birdstrike increases. To improve pilot protection, the Air Force requested a one-piece, wrap around windscreen be designed and developed to replace the original three-piece design. Three main requirements were placed on the new design. First, the unit had to be able to withstand a 500 knot, 4 pound bird strike with no debris entering the cockpit. Next, the windscreen had to be compatible with a Heads Up Display, or HUD, and the third requirement was that the windscreen must be quickly changeable for easier maintenance. Adding new composite technology to existing impact-resistant transparency technology has resulted in all of these requirements being met, with an all composite frame.

Two previous programs led to the development of the all-composite frame. The T-38 composite bow frame request initiated all the work of integrating composites into the realm of transparencies. The second, and much more influential program, was the A-7 One Piece Windscreen and Bow Frame replacement program. This program, like the F-4, set out to replace the existing three piece windscreen and metallic arch with a one piece wrap around windscreen with a composite aft arch, but leaving the rest of the frame metallic. By meeting the 480 knot, 4 pound bird strike requirement, much knowledge was gained in understanding how to combine these two technologies. Having gained this understanding, the next logical step was to attempt the all composite frame.

The all composite frame assembly consists of the following components: aft arch or bow frame, left and right inside longeron, forward arch, left and right, forward and aft fairing supports, and a bulkhead plate. (See Figure 1.) The four basic materials used to construct these parts are S-2 Fiberglass fabric, S-2 unidirectional tape, Kevlar* fabric, and

*Kevlar is a registered trademark of E. I. duPont de Nemours & Company.

Kevlar unidirectional tape, all preimpregnated with a 250 degree Fahrenheit curing epoxy resin. The bow frame is the only component to use all four materials. The rest of the components use only the S-2 Fiberglass fabric or a combination of the S-2 Fiberglass fabric and unidirectional tape. Let us begin with a look at the bow frame.

The bow frame is the main component of the composite assembly. The main materials being used to construct the bow frame are the unidirectional tapes, with plies of fabric placed at calculated intervals to obtain a more even distribution of loading when that load is applied. The Kevlar materials are used for increased stiffness and toughness, while the fiberglass materials are used for strength. The usage ratio of Kevlar to fiberglass is approximately 2:1, while the usage of unidirectional tape to fabric is nearly 8:1.

The arch works in the following manner. When a birdstrike is sustained, similar to what this unit was required to withstand, over 100,000 pounds of force is instantaneously applied to the windscreen and arch. If the arch were designed to withstand this amount of loading, it would be extremely stiff and the windscreen would fail before the arch could begin to do its work. So that the windscreen and arch can work together, the arch has been designed to withstand approximately 30,000 pounds of load before first ply failure. Much of the rest of the energy is absorbed by more plies failing, along with the mounting brackets, called clevis brackets, pivoting outward under the load. By absorbing the energy this way, very little of the initially very large load is applied to the frame of the aircraft. This not only saves the pilot, but also saves on the replacement down time, if not the actual loss of the aircraft.

The rest of the frame, as stated earlier, is made of fiberglass fabric with or without unidirectional tape. Since these components see much less of the impact loads of a birdstrike but will be affected by flight loads and cockpit pressurization for flight, material strength, not stiffness, becomes the driving factor in material choice. The inside longeron is the only other component to use the unidirectional tape as a material component. Much of the tape used in the inside longeron is oriented 90 degrees to the length of the part to give strength to the part during the compressive action of a birdstrike.

To meet the requirement of quick changeability, two new systems had to be developed. The first of these involved sealing. Typically, wet sealants requiring 12-24 hours to set up

were used to seal the windshield to the frame. This made change-out time for the original side panels approximately 24-36 hours, not including changes or repairs to the center piece of glass. To meet the goal of a complete windshield change in 2 hours or less, a dry sealing system had to be created.

Several different materials were tested for compressability, producability, and compatability with the windscreen. By processing a medium durometer material into flat strips, bulbed pieces, and formed shapes, the sealing problem has been solved. These seals will eliminate the long time periods of waiting for the wet sealants to dry, but still would do nothing for the tedious process of handling and starting each individual washer and nut for attaching the windshield.

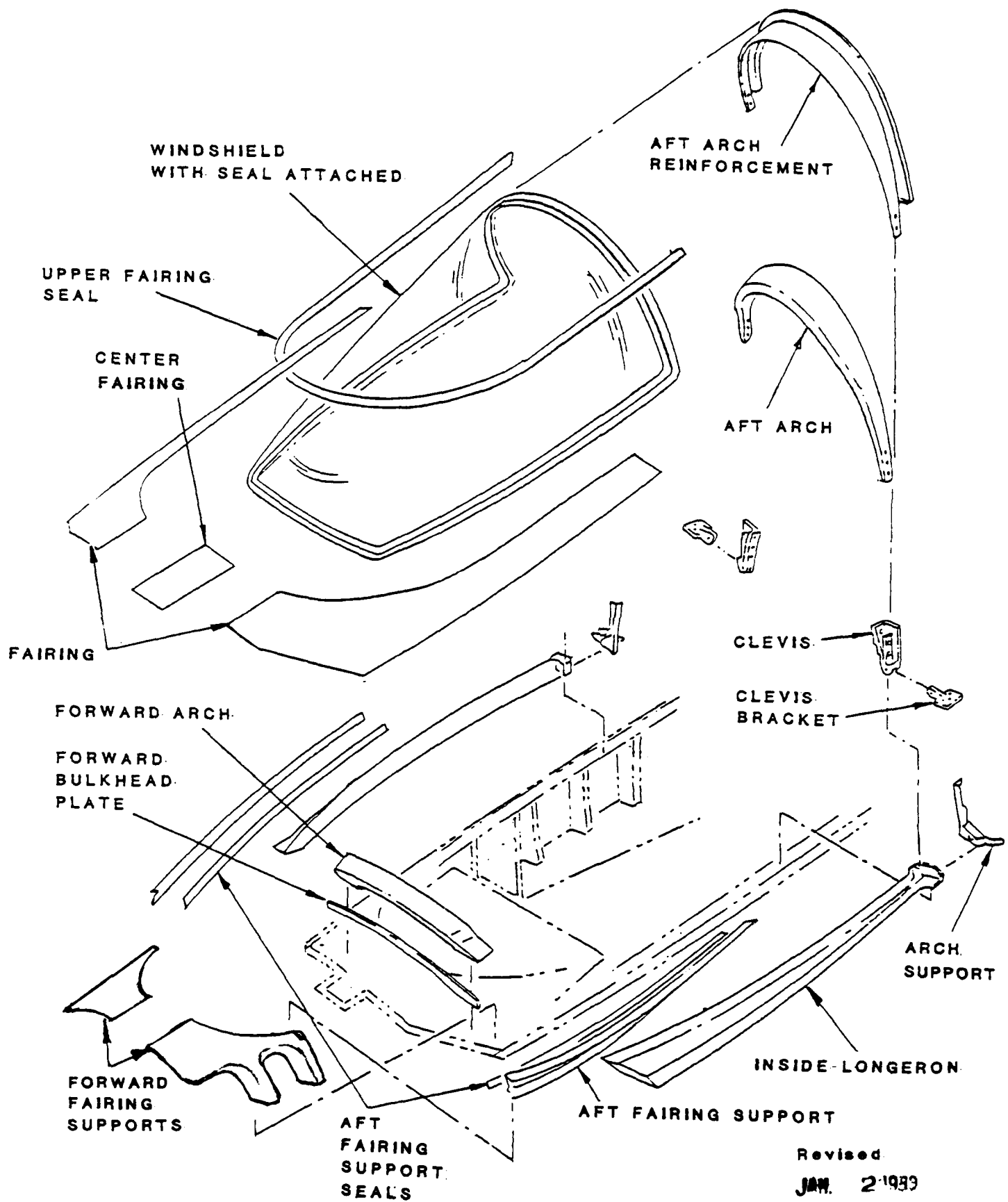
The bolt, washer, and nut attachment system also needed revision in order to meet the required change-out time. Removing the washer and nut attachment system would not only speed up windscreen change time, but would also reduce Foreign Object Damage, or FOD. One option, which was replacing them with nutplates, would add 3 times as many holes to drill into the composite, as well as weakening the composites and creating sealing problems. The fastener developed for this program is called a racetrack fastener, and basically is an internal nut with an external washer or bearing surface (see Figure 2). This fastener has ribs on the throat which, when pressed into the composite, set against rotation and hold the fastener in position during removal and reinstallation of the windscreen. The fastener also reduces the normal protrusion of the washer and nut system into the cockpit area from .313 inches to .080 inches.

To even further reduce FOD, a Thin-Head Rivnut*, produced by BFGoodrich Co., will be used in lieu of washers and nuts to attach the frame to the aircraft sill. This fastener, similar to a jack-screw, will be permanently installed in the sill before attaching the frame, thus eliminating the difficult task of starting nuts blindly.

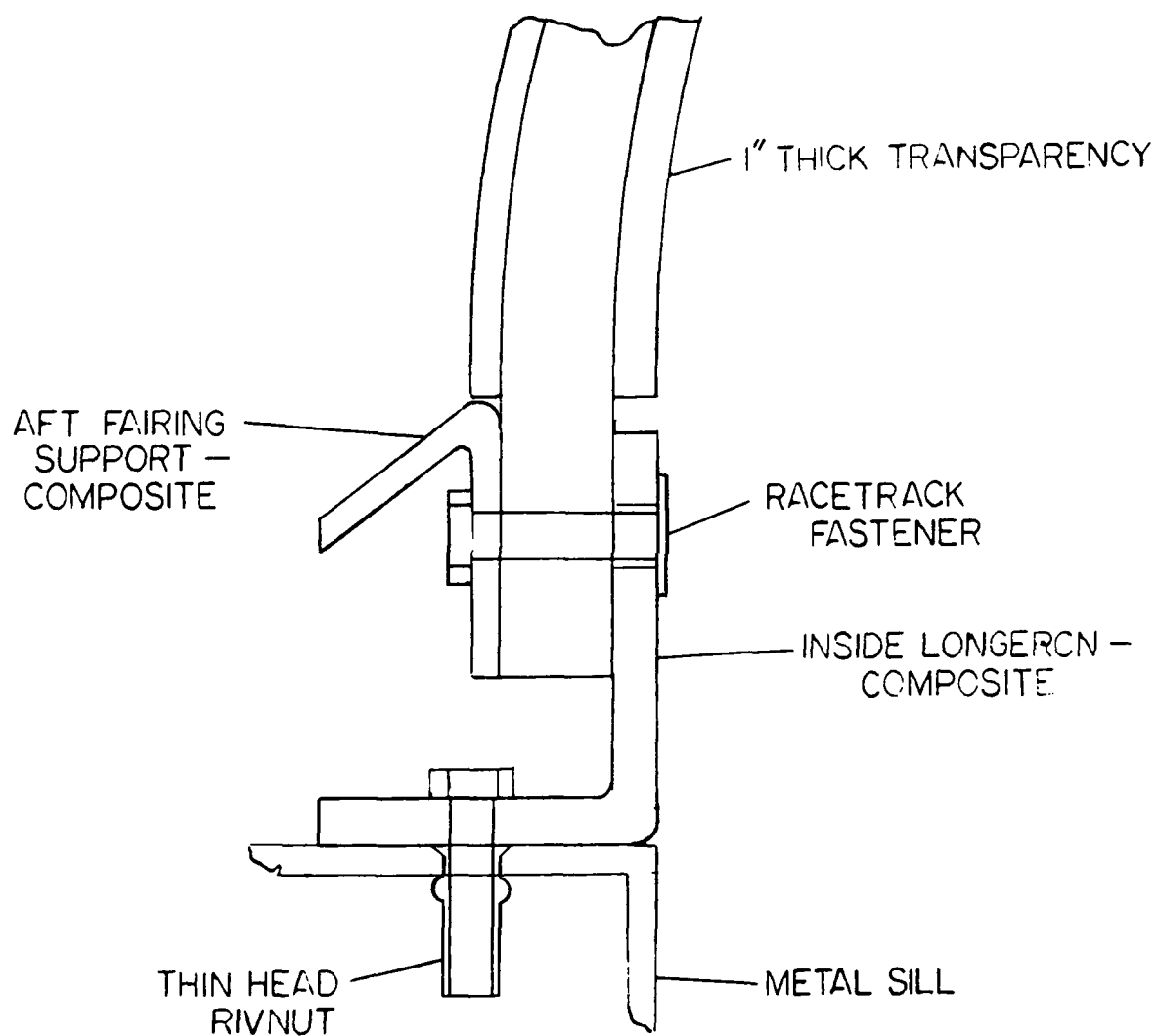
By learning from previous programs and developing new and innovative solutions to existing problems, Texstar, Inc. has successfully met the goals and objectives of the F-4 One Piece Windscreen Program. And by meeting those goals, the service life of the F-4 aircraft, as well as increasing mission capability and improving pilot safety, can now be extended well beyond the year 2000.

*Rivnut is a registered trademark of the BFGoodrich Co.

F-4 ONE PIECE WINDSCREEN



F-4 ONE-PIECE WINDSCREEN BASIC ASSEMBLY



VERSATILE APPLICATIONS OF POLYURETHANES IN
AIRCRAFT TRANSPARENCIES

Dr. William Lewis
Dr. Janet Andrechak

Swedlow, Inc.

VERSATILE APPLICATIONS OF POLYURETHANES IN AIRCRAFT TRANSPARENCIES

Dr. William Lewis
Dr. Janet Andrechak

SWEDLOW, INC.

ABSTRACT

The broad utility of polyurethanes in transparencies is due to their retention of desirable properties over an extremely wide compositional range. Relatively soft castable or sheet interlayer formulations provide elasticity, adhesion, manufacturing ease, and operability over wide temperature ranges. Intermediate hardness coatable or sheet protective liners are abrasion resistant and stable in exterior environments. Rigid sheets of polyurethane are being considered as high-temperature resistant exterior face plies. An overview of these current and developmental applications will be presented, with respect to chemistry, properties, and performance in aircraft transparencies.

INTRODUCTION

Polyurethanes are synthesized by condensation reactions between isocyanates and hydroxyl-functional compounds, as illustrated in Figure 1. Typically, diisocyanates and high molecular weight but liquid diols for flexibility, and short-chain diols for strength are combined in a single formulation. Examples of some commercially available raw materials are shown in Figure 2.

On a molecular level, polyurethanes are segmented copolymers. Their "soft segments" comprising various high molecular weight polyols are tied together and usually capped with isocyanate-functional materials in an initial stage, or "pre-polymer" reaction. These polyols form the "soft segment" of the polyurethane. The prepolymer may then be further reacted with chain extenders, typically low molecular weight diols, to form the urethane "hard segments". These hard segments give strength to the polyurethane through hydrogen bonding between the polar, closely spaced urethane linkages on adjacent chains. The relative proportions and degree of phase separation between the hard and soft segments on a molecular scale determine the bulk physical properties of polyurethanes. The phase separation is controlled by the polyol type and molecular weight, the compatibility of the monomers, the symmetry of the isocyanate and chain extender, the degree of hydrogen bonding, the monomer reactivity, and the temperature. Figures 3 and 4 illustrate these concepts: hydrogen bonding of the urethane hard segment, the alignment of the hard segments, and the phase separation of hydrogen-bonded hard segment groups.

With the addition of crosslinkers such as triols or polyisocyanates to a urethane system, the urethane physical properties shift from those of a thermoplastic to a thermoset. The degree of crosslinking affects the hardness, flexibility, toughness, and the thermal stability of the urethane polymer. Although added crosslinks disrupt the alignment of adjacent chains somewhat, they do not melt at high temperatures, in contrast to the inter-chain hydrogen bonds.

POLYURETHANE INTERLAYERS

Interlayer Applications

The traditional role of polyurethanes as interlayer materials has been intermediate between silicone rubbers and polyvinyl butyral resins (PVB). Urethanes are significantly less expensive than silicones, and have offered a wider service temperature range than PVB. Emerging needs within the aerospace industry require materials which will maintain their performance characteristics over the widest possible temperature range, such as silicones, but be cost competitive in the total manufacturing scheme.

Swedlow is developing new polyurethane materials to meet these emerging performance needs. Thermoset urethanes with effective additive stabilizers are being developed to meet the higher temperature use requirements. Urethanes are also being formulated with lower Tg values to extend the low-temperature serviceability of the interlayer. Lower modulus urethanes are being developed which may extend use of urethanes into laminate applications combining glass and plastic plies.

Physical Property Comparisons

As shown in Table 1, physical properties of current typical thermoplastic and thermoset urethane formulations range between typical silicone and PVB properties. PVB is low in cost and easy to process, but very limited in its service temperature range. Silicone has the widest temperature range, but is low in tear strength and toughness, difficult to process, sometimes marginal in adhesion, and low in stiffness for some applications. Polyurethanes, with their wide latitude of compositional variations and inherent toughness and adhesive qualities, can be formulated to obtain most of the desired balance of physical properties for interlayer applications.

The characteristics of three developmental formulations of polyurethanes prepared at Swedlow are presented in Table 2. As shown, we have extended the upper temperature range of thermoset interlayers, while maintaining most of the desirable low temperature performance of thermoplastic urethanes and silicones. We have also identified formulations with properties approaching silicones in modulus, to minimize stresses in glass/plastic laminates.

Manufacturing Issues

Polyurethane interlayers can be manufactured as thermoplastic sheets which are laid up, laminated, and formed. At Swedlow, thermoset interlayers are also processed using conventional "cast-in-place" processes. Approaches which will allow lamination of thermoset sheets are being developed.

Performance Data

The optics of properly formulated and manufactured polyurethane interlayers are outstanding, with none of the haze problems that plague some silicone formulations. Adhesion is also outstanding, with failure typically occurring cohesively within the interlayer at well over 1000 psi. Adhesion is maintained even at polycarbonate processing temperatures in excess of 300°F. Properties, as noted, extend over a wide range of formulations. Service life, based on accelerated tests, is expected to be outstanding.

POLYURETHANE SHEET AND COATABLE PROTECTIVE LINERS

Liner Applications

Thermoset polyurethanes can be used as exterior or interior protective layers or "liners" for aircraft transparencies. Such liners can protect the underlying substrate against abrasion and varying environmental conditions. In some applications, the liner protects a conductive coating on the exterior surface of the transparency.

The liner must be optically acceptable, exhibit heat stability, maintain adhesion to the substrate, resist erosion and resist static charging problems, in addition to protecting coatings and the substrate. The liner must maintain these characteristics while being exposed to all the rigors of weather and high speed flight.

Physical Property Spectrum

A general polyurethane liner formulation may consist of polyether diols and triols, an aliphatic diisocyanate, and a chain extender, such as 1,4-butanediol. By varying the percentage of hard segments and the molecular weight between crosslinks, it is possible to produce liner formulations covering a broad spectrum of physical properties. Table 3 presents a comparison of the physical properties of three typical formulations.

Although urethanes are properly viewed as tailorable polymers, trade-offs do occur. For example, a harder polyurethane formulation will in general have excellent weatherability and solvent resistance, but rain, hail, and dust erosion resistance may decrease as the resilience of the polymer decreases.

Manufacturing Issues

Polyurethane liners are typically processed to a thickness of about two to upwards of 20 mils. With the use of Swedlow proprietary technology, urethane liners can be prepared in sheet form and laminated. Alternatively, liners have also been produced using coating or casting techniques, which extend liner applications to compound-curved shapes.

Performance

Polyurethane liners maintain adhesion to ITO coated glass substrates at temperatures in excess of 200°F. Liner systems for protection of conductive coatings on plastics are emerging. Polyurethane liners of appropriate hardness show excellent resistance to rain, dust, fog, salt spray, cleaning solvents, and aircraft fluids. Where precipitation static buildup is anticipated, the bulk resistivity of the liner can be adjusted by proprietary methods to drain charge through to the underlying coating. Mar and abrasion resistance, and weatherability of properly formulated and stabilized liners are excellent.

HIGH TEMPERATURE RESISTANT EXTERIOR FACE PLIES

In aircraft transparency applications, there is a growing need for high temperature, weatherable, outer ply materials. GAC-590 is a transparent thermoset urethane engineered to meet these

requirements. Initially developed at Loral, it is currently being jointly developed by Loral and Swedlow.*

GAC-590 is a highly crosslinked urethane based on chemistry similar to the liners and interlayers discussed above. Its Tg and heat distortion temperature are unusually high, due to the combined effects of hydrogen bonding and a tightly crosslinked network. GAC-590 also exhibits good environmental stability, chemical resistance, abrasion resistance, and adhesion of coatings.

The physical properties of GAC-590 are presented in Table 4, with comparative data for acrylic and polycarbonate. GAC-590 is comparable to polycarbonate, and superior to acrylic in its high temperature properties. Its outstanding features are its chemical agent resistance, excellent weatherability, and abrasion resistance.

Further information will be given in a companion paper at this conference.

SUMMARY AND CONCLUSION

Using urethanes as building blocks, materials as soft as silicones or as hard as acrylics, with serviceability from -50° to 350°F, and outstanding weatherability and other properties have been formulated. Their use as interlayers, liners, or heat-resistant outer plies extends the range of options for material selection in aircraft transparency design, and helps to meet the emerging challenges in this dynamic industry.

*GAC-590 is a trademark of Loral Systems Group. In products sold by Swedlow, the material designation will be Acrivue 590.

FIGURE 1

REACTION OF ISOCYANATES AND ALCOHOLS TO
FORM URETHANES

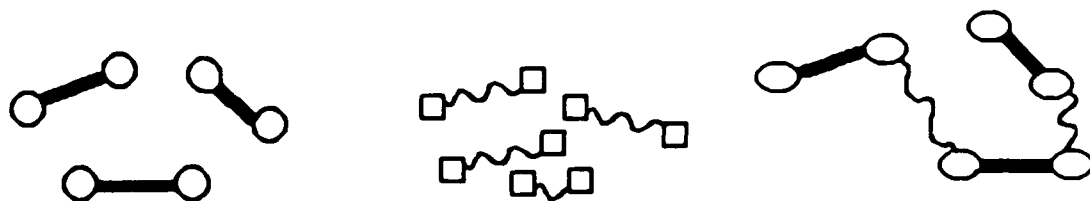
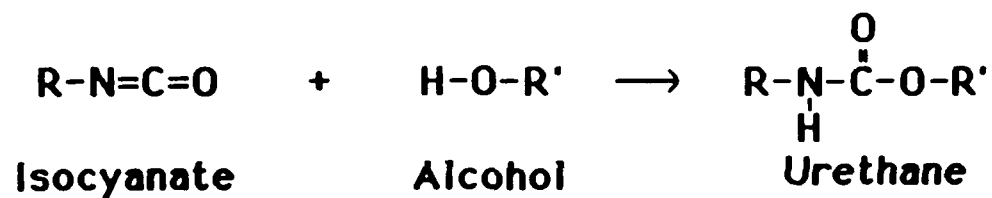
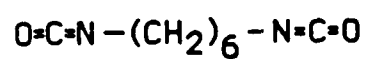
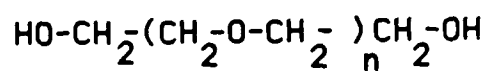


FIGURE 2

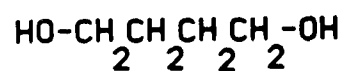
BASIC RAW MATERIALS FOR POLYURETHANES



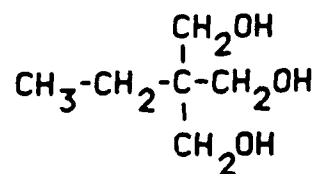
Hexamethylene
Diisocyanate



Polyether Diol



Butenediol



Trimethylolpropane

FIGURE 3

**HYDROGEN BONDING BETWEEN
URETHANE GROUPS ON ADJACENT CHAINS**

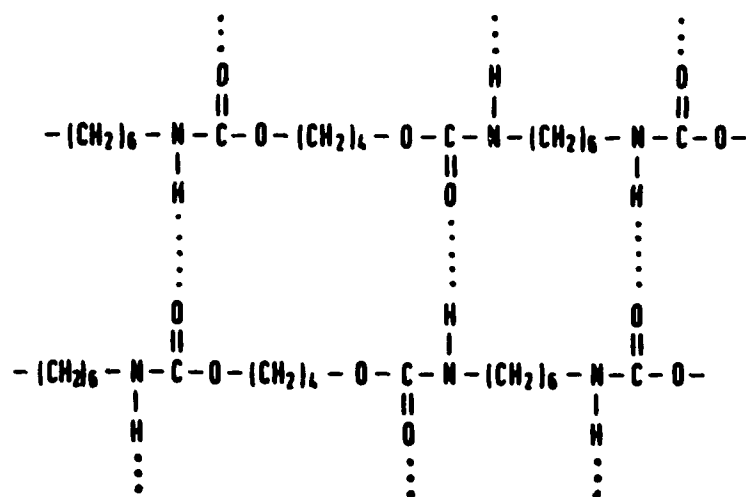
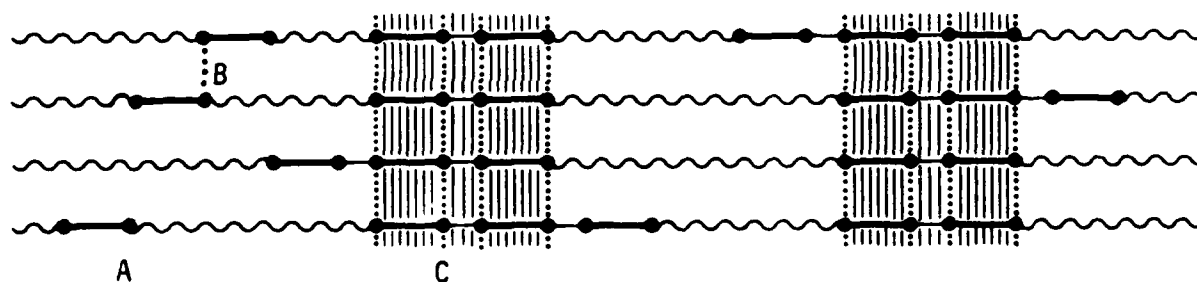


FIGURE 4
INTERCHAIN INTERACTION, ALIGNMENT AND
PHASE SEPARATION OF HARD SEGMENTS



A = Isolated Urethane Groups
B = Interchain Interaction (Hydrogen Bonding)
C = Phase-separated Hard Segments

TABLE 1
PHYSICAL PROPERTIES OF INTERLAYER MATERIALS

	PVB	PUR-1	PUR-2	SILICONE
Tensile Strength psi	3000-4500	1500-2500	3000-4500	350-800
% Elongation	180-250	350-600	200-350	300-600
Tensile Modulus 100% Elongation, psi	500-3000	500-1000	500-800	50-100
Tear Strength, P.I.T.	--	400-600	220-360	20-80
Shore "A" Hardness	54-98	70-85	80-95	25-60
Useful Service Range	0 to 150°F	-50 to 200°F	0 to 300°F	-100 to 350°F
Crosslinked?	No	No	Yes	Yes

TABLE 2
Properties of Developmental Thermoset
Polyurethane Interlayers

	SS-6845	SS-6864	SS-6865
Tensile Strength, psi	3500	1200	4000
Elongation, %	250	550	600
Tensile Modulus, psi	700	200	450
Tear Strength, pit	250	100	250
Shore A	85-90	55-60	55-60
Service Range	0-350°F	-40 to 350°F	-10 to 350°F

TABLE 3**Properties of Polyurethane Protective Liners**

	SOFT	MEDIUM (SS-6831)	HARD (SS-6858)
Tensile Strength, psi	2800	4500	5500
Elongation, %	225	180	150
Tensile Modulus, psi	500	1800	3500
Tear Strength, pit	95	450	1100
Shore "D" Hardness	31	62	67

TABLE 4
Physical Properties of GAC-590
Compared to Acrylic and Polycarbonate

	GAC-590	ACRIVUE 350	POLY- CARBONATE
Tensile Strength, psi	12,000	>9000	8400
Elongation, %	5	5	110
Flex Strength, psi	16,000	16,000	13,500
HDT, °F	285	238	280
Shore "D"	90	-	-
LT/Haze, %	91.6/1.0	92.0/1.0	89.1/0.5
Taber, 500 revs., Δ% Haze	3.0	35	37

T-38 COMPOSITE BIRD-IMPACT-RESISTANT-WINDSHIELD FRAME

S. J. Cieslak
F. N. Smith

Alcoa Technical Center

T-38 COMPOSITE BIRD-IMPACT-RESISTANT-WINDSHIELD FRAME

By

S. J. CIESLAK AND F. N. SMITH
ALCOA TECHNICAL CENTER
ALCOA CENTER, PA 15069

ABSTRACT

In November, 1988, Alcoa's Composites Manufacturing Technology Center was awarded a contract to complete the work of an original Sierra Technologies Corporation (formerly Sierra Composite Design) contract awarded by PPG Industries, Huntsville, Alabama, in April, 1987. The contract is to design and build 14 prototypes of a composite bird-impact-resistant-windshield frame for the Air Force T-38 jet trainer aircraft. A composite windshield frame was determined to be desirable to replace the cast-magnesium windshield frames now being used. The composite windshield frames would be better able to absorb the impact of a bird-strike, allow improved visibility, and offer other advantages over the metal frames.

Specific design criteria for the composite frames were identified in a Statement of Work prepared by the Air Force:

1. The main criterion was that the windshield and frame assembly must be capable of withstanding a four pound bird-strike at 400 knots (Kinetic energy at impact, 28,300 ft lb).
2. The frame must have consistent external dimensions, minimum weight, and maximum life.
3. Improved visibility for the crew over that of an experimental composite-reinforced cast-magnesium frame was necessary. This reinforced frame was developed to test the concept of composite frames.
4. Minimum cost was important.
5. Other criteria included ease of repair, improved maintainability, improved life span, corrosion resistance, and damage tolerance.

The design concepts for this project suggest that a "synergistic hybrid of fibers" would achieve a balance of strength, stiffness, and resiliency tailored to the structural character of the Bird-Impact-Resistant-Windshield transparent panel. Our design analysis dictated lower modulus materials for the primary structure, reinforced locally with a higher modulus fiber in regions of high loading.

INTRODUCTION

The Northrop T-38 Talon Aircraft continues to serve as the USAF's main supersonic trainer. When production ended in early 1972, approximately 1,200 T-38s had been delivered to the USAF. Original deliveries began in 1961. At the present time, over 800 T-38 aircraft are utilized which have an average age of 22 years.

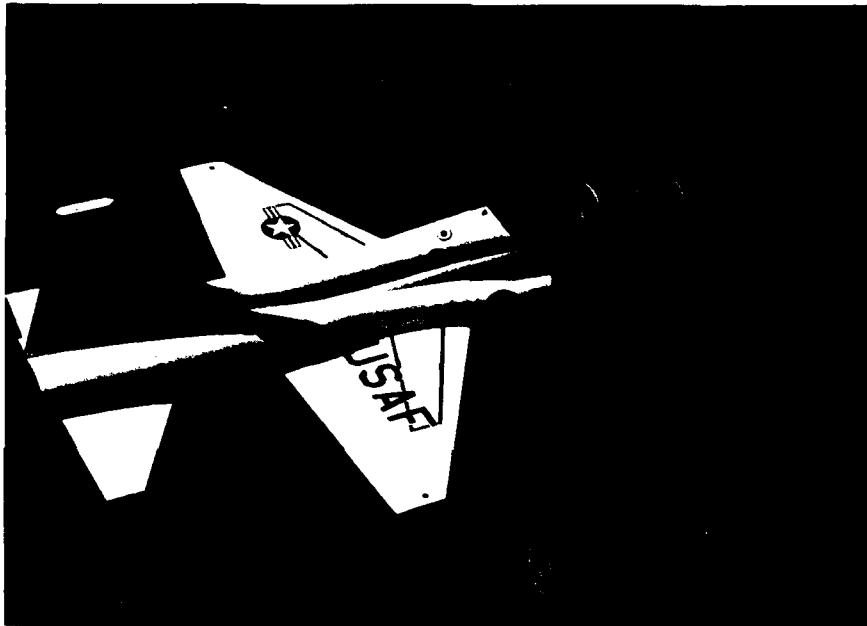


Figure 1

The T-38 Talon continues to serve the USAF training requirements.

The longevity of the T-38 has led to corrosion problems on the cast magnesium forward windshield frame. A Bird-Impact-Resistant-Windscreen (BIRW) has recently been developed for the T-38 consisting of the current cast magnesium frame with a composite aft arch reinforcement, and a laminated polycarbonate transparent panel. The composite aft arch (bow) reinforcement was necessary because the current cast magnesium frame does not provide sufficient impact resistance. As can be seen in Figure 2, an S-glass/Kevlar combination was added to the original magnesium bow as an interim solution. However, this interim solution will not meet the windshield life assembly objectives because of the progressive magnesium corrosion.

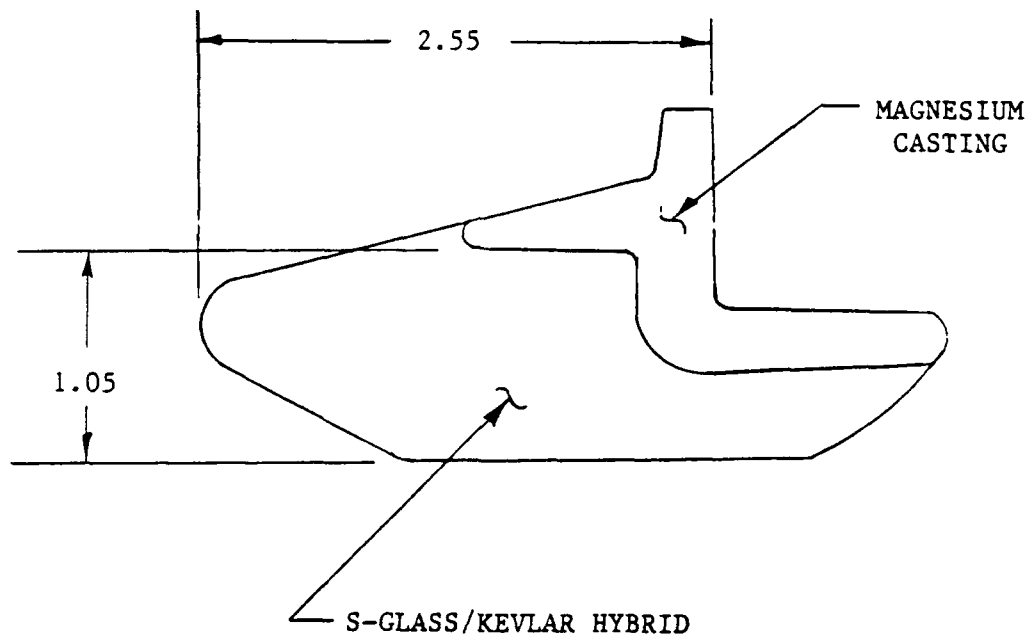


Figure 2

The S-Glass/Kevlar add on reinforcement to the cast magnesium windshield frame arch was based on work completed by the University of Dayton Research Institute (UDRI)

Air Force Composite Frame Program

In order to find a more long-term solution, the Fighter, Tactical, Trainer System, Program Management Division, Directorate of Material Management, San Antonio Air Logistics Center, Kelly Air Force Base, Texas, issued a Statement of Work in September, 1986 to develop an all-composite forward windshield frame, for the T-38.

Specific design criteria for the composite frames were:

1. The ability of the windshield and frame assembly to withstand a four pound bird-strike at 400 knots.
2. The frame must have consistent external dimensions, minimum weight, and maximum life.
3. Increasing the windshield assembly visual area over the interim aft arch reinforcement.
4. Other design criteria included minimum cost, ease of repair, improved maintainability, corrosion resistance and damage tolerance.

Contract Awards

Kelly Air Force Base awarded a contract to PPG Industries of Huntsville, Alabama, in April, 1987. PPG chose Sierra Composite Design as a subcontractor to design and build 14 prototype composite bird-impact-resistant-windshield frames. In November 1988, Alcoa Composites Manufacturing Technology Center was awarded a contract to finish the assembly of the composite prototype frames.

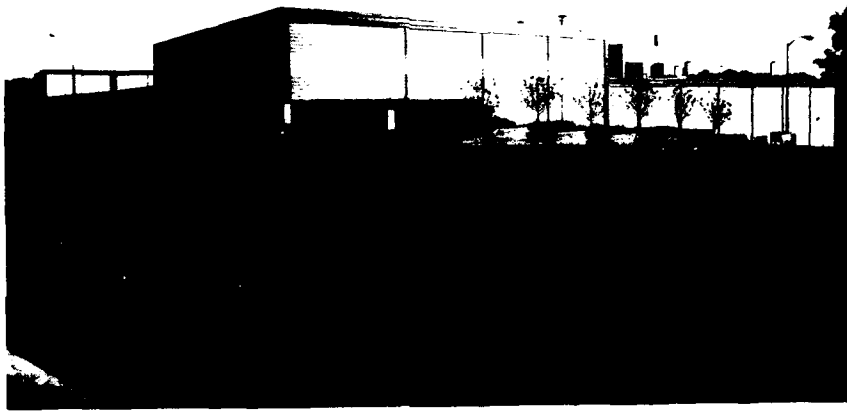


Figure 3
View of Alcoa Laboratories, Composites Manufacturing Technology Center Complex
near Pittsburgh, PA.

The current design is a multi-piece assembly consisting of the bow, outer skin, lower skin, bulkhead, fairing and metal fittings and attachment hardware.

Bow Design

The bow is the critical portion of the frame with respect to bird-strike loading. The hybrid composite/magnesium windshield frame bow (Figure 2) was used as a model for structural design of the all-composite bow because it successfully passed the 400 knot, four-pound bird strike test. The all-composite bow was designed to have bending and torsional stiffness approximating the hybrid design. The hybrid bow consists of AZ91C magnesium and Kevlar/S-glass reinforcement. In designing a new all-composite bow, a 100% Kevlar bow design was chosen over a hybrid laminate combination of Kevlar/S-glass due to an engineering

analysis that it could have better energy absorbing characteristics as well as simplify the manufacturing process and quality control requirements.

Prototype Bow Tests

Three development bows were built and attached to magnesium frames. Virgin transparencies were installed and the assemblies were subjected to the bird-strike tests at PPG. Tests were completed in June, 1987. The three bow designs were "standard," "soft," and "stiff" bow designs. All three designs were successful from a physical damage standpoint. From a performance standpoint, the "stiff" bow was chosen as the T-38 bow design with minor adjustments made in the section properties based on a deflection analysis.

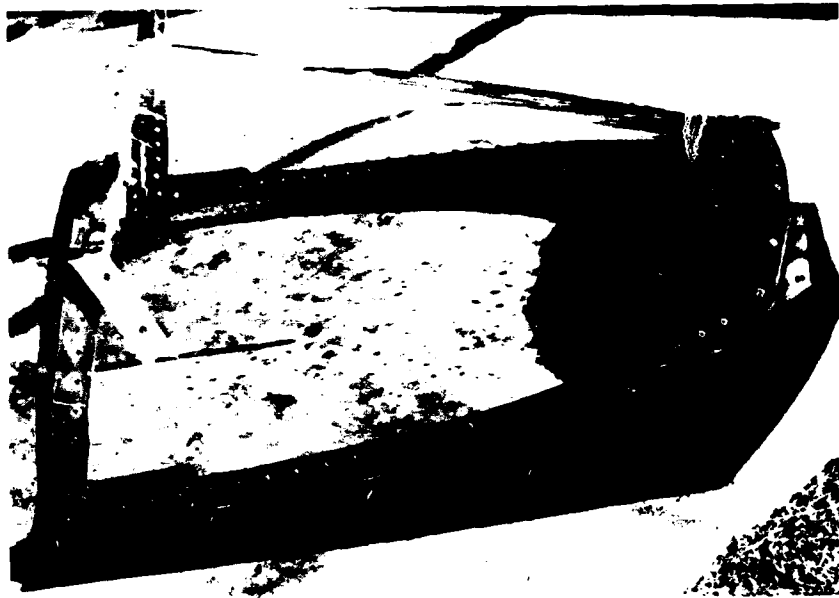


Figure 4
One of the prototype bow assemblies after a PPG bird strike test.

The frame, outer skin, lower skin, bulkhead and fairing were designed using graphite epoxy based on cabin pressure loads.

Pre-Prototype Design Summary

As a result of design reviews with Kelly AFB, Sierra Composite Design, and PPG personnel, the current all-composite windshield frame is expected to meet the original design goals. Figures 5 and 6 show the installation of the frame and the frame/transparency on a T-38 during preliminary fit checks.

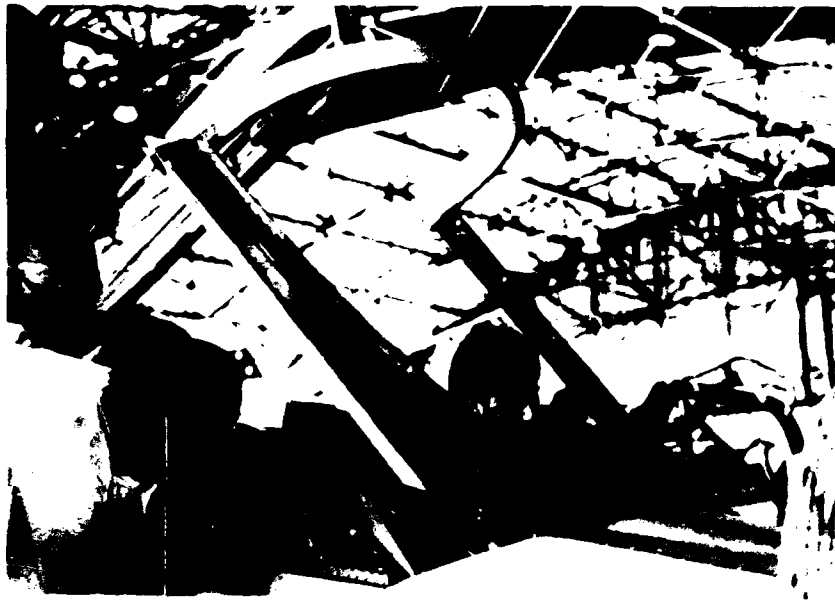


Figure 5
The all-composite bow is bolted to the bulkhead hinges of a T-38.



Figure 6
The bird-impact resistant-windscreen (BIRW) and frame installed on a T-38.

The general geometric configuration is maintained. The elimination of the vertical flange on the bow and the doubler on the pressure bulkhead must be reviewed for their service impact.

The most critical loading condition is the impact of a four pound bird at 400 knots. The development tests have shown that the bow design presented here is capable of withstanding those loads. The remainder of the frame is a relatively straightforward design but must still be reviewed as a result of obtaining information from the T-38 loads document.

The visibility for the crew is significantly improved over that available with the hybrid reinforced magnesium bow. It does not provide the level of visibility available with the magnesium bow alone. However, that bow will not meet the load requirements.

The all-composite frames will be fabricated in a dimensionally stable composite tooling system to produce dimensionally uniform parts.

The use of large scale co-cured parts to minimize the parts count and the secondary bonding requirements will result in minimal production costs. Figure 7 shows the bow frame assembly, bulkhead doubler and fairing.



Figure 7
All-composite windshield frame components.

The composite parts are designed to be readily repaired at any service center with facilities to perform "in situ" bonding. The damage associated with a major bird-strike incident will require replacement of the frame and transparency.

Development costs have been reduced by using the data obtained by the UDRI study and by drawing on the design experience of Sierra Composite Design.

Maintainability, life, corrosion resistance, and damage tolerance have all been improved by using appropriate composite materials for the frame.

A complete weight study has not been completed. Initial calculations show that the composite bow is 47% lighter than the UDRI reinforced bow. The remainder of the frame will, after final design, result in a reduction of weight for the complete assembly.

The pre-prototype design phase has been successfully completed. Alcoa and PPG Industries are continuing the program to manufacture the bird-strike and flight test frames.

Current Prototype Production Status

The fabrication of the composite frames is underway at Alcoa's Composite Manufacturing Technology Center, Alcoa Center, Pennsylvania with completion of all frames expected by 89/03/31. The frames are an assembly of an outer skin/bow, inner skin, and bulkhead doubler. Figure 8 shows the underside view of the outer skin/bow. The aluminum joints at the base of the photo provide hard attach points.



Figure 8
Underside of all-composite frame with fairing and bulkhead doubler in foreground.

The fabrication plan divides the work force into five teams, each responsible for one component or bonding. This approach maximizes the learning curve benefit and ensures on-time delivery of the frames and fairings.

Materials/Method of Assembly

The materials used in the frame assembly are fiber-reinforced organic matrix composites. The outer skin is an eight-ply laminate of graphite/epoxy fabric. The bow fabrication is incorporated into the outer skin prior to curing. The bow is a 77-ply laminate, consisting of aramid/epoxy fabric and tape. The outer six aramid/epoxy plies are wrap-around plies within which the aramid/epoxy fabric and tape plies are stacked. Aluminum support members are placed at the feet of the bow during lay-up. Figure 9 is a plan view of the composite design.

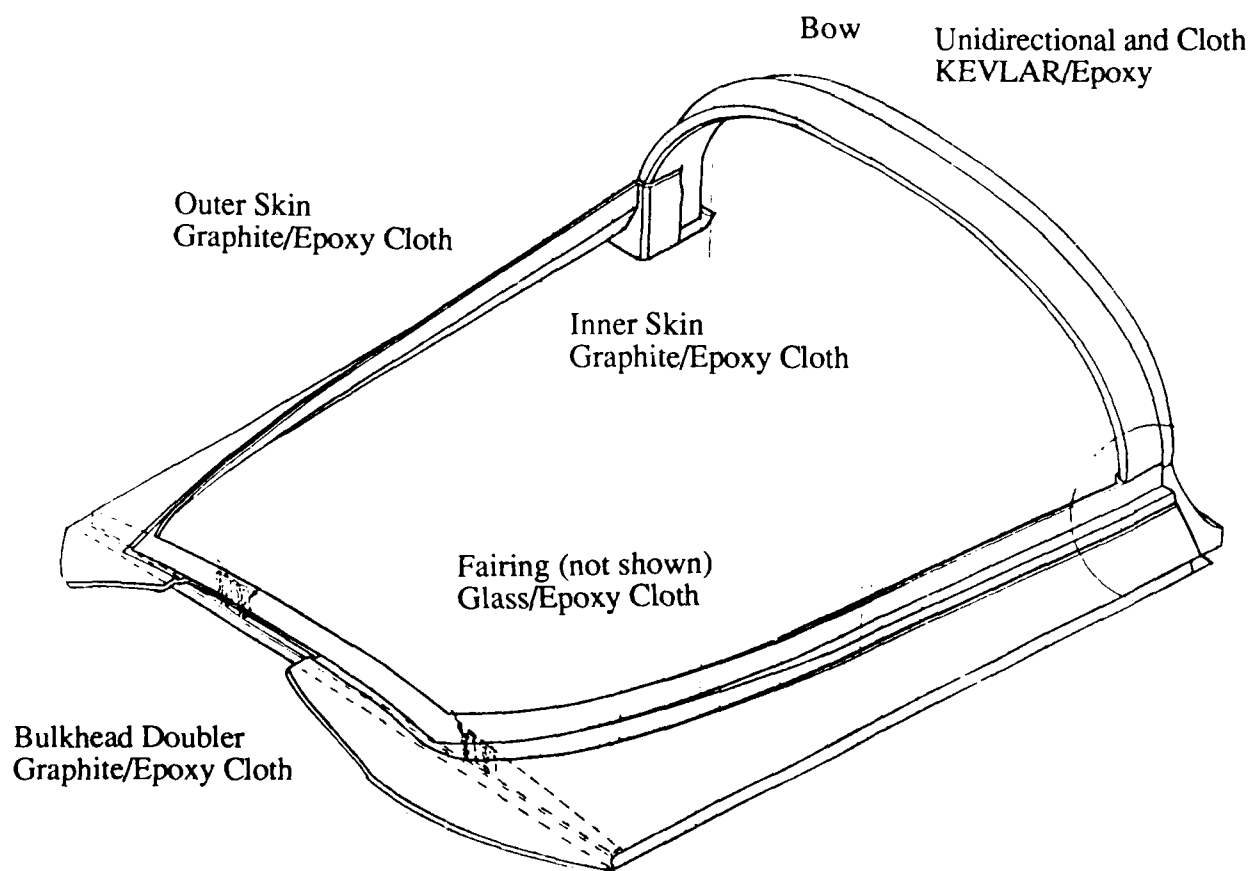


Figure 9
All-composite frame diagram.

The inner skin and bulkhead doubler are eight-ply laminates of graphite/epoxy with exterior surface plies of fiberglass/epoxy. The fairing is 12-ply fiberglass/epoxy laminate. The frame assembly is bonded with a matte type 250°F adhesive.

The current technique for fabrication of the composite frames is hand lay-up. Conversion to successful production depends on incorporation of automated processes to reduce the labor required to fabricate each frame. The use of a Gerber table for ply cutting and automatic tape laying for the bow plies are two strong candidates for automation. A completed frame/transparency assembly can be seen in Figure 10.



Figure 10
A completed frame/transparency assembly.

Bird-Strike Testing

The current development program includes bird-strike testing at PPG Industries' facility in Huntsville, Alabama. The windshield assembly must withstand the impact of a four-lb bird at a velocity of 400 knots at each of four locations. Six bird strike tests are required, four at ambient temperatures and two at 200 \pm 15°F. The primary test data are high-speed (5000 frames/second nominal) motion pictures generated from two cameras positioned to obtain an unobstructed view of the inside of the windshield assembly. A third camera is positioned to obtain a side view of the windshield assembly. Bird-strike tests are scheduled for late January, 1989.

Flight Testing

Flight testing will be conducted by the Air Force after a prototype fit demonstration and flight certification. The prototype windshield assembly will remain on the aircraft for a minimum of 25 hours during which operational records, the condition of the windshield assembly, and air crew comments will be tracked and recorded by the Air Force. Once flight certification is obtained, operational test and evaluation will be initiated. Five additional windshield assemblies will be installed on operational T-38 aircraft for a period of six months.

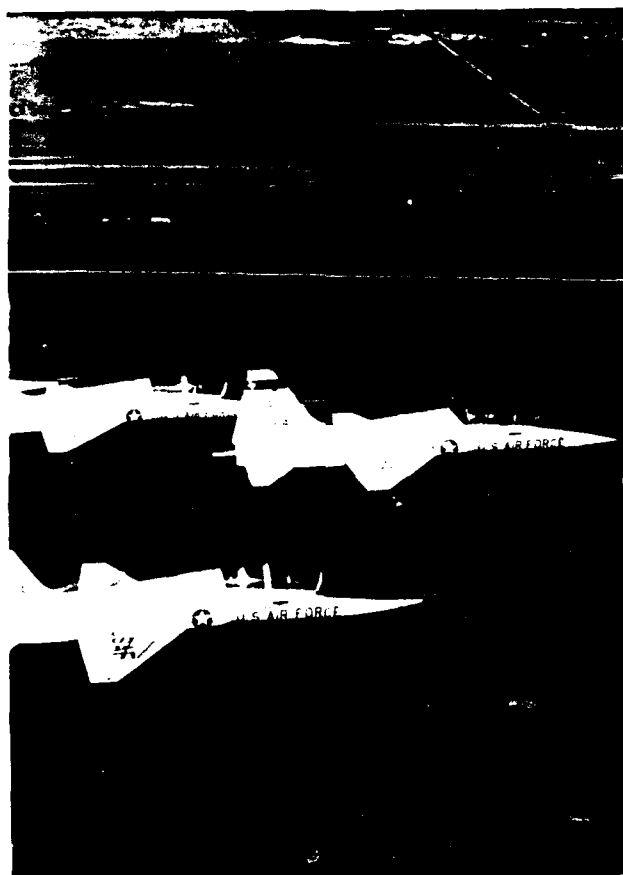


Figure 11
Three T-38's fly a mission near Reese AFB.

Summary and Conclusion

An all-composite windshield frame for a T-38 aircraft has been designed and is currently in the prototype production phase at Alcoa. PPG Industries will test the prototype frames at its bird-strike test facility in Huntsville, Alabama. Upon successful completion of the test program, flight testing will commence. Given successful manufacturing, bird-strike and flight testing, it is expected that a plan to retrofit the T-38 fleet in the early 1990s will take place.

References

1. "Statement of Work for Development of T-38 Composite Forward Windshield Frame," Fighter, Tactical, Trainer System, San Antonio Air Logistics Center, Kelly Air Force Base, Texas (1986 September 05).
2. Jacobsen, R. A., "T-38 Composite Windshield Frame Pre-Prototype Design Report - All-Composite Frame for T-38 Forward Windshield," Sierra Composite Design, Sparks, Nevada, (1987 June 30).
3. Jacobsen, R. A., "T-38 Composite Windshield Frame First Interim Report - All-Composite Frame for T-38 Forward Windshield," Sierra Composite Design, Sparks, Nevada (1987 September 01).
4. Salls, M. A. "T-38 Composite Windshield Frame Prototype Design Report - All-Composite Frame for T-38 Forward Windshield," Sierra Composite Design, Sparks, Nevada (1988 June 20).
5. "Fabrication of Prototype Hybrid Composite Arch Reinforcement for the T-38 Aircraft," UDR-TM-85-20, University of Dayton Research Institute, May, 1985.

NEW LOW VOLTAGE HEATING ELEMENT DESIGN FOR
AIRCRAFT TRANSPARENCIES

Charles R. Graham

PPG Industries

Title: New Low Voltage Heating Element Design for Aircraft Transparencies

Author: Charles R. Graham
Senior Engineering Associate
PPG Industries
Glass Research & Development

Abstract:

A major milestone has been achieved in the development of a new low voltage heating element for aircraft transparencies which offers superior performance to conventional systems. An innovative design concept will be described that permits significant improvement in optical quality at de-icing power densities, an important feature since "hot optics" distortion is a characteristic of low voltage heated aircraft transparencies which use resistive wire heating elements.

The new heating element design incorporates a fine mesh electroformed metal grid which combines high visible transmittance and low electrical resistivity with inherent uniformity in power dissipation. Collectively, these attributes provide a transparency which exhibits the optical clarity of a transparent conductive film and the de-icing capacity of a conventional resistive wire unit.

This technical report will describe basic concepts in the design of low voltage heating elements for aircraft transparencies, with the primary focus being directed towards factors that affect heating performance and optical clarity. The mechanisms which contribute to "hot optics" distortion phenomena will be described in terms of relevant physical properties of the heating element and interlayer materials. Depending upon the configuration and dimensions of the heating element, thermally induced gradients in the interlayer's refractive index can have a pronounced effect upon the observed degree of optical distortion. This effect can be enhanced or minimized by careful selection of key design parameters. It will be demonstrated that the unique design of the new heating element will meet required performance levels while at the same time minimizing the "hot optics" distortion effects.

1.0 Introduction

For over twenty years, PPG has served the aircraft industry with three types of heated aircraft transparency heating element designs: NESAS[®] coating (chemical vapor deposited pyrolytic coating), NESATRON[®] coating (vacuum deposited thin film), and AIRCON[®] transparency (sewn resistive wire). Each product has been designed to integrate a heating element into the aircraft transparency design to support the necessary de-fogging and de-icing heating function and at the same time comply with the demanding structural and optical performance specifications of the unit.

In this technical report, the primary focus of attention will be directed toward the design of heating elements which specifically support the class of aircraft having low voltage aircraft power distribution systems (typically 28 volts DC). At this voltage level, a low resistance heating element capable of carrying high current loads would be necessary to achieve the power density requirements.

Ideally, a transparent conductive film heating element would be highly desirable. Unfortunately, a conductive thin-film meeting the requisite resistivity criteria would also be exceptionally thick, such that the luminous transmittance of the transparency would be well below the 70% minimum requirement. Thus, the only realistic approach to accomplish the low resistance design goal is to utilize very thin resistive wire heating elements spaced sufficiently apart to gain adequate transmittance.

The presence of a resistive metal heating element embedded in the interlayer material introduces optical performance design issues that are not present in the design of the transparent conductive heating elements.

Several key factors in the design of the basic transparency contribute to minimizing optical distortion, when no power has been applied to the heating element. Although these design factors are an important concern for the overall optical performance of the heated aircraft transparency; the primary design issue addressed by this report will be the optical distortion uniquely induced by applying electrical power to the heating element.

This technical paper describes the basic mechanisms as to how and under what conditions the heater element will affect the optical performance of the transparency. Technical solutions will indicate how these effects can be minimized in the design of the present resistive wire heating element or by a new approach to utilize a fine mesh resistive metal heating element.

2.0 Low voltage heated aircraft designs

In terms of the critical task of heating the outboard glass surface, the resistive metal heating element emulates the uniform heating characteristics of a transparent conductive film quite well. In terms of the localized heating of the interlayer material, the hot metal embedded in the interlayer can generate uniquely shaped heating profiles which can differ significantly from the uniform heating profile produced by the transparent conductive film heating element. In some cases, these heating profiles can induce severe thermal gradients which can affect the optical clarity of the transparency by

modifying the interlayer material's index of refraction. This type of optical distortion is commonly referred to as "hot optics" distortion.

The critical design issue is the development of a resistive metal heating element configuration which can emulate the uniform heating characteristics of the transparent conductive film on both a localized and a global basis.

2.0 Hot optics distortion effect

3.1 Description

One critical measure of optical performance of a transparency is the relative degree of optical distortion (optical clarity of a viewed object). When the basic conditions for hot optics distortion are present, the result is a severe degradation of the optical clarity of viewed objects when the power has been applied to the heating element. Upon closer examination, the presence of index of refraction gradients in the interlayer material are observed at the interface between the interlayer material and the hot metal elements.

3.2 Basic physical mechanisms

A necessary condition for the presence of hot optic distortion is the existence of a relatively large temperature differential between the surface temperature of the resistive metal heating element and the ambient temperature of the interlayer material in close proximity to the heating element. The localized thermal gradients, resulting from this temperature differential, will produce corresponding gradients in the interlayer's density and index of refraction. The severity of the index of refraction gradient is directly proportional to the severity of the hot optics distortion.

Also, the absence of these thermal gradients will be consistent with the absence of hot optics distortion, thus the factors that contribute to producing these thermal gradients should be considered in the design of the resistive metal heating elements.

The presence of large temperature differential is a function of the interlayer's thermoplastic physical property attribute, the relatively low thermal conductivity, the ambient temperature, and heating element's temperature (function of power density). This functional relationship can be defined in terms of the power density and the relative separation (or isolation) of the individual heating elements from adjacent heating elements or other heating sources.

In principle, for a given heating element separation, there exists a critical power density level; when exceeded, the hot optics distortion effect will be present. This power density optical distortion threshold value will increase as the relative heating element separation is reduced. In effect, the more heating profiles from adjacent heating sources overlap and re-inforce, then there is less opportunity for the thermal gradients to develop.

3.3 Minimization measures

The design objective would be to increase the power density optical distortion threshold above the maximum power density requirement for the heated transparency.

For new or revised product design applications, the resistive wire spacing can be minimized thus increasing the power density threshold to a point where hot optics distortion can be significantly reduced. It should be noted that any adjustment in the resistive wire separation will also require a corresponding change in the wire resistivity to assure the bus to bus resistance specification is maintained. In practice, there may not be sufficient latitude within the resistive wire design parameters to assure the optical spacing and still achieve the power density specifications.

In the fine mesh resistive metal heating element case, an additional factor will significantly contribute to increasing the power density threshold to the necessary level. Differing from the parallel resistive wire elements, the fine mesh has a metal cross member equally spaced with the current carrying elements (grid-like pattern).

In a resistive circuit network, current flow will follow the path of least resistance and due to the symmetry of this network, there will be little or no current flow in these cross members. These elements will still contribute significantly to heating the interlayer material by becoming an additional source of heating, since the metal in the cross member is a very efficient thermal conductor.

In one test, a resistive wire and a fine mesh resistive metal heated aircraft transparency, having the same power requirements, were compared. For both heaters, the power density level (de-icing) and the spacing of the electrical current carrying elements were effectively the same. The hot optics distortion was present in the resistive wire heating element design, but not in the fine mesh resistive metal heating element design. In another test, the previous resistive wire heating element design was re-designed to minimize the resistive wire spacing which resulted in a similar hot optic distortion reduction improvement.

4.0 Heating element design approach

4.1 Resistive wire heating element

The basic design approach used for many years for PPG's AIRCON resistive wire heating element product has been to precisely sew a very fine resistive wire into the surface of an interlayer mat. The wires are sewn, in a sinusoidal pattern, adjacent to each other between two busbars, the heating element is electrically equivalent to a large set of parallel resistors. The determination of the bus to bus resistance for the resistive wire heating element is a function of the metal's wire resistivity, distance between the busbars, width of busbar, and number of wires.

4.2 Fine mesh resistive metal heating element

This fine mesh resistive metal heating element would be fabricated by high precision electroforming techniques to form a grid-like pattern. This unique approach offers design options which can minimize the impact of the resistive metal heating element on the optical performance of a heated aircraft transparency.

The fine mesh resistive metal heating element design concept is presently at the prototype development stage at PPG Glass R&D, Harmarville, PA. Fine-line large format photolithography imaging techniques are used to form the basic electroform mold in very thin photoresist which has been laminated on a stainless steel mandrel. The unique pattern imaged as the electroform mold is defined as a symmetrical network of inter-connecting circles and arcs.

The bus to bus resistance for a fine mesh resistive metal heating element is a function of the pattern resistivity. In this context, the pattern resistivity is an empirically determined measure similar to the sheet resistivity measure for a transparent conductive thin-film and expressed in the same terms (ohms per square). Pattern resistivity is a function of metal's volume resistivity, line width of individual elements, electroform thickness, pattern style, and pattern density. Once the minimum pattern density (lines/inch) which can increase the power density threshold beyond the maximum power density requirement has been determined, then the parameters to achieve target pattern resistivity can be established. There is sufficient latitude in these electroforming parameters (metal selection, thickness, and line width) to obtain a broad range of pattern resistivities.

4.3 Non-rectangular shaped heating elements

The cross-sectional area to be heated in many transparency designs require a non-rectangular shaped layout for the heating element. To assure uniform power density distribution (or some unique heating profile), incremental adjustment in the heating element's bus to bus resistance would be required to account for the change in the distance between busbars. Extra attention will be required to assure that the method to adjust the bus to bus resistance does not introduce the conditions for hot optic distortion.

The usual technique to vary the bus to bus resistance, for resistive wire heating elements, is to select combinations of wire size, wire resistivity, or wire spacing. The incremental change from one zone to another is as small as possible to assure uniform heating as well as minimum impact on aesthetic appearance.

In principle, several technical approaches have been discussed to control the processing conditions which can produce a fine mesh resistive metal heating element. The design objective would be to attempt to maintain the same pattern density and vary the parameters that control the pattern resistivity in the following order of preference: metal resistivity, electroform thickness, line width, pattern style, and/or pattern density.

5.0 Conclusion

This paper's discussion on the design of resistive wire heating elements and on physical mechanisms that produce hot optics distortion has given some insight on why hot optic distortion is present in some heated aircraft transparencies and not in others.

The research design approach of the fine mesh resistive metal heating element is one technique to bridge the technology gap between the resistive wire and transparent conductive thin-film heating element by offering the positive attributes of both technical approaches.

Acknowledgements:

I wish to acknowledge the excellent technical contributions of R. L. Emmert and J. E. Simpson in this research project effort.

SESSION III

UNDERSTANDING CURRENT MATERIALS (PART A)

Chairman: K. Armstrong
British Airways
Middlesex, England

Co-Chairman: B. S. West
University of Dayton
Dayton, Ohio

Coordinator: B. L. Boman
McDonnell Aircraft Co.
St. Louis, Missouri

WEATHERING OF PLAIN AND COATED POLYCARBONATE:
A COLLABORATIVE STUDY CARRIED OUT BY TECHNICAL PANEL PTP3
OF THE TECHNICAL COOPERATION PROGRAM

Peter Burchill
National Research Laboratory

W. B. Moniz
Naval Research Laboratory

Weathering of Plain and Coated Polycarbonate: A Collaborative
Study Carried Out by Technical Panel PTP3 of The Technical
Cooperation Program

Collated by:

Peter Burchill*
Materials Research Laboratory
Ascot Vale
Victoria 3032
Australia
and
W. B. Moniz
Chemistry Division
Naval Research Laboratory
Washington, D. C. 20375-5000

Abstract

In 1981 an international collaborative program was set up to assess the performance of polycarbonate then available as plain sheets and with an abrasion resistant coating. Plain and coated sheets from General Electric Corporation, USA (LEXAN) and from Bayer, Germany (MAKROLON) were exposed to a tropical environment in Queensland, Australia. Various properties were measured at laboratories in Australia, Canada, UK, and USA. The coating provides considerable protection to the polycarbonate towards abrasion as assessed by a wiper test. Uncoated material showed surface damage after 2000 strokes while coated material did not show similar damage until 20000 strokes. The coating on LEXAN was assessed as slightly superior to that on MAKROLON. However, after as little as 12 months weathering there was considerable damage to the surface of the uncoated polycarbonate such that abrasion resistance was not measured, while the coated material had a blotchy appearance suggesting the coating was beginning to detach. Losses in elongation to break, in craze resistance, and in rain erosion resistance were also found. The coating, though, appears to slow down the degradation of the polycarbonate in that yellowing occurs less readily. Overall, the surface coatings evaluated did not possess adequate durability nor provide long term protection for the polycarbonate. Surface material in the weathered sheets was analyzed for changes in molecular weight and UV absorber content and depth profiles obtained showing that degradation is confined to a layer only 50 μm thick. A comparison with a polycarbonate weathering trial set up in 1976 showed that no improvement had occurred in stabilizing this polymer against photo-degradation.

*Visiting Scientist at NRL, 1988-89, under the Navy Exchange Scientist Program

INTRODUCTION

In 1981, panel PTP-3, (Organic Materials) of The Technical Cooperation Program (TTCP) recognized that an assessment of the properties of commercially available polycarbonate sheet would be a worthwhile subject for an international collaborative study. The major attractions of polycarbonate are its transparency, and its resistance to impact over a wide range of temperature from sub-zero to over 100°C. However, serious deficiencies were noticed very early in its commercialization. It is more easily scratched than polymethylmethacrylate (a material it would replace), it is subject to environmental stress cracking, and it is degraded by sunlight. Over the years manufacturers achieved better control over molecular weight, and found methods to improve color, weatherability and scratch resistance. This material now is important in glazings, as visors and in riot shields.

Over the period 1982-1986, the TTCP study assessed the environmental performance of stabilized surface coated polycarbonate by an outdoor exposure of both coated and uncoated UV-stabilized sheet material. Materials from two major suppliers were chosen for the study: LEXAN 9034-112, and LEXAN MR-5 from General Electric Corporation, USA; and MAKROLON LS and MAKROLON Hard 281 from Bayer, Germany. The main purposes were:

- a) to determine if the coating remains on the polycarbonate and continues to provide abrasion resistance
- b) to assess the weathering resistance of current materials
- c) to identify methods of characterization of polycarbonate, the stabilizers, and the surface treatments.

Four countries were involved in this study: Australia, Canada, UK and USA.

TRIAL CONDITIONS

The materials as 375 x 375 x 3mm sheets were exposed at the Joint Trials and Tropical Research Establishment (JTTRE), Innisfail, Queensland, Australia, in the hot/wet cleared site. The sheets were supported at 45° facing north, coated side uppermost. Innisfail has a hot, wet climate with a yearly average temperature of 24°C and mean annual maximum and minimum temperatures of 28°C and 19°C. The yearly average relative humidity is 81% with mean annual maximum and minimum values of 94% and 60%. Exposures began in April 1982 and continued for a period of four years, with removal of samples for assessment at 6, 12, 18, 24, 36, and 48 months. Parallel sets of control samples were maintained in the dark under controlled temperature and humidity in order to provide differentiation of weather-induced vs. age-induced changes.

PROPERTY EVALUATION AND ANALYSIS

The following assessments were performed on the control and the weathered materials: visual appearance, rain erosion and abrasion resistance, chemical degradation, tensile and impact properties, stress cracking, and comparison with a polycarbonate weathering trial of 1976.

Visual Appearance

Examination of unweathered materials by Nomarski differential interference microscopy revealed that apart from some scratches both surfaces of the coated and plain LEXAN samples were extremely smooth. One surface of the uncoated MAKROLON samples exhibited fine 'ripple' lines, all oriented in the same direction and typically separated by about 10 μm . From the intensity profile of the Nomarski image it would appear that these lines were fine grooves in the otherwise smooth surface. The coated MAKROLON surfaces exhibited undulations up to a height of about 50 nm typically over a length of 20 μm or more.

Examination of the materials between crossed polarisers showed that they all exhibited considerable birefringence. With the uncoated materials, a reasonable extinction could be obtained at 90° intervals as the specimens were rotated in their own plane between the polarisers, i.e. as would be obtained from a uniaxial crystal. No such extinction was noted with the coated specimens and, in fact, with the coated MAKROLON specimens there was little change in the light output as they were rotated between the crossed polarisers. It would appear that birefringence had been significantly affected by the coating process.

The reflectance spectra from both the coated polycarbonates exhibited strong sinusoidal variations and from the wavelength separation of adjacent transmittance peaks the coating thickness was calculated to be of the order of 5 μm . From the amplitude of these sinusoidal variations it was concluded that the refractive index of the coatings was about 0.1 below that of the polycarbonate substrate ($n = 1.59$). The coatings therefore produce a small antireflection effect, the overall reduction in reflectance through the visible spectrum being between 1 and 1.5 percent per surface relative to the 5 percent reflectance from an uncoated polycarbonate surface.

After 12 months of weathering all uncoated samples had taken on a pale yellow tint, and all were fogged to a degree that would make them unacceptable as transparencies. Image visibility of an object viewed through the material was badly affected. Examination in transmitted light using the

Interphako interference microscope allowed a good assessment of surface damage to be made. In addition to a general roughness of the order of $1\text{ }\mu\text{m}$ in magnitude, there were many steep sided pits with depths up to $10\text{ }\mu\text{m}$ and lateral dimensions of $20\text{ }\mu\text{m}$. From interference fringes areas about $30\text{ }\mu\text{m}$ in size with a height $2\text{-}3\text{ }\mu\text{m}$ about the general level were also found.

The weathered surface of the coated LEXAN had deteriorated considerably after 12 months, giving a rather 'patchy' appearance. Optical microscopy showed that the surface could be divided into three types of regions:

- 1) Areas having normal level of reflectance, exhibiting little surface structure but not as smooth as an unweathered coating
- 2) Small areas interspersed within (1) having a higher reflectance and showing interference colors
- 3) Areas having more scatter and with surface scratches and fine debris making up about 50% of the total area and at a level $3\text{-}4\text{ }\mu\text{m}$ below that of type (1).

It would appear that in type (3) areas part or all the coating has been removed by weathering. Type 2 areas are intermediate stages in the weathering, with the coating separating from the substrate and the interference fringes arising from this separation.

The coating on MAKROLON was much better in that weathered surfaces could not be distinguished from unexposed ones by the eye. However, interference microscopy showed that the surface roughness was greater in weathered material with a peak to valley height of about $0.3\text{ }\mu\text{m}$, several times larger than that of the unexposed surface.

Scanning electron microscopy of weathered uncoated material gave similar evidence of surface damage. Crazes, blotches, mottled areas, and furrowing were observed. Coated LEXAN showed lines, wrinkles and mottling of the surface with occasional craze or crack. The appearance of coated MAKROLON was superior, with some banding and a few crazes or cracks in the surface.

Haze measurements on material exposed for 12 months also showed that the coating provides protection of the polycarbonate surface from becoming rough. The surface damage and yellowing increase with exposure time, and after 24 months there was little if any coating left on the surface of the coated materials whether LEXAN or MAKROLON. The coating on MAKROLON was superior to that on LEXAN in terms of protection against weathering.

Rain Erosion and Abrasion Resistance

Rain erosion resistance was evaluated using a rig originally described by Fyall and Strain (Ref. 1). The holders at the end of a 3.2 m long arm were set to allow impact at 90° and 60°. A speed of 223 m/s (430 knots) was used with a simulated rain field of 25 mm/h having a predominant drop size of 2 mm diameter. Damage was assessed through weight loss and haze measurements.

Measurements on unexposed material show that at 60° and 90° impact these coatings on polycarbonate provide no protection and in fact degrade the performance with respect to the appearance of haze and weight loss, Table (1) and Figures 1 and 2. For the exposed materials haze increases rapidly on rain erosion, giving very high values (Table 1). Weight loss due to erosion on the exposed material after an induction period of some 15 minutes was very rapid compared to unexposed material and was seen in both coated and uncoated materials. erosion rates appear greater after weathering. There appears to be no difference in the level of protection provided by the coatings on LEXAN or MAKROLON.

Abrasion resistance was assessed using the NPL abrasion machine under standard conditions, i.e. a slurry of B.S. coarse dust in distilled water (10 g per 100 cm³), a wiper speed of about 300 strokes per minute and a wiper loading of approximately 10 g per cm length of blade. Tests were carried out with the number of strokes ranging between 2000 and 20,000.

Incident light microscopy indicated that after 2000 strokes all of the abraded areas of the uncoated polycarbonates had been damaged.

Roughness average values (R_a) measured on the RPI Talystep ranged between 55 and 100 nm compared to values of a few nm for the unabraded surfaces. Image contrast of a distant object was reduced significantly by viewing it through the abraded windows. A further very marked loss of image contrast was obtained when abrasion of the uncoated specimens was continued up to 10,000 strokes. Measured R_a values were then above 100 nm.

Abrasion testing of the coated material showed that the coatings produced a considerable degree of protection to the polycarbonate substrates. After 2000 strokes only a few scratches were visible by incident light microscopy, these ranging from fine scratches to reasonably deep grooves; well over 90 percent of the abraded surfaces of the LEXAN and MAKROLON coatings remained undamaged. After 10,000 abrasion strokes slight deterioration in image quality of an object viewed through the abraded material was detectable. This

became more marked after 20,000 strokes, a somewhat larger reduction in image contrast being produced by the coated MAKROLON abraded specimens compared to the coated LEXAN ones. Even after 20,000 abrasion strokes approximately 50 percent of the center of the abraded areas appeared undamaged as assessed by incident light microscopy, although in the more heavily abraded regions at the ends of the wiper blade stroke almost all the surface had suffered some damage. From this microscopical examination it was concluded that damage to either coating was of comparable magnitude, the LEXAN coatings probably being slightly superior in their abrasion resistance. A similar conclusion was reached from examination by interference microscopy and profilometry; abrasion grooves produced by the silica particles appeared, in general, to be somewhat deeper and wider on the coated MAKROLON.

Chemical Degradation

Infra-red Analysis. Infra-red spectroscopy was employed to show the degradation of the polycarbonate. A reflectance technique was used which records the spectra of surface material to a depth of 1-5 μm . Both uncoated materials show substantial degradation after environmental exposure, the significant spectral changes being:

1. Appearance of a carbonyl peak at 1730 cm^{-1}
2. Appearance of a broad peak at 1600 cm^{-1}
3. Decrease in intensity of absorption at 1780 cm^{-1}
4. Additional peak near 1220 cm^{-1} while that at 1200 cm^{-1} decreases in intensity.

MAKROLON appears to degrade slightly more rapidly than LEXAN and for both samples this degradation is significant after only 12 months; the spectra after 18 months show only a little more damage in the 1 μm surface zone sampled.

The spectra indicate the formation of breakdown products. These products arise from photolysis and hydrolysis of the carbonate link and further reactions with oxygen (SCHEME 1). These spectral changes can be explained from work done on model systems under ideal conditions.

With the coated polycarbonates, the coating thickness is such that the polycarbonate is not detected by reflectance. Changes do occur in the spectra of the coating on weathering, and are greater in the MAKROLON coating. The coatings, which are organo-silicate/silicic acid based polymers, are different and that on MAKROLON showed a greater degree of oxidation upon weathering.

Molecular Weight. Polymer molecular weight is very critical in the performance of polycarbonate. This parameter was measured in two laboratories and the results are given in Table (2). Each laboratory found no difference in molecular weight and its distribution for plain and coated polycarbonate from the same manufacturer. However, the molecular weights determined by the two laboratories differed, probably reflecting the difficulty of the measurement and the different assumptions made in analyzing the data. Both laboratories used size exclusion chromatography, and applied the universal calibration method based on polystyrene standards.

On exposure, reductions in the molecular weight of surface material can be seen after 12 months. Coatings did not prevent those processes which result in polymer chain scission and it was not possible to show that the processes were retarded by the coatings. Figures (3,4) show the changes in molecular weight (M_w) with depth and that damage is occurring to 100 μm .

Stabilizer. In all of the materials the UV stabilizer was the same: 2-(2-hydroxy-5-*t*-octylphenyl)-benzotriazole (Cyasorb UV 5411- American Cyanamid Corp.) The bulk concentration was 0.3% w/w except in some coated MAKROLON specimens in which it was 0.2% w/w. Stabilizer concentration at the surface of the coated polycarbonate was much higher - up to 0.7% w/w. It would appear that the stabilizer accumulates preferentially at the polycarbonate/coating interface, though incompatibility of the stabilizer with the polycarbonate does not appear to be a problem. The surface layer concentration of uncoated sheet was the same as the bulk concentration.

Exposure of these materials reduces the stabilizer concentration in the surface which receives the full force of the weather. In the coated material, after 12 months exposure the surface concentration is still higher than the bulk concentration, and the coating is still largely intact. After 24 months the surface concentrations are much lower than bulk in all cases. This reduction in concentration is due to reaction of the stabilizer with free radicals produced in the photolysis of the polycarbonate by sunlight and the subsequent oxidation reactions. Figure (4) shows the variations in concentration of stabilizers with depth for coated LEXAN after 24 months. Other materials show similar changes and the depleted layer is about 80-100 μm thick.

Yellowing. The yellowing of these polycarbonate materials was measured according to ASTM D1925-70, and the results are shown in Figure 5. Using a subjective assessment that polycarbonate with a yellowness index greater than 4 is unacceptable, the exposure times to reach this at JTRE were

MAKROLON - uncoated	7 months
LEXAN - uncoated	9 months
LEXAN - coated	13 months
MAKROLON - coated	19 months

The coating appears to inhibit yellowing, significantly so with coated MAKROLON (see Figure 5).

Tensile and Impact Properties

Table 3 gives the yield strength, elongation at break, and the impact strength of these materials, after 18 months exposure, and unexposed. The stress/strain properties show no change in yield strength of the polycarbonate with weathering. However, there is a progressive decrease in elongation to break which after 18 months is about half that of the unexposed material. This decrease in ductility is indicative of an embrittled surface, manifested by the large number of small cracks which appear in the surface of the test specimens as the plastic begins to yield. This embrittlement also produces a decrease in impact strength.

Stress Cracking

The stress cracking of the polycarbonates was assessed by a critical strain method described in Ref. 2. A 2:1 (v/v) mixture of ethanol: 2-ethoxyethanol was applied to the weathered surface of specimens. The critical strain to produce cracking of the polycarbonate or separation of the coating from the substrate was compared with that of unexposed controls. The results for 6, 12 and 18 months are given in Table 4.

The resistances of all four materials are considerably reduced by weathering. Uncoated LEXAN and MAKROLON gave similar results, and over the first 12 months of exposure their critical strain decreased to less than half the control values. Continued weathering produced no further decrease in the critical strain. Coated materials showed considerable differences after 6 months exposure; the MAKROLON being more seriously affected than the LEXAN. After 12 and 18 months exposure the results for both materials were similar and the same as those for uncoated polycarbonate.

Polycarbonate Trial of 1976

In 1976 a weathering trial of MAKROLON M2803 was carried out at JTTRE. This plastic contained a different UV-stabilizer: p-methoxybenzylidene malonate (Cyasorb 3100). Measurements of the molecular weight change with depth showed that after 2 and 6 years of weathering, the thickness of the

degraded layer was $\leq 15 \mu\text{m}$ and $\sim 85 \mu\text{m}$, respectively. The stabilizer content was only 1% at the surface compared with nearly 4% in the bulk material. Compared to the recent trial this stabilizer content is 10 times greater. Comparison of the bulk molecular weight and its distribution showed that there was no difference between the polycarbonates used in the two trials.

The 1976 polycarbonate started to yellow immediately on exposure with no indication of an induction period which was seen with the recent materials. The time taken to reach a yellowness index of 4 was greater than that of uncoated MAKROLON in the recent trial, however ultimate yellowness levels were much greater (Figure 5).

SUMMARY AND CONCLUSIONS

Polycarbonate coatings available from Bayer and GE in 1981 (Bayer MAKROLON Hard 281 and GE LEXAN MR-5) did not confer long term protection against weathering. The coatings provided considerable improvement in resistance to abrasion, but did not reduce the rapid development of haze from rain erosion. After tropical weathering for several months, changes in the coating introduced optical aberrations and permitted degradation of the underlying polycarbonate. Elongation to break and impact strength decreased markedly after 18 months of weathering, although yield strength in all samples was virtually unaffected. Coated polycarbonate yellowed to an unacceptable degree in 13 to 19 months, versus 7 to 9 months for uncoated polycarbonate. Depth-profiling characterization procedures were able to analyze the coatings, the decreases in polymer molecular weight, the degradation products, and the depletion and migration of UV stabilizers that accompanied the weathering processes.

ACKNOWLEDGEMENTS

The collators acknowledge with thanks the contributions of the numerous scientists who carried out this study under the auspices of the following laboratories: Joint Trials and Tropical Research Establishment, Materials Research Laboratory (Australia); Defence Research Establishment, Pacific (Canada); Royal Armament R & D Establishment Waltham Abbey, Royal aerospace Establishment, National Physical Laboratory, Admiralty Research Establishment DQA/TS (United Kingdom); Army Materials Technology Laboratory, Naval Research Laboratory, Air Force Wright Aeronautical Laboratories (United States).

References

1. A. A. Fyall and R.N.C. Strain, "A whirling arm test rig for the assessment of the rain erosion of materials", RAE Technical Report Chem 509 (1956).
2. MQAD Technical Paper No. 691. Available through Admiralty Research Establishment DQA/TS.

TABLE 1

Effect of Weathering on Haze of Stabilized
and Coated or Plain Polycarbonate

<u>Material</u>	<u>Coating</u>	<u>Weather Months</u>	<u>% Haze As Received</u>	<u>Rain Eroded #</u>
LEXAN	No	0	0.8	7.9
LEXAN	Yes	0	0.7	15.1
MAKROLON	No	0	1.2	9.2
MAKROLON	Yes	0	1.0	52.7
LEXAN	No	12	32	100
LEXAN	Yes	12	3.2	61
MAKROLON	No	12	32	100
MAKROLON	Yes	12	1.6	98

#5 minutes at an impact angle of 90°

TABLE 2

Molecular Weight Measurements

Lab A		Lab B	
	M_n	M_w	
			M_n
			M_w
LEXAN	24000	44000	17000
			38000
MAKROLON	24000	42000	16000
			37000

 M_n Number average molecular weight M_w Weight average molecular weight

TABLE 3

Mechanical Properties of Coated and Plain Polycarbonate
at 0 and 18 Months Exposure

Material	Property						
	Yield Strength #		Elongation at Break #		Impact Energy to Break N_m		
	MPa		%				
	0 months	18	0 months	18			
Lexan	U	63	63	184	104	71	57
	C	67	67	140	123	86	77
Makrolon	U	65	65	196	103	86	53
	C	66	66	105	51	87	2.6

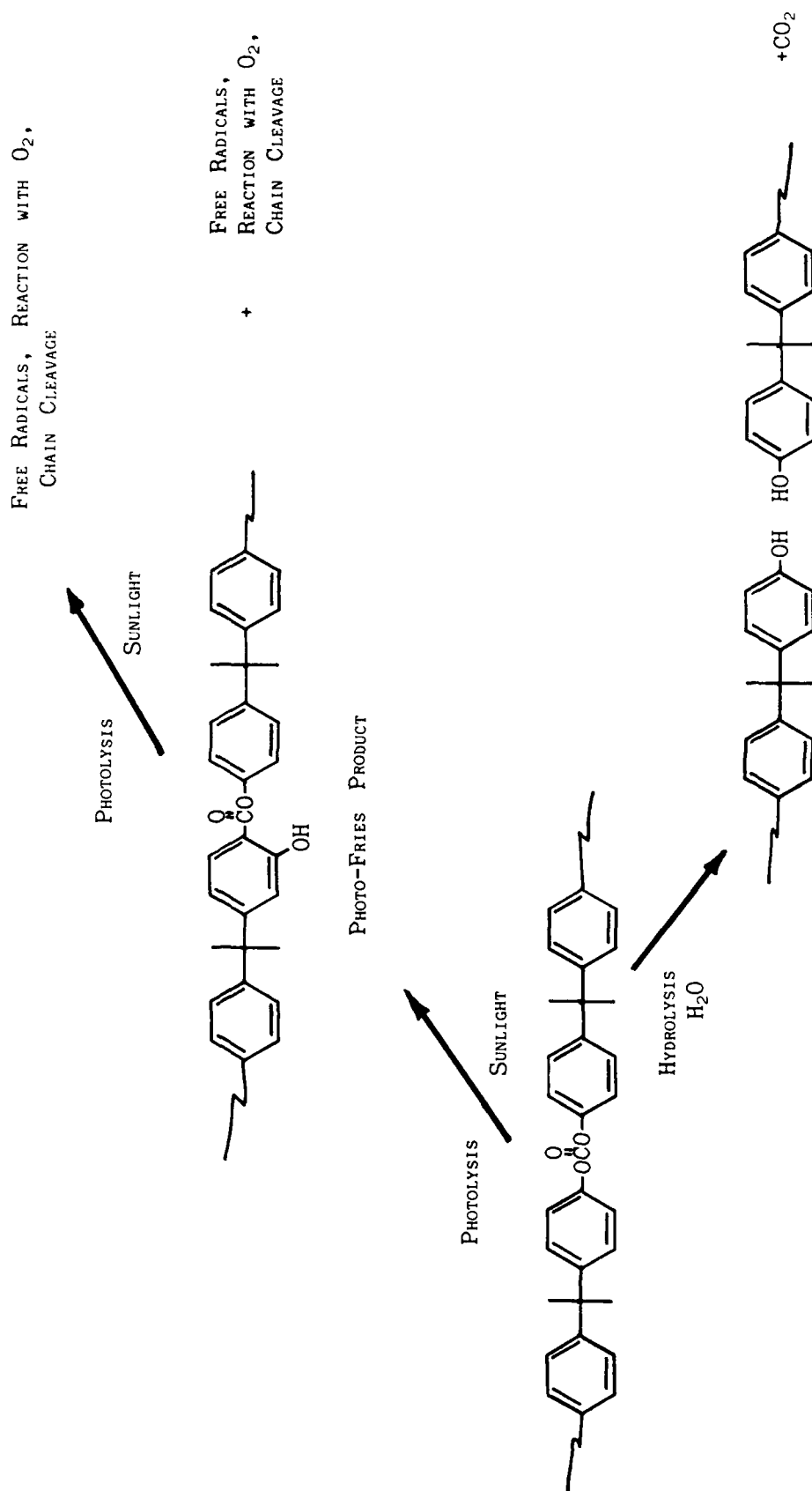
Tested according to ASTM D 638M-81 at a crosshead speed of 5 mm/min.

TABLE 4

Critical Strain for Stress Cracking of Polycarbonate Materials

<u>Material</u>	<u>Controls</u>		<u>Exposure Times</u>		
	<u>1</u>	<u>2</u>	<u>6 Months</u>	<u>12 months</u>	<u>18 months</u>
LEXAN uncoated	0.60	0.74	0.41	0.31	0.33
LEXAN coated	0.69	0.65	0.58	0.20	0.29
MAKROLON uncoated	0.67	0.76	0.44	0.31	0.32
MAKROLON coated	0.74	0.57	0.27	0.24	0.26

CHEMICAL DEGRADATION OF POLYCARBONATE



Scheme 1

MODES OF IMPACT FAILURE

Gerald L. Robbins, Ph.D.
Mobay Corporation

MODES OF IMPACT FAILURE

Presented
January 17, 1989
CONFERENCE ON AEROSPACE TRANSPARENT
MATERIALS AND ENCLOSURES
Hyatt Regency Hotel
Monterey, California

Gerald L. Robbins, Ph.D.
Materials Specialist
Mobay Corporation
Plastics & Rubber Division
Mobay Road
Pittsburgh, PA. 15205

Introduction

The rapidly changing field of the aerospace industry has incorporated new technologies over the years to improve performance using advanced polymer materials. One target area has been aircraft transparencies, where glass has been replaced by clear engineering thermoplastics. The preferred clear high performance polymer is polycarbonate, which is the material of choice for military aircraft canopies on the B-1, F-111, and F-16. Polycarbonate is selected for this critical application because it possesses a high degree of clarity and brightness, low haze, and can be thermoformed into the canopies while maintaining its excellent impact strength. Polycarbonate also has high tensile strength, high heat deflection temperatures, and maintains excellent ductility in this critical application.

Polycarbonate can also be laminated with other clear materials such as urethane or silicone rubbers which are used as interlayers between several polycarbonate sheets to improve the overall thermoformed canopy properties. In addition, a top laminate of acrylic sheet and a mar resistant coating provide weatherability and UV protection while improving the scratch resistance of the canopy.

The polycarbonate resin chosen for military canopies has a high degree of transparency and extremely low haze for the outstanding visibility required by the pilot. The overall clarity of the composite structure must be maintained at an acceptable level for the finished canopy and still maintain impact strength. Clarity can be readily measured by several visual and photometric methods while the impact strength of the polycarbonate is measured by a variety of different physical test methods. These methods can vary in many ways from some simple techniques such as impacting a notched bar using the Izod Impact Test to impacting a flat surface with the Drop Dart and Instrumented Impact Tests. Other, more realistic and costly methods using Bird Strike Impact techniques to evaluate finished composite canopy structures using simulated flight conditions are also used. An impact test is needed which evaluates polycarbonate sheet performance before the costly process of preparing the final laminated canopy and Bird Impact Testing.

Mobay Corporation, a major polycarbonate resin supplier to the aerospace industry, is constantly evaluating improved methods for determining the impact strength of sheet. Each sheet manufacturing company must comply with military specification MIL-P-83310. The mil spec states that 0.125" sheet must have a minimum 12 ft-lbs/inch notched izod impact strength while 0.250" sheet have 2.5 ft-lbs/inch notch strength. While this specification clearly states the notch impact strength requirement it can be misleading because it does not specify how the sample is to be prepared. This paper will demonstrate that the same grade of polycarbonate resin can have widely varying impact strengths if the sample is extruded rather than injection molded

and that post-production thermal treatments can alter the initial notch impact results. This can, and has, led to different interpretations by the sheet suppliers and to confusion of notched impact results by the canopy manufacturers.

This paper will show how the notched izod impact strength is directly related to the stress in the extruded or injection molded part and that post-production heating of the part can reduce the izod impact results. Because of this, consideration should be given to eliminating notched izod impact as a specification for polycarbonate sheet used in military transparencies.

Notched Izod Impact

It is a well known fact that notched izod impact of polycarbonate having a specific thickness can vary considerably depending upon the internal stress of the part. Parts having high internal stress will have higher notched izod impact strength than parts with lower internal stress. Internal stress is dictated by the conditions of manufacturing the part. Additional factors, such as post manufacturing thermal treatment of the part can lower the initial notched izod impact by reducing the internal stress. For example, a 0.125" izod bar having a notching radius of 0.010" which is molded with a 550°F melt temperature, 150°F mold temperature, 15,000 PSI clamp pressure, and a slow injection rate will typically have 17 ft-lbs/inch notched impact strength. Now, if an identical sample is taken and "annealed", it will yield a much lower notched impact strength of 3-4 ft-lbs/inch. "Annealing" is defined as maintaining the bar at an elevated temperature (i.e. 250-300°F) for a specific time period (1-3 hours). The higher the temperature of annealing, the shorter the time period needed to reduce the internal stress of the part and, consequently, the lower the notched izod impact strength. The loss of notched impact strength is due to a reduction of the internal stress in the sample. This can visually be determined by viewing a sample with polarized light before and after annealing and counting the number of birefringence lines. The number of birefringence patterns in the sample will decrease upon annealing which coincide with lower internal stress in the part. After annealing a polycarbonate part the number of birefringence lines are reduced.

There is a considerable difference in the amount of stress in a part as the process changes when comparing extrusion to injection molding. The extrusion process is a lower pressure process than injection molding and does not yield the high internal stresses needed to produce the high notch impact strengths. The notch impact strength of an extruded part is usually less than 2.5 ft-lbs/inch for a 0.250 inch sample for sheet while normal injection molding conditions yield notch impact results greater than 2.5 ft-lbs/inch.

Furthermore, the post production process of making the aircraft canopy lowers the initial notch impact strength of the sheet. The thermoform process transforming polycarbonate sheet into a canopy structure is, essentially, an "annealing" process. The polycarbonate is held at some elevated temperature above the glass transition of 300°F for a set period of time allowing the material to drape and fill the shape of the canopy mold. This forming process reduces the internal stress of the polycarbonate. Therefore, it is not important to know the initial notch impact value of the sheet. Rather it is more important to know the final impact strength of the sheet after completion of the thermoforming process.

Notched Izod Test Results

Figures 1 and 2 show the notch impact strength of recently produced 0.250" polycarbonate sheets from suppliers A and B, which have been extruded for military aircraft canopies. Neither of the manufacturers sheet meets the required 2.5 ft-lbs/inch of notch as a general rule. Figure 3 compares the notch izod impact results for sheet from the two different manufacturers.

If the parts have a higher internal stress, such as by injection molding the bars, then the notch impact results are dramatically changed. Figure 4 compares the notched impact of sheet to injection molded polycarbonate resin which is used to make sheet for aircraft canopies. Two different molding conditions are used to mold the bars, with one producing a higher stress level in the part. The highly stressed bars were molded using a slower injection speed and lowering the mold temperature while the bars with lower stress were made using normal molding conditions. It is obvious that changing the mold conditions for the material can dramatically change the notch impact. When using an equivalent resin, the notch impact strength of the molded parts, regardless of mold conditions, is higher than the extruded sheet. The notch impact strength of polycarbonate is very dependent upon the amount of internal stress in the bar. The rule of thumb is the higher the internal stress the higher the notch impact strength of the part.

Another factor when considering impact strength is the age of the part. Does a 2 year old part have the same notched impact strength of a recently made part? Figures 5 and 6 give the notched impact strength of sheet which is two (2) years old. Comparing the sheet from two suppliers in Figure 7 shows each to average under the required 2.5 ft-lbs/inch notch strength. Note the average impact strength of 2.3 ft-lbs/inch is unchanged after two years aging from recently prepared sheet as shown in Figures 8 and 9.

Another method to demonstrate that injection molded parts have higher impact strength than extruded sheet is to cut up and regrind sheet and mold the regrind into parts and test for notch impact. Figures 10 and

11 compare notch izod impact of injection molded bars made from regrind sheet material of Suppliers A and B to the original sheet. The average notch impact strength is slightly different between the two suppliers, with sample A having 2.6 while B is 2.5 ft-lbs/inch. Both values are above the original impact strength of 2.3 and 2.35 ft-lbs/inch of the sheet used to make the molded bars. Again, the increase in notch impact strength for the regrind is due to the increased internal stress of the molded bars even though an additional heat history has been applied to the molded material. The injection molded bars are made using normal molding conditions without any attempt to produce a higher internal stress in the parts.

Figure 12 compares the notch impact strength of bars injection molded from regrind sheet and bars molded from virgin resin. Although the regrind sheet has an additional processing heat history, the average impact strength is similar to the virgin resin. All the bars are made at one injection molding condition producing equivalent internal stresses. The results are that each sample yields equivalent notch impacts.

Instrumented Impact

Military and aircraft manufacturers are concerned with the impact strength of the canopy when struck by an object (i.e. bird) during a flight operation. During flight of the aircraft, the object impacts at a smooth, curved surface and not at a notch. Therefore, it is more important to understand the phenomenon of impact upon a flat polycarbonate surface than at a notch.

One technique to measure impact on a flat surface is instrumented impact. It is similar to drop dart impact in that the dart strikes a flat surface with the energy and force to penetrate the sample being measured. The difference between the falling dart and instrumented impact test is that the instrumented dart method hits the flat sample at a constant velocity and continues at this velocity to penetrate the sample rather than having a dart of known weight strike the sample at a velocity due to gravity. Drop dart impact decelerates upon striking the sample while the instrumented method maintains a constant speed during impact. Information obtained using the instrumented impact method is more reproducible and fewer samples are needed to obtain an impact energy. For example, as many as 30-40 samples are required to determine the drop dart impact while only one sample is needed for instrumented impact. In addition to the impact energy value obtained, the force required to penetrate the sample as shown in Figure 13 is also given for the instrumented dart method.

Figures 14 and 15 compare the similar impact results of extruded sheet from Suppliers A and B by instrumented dart. Even after aging sheet for 10 days at 250°F, Figure 16 shows the instrumented impact strength to be retained. Figures 17 and 18 demonstrate that thermally aging

polycarbonate sheet as little as two hours can significantly lower the notch izod impact but does not alter the instrumented impact strength. The process of drying the sheet and forming the canopy can reduce the notch impact strength of the polycarbonate without affecting the instrumented impact.

Obviously notched impact is strongly affected by the internal stress of the part. Notched impact gives more information about the manner in which the part is produced and how it has been treated after production rather than the quality of the material to produce the part. Notched izod may or may not give any information about the quality of the material in the part. To get meaningful notch impact data, the method of production for the part to be tested must also be specified. Finally, since the sheet must be heated above the glass transition temperature to form the canopy, the initial notch impact strength becomes of very limited value. It is better, perhaps, to specify a drop dart or instrumented dart impact test where results do not change even when the polycarbonate has been produced with different extrusion conditions, heated above the glass transition temperature, annealed, or held at an elevated temperature for a long period of time. A more meaningful approach to determine the impact strength of polycarbonate would utilize some type of dropping weight test such as instrumented or dart impact rather than notched izod impact.

It is obvious that notched izod impacts are significantly reduced after annealing which lowers the internal stress. The question then to be answered is whether the drilling of holes in a canopy, which is a notching process, alters and reduces the impact resistance of the canopy upon bird impact? Should alternatives other than drilling holes in the canopy be considered to reduce or eliminate the risk of low notch impact strength when attaching the canopy to an aircraft? There are a number of designs presently in use which attach polycarbonate windshields without the need for drilling holes that can withstand high speed impacts. Some of these designs are approved for use by the Federal Railroad Administration for windshields in high speed trains traveling up to 80 miles per hour that must withstand an impact from a 16 pound cinder block hung from a stationary object such as a railroad trestle. Additionally, other design features incorporating a positive engagement of the canopy to the frame which eliminates the possibility of sucking the canopy from the aircraft when traveling at supersonic speeds must be taken into account. Finally, the contraction and expansion of the canopy structure in a positive engagement frame to allow the polycarbonate to withstand a bird strike at high velocity must be considered.

Conclusion

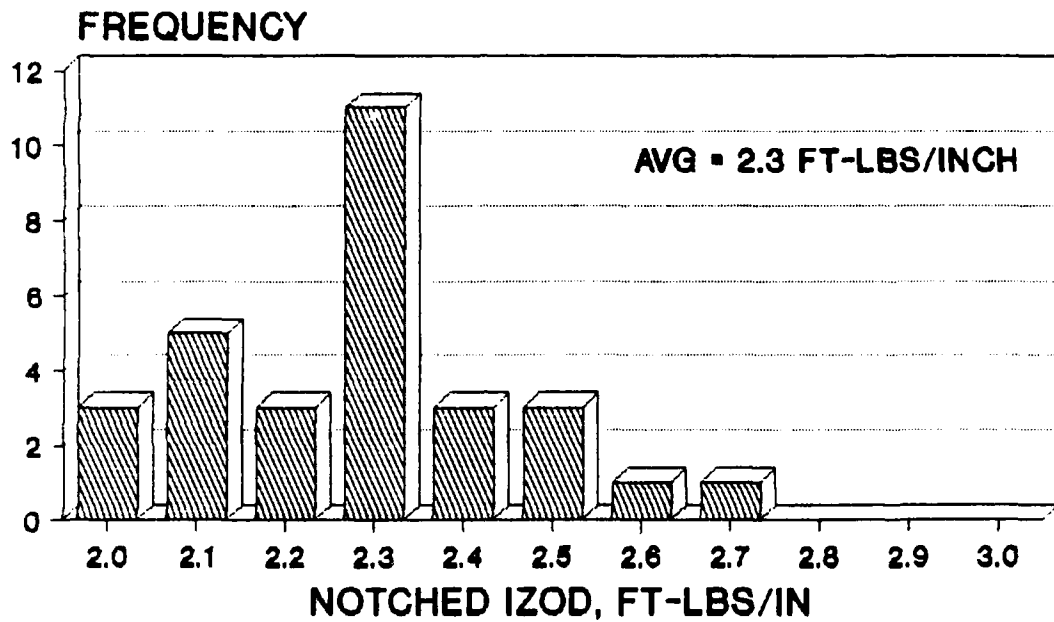
1. The amount of internal stress in a part or the amount of thermal annealing has little effect on the instrumented or drop dart impact.

2. Notched impact strength of polycarbonate is dependent upon the internal stress of the part.
3. An injection molded bar has higher notched izod impact strength than does a part extruded with the same polycarbonate resin.
4. Thermally annealing a molded or extruded part will significantly reduce the notched izod impact strength of that part.
5. Other designs should be considered which eliminate the need for drilling holes in the canopy to attach to the aircraft frame.

Acknowledgements

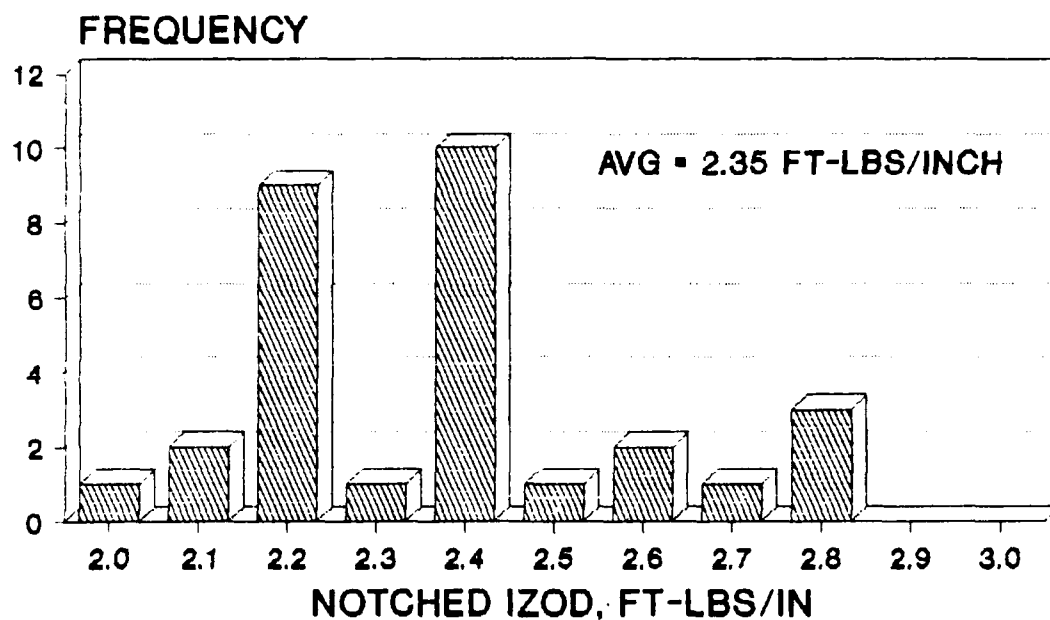
The author would like to thank several members of the Mobay staff including Tom Barclay, Bob Cannon, Regina Cole, and Walter Heckla. In addition, thanks to Don Carroll of Rohm & Haas and Pat Walters of PPG for supplying the extruded polycarbonate sheets for this study.

0.250 INCH SHEET, SUPPLIER A IMPACT STRENGTH OF CURRENT INVENTORY



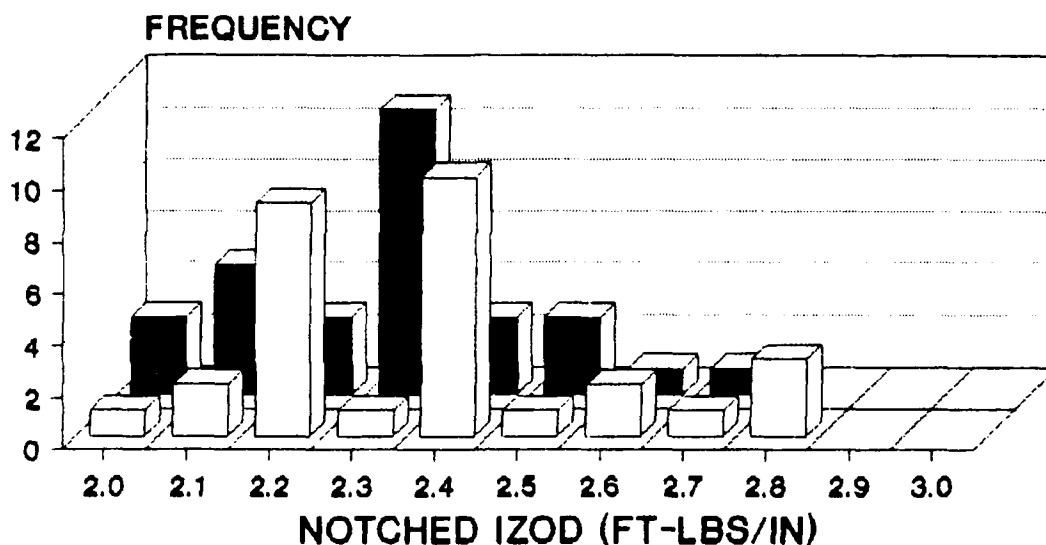
**SAMPLES CUT FROM SHEET
TOTAL: 30 TEST SPECIMENS**

0.250 INCH SHEET, SUPPLIER B IMPACT STRENGTH OF CURRENT INVENTORY



SAMPLES CUT FROM SHEET
TOTAL: 30 TEST SPECIMENS

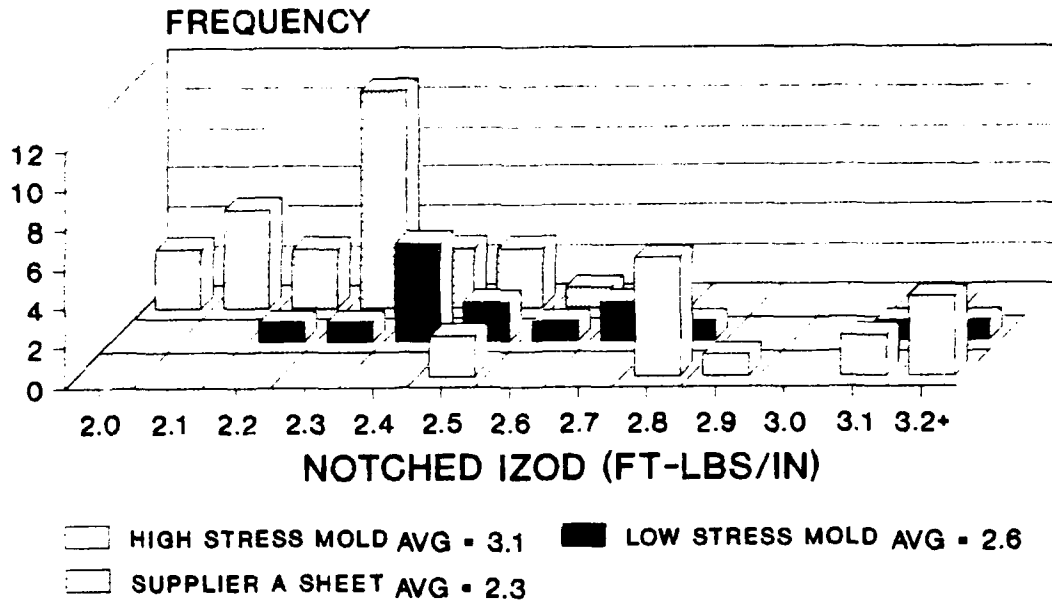
NOTCHED IZOD OF CURRENT SHEET COMPARISON OF SUPPLIER A AND B



SUPPLIER B
 SUPPLIER A
 AVG = 2.35 FT-LBS/INCH AVG = 2.3 FT-LBS/INCH

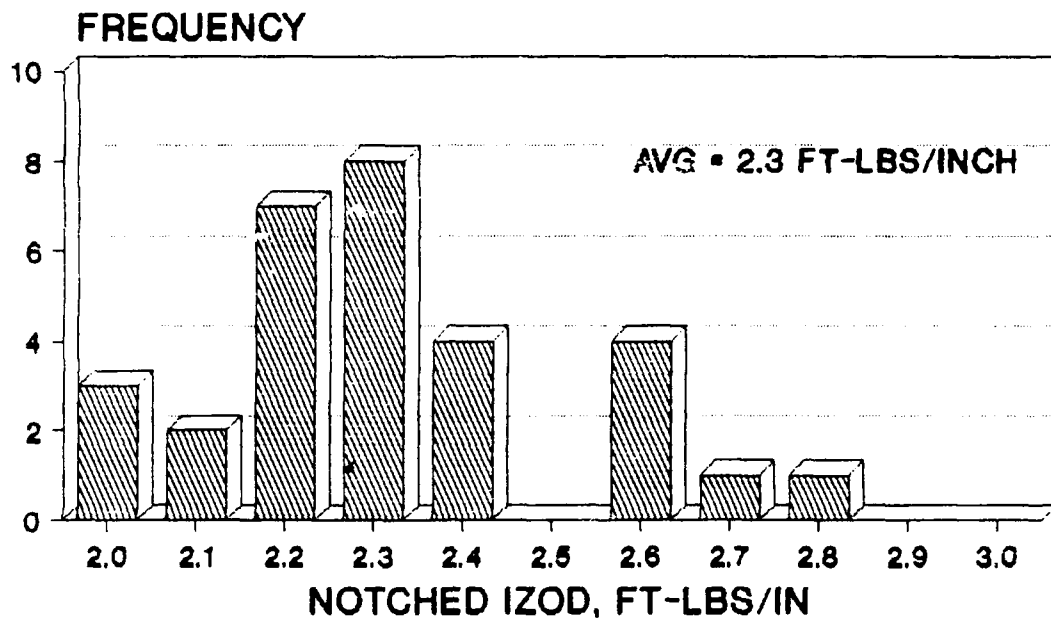
TOTAL: 30 SPECIMENS EACH
SAMPLES CUT FROM 0.250" SHEET

NOTCHED IZOD COMPARISON HIGH & LOW STRESS MOLDED vs SHEET A



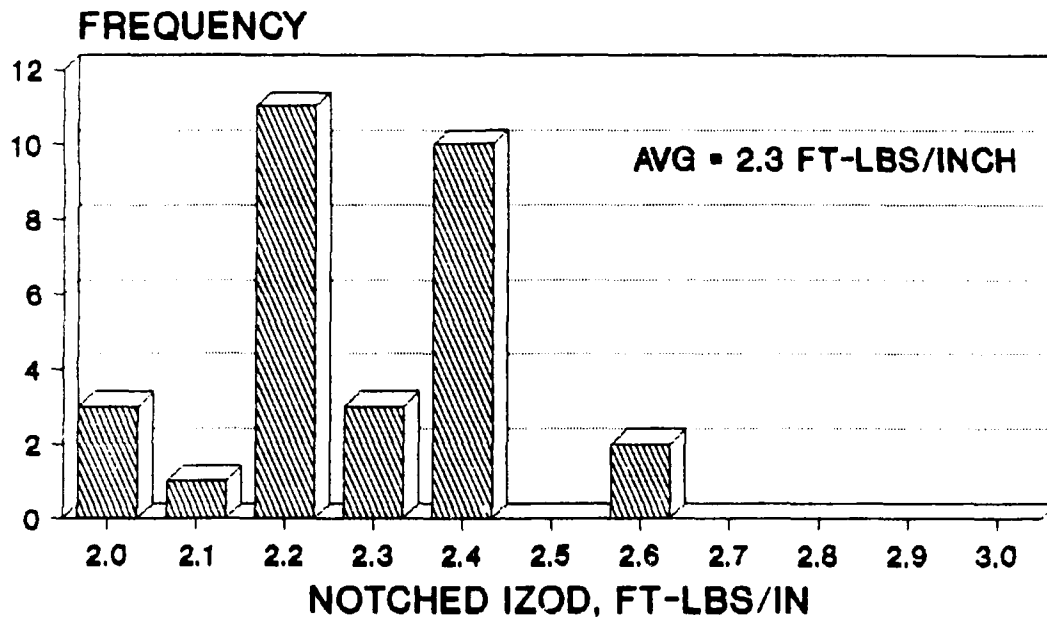
SPECIMENS ARE 0.250"

**0.250 INCH SHEET, SUPPLIER A
IMPACT STRENGTH OF 2 YR OLD INVENTORY**



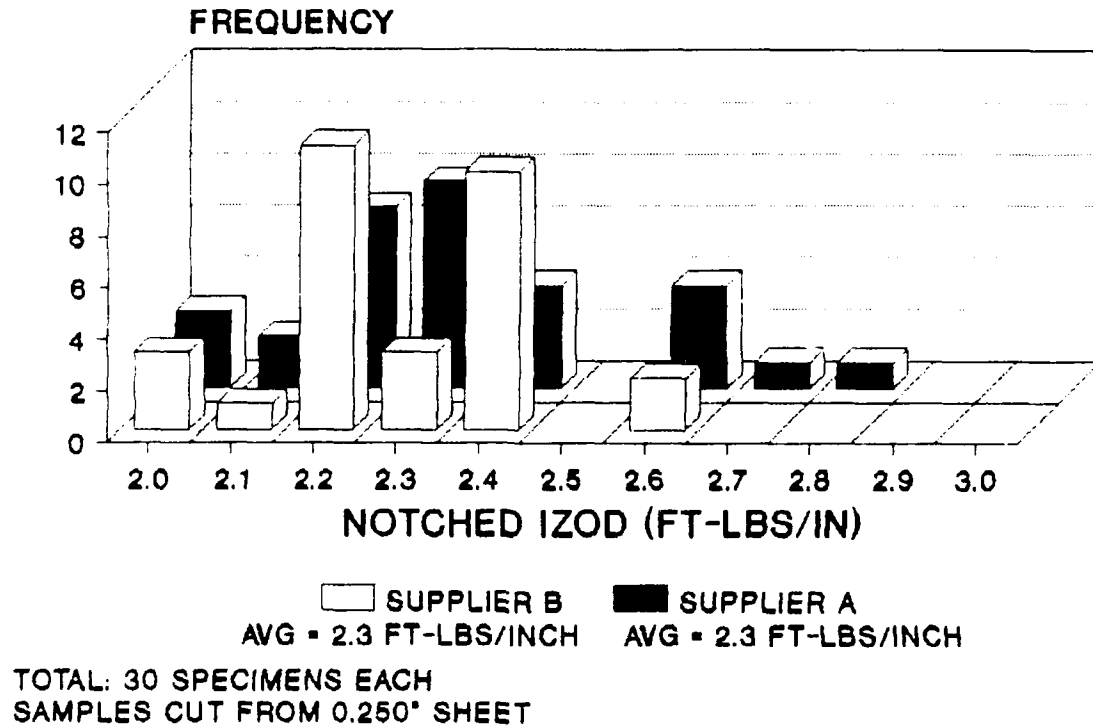
**SAMPLES CUT FROM SHEET
TOTAL: 30 TEST SPECIMENS**

**0.250 INCH SHEET, SUPPLIER B
IMPACT STRENGTH OF 2 YR OLD INVENTORY**

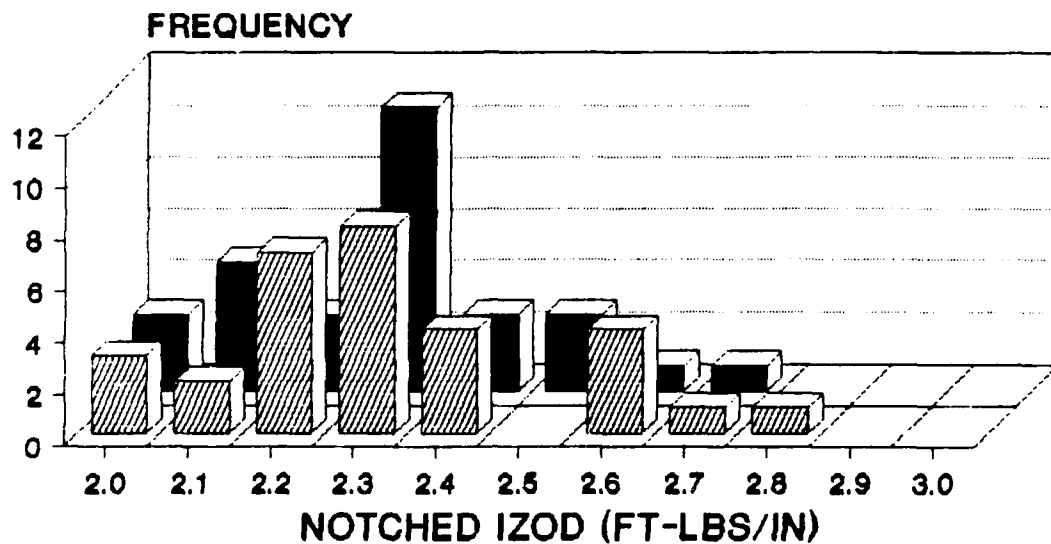


**SAMPLES CUT FROM SHEET
TOTAL: 30 TEST SPECIMENS**

NOTCHED IZOD OF 2 YR OLD SHEET COMPARISON OF SUPPLIER A AND B



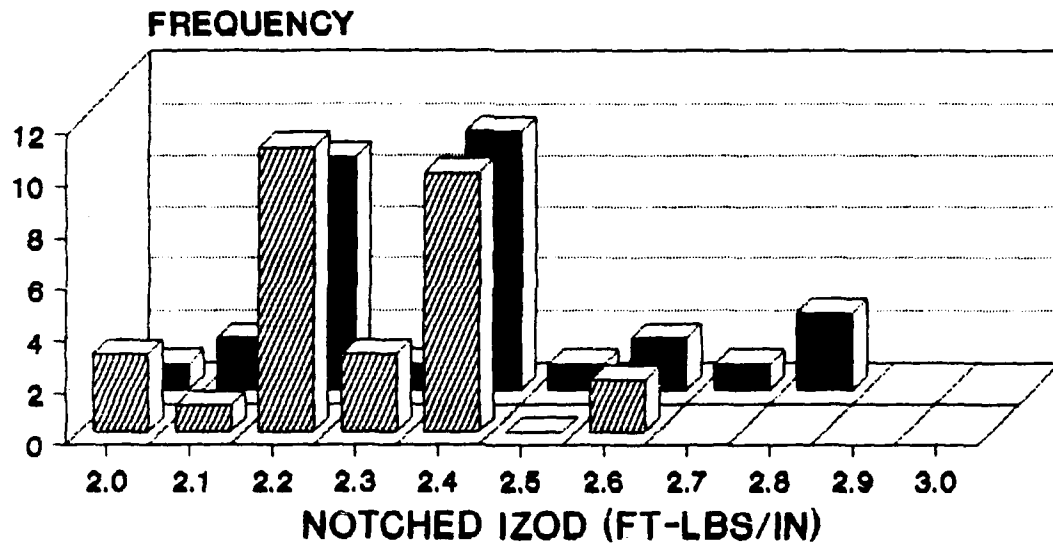
NOTCHED IZOD: SUPPLIER A CURRENT vs 2 YEAR OLD INVENTORY



 2 YR OLD SHEET	 CURRENT SHEET
AVG = 2.3 FT-LBS/INCH	AVG = 2.3 FT-LBS/INCH

TOTAL: 30 SPECIMENS EACH
SAMPLES CUT FROM 0.250" SHEET

NOTCHED IZOD: SUPPLIER B **CURRENT vs 2 YEAR OLD INVENTORY**

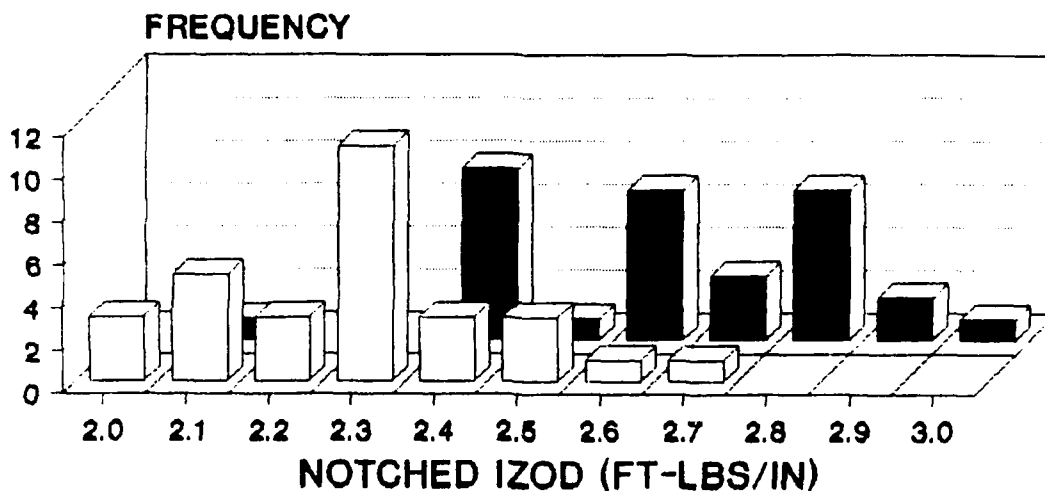




2 YR OLD SHEET
 AVE: 2.3 FT-LBS/IN

CURRENT SHEET
 AVE: 2.35 FT-LBS/IN

TOTAL: 30 SPECIMENS EACH
SAMPLES CUT FROM 0.250" SHEET

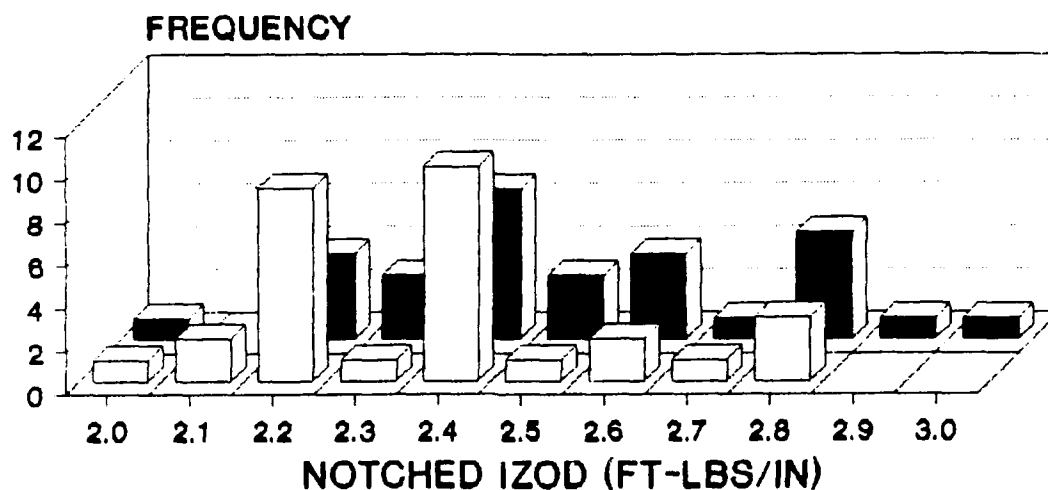
IZOD OF SUPPLIER A SHEET vs REGRIND **COMPARISON OF SHEET vs REGRIND OF SHEET** **INJECTION MOLDED INTO BARS**



 SUPPLIER A SHEET	 INJ-MOLD REGRIND
AVG = 2.3 FT-LBS/INCH	AVG = 2.6 FT-LBS/INCH

0.250" SPECIMENS
INJ-MOLDED BARS HAVE 2 HEAT CYCLES

IZOD OF SUPPLIER B SHEET vs REGRIND **COMPARISON OF SHEET vs REGRIND OF SHEET** **INJECTION MOLDED INTO BARS**



 **SUPPLIER B SHEET**
 AVG = 2.35 FT-LBS/INCH

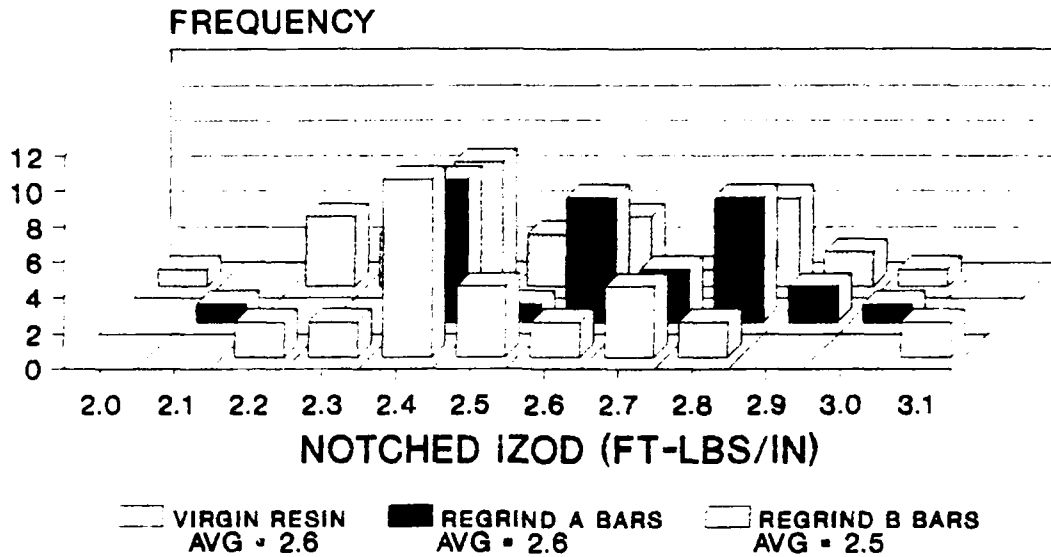
 **INJ-MOLD REGRIND**
 AVG = 2.5 FT-LBS/INCH

0.250" SPECIMENS

INJ-MOLDED BARS HAVE 2 HEAT CYCLES

NOTCHED IZOD IMPACT STRENGTH

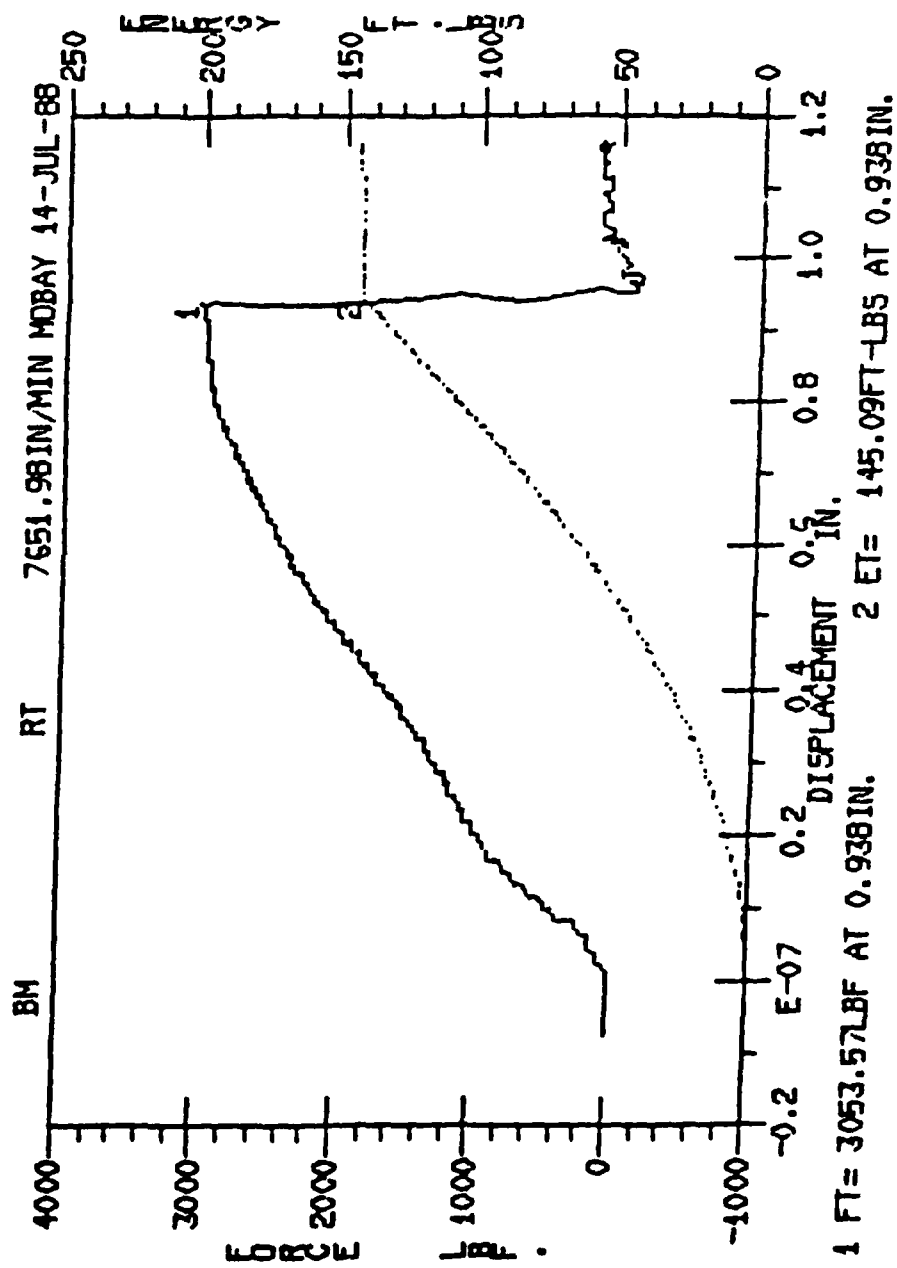
A & B SHEET REGRIND vs VIRGIN RESIN
INJECTION MOLDED INTO BARS



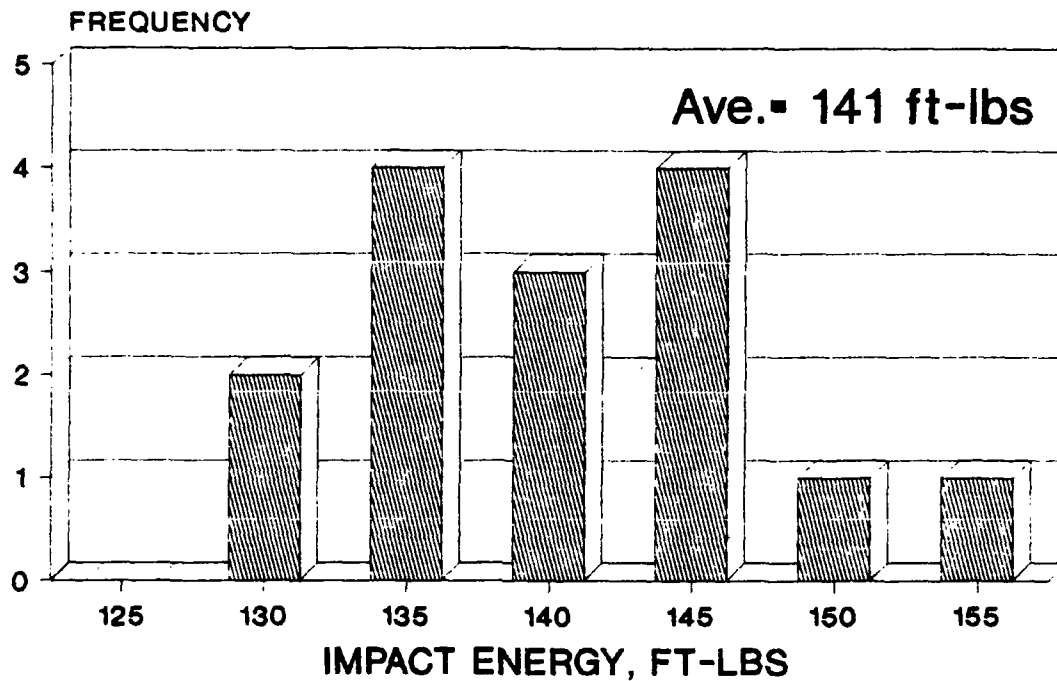
0.250" SPECIMENS
BARS MOLDED WITH EQUIVALENT STRESS
REGRIND SPECIMENS HAVE 2 HEAT HISTORIES

INSTRUMENTED DART IMPACT

GRAPHIC DISPLAY OF FORCE AND ENERGY REQUIRED TO PENETRATE THE SAMPLE

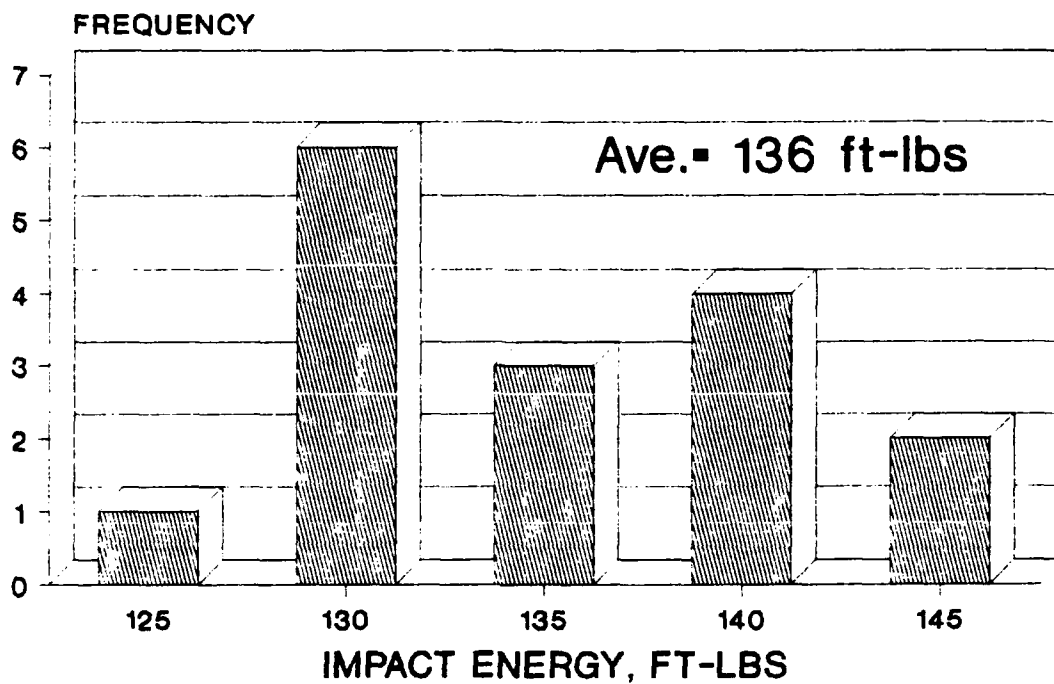


SUPPLIER A SHEET
INSTRUMENTED IMPACT OF CURRENT INVENTORY



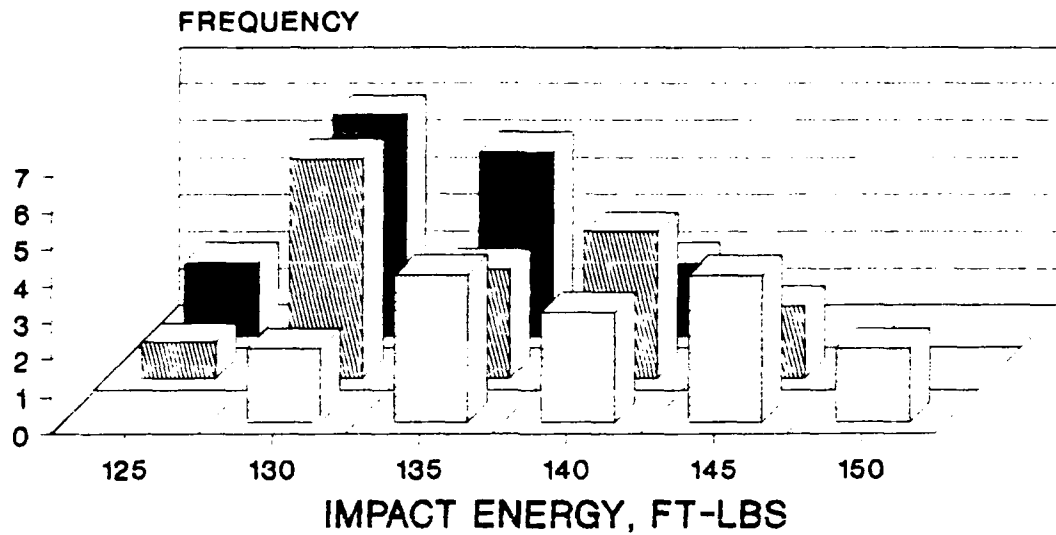
TOTAL: 15 TEST SPECIMENS
INSTRUMENTED IMPACT SPEED = 7500 In/min

SUPPLIER B SHEET
INSTRUMENTED IMPACT OF CURRENT INVENTORY



TOTAL: 16 TEST SPECIMENS
INSTRUMENTED IMPACT SPEED • 7500 In/min

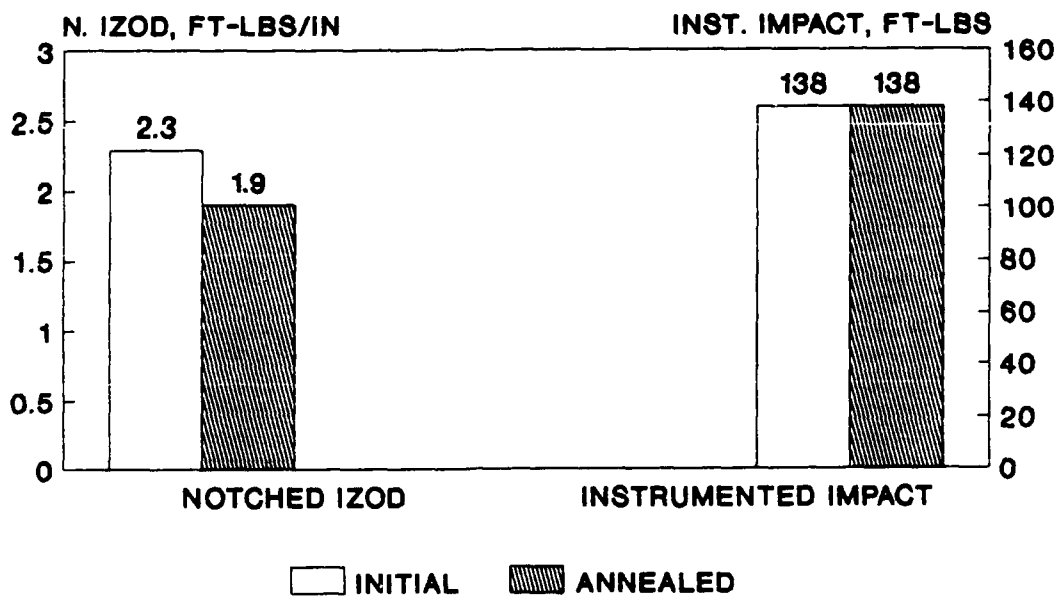
INSTRUMENTED IMPACT SUPPLIERS A & B vs AGED SHEET



 SUPPLIER A AVG = 141 ft-lbs	 SUPPLIER B AVG = 136 ft-lbs	 AGED SHEET AVG = 131 ft-lbs
---	---	--

IMPACT SPEED = 7500 in/min; 0.5 IN. DART
 SAMPLES TAKEN FROM 0.250" SHEET
 SHEET AGED AT 250F FOR 10 DAYS

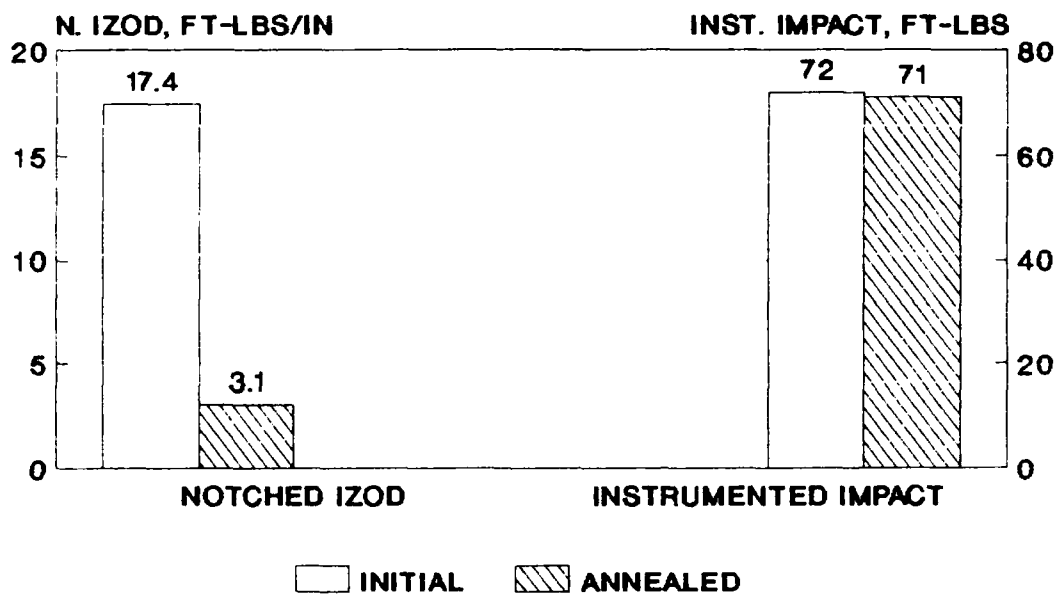
NOTCHED IZOD and INSTRUMENTED IMPACT INITIAL vs ANNEALED SAMPLES



SAMPLES ARE 0.250 INCH

SAMPLES AGED 2 HRS AT 250F

NOTCHED IZOD and INSTRUMENTED IMPACT INITIAL vs ANNEALED SAMPLES



SAMPLES ARE 0.125 INCH

SAMPLES AGED 2 HRS AT 250F

SILICONE INTERLAYER ADHESION CHARACTERISTICS

Dr. Cliff Juengst
Don LeMasters
Hai-Tao Wang

Swedlow, Inc.

SILICONE INTERLAYER ADHESION CHARACTERISTICS

Dr. Cliff Juengst
Mr. Don LeMasters
Mr. Hai-Tao Wang

SWEDLOW, INC.

ABSTRACT

Silicone adhesion presents a challenge for aircraft transparency manufacturers. Several factors affect the adhesion of silicone to acrylic, polycarbonate and electrically conductive glass surfaces. These factors are discussed. Bond adhesion test methods are reviewed. Sample preparation and testing procedures are shown for glass windshield programs. Representative bond adhesion values and failure modes from these tests are noted.

Loss of silicone adhesion limits the service life of windshields. Delamination of the silicone interlayer has been a recurring problem with the B1-B windshield. The failures are time-dependent, and are believed to be due in part to low residual stress in the interlayer, temperature and humidity. Results of time-dependent adhesion failure studies employing fixed strains, elevated temperature and humidity exposure are presented.

INTRODUCTION

Silicone interlayers are employed in laminated transparencies in many high-performance aircraft, including the B1-B, F-14 and F-111. Silicone is often selected for the most demanding applications due to its outstanding mechanical properties and excellent thermal stability. The very low glass transition temperature, $<-100^{\circ}\text{C}$, and thermal-oxidative stability to $>300^{\circ}\text{C}$, allow silicone interlayers to maintain low modulus and other elastomeric properties throughout the operating temperature range of modern aircraft.

The excellent elastomeric properties of silicone interlayers allow each ply in a laminate to expand and contract as temperature varies without transmitting high stresses to the bond line or to the other bonded ply. This is especially important where there are large differences in thermal coefficients of expansion of the two plies, such as in glass/plastic laminates. An example of such an application is the B1-B windshield, where silicone is used between the glass outer and polycarbonate structural ply. Silicone is also used in the B1-B windshield between the thin inner polycarbonate spall shield and the structural ply, to decouple the plies and prevent crack propagation during projectile impact.

In all-plastic laminated transparencies, a silicone interlayer is often selected primarily for its thermal stability. Examples of such applications are windshields in F-14 and F-111 aircraft, where silicone is used to bond thin as-cast acrylic outer plies to plastic structural components. In these applications, the low modulus of silicone over a wide temperature range also reduces outer ply cracking, which can occur due to sharp thermal gradients experienced under some flight conditions. Transparencies for advanced aircraft with even higher operating temperature requirements are also being designed with silicone interlayers.

CHEMISTRY OF SILICONE INTERLAYERS

Silicone elastomers employed as interlayers are a mixture of polydimethylsiloxanes and filler. The polydimethylsiloxanes contain chemical functional sites which react during the cure to form a crosslinked network. Cure chemistry is most commonly vinyl-hydride addition polymerization catalyzed by a platinum compound (Figure 1). The filler is chemically bonded to the matrix to provide effective reinforcement, and also must be in very small particulate form or be compatible with the matrix to maintain transparency.

Silicone interlayers are commonly cast from a liquid resin mix, which cures to a crosslinked elastomer and develops adhesion to substrates at a moderately elevated temperature. Swedlow SS-5272Y HT silicone is an example of such a

cast-in-place resin. Physical properties available from these types of materials are shown in Figure 2. The wide range of properties that can be obtained from cast-in-place silicones allows tailoring of the interlayer to yield optimum properties for a given application. Alternatively, silicone interlayer material is available in B-staged sheet form from Dow Corning (X4-4643). This material requires heat and pressure to laminate transparency components together and develop full mechanical properties.

BONDING SILICONE INTERLAYERS

The inherent properties of silicone elastomers present special problems in bonding them to other substrates. The low surface energy of polydimethylsiloxane allows uncured liquid resin to spread evenly (i.e., wet out) over most surfaces. However, lack of other bonding modes (i.e. electrostatic or chemical) prevents formation of a strong adhesive bond to the substrate, so adhesion is due solely to weak intermolecular forces. Incidentally, this is why silicone fluids are often used as release agents.

The key to achieving high adhesion with silicone elastomers is to maximize chemical compatibility between the silicone and the substrate. This requires use of an effective primer coating. The primer must form a high optical quality film on the substrate, must contain reactive sites or other functional groups which result in high adhesion to both silicone and substrate, must be transparent, and must be stable to the environments experienced in service.

Primers are usually applied as dilute solutions in organic solvents by spray, flow or wipe coating processes. With substrates which are sensitive to solvent attack, such as polycarbonate, the selection of solvent carriers for the primer is severely limited. Plastic substrates also limit the maximum temperature which can be used to dry or cure the primer film. These limitations can present significant problems in primer development.

ADHESION TESTS

Three adhesion tests are commonly used to characterize silicone/substrate adhesion. The simplest procedure is the tensile test, which is used for quality control purposes on many transparency programs. The typical tensile specimen is shown in Figure 3. The measured tensile strength is normally between 150 and 450 psi depending on the silicone formulation, cure cycle, interlayer thickness and rate of loading. Ideally, the failure should be cohesive in the silicone. This indicates that the full strength of the silicone is being used. Cohesive failure occurs in the silicone in a plane perpendicular to the direction of applied force.

The peel test is also widely used, especially to measure silicone/glass adhesion (Figure 4). The test is run after initiating the peel with a razor blade at the

glass surface. The peel force is perpendicular to the plane of the bar. Typical peel strengths are 12 to 60 pounds per inch width (piw) with cohesive failure, which is 45 degrees offset from the direction of the peel force (Figure 5).

The shear test is the most difficult to duplicate reliably. Three- and five-ply shear specimens are shown in Figure 6. The five-ply specimen is more difficult to fabricate, but the five-ply fixture controls the specimen geometry better and reduces the degree of tensile and peel forces introduced at high strains. Normal shear strengths range from 100 to 250 psi. Failure usually initiates at the silicone/substrate interface, and spreads in a plane into the silicone at a 30-60 degree angle from the direction of applied force.

ENVIRONMENTAL EFFECTS

The interlayer in laminated transparencies can be exposed to cleaning fluids and fuels during routine operation and maintenance with some designs. Exposure times to such chemicals are relatively short, so only chemicals which are aggressive and rapidly absorbed will affect the bond line. On the other hand, water, especially water vapor, is ever present. While a silicone elastomer will resist absorption of liquid water due to its low surface energy, water vapor readily migrates into the material and can reach the bond line unless an effective barrier is present. Depending on the primer chemistry, degradation of the bond might occur by hydrolysis of silicon/oxygen bonds or disruption of electrostatic bonding sites. Thus, water absorption over a long period of time might lead to adhesive failure, and is a factor which must be evaluated to fully characterize a silicone/primer system.

The effect of water on the adhesion of silicone to ITO-coated glass was evaluated with two primers using a 90 degree peel test. The test specimen configuration used is shown in Figure 4, with a 0.200" thick interlayer. The same lot of a standard cast-in-place silicone was used for all samples. Primers used were Swedlow SS-6569, a conventional glass primer, and SS-6849, a developmental primer designed for improved resistance to water. Sets of peel specimens made using the two primers were exposed to water vapor under accelerated conditions (120°F/ 100%RH), and peel strengths were determined periodically. Results are plotted in Figures 7 and 8.

Figure 7 shows that water exposure causes rapid reduction in peel strength with SS-6569 over the first 100 hours exposure, while strength is essentially unaffected with SS-6849. Figure 8 shows that the failure mode shifts from cohesive to adhesive with both primers as exposure time increases. With SS-6569, the transition occurs during the first 50-100 hours; with SS-6849, after 200-300 hours. These results illustrate the dramatic effect water can have on bond strength, and show that primers that are apparently equivalent based on standard tests can have much different performance when water exposure is introduced as a variable.

TIME-DEPENDENT PROPERTIES

Adhesion tests described above are useful to characterize and compare silicone interlayers and primers, but do not represent conditions experienced by transparencies in service, where bond lines are subjected to small constant or cyclic strains coupled with environmental exposure. For a large glass-faced polycarbonate transparency, a fixed strain may be as high as 0.25-0.30 radians in shear and 0.01 in tensile. This leads to a residual stress that can be as high as 40 psi.

To better duplicate actual loading conditions, time-dependent adhesion tests were run on specimens at strains below the failure point observed in short-term tests. Tests were run in both tensile and shear modes, and with both glass and polycarbonate substrates. Figure 9 shows test specimens used for this study. The test fixture holds block "A" fixed, and flat plates apply a tensile or shear strain to block "B". Samples were all made using the same lot of standard cast-in-place silicone. Several sets of data were gathered at different temperatures and fixed strains. The data allow a time-temperature relationship to be developed for different strains, which provides a means to estimate the time to adhesive failure at different operating temperatures and fixed strains.

Figures 10 and 11 show typical plots of time to failure versus tensile or shear strain for silicone/glass samples at 150°F, and Figures 12 and 13 show corresponding plots for silicone/polycarbonate samples. Mixed failure modes (cohesive/adhesive) were observed in many of these specimens. In general, higher strain loads result in cohesive failure while the lower strain loads lead to interfacial adhesive failure between the silicone and the substrate.

Humidity exposure was added as a variable in some of the studies. Figure 14 shows plots of time to failure versus shear strain of samples exposed at 100°F and 100% RH along with samples exposed at 100°F under dry conditions. Partial results of a similar study using tensile loads are summarized in Figure 15.

A number of important conclusions were drawn from the data shown in Figures 10-15:

1. Silicone/substrate bond strength is a strongly time-dependent property. Relatively low tensile or shear loads operating over long periods of time can cause adhesion failure.
2. Bond strength appears to have a stronger dependence on loading time with residual tensile strains than with residual shear strains.

3. Exposure to water vapor results in a marked reduction in time to failure under constant load conditions.

A limited understanding of these factors at the time the B1-B windshield was designed and developed resulted in design inadequacies, which has led to a relatively high frequency of silicone interlayer delamination in the field. Even though silicone is the best interlayer for this application, its properties and limitations are still not adequately characterized. Effects of environmental exposure and time-dependency of properties are two areas where a better understanding is needed.

CONCLUSIONS

1. Silicone elastomers have an attractive balance of properties which make them the preferred interlayer for many high-performance aircraft transparencies.
2. The inherent properties of silicones present special problems in bonding to other substrates. Primers that are specially-designed for the silicone and substrate are required for high adhesion.
3. Adhesion of silicones is strongly time-dependent. Low residual strains operating over long time periods can cause adhesion failure in laminated transparencies.
4. Exposure of silicone/substrate bond lines to water vapor causes rapid reduction in adhesion with current primers. The effect can be reduced by use of primers which are more resistant to water, such as SS-6849.
5. The limitations of silicones and detrimental effects of residual strains and water exposure must be taken into account in transparency designs. Residual strains should be minimized, and bond lines should be protected from environmental exposure.
6. Additional work is needed to better define design limits of current silicones, to develop an understanding of the mechanism of the time-dependency of adhesion and observation of mixed failure modes, and to develop an understanding of the mechanisms by which water degrades adhesion. Work should also continue to develop tougher transparent silicones and improved primer systems.

FIGURE 1
VINYL-HYDRIDE ADDITION POLYMERIZATION

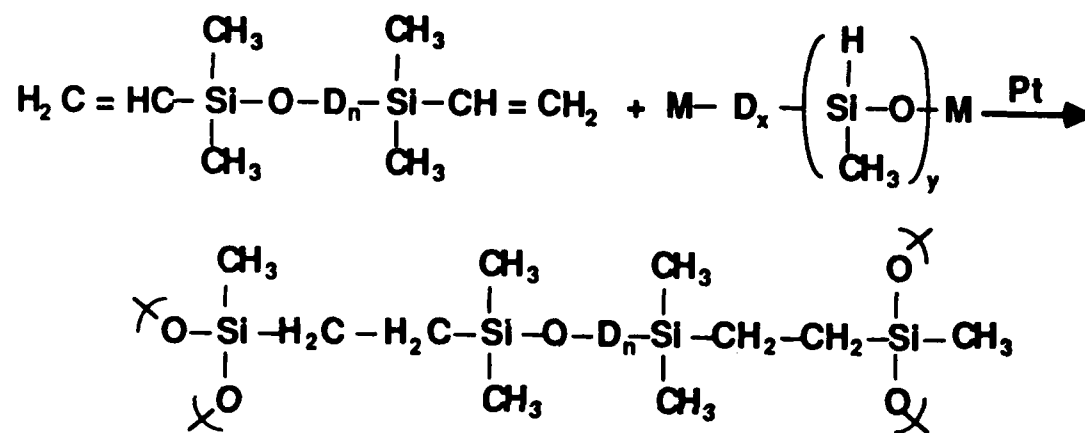


FIGURE 2
PHYSICAL PROPERTIES OF CURED SILICONE RESIN

	ASTM	MINIMUM	MAXIMUM
Tensile Strength(psi)	D412	360	820
Ultimate Elongation(%)	D412	320	600
Modulus (psi)			
100%		51	680
200%		140	690
300%		270	750
Shore "A" Hardness	D2240	25	60
Tear Strength(ppi) ¹	D624	21	77

¹ ppi = Pounds per inch thickness

FIGURE 3
BOND TENSILE SPECIMEN CONFIGURATION

SPECIMEN DIMENSIONS AND TOLERANCES

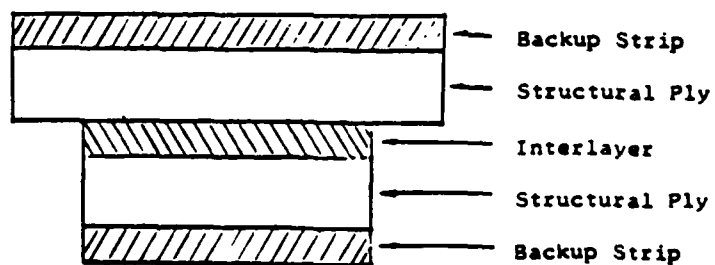
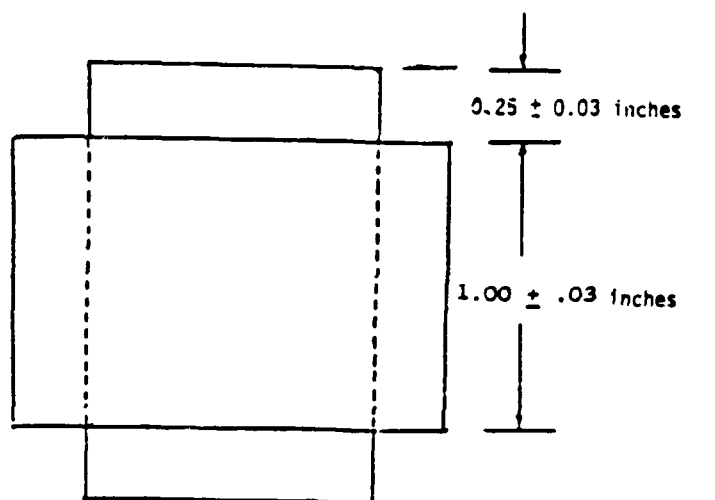


FIGURE 4
SILICONE INTERLAYER PEEL BAR CONFIGURATION

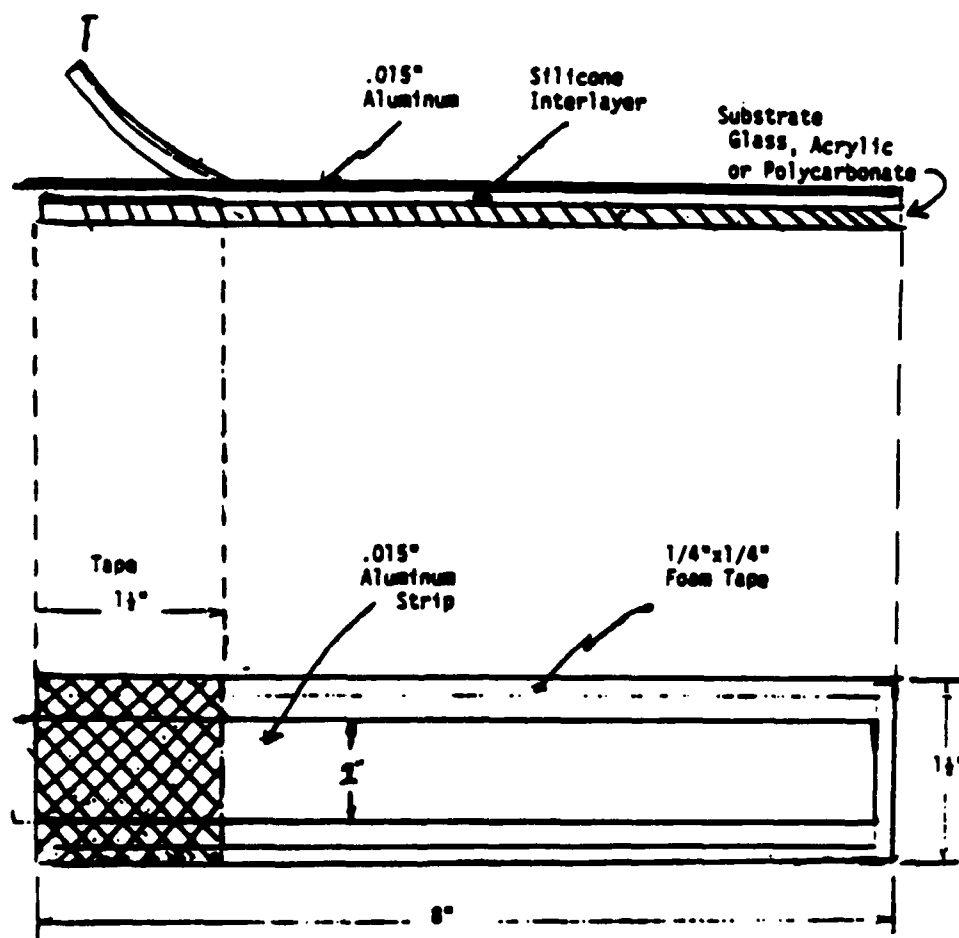


FIGURE 5
SHEAR PLANES IN THE SILICONE FROM COHESIVE FAILURE
IN THE 90 DEGREE PEEL TEST

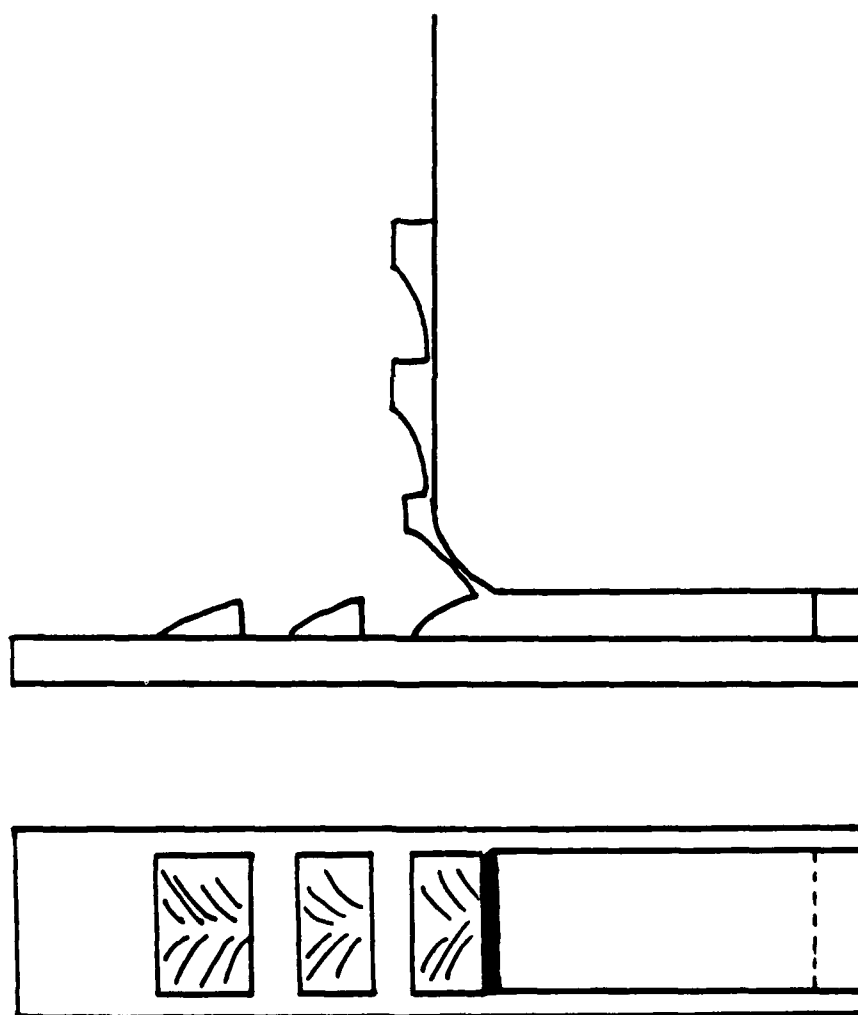
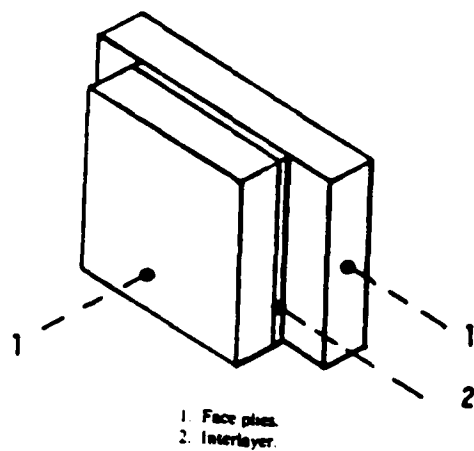
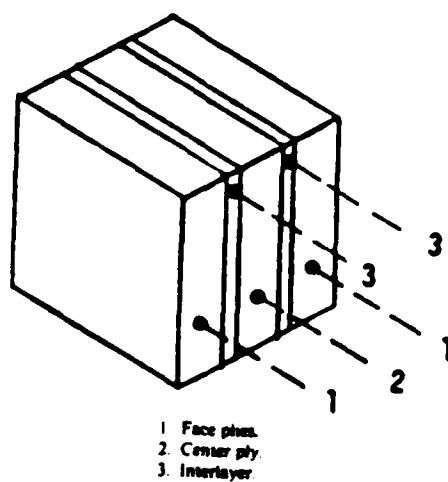


FIGURE 6
THREE-PLY AND FIVE-PLY TEST SPECIMENS CONFIGURATIONS



THREE-PLY SPECIMEN



FIVE-PLY SPECIMEN

FIGURE 7

PEEL STRENGTH AFTER HUMIDITY EXPOSURE
(120°F/100% Relative Humidity)

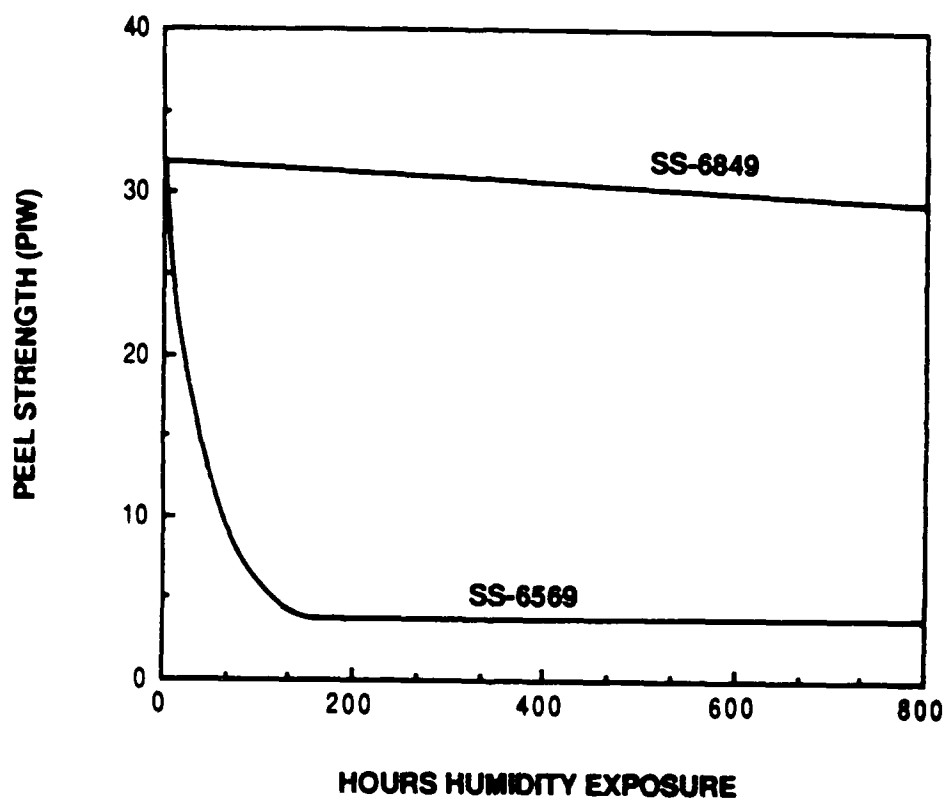


FIGURE 8
FAILURE MODE OF PEEL BARS AFTER HUMIDITY EXPOSURE
(120°F/100% Relative Humidity)

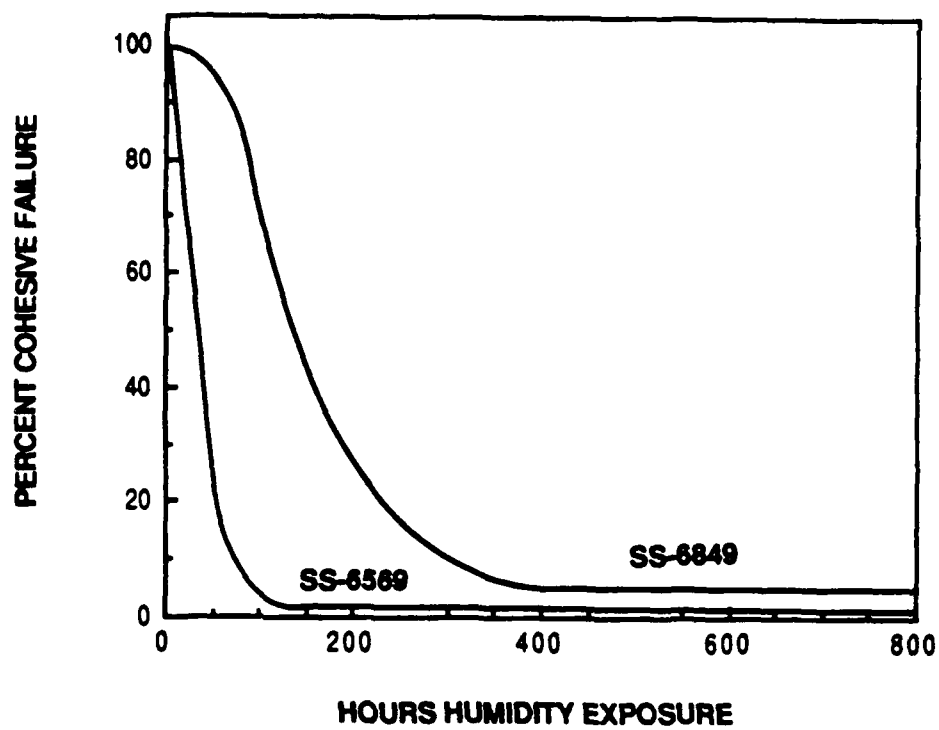


FIGURE 9
TEST SPECIMEN FOR FIXED STRAIN TIME DEPENDENT
FAILURE TESTS

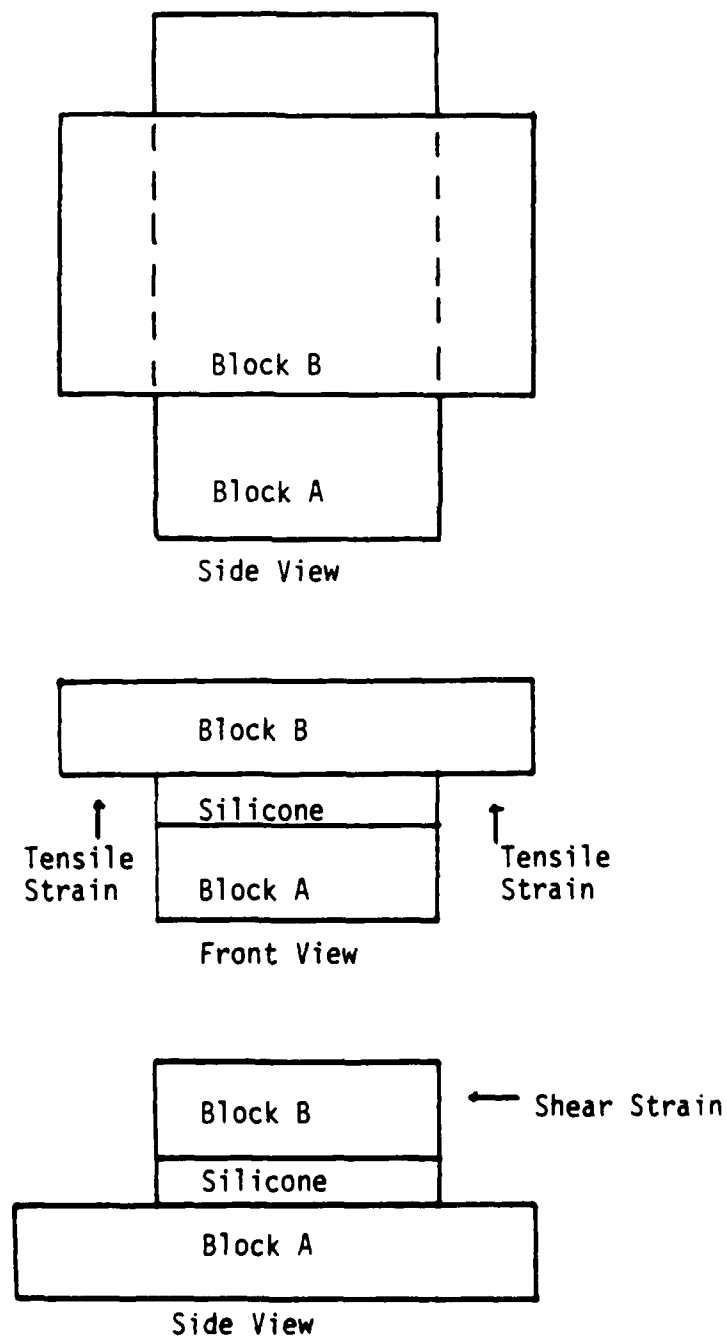


FIGURE 10
SILICONE TIME DEPENDENT ADHESION FAILURE - GLASS
SUBSTRATES
(150°F, TENSILE STRAIN)

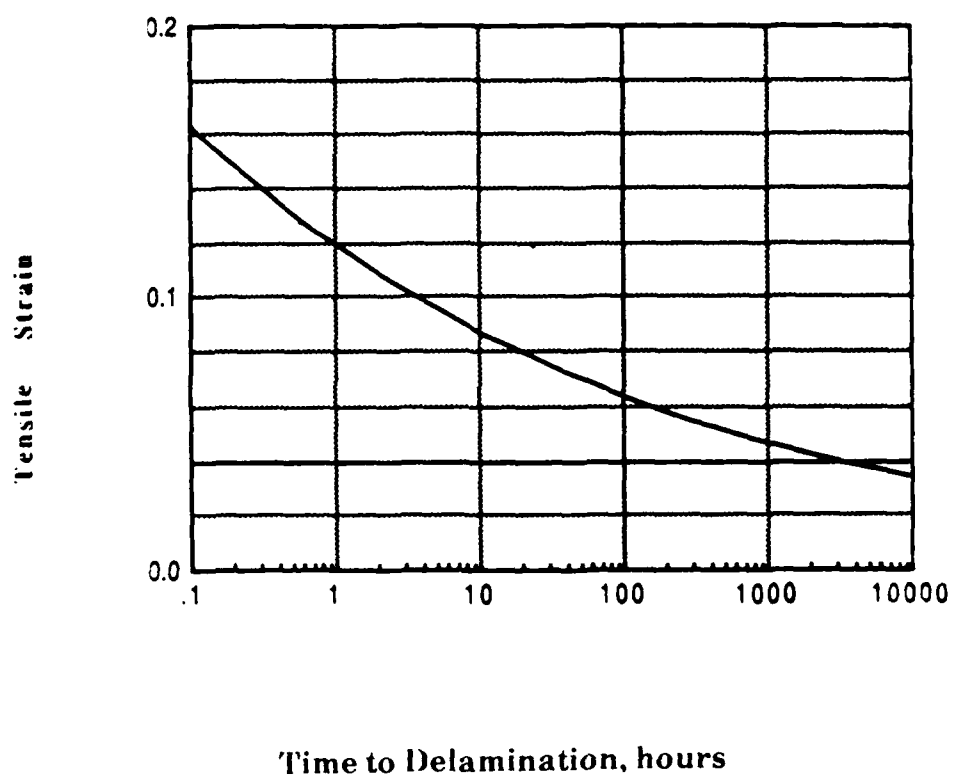


FIGURE 11
SILICONE TIME DEPENDENT ADHESION FAILURE - GLASS
SUBSTRATES
(150°F, SHEAR STRAIN)

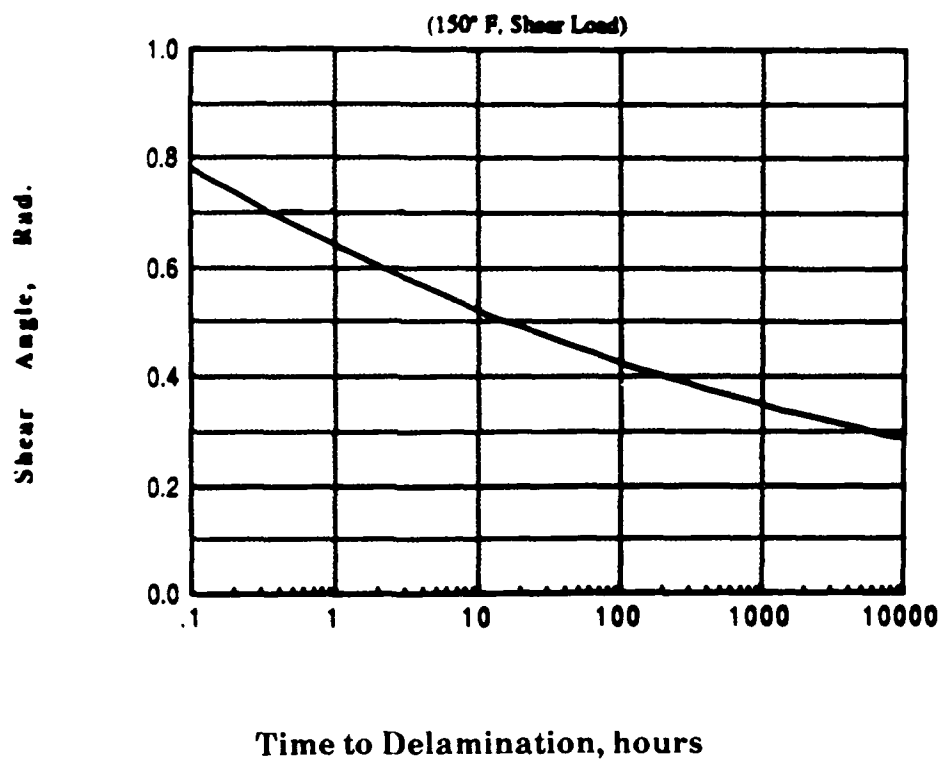


FIGURE 12
SILICONE TIME DEPENDENT ADHESION FAILURE
POLYCARBONATE SUBSTRATES
(150°F, TENSILE STRAIN)

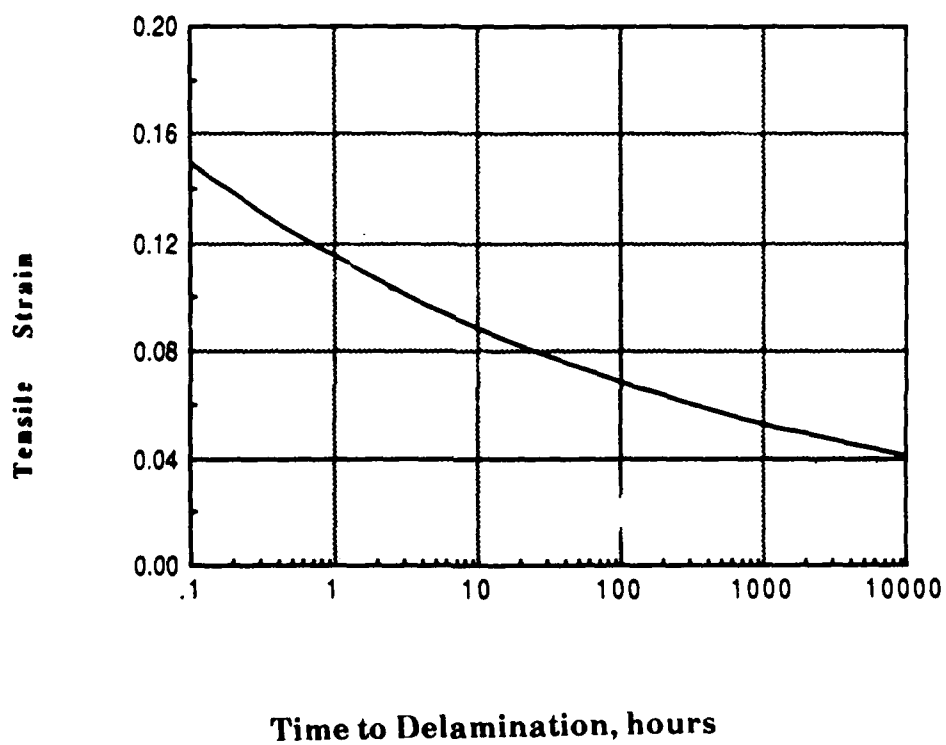


FIGURE 13
SILICONE TIME DEPENDENT ADHESION FAILURE
POLYCARBONATE SUBSTRATES
(150°F, SHEAR STRAIN)

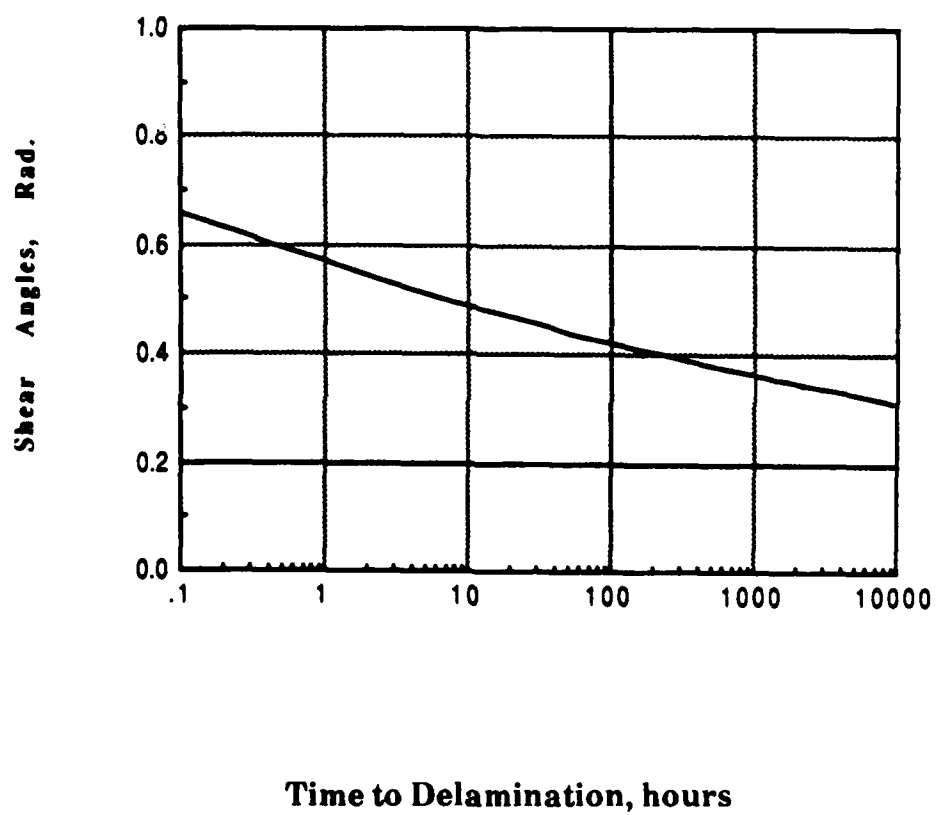


FIGURE 14
SILICONE TIME DEPENDENT ADHESION FAILURE
POLYCARBONATE SUBSTRATES
(100°F, 100% RELATIVE HUMIDITY, SHEAR STRAIN)

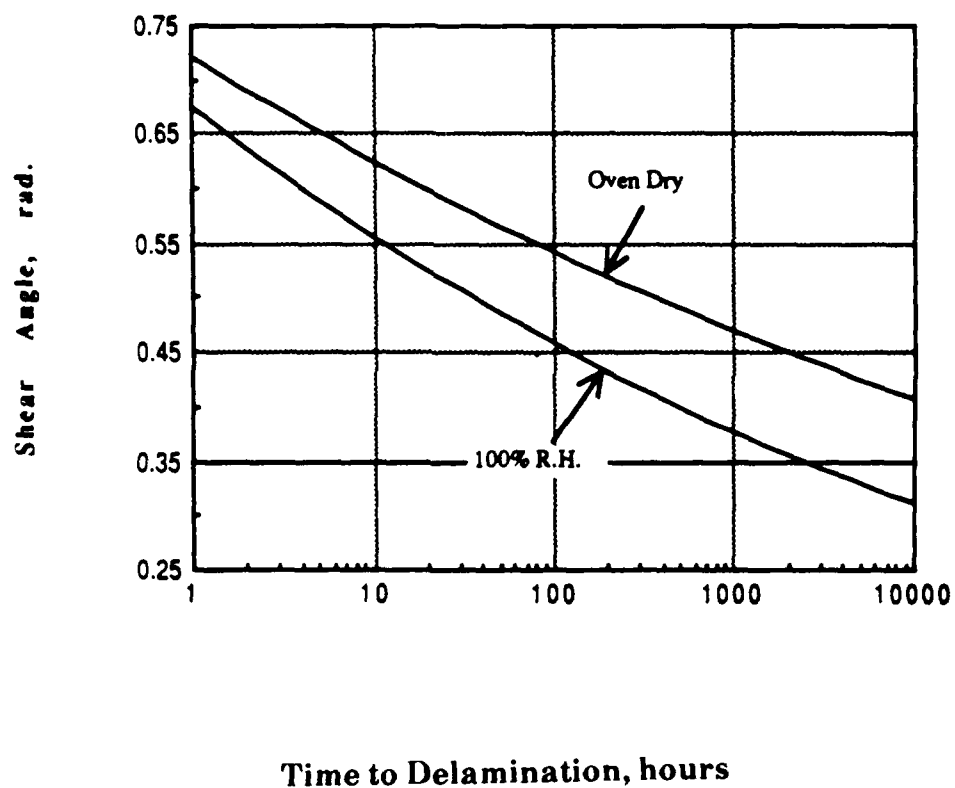
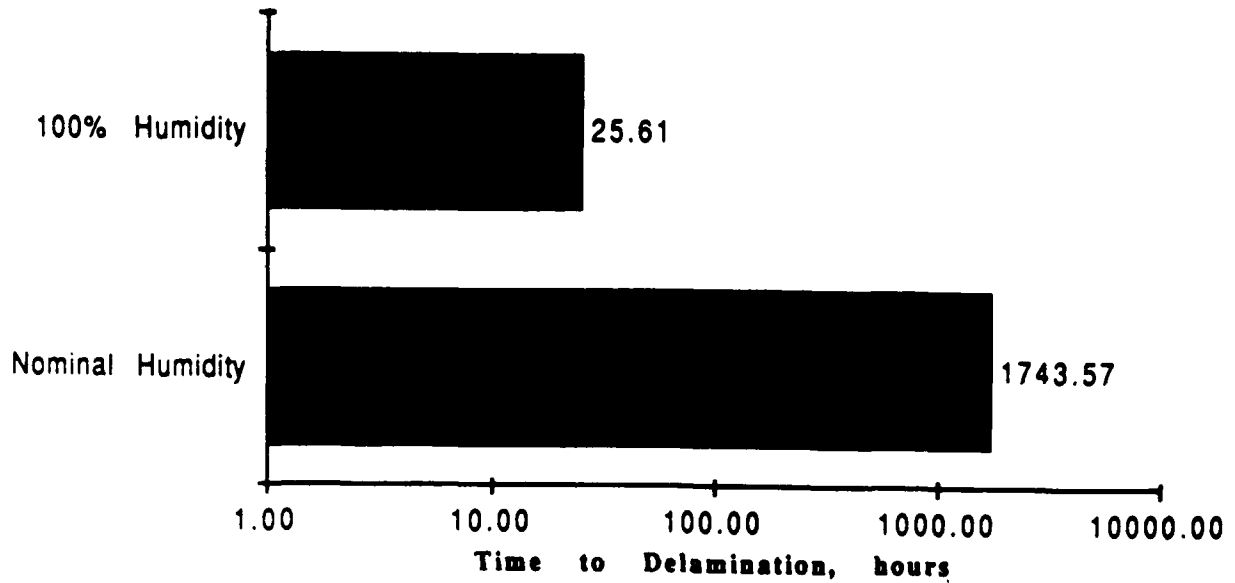


FIGURE 15
SILICONE TIME DEPENDENT ADHESION FAILURE
POLYCARBONATE SUBSTRATES
(100°F, 100% RELATIVE HUMIDITY, 0.11 TENSILE STRAIN)



TRANSPARENT CONDUCTIVE COATINGS

Dr. Harold Gurev
Dr. Mohammad Nisar

Swedlow, Inc.

TRANSPARENT CONDUCTIVE COATINGS

Dr. Harold Gurev
Dr. Mohammad Nisar

SWEDLOW, INC.

ABSTRACT

Transparent conductive coatings (TCC) for aerospace transparency applications fall into two distinct classes: semiconducting oxides and semitransparent thin metal films. A theoretical consideration of material properties which govern electrical conductivity as well as optical transparency shows that these two classes of TCC function in widely different modes because of differences in carrier concentration and mobility as well as band gap energy.

Solid state theory is utilized to predict fundamental limits on the performance of each class. The need to characterize the carrier concentration of semiconductor film products, as well as their electrical conductivity, to control their optical performance as TCC is discussed.

The transmittance of semitransparent thin metal films can be enhanced by sandwiching them between dielectric layers designed to suppress reflectance at each metal interface. Theoretical predictions of the performance of several enhanced gold and silver stack designs are compared to measured values of experimental deposits. The performance of these stacks is compared to typical ITO films deposited on a range of polymers (including polycarbonate, stretched acrylic, GAC-590). The inherent advantages and disadvantages of enhanced gold TCC versus ITO are discussed.

INTRODUCTION

Transparent, conductive coatings (TCC's) are playing an increasing role in the design of high performance aircraft transparencies. Two general classes of coatings can be engineered to satisfy these requirements.; wide gap semiconductors (notably oxides of such metals as In, Sn, Zn, Cd) and semitransparent noble metal films. These two classes are quite dissimilar in their structure as well as the physical manner in which they provide both electrical conductivity and optical transparency. We will explore the operative mechanisms in their optical action through use of the Drude¹ model of the interactions of light with free electrons. This approach will allow us to describe the inherent limitations on electrical conductivity and optical transparency for each class of TCC for specific applications.

We will then proceed to discuss the levels of performance which have been demonstrated with these TCC's on various polymer substrates.

THEORY

The Drude model describes an optical model for conductive materials based on a gas of free electrons. A conductor is described by two parameters: the density of free electrons and the scattering mechanisms operative. Over a limited spectral region, centered on the visible range, this model has been found to describe well the optical properties of metals and doped semiconductors²⁻⁴. The general features of a Drude material are shown in Fig. 1.

Absorption

Absorption occurs when the light frequency is low enough that the electrons can suffer many collisions during each alternation of the light's electrical field. The collision process gives rise to absorption. As frequency is increased, the free electrons can no longer respond to the shorter period of the alternating field and absorption falls. (At high frequency where the electric field is strong enough to cause interband transitions of bound electrons, strong absorption is again encountered in the UV).

Reflection

At low frequencies, the many collisions of the free electrons causes the electron cloud to reflect incoming light by scattering its electric field. As frequency of the incoming light increases, the screening action becomes weaker until, at the plasma frequency (ω_p) high infrared reflection is no longer produced. ω_p is proportional to the square root of electron density.

Fundamental Differences between Metals and Semi Conductor Films

The spectral properties of a wide band gap semiconductor, i.e. indium tin oxide, (ITO) are illustrated in Figure 2. Because electron density is low for such a material, the plasma frequency is below the visible range. Absorption will also be low through the visible range because of the low electron density.

Note that the carrier density of an ITO coating will depend on doping level; both by control of the Sn/In ratio as well as the degree of oxygen deficiency. By proper control of carrier density, high transmission can be provided in the visible by pushing the plasma frequency well into the NIR and suppressing free carrier absorption. We pay two prices for this engineering of "Drude properties" which can be especially important in the coating of polymers to low sheet resistance values.

1. The rather low electron density (as compared to a noble metal) requires that the ITO be much thicker for comparable sheet resistivity.
2. This situation is aggravated in ITO when coated on temperature-sensitive substrates. The structure of low temperature deposited ITO tends to be less ordered, providing more imperfections which limit carrier mobility and thus impede current flow. Since resistivity depends on the product of carrier concentration and mobility, ITO films deposited on polymers suffer a further thickness penalty.

For example, 10 ohm/sq. gold films have a bulk resistivity of near 10^{-5} ohm cm; typical ITO deposited on polymers is over 4×10^{-4} ohm cm. Hence an ITO film must be nearly 40 times thicker than a gold film of the same resistance.

Let us now consider the performance of a semitransparent noble metal film (Ag or Au) as described by the Drude model (Figure 3)⁵. As discussed previously, Au films can be quite thin to obtain high conductivity. This is fortunate because it limits the free-carrier absorption loss. However, the high density of free electrons pushes the plasma frequency into the UV, so the entire visible range transparency is dominated by gold's reflectance. Suppress the reflectance, and noble metal films become more effective TCC's. Such action is typically produced by the use of a sandwich of properly

designed antireflective dielectric layers around this gold. Several theoretical designs and measured performance are considered.

Calculated Optical Performance of Enhanced Metal TCC's

Calculated spectral values of transmittance and reflectance of a bare silver film, 150 Å thick, on an acrylic substrate are presented in Figure 4. The same values for a bare 150 Å gold film are shown in Figure 5. While silver has a small absorptance across the visible range, gold exhibits a strong intrinsic absorptance in the blue end of the spectrum which produces its characteristic color. From a phenomenological viewpoint, bound electrons in silver are more strongly bound requiring UV light of 3.8 eV to cause interband transitions, while these electrons in gold are more weakly bound and visible light of 2.2 eV (5635 Å) will excite them.

We then proceed to calculate the efficiency of a simple anti-reflecting optical stack to enhance transmission by suppressing reflectance of the noble metal layer's interfaces. Compare the performance of a typical $\text{TiO}_2\text{-Ag-TiO}_2\text{-SiO}_2$ design (Figure 6) with a $\text{TiO}_2\text{-Au-TiO}_2\text{-SiO}_2$ design (Figure 7). The blue absorptance of the Au design cannot be eliminated by anti-reflection designs, hence Ag designs will have superior optical performance. (Unfortunately the chemical reactivity of silver severely limits its practical application in corrosive media, including the atmosphere, without hermetic sealing. This is in sharp contrast to the chemical inertness of gold films.)

PROPERTIES OF TCC's ON PLASTIC TRANSPARENCIES

We have coated both types of TCC's on a variety of polymers, including stretched acrylic, polycarbonate and GAC-590. ITO has been sputtered and enhanced gold deposited by several proprietary processes. Figure 8 presents the spectral transmission curve for a typical ITO coating on stretched acrylic, to a sheet resistivity of 15 ohm/sq. Figure 9 shows the transmittance of a typical enhanced gold coating (of a $\text{TiO}_2\text{-Au-TiO}_2\text{-SiO}_2$ design) on stretched acrylic at a sheet resistivity of 4 ohm/sq.

The general optical performance of our coatings on plastic can be compared by reference to Figure 10 which plots the % LT of a series of coatings prepared by the ITO process, the enhanced gold process, and single layer bare gold.

As predicted by theoretical analysis, the sandwiching of the gold layer between anti reflecting dielectrics does appreciably improve the light transmission at sheet resistance as low as 3.5 ohm/sq..

The calculated value represents an upper bound on the performance of enhanced gold coatings which can be approached as the stoichiometry and density of the dielectric layers are improved to bring their optical constants closer to bulk values. The perfection of these layers is often limited by low substrate temperatures required for polymer deposition which prevents thermal activation of oxidation during deposition as well as restricting adatom mobility needed to obtain high packing density of the deposited oxide. Thus the fundamental restraint on the properties of TCC's on temperature-sensitive polymer substrates affects both the dielectric oxides of the enhanced gold stack as well as the conductive oxides as described earlier. While high performance TCC's on glass (especially ITO) have long been available, high performance TCC's on polymers are newly emerging technologies.

It is readily apparent that ITO films are superior in transmittance to enhanced gold over the entire range of resistance values tested. However resistance measurements during 3 point bending tests of acrylic coated with ITO and with enhanced gold (Figure 11) showed that the ITO begins to lose conductivity, by microcracking, at a strain as low as 0.6% while enhanced gold can be strained to 2.5%. The gold layer is inherently more ductile than the ITO which is a brittle oxide ceramic. We believe that the dielectric layers in the gold stack also crack at some level of tensile strain, but these cracks do not propagate into the gold layer, nor are they visible to the naked eye.

The inertness of gold does pose one technical challenge to the film designer; achieving required adhesion to the sandwiching oxide layers. Since gold forms no oxide, adhesion by mutual oxide solubility which occurs generally at metal-oxide interfaces is not possible. Proprietary film stack design modifications and refinements in deposition technologies have provided solutions to the adhesion problem.

The durability of TCC on plastic transparency substrates has been extensively measured. The results obtained on typical samples and reported in Table I for bare gold, enhanced gold and ITO, all were overcoated with polysiloxane abrasion resistant coatings (ARC) or polyurethane protective liners. These tests demonstrate that enhanced gold and ITO have excellent durability characteristics and that the enhanced gold avoids the microcracking due to thermal

stresses found in ITO samples, when exposed to extremes of temperature.

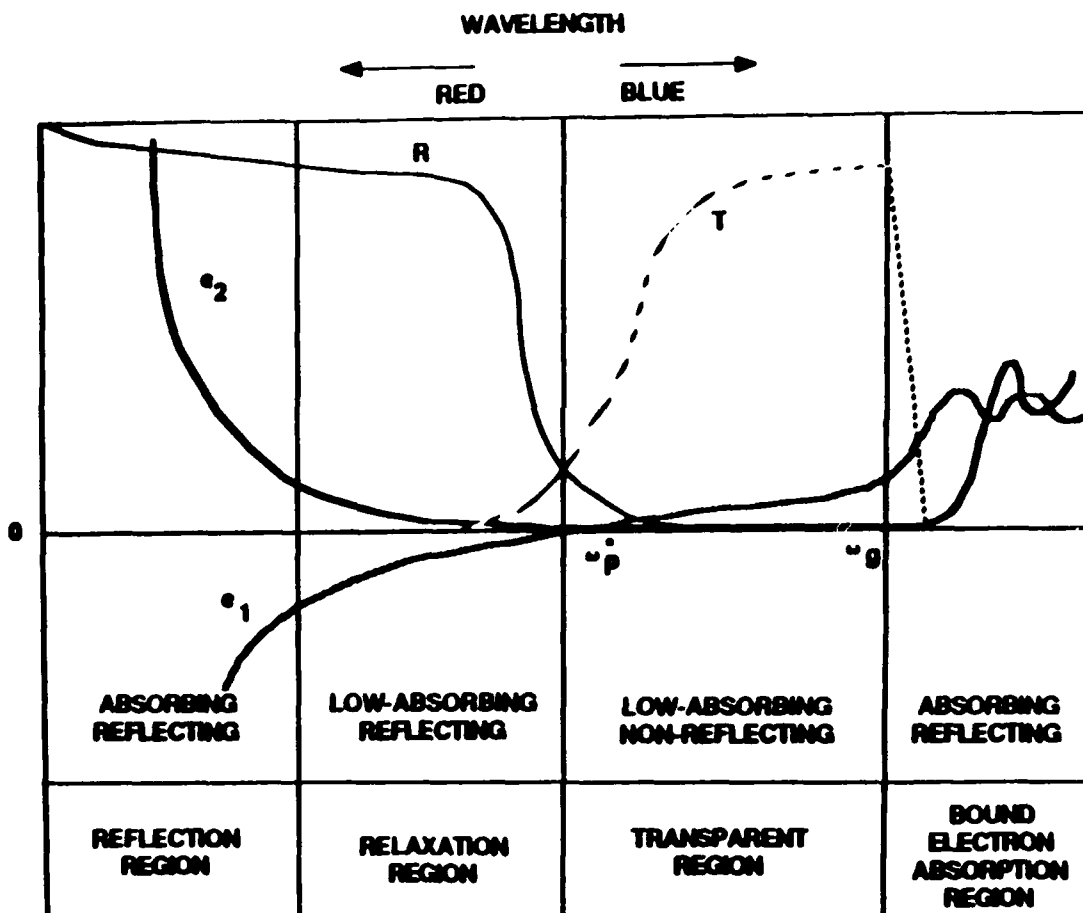
CONCLUSIONS

1. The use of ITO on plastic transparencies will be limited by the sensitivity of the application to microcracking conditions. Enhanced gold will withstand strains which are four times higher.
2. TCC's with transmission near 70-72% LT and sheet resistance near 3.5 ohm/sq. have been demonstrated by enhanced gold technology.
3. The performance of enhanced gold TCC's can be readily tailored to specific application by adjustment of the thickness of the component layers in the optical stack design.
4. Significant improvement in % LT could be realized with enhanced silver designs if the silver could be adequately protected from atmospheric corrosion.
5. Properly engineered enhanced gold TCC's provide durability suitable for the aircraft environment.

REFERENCES

1. P. Drude, Z. Phys. 1 (1900) 161.
2. K.L. Chopra et al, Thin Solid Films, 102 (1983) 1-46.
3. G. Frank et al, Appl. Physics, A27, (1982) 197-206.
4. C.M. Lampert, Solar Energy Materials, 6 (1981) 1-25.
5. B. Karlsson, et al, Proc. SPIE, 327 (1982) 156-179.

FIGURE 1
OPTICAL BEHAVIOR OF DRUDE MATERIAL



The response of free electron gas varies with wavelength causing characteristic changes in reflectance (R), transmittance (T) and dielectric constants (ϵ_1 , ϵ_2) (Ref.5)

FIGURE 2
SPECTRAL PROPERTIES OF A TRANSPARENT
REGION THM

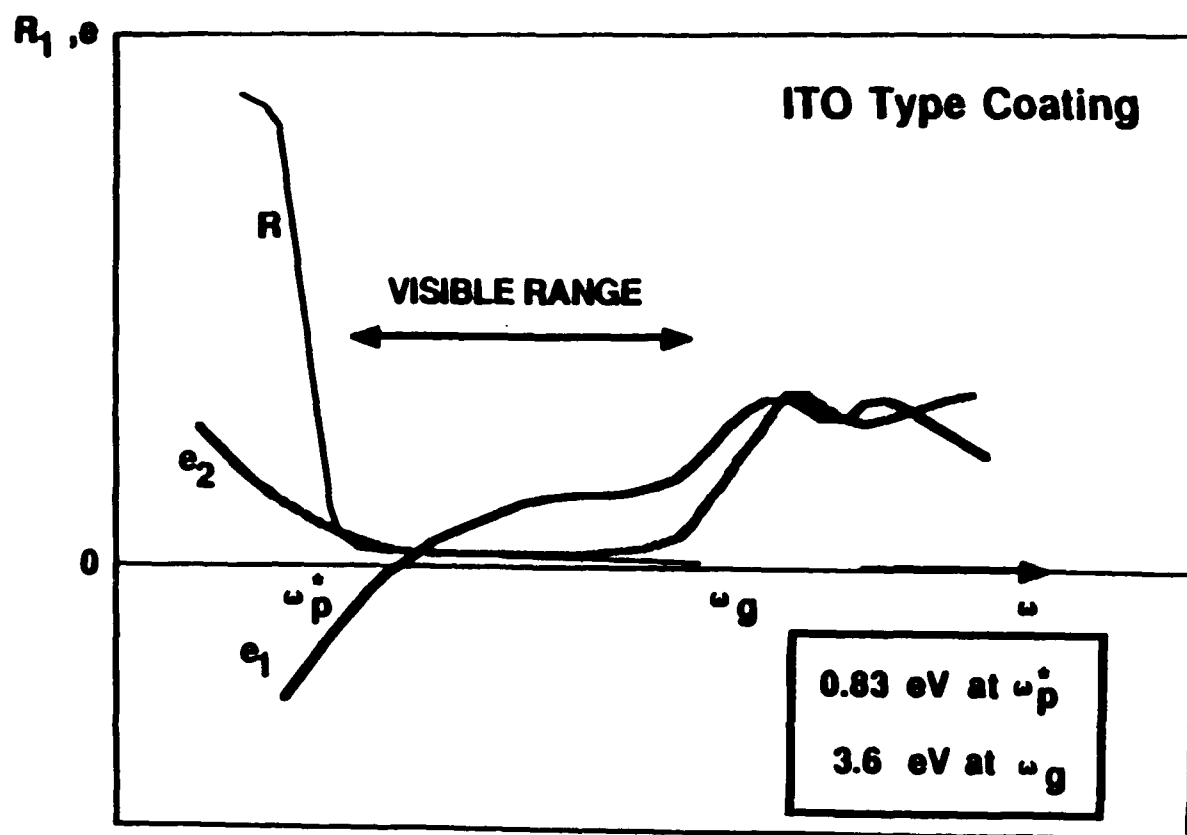


FIGURE 3

SPECTRAL PROPERTIES OF A RELAXATION
REGION REFLECTANCE LIMITED THM

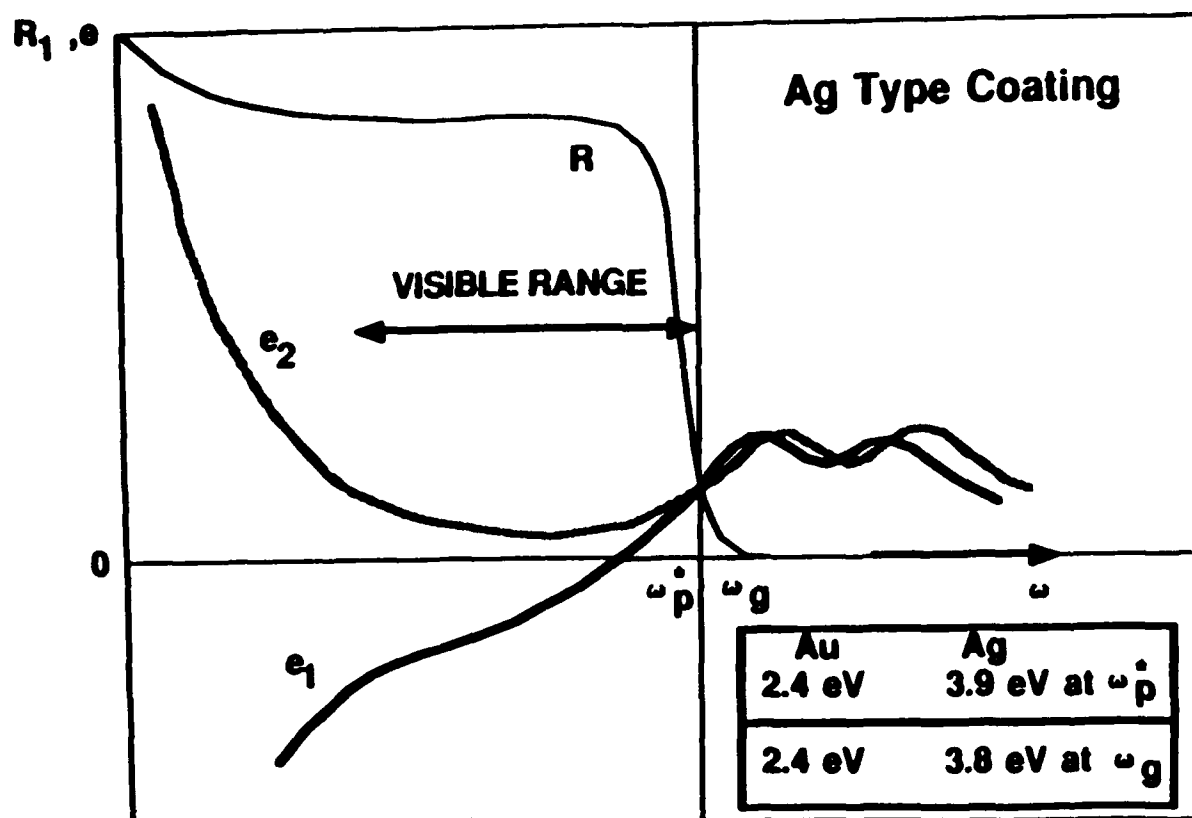


FIGURE 4
BARE SILVER ON ACRYLIC
150 Angstrom Thick Silver Coating on 0.25" Thick
Acrylic Sheet

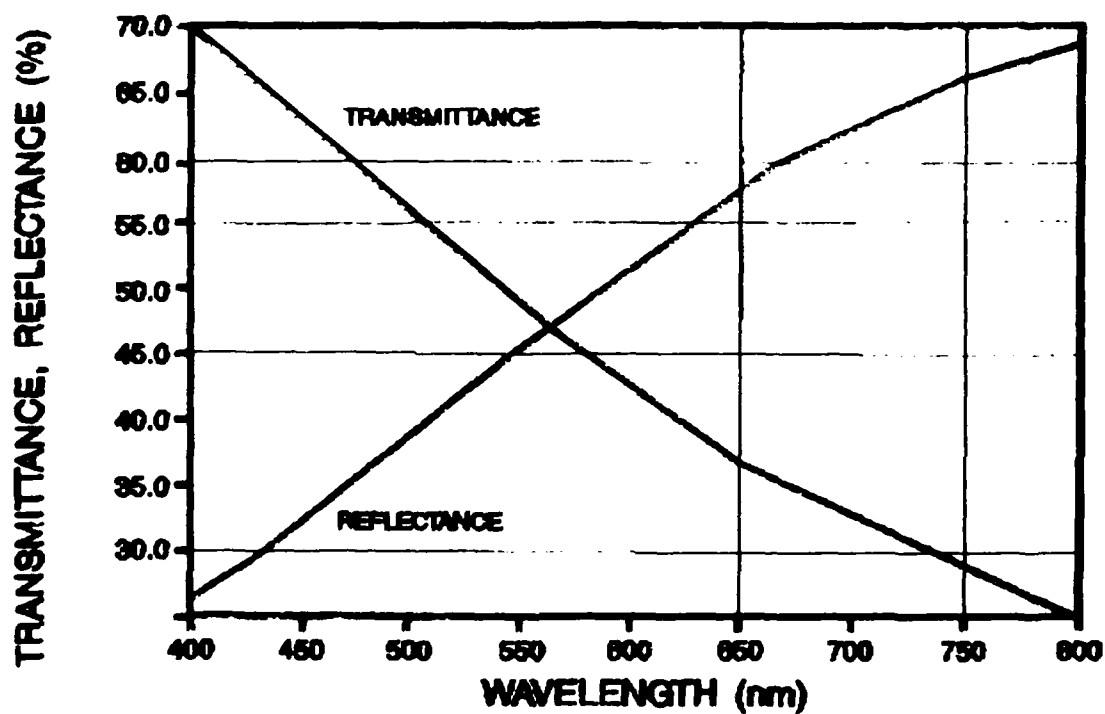


FIGURE 5

BARE GOLD ON ACRYLIC

150 Angstrom Thick Gold Coating on 0.25" Thick Acrylic Sheet

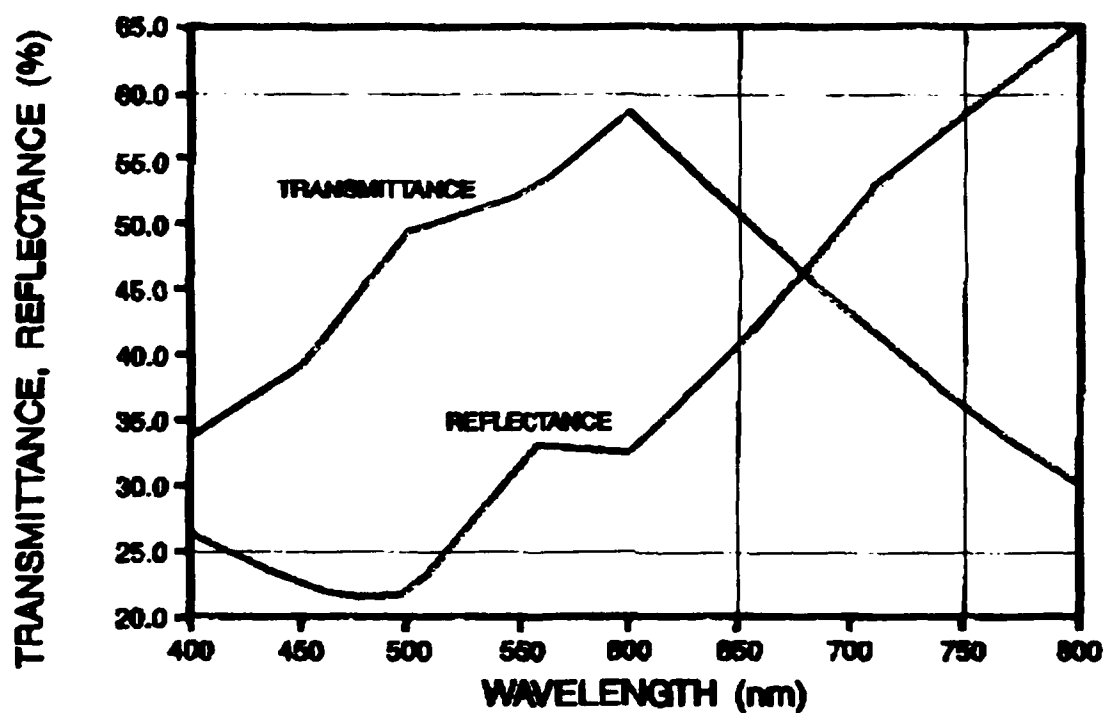


FIGURE 6
ENHANCED SILVER ON ACRYLIC

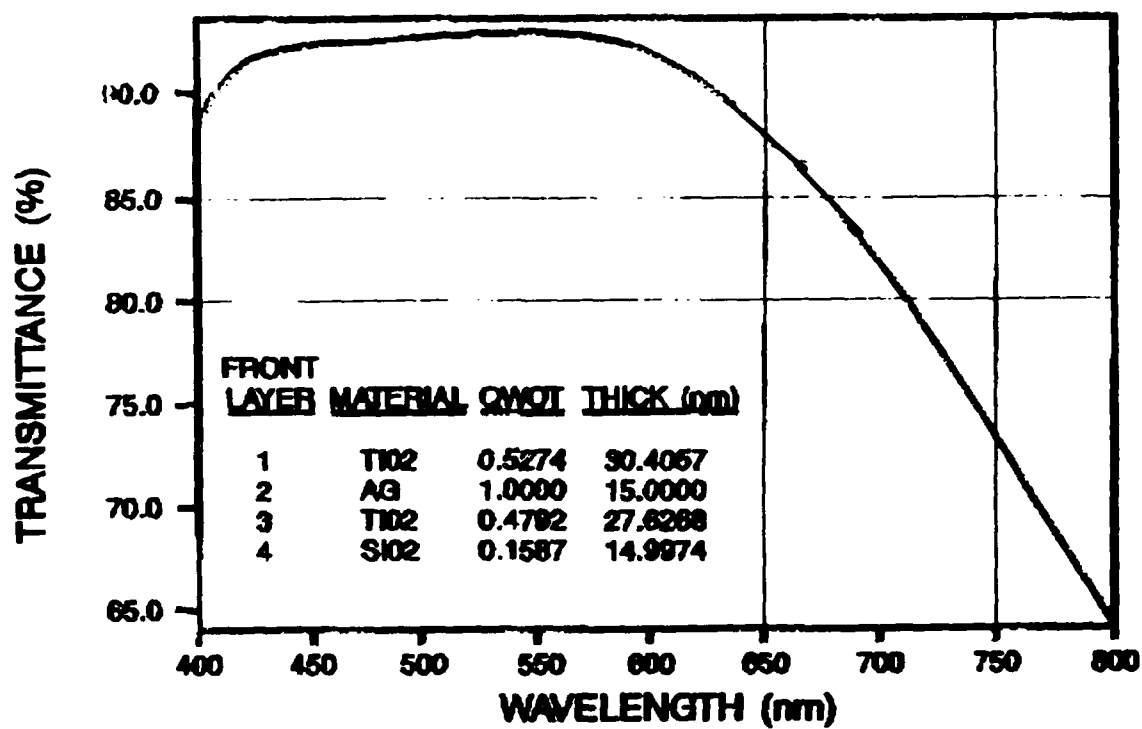


FIGURE 7
ENHANCED GOLD ON ACRYLIC

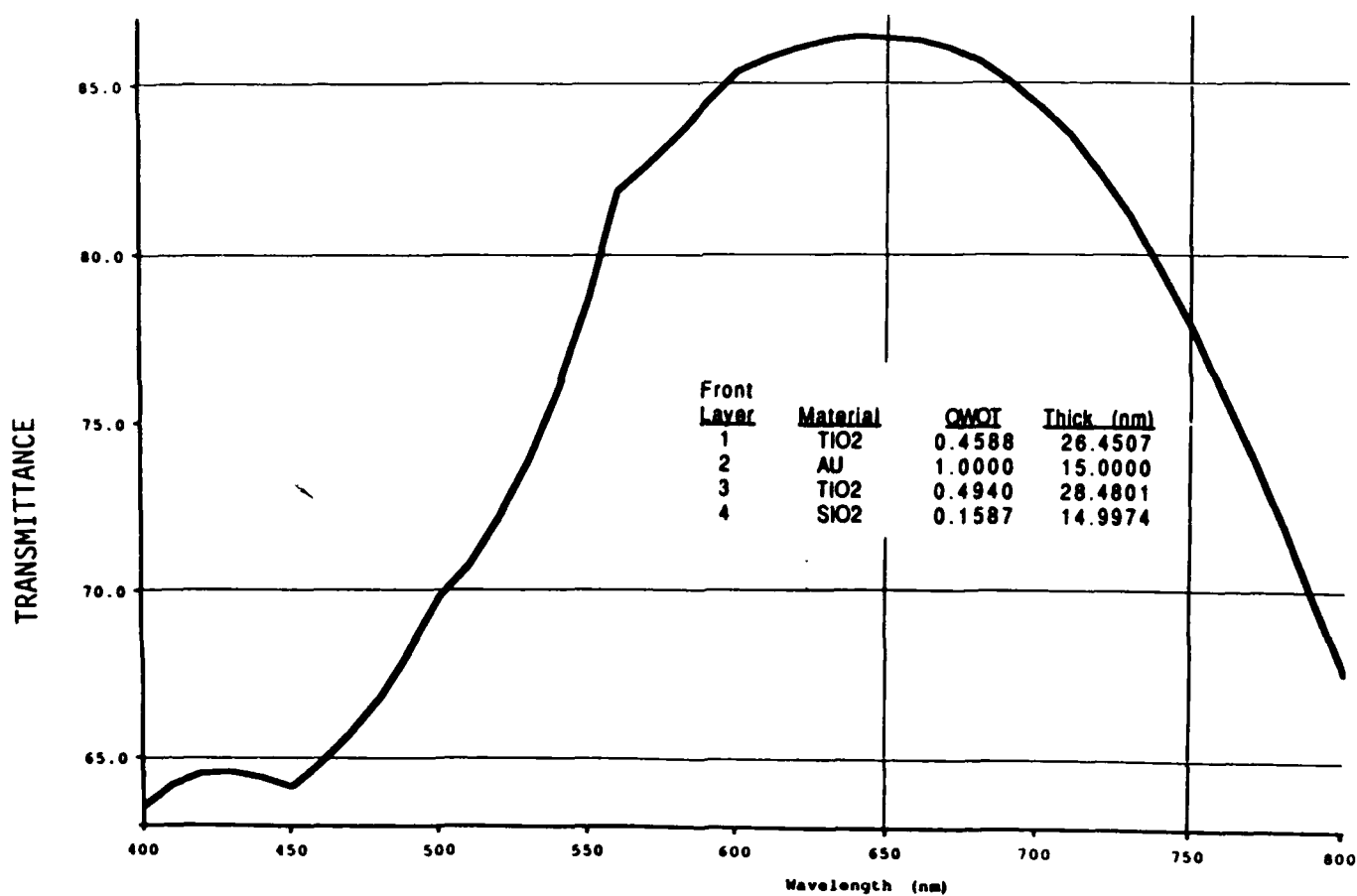


FIGURE 8
TRANSMITTANCE OF TYPICAL 15 OHM/SQ.
ITO FILM ON STRETCHED ACRYLIC
(LT = 76.9%)

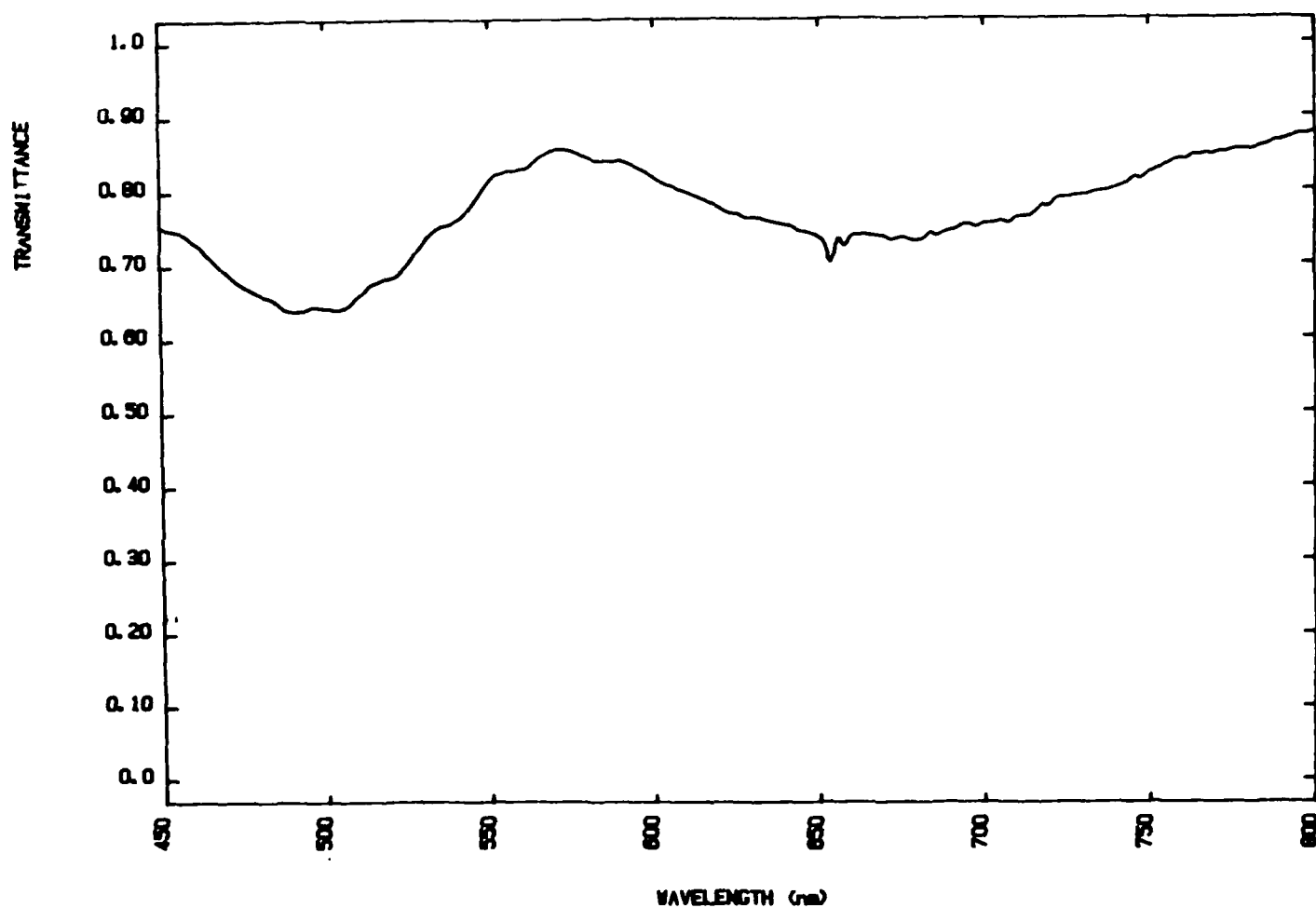


FIGURE 9

**TRANSMITTANCE OF TYPICAL 4.3 OHM/SQ.
ENHANCED GOLD ON STRETCHED ACRYLIC
(LT = 68.7%)**

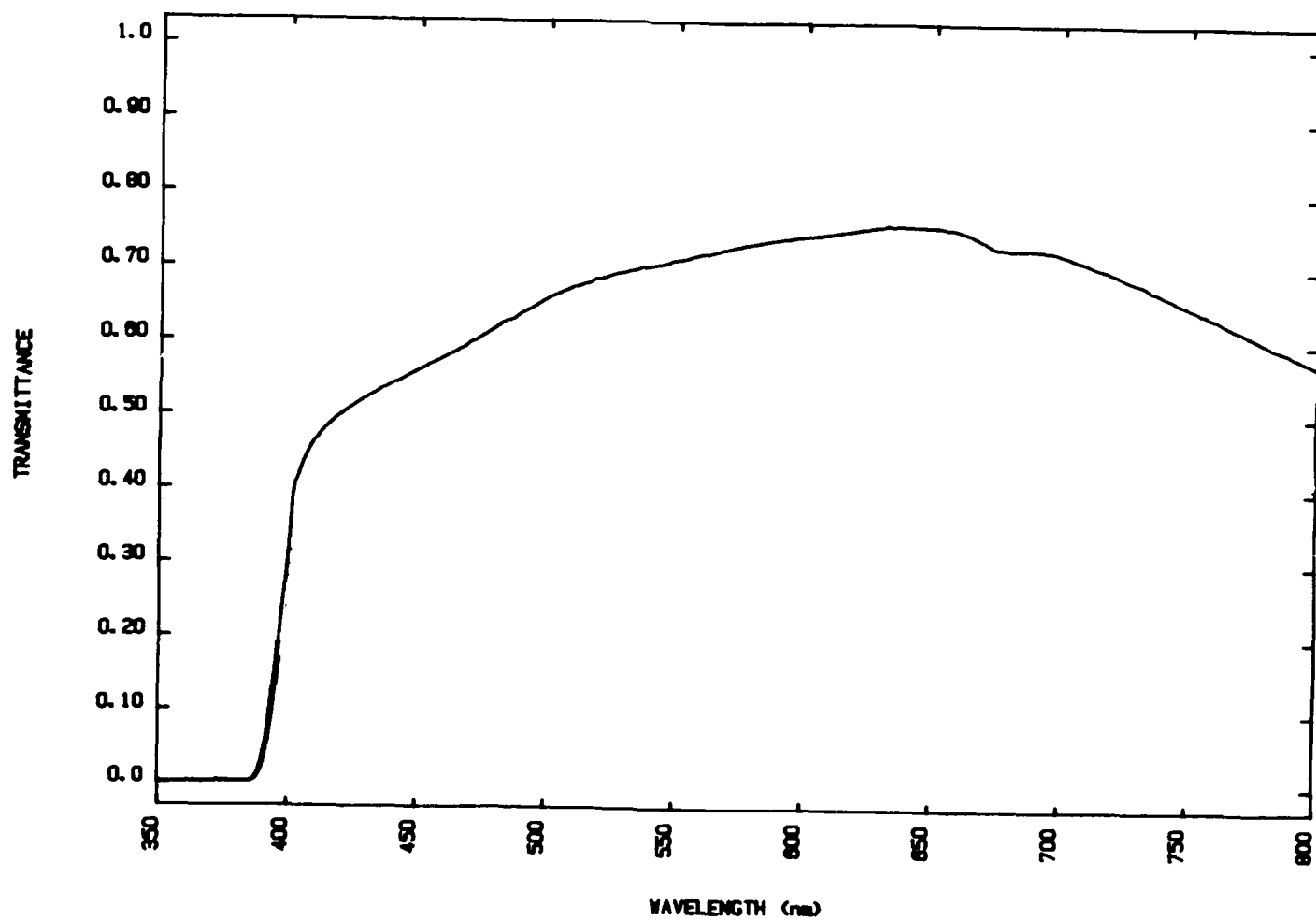


FIGURE 10
VISIBLE LIGHT TRANSMISSION OF VARIOUS
ELECTRICALLY CONDUCTIVE COATINGS

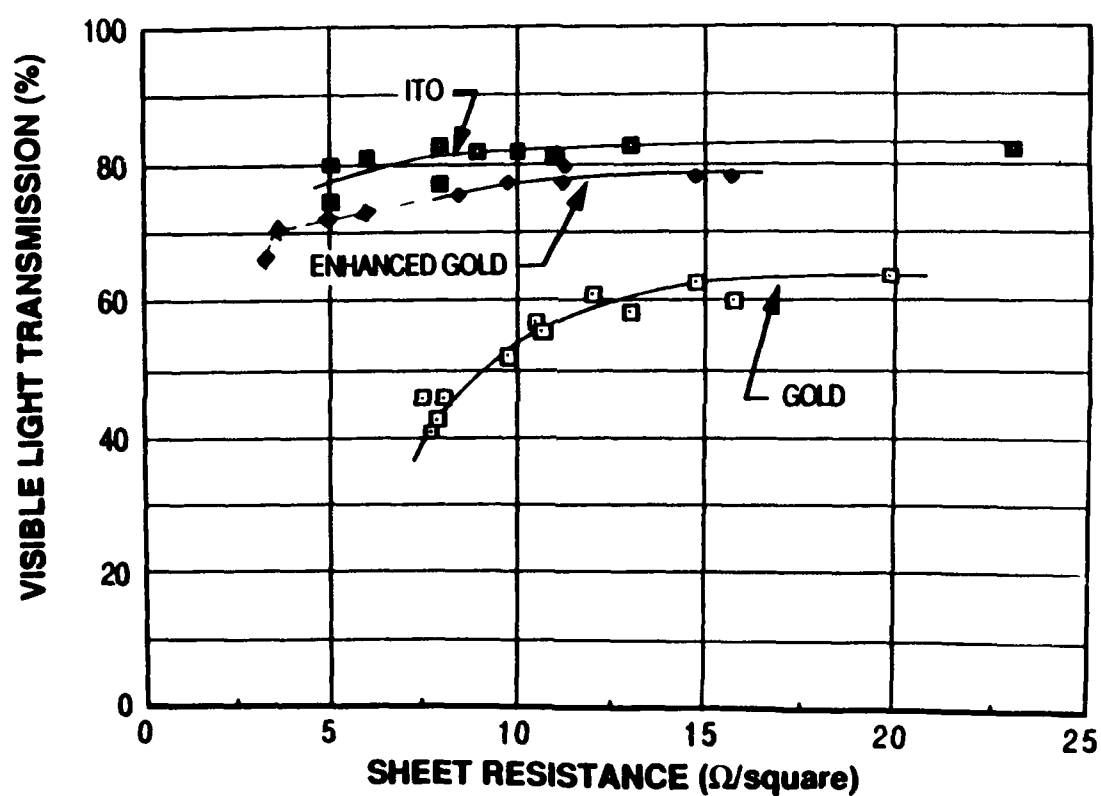


FIGURE 11

**STRAIN ALLOWABLE FOR SWEDLOW
ENHANCED GOLD AND ITO**

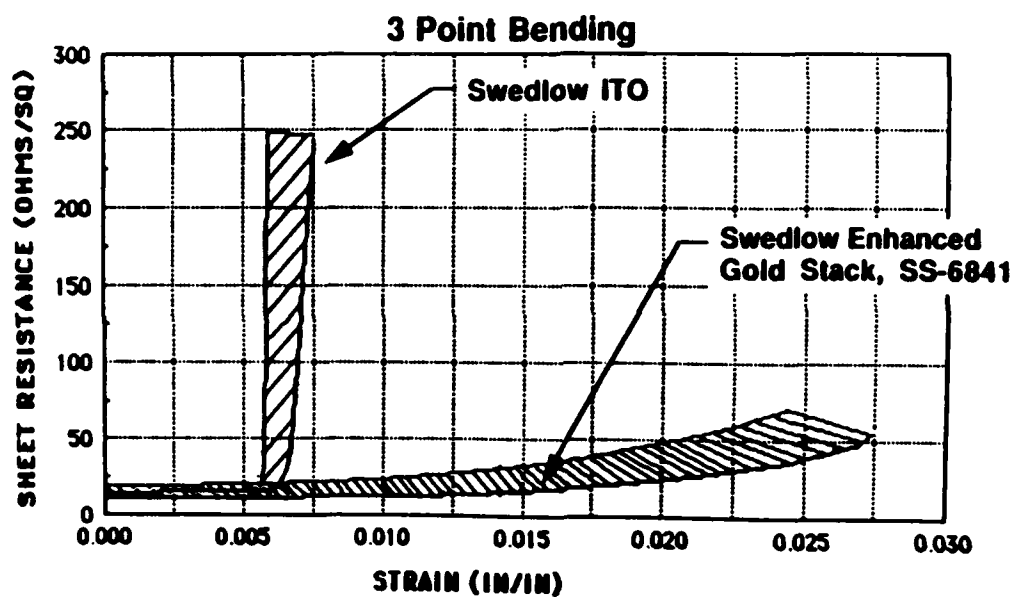


TABLE 1
**COMPARISON OF PROPERTIES OF TCC'S ON EITHER STRETCHED ACRYLIC
OR POLYCARBONATE WITH ARC OVERCOAT**

	ENHANCED GOLD	SINGLE LAYER GOLD	ITO
OPTICAL			
LT, % Visible	78	65	82
LT, % 800-900nm	70	50	75
Haze, %	<1.5	<1.5	<1.5
ABRASION RESISTANCE			
Taber Abrasion			
Delta % Haze			
100 revs	1-2	1-4	1-2
200 revs	2-4	2-10	2-4
500 revs	6-10	20-40	6-10
Steel Wool	Good	Good	Good
ADHESION			
Tape Pull, 3M 600, %	100	100	100
Tape Pull, 3M 250, %	100	100	100
Cross Hatch Tape Pull, 3M 600, %	100	50-100	100
DURABILITY			
Thermal Soak -60°F/24 hrs plus 200°F/24 hrs.	NO CHANGE	NO CHANGE	NO CHANGE
Thermal Cycling -60°/200°F/24 hrs 5 Cycles	NO CHANGE	NO CHANGE	MICRO- CRACKING
Thermal Soak 340°F/12 hrs. on GAC-590 No ARC	NO CHANGE	NOT DETERMINED	FAILS
Humidity Exposure 105°F/95% RH Time to Fail	>1000 hrs	<200	>1000

ACRYLIC AIRCRAFT GLAZING MATERIALS PERFORMANCE
OF PMMA WITH LOW WATER ABSORPTION

G. G. Schreyer
Rohm GmbH

F. J. Hewitt
CYRO Industries

Acrylic Aircraft Glazing Materials
Performance of PMMA with Low Water Absorption

G.G. Schreyer and
Röhm GmbH
Postfach 4242
D-6100 Darmstadt
Federal Republic of Germany

F.J. Hewitt
CYRO Industries
25 Executive Blvd.
Orange, CT 06477-0550

Abstract

K. Ewald and G.G. Schreyer have demonstrated that the water absorption of the glazing material, the stretching procedure and especially the details of the fabrication process are the key factors for the crazing behavior or the service life of a cabin window. A cabin window performance study done on windows made by various manufacturers from sheets with different crosslinking systems/water absorption confirms these findings. The test results show that the mechanical performance (including solvent induced crazing behavior) of stretched PMMA with low water absorption is at least as good as that of material with high water absorption.

The material when tested in accordance with the requirements of MIL-P-25690 fulfills and shows less crazing under actual flight conditions than standard material (high water absorption).

Surprisingly it was found that cabin windows made from PMMA of high craze resistance can show mechanical properties and solvent induced crazing behavior inferior to that of windows made from materials with lower solvent craze resistance (low water absorption). The poor craze resistance of such windows against chemicals as isopropanol or a toluene/isobutylacetate mixture stems from improper fabrication resulting in too high stresses and too many imperfections in the surface of the window.

Discussion

K. Ewald and G.G. Schreyer have previously demonstrated that the crazing behavior or the service life of a cabin window depends significantly on

- * the water absorption of the acrylic material and
- * the surface quality of the window.

Figure 1 shows the updated results of the Lufthansa B 747 flight tests using cabin windows which have been made from materials with different water absorption and which exhibit surface qualities between very poor and very good. (We thank K. Ewald and Lufthansa for providing this data to us.)

Figure (Slide) 1
LUFTHANSA - B 747
Cabin Window Flight Test

The test results demonstrate clearly: low water absorption = longer service life.

The wide scatter, found for each different level of water absorption, is the result of an extreme variation of the surface quality.

The water absorption that the acrylic glazing material exhibits is a result of the combination of the water absorption of the basic acrylic (PMMA) and of the crosslinker, used to improve the craze resistance of the acrylic against deicing fluids, lacquer thinners, etc.

Figure 2 shows the chemistry and the water absorption of the acrylics used in our investigations.

Figure (Slide) 2
Acrylic Aircraft Glazing
Chemistry and Water Absorption

As the Figure clearly shows, going from a hydrophobic to a hydrophilic crosslinker can easily double the water absorption of the acrylic glazing material. This corresponds to approximately 2.5 times higher stresses in the surface of the cabin window during the desorption phases (drying). As has been demonstrated earlier, the desorption stresses, superimposed with thermomechanical stresses, cause the crazing in actual flight service.

Surface quality, meaning physical-chemical material performance and induced thermomechanical stresses in the surface, combined with surface imperfections, depends on things as described in Figure 3.

Figure (Slide) 3
Acrylic Aircraft Glazing
"Surface Quality"

How important good surface quality is can be derived from Figure 4. This table compares some key properties of stretched PMMA, Type A to those of stretched PMMA, Type B. In the case of the Type A material, stretching and window manufacturing have been done by different European companies (S/1 and W/2). In the case of the Type B material two different U.S. companies, No. 3 and No. 4, did both, the stretching and window manufacturing operations. As shown in Figure 1, Type B material has a high crosslinking density. Type A material has a low crosslinking density. Therefore windows made from Type B PMMA would be expected to show higher solvent induced stress to craze values than windows made from Type A PMMA. This is only true in one case where Company No. 4 stretched the material and made the windows. In the case of Company No. 3, the solvent crazing behavior of the B-window is actually inferior to that of the A-window, the reason here being poor surface quality, not the inherent quality of the material.

Figure (Slide) 4
Crazing Behavior of Cabin Windows.
Influence of Material, Stretching Procedure
and Window Fabrication

We also must recognize that all the physical properties and especially the stress to craze value of the stretched Type A material/window fulfil the requirements of MIL-P-25690 for stretched acrylics (3000 psi). This justifies and recommends again the use of this type of PMMA for cabin windows. Type A material corresponds to materials, which are traditionally used in Europe for canopies and cabin windows. Type B corresponds to one of the materials frequently used in the U.S.

Figure No. 5 shows the same type of data for stretched sheet and windows made from Type B 1 material, another material with high crosslinking density and high water absorption. As we can see, various stretched sheets from

one and the same stretcher show significant differences in the stress to craze values, with isopropanol used as crazing agent.

Figure (Slide) 5
Crazing Behavior of Cabin Windows.
Influence of Material, Stretching Procedure
and Window Fabrication

Sheets with values above 4000 psi are observed as well as sheets below 3000 psi, the requirement of MIL-P-25690.

Windows made by Company No. 5 from Type B material have solvent stress to craze values which are inferior to windows made by Company No. 2 from Type A material. We would have expected Type B material to be better than Type A.

I should point out here that all cabin windows, evaluated in our study, have been sampled from commercial airplanes before crazing took place.

As a result of our work we can state: windows made from Type A material, which is presently not qualifiable as MIL-P-8184 material, can perform better in actual service than windows made from the B 1 product which fulfils the stress to solvent craze requirements of MIL-P-8184.

This is the principal anomaly of the stress to craze test in MIL-P-8184. This specification actually eliminates the materials which have the best in-flight service life.

As a consequence of the results shown in Figures 4 and 5 we wanted to evaluate, how

- (1) stretching improves the stress to craze values of PMMA, both Type A and Type B, and also
- (2) how the stress to craze values found, would compare to the stress to craze requirements of the most recent redraft proposal of MIL-P-8184 E.

As discussed during several meetings of the ASTM F 7.08 Group (Aerospace Transparent Enclosures and Materials) windows made from Class 2 material - as defined in the proposed MIL-P-8184 E - have longer service life under actual flight conditions but are less resistant to crazing caused by chemicals as isopropanol or toluene/isobutyl acetate¹⁾ in the unstretched state. This is caused

¹⁾ replacing lacquer thinners

by the replacement of the hydrophilic crosslinking system used in Type B PMMA by a hydrophobic system.

Figure (Slide) 6
Stress to Craze Behavior of Typical Class 1
and Class 2 PMMA Sheet.
Unstretched and Stretched (PSI)

Figure 6 shows that stretching leads to a significant improvement of Type A PMMA if good surface quality is achieved. If not, and this happened in the case of the B 1 product of our evaluation, the stretched sheet can be less craze resistant than the unstretched product.

This can be seen from Figure 6 where cabin windows in use were measured. The values added in parentheses are those which we believe could be achieved if the surface quality were better.

What we found demonstrates that it does not make too much sense to characterize the quality of a cabin window made from stretched PMMA sheet by tests done on the unstretched sheet. The crazing test should be done on samples taken from the windows, canopies, etc.

This Figure shows that stretched PMMA Type A does fulfil the stress to craze requirements of MIL-P-25690.

Looking at the stress to craze behavior of the unstretched PMMA Type A, we propose that stress to craze values of MIL-P-8184 E (newest proposal) should be lowered from 2500 to 2000 in the case of isopropanol and from 2000 to 1500 if toluene/isobutylacetate (1/2) is used as crazing agent.

These values correspond to the tests done on "dry" material. The values for "wet" conditions have to be changed correspondingly.

The Lufthansa flight tests have clearly demonstrated the excellent performance of the PMMA/Type A regarding service life.

For cabin windows manufactured from this material, when stretched sheet and windows are made with good surface quality, Lufthansa expects 20-25,000 hours of service life compared to 5-10,000 hours windows show today.

Another demonstration of the quality of Type A PMMA is given in Figure No. 7. This figure shows the different types of aircraft with windows, canopies, etc. made from Type A material by a French manufacturer.

Figure (Slide) 7

Application of PMMA Type A for Windows, Canopies, etc.

Let me close my presentation with this summary:

PMMA made with hydrophobic crosslinkers has the highest potential for long service life.

Therefore, the revision of MIL-P-8184 E should allow the manufacturers to use such material to make stretched sheet and glazing.

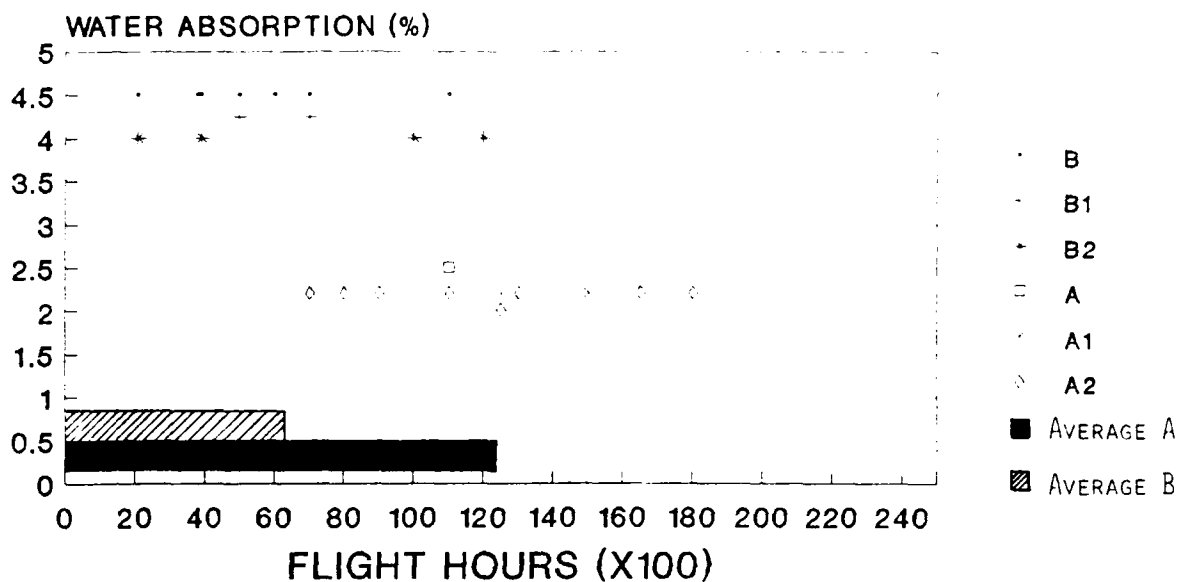
Better surface quality of stretched sheet and glazing is needed. The grinding and polishing technologies developed by Lufthansa and other companies are the key to this necessary quality improvement.

FJH/GGS/mb

Attachments: Figures 1-7

FIGURE 1

LUFTHANSA - B 747 CABIN WINDOW FLIGHT TEST Removal after excessive crazing



Water absorption saturation
at 60 degrees centigrade

Figure 2

ACRYLIC AIRCRAFT GLAZING
CHEMISTRY AND WATER ABSORPTION

Material Code	Type	Crosslinker Amount	Water Abs. % 60 °C, Sat.	Service life (flight hours)*)		X-Linking density
				minimum	maximum	
B	Hydrophilic	High 8-15 %	4,8	4000	8000	High
B 1	Hydrophilic	8-15 %	4,5	4000	7000	↓
B 2	Hydrophilic	8-15 %	4,1	2000	12000	
A 2	A/B combination		2,8	14000	
A 1	A/B combination		2,6	12000	14000	
A	Hydrophobic	Low 0,1-2 %	2,5	6000	> 18000	Low

*) Hours to removal of cabin windows after excessive crazing.
 Values strongly depending on Surface Quality!

Figure 3

ACRYLIC AIRCRAFT GLAZING

"SURFACE QUALITY"

Physical-Chemical Material Performance

- * Molecular Structure - Crosslinking situation
- * UV-Stability

Processing of Acrylic Sheet

- * Type of Stretching Operation
- * Thermo-mechanical Stress build up
- * Grinding-, Polishing-Procedure/Quality.
Surface imperfections
- * Post Treatment (thermal-mechanical)
- * Internal Stresses

Fabrication of Cabin Window

- * Surface Protection
- * Forming Process (Temperature - Time - History)
- * Polishing Procedure
- * Internal Stresses

Maintenance Situation

- * Cleaning Procedures - Chemical aspects
- * Cleaning Procedures - Mechanical aspects

Figure 4

Crazing Behaviour of Cabin Windows. Influence
of Material, Stretching procedure and Window Fabrication

Property	Unit	PMMA Type A stretched	PMMA Type B stretched		
Stretch./Comp.Code		S/1	S/3	S/4	S/4
Window/Manuf. Code		W/2	W/3	W/4	W/4
Airplane		Airbus	Airbus	B 747	B 737
Thickness	mm	9.6-9.8	9.6-10.0	8.6-9.1	9.4-9.6
Degree of stretching	%	71-79	67-69	67-92	70-75
Birefringence	$\cdot 10^{-6}$	17-21	10.1	79-91	11.5-21.1
Waterabsorption	%				
Sat. 23 °C		2.2	4.5	4.5	4.5
Sat. 60 °C		2.5	4.8	> 4.2	> 4.2
Stress to Craze ¹⁾					
Isopropanol					
Dry ²⁾	PSI	3085-3486	3057-3129	4129-5014	3900-4114
Wet ³⁾	PSI	2457-2843	2500-2729	3457->4570	3400-4186

1)According to MIL-P-25690

2)after 1 week 23 °C, 50 % r.H

3)after 30 days in water, 23 °C

Figure 5

Crazing Behaviour of Cabin Windows. Influence
of Material, Stretching procedure and Window Fabrication

Property	Unit	PMMA Type A stretched	PMMA Type B 1 stretched				
Sheet/Window.		Window	Window	Window	Sheet	Sheet	Sheet
Stretch./Comp. Code		S/1	S/6	S/5	S/6	S/6	S/6
Window/Manuf. Code		W/2	W/1	W/5	-	-	-
Thickness	mm	9.6-9.8	9.3-9.5	9.1-9.2	9.3	9.3	9.5
Degree of stretching	%	71-79	71-75	67-76	70-74	72-75	71-77
Birefringence	$\cdot 10^{-6}$	17-21	11.4-23.2	5.6-21.8	15.5	8.2	20
Waterabsorption	%						
Sat. 23 °C		2.2	4.2	-	-	-	-
Sat. 60 °C		2.5	4.3-4.5	-	4.4	4.4	-
Stress to Craze ¹⁾							
Isopropanol							
Dry ²⁾	PSI	3085-3486	3457-3900	2143-2257	3257-3457	2886-3186	4386
Wet ³⁾	PSI	2457-2843	2814-3314	857- 900	2171-2243	1986-2028	3214

1)According to MIL-P-25690

2)after 1 week 23 °C, 50 % r.H

3)after 30 days in water, 23 °C

Figure b

**Stress to Craze Behaviour of typical Class 1
and Class 2 PMMA. Unstretched and stretched (PSI)**

Crazing Agent	Class 1 (PMMA Type B 1)		Class 2 (PMMA Type A)	
	unstretched	stretched ⁴⁾	unstretched	stretched ⁵⁾
	4.3 % water absorption (23 °C)		2.2 % water absorption (23 °C)	
Isopropanol				
min.	3071	2214	2143	3286
max.	3429	2357	2929	3614
average	3286	2271 ⁶⁾ (4000-4400)	2429	3414
Mil-Requirement	2500 ¹⁾	3000 ³⁾	2500 ¹⁾ 2200 ²⁾	3000 ³⁾
Toluene/Isobutylac. 1/2				
min.	2714	2057	1286	2214
max.	> 3143	2171	1857	2500
average	> 2714	2183 ⁶⁾ (3000-3400)	1571	2386
Mil-Requirement	2500 ¹⁾	none	2000 ¹⁾ 1500 ²⁾	none
Sample Preconditioning	2h 120 °C 48h 23 °C, 50%r.H.	1 Week 23 °C, 50%r.H.	2h 120 °C 48h 23 °C, 50%r.H.	1 Week 23 °C, 50%r.H.

1) MIL-P-8184 E

2) MIL-P-8184 E Modification (CYRO proposal)

3) MIL-P-25690

4) Stretched by Company no 6 (USA)

5) Stretched by Company no 1 (Europe)

6) Craze enhanced, poor surface quality

Figure 7

Application of PMMA Type A
for windows, canopies etc.

(Company no 1)

Airbus 320

310

300

Falcon 900

50

10

Casa 212

235

Mirage 2000

III

Etendard IV

Transall

Breguet 1150 ATL 1

ATL 2

Jaguar

Helicopters

SESSION III

UNDERSTANDING CURRENT MATERIALS (PART B)

Chairman: B. S. West
University of Dayton
Dayton, Ohio

Co-Chairman: K. Armstrong
British Airways
Middlesex, England

Coordinator: B. L. Boman
McDonnell Aircraft Co.
St. Louis, Missouri

THE RAIN EROSION OF SOME AS-CAST AND
PRESSED/STRETCHED ACRYLIC MATERIALS

N. S. Corney
E. M. Minter
P. Tattershall

Royal Aircraft Establishment

THE RAIN EROSION OF SOME AS-CAST AND PRESSED/STRETCHED ACRYLIC MATERIALS

by

N S Corney, E M Minter, and P Tattershall

Royal Aerospace Establishment,
Farnborough,
Hampshire,
England

ABSTRACT

The multiple water drop erosion of polymethylmethacrylate has been studied using as-cast material from three sources, pressed material from three as-cast materials and one stretched material. The investigation was performed using the RAE Rain Erosion Facility at a nominal intensity of 25 mm/h at a speed of 223 m/s over a range of impact angles. The erosion rate was determined by measurement of changes in weight and white light transmission and haze.

The three as-cast materials behaved in very similar fashion, at impact angles of 90° and 60° slight surface damage in the early stages of erosion resulted in large changes in the measured optical properties. With increasing erosion significant weight losses occurred indicating deep penetration and bulk removal of material. At 30° impact angle steady changes in optical properties and weight loss occurred simultaneously whilst there was an intermediate behaviour at 45°.

All the pressed and stretched materials showed similar erosion behaviour and exhibited lower erosion resistance than did the as-cast materials.

The rates of erosion as determined by weight changes were approximately proportional to the seventh power of the resolved component of velocity normal to the material surface.

1 INTRODUCTION

The erosion of polymethylmethacrylate (PMMA) at sonic and sub-sonic speeds in a simulated rainfield environment was the subject of early investigations (1, 2) and more recently (3) a detailed study of the erosion mechanism has been reported. The work described in this paper was aimed at examining the erosion of as-cast PMMA materials from three manufacturers and comparing their performance with that of three pressed and one stretched PMMA materials. Little attention, other than that reported in (4, 5) has been focussed on the influence of varying material properties, caused by the different processing methods, on the susceptibility to rain erosion in spite of the widespread application of the latter materials in bird-strike-resistant transparencies. This work is a continuation of that reported briefly in the literature (6).

2 MATERIALS

Details of the materials used in this work are given in Table 1. The three pressed materials were produced by one manufacturer from three as-cast materials from three different suppliers. It is important to realise that the pressed and stretched materials were not necessarily derived from the same as-cast materials as used in this work.

All materials were cut into 25 mm square specimens before removing the protective covering and were then washed in warm water to remove final traces of covering and adhesive.

3 EXPERIMENTAL

Evaluation of the rain erosion resistance of these materials was carried out using the refurbished RAE Rain Erosion Facility described originally by Fyall and Strain (7), recent modifications being described in (6). All work was done at a standard speed of 223 m/s with a simulated rainfield of nominal intensity of 25 mm/h and a predominant drop diameter of 2 mm. Specimen holders were available for impact angles from 90° to 30° in 15° increments. Initially and after each erosion exposure, specimens were dried at 65°C for 30 min before weighing and measurement of white light transmission and haze using a Gardner XL-211 Hazegard hazemeter to the method of ASTM D-1003.

Most of the results were obtained on duplicate specimens exposed simultaneously in successive erosion exposures with property measurements after each incremental exposure. However, in some cases, separate specimens were exposed for the required progressively increasing periods before making measurements on the whole set of specimens. This procedure had the advantage of producing a set of specimens for visual comparison of erosion damage.

Despite care in handling the specimens, occasional handling damage was noted in the form of light scratches and may account for some observed differences for duplicate specimens.

4 RESULTS AND DISCUSSION

Results are presented in Figures 1-7 as plots of haze, transmission and weight loss as a function of erosion time for the various impact angles used. The 75° impact angle was not used for all materials due to the unavailability of a holder capable of accommodating the thicker specimens.

4.1 As-Cast Materials

Figures 1-3 show that all three materials examined behaved in a very similar manner and that reasonably good agreement was obtained between duplicate specimens. It can be seen that, in each case, at 90°, 75° and 60° impact angles, the major changes in optical properties occur before a steady rate of weight loss is established. At 30° impact angle, steady changes of optical properties and weight loss take place simultaneously, while at 45° impact angle there is intermediate behaviour.

As would be expected from well established observations of rain erosion on angled surfaces, the rates of change of optical properties and weight loss decrease with reduction of impact angle.

4.2 Pressed and Stretched Materials

Figures 4-7 show a general similarity of form for these materials and again show reasonably good agreement between duplicate specimens. One notes that changes in optical properties, particularly at the larger impact angles, precede weight loss although the changes in all parameters are very rapid at impact angles close to the normal.

The erosion rates of the pressed and stretched materials are in all cases greater than those for the as-cast materials although transmission after erosion at 60° and 45° impact angles appears to reach a quasi-steady value after an initial rapid deterioration. By the time this quasi-steady value is reached, however, the haze is at a very high value which would render the transparency unserviceable.

From a smaller data set, it was concluded in (6) that pressed and stretched materials showed poorer rain erosion resistance than as-cast materials. In that paper it was observed that since the fracture toughness and impact strength of pressed and stretched materials are almost double those of as-cast PMMA, it might be expected that the rain erosion resistance of the pressed and stretched would be greater than the as-cast materials. Oberst (8) concluded however, that the extent of rain erosion damage to plastics cannot always be correlated with their impact strengths.

4.3 Effect of Impact Angle on Erosion Rate

The generally accepted relationship between steady erosion rate R and impact angle ϕ at constant speed is given by

$$R = k \sin^x \phi$$

where k and x are constants. The data in Figures 1-7 have been examined to determine the steady erosion rates where such conditions have been reached and the rates have been used to calculate the value of x , with the results being given in Table 2. In view of the imperfect nature of the data (uncertainty of whether steady erosion conditions have been reached) it is, perhaps, not surprising to find some variability between and within groups. Earlier work (2) had found values of x between 5 and 7 for weight measurements which is somewhat lower than the bulk of our findings. This may possibly be explained by the uncertainties noted. For haze and transmission measurements the value of x found in this work is approximately 5.

5 CONCLUSIONS

The study of rain erosion of three as-cast PMMA materials at a speed of 223 m/s in a simulated rainfield of 25 mm/h nominal intensity has shown that the materials exhibit very similar behaviour, with the early stages of erosion being highlighted by changes in white light haze and transmission and the later stages by weight loss.

Three pressed and one stretched PMMA all showed similar erosion characteristics although the erosion rates were greater than those recorded for the as-cast materials.

The rates of erosion as determined by weight measurements were approximately proportional to the seventh power and by haze and transmission measurements were approximately proportional to the fifth power of the resolved component of velocity normal to the material surface.

6 ACKNOWLEDGEMENTS

The authors are grateful to British Aerospace plc (Hamble and Kingston sites) and Lucas Aerospace for the provision of samples for this work. The use of the Gardner Hazemeter was by kind permission of the Commandant, RAF Institute of Aviation Medicine.

TABLE 1
DETAILS OF MATERIALS EXAMINED

Identification	Other Details
C1	Cast material supplied by Lucas Aerospace, 2.7 mm thick
C2	Cast material specification DTD 5592, 5.6 mm thick
C3	Cast material supplied by BAe Hamble, 8.2 mm thick
P1	Pressed material supplied by Lucas Aerospace, 6.6 mm thick
P2	Pressed material supplied by Lucas Aerospace, 5.4 mm thick
P3	Pressed material supplied by Lucas Aerospace, 6.7 mm thick
S1	Stretched material supplied by BAe Kingston, 8.2 mm thick

TABLE 2
VALUES OF EXPONENT \times RELATING EROSION RATE TO IMPACT
ANGLE

Material	Exponent for		
	Haze	Transmission	Weight Loss
C1	8.6	6.7	11.8
C2	4.3	3.1	6.6
C3	5.3	5.2	6.5
P1	3.8	6.4	7.1
P2	3.6	5.0	7.0
P3	4.6	5.6	6.8
S1	5.1	7.3	8.7

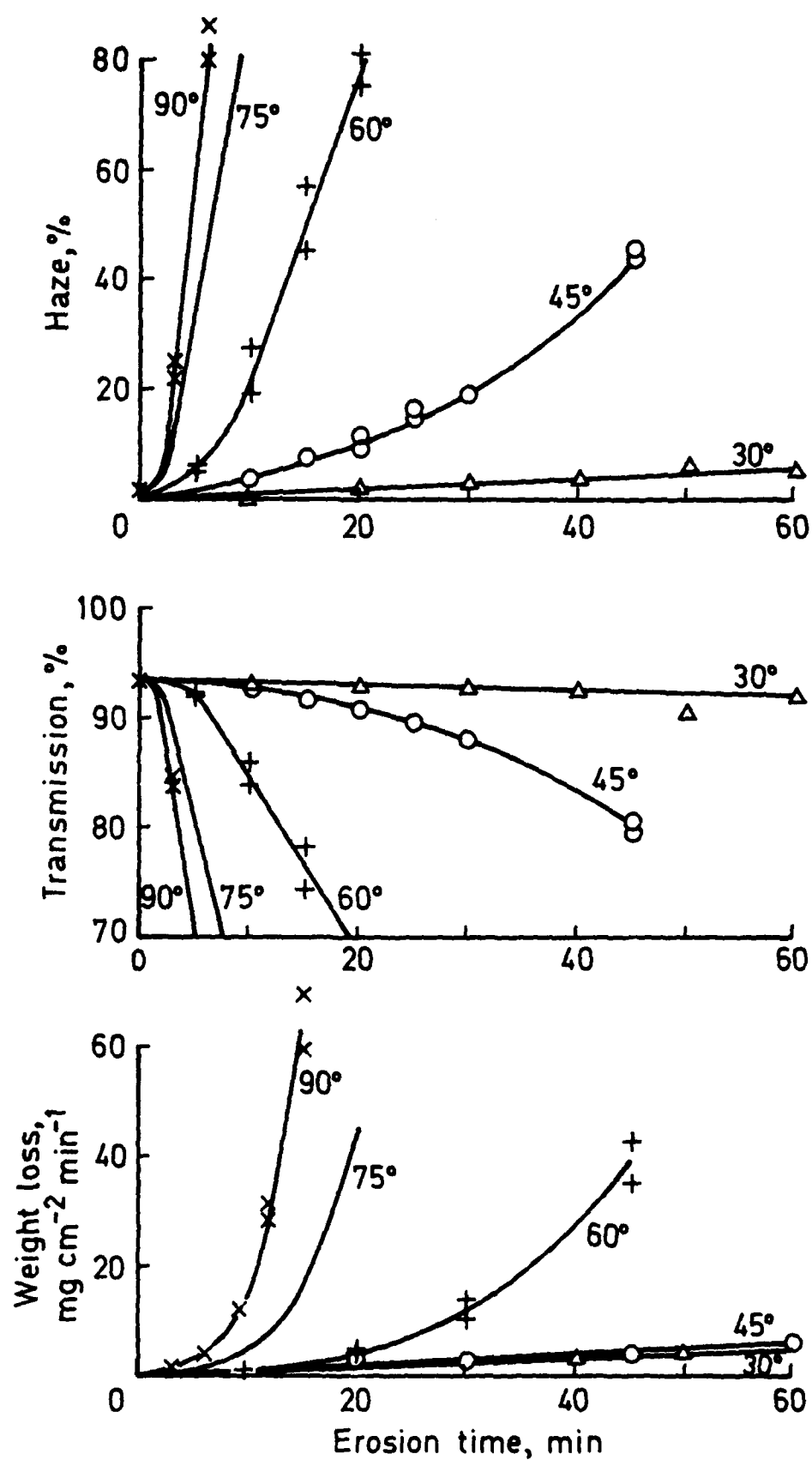


Fig 1 Rain erosion of as-cast acrylic C1

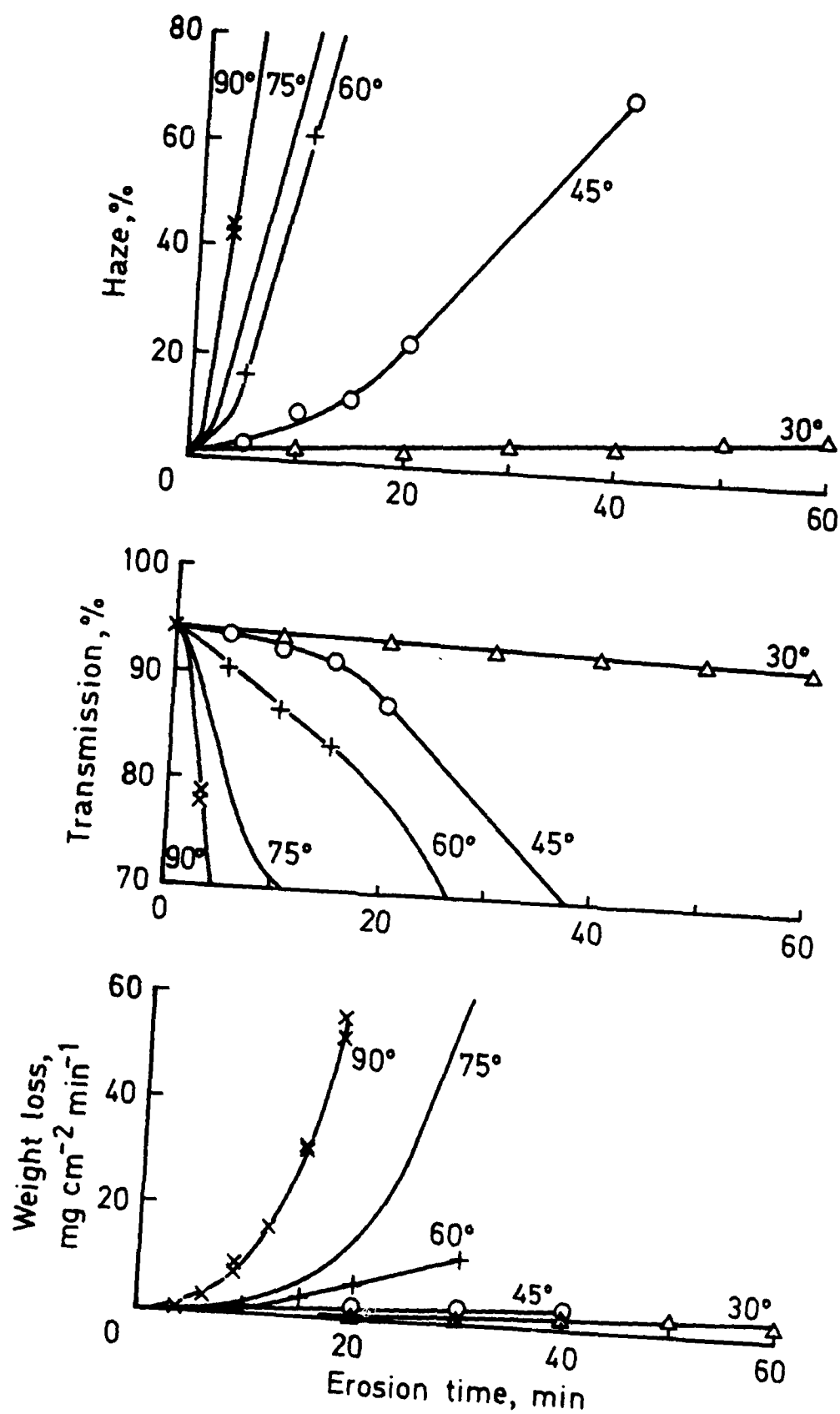


Fig 2 Rain erosion of as-cast acrylic C2

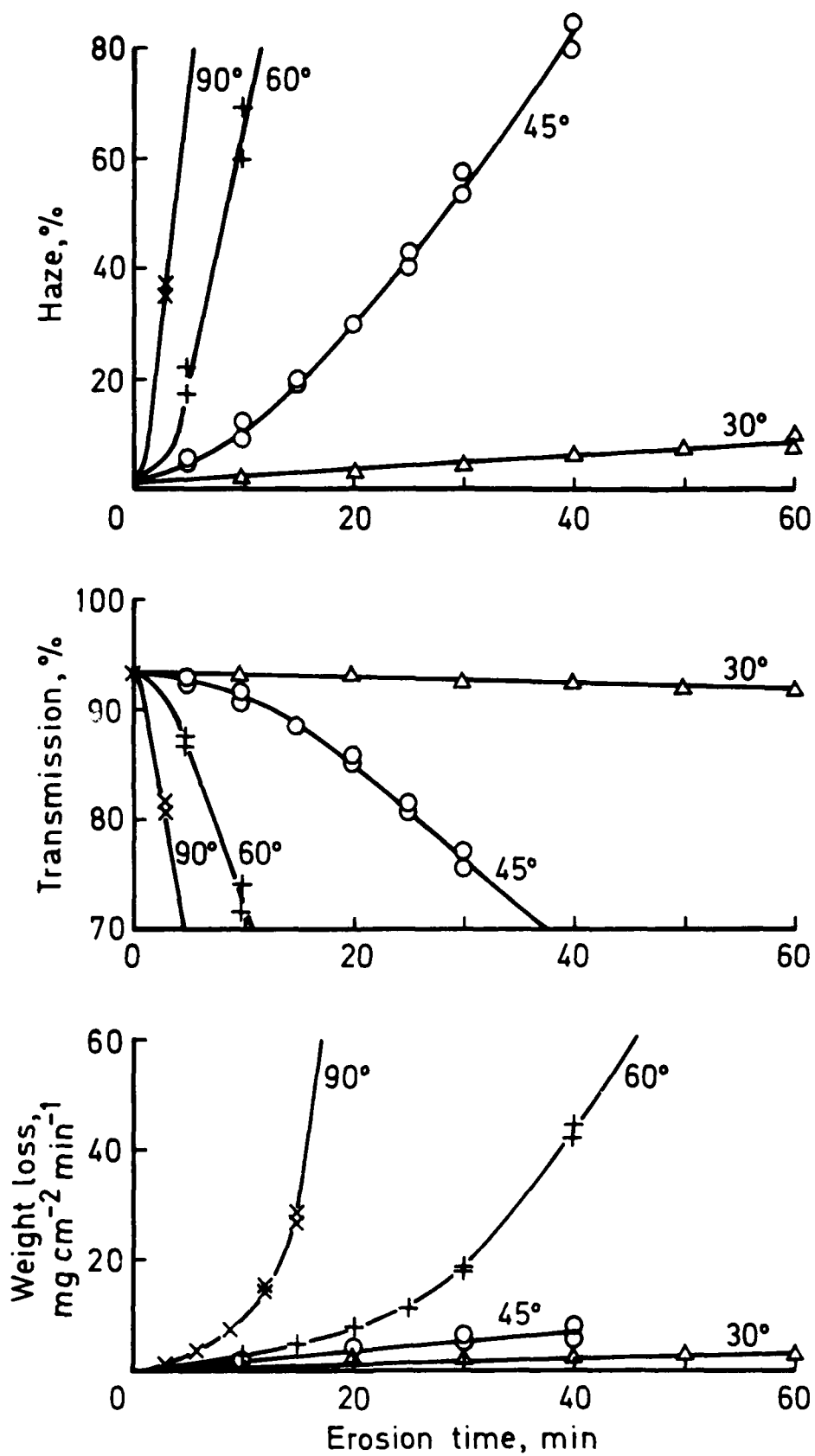


Fig 3 Rain erosion of as-cast acrylic C3

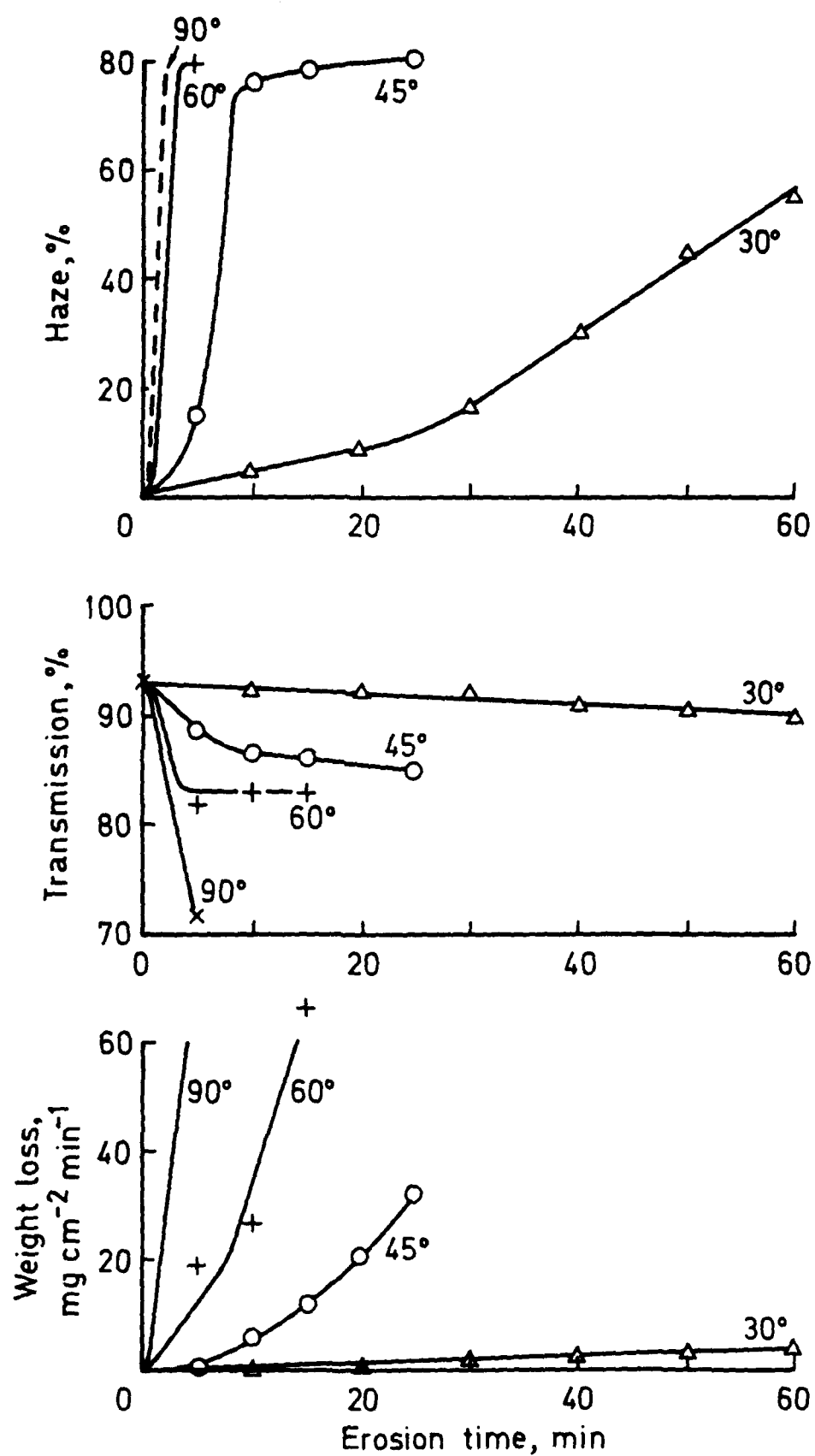


Fig 4 Rain erosion of pressed acrylic P1

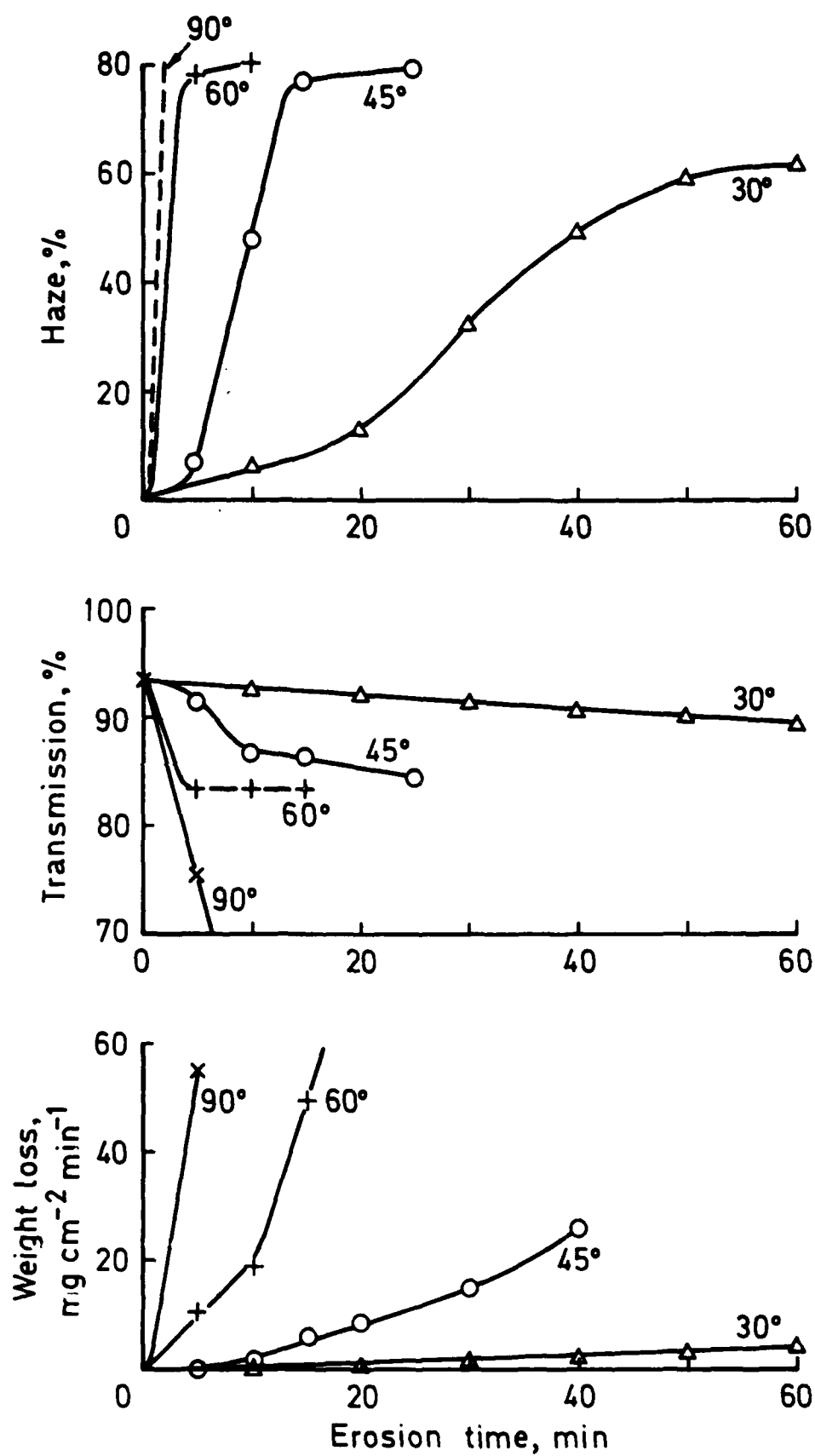


Fig 5 Rain erosion of pressed acrylic P2

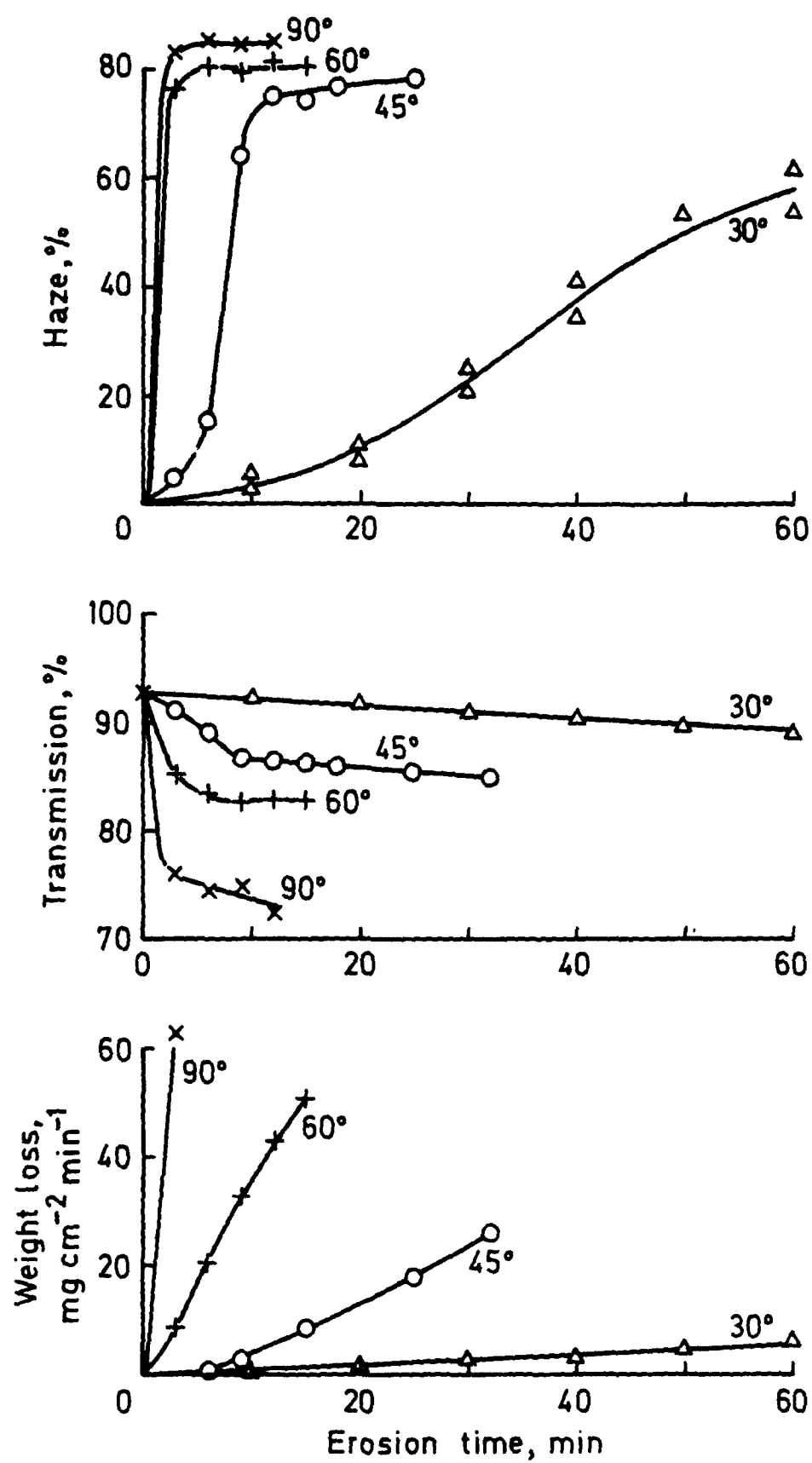


Fig 6 Rain erosion of pressed acrylic P3

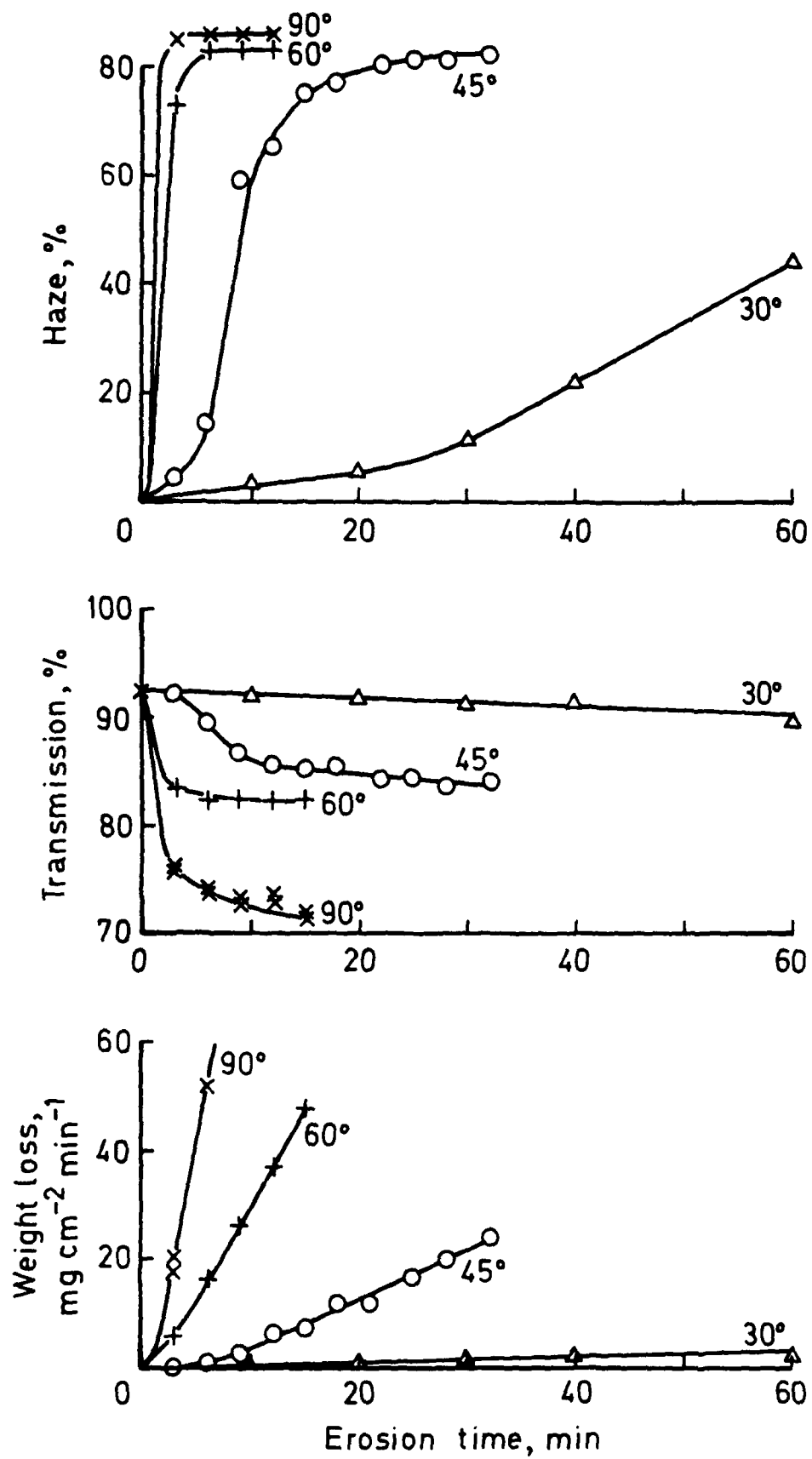


Fig 7 Rain erosion of stretched acrylic S1

REFERENCES

- 1 Fyall A A J Roy Aero Soc 66, 447-453 (1962)
 King, R B
 Strain, R N C
- 2 Hoff, G Material destruction by liquid impact.
 Langbein, G Erosion by cavitation or impingement.
 Rieger, H ASTM STP 408, 42-69 (1967).
- 3 Adler, W F Rain erosion behaviour of polymethylmethacrylate.
 Hooker, S V J Mat Sci, 13, 1015-1025 (1978).
- 4 King, R B Rain Erosion Part X. An assessment of various
 materials.
 RAE Technical Report 75009 (1975).
- 5 Peterso. , T L Rain erosion behaviour of transparent plastics and
 protective coatings. Conf on Aerospace
 Transparencies and Enclosures.
 AFML-TR-76-55 (1976).
- 6 Corney, N S The rain erosion of some transparent materials for
 Minter, E M aerospace applications.
 Proc 7th Int Conf on Erosion by Liquid and Solid
 Impact (ed Field, JE & Dear, JP) Paper 6,
 Cambridge (1987).
- 7 Fyall, A A A whirling arm test rig for the assessment of the
 Strain, R N C rain erosion of materials.
 RAE Technical Report CHEM 509 (1956).
- 8 Oberst, H Rain erosion and molecular properties of synthetic
 materials.
 RAE Library Translation 1335 (1968).

Copyright (C) Controller HMSO London 1988

EFFECTS OF SOLVENTS ON CRAZE INITIATION AND
CRACK PROPAGATION IN TRANSPARENT POLYMERS

Janice J. Vanselow
Alex J. Hsieh
Jennie H. Brown

U.S. Army Materials
Technology Laboratory

John I. Stevens

U.S. Army Chemical Research,
Development and Engineering
Center

EFFECTS OF SOLVENTS ON CRAZE INITIATION AND CRACK PROPAGATION IN TRANSPARENT POLYMERS

Janice J. Vanselow, Alex J. Hsieh, Jennie H. Brown
Polymer Research Branch
U.S. Army Materials Technology Laboratory
Watertown, Massachusetts 02172

John I. Stevens
Research Directorate
U.S. Army Chemical Research, Development and Engineering Center
Aberdeen Proving Ground, Maryland 21010-5423

ABSTRACT

Transparent polymers being considered for use in Army systems must be evaluated for resistance to crack and craze growth in a chemical environment. Current tests for determining craze initiation include environmental stress crazing tests based on ASTM D-790 and ASTM F-484. Results for a series of cast and biaxially stretched poly (methylemethacrylate) (PMMA) materials, as well as several formulations of polycarbonate, show a range of critical strain measurements in crazing solvents. A polyurethane based thermoset material showed superior resistance to crazing in several of these solvents. The effect of solvents on crack propagation in transparent polymers is demonstrated by a dead weight loading apparatus and compact tension specimens based on ASTM E-399. Samples of PMMA are tested in o-xylene, water, and air. Immersion testing is also used for comparison.

INTRODUCTION

The U.S. Army Materials Technology Laboratory (MTL) has been working in conjunction with the U.S. Army Chemical Research, Development, and Engineering Center (CRDEC) for the past four years (FY 85-88) on evaluating the susceptibility of transparent polymers to failure when exposed to chemicals. This is in response to the NBC Contamination Survivability of Army Materiel policy, AR 70-71, which requires that all Army system materiel be hardened against degradation in a chemical warfare (CW) environment. This includes the ability to be decontaminated.

Polycarbonate (PC) and poly(methylmethacrylate) (PMMA) are known to craze while under mechanical stress. This behavior is enhanced by exposure to organic solvents (1,2). In order to determine the level of degradation in a chemical warfare environment of currently produced transparent materials, environmental stress crazing (ESC) and crack growth studies have been underway at MTL and CRDEC.

This report summarizes much of the work that has been done on solvent induced craze initiation and crack propagation of transparent polymers, including current studies on the effects of water sorption on crack propagation of a PMMA polymer.

EXPERIMENTATION

Solvents and Materials

Several of the solvents chosen for these studies are considered simulants for chemical agents. Simulants are chosen based on molecular weight, density, vapor pressure, and total solubility parameters similar to the actual agents, GD, HD, and VX. CRDEC has suggested several simulants in its recent report (3). MTL has been using diisopropylmethylphosphonate (DIMP) for GD, and 1,5 dichloropentane (DCP) for HD.

Much work has also been done with the universal decontaminant, DS2, which consists of 70% diethylenetriamine (DETA), 28% methylcellosolve (MECL) and 2% sodium hydroxide (NaOH) by weight. It has been determined that DETA is the most aggressive component of DS2 in environmental stress crazing studies of polycarbonate (4). DETA has also been used for some baseline comparisons

between MTL and CRDEC work. MECL has been shown to be aggressive in crack propagation studies (5).

Crack propagation studies with PC and PMMA have been done with several organic solvents (5,6). O-xylene was chosen as a cracking agent for PMMA based on its total solubility parameter and its tendency to crack and craze this polymer. It is also non-corrosive towards the current apparatus being used for these studies.

Samples of materials have been acquired through several sources. These sources are included in the references. Most samples were collected through distributors wishing to gain solvent resistance information.

ESC Test Development

The most widely used test, to this point, has been the static three-point-bend stress crazing test, based on the geometry of the ASTM D-790 flexure test (4). This test is appropriate since it only requires a small amount of liquid. Literature values of this test with PC and several crazing agents are available (1). The procedure and fixture for this three-point-bend ESC test were developed at MTL and revised by CRDEC to be suitable for chemical agent testing (3). CRDEC added the use of a video camera to record results so that constant monitoring in a hazardous environment is not required. CRDEC has also initiated the use of a laser for detecting craze initiation, which promises to be a significant improvement over the visual method.

MTL has also been implementing the ASTM F-484 ESC test, which uses a cantilever beam specimen, for comparison to the three-point-bend test. Results indicate a critical stress level where crazing initiates as opposed to a critical strain level. This test is recommended by the MIL-SPEC P-83310 for PC, although the ASTM version specifies PMMA with appropriate conditioning requirements. MTL has been using this test for both materials (6,7). Again, the cantilever beam ESC test only requires a small amount of liquid and, thus, could be used for agent testing as well. The apparatus, however, is a bit more cumbersome, and larger samples are required. In addition, a material with a relatively low flexural modulus or stiffness can not be tested with a cantilever beam specimen since the critical stress will be difficult to calculate with a deflection greater than fifteen degrees.

Crack Propagation Test Development

In order to determine a material's resistance to crack propagation when exposed to solvents, MTL has been using a dead weight loading apparatus with compact tension (CT) specimens based on ASTM E-399 (5,6,7). This test has been improved over conventional studies (8) by limiting the amount of liquid. Instead of immersing the sample in solvent, the test liquid is added dropwise to just the crack area. This test also has some advantage over the ESC tests since a full set of data showing how the crack increment varies with time, can be acquired from one sample. To determine critical strain from the ESC tests, several specimens must be tested. The specimen preparation for the crack growth studies, however, is more complex than the testing bars required for ESC studies. It is important to distinguish the difference between resistance to crack propagation when exposed to solvent which is determined in this test, and resistance to craze initiation which is determined in ESC tests. A material can be more or less resistant depending on which test is used (6).

RESULTS AND DISCUSSION

In Table 1, critical strain measurements for several formulations of PC samples are shown from MTL and CRDEC work during the past few years. This collection reflects the range of values that can occur when different formulations are used as well as possible differences due to test locations. In the case of Lexan 9034, one critical strain value was determined at MTL and the other at CRDEC; this is indicated with superscripted numbers which refer to references where these results were originally reported.

In order to compare some craze initiation studies which have been done on PMMA samples, critical stress measurements which result from the ASTM F-484 ESC test, can be converted to critical strain measurements by dividing by the flexural modulus. Table 2 illustrates this by converting critical stress measurements made on a series of PMMA materials (6) to critical strain values. These PMMA samples, under the trade name, Acrivue, are a series of cast (320, 350AC, 351) and biaxially stretched (350S, 352S) acrylics from Swedlow, Inc. Their formulations differ in molecular weight as well as crosslinking agents, not further described by the manufacturer. In Table 3, the critical strain values for the Acrivue materials are similarly obtained and compared to critical strain measurements made at CRDEC with the

three-point-bend apparatus and the laser equipment (3). The Polycast samples were acquired from LORAL Systems Division. It should be noted that the variation in critical strain measurements with different formulations of PMMA can be just as large, if not larger, than the variation in those of PC. In addition, the Polycast 76 material appears to have the best resistance to solvent induced craze initiation of the cast acrylics.

CRDEC also tested GAC 590, a polyurethane based thermoset from LORAL Systems Division, and found the critical strain measurements to be greater than 3.1% in both DCP and DIMP (3). This was the best result of all transparent materials tested.

Table 1. Critical Strain Measurements for Polycarbonate

<u>Name</u>	<u>Critical Strain</u> <u>in DETA(%)</u>	<u>Critical Strain</u> <u>in DCP(%)</u>	<u>Critical Strain</u> <u>in DS2(%)</u>
Lexan 9034	0.24 ⁷ , 0.30 ⁹		
SL3000(GE)	0.34 ⁴	0.40 ⁴	0.32 ⁴
Makrolon	0.30 ⁹		0.31 ¹⁰
Lexan MR5	0.55 ⁹	0.87 ³	0.59 ¹⁰
PC from Swedlow			0.30 ⁶ , 0.27 ⁶

Table 2. Calculated Critical Strains for PMMA Samples
Tested in DS2 via ASTM F 484

<u>Name</u>	<u>Critical Stress</u> (psi)	<u>Flexural Modulus</u> (psi x 10 ⁻³)	<u>Critical Strain</u> (%)
Acrivue 320	1300	450	0.29
Acrivue 350AC	1400	470	0.30
Acrivue 351	2900	460	0.64
Acrivue 350S	3200	450	0.70
Acrivue 352S	5500	450	1.22

Table 3. Critical Strain Measurements for Several PMMA Formulations

<u>Material</u>	Critical Strain <u>in DCP(%)</u>	Critical Strain <u>in DIMP(%)</u>
Acrivue 320	0.13	0.33
Acrivue 350AC	0.28	0.43
Acrivue 351	0.43	0.65
Polycast 76*	0.60	0.87
Acrivue 350S	0.78	1.22
Acrivue 352S	1.22	1.33
Poly 76S (LORAL)*	0.87	1.50

*See reference (3)

Crack Propagation and Water Sorption Studies of PMMA

Water sorption (11) has been shown to significantly affect ESC measurements of PMMA materials. The samples tested at MTL were in a hood and contained less than 0.1% by weight of water. Table 4 shows the amount of water these acrylic materials will adsorb in 30 days.

Solubility parameters, δ , can be used to predict a region of crazing based on the difference between the total solubility parameter of the solvent and that of the polymer (1). The total solubility parameter of water is 23.4 (cal/cm³)^{1/2} (12). PMMA or acrylic materials have a range of total solubility parameters of 8.9-12.7 (cal/cm³)^{1/2} (12). The large difference between the δ of water and that of PMMA suggests that crazing and cracking would not occur. The δ of o-xylene is 8.8 (cal/cm³)^{1/2} (12). The closeness of the δ 's of o-xylene and PMMA suggest that crazing and cracking in PMMA will occur when exposed to this solvent.

In Figure 1, the effect of o-xylene on the craze/crack propagation in a PMMA sample is illustrated. The designation craze/crack is used since this test can not distinguish between the two phenomena. The three samples of Acrivue 320 are tested at initial stress intensity factors (K_I) of 0.60-0.68 MPa*m^{1/2} which correspond to 45-50% of its fracture toughness (6). Although water is known to plasticize PMMA and, thus, reduce its resistance to solvent induced stress

crazing (11), when used independently in this craze/crack propagation test, it does not act as a crazing or cracking agent. A follow up study is suggested which tests a moist sample of PMMA which is subsequently exposed to a crazing agent such as o-xylene.

Immersion results show a significant weight gain in water of PMMA samples, however, no surface crazing occurs. In o-xylene, weight loss is demonstrated in four out of five of the samples. This indicates more aggressive behavior than in water due to dissolution. The fifth sample, Acrivue 352S, shows less weight gain than in water, but the surface crazes which result indicate aggressive behavior on the part of o-xylene. Acrivue 320 was most affected by the solvent, since significant surface crazing was seen, as well as a higher weight loss. Previous craze/crack propagation studies verify the higher susceptibility of Acrivue 320 (6). The crack propagation studies demonstrate the aggressiveness of o-xylene in a much shorter time frame than that required for detection of surface crazing.

It should be noted that the range of values for solubility parameters for PMMA and PC ($9.5-10.5 \text{ (cal/cm}^3)^{1/2}$) (12), as opposed to a single value, is due to the large number of formulations in which these polymers exist. This is illustrated by the variation in ESC results shown in Tables 1, 2 and 3.

Table 4. Immersion Results - Percent Weight Uptake in (24 Hours)30 Days

<u>Material</u>	<u>Water</u>	<u>o-xylene</u>
Acrivue 320	(0.19)0.91	(-0.04)-0.48*
Acrivue 350AC	(0.27)1.49	(0.02)-0.13
Acrivue 351	(0.25)0.90	(0.02)-0.11
Acrivue 350S	(0.45)1.46	(0.09)-0.02
Acrivue 352S	(0.15)0.99	(0.28) 0.67*

* surface crazing

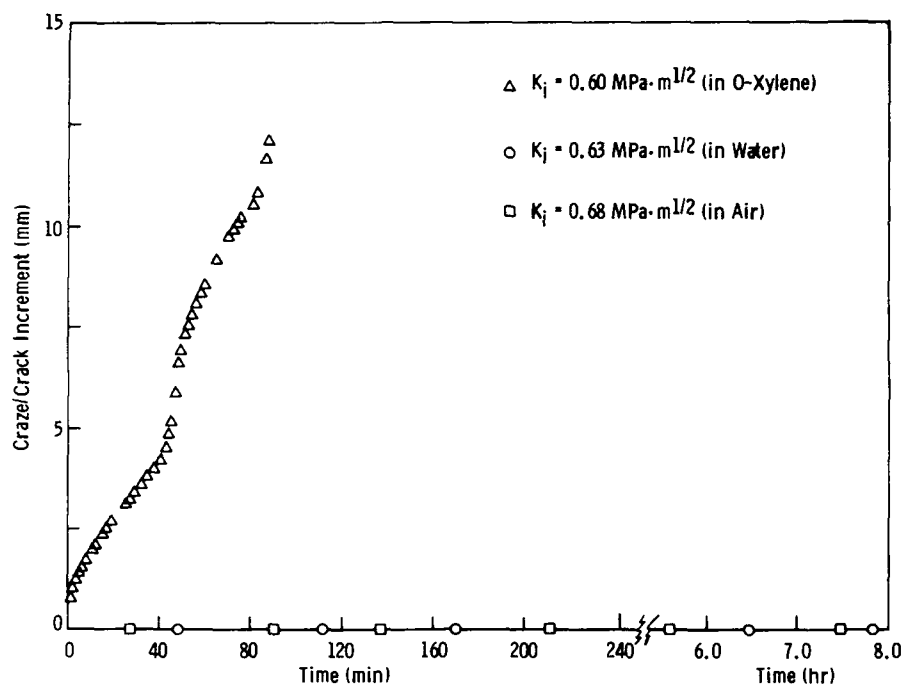


Figure 1. Craze/Crack Growth Curves for Acrivue 320 in o-xylene, water and air.

SUMMARY

The results which have been summarized here identify some of the concerns that must be recognized when conducting different types of tests for chemical resistance. This includes careful identification of nominally similar samples, as in the case of PMMA and PC, and also includes specific identification of the property desired, such as resistance to craze initiation or to crack propagation. Future studies are necessary to continue to assess newly developed transparent polymers being considered for use in Army systems. In addition, modifications should be made to the crack propagation apparatus to prepare it for chemical agent studies.

REFERENCES

1. C.H.M. Jacques, M.G. Wyzgoski, "Prediction of Environmental Stress Cracking of Polycarbonate from Solubility Considerations", J. Appl. Pol. Sci., vol. 23, 1979, pp. 1153-1166.
2. P.J. Burchill, G. Mathys, R.H. Stacewicz, "Analysis and Properties of Some Commercial Poly(methylmethacrylate)-based Materials", J. Mat. Sci., vol 22, 1987, pp 483-487.
3. R. Lewis, S. Liebman, L. Isaacson, E.W. Sarver, P.S. Grasso, "Chemical Agent Simulants for Testing Transparent Materials", presented at the 1988 U.S. Army CRDEC Scientific Conference on Chemical Defense Research (Nov. 15-18, 1988). To be published in the Proceedings.
4. L.H. Lee, J.J. Vanselow, "Chemical Degradation and Stress Cracking of Polycarbonate in DS2", MTL TR 87-46, September 1987.
5. A.J. Hsieh, J.J. Vanselow, "Environmental Stress Cracking and Cracking of Transparent Polymers", MTL-TR to be published.
6. J.J. Vanselow, A.J. Hsieh, J.H. Brown, "Environmentally Induced Discontinuities in Transparent Polymers", presented at the 1988 U.S. Army CRDEC Scientific Conference on Chemical Defense Research (Nov. 15-18, 1988). To be published in the Proceedings.
7. J.J. Vanselow, A. Hsieh, "Evaluation of Transparent Polymers for Chemically Hardened Army Systems", MTL-TR 88-24, July 1988.
8. C. Lhymn, J.M. Schultz, "Environmental Testing of a Glass-Fiber Reinforced Thermoplastic", Polymer Eng. and Sci., vol. 24, no. 13, Sept., 1984.
9. J.J. Vanselow, V. Henderson, J. Stevens, "Crazing and Cracking in Transparent Materials", Proceedings of the 1987 US Army CRDEC Scientific Conference on Chemical Defense Research, CRDEC-SP-88013, p.1301, April 1988.
10. J.J. Vanselow, L.H. Lee, "Stress Cracking of Thermoplastics", Proceedings of the 1986 US Army CRDEC Scientific Conference on Chemical Defense Research, CRDEC-SP-87008, p.581, June 1987.
11. P.J. Burchill, R.H. Stacewicz, "Effect of Water on the Crazing of a Crosslinked Poly(methylmethacrylate)", J. Mat. Sci. Let., v.1, 1982, pp. 448-450.
12. J. Brandup, E.H. Immergut, "Polymer Handbook", 2nd ed., John-Wiley & Sons, New York, 1975.

ACRYLIC MATERIALS FOR AIRCRAFT TRANSPARENCIES:
STRUCTURE AND EFFECTS OF ENVIRONMENT AND AGE
ON CRAZE RESISTANCE

P. J. Burchill
R. H. Stacewicz
G. Mathys
R. G. Davidson

Materials Research
Laboratory

ACRYLIC MATERIALS FOR AIRCRAFT TRANSPARENCIES: STRUCTURE AND EFFECTS OF ENVIRONMENT AND AGE ON CRAZE RESISTANCE

P. J. Burchill, R. H. Stacewicz, G. Mathys and R. G. Davidson

Materials Research Laboratory
Ascot Vale
Victoria 3032
Australia

Abstract

There are several manufacturers of acrylic materials which qualify to be used for windows in aircraft. Despite specification acceptability these materials are not similar chemically and such differences affect their long term behavior, especially in terms of water absorption and its effect on craze resistance. A comparison has been made of the properties of the unmodified acrylic with those which have been modified during the polymerization with various co-monomers. These co-monomers are either methacrylamides or difunctional methacrylic esters. A method of identifying the plastic will be outlined.

Craze resistance of these plastics decreases linearly with water content by about 8 MPa per one percent of water absorbed. However, because water solubilities at saturation are quite different in these materials, the rates at which craze resistance is reduced vary, with methacrylamide modified polymers being most severely effected. Water absorption is accompanied by swelling of the polymer and this dimensional change at saturation varies between 0.5% and 1.5% depending on the polymer. Procedures based on craze resistance or swelling for selection of an acrylic material will be discussed.

An exposure trial of various acrylic materials at a tropical site in Queensland, Australia has shown that the laboratory results on craze resistance are realistic. However, at the same time it showed that age of the material has an effect, that a small applied tensile load may be beneficial, and that the effect of sunlight is small. Craze resistances of material exposed for 2 years were greater than expected. This aging affect has also been observed in the laboratory with dry material. The exposure trial also showed that cleaning of acrylic can be very critical in a hot/humid environment. With the wrong fluid, crazing can readily occur without the presence of an external tensile load.

Introduction

The improvement in mechanical properties obtained by cross-linking poly(methylmethacrylate) (PMMA) has led to the wide use of the modified form of this polymer (modified acrylic) for aircraft transparencies. There are various means by which cross-links can be introduced into the base polymer, and the method used varies with each manufacturer. Even though the materials from different sources pass the specifications for use in aircraft they are not the same chemically. These differences show up in the craze resistance of these materials and the response of craze resistance to the environment.

It has been observed that primary causes for rejection of a transparency after a number of years in service are loss of clarity and distortion. The causes of these poor optical properties are scratches, crazes, microcracks, and changes in thickness and shape which cause visual distortion. In the F111C aircraft used by the Royal Australian Air Force (RAAF), scratches, and distortion which results from overheating are mainly caused by abuse and are largely avoidable. Crazes and micro-cracks, though they may arise from abuse, are believed to be the outcome of the effect of the service environment on the material. This RAAF environment consists of exposure to ground conditions, which are warm to hot and humid, to large temperature variations during flight, and to cleaning agents.

This paper considers the chemical structure of PMMA based materials, the influence of a tropical environment, and the age of the materials on their resistance towards crazing.

Material Composition

The commercial modified acrylics studied contained 5% or less of a co-monomer which provided points for the formation of cross-links. From infra-red spectra of the materials it was possible to show in some cases that a modifier was present. It was not possible though to identify the modifier by infra-red analysis of the bulk material, but its type could be determined; thus, amides and triazines were shown to be present in some of the materials. Through extraction of large quantities of these plastics, small amounts of unreacted monomers can be obtained, and identified. Table 1 gives a list of the acrylics studied and the cross-link providing monomer found. Information on the co-monomers was also obtained by heating the plastics with alkali and recovering the low molecular weight material [1].

The cross-link density found in these polymers was not uniform between manufacturers, though apart from Material B similar improvements in craze resistance towards isopropanol has been found relative to the unmodified acrylic. The low

density (high molecular weight between cross-links) found with sym-triallyltriazine (Material B) is a result of its low reactivity. With the neo-pentylglycol dimethacrylate containing Material (E) the highest cross-link density was found reflecting the fact that this link is formed by the same type of chemical reaction that produces the polymer. Moreover, with this co-monomer a higher cross-link density is required to give the same improvement in properties observed with methacrylamide modified acrylics, [1].

The similarity in co-monomers used by three manufacturers means that it can be a lengthy procedure to identify the material source of an acrylic transparency that has been rejected from service. This problem has been solved using a technique known as evolved gas analysis [2,3]. Samples of about 5 milligrams were pyrolysed at 10°C/min from ambient to 600°C in a stream of nitrogen (50 ml/min). The gas stream was passed through a gas cell in a FTIR spectrometer to obtain spectra of the evolved gases for every 2°C increase in temperature. Compounds were identified from their infra-red spectra and evolution profiles were constructed of absorbance against temperature.

The gases most commonly evolved were methylmethacrylate, methanol and carbon dioxide, and sometimes formaldehyde. The shape of the evolution profiles, especially for methanol, was found to be characteristic for each type of acrylic. Methacrylamide modified acrylics were readily distinguished, figure 1. Acrylics containing multi-functional methacrylate ester co-monomers were more difficult to characterize by this method. However, the decrease in yield of methylmethacrylate, and the evolution profiles obtained by monitoring absorbance at different infra-red frequencies in the ester absorption band provided means to identify the plastic, [3].

Water Absorption, Swelling and Craze Resistance

Craze resistance of a material is the minimum tensile force under given experimental conditions that must be applied to a specimen to cause crazing in the presence of an active liquid. The craze resistance of these plastics under standard laboratory conditions has been reported [1], and this resistance related to the changes in chemical structure of PMMA brought about by the co-monomers. With isopropanol, the most usual fluid applied in such tests, the craze resistances are similar (except B) and much greater than that of unmodified PMMA. The co-monomers also change other properties of the base polymer and so may have a detrimental effect on the long term performance of the material.

The pure polymer, PMMA, absorbs about 2.4 weight percent of water at saturation. Introduction of polar groups into the

polymer will increase the amount of water absorbed, and this has been observed in methacrylamide modified acrylics. Table 2 gives the solubility of water at 25°C and its diffusion coefficient for five cross-linked PMMA's, together with the associated volume expansion. The values can be compared to those for pure PMMA - Material U.

Absorption of water measured by the change in weight with time is practically Fickian for all these polymers, as is shown in figure 2, giving the initial part of the absorption curve for Material D. Departure from this ideal nature is most noticeable at long absorption times for the methacrylamide containing plastics. Figure 3 shows the increase in length that occurs as water is absorbed by a thin strip. Desorption of water is responsible for the tensile stresses that develop in surfaces due to restraint of shrinkage by underlying material. The magnitudes of the swellings given in Table 2 and the Young's modulus of these materials which is about 3 GPa shows that stresses of the order of 20 MPa can be developed easily. Such stresses are sufficient to cause crazes to form in the surface without having to apply an external force when there is an active liquid present.

Figure 4 shows the minimum external stress to produce crazes using isopropanol that needed to be applied to D which contained different concentrations of water. As the water content is increased, stress due to desorption increases but the sum of the external and desorption stresses is constant [5]. Previous work has shown that the minimum applied stress to produce crazing in all these materials decreased by 8 MPa for each percent of water absorbed. The time required to reach a particular water content for a given thickness depends on the square of the solubility and on the diffusion coefficient. Materials A, C, and D absorb water more rapidly than the others and so the craze resistance of dry material placed in water for a given time will decrease more than that of B, E and U. Hence tests for material selection and suitability could be based on the change in length of a specimen or the decrease in craze resistance for a given immersion time in water.

Exposure to a Tropical Environment

Proof of accelerated laboratory tests is found in the behavior of materials towards outdoor weathering. Materials A, C and U have been exposed to a tropical environment at the Joint Trials and Tropical Research Establishment in Innisfail, Queensland. They were exposed as bars at either open or sheltered from direct rain and sunlight sites. After 2 years, the specimens were cleaned, then loaded as cantilevers and treated with isopropanol. Material C required no external stress to produce crazing. Materials A and U both showed

better than expected craze resistances given the amount of water they had absorbed which was 77% of saturation, Table 3. The results showed that the main environmental factor in the reduction of craze resistance is absorbed water. Sunlight had only a small effect in causing further reduction. The same result was obtained when the materials were exposed as loaded cantilevers, maximum outer fiber stress was 13.8 MPa. Material A in both sites and C from the shaded sites showed small increases in craze resistance due to load. However, material C showed much greater sensitivity towards sunlight, and after 2 years the loaded specimens began to break in the field. In addition, these results also showed that in highly humid environments the unmodified PMMA performs better than a PMMA modified with methacrylamides, [8].

Exposure of sheets of A as a laminate with polycarbonate and a transparent rubber interlayer was also done to simulate weathering of a laminated transparency and the effect of cleaning. The acrylic outer surface was washed weekly with either water, or a water-isopropanol mixture (1:1 v/v) or isopropanol at the exposure site. Those laminates which were washed with isopropanol showed some crazing after 6 months. After 2 years, the isopropanol washed laminates were highly crazed while laminates washed with the other liquids were not.

Effect of Age

When the craze resistances of the specimens which had been exposed for 2 years were compared with expected values based on laboratory experiments, it was observed that the weathered material had a much higher resistance. The laboratory experiment is in the form of an accelerated test in that samples are immersed in water for a given time and tested immediately. Thus, for water contents less than saturation, the water concentration in the material varies with depth, and the material is not at equilibrium. This is not important in relating fall in craze resistance with water content because the decrease only depends on the average concentration [5]. However, as has been observed with the effects of thermal history on mechanical properties, similar effects may be occurring with water content history. Aging results in density increases as the polymer chains pack more closely, and there are increases in modulus and yield strength [6,7]. The better than expected craze resistance may be due to an aging effect.

A test for aging effects has been performed by conditioning many specimens and storing them in a dry atmosphere for six months. Half the specimens were then reconditioned to destroy any aging effect and their craze resistance compared with that of old material immediately. The

results are given in Table 4 where it can be seen that all the five materials tested showed that 6 months aging had produced 20% or greater increase in craze resistance.

Conclusion

The craze resistance of acrylic materials for aircraft transparencies has been shown to be dependent on both the environment and on small chemical differences in the polymers. For use in highly humid conditions the unmodified acrylic or those modified by multifunctional methacrylate esters will give better service. In dry environments, all the modified acrylics would be better than the unmodified material, however, the toughness of the material would become a consideration. Previous work [1] has shown that of the modified acrylics those containing methacrylamides are tougher. Furthermore, because of an aging effect, if the materials can reach equilibrium with their environment then performance which is better than expected from laboratory tests may be observed.

References

1. P. J. Burchill, G. Mathys and R. H. Stacewicz, Journal of Materials Science 1987, 22, 483.
2. R. G. Davidson, Journal of Applied Polymer Science 1987, 34, 1631.
3. R. G. Davidson, Microchimica Acta, in press.
4. R. G. Davidson, Journal of Analysis and Applied Pyrolysis, (submitted for publication).
5. P. J. Burchill and R. H. Stacewicz, Journal of Materials Science, Letters 1982, 1, 448.
6. L.C.E. Struik in "Physical Aging in Amorphous Polymers and other Materials", Elsevier, Amsterdam, 1978.
7. E.S.W. Kong in "Advances in Polymer Science", Vol. 80, 1986.
8. P. J. Burchill and R. H. Stacewicz, Materials Forum, in press.

Figure Captions

1. Methanol evolution profiles for Plexiglas-55 and Polycast-76: concentration in the gas stream variation with temperature.
2. Absorption of water (% w/w) against time (days^{1/2}) for material D.
3. Increase in length (%) against time (S^{1/2}) for material D on immersion in water.
4. Variation in external stress that has to be applied to material D to produce crazing with water content (% w/w).

Table 1

Modified Acrylics

Identifier	Material	Co-monomers	M _n [#]	Manufacturer
A	Plexiglas 55	methoxymethylmethacryl- amide + methacrylamide	11300	Rohm & Haas
B	Plexiglas 249	sym-triallyltriazine	139000	Roehm GmbH
C	Polycast 76	methacrylamide + formaldehyde	20000	Polycast Corp.
D	Acivue A	hydroxymethyl- methacrylamide	25000	Swedlow Inc.
E	S-708	neo-pentylglycol- dimethacrylate	3700	"

Number average molecular weight between cross-links

Table 2

Water Absorption at 25°C

Material	Diffusion Coefficient ($\text{m}^2\text{sec}^{-1} \times 10^{13}$)	Solubility % (w/w)	Swelling % (v/v)
A	3.0	3.7	2.3
B	4.7	2.4	1.3
C	3.2	4.9	3.7
D	-	-	2.8
E	5.5	2.4	1.3
U	5.1	2.4	1.3

Table 3

Craze Resistance of Exposed Bars and Controls (MPa)
towards isopropanol

Material	Control	Shaded Site	Open Site	Open Site Loaded	Expected Resistance
A	23.4	9.6	7.0	12.5	1
U	18.0	11.7	10.7	11.8	4

Table 4

Effect of Age on Craze Resistance (MPa) towards Isopropanol

Material	Old	New	% Increase on Aging
A	24.6	19.2	28
B	21.3	14.8	44
C	27.5	21.6	27
D	35.9	26.2	37
U	15.8	13.2	20

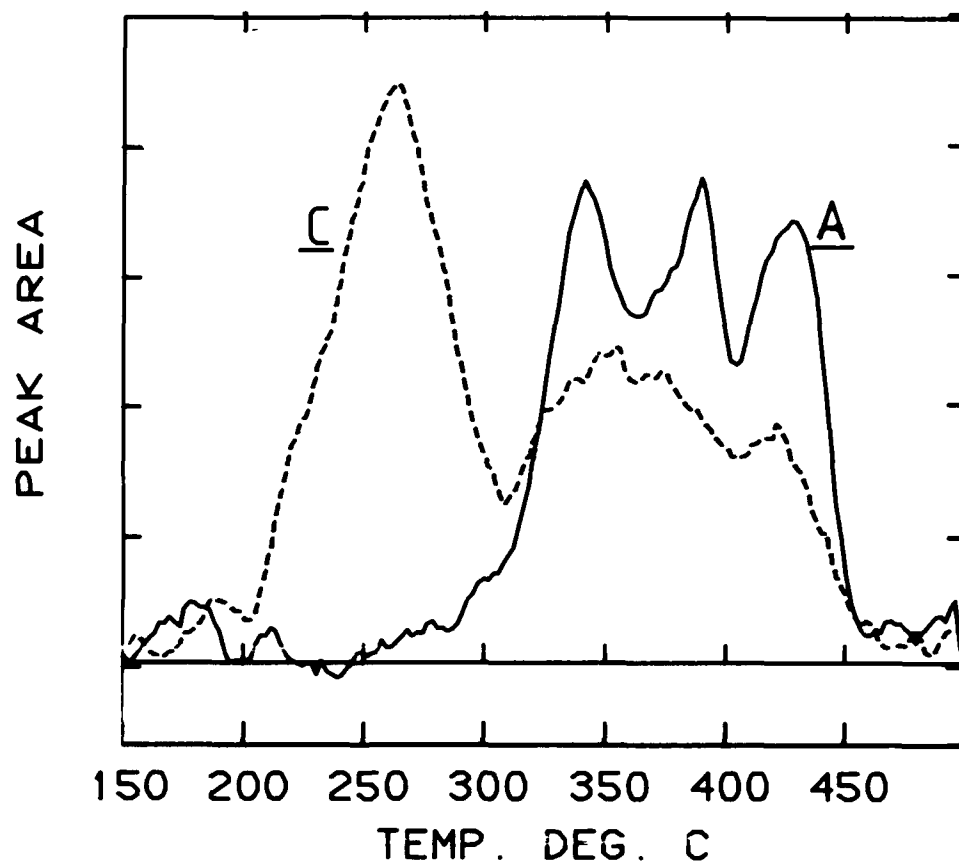


Figure 1. Acrylic Materials for Aircraft Transparencies: Structure and Effects of Environment and Age on Craze Resistance.

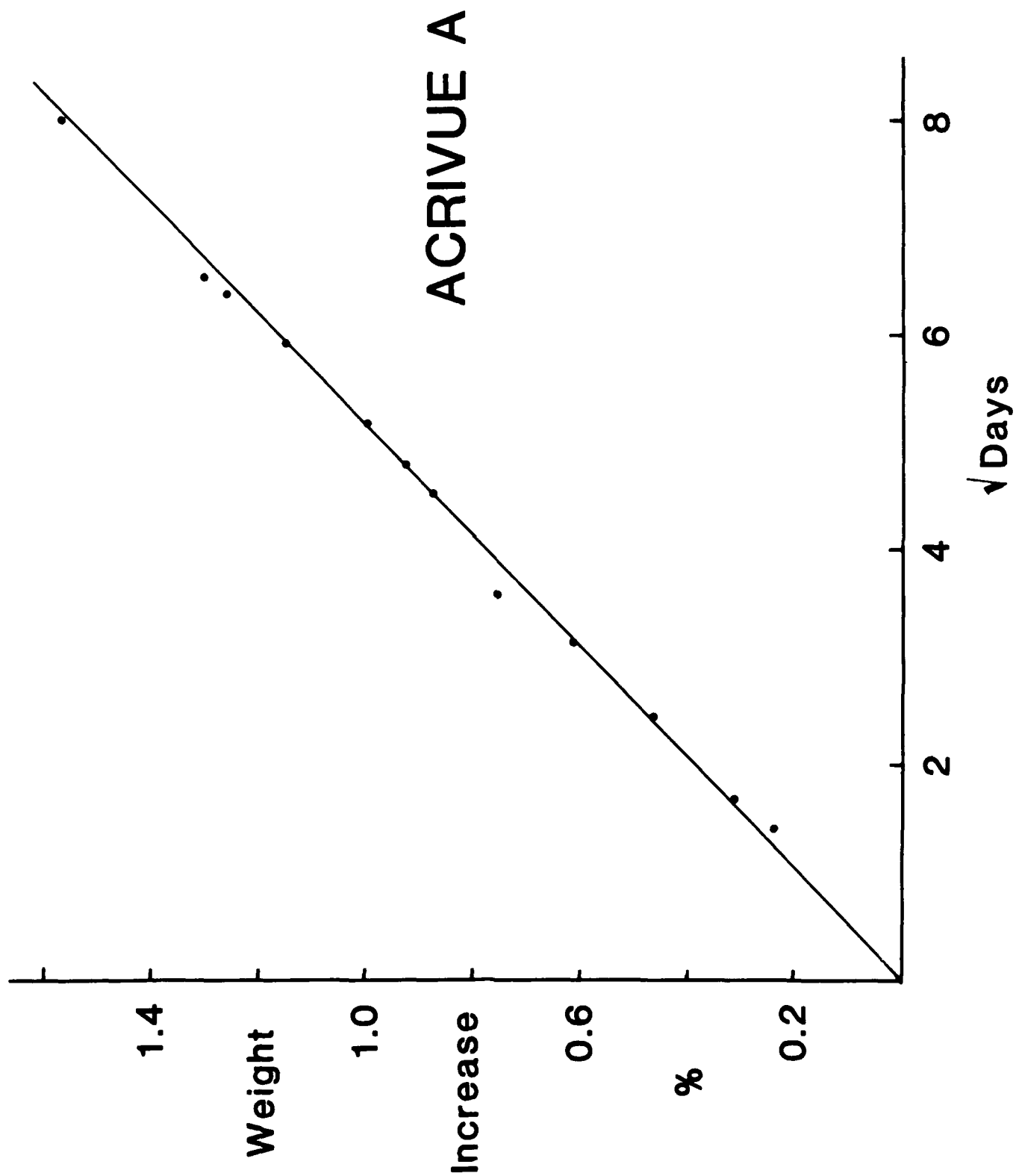


Figure 2

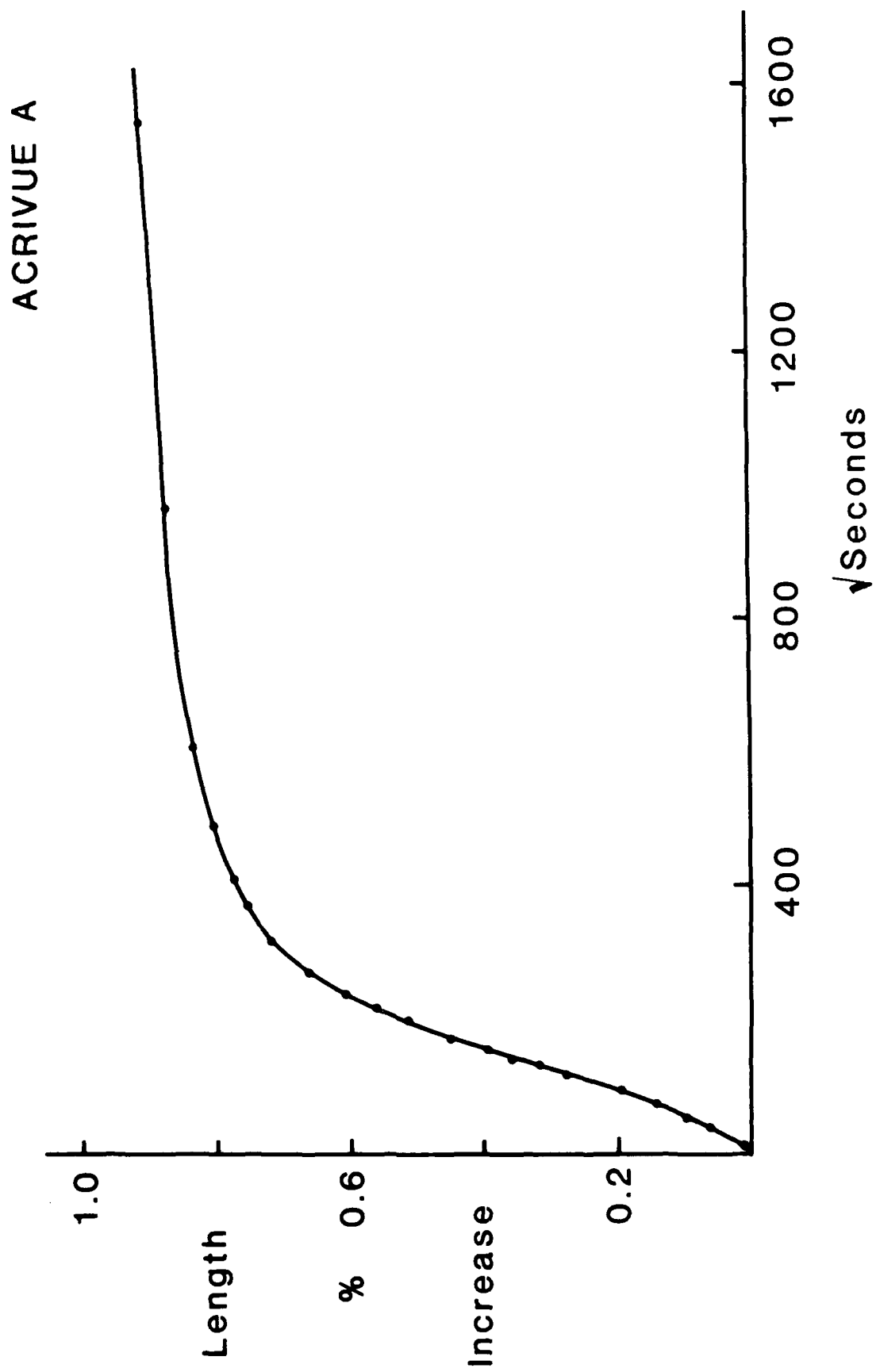


Figure 3

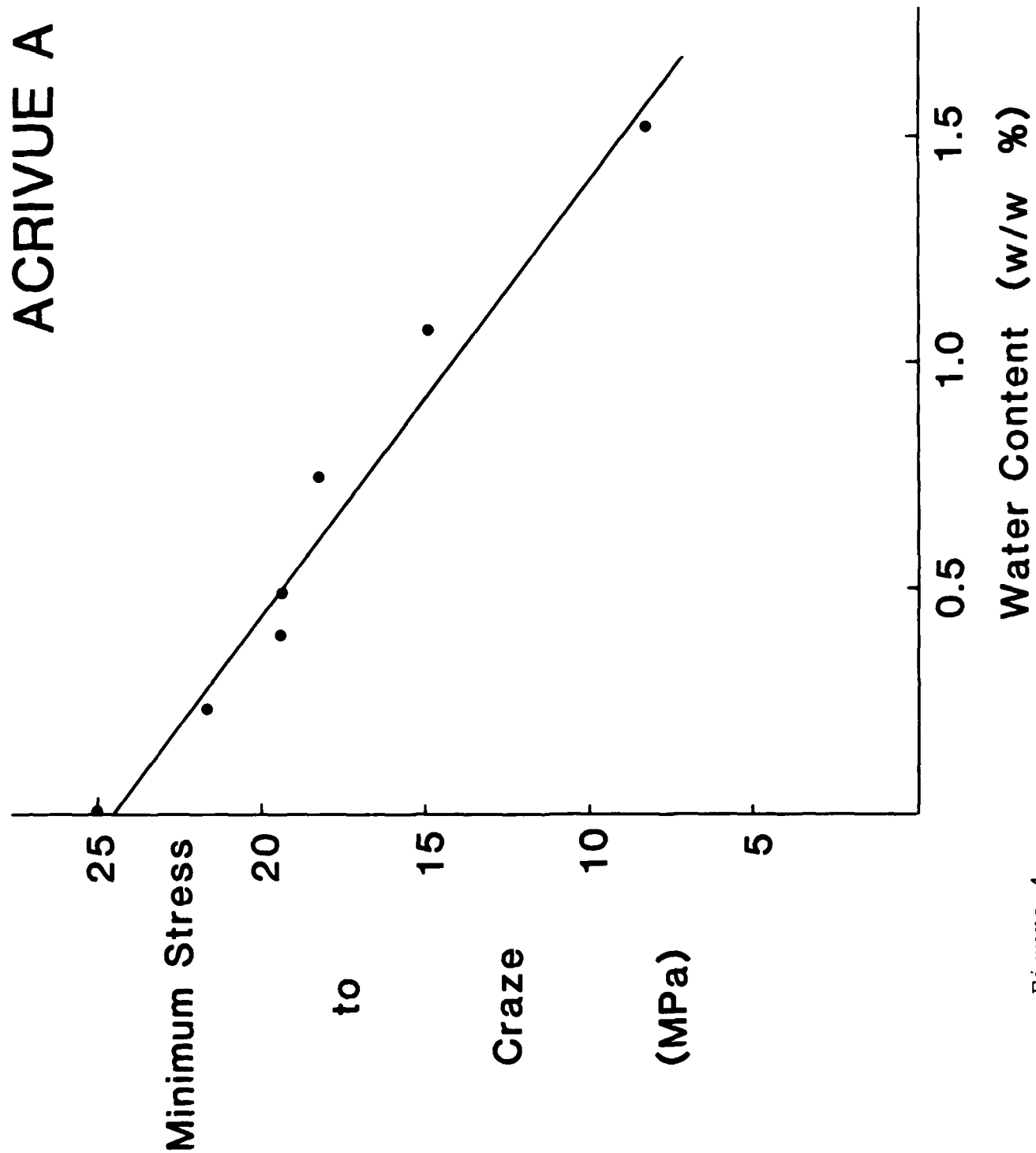


Figure 4

THE CAUSE AND EFFECT OF STRUCTURAL DEGRADATION
OF IN-SERVICE AGED F-111 ADBIRT WINDSHIELD TRANSPARENCIES

Daniel R. Bowman
Blaine S. West

University of Dayton

THE CAUSE AND EFFECT OF STRUCTURAL DEGRADATION OF IN-SERVICE
AGED F-111 ADBIRT WINDSHIELD TRANSPARENCIES*

Daniel R. Bowman and Blaine S. West, UDRI
University of Dayton Research Institute
Dayton, Ohio 45469
(513) 229-3018

ABSTRACT

A test program consisting of 22 full-scale birdstrike tests of F-111 ADBIRT windshield transparencies was conducted. Test hardware was developed to simulate flight structure, and four-pound artificial birds were used to impact the transparencies at the most critical location, the upper inboard corner. Testing was completed on windshield panels ranging from unaged baseline windshields to windshields which had been in service for more than five years. The structural integrity of F-111 ADBIRT windshield transparencies was found to be significantly reduced by in-service aging. Capability envelopes were developed for each vendor's windshield, relating bird impact resistance capability to installed age.

A follow-on test program was conducted consisting of: laboratory coupon tests of in-service aged and baseline F-111 ADBIRT windshield coupons; research of polycarbonate degradation and craze testing; fractography; and finite element analysis of the windshield edge attachment. Coupon testing completed to date indicates no degradation in bulk polycarbonate properties. Analysis of the edge attachment revealed numerous fatigue cracks at the edges and in the vicinity of the bolt holes. A literature search of craze testing indicated that the sealants used for the F-111 have been found to craze polycarbonate. Finite element analysis showed significant tensile stresses at the edges for various load cases. These stresses were high enough to propagate existing cracks, and in several cases the stresses were high enough to initiate cracks.

SECTION 1
BACKGROUND AND OBJECTIVES

Since 1979, the service life of the F-111 ADBIRT transparencies has been dictated by qualitative visual inspection. Parts have been removed from service when optical defects developed, such as scratches, acrylic crazing, rainbowing, and interlayer discoloration; and when structural defects developed, such as birdstrike damage, surface cracks, and delamination.

The first indication of possible ADBIRT in-service degradation was discovered in a program entitled Flightline Thermal Environment Testing of F-111 Transparencies,¹ completed in 1981, in which several thermally cycled

*Performed under Contract F33615-84-C-3404 for the Air Force Wright Aeronautical Laboratories, Flight Dynamics Laboratory, Wright-Patterson Air Force Base, Ohio.

and in-service aged transparencies were birdstrike tested. The testing undertaken indicated significant degradation; however, only a limited number of transparencies were tested. In 1985, the UDRI conducted a general transparency testing methodology program² in which coupons from various transparencies including the F-111 ADBIRT windshields were laboratory aged using ultraviolet light combined with heat and humidity and subjected to a series of laboratory tests to ascertain structural and optical durability. This program was part of a larger and more complete effort by Mr. Malcolm Kelley of AFWAL/FIER to develop a transparency durability/life cycle database from both laboratory coupon testing and field tracking of failed windshields. In instrumented impact beam tests, F-111 coupons which had been subjected to three "equivalent" years of laboratory aging showed a 40% reduction in energy absorption (a direct indication of bird impact resistance capability). It was suspected that some combination of age, service loading, thermal cycling, UV radiation, and moisture contributed to eventually degrade the impact strength of transparencies. However, at the time it was also hypothesized that the laboratory aging might be too severe.

On 13 June 1986, an F-111A Sierracin BIRT canopy transparency, installed in May 1979, broke out of its frame while the aircraft was in flight at Mach 1.9 and 45,000 feet altitude. On 15 February 1987, an F-111D had a birdstrike on the right windshield while flying at 500 feet AGL and 480 knots. The bird punched through near the center beam, leaving a hole larger than a softball, and damaging or destroying several circuit breaker panels and other small items on the aft bulkhead. Bird weight was estimated at 4.8 pounds. The transparency was a Sierracin ADBIRT windshield installed in May 1980. It was speculated that the effects of in-service aging may have contributed to these failures, since both failures were uncharacteristic of new transparencies.

This paper documents full-scale birdstrike and laboratory coupon testing of new and in-service aged F-111 windshields. The main objectives of this effort were: (1) to determine the effect of in-service aging on the bird impact resistance capability of the F-111 windshield; (2) to reproduce full-scale windshield degradation trends in the laboratory, correlating coupon testing with full-scale birdstrike testing; and (3) to determine the cause of degradation.

SECTION 2 TEST ARTICLE AND TEST MATRIX

2.1 TEST ARTICLE

The basic test articles were new and in-service aged right-hand F-111 ADBIRT windshield transparencies. The cross-section is illustrated in Figure 1. Transparencies with a known in-service life (actual time on the airplane) were tested because time on the airplane was suspected to affect degradation. To eliminate geographical location as a variable, full-scale birdstrike testing was limited to windshields from one geographical area (Cannon AFB, where the in-service failures occurred, and Mountain Home AFB,

which has a similar climate).* These two bases were chosen as a worst case, using the logic that the UK bases hangar their planes which protects them from the climate, and the Plattsburgh and Pease bases do not receive as much sun as the Cannon and Mountain Home bases. Two transparencies from the United Kingdom were also full-scale tested as a spot check on the significance of geographical location.

2.2 TEST MATRIX

This program consisted of 22 full-scale birdstrike tests and a number of coupon test specimens. The full-scale birdstrike test matrix is shown in Table 1. The coupon test matrix is shown in Table 2. The experimental coupon test phase was primarily based on the recommended aircraft transparency test methodology for durability evaluation, documented in References 2 and 3. Additional exploration tests were developed as required.

SECTION 3 FULL-SCALE BIRDSTRIKE TESTS

3.1 TEST SETUP

General Test Considerations

An F-111E crew escape module served as the basic test-bed. The use of an actual crew enclosure reduced the cost of frame development and allowed for more realistic testing. The aft arch and forward center beam were expected to sustain damage during transparency testing. Consequently, it was desirable to design a replaceable center beam and aft arch to preclude the sacrifice of a large amount of expensive and unavailable flight structure.

Historically, full scale birdstrike testing of aircraft transparencies has been accomplished either on a hardstand (rigid fixturing) or actual flight hardware. This program is one of the first to bridge the gap between hardstand birdstrike testing and flight hardware birdstrike testing. Hardstand testing is reasonably economical; however, the validity of test results achieved on a rigid hardstand are questionable because most aircraft support systems are flexible, not rigid, and birdstrike resistance capability for a transparency system can be very dependent on support structure stiffness. For instance, if the aft windshield arch is too stiff, peak loads will increase and the windshield will tear at the aft arch behind the impact point; if the aft arch is too flexible the windshield may fail due to excessive deflection. The stiffness and strength of the aft arch need to be closely tailored to the windshield stiffness and strength to optimize system bird impact resistance. Flight hardware testing provides optimal test results; however, flight hardware is expensive and often in short supply. Therefore, a suitable alternative is desirable. The best

*NOTE: The F-111 bases are located in three geographical areas. Group 1: Western U.S.-Cannon and Mt. Home, Group 2: Northeastern U.S.-Plattsburgh and Pease, and Group 3: United Kingdom-Lakenheath and Upper Heyford.

alternative is simulated flight hardware, which can be designed at a reasonable cost with stiffness and strength values close to actual flight hardware values for realistic system structural response.

3.2 HARDWARE DESIGN AND FABRICATION

Test hardware was developed in accordance with the following material and geometric constraints. The material used should be readily available, reasonably priced, machinable, weldable, and tough. The cross-sectional engineering properties should match the properties of the flight hardware as closely as practical under the constraints of material and fabrication methods; the F-111 windshield is extremely sensitive to small changes in aft arch stiffness as evidenced by the work accomplished by UDRI to develop an aft arch reinforcement for the BIRT.⁴ In addition, the cross-sectional shape must be similar to the existing shape to allow the canopy to fit against the aft arch without interference.

A 4130 chrome-moly steel was chosen to satisfy the material constraints. It was decided that it would be advantageous to build the aft arch in two pieces (the production arch is one piece) to allow change-out of damaged right-hand arches without requiring changeout of the left-hand windshield which was not being tested.

Three centerbeams, one left-hand arch, and six right-hand arches were constructed. The arch/centerbeam assembly is illustrated in Figure 2. Grade 8 alloy capscrews were used for all arch-to-sill and arch-to-centerbeam connections. Flight hardware fasteners for the windshield were located, but the price per fastener was unreasonable, and delivery could not be achieved prior to testing. Equivalent strength and ductility fasteners (NAS 1203 and NAS 1204) were substituted.

3.3 TEST PROCEDURE

A brief summary of the test plan follows. The windshields were installed in the crew module per the applicable Technical Order, except that a neoprene 1/8" sponge gasket was used in place of sealant. Artificial four-pound gelatin birds were used to impact the transparencies at the most critical location, the upper inboard corner. A baseline capability was established with the new optical reject transparencies. The in-service aged transparencies were then tested. Each test was documented with high speed films and still photographs. The windshield test article was removed and the aft arch was inspected for damage after each test. Damaged arches were removed and replaced. The damaged arches were annealed, reformed to correct shape, rewelded where required, reheat treated to a Rockwell hardness of C35.5-C37.0, and then reused.

3.4 BIRDSTRIKE TEST RESULTS

Table 3 presents a summary of the 22 birdstrike tests. Figure 3 depicts a birdstrike tested baseline transparency, and Figures 4-7 depict characteristic birdstrike tested in-service aged transparencies.

3.5 DISCUSSION OF FULL-SCALE BIRDSTRIKE TESTING

The Effect of In-Service Aging on Bird Impact Resistance

No relationship was discovered between total age and birdstrike resistance capability, although at least one source in the literature indicates a reduction in bare polycarbonate impact strength with absolute age.⁵ A plot of birdstrike resistance capability versus installed age (date of installation subtracted from date of removal) is presented for each vendor in Figure 8. Note that a predicted capability curve for 0.725" stretched acrylic is included.* This plot indicates a definite relationship between installed age and degradation. The actual cause of degradation was thought to be a complex combination of extrinsic factors including absolute age, installed age, geographic location, and more specific intrinsic factors such as total UV exposure, thermal history, fatigue, hydrolysis, and molecular attack. Table 4 presents a comparison of baseline and in-service aged windshield birdstrike resistance.

Full scale tests on the two transparencies which were from the UK indicated no significant difference in capability compared to the Cannon and Mountain Home windshields. The UK windshields were expected to perform better (show less degradation with age) if UV or flightline thermal history is causing the degradation, because the aircraft at the UK are kept in hangars out of the sun.

The structural integrity of F-111 ADBIRT windshields is significantly reduced by in-service aging. Results of the bird impact tests indicate that the windshield capability is reduced to 360 knots after two years (40% in terms of impact energy) and reaches an asymptotic minimum value of 325 knots at an installed age of five years. There is also a change in failure mode between the degraded and baseline windshields. When shot at velocities exceeding their capability, new windshields are ductile and crack resistant, absorb energy, and maintain coherency (no spalling). The degraded windshields, however, have decreased crack tolerance, absorb little energy (minimum plastic deformation), and have a tendency to spall. The effect of increasing velocity (and strain rate) on transparency damage is depicted in Figure 9.

Analysis of the birdstrike films and the failed transparencies indicated that cracking and subsequent failure paths were initiated at the bolt holes behind the impact point. This was expected, because the bolt holes are sites of stress concentration. The F-111 ADBIRT windshield is especially sensitive to edge attachment failure at the aft arch because of the limited distance between the fasteners and the edge of the windshield. The edge distance is dictated by the aft arch forward flange geometry and is

*This curve was estimated from historical birdstrike data including edge attachment effects from Reference 6, flexure beam test data of laboratory aged acrylic from Reference 2, and laboratory testing of coupon specimens from in-service aged T-38 acrylic windshields from Reference 7.

approximately half an optimal edge distance. One good indication of polycarbonate ductility is the amount of bolt hole deformation behind the impact point. As the transparencies age, bolt hole deformation decreases and the chance of developing cracks at the bolt holes increases. This is an indication of decreased fracture toughness and possible embrittlement. Fracture toughness describes a material's ability to resist crack propagation. A decrease in fracture toughness means that the material is more notch sensitive and has less resistance to crack growth. Polycarbonate embrittlement is characterized by a decrease in plastic deformation and ultimate stress.⁸ In addition, it was hypothesized that as the polycarbonate becomes degraded the strain rate sensitivity may increase. At low impact velocities the critical fracture toughness or embrittlement strain and/or strain rate is not exceeded, resulting in normal elastic-plastic behavior; but at high velocities the critical strain and/or strain rate may be exceeded, resulting in elastic response followed by brittle failure (unstable crack growth) with little or no plastic deformation evident. The amount of crack branching into the polycarbonate plies from the edge attachment and punch-through failures were thought to be evidence that the polycarbonate properties were changing throughout the windshield, not just at the edge attachment.

SECTION 4 EXPERIMENTAL COUPON TESTS

4.1 HAZE/TRANSMITTANCE

The standard FTM406-Method 3022 coupon, 1-1/2" square was used. An XL 211 Hazeguard system was used to measure haze/transmittance as per Federal Test Method Standard FTM406, Method 3022.

There appears to be a trend of increased haze with increased service life, which may be related to scratches, crazing, and other surface defects. No trend could be detected from percent transmittance data, and the observed scatter in the data may be related to manufacturing variations. The F-111 ADBIRT Transparency acceptance Test Procedure 601 limits percent haze to a maximum of three percent and percent transmittance to a minimum of 84 percent for new transparencies without metallic coatings. All of the aged transparencies tested had haze values above three percent, and the transmittance values were all above 85 percent on the average.

4.2 INTERLAMINAR BOND INTEGRITY

4.2.1 Torsional Shear

Specimens were machined Using ASTM D229-76 as a guideline, having an annular test area of 0.245 sq. in. Torsional shear tests were conducted at an angular displacement rate of 10 degrees/minute, resulting in an equivalent average linear shear displacement rate (equivalent average linear shear displacement rate = average angular displacement rate $\times (\pi/360) \times (r_i + r_o)/2$) of 0.055 in/min. Specimens were tested by holding one surface ply stationary with an aluminum fixturing socket attached to the closed loop MTS system load cell and applying a torque to the other ply through a fixturing socket attached to the actuator. Torsional shear test results are summarized in Table 5. The interlayer properties have obviously undergone significant change. Sierracin's silicone interlayer, which is between the

acrylic and polycarbonate plies, develops higher ultimate shear stress, shear modulus, and absorbed energy with increased in-service age. This may be caused by additional cross-linking with time, or by the loss of a plasticizer within the silicone. The urethane interlayers for both manufacturers are experiencing large reductions in angular displacement, ultimate shear strength, shear modulus, and absorbed energy with increased in-service age. The effect on full-scale birdstrike resistance of these reductions is unknown. However, previous testing completed at UDRI indicates that interlayer properties can strongly affect transparency performance. It is of interest to note that the baseline shear strength of PPG's urethane is nearly twice that of Sierracin. This agrees with earlier testing documented in AFWAL-TR-83-3063.

4.2.2 Flatwise Tension

Using ASTM F521-77 as a guideline, the 2-inch square standard specimen was modified to 1-inch square to minimize the effects of transparency curvature. The specimen test area was undercut, to ensure failure in the test interlayer and to eliminate specimen-to-fixture bondline failure. Specimens were bonded to one-inch square loading blocks using a room temperature curing adhesive. An alignment fixture was used to center the specimen and align the loading blocks to ensure a true tensile load. Tests were conducted at a loading rate of 100 lb/sec in an MTS electrohydraulic closed loop test machine. Load versus displacement data was recorded.

Flatwise tension test results are shown in Table 6. The urethane interlayer between the polycarbonate plies is experiencing significant degradation. Similar to the torsional shear results, the Sierracin silicone interlayer, which is between the acrylic and polycarbonate plies, becomes stiffer and stronger with increased installed age. The PPG urethane acrylic/polycarbonate interlayer properties are not changing significantly.

4.3 IMPACT-HIGH RATE MTS BEAM

The three-point loaded beam specimens were machined to t inches thick, $2t$ inches wide, and $15t$ inches long, where $t = 0.75$ inches (the nominal thickness). Specimens were cut from the transparencies so as to minimize curvature along the beam length and equalize the curvature between replicates. The "high-rate" MTS beam test is an instrumented flexure test utilizing three-point simply-supported loading. The MTS test machine used to conduct these tests is a high performance electrohydraulic closed loop test system with high level control and data gathering capabilities. A mounting fixture was used to provide three-point simply-supported loading to the center of each beam specimen; the contact radius of each loading support being $3/8$ inch. The span between supports was $6t$ with an overhang of $4t$ at each end. The specimen was centered in the fixture with the test surface down, producing tension in the test surface under investigation. Displacement rates were controlled to the nominal reported velocities of 2,000 or 40,000 inches/minute. Peak displacement was set at a selected value of 3.25 inches.

Plots of failure energy versus installed age are shown in figures 10 and 11 for the 40,000 in/min impact beam results. The 2,000 in/min trends

were similar. Overall averages by manufacturer for all specimens are shown in Tables 7 and 8.

Testing completed with the acrylic ply in compression indicated that the interior surface of the inboard polycarbonate ply did not appear to be embrittled except for two PPG windshields, full-scale tests 9 and 22, where failure initiated at the coating surface. These windshields had experienced interior coating degradation - the coating had become an opaque, milky-white color as if the surface had crystallized or oxidized. Testing completed with the acrylic ply in tension indicated that the outboard surface of the outboard polycarbonate ply is not embrittled. From the plots of energy-to-failure versus installed age, there are no recognizable patterns. The data exhibits normal scatter which does not appear to be related to age. Overall results indicate that for this test at the tested strain rates (approximately 7.1 in/in/sec for 2000 in/min and 142 in/in/sec for 40,000 in/min displacement rates) there is no embrittlement or relationship between cross-section structural performance and age.

The overall averages presented in Tables 7 and 8 are of interest for making comparisons between each manufacturer's cross-section. For acrylic in tension, peak load and energy-to-failure are very similar for the two manufacturers. In tests conducted with the acrylic in tension, the differences in peak load and energy are small because the load carrying capacity of the beam cross-section is reduced immediately when the acrylic fails, reducing the effective depth of the cross-section and eliminating the effect of the stiffer urethane interlayer. For acrylic in compression, peak load and energy-to-failure are significantly higher for PPG. This can be attributed to the fact that the PPG windshield has a urethane interlayer between the acrylic surface ply and the outboard polycarbonate structural ply, while the Sierracin windshield uses a silicone interlayer. The urethane is much stiffer and provides better shear coupling than the silicone between the acrylic and polycarbonate. Even though the acrylic crushes early in the testing event, load continues to increase with little change in stiffness because the acrylic still carries load in compression. For bending in either direction (acrylic in tension or compression) the PPG cross-section is stiffer initially than the Sierracin cross-section.

4.4 IMPACT-FALLING WEIGHT

The three point loaded falling weight beam specimens, loading nose geometry, and span were the same as used for the MTS beam test. The specimens were tested in accordance with ASTM test method F736-81. Test results are summarized in Table 9.

The falling weight test has been used primarily for monolithic acrylic and polycarbonate specimens. The threshold of failure energy has been defined for polycarbonate as the energy required to open a visible crack, and for acrylic as the energy required to fracture the specimen. The F-111 ADBIRT laminate is not as stiff as the monolithic specimens and consequently some of the specimens pushed through the supports prior to the development of a visible open crack in either structural polycarbonate ply. The energy required to push the specimen through the supports is a function of stiffness and overall strength. No pattern can be determined from the falling weight results.

4.5 SPLIT HOPKINSON BAR

The Split Hopkinson bar provides one of the few research tools for investigating the behavior of materials under uniaxial stress loading at strain rates above 300s^{-1} . The University's Hopkinson bar has been designed to measure tensile, as well as compressive, stress-strain relationships. Both tensile and compressive tests were planned to evaluate baseline and in-service aged polycarbonate properties. This testing was not completed in time for approval of publication.

4.6 AIR CANNON

Plate specimens 10 inches square were cut from six different windshields. Edges remained as band sawed. Additional specimens, 12 inches square, were cut from Rohm and Haas and from General Electric aircraft grade 0.31 inch polycarbonate sheet. This material had been stored at UDRI in a warehouse type environment for approximately seven years. This sheet was used for an earlier program at UDRI which included air cannon testing⁹.

The projectile was a commercially available one inch diameter steel ball bearing. The sabots were stripped from the projectiles in the stripper section of the gun to keep the sabot from traveling on into the test specimen. A "picture frame" fixture with a ten-inch square opening was used to support the specimens. The specimens were taped to the front of the frame (i.e., the side facing the oncoming projectile), to achieve a simply supported edge condition.

Failure energy was defined as the minimum energy absorbed by the specimen that produced a visible, open crack. The failure energy was taken to be equal to the kinetic energy of the projectile (that is, all the projectile kinetic energy was assumed to be absorbed by the plate). The computed strain rate values are time-averaged values rather than instantaneous values; that is, they represent the average strain rate over the impact event duration rather than the strain rate at one specific instant of time.

Test data for the 10-inch square air cannon specimens cut from the F-111 windshields is shown in Table 10 and plotted in Figure 12. PPG specimens had significantly higher threshold energies than Sierracin specimens. Specimens from both manufacturers showed only a small decrease in impact energy with increasing installed age. This decrease may not be a function of the structural plies, but may be caused by degradation of the interlayer properties as noted earlier.

As a check of the effect of aging in a warehouse environment, air cannon testing on the 0.31-inch-thick seven year old polycarbonate sheet from General Electric and from Rohm and Haas was repeated. The specimen size (12" square), frame size (10" square), support condition (simply supported), and projectile size (1" diameter steel ball bearing) were all the same as for the earlier air cannon testing. The results of this testing are summarized and compared with earlier testing in Table 3.15. Note that the threshold energy actually increased for both manufacturers after the material had been aged in a warehouse environment, although the increases may not be statistically significant.

4.7 TENSILE EDGE ATTACHMENT

The edge attachment beams were cut from the transparencies at the aft arch. The specimen geometry is shown in Figure 13. The edge attachment specimens were tested with the fastener end mounted in a fixture which simulated the fixity and attachments of the actual transparency design; the other end included a 0.9" diameter hole which was pin-loaded. The test specimens were tensile loaded at a displacement rate of 500 in/min. using an electrohydraulic closed loop MTS test machine.

Table 12 is a summary of the edge-attachment test data. The specimens which failed at high peak loads and energies to failure exhibited ductile behavior. The specimens which failed at low peak loads and energies to failure exhibited brittle failure. The aged specimens had some cracks prior to being tested. In general, cracks running from the edge to the bolt hole had marginal effect on edge strength. However, cracks running from one bolt hole to the next appeared to have contributed to the brittle failure mechanism. The integrity of the adhesive bond between the metal bearing strip/edge retainer and the inboard polycarbonate ply has a significant effect on edge strength. This can readily be seen by comparing two of the aged PPG groups. The 25 1/2 month installed age PPG specimens experienced brittle failure, with little contribution of strength from the edge retainer, while the 40 month installed age PPG specimens failed in a ductile manner, with the metal edge retainer/transparency bond maintaining structural integrity of sufficient degree to cause plastic deformation and eventual tearing failure of the retainer behind the bolt holes. In fact, the ductile failure mode of these specimens may be partially attributable to the excellent adhesion of the retainer. The importance of the metal edge retainer is immediately obvious when comparing the Sierracin edge attachment group with the greatest in-service age 6y 4 3/4m (which has no metal retainer) with the other Sierracin edge attachment groups.

4.8 TENSILE TESTING

Both pseudo static and high strain rate ($\approx 200s^{-1}$) tensile testing was planned for baseline and in-service aged polycarbonate. This testing was not completed in time for approval of publication.

4.9 FRACTURE TOUGHNESS AND FATIGUE CRACK GROWTH

Fracture toughness and fatigue crack growth testing were not completed in time for approval of publication.

4.10 DYNAMIC MECHANICAL ANALYSIS (DMA)

Dynamic mechanical analysis (DMA) was used to analyze the individual acrylic and polycarbonate plies of baseline and an in-service aged PPG and Sierracin windshields. Specimens were cut from the bulk windshield material away from the edges. Each layer was analyzed from -175° to $250^{\circ}C$ using a $2^{\circ}C/min$. heating rate at a fixed frequency of 1.0 Hz using a Dupont 983 dynamic mechanical analyzer.

Results from only several tests were completed in time for approval of publication. DMA scans of baseline and in-service aged PPG specimens are

shown in Figures 14, 15, and 16. Determination of the glass transition temperatures, T_g , for each polymeric layer (using the maximum of the loss modulus curve, E''), indicated the following:

Manufacturer Sequence No. Installed Age	Ply	T_g , °C
PPG Baseline	Acrylic	128
	Outboard Polycarbonate	159
	Inboard Polycarbonate	156
PPG #69 3y 4m	Acrylic	115
	Outboard Polycarbonate	153
	Inboard Polycarbonate	155

In addition to the 13°C difference in T_g of the two acrylic layers, differences in the scans of the polycarbonate layers were also observed. These differences were seen as secondary transitions in the 0° to 100°C range. How these differences relate to transparency performance is being evaluated.

4.11 DIFFERENTIAL SCANNING COLORIMETRY (DSC)

DSC testing was not completed in time for approval of publication.

4.12 GEL PERMEATION CHROMATOGRAPHY (GPC)

GPC testing was not completed in time for approval of publication.

SECTION 5 SUPPORTING INVESTIGATIONS

5.1 POLYCARBONATE DEGRADATION

The degradation, stability, and life expectancy of polycarbonate have been the subject of much research. In this section the term degradation will refer to a decrease in toughness (area under the stress-strain curve). Polycarbonate degradation is caused by any one or a combination of five conditional irritants, including UV light, thermal history, moisture, chemical attack, and fatigue.^{10,11}

Ultraviolet light provides energy to the polycarbonate, causing a photochemical reduction in molecular weight via bond scission. Degradation is limited almost entirely to the surface. This degradation is evidenced by a reduction in molecular weight and a corresponding reduction in elongation to break and impact energy. The degraded surface is essentially a flawed zone (with microcracking in the top 5-10 micrometers) which allows crack propagation into the undegraded bulk of the polycarbonate. Photo-degraded polycarbonate characteristically begins to darken and show visible surface damage.^{12,13}

Laminated polycarbonate with a surface acrylic ply would not be likely to experience UV degradation because the surface acrylic ply should absorb

most of the UV light. Any UV light which penetrates the acrylic and the first interlayer should be minimal, and would be absorbed by the outboard surface of the first outboard polycarbonate ply. For these reasons, it is doubtful if UV degradation is affecting the F-111.

Thermal history has a large effect on the properties of polycarbonate. When polycarbonate sheet is extruded and then cooled below the glass transition temperature (the temperature at which the material begins to change from a glassy solid to a rubbery material, $T_g \approx 150^\circ\text{C}$ (302°F)), the long chain polymers are frozen in place. The differential cooling rate between the surface and the interior of the polycarbonate causes residual stresses to develop, with compression at the surface and tension in the interior of the material. Cold working of polycarbonate also causes residual stress to develop. This residual compressive stress at the surface of the polycarbonate sheet allows ductile yielding around flaws. As the polycarbonate experiences time at temperature (thermal history), these residual stresses are relieved. Once the residual stresses fall below a critical value the polycarbonate tends to fail in a brittle manner in the vicinity of a flaw. These results can be obtained for 0.25" and thinner polycarbonate sheet. Polycarbonate sheet thicker than 0.25" does not appear to be affected by residual stresses, exhibiting brittle failure in notched Izod tests regardless of thermal history. It is important to note that these residual stresses affect only the notch sensitivity of the polycarbonate.¹⁴⁻¹⁶

Pielstocker^{17,18} and many others¹⁹⁻³² attribute thermal degradation of the bulk polycarbonate to a different mechanism. Once polycarbonate cools below T_g during manufacture, molecular mobility is significantly reduced and polymer chains are frozen in place, with quenching producing the highest degree of frozen disorder. As the polycarbonate experiences thermal history, annealing below 130°C (266°F), the polymer chains move to a more preferred orientation (which is more ordered). Of course, the higher the temperature and the greater the time at temperature, the greater the amount of molecular movement and ordering. This reordering increases the polycarbonate density. There is no evidence of molecular weight change or crystallization. The more ordered structure develops higher yield stress but lower elongation, eventually resulting in embrittlement. Above 130°C this ordering begins to compete with a disordering effect at the onset of the glass transition which results in the rotation of the polymer chains and a subsequent decrease in all properties.

It is of interest to note that the effect of annealing (time at temperature) and subsequent embrittlement can be reduced by heating the polycarbonate to a temperature around T_g and then quenching the polycarbonate. This reorients the polymer structure, again freezing residual stresses, and molecular disorder.

Table 13 presents the time at temperature for 304 hours (one equivalent year) of F-111 flight time temperature as simulated at the Pressure Thermal Lab in Building 65 at WPAFB. This does not include time on the flightline where temperatures as high as 93°C (200°F) have been reported in the F-111 cockpits. Obviously, the F-111 is experiencing significant thermal history

and there is a likelihood that this thermal history is affecting the polycarbonate on the F-111 ADBIRT transparencies.

At room temperature, moisture appears to have minimal effect on polycarbonate properties. However, at elevated temperature, hydrolysis (which is a chemical reaction causing bond scission) takes place, causing a molecular weight reduction. In addition, water acts as a plasticizer (permits easier flow, more plastic behavior), enhancing the rate of molecular reordering of the type mentioned above. The end result is that moisture degrades polycarbonate via two mechanisms: molecular weight reduction by hydrolysis and accelerated reordering at annealing temperatures.³³⁻³⁵ Consequently, the presence of moisture in the F-111 in combination with thermal history is a potential cause of degradation.

Chemical attack is similar to hydrolysis or UV degradation in that it may cause a decrease in molecular weight, or a chemical can act as a plasticizer or antiplasticizer (an antiplasticizer may increase cross-linking between molecular chains, making the material harder and more brittle). The chemical attack can be caused by a cross-section component such as the urethane or silicone interlayer, or by any processing chemical or contaminant which is present in the cross-section. Again, temperature may accelerate any chemical reaction. Several polymer chemists contacted suggest the possibility that the urethane interlayer itself is degrading, permeating the polycarbonate and acting as either a plasticizer or an antiplasticizer, in either case degrading the polycarbonate. Also it should be realized that any type of adhesive bond, such as the one between the polycarbonate and the urethane, makes use of a chemical attack type mechanism which creates the good adhesion. Consequently, there is a possibility of continued attack.

Fatigue will also degrade polycarbonate.^{36,37} This stress is caused by a combination of flight loadings, cabin pressure, and thermal expansion or contraction. Undegraded polycarbonate has a limiting fatigue strength of more than ± 1000 psi up through 10^7 cycles according to GE and Mobay manufacturing literature. It is doubtful that the fatigue limit of the bulk material is being approached in stress magnitude or cycles; however, it is possible that the fatigue life is reduced in combination with the previously mentioned degradation mechanisms and stress concentration sites caused by geometry, crazing or inherent flaws. In fact, it is highly likely that the degradation is caused by a synergistic effect in which each of the five irritants may have some effect which is further enhanced by the other factors.

5.2 WINDSHIELD DIMENSIONAL ANALYSIS

Physical measurements of new and various in-service aged F-111 ADBIRT windshields from both vendors were made to analyze dimensional variation. Figure 17 illustrates the dimensions measured, and Table 14 summarizes the measurements. The aft arch height was the only measurement for which the correct fit dimension was easily determined. Forward arch height, forward beam height, and forward sill height are included to show relative variation. From these measurements it is obvious that there is dimensional variation even for new windshields. The significance of the variation is difficult to quantify. By itself, minor dimensional variation is probably not a problem, but may accelerate degradation in combination with other

factors because installation of windshields which fit poorly will cause stress to be introduced in the windshield.

5.3 CRAZE TESTING

Craze testing of various chemicals and sealants used to install or clean aircraft windshields was researched. General Dynamics, under contract F33657-75-C-0310, evaluated the compatibility of various sealants with polycarbonate for the F-16.³⁸ A dogbone tensile specimen was used with a 0.250" hole in the necked-down area for stress concentration. The results of this testing are shown in Table 15. The only sealant tested which did not cause stress cracks was RTV 630, a rubber sealing compound which has low peel and tear strength. Of the other sealants tested, PR 1425, which has a high tear strength, was the least aggressive. The base material for PR 1425 produced pinpoint sized stress cracks.

In a similar evaluation conducted by the UDRI Elastomers Lab, under Contract F33615-84-C-5130, nine polysulfide sealants were used to evaluate potential stress cracking of Lexan SL-3000 polycarbonate dogbone specimens under a constant tensile stress of 2,000 psi at a temperature of 180°F for 48 hours. The nine sealants included:

PR 383, PR 1425, PR 1725, PR 1750, PS 899, RW-2178-71 (Products Research Chemical Corp.

GC 408, CG 409 (Goal Chemical)

CS 3204, CS 3204-Solvent Free (Chem Seal)

Results of the stress-cracking testing indicated that cracking around the periphery of the hole was observed for all sealant samples, except for PR 1425, immediately following testing.

Additional craze testing was conducted by UDRI, using the less severe cantilever beam at 2,000 psi, room temperature, 45°F, and 180°F for 24 hours. The results of this testing are shown in Table 16.

The sealant used for the F-111 windshield and canopy is PS 899, a polysulfide based two-part sealant. It is possible that the PS 899 causes crazing at the transparency edge and inside the bolt hole at the polycarbonate surface. These crazed areas could then crack and grow with cyclic temperature and cabin pressure loads.

Other possible crazing agents include approved cleaning agents which may soak the edge of the transparency and the interior of the bolt holes, causing crazing and cracking similar to the recent F-16 problem.

Approved chemicals (T.O 1F-111(b) A-2-2-1, Section VI, Paragraphs 6-1 to 6-101) for the F-111 windshield and canopy are shown below.

<u>Nomenclature</u>	<u>Part Number or Specification</u>	<u>Application</u>
Sealant	MIL-S-83430, Class B-1/2 and Class B-2 (Pro-Seal 899)	Seal around ends and canopy
Primer	EC1945B (3M Company)	Prime metal wherever PS 899 sealant is applied
Sealant	Dow Corning 94-002	Reseal damaged sealant at transparency edge
Petroleum Jelly	Commercial	Applied along the bolt line
Cleaner	Fed Spec P-P-560	Used for transparency cleaning
Cleaner	Isopropyl Alcohol Fed Spec TT-I-735A	Used for transparency cleaning
Cleaner	Aliphatic Naptha Fed Spec TT-N-95 Type 2	Used for transparency cleaning

None of the listed chemicals are required to be specifically tested and approved for use with polycarbonate. Craze testing has only been required with acrylic for the transparency cleaners listed.

5.4 FRACTOGRAPHY (CRACK & FAILURE SURFACE ANALYSIS)

A number of the service-aged F-111 windshield edges were carefully studied at UDRI. The sealant at the outside edges, the glass/phenolic edge reinforcement, and the aft arch bearing strip were removed to determine the condition of the polycarbonate in the vicinity of the edge and the bolt holes.

A significant number of cracks were discovered and documented. Analysis of the crack documentation was completed to determine patterns in crack location (sill, center beam, aft arch, forward arch, inboard polycarbonate ply, outboard polycarbonate ply), direction of travel, and length. Most of the transparencies have a significant number of cracks and, as would be expected, the number of cracks increase as installed age increases. Figures 18 and 19 are plots of the total number of cracks per ply in the studied windshields versus installed age. The most important result noted is that the majority of the cracks are occurring in the inboard polycarbonate ply.

The failure surfaces of two specimens from the previously completed edge attachment testing and one of the cracks discovered in the edge attachment crack analysis were photographed with optical and scanning electron microscopes. Figure 20 is a photograph of a PPG baseline edge attachment test failure surface. This surface is typical of a ductile tearing mode with "river" patterns. Figure 21 is a photograph of a PPG

service aged edge attachment test failure surface (Sequence #643, installed age 2y 1.5m). This surface shows crack initiation at the top of the photograph, followed by semicircular fatigue striations. It is likely that each of these striations corresponds to one load cycle. It is obvious that the existence of this fatigue crack prior to the edge attachment test compromised the integrity of the edge attachment. The baseline specimen failure energy was 1417 in-lbs, and the in-service aged specimen failure energy was only 400 in-lbs. This test indicates that fatigue cracks significantly degrade structural capability and change the failure mode from ductile to brittle.

Figure 22 is a photograph of a fatigue crack from a service aged PPG windshield (Sequence #809, installed age > 5 y 1m). The semicircular fatigue striations are obvious. The existence of fatigue cracks (and it should be noted that many probably exist which are too small to be seen with the naked eye) is most likely the direct cause of the reduced birdstrike capability of service-aged windshields. As the number of cracks increase and as the size of the cracks increase, the windshield capability is reduced.

5.5 FINITE ELEMENT ANALYSIS OF EDGE ATTACHMENT

A finite element model of the aft edge of the F-111 ADBIRT windshield was constructed. The objective of this study was to obtain an approximation of the state of stress for various cabin pressure and temperature loadings in the vicinity of the windshield edge attachment to determine if stress levels are high enough to initiate fatigue cracking independent of chemical or environmental crazing and stress cracking.

Five different loading cases were evaluated:

	Cabin Pressure psi	Cockpit Temperature °F	External Temperature °F	Max Tensile Stress @ Bolt Hole psi
1.	9.15	75	75	6000
2.	9.15	75	350	yielded
3.	6.06	75	30	8000
4.	0	30	30	yielded
5.	0	200	100	yielded

In all but the first case, the maximum stresses were in the outboard ply, while the majority of the cracks (visible size) were found in the inboard ply. This would imply either that an unknown loading case is causing cracks in the inboard ply, or that some other mechanism, such as chemical crazing/cracking, is initiating the cracks. Also, many cracks were discovered which initiated at the edge of the windshield, while the FEA indicated relatively low tensile stresses (< 3000 psi) along the edge. This also would indicate that something besides, or in addition to, stress is starting the cracks. The coupon testing completed to date has not included local effects in the vicinity of the edges. It is possible that polycarbonate properties are changing at these edges (boundaries). These changes are extremely difficult to detect as they may involve only the outer skin of the polycarbonate (on the order of 5-10 microns in thickness).

SECTION 6 CONCLUSIONS

The structural integrity of in-service aged F-111 ADBIRT windshield was found to be significantly reduced by in-service aging. Results of the bird impact tests indicated that the windshield capability is reduced from a 470 knot baseline capability (as tested on simulated flight hardware) to 360 knots after two years (40% in terms of impact energy) and reaches an asymptotic minimum value of 325 knots at an installed age of five years. In addition, there was a change in failure mode of the degraded windshields. When shot at velocities exceeding their capability, new windshields are ductile and crack resistant, absorb energy, and maintain coherency (no spalling). The degraded windshields, however, have decreased crack tolerance, absorb little energy (minimum plastic deformation), and have a tendency to spall.

Experimental laboratory coupon testing will continue at UDRI. To date testing has indicated no major changes in the bulk polycarbonate properties. The bulk interlayer material properties changed significantly; however, these changes did not appear to affect overall laminate performance. The edge attachment tests revealed gross differences between failure modes of new and in-service aged coupons; that is, ductile failure for some specimens versus brittle failure (initiating at fatigue cracks) for other specimens. The inconsistencies among the edge attachment tests can be attributed to the integrity of the adhesive between the metal bearing strip and the inboard polycarbonate ply. Those specimens with good bearing strip adhesion developed high edge strength and toughness even in the presence of fatigue cracks. It is important to note, however, that this adhesion or lack thereof did not appear to significantly affect full-scale testing. This is probably because hole-to-hole cracking dominates failure initiation in service-aged parts. Another difference is that the loading in the edge attachment test is uniaxial while in an actual birdstrike it is certainly triaxial and applied at a significantly higher rate.

Investigation of the sealants, cleaner, and other chemicals used to install or clean aircraft windshields indicated that the sealant used for the F-111 is an aggressive agent known to cause polycarbonate crazing. It is possible that the sealant causes crazing or stress cracking. Other possible crazing agents include approved cleaning agents which may soak the edge of the transparency and the interior of the bolt holes, causing crazing and cracking similar to the recent F-16 problems. These initial crazes or small stress cracks are then propagated by the cyclic pressure thermal loads associated with flight and the thermal fluctuations on the flightline.

The fatigue crack tabulation and analysis brought to light the significance and magnitude of the crack problem. Virtually none of the in-service aged windshields studied were crack-free. The finite element analysis of the edge attachment for the different load cases showed significant tensile stresses. In several of the cases those stresses were large enough to initiate cracks, and in all cases large enough to propagate existing cracks.

REFERENCES

1. Simmons, Robert J., Flightline Thermal Environment Testing of F-111 Transparencies, AFWAL-TR-83-3062, July 1983.
2. Clayton, K. I., West, B. S., and Bowman, D. R., Aircraft Transparency Test Methodology, AFWAL-TR-85-3125, March 1986.
3. Clayton, Kenneth I. and West, Blaine S., Aircraft Transparency Testing Methodology and Evaluation Criteria - Part II, Methodology Development for Improved Durability, AFWAL-TR-83-3045 Part II, April 1983.
4. West, Blaine S., Design and Testing of F-111 Bird Resistant Windshield/Support Structure, Volume 1 - Design and Verification Testing, AFWAL-TR-76-01, October 1976.
5. Heath, J. B. R. and Gould, R. W., "Degradation of the Bird Impact Resistance of Polycarbonate," Conference on Aerospace Transparent Materials and Structures, Scottsdale, AZ, July 1983.
6. Lawrence, J. H., Guidelines for the Design of Aircraft Windshield/Canopy Systems, AFWAL-TR-80-3003, February 1980.
7. Ursell, C. R., Investigation of the Effect of Age on the Structural Integrity of F-5 Canopies, Southwest Research Institute Project No. 03-6116-001, June 1981.
8. Yamasaki, R. S. and Blaga, A., "Degradation of Polycarbonate Sheeting on Outdoor Exposure, Relationship Between Changes in Molecular Weight and Tensile Properties," International Union of Testing and Research Laboratories for Materials and Structures, Vol. 10, No. 58, July-August 1977.
9. Clayton, Kenneth I., Stenger, Gregory J., West, Blaine S., and Johnson, Paul E., Development of an Impact Resistant Test Method for Polycarbonate, AFWAL-TR-83-3128, February 1984.
10. Davis, A. and Golden, J. H., "Stability of Polycarbonate," J. Macromol. Sci. - Revs. Macromol. Chem., C3(1), 1969, pp. 45-68.
11. Ram, A., Zilber, O. and Kenig, S., "Life Expectation of Polycarbonate," Polymer Engineering and Science, Vol. 25, No. 9, June 1985, pp. 535-540.
12. Yamasaki, R. S. and Blaga, A., pp. 197-203.
13. Sherman, E. J., Ram, A., and Kenig, S., "Tensile Failure of Weathered Polycarbonate," Polymer Engineering and Science, Vol. 22, No. 8, mid-June 1982, pp. 457-465.
14. Broutman, L. J. and Krishnakumar, S. M., "Impact Strength of Polymers: 1. The Effect of Thermal Treatment and Residual Stress," Polymer Engineering and Science, Vol. 16, No. 2, February 1976, pp. 74-81.

15. Thakkar, B. S. and Broutman, L. J., "Impact Strength of Polymers: 3. The Effect of Annealing on Coldworked Polycarbonates," *Polymer Engineering and Science*, Vol. 21, No. 3, February 1981, pp. 155-162.
16. Ram, A., Zilber, O. and Kenig, S., "Residual Stresses and Toughness of Polycarbonate Exposed to Environmental Conditions," *Polymer Engineering and Science*, Vol. 25, No. 9, June 1985, pp. 577-581.
17. Pielstocker, G., *Kunststoffe*, Vol. 51, 1961, p. 509.
18. Pielstocker, G., *Brit. Plastics*, Vol. 35, 1962, p. 365.
19. Golden, J. H., Hammant, B. L. and Hazell, E. A., "The Effect of Thermal Pretreatment on the Strength of Polycarbonate," *Journal of Applied Polymer Science*, Vol. 11, January 1967, pp. 1571-1579.
20. Neki, K. and Geil, P. H., "Morphology-Property Studies of Amorphous Polycarbonate," *J. Macromol. Sci-Phys.*, B8(1-2), 1973, pp. 295-341.
21. Morgan, R. J. and O'Neal, J. E., "The Effect of Thermal History on the Mechanical Properties of Crystallinity of Polycarbonate," *MDRL 75-37*, Nov. 1975.
22. Ryan, J. T., "Impact and Yield Properties of Polycarbonate as a Function of Strain Rate, Molecular Weight, Thermal History, and Temperature," *Polymer Engineering and Science*, Vol. 18, No. 4, March 1978, pp. 264-267.
23. Pitman, G. L., Ward, I. M., and Duckett, R. A., "The Effect of Thermal Pre-Treatment and Molecular Weight on the Impact Behaviour of Polycarbonate," *Journal of Materials Science*, Vol. 13, No. 10, October 1978, pp. 2092-2104.
24. Yakouchi, M. and Kobayashi, Y., "Effect of Heat Pretreatment and Strain Rate on Tensile Properties of Polycarbonate Sheet," *Journal of Applied Polymer Science*, Vol. 26, No. 2, Feb. 1981, pp. 431-440.
25. Parvin, M., "The Effect of Annealing on Fracture Behaviour of Polycarbonate," *Journal of Materials Science*, Vol. 16, No. 7, 1981, pp. 1796-1800.
26. Heath, J. B. R. and Gould, R. W., "Degradation of the Bird Impact Resistance of Polycarbonate," *SAMPE Quarterly*, Oct. 1982, pp. 20-29.
27. Varadarajan, K. and Boyer, R. F., "Effects of Thermal History, Crystallinity, and Solvent on the Transitions and Relaxations in poly(bisphenol-A carbonate)," *Journal of Polymer Science: Polymer Physics edition*, Vol. 20, No. 1, January 1982, pp. 141-154.
28. Bauwens-Crowet, C. and Bauwens, J.-C., "The Relationship Between the Effect of Thermal Pre-treatment and the Viscoelastic Behaviour of Polycarbonate in the Glassy State," *Journal of Materials Science*, Vol. 14, No. 8, 1979, pp. 1817-1826.

29. Bauwens-Crowet, C. and Bauwens, J.-C., "Annealing of Polycarbonate Below the Glass Transition: Quantitative Interpretation of the Effect of Yield Stress and Differential Scanning Calorimetry Measurements," *Polymer*, Vol. 23, Oct. 1982, pp. 1599-1604.
30. Bauwens, J.-C., "Attempt to Correlate the Yield Processes Above and Below the Glass Transition in Glassy Polymers," *Polymer*, Vol. 25, No. 10, Oct. 1984, pp. 1523-1526.
31. Bubeck, R. A. and Bales, S. E., "Changes in Yield and Deformation of Polycarbonates Caused by Physical Aging," *Polymer Engineering and Science*, Vol. 24, No. 10, mid-oct. 1984, pp. 1142-1148.
32. Zurimendi, J. A., Biddlestone, F., Hay, J. N., and Haward, R. N., "Physical Factors Affecting the Impact Strength of Polycarbonate," *Journal of Materials Science*, Vol. 17, No. 1, January 1982, pp. 199-203.
33. Long, T. S. and Sokol, R. J., "Molding Polycarbonate: Moisture Degradation Effect on Physical and Chemical Properties," *Polymer Engineering and Science*, Vol. 14, No. 12, December 1974, pp. 817-822.
34. Gardner, R. J. and Martin, J. R., "Humid Aging of Plastics, Part II, Effect of Molecular Weight on Mechanical Properties of Polycarbonate," *SPE Technical Paper No. 24*, 1978, pp. 328-331.
35. Bair, H. E., Falcone, D. R., Hellman, M. Y., Johnson, G. E., and Kelleher, P. G., "Hydrolysis of Polycarbonate to Yield BPA," *Journal of Applied Polymer Science*, Vol. 26, No. 6, June 1981, pp. 1777-1786.
36. MacKay, M. E., Teng, T.-G., and Schultz, J. M., "Craze Roles in the Fatigue of Polycarbonate," *Journal of Materials Science*, Vol. 14, No. 1, January 1979, pp. 221-227.
37. Gotham, K. V. and Wright, D. C., "Fatigue in Polycarbonate," *Plastics and Rubber Processing and Applications*, Vol. 4, No. 1, 1984, pp. 43-51.
38. Head, S. W., "Evaluation of Sealing Materials Used on F-16 Polycarbonate Transparencies," *General Dynamics 16PR937*, December 1980.

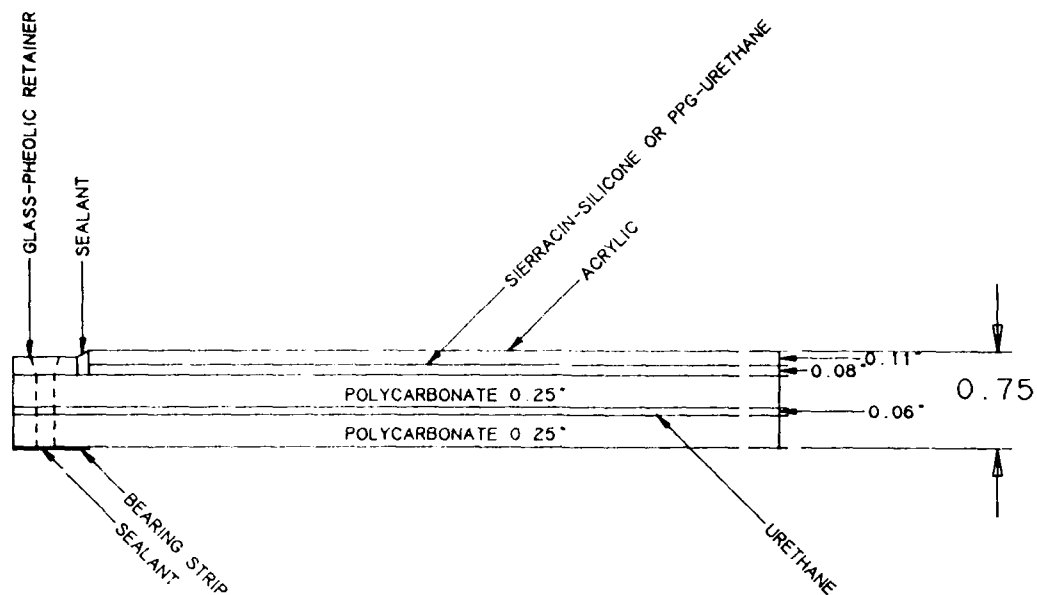


Figure 1. F-111 ADRIART Transparency Nominal Cross-Section.

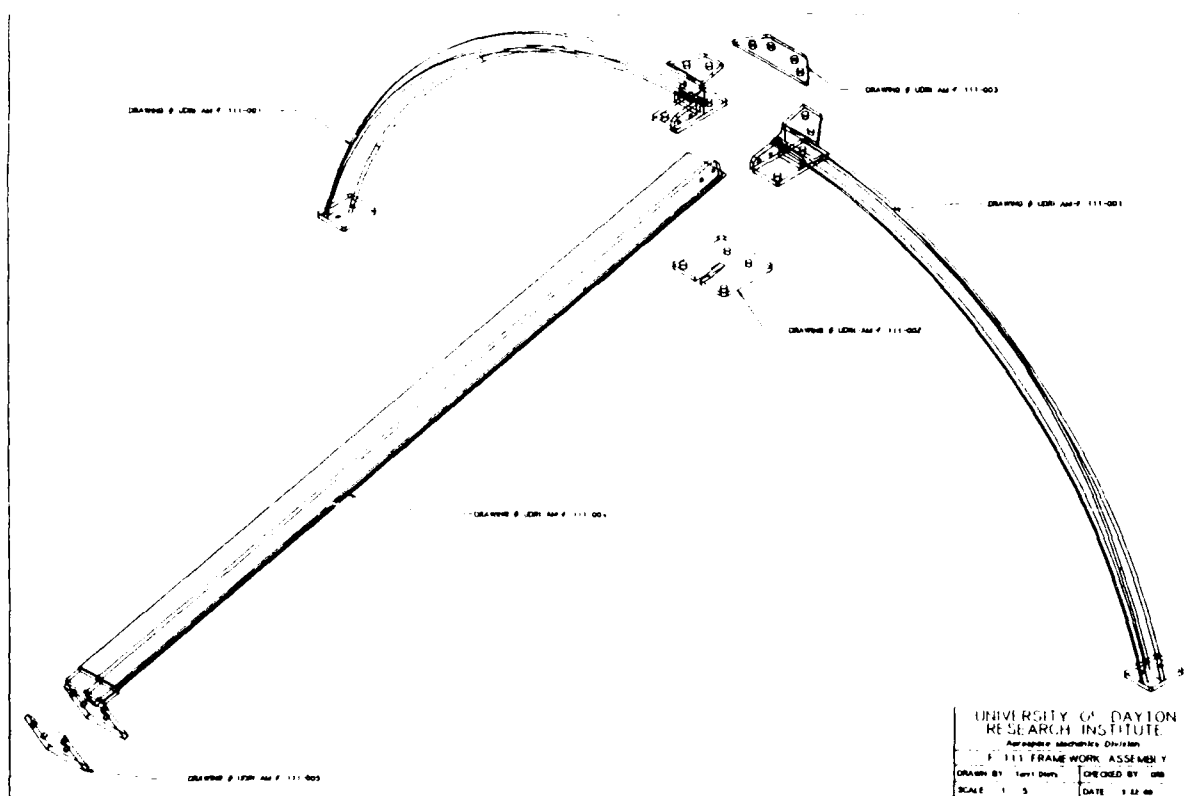


Figure 2. UDRI Arch/Center Beam Assembly.

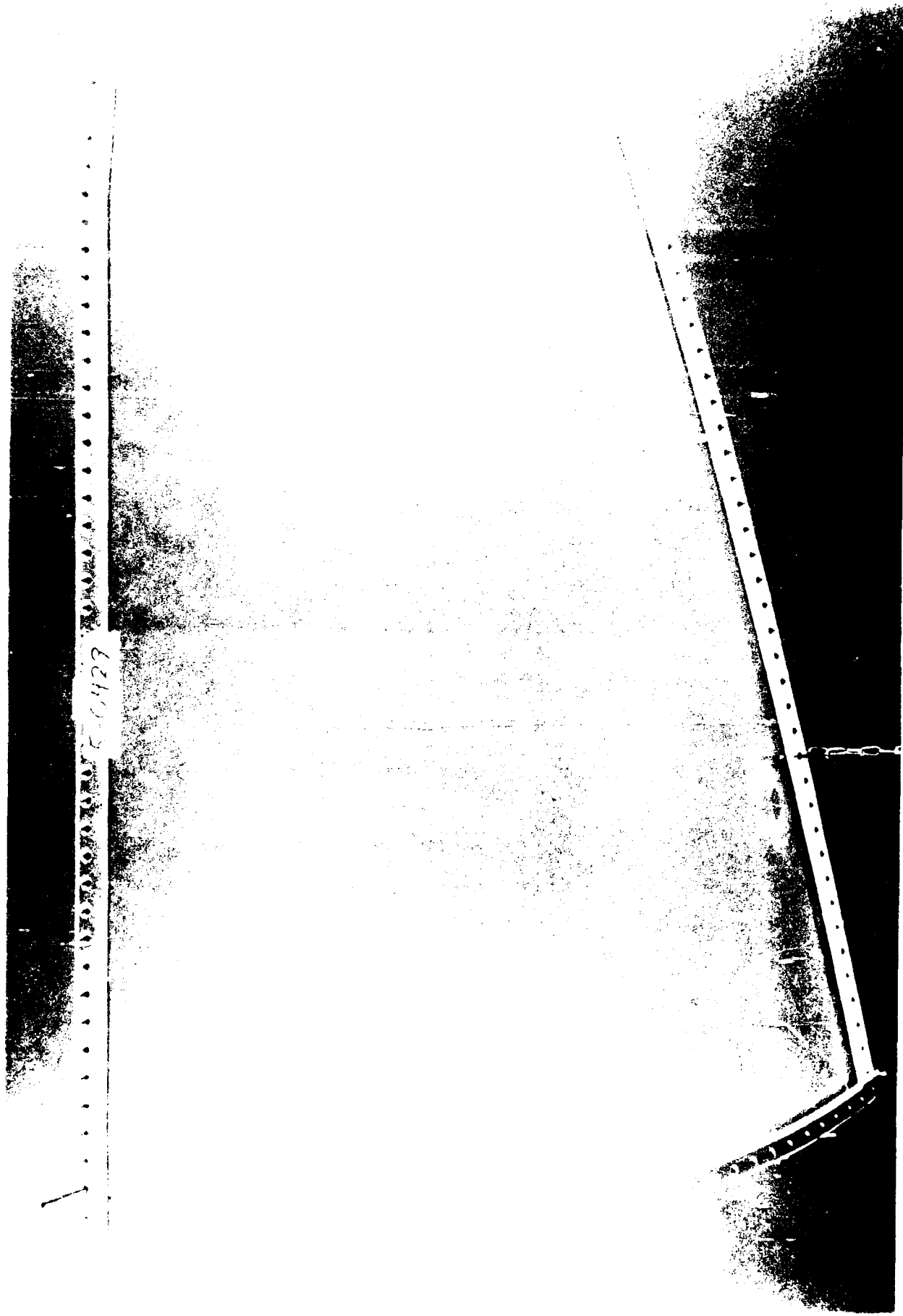


Figure 3. Test No. 3, Shot No. 5-0429.



Figure 4. Test No. 9, Shot No. 5-0435.



Figure 5. Test No. 14, Shot No. 5-0440.



Figure 6. Detail of damage to No. 5-0444.

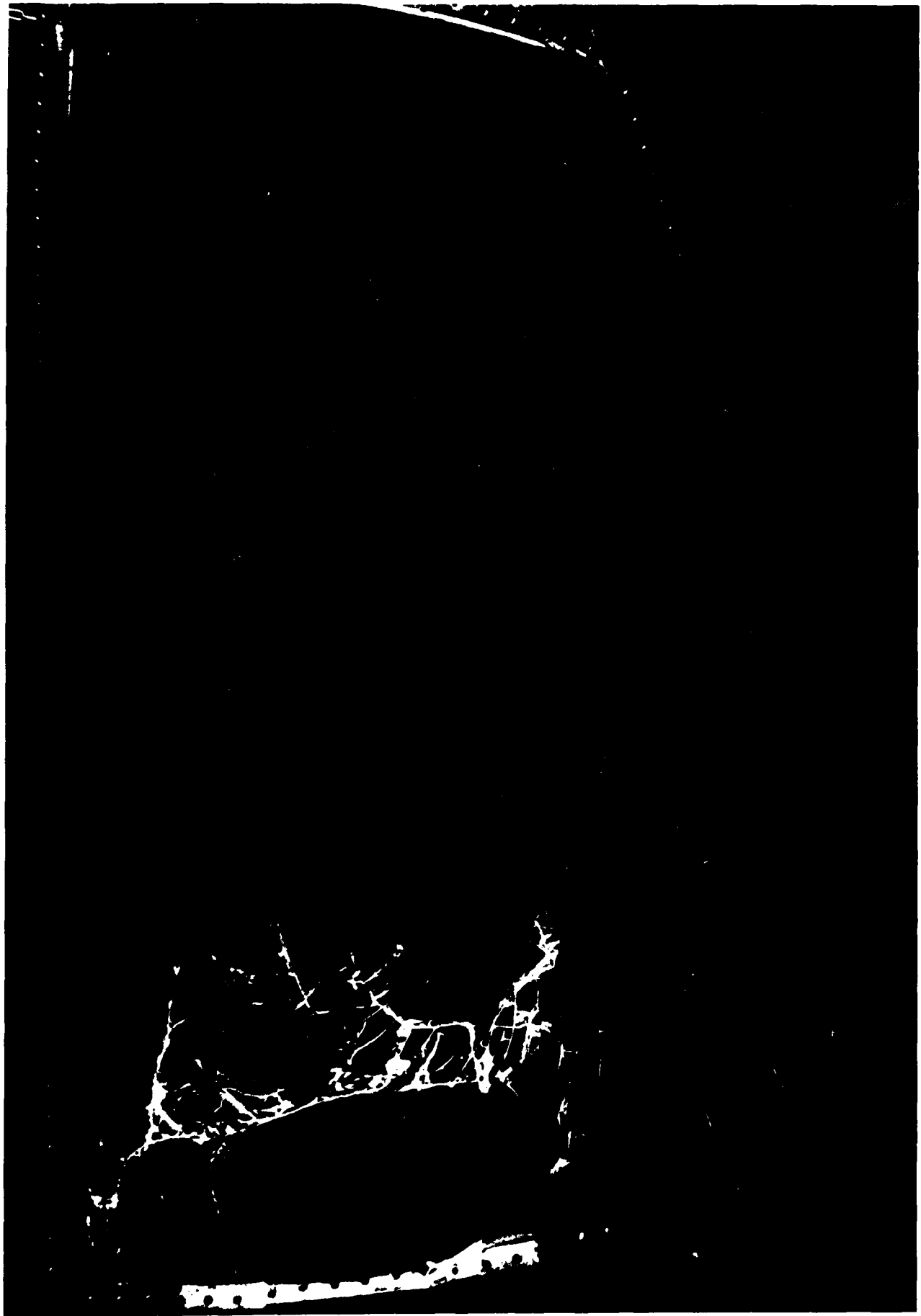


Figure 7. Test No. 2, Shot No. 5-0428.

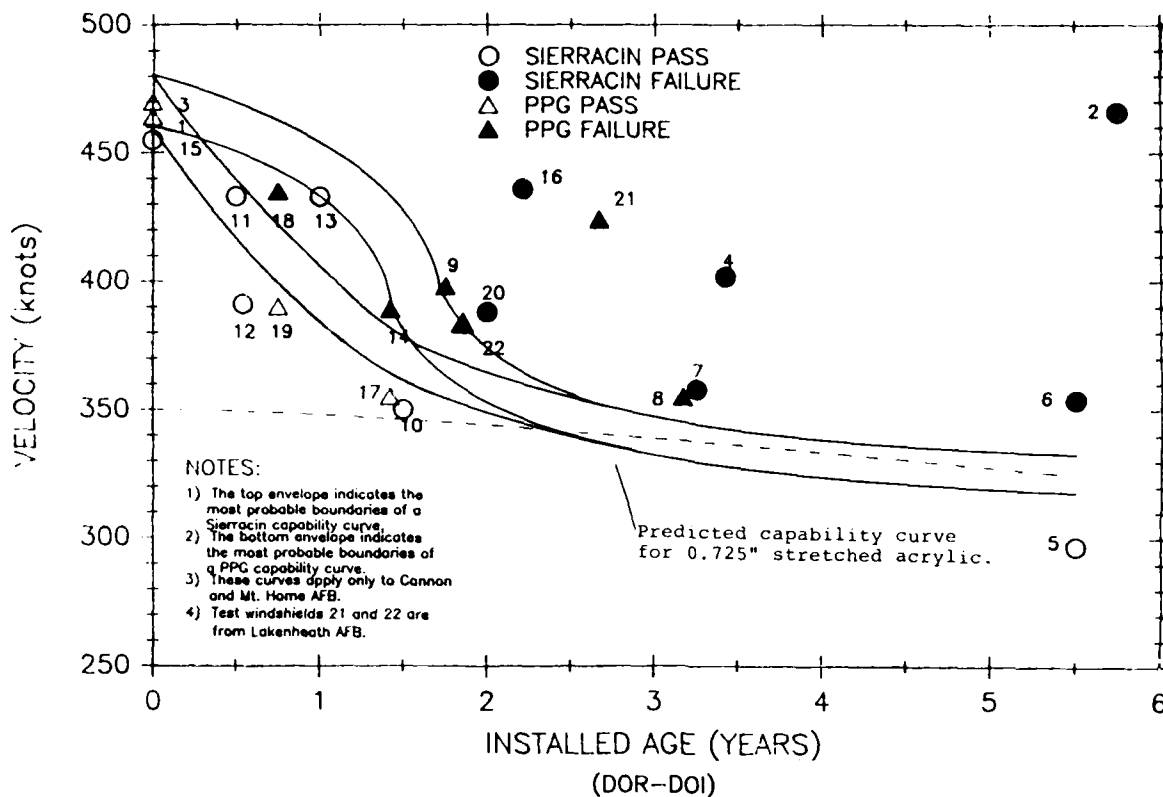


Figure 8. Capability Envelopes for Sierracin and PPG Transparencies.

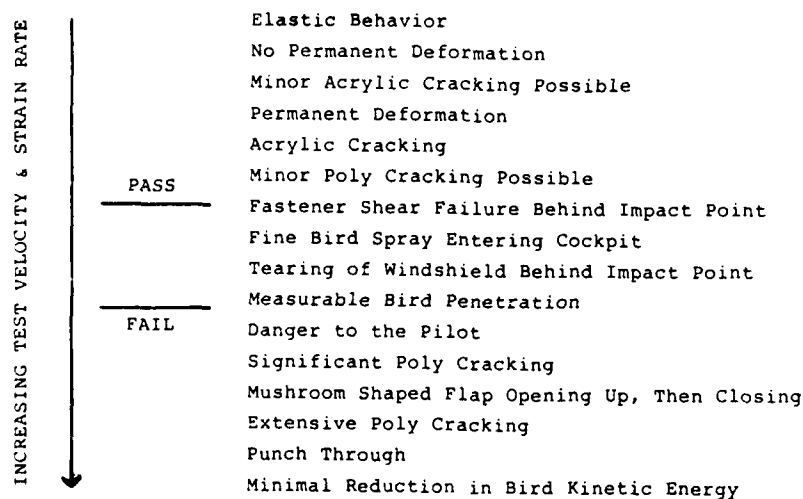


Figure 9. Effect of Increasing Test Velocity on Windshield Damage for Service-Aged Windshields.

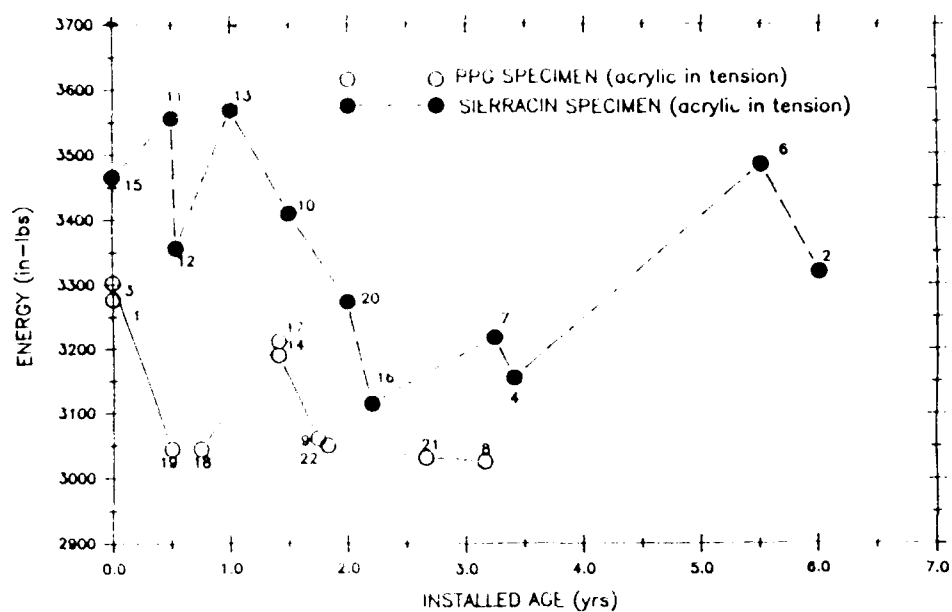


Figure 10. 40,000 in/min Impact Beam Energy vs. Installed Age, Acrylic in Tension.

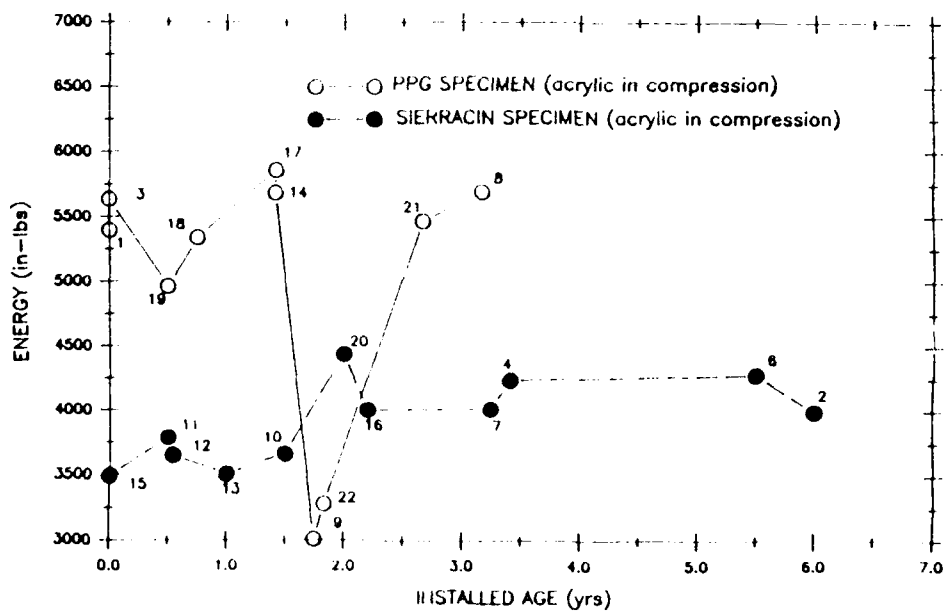


Figure 11. 40,000 in/min Impact Beam Energy vs. Installed Age, Acrylic in Compression.

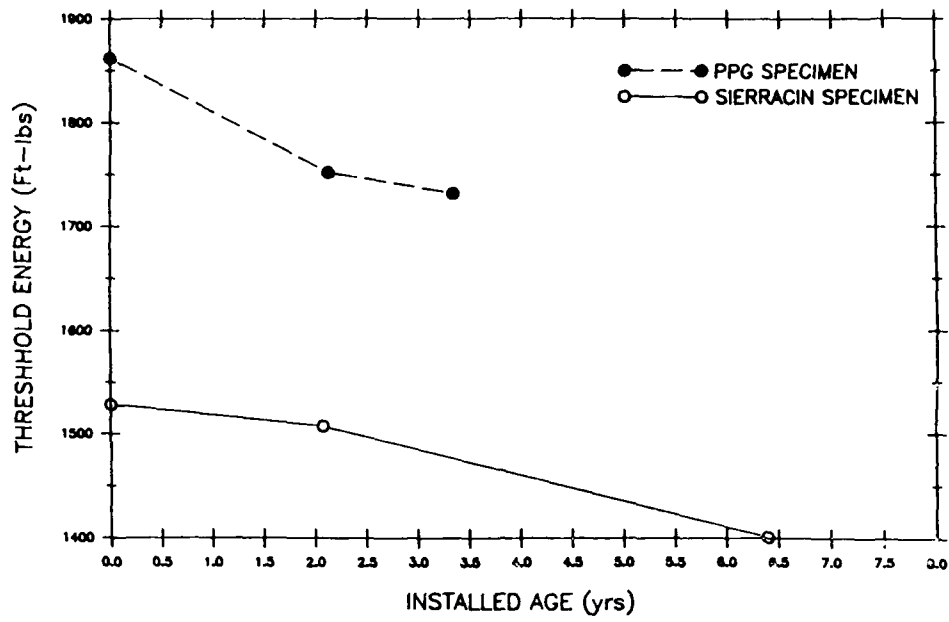


Figure 12. The Effect of Installed Age on Air Cannon Threshold Energy.

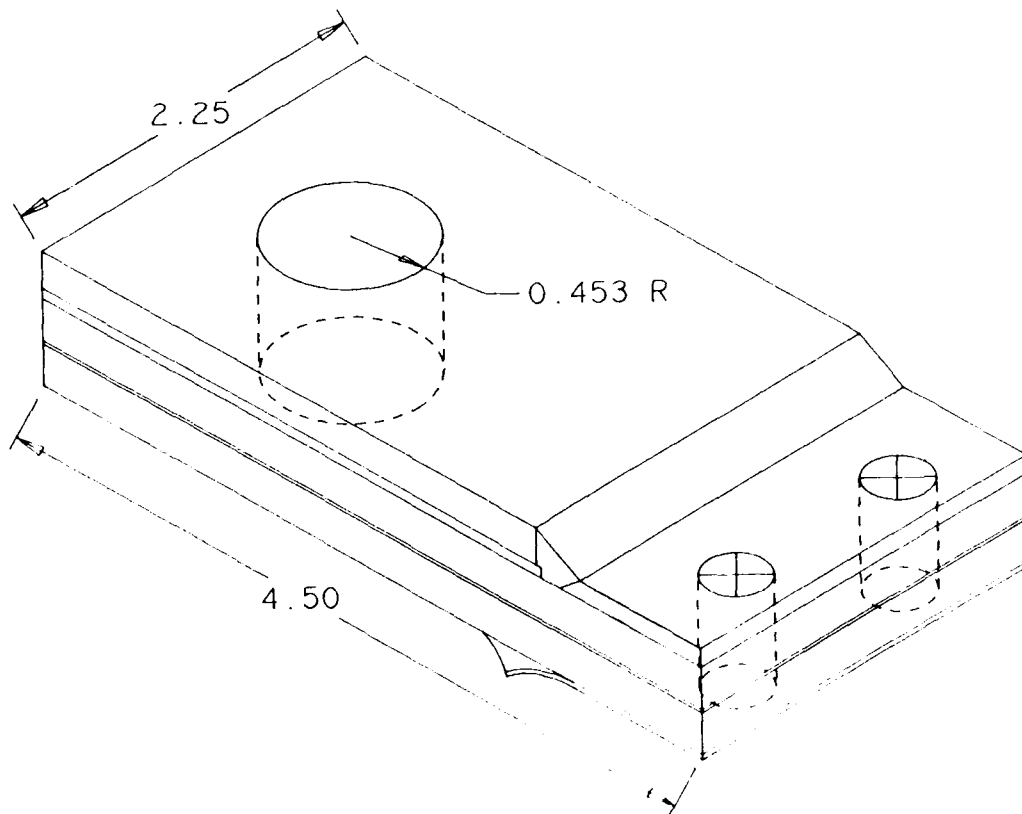


Figure 13. Edge Attachment Test Specimen.

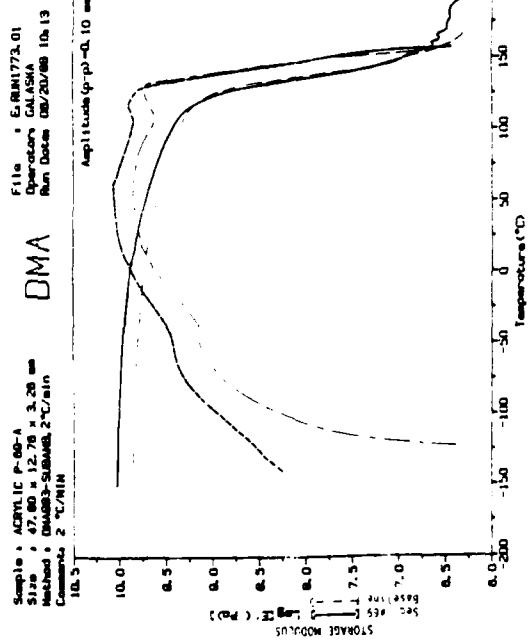


Figure 14. PPG Baseline and In-Service Aged Acrylic DMA Scans.

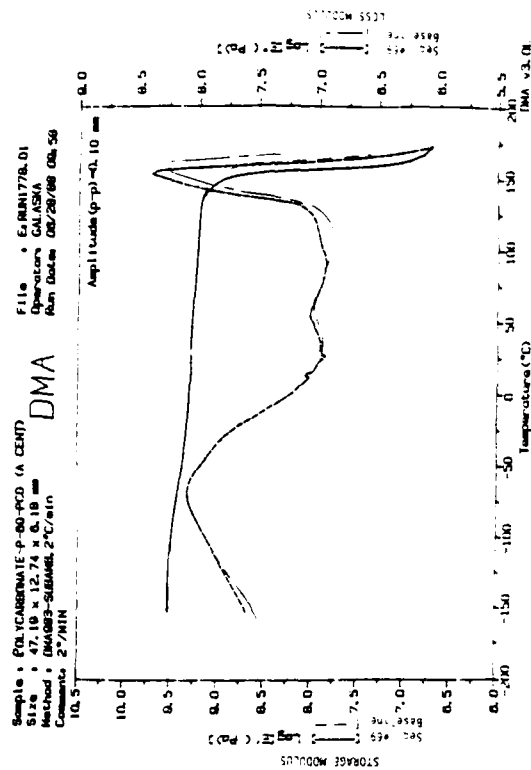


Figure 15. PPG Baseline and In-Service Aged Outboard Polycarbonate DMA Scans.

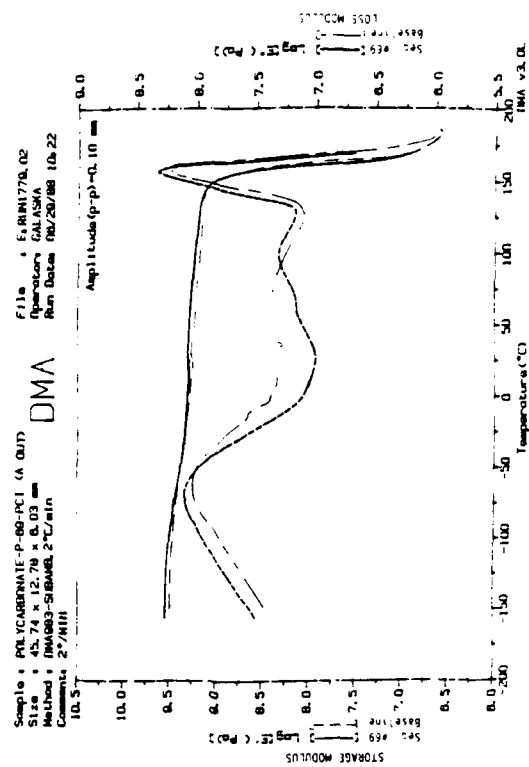


Figure 16. PPG Baseline and In-Service Aged Inboard Polycarbonate DMA Scans.

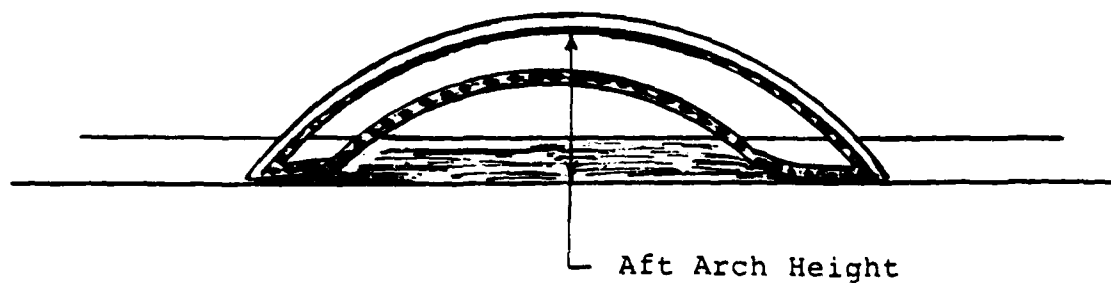
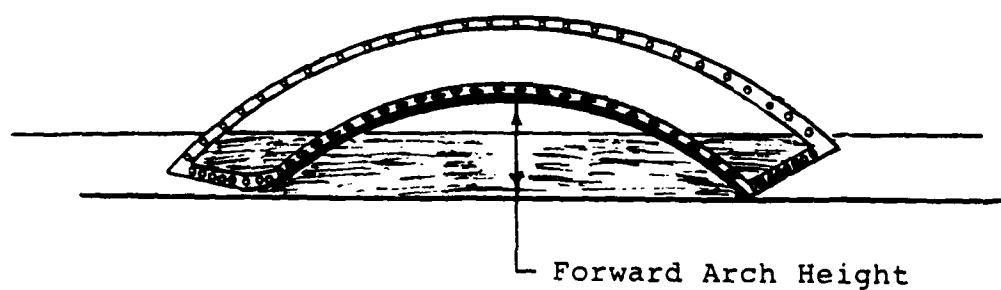
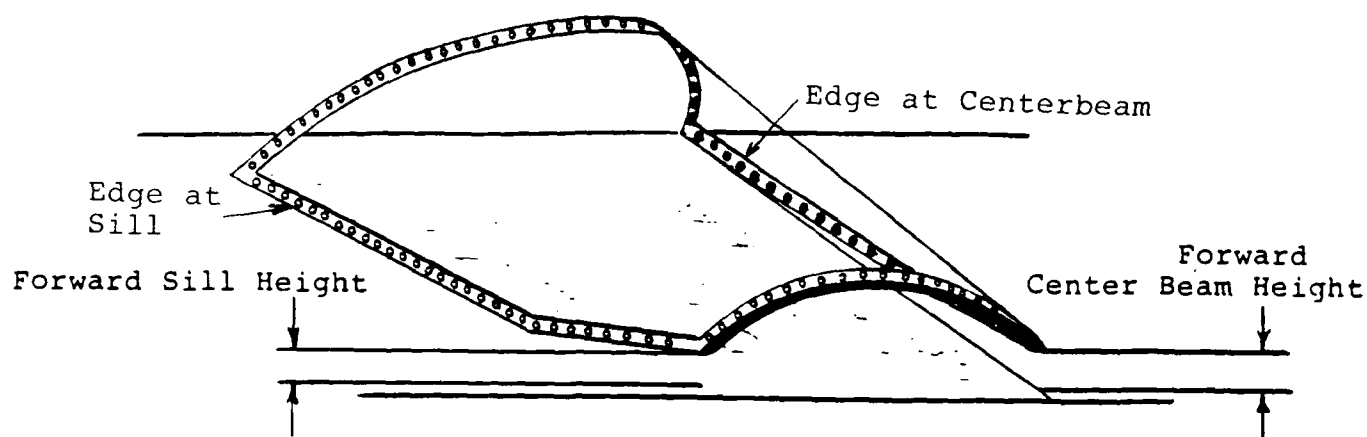


Figure 17. F-111 ADBIRT Physical Measurements.

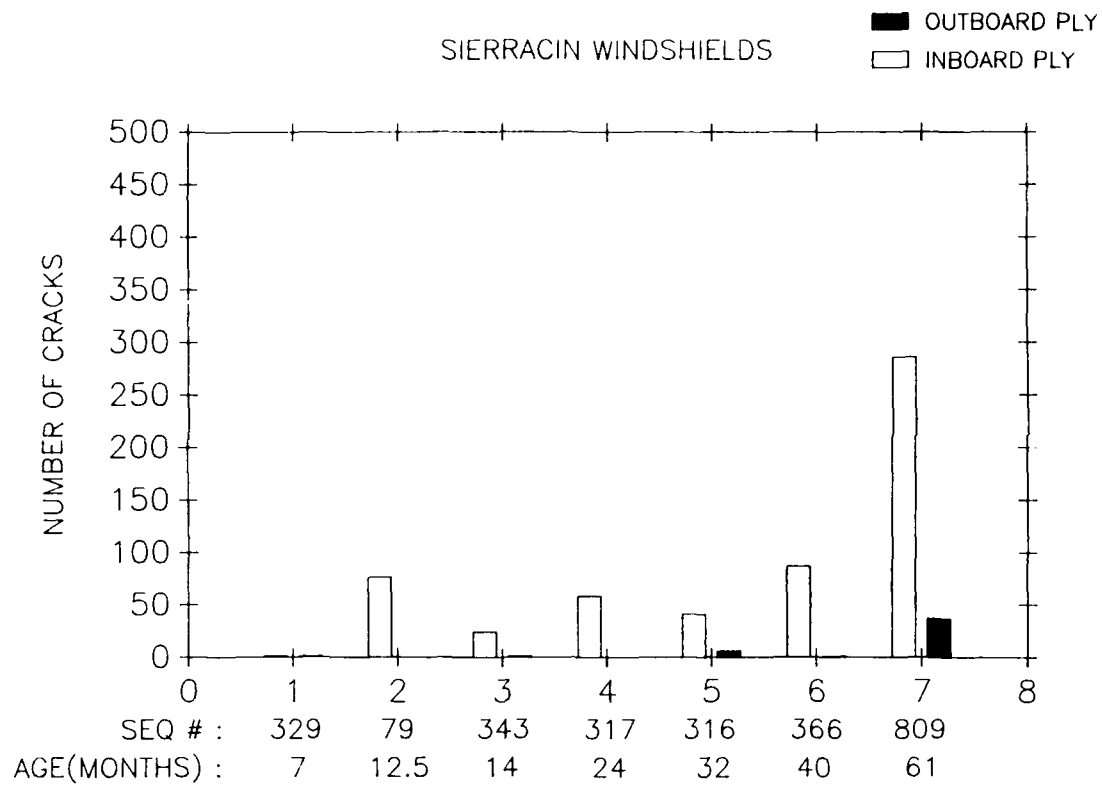


Figure 18. Number of Cracks by Ply, Sierracin.

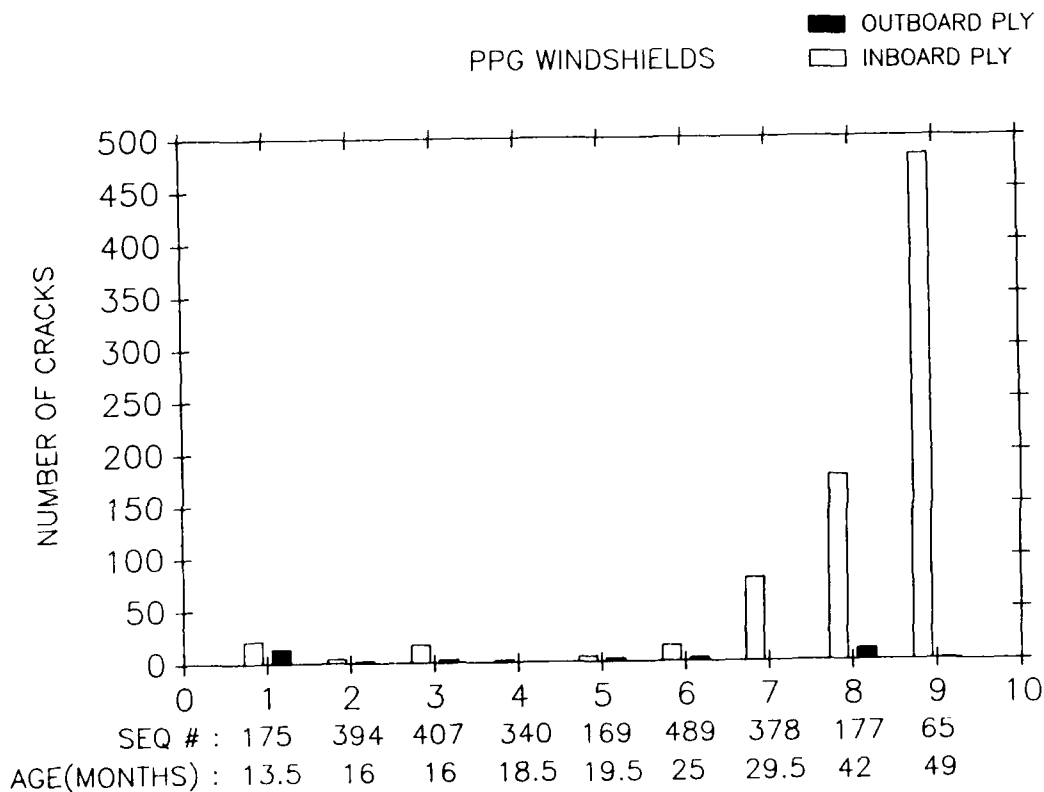


Figure 19. Number of Cracks by Ply, PPG.



Figure 20. Edge Attachment Test Failure Surface Detail, PPG Baseline.



0830 15KW X75 100PM W035

Figure 21. Edge Attachment Test Fatigue Crack/Failure Surface Detail, PPG Sequence #643, Installed Age 2 yr. 1.5m.

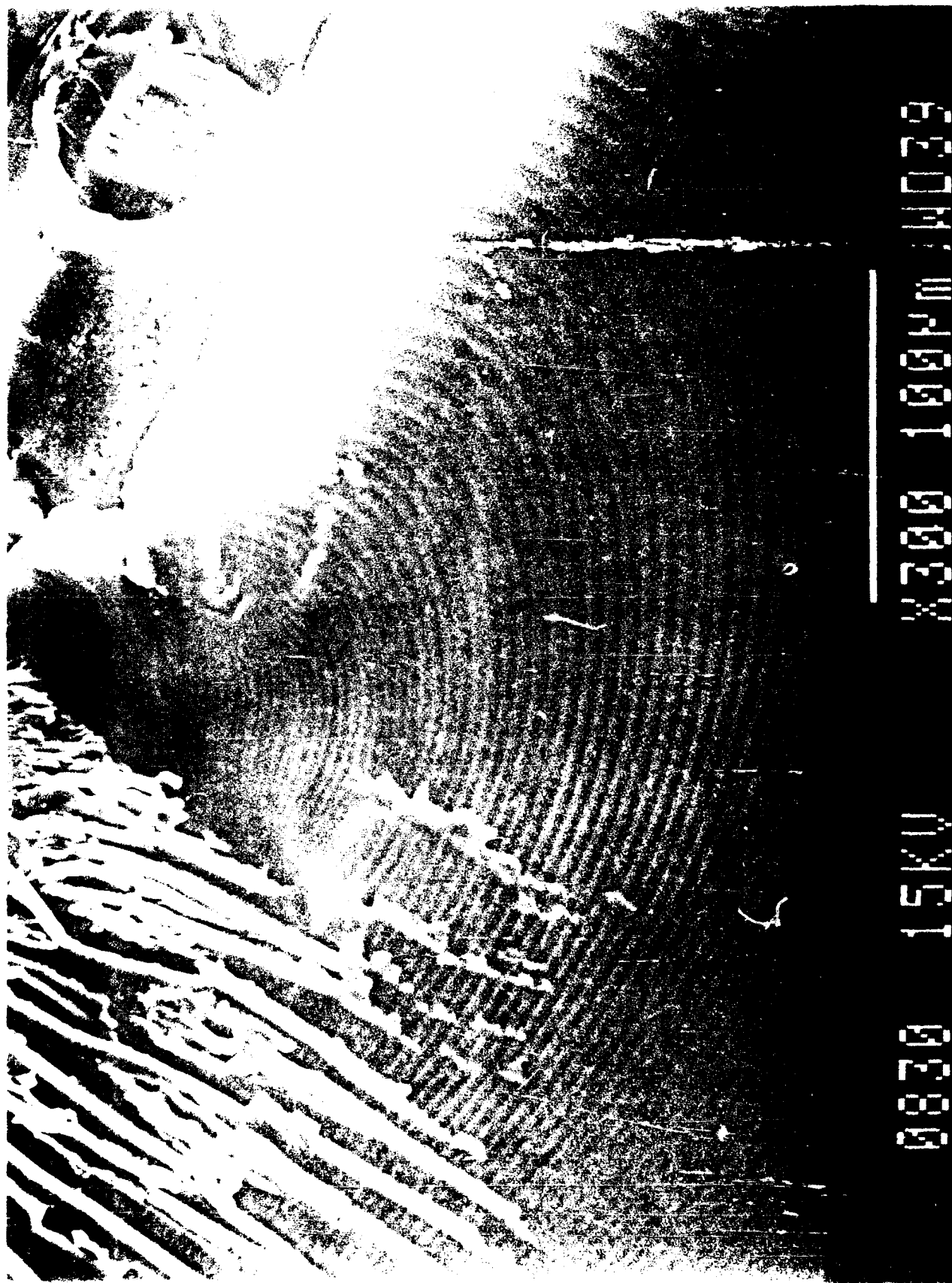


Figure 22. Fatigue Crack Detail PPG Sequence #809, Installed Age Greater Than 5y 1m.

TABLE 1
FULL SCALE BIRDSTRIKE TEST MATRIX

Quantity	Installed Age	Manufacturer	Test	Specimen ID
0	4-6 years	PPG	Haze/Transmittance	T
4	4-6 years	Sierracin	Interlaminar Bond Integrity	TS
			Torsional Shear	FT
1	3-4 years	PPG	Flatwise Tension	
2	3-4 years	Sierracin	MTS Three Point Beam	L
			2,000 in/min	H
			40,000 in/min	
1	2-3 years	PPG	Falling Weight Three Point Beam	FW
2	2-3 years	Sierracin	Split Hopkinson Bar	SH
4	1-2 years	PPG	Air Cannon	AC
2	1-2 years	Sierracin	Tensile Edge Attachment	EA
0	0-1 years	PPG	Tensile Testing	TEN
3	0-1 years	Sierracin	Fracture Toughness	CT
2	0 years	PPG	Fatigue Crack Growth	FC
1	0 years	Sierracin	Dynamic Mechanical Analysis	DMA
			Differential Scanning Calorimetry	DSC
Total 22			Gel Permeation Chromatography	GPC

TABLE 3
BRIEF F-111 TEST SUMMARY

Test Date	Test No.	Seq. No.	Mfg. S/N	DOM	DOI	DOR	Service Life DOR-DOM	Installed Life DOR-DOI	Base	Test Velocity	Comments/Brief Summary of Results
5-12-87	1	Baseline	PPG 151901-104	6-85-11-85						464 kts	Pass-sheared arch/sill connection bolts and a centerbeam connection bolt. Arch permanently deformed and requires modification.
5-14-87	2	89	Sier 192	8-79	9-26-79	After 6/85	5y 10m-6y 4m	5y 6m-6y	Cannon	466 kts	Catastrophic failure-punched large hole. No arch damage.
6-1-87	3	Baseline	PPG	6-85-11-85						470 kts	Pass-with modified arch-UDRI system capability. Arch permanently deformed.
6-4-87	4	135	Sier 102	6-79	5-6-80	10-83	4y 5m	3y 5m	Cannon	402 kts	Failure-large flap opened up and then closed. No arch damage
6-8-87	5	632	Sier 200	9-79	1-21-81	7-24-86	5y 11m	5y 6m	Cannon	297 kts	Pass - minimal acrylic cracking - W/S still in elastic range. No arch damage.
6-9-87	6	632	Sier 200	9-79	1-21-81	7-24-86	5y 11m	5y 6m	Cannon	354 kts	Failure - large flap opened up and then closed. Extensive cracking of all plies. No arch damage.
6-11-87	7	22	Sier 132	5-79	5-18-82	3-85	6y 3m	3y 3m	Cannon	358 kts	Failure - large flap opened up and then closed. Poly plies spalled off in places. No arch damage.
6-15-87	8	528	PPG 16-087	8-8-80	4-24-82	7-25-85	5y	3y 2m	Mt. Home	366 kts	Failure - W/S tore through bolt holes for 12" at aft arch. No arch damage.
6-17-87	9	144	PPG 16-660	7-22-83	12-15-83	9-17-85	2y 11m	1y 9m	Cannon	398 kts	Failure - W/S tore all along along aft arch. No arch damage
6-18-87	10	143	Sier 514	6-82	8-30-82	3-15-84	2y	1y 6m	Cannon	350 kts	Pass - minimal acrylic cracking. Minor permanent arch deformation
6-24-87	11	558	Sier 92	7-84	8-7-85	2-7-86	1y 7m	6m	Mt. Home	433 kts	Marginal pass-some acrylic cracking. No polycarbonate failure. 13 bolts sheared behind impact point. Negligible bird penetration. Permanent arch deformation
6-25-87	12	351	Sier 692	11-82	3-29-85	10-11-85	2y 11m	6.5m	Mt. Home	391 kts	Pass-small pocket behind the impact point. Permanent arch deformation.
6-29-87	13	UD #12	Sier 522	7-82	8-2-82	11-8-83	1y 4m	1y	Mt. Home	433 kts	Marginal pass - same as #11. Minor bird penetration. Permanent arch deformation.
7-6-87	14	UD #11	PPG 16-245	11-18-80	4-2-82	8-30-83	2y 9m	1y 5m	Mt. Home	389 kts	Failure- W/S tore along aft arch for 18". Flap opened up. Extensive cracking. Permanent arch deformation.
7-13-87	15	551	Sier 248	2-85	-	-	-	0		455 kts	Pass - small pocket behind impact point. 10 bolts sheared behind impact point. No polycarbonate cracking. Permanent arch deformation.
7-15-87	16	582	Sier 052	6-84	8-13-84	10-17-86	2y 4m	2y 2.5m	Mt. Home	436 kts	Failure - w/s tore along aft arch for 8". 16 bolts sheared behind impact point. Extensive cracking. Permanent arch deformation.
8-5-87	17	140	PPG 16-432	8-26-81	8-30-82	1-23-84	2y 5m	1y 5m	Cannon	355 kts	Pass - no permanent deformation. No damage except unusual acrylic cracking near front sill, and one 3" middle ply polycarbonate crack.
8-7-87	18	623	PPG 030	1-28-85	6-20-85	3-26-86	1y 2m	9m	Cannon	435 kts	Failure - w/s tore along aft arch for 8". Flap opened up. Permanent arch deformation.
8-11-87	19	148	PPG 002	1-3-85	1-85/6-85	1-9-86	1y	6m-12m	Cannon	390 kts	Pass - small pocket at impact point. Extensive acrylic cracking away from impact point. Permanent arch deformation.
8-17-87	20	88	Sier 264	10-81	4-10-83	4-11-85	3y 6m	2y	Cannon	388 kts	Failure - w/s tore along aft arch for 8". Flap opened up. Permanent arch deformation.
8-20-87	21	615	PPG 16-292	2-11-81	5-11-84	1-5-87	5y 11m	2y 8m	Lakenheath	424 kts	Failure - w/s tore along aft arch for 10". Flap opened up. Permanent arch deformation.
8-26-87	22	548	PPG 16-580	8-18-83	1-26-84	12-6-85	2y 4m	1y 10m	Lakenheath	383 kts	Failure - w/s tore along aft arch for 6". Permanent arch deformation.

TABLE 4
COMPARISON OF BASELINE AND IN-SERVICE AGED WINDSHIELD
BIRDSTRIKE RESISTANCE CAPABILITIES

Transparency	Installed Age (years)	Capability (knots)	% Reduction* in Velocity	% Reduction** in Energy
Baseline	0	470		
PPG	1	395	16.0	29.4
	2	355	24.5	42.9
	3	333	29.1	49.8
	4	325	30.9	52.2
Sierracin	1	440	6.4	12.4
	2	365	22.3	39.7
	3	337	28.3	48.6
	4	325	30.9	52.2

* Reduction = $\frac{\text{Baseline} - \text{Reduced Capability}}{\text{Baseline}} \times 100\%$

** Reduction = $\frac{\text{Baseline}^2 - \text{Reduced Capability}^2}{\text{Baseline}^2} \times 100\%$

These capabilities were determined from the test program. Actual baseline capability on flight structure is 490 knots. Because of the nature of the failures and the embrittlement of the polycarbonate, it is not appropriate to scale up the capability for all age groups 20 knots.

TABLE 5
COMPARATIVE SUMMARY OF TORSIONAL SHEAR TEST DATA

Full-Scale Test No. Manufacturer Service Life	Interlayer*	Average Angular Displacement	% Change from Baseline	Avg. Ult. Shear Stress (psi)	% Change from Baseline	Avg. Shear Modulus (psi)	% Change from Baseline	Average Energy (in. #)	% Change from Baseline
Test #3 PPG Baseline	A/P U	35.7*	-	1830	-	615	-	49.9	-
Test #8 PPG 3y 2m	A/P U	35.7*	0	1696	-7.3	564	-9.3	60.8	+21.8
Test #15 Sierr Baseline	A/P S	30.3*	-	123.5	-	36.5	-	2.63	-
Test #7 Sierr 3y 3m	A/P S	18.0*	-40.6	193.6	+56.8	90.0	+146.6	2.86	+8.7
Test #546 Sierr 5y 6m	A/P S	20.4*	-32.7	227.4	+84.1	97.6	+167.4	3.41	+29.7
Test #3 PPG Baseline	P/P U	28.5*	-	3984	-	836	-	104	-
Test #8 PPG 3y 2m	P/P U	23.9*	-16.1	2506	-36.6	653	-21.9	61.2	-42.8
Test #15 Sierr Baseline	P/P U	40.8*	-	2141	-	458	-	51.7	-
Test #1 Sierr 3y 3m	P/P U	11.6*	-71.6	245.7	-88.5	270	-41.0	2.81	-94.6
Test #546 Sierr 5y 6m	P/P U	38.5*	-5.6	747.8	-65.1	221	-51.7	25.6	-50.5

* U denotes urethane
S denotes silicone

TABLE 6
FLATWISE TENSION SUMMARY

		<u>POLY/POLY INTERLAYER</u>					
		Ultimate					
Full-Scale Test #/Mfgr/ Installed Age	Interlayer	<u>Tensile Stress</u>		<u>Tensile Modulus</u>		<u>Energy</u>	
		psi Average	Percent Change	psi Average	Percent Change	in. lbs. Average	Percent Change
Test #3/PPG/ Baseline	U	3004	-	5490	-	223.9	-
Test #8 PPG/3y 2m	U	2759	-8.16	5041	-8.18	115.9	-48.24
Test #15/Sier/ Baseline	U	2474	-	6724	-	208.1	-
Test #7/Sier/ 3y 3m	U	1027	-58.49	4689	-30.26	22.0	-89.43
Tests #5 & #6 Sier/3y 3m	U	1340	-45.84	5522	-17.88	86.5	-58.43

		<u>ACRYLIC/POLY INTERLAYER</u>					
		Ultimate					
Full-Scale Test #/Mfgr/ Installed Age	Interlayer	<u>Tensile Stress</u>		<u>Tensile Modulus</u>		<u>Energy</u>	
		psi Average	Percent Change	psi Average	Percent Change	in. lbs. Average	Percent Change
Test #3/PPG/ Baseline	U	2429	-	8376	-	100.6	-
Test #8/PPG/ 3y 2m	U	2279	-6.18	8272	-1.24	103.4	2.78
Test #15/Sier/ Baseline	S	315	-	1017	-	21.2	-
Test #7/Sier/ 3y 3m	S	346	9.84	1402	37.86	11.4	-46.23
Tests #5 & #6 Sier/3y 3m	S	458	31.22	1318	29.60	22.5	6.13

TABLE 7
2000 IN/MIN IMPACT BEAM SUMMARY

ACRYLIC IN TENSION

	Average Modulus	(Standard Deviation)	Average Peak Load	(Standard Deviation)	Average Energy	(Standard Deviation)
PPG	275.1	(73.25)	1313.9	(79.77)	2673.6	(137.8)
Sierracin	103.03	(15.05)	1359.3	(84.79)	2740.6	(206.7)

ACRYLIC IN COMPRESSION

	Average Modulus	(Standard Deviation)	Average Peak Load	(Standard Deviation)	Average Energy	(Standard Deviation)
PPG	203.4	(8.3)	2256	(76.5)	4153	(871.2)
Sierracin	100.7	(15.7)	1847	(131.3)	3270	(570.2)

TABLE 8
40,000 IN/MIN IMPACT BEAM SUMMARY

ACRYLIC IN TENSION

	Average Modulus ksi	(Standard Deviation)	Average Peak Load lbs.	(Standard Deviation)	Average Energy in-lbs.	(Standard Deviation)
PPG	561	(86)	2178	(75)	3124	(109)
Sierracin	443	(131)	1993	(153)	3357	(156)

ACRYLIC IN COMPRESSION

	Average Modulus ksi	(Standard Deviation)	Average Peak Load lbs.	(Standard Deviation)	Average Energy in-lbs.	(Standard Deviation)
PPG	518	(97)	2872	(188)	5033	(1026)
Sierracin	373	(128)	2330	(142)	3917	(321)

TABLE 9
DATA SUMMARY, FALLING WEIGHT TESTS

Manufacturer	Sequence Number	Installed Age	Compression Surface	Threshold of Failure Energy (in. lbs.)	Strain Rate (in/in/sec)
PPG	Baseline	0	P	2978*	86
			A	5000	89
PPG	643	2y 1.5m	P	3080*	78
			A	5276	93
PPG	69	3y 4m	P	2966*	77
			A	4462*	84
Sierracin	Baseline	0	P	3960*	92
			A	3398	82
Sierracin	417	2y 1m	P	4083*	96
			A	3775*	92
Sierracin	624	6y 4.75m	P	2938	79
			A	4023*	91

*Specimens pushed through supports -- no failure

TABLE 10

F-111 ADBIRT WINDSHIELD
AIR CANNON TESTING DATA SUMMARY

Specimen ID No.	Mfgr. Seq. # & Installed Age	Impactor Type	Impactor Mass (gm)	Velocity (ft-sec)	Energy (ft-lbs)	Failure Type**	Threshold Velocity	Threshold Energy	Percent Reduction
AC-P-2	PPG (Baseline)	1" Dia.	66.7	802	1470	D	902.5	1862	-
AC-P-3		Steel		869	1726	D			
AC-P-4		Sphere		894	1827	D			
AC-P-6				897	1839	D			
AC-D-5				908	1885	P(2P)			
AC-P-1				911	1897	P(2P)			
AC-P-13	PPG Seq. #693 2y 1.5m	1" Dia.	66.7	772	1362	D	875.5	1752	5.91
AC-P-15		Steel		871	1734	D			
AC-P-18		Sphere		880	1770	P(MP)			
AC-P-16				892	1819	P(3P)			
AC-P-17				892	1819	P(MP)			
AC-P-14				897	1839	P(MP)			
AC-P-9	PPG Seq. #69 3y 4m	1" Dia.	66.7	868	1722	D	871	1732	6.98
AC-P-8		Steel		871	1734	D			
AC-P-7		Sphere		871	1734	P(3P)			
AC-P-10				878	1762	P(MP)			
AC-P-11				-	-	-			
AC-P-12				-	-	-			
AC-S-5	Sierracin Baseline	1" Dia.	66.7	804	1478	D	817.5	1528	-
AC-S-6		Steel		831	1578	P(MP)			
AC-S-4		Sphere		851	1655	P(3P)			
AC-S-3				860	1690	P(MP)			
AC-S-2				881	1774	P(3P)			
AC-S-1				908	1885	P(MP)			
AC-S-10	Sierracin Seq. #417 2y 1m	1" Dia.	66.7	806	1485	D	812.0	1507	1.37
AC-S-7		Steel		809	1496	D			
AC-S-11		Sphere		815	1518	P(3P)			
AC-S-9				822	1544	P(3P)			
AC-S-8				831	1578	P(MP)			
AC-S-12				-	-	-			
AC-S-14	Sierracin Seq. #624 6y 4.75m	1" Dia.	66.7	759	1317	D	783.0	1401	8.31
AC-S-15		Steel		783	1401	D			
AC-S-17		Sphere		783	1401	D			
AC-S-16				790	1427	P(3P)			
AC-S-13				803	1474	P(3P)			
AC-S-18				-	-	-			

**D Ductile Deformation
P(2P) - Penetration (2 petals)

P(3P) - Penetration (3 petals)
P(MP) - Penetration (multiple petals)

TABLE 11

AIR CANNON TESTING DATA SUMMARY FOR
0.31 INCH AIRCRAFT GRADE POLYCARBONATE SHEET

Specimen ID No.	Mfrg. and Total Age	Impactor Type	Impactor Mass (gm)	Velocity (ft-sec)	Energy (ft-lbs)	Failure Type**	Threshold Velocity (ft/sec)	Threshold Energy (ft-lbs)	% Change in Energy
AA-1*	General Electric (Baseline)	1" Dia. Steel Sphere	66.7	473	510	D	651	970	-
AA-3				597	810	D			
AA-6				627	900	D			
AA-7				637	930	D			
AA-4				651	970	F			
AA-8				656	980	D			
AA-5				666	1010	P			
AA-2				709	1150	P			
AC-GE-1	General Electric (Approx. 7 yrs.)	1" Dia. Steel Sphere	66.7	646	954	D	668.5	1022	+5.36
AC-GE-5				655	981	D			
AC-GE-3				667	1017	D			
AC-GE-4				670	1026	P(2P)			
AC-GE-2				679	1054	P(2P)			
AA-2R*	Rohm & Haas Baseline	1" Dia. Steel Sphere	66.7	644	950	F	644	950	-
AA-1R				808	1490	P			
AC-RH-2	Rohm & Haas (Approx. 7 yrs.)	1" Dia. Steel Sphere	66.7	624	890	D	653.5	976	+2.74
AC-RH-1				650	966	D			
AC-RH-3				652	972	D			
AC-RH-7				655	981	P(2P)			
AC-RH-5				667	1017	P(3P)			
AC-RH-6				679	1054	P(3P)			
AC-RH-4				688	1082	P(3P)			

*Development of an Impact Resistant Test Method for Polycarbonate," February 1984, AFWAL-TR-83-3128.

**D - Ductile Deformation

P(3P) - Penetration (3 petals)

P(2P) - Penetration (2 petals)

P(MP) - Penetration (multiple petals)

TABLE 12
EDGE ATTACHMENT TEST RESULTS

Specimen I.D.	Manuf./ Seq. No./ DOM Installed Age	Peak Load (lbs.)	Average (Standard Dev.)	Failure Energy (in.lbs.)	Average (Standard Dev.)	Failure Mode
EA-P-1	PPG Baseline	3428		1493		DF, AFGPR/BH, AFMR
2		3302	3335	1532	1621	DF, BH, AFMR
3		2962	(216)	1628	(176)	DF/BF, BH, AFMR
4		3580		1858		DF, BH, AFMR
5		3472		1800		DF/BF, BH, AFMR
6		3265		1417		DF, AFGPR/BH, AFMR
32	PPG	3995	3969	1760	1827	DF, BH, AFMR
33	Seq. #137	3410	(828.1)	1410	(332.5)	DF, AFGPR, AFMR
34	11-2-81	3615		1825		DF, BH, AFMR
35	1y 10m	5390		2340		DF/BF, BH, AFMR
36		3435		1800		DF/BF, BH, AFMR
7	PPG	2972		245		BF, AFGPR, AFMR
8	Seq. #643	3342	3115	400	339	BF, AFGPR, AFMR
9	8-20-81	2912	(179)	265	(100)	BF, AFGPR, AFMR
10	2y 1.5m	3240		302		BF, AFGPR, AFMR
11		3110		484		BF, AFGPR, AFMR
EA-P-20	PPG	2920	3322	230	565	BF, AFGPR, AFMR
21	Seq. #824	2680	(634.9)	165	(681.7)	BF, AFGPR, AFMR
22	9-10-81	3000		220		BF, AFGPR, AFMR
23	2y 11m	3975		1770		DF/BF, BH, CFMR
24		4035		440		BF, CFMR, AFMR
13	PPG	3145		1110		DF, AFGPR, AFMR
14	Seq. #63	2540	3954	257	1445	BF, AFGPR, AFMR
15	6-4-81	4405	(1053)	1480	(811)	DF, AFGPR, DMR/AFMR
16	3y 4m	4830		2197		DF, AFGPR, DFMR
17		4852		2181		DF, AFGPR/BH, DFMR
26	PPG	5315	5281	2690	2795	DF, BH, DFMR
27	Seq. #42	5325	(46.8)	2975	(160.9)	DF, BH, DFMR
28	7-17-81	5215		2630		DF, AFGPR, DFMR
29	3y 8.5m	5300		2720		DF, BH, DMR/DFMR
30		5250		2960		DF/BF, BH, DFMR
EA-S-1	Sierracin	4650		1713		DF, BH, DMR/CFMR
2	Baseline	4725	4834	1708	1929	DF, AFGPR, DMR/CFMR
3		4900	(174)	2091	(174)	DF, BH, DMR/CFMR
4		4738		2039		DF, BH, DMR/CFMR
5		4850		2054		DF, BH, DMR/CFMR
6		5138		1966		
EA-S-20	Sierracin	2645	3617	370	941	BF, AFGPR, CFMR
21	Seq. #935	2550	(862)	370	(572)	BF, AFGPR, CFMR
22	11-79	4050		975		DF/BF, AFGPR, CFMR
23	1y 5m	4565		1920		DF, BH, DMR/CFMR
24		3540		920		DF/BF, AFGPR, CFMR
25		4350		1090		DF/BF, AFGPR, DMR/CFMR
8	Sierracin	5275	5057	2231	1876	DF, BH, DMR, AFMR
9	Seq. #417	5250	(334)	2228	(527)	DF, BH, DMR/CFMR
10	1-82	4563		1115		DF/BF, CFMR, DMR/CFMR
11	2y 1m	5138		1930		DF, BH, CFMR
EA-S-27	Sierracin	4840	4840	1370	1835	DF/BF, AFGPR, DMR/CFMR
28	Seq. #312	4845	(517)	1490	(684)	DF/BF, AFGPR, DMR/CFMR
29	6-82	3995		1190		DF/BF, AFGPR, DMR/CFMR
30	3y 3m	5300		2385		DF, BH, DMR/CFMR
31		5220		2740		DF, BH, DMR/CFMR
13	Sierracin	2388		188		BF, AFGPR*
14	Seq. #624	1813	2048	138	146	BF, AFGPR*
15	10-79	2238	(258)	157	(32)	BF, AFGPR*
16	6y 4 3/4m	1988		148		BF, AFGPR*
17		1813		101		BF, AFGPR*

*This group did not have a metal bearing strip/edge retainer

Legend:

BF - Brittle failure of polycarbonate plies
 DF - Ductile failure of polycarbonate plies
 BH - Bolt Head pulled through glass phenolic retainer
 AFGPR - Adhesive failure of bond line between glass phenolic retainer and polycarbonate
 CFMR - Cohesive failure of bond line between glass phenolic retainer and polycarbonate
 AFMR - Adhesive failure of bond line between metal retainer and polycarbonate
 CFMR - Cohesive failure of bond line between metal retainer and polycarbonate
 DFMR - Ductile failure of metal retainer
 DMR - Ductile deformation of metal retainer

TABLE 13

FLIGHT TIME AT TEMPERATURE

Temperature °F	°C	Hours/Years
25	-4	14.4
30	-1	36.2
40	4	19.8
45	7	12.0
65	18	23.3
70	21	14.4
95	35	1.7
100	38	0.7
105	41	129.2
110	43	1.9
120	49	38.3
125	52	0.9
145	63	1.5
170	77	0.7
175	79	0.7
185	85	0.7
195	91	0.7
200	93	1.6
210	99	4.0
265	129	0.6
355	179	0.3
304.0 HOURS		

Composite test profile from Mountain Home, Lakenheath,
Red Flag, and Functional Check flight profiles.

TABLE 14

SUMMARY OF PHYSICAL MEASUREMENTS ON VARIOUS
F-111 ADBIRT WINDSHIELDS

Date of Measurement Time	Sequence Number	Mfg.	S/N	Aft. Arch. Height	Variation From Correct Fit Dimension*	Forward Arch. Height	Forward Still Height
11/87	Baseline	Ster	051	6 1/8	7/16	2	3 1/8 1/4
	Baseline	Ster	053	5 7/8	3/16	1 13/16	3 5/16 3/16
	Baseline	Ster	055	6	5/16	2	3 3/16 5/16
	Baseline	Ster	057	5 9/16	-1/8	2 1/4	3 5/16 1/4
5/84	622	Ster	994	5 7/8	3/16	2 3/16	2 15/16 3/8
2/84	577	Ster	850	5 3/4	1/16	2 3/16	3 3/16 3/8
3/83	617	Ster	288	5 13/16	1/8	2 1/4	3 3/16 5/16
5/82	UD-9	Ster	439	5 3/4	1/16	2 5/16	3 1/8 1/2
4/82	UD-22	Ster	358	5 5/8	-1/16	2 1/4	3 1/4 3/8
7/81	57	Ster	418	5 11/16	0	2 1/4	3 5/16 5/16
10/79	624	Ster	200	5 13/16	1/8	2 3/16	3 5/16 3/8
9/79	UD-20	Ster	201	5 25/32	3/32	2 5/16	3 5/16 3/8
10/78	UD-10	Ster	5	5 13/16	1/8	2 1/8	3 5/16 3/8
5/1/86	Baseline	PPG	86-H	5 3/8	-5/16	2 1/4	3 1/2 1/4
			05-01				
			1668				
5/1/86	Baseline	PPG	86-H	5 1/2	-3/16	2 3/16	3 1/8 3/16
			05-01				
			1669				
8/4/86	Baseline	PPG	86-H	5 3/8	-5/16	2 3/16	3 5/16 7/16
			08-04				
			1810				
8/7/86	Baseline	PPG	86-H	5 1/2	3/16	2 1/16	3 3/16 5/16
			08-07				
			1813				
85	Baseline	PPG	85	5 1/8	1/16	2 1/4	3 3/8 1/4
12/18/85	640	PPG	85-H	5 17/32	-5/32	2 3/16	3 1/2 3/8
			12-18				
			1249				
6/22/83	531	PPG	16-637	5 1/2	-3/16	2 1/8	3 5/8 3/8
6/8/83	UD-18	PPG	16-629	5 15/32	-7/32	2 3/16	3 3/4 5/16
5/31/83	4	PPG	15-627	5 5/8	-1/16	2 1/8	3 1/16 3/8
3/29/83	536	PPG	16-595	5 7/16	-1/4	2 3/16	3 7/16 5/16
3/17/81	530	PPG	19-18	6 7/32	17/32	2 3/8	3 5/16 5/16
12/13/81	UD-15	PPG	81			2 7/16	3 7/16 5/16
			Lot 79				
8/20/81	643	PPG	16-437	5 11/16	0	2 3/16	3 9/16 5/16
6/1/81	UD-21	PPG	16-345	5 7/8	3/16	2 5/16	3 11/16 7/16
10/20/80	UD-13	PPG	16-202	5 25/32	3/32	2 1/4	3 11/16 5/16
9/29/80	UD-14	PPG	16-168	5 25/32	3/32	2 5/16	3 1/16 5/16

TABLE 15

RESULTS OF POLYCARBONATE STRESS TESTS
WITH AGGRESSIVE AGENTS

CONTAMINANT	LOAD PSI	TEMP °F	TIME HRS	RESULTS
Control	2000	180	48	No cracking
Prod Res PR 1425	2000	180	48	No cracking
Prod Res PR 1425 Accel Only	2000	180	48	No cracking
Prod Res PR 1725 Base Only	2000	180	48	Pinpoint stress crack each side of hole
Prod Res 1725	2000	180	48	No cracking
Prod Res PR 1725	2000	180	48	Severe stress cracking
Prod Res PR 1725 Base Only	2000	180	48	Light stress cracks
DAPCO #73 Comp "B"	2000	180	2-3	SX broke
DAPCO #73 Comp "A"	2000	180	48	Stress cracks at hole
DAPCO #73 A & B Mixed	2000	180	48	Stress cracks at hole
Control	3000	RT	50	Light stress cracks
Polybutene	3000	RT	50	Light stress cracks
Proseal 899 Accel	3000	RT	50	Cracked
Proseal 899 Base	3000	RT	50	Cracked
Prod Res PR 1750 Mixed Sealant	3000	RT	50	Cracked
RTV 630	3000	RT	50	No cracks
Uralane 5754	3000	RT	50	Light stress cracks
Prod Res PR 1725	3000	RT	50	Light stress cracks
Control	3000	180	50	Light stress cracks
Prod Res 1425	3000	180	50	Light stress cracks
Uralane Adhesive	3000	180	50	Light stress cracks

TABLE 16

WINDSHIELD SEALANT EVALUATIONS
CANTILEVER STRESS CRAZING @ 2000 PSI

	R.T.	95°F	180°F
Blank Specimens	None	None	None
PR 1422	None	None	Crazed
PR 1425	None	---	None
PR 1725	None	---	None
PR 1750	None	---	None
PR 383	None	None	Crazed
PS 899	None	---	None
RW-2178-71	None	None	Crazed
GC 408	None	None	Crazed
GC 409	None	---	None
CS 3204	None	---	None
CS 3204/SF	None	None	Crazed
DC 799	None	Crazed (1)	Crazed
GE 87-386-001A	None	None	Crazed (1)

NOTE: (1) One of three samples crazed.

ACRYLIC WINDOW CRAZING

Klaus Ewald

Lufthansa German Airlines

ACRYLIC WINDOW CRAZING

Klaus Ewald
Lufthansa German Airlines
Aircraft Engineering Department
Structures Group
Frankfurt - West-Germany

Presented at the
15th Conference On Aerospace Transparent
Materials And Enclosures

16. - 20. January 1989
Hyatt Regency
Monterey, California

Abstract

Since 1980/81 a steady increase in craze damage on acrylic cockpit and passenger cabin windows was realized. Findings gave some strong evidence on material and/or process changes related primary source.

Denying this, manufacturers failed to initiate corrective action in time.

When the problem was growing epidemically, placing a tremendous burden on airlines to provide undisturbed view for pilots and passengers, a fantastic problem causing theory was presented in 1983 with great emphases - sulfuric acid from a volcano eruption.

Even no acid was ever confirmed on an aircraft and all visible signs were in contradiction, this theory was eagerly adopted nearly worldwide, influencing the whole industrie.

It was no surprise, when nearly no reaction could be realized when the acid ceased in 1984/1985 and the problem did not disappear.

This paper highlights the findings of an 8 years study performed on 7 flight test aircraft with some 700 windows involved as well as extensive laboratory testing.

The data obtained give overwhelming evidence that the problem was and still is being caused by a tough competition caused by strong aircraft manufacturer's demand for cheaper windows.

Findings clearly indicate that material changes have had some influence, but speeding up the manufacturing process must be considered as the prime reason. Some unrealistic and misleading specification requirements have to be taken into consideration also.

At the end the question has to be raised: why are real service experience and sound findings rated at a lower level compared to unconfirmed hypothesis, but published by influential parties and why seems a close multilateral cooperation to solve the problem be impossible or even undesirable?

Looking back in crazing history as experienced by Lufthansa German Airlines since introduction of jet aircraft in 1960, with special attention to the more recent past of the last 8 years, it becomes more and more obvious that something mysterious and/or even magic must have been involved when facts and findings are compared with official announcements and corrective actions as presented and introduced (or better not introduced) by those parties claiming to have the overall responsibility for aircraft windows.

Therefore I like to start my report with the same phrase fairytales normally begin:

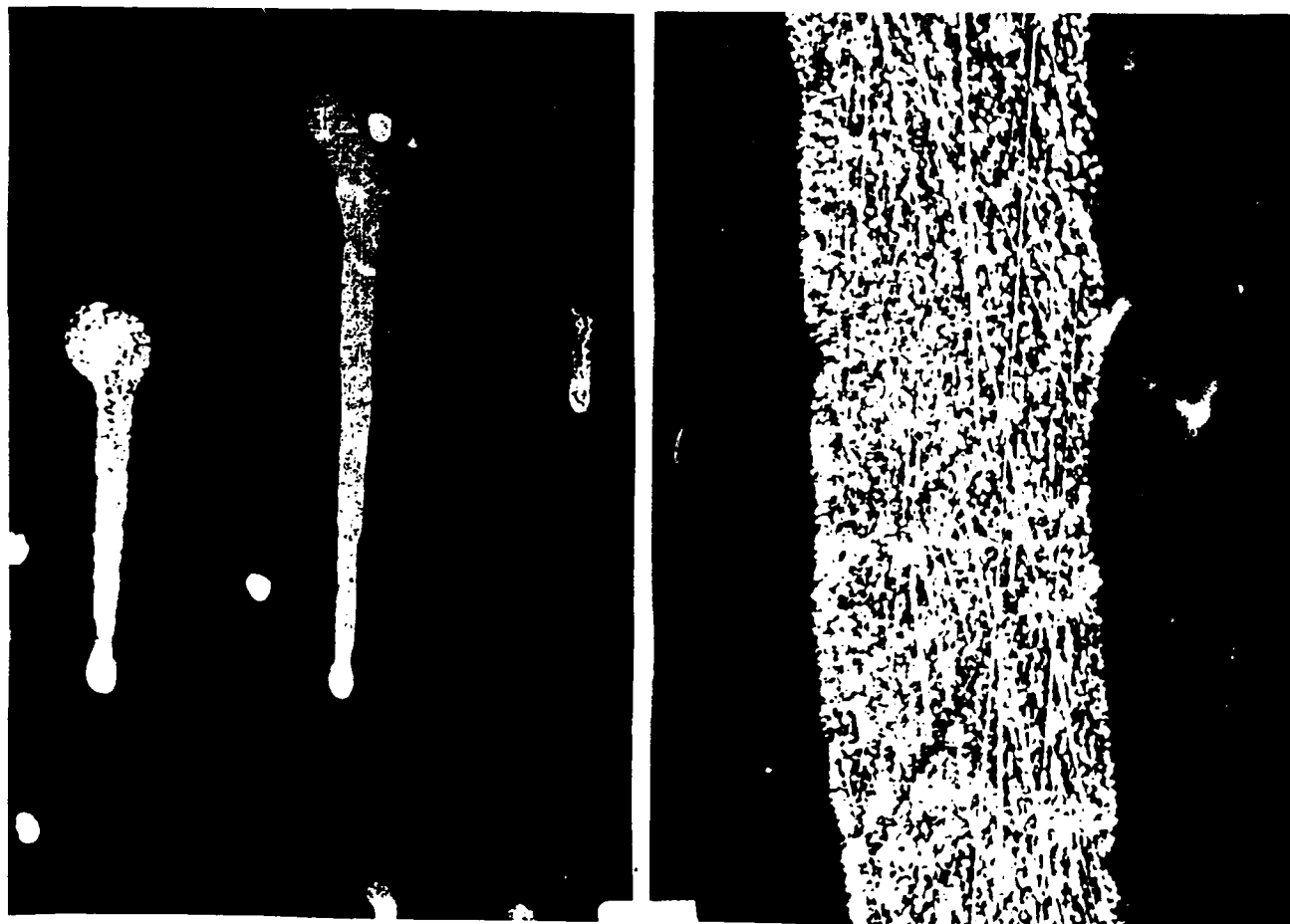
Once upon a time we had good quality and long lasting acrylic windows.

I am awful sorry, this is not the fairytale, this is the truth!

But I will come back to the fairytale, later. First the truth.

For more than a decade no problems emerged from the use of stretched acrylic as clazing material on jet aircraft operated by Lufthansa. The main reason for window removal was the result of lack of care by those maintaining the aircraft.

Scratches, paint stripper damage, and crazing caused by the use of detrimental solvents made premature replacements mandatory.



Since 1973/74 an increasing number of craze damaged windows was reported by some airlines and later acknowledged by the affected aircraft manufacturer. One airline later made the attempt to relate this problem to the introduction of a new stretching method, which uses a pressing process rather than stretching. They had to fail mainly due to three circumstances: lack of interest and support by the industrie, lack of suitable investigation methodes, and lack of interest by most airlines. This time not due to a general lack of interest, because crazing on acrylic windows was not considered as a major problem or a problem at all. Lack of interest by the airlines this time was created, because most airlines were not, or just slightly affect by the problem. Only windows from one small source were affected and most airlines, including Lufthansa, had none or just a few of these windows installed.

Today we are in a position to prove that the suspicion was correct.

Using the press stretching method, nobody is able to gain as good results as with tension stretching. In most cases the quality will be less than marginal.

The first real crazing problem within our fleet developed shortly after introduction of a new aircraft type in 1975/76, using a new type of as-cast acrylic for passenger cabin window application.

In early 1980 the material manufacturer performed a thorough inspection of acrylic cabin windows on all 5 remaining types of aircraft operated by Lufthansa and was convinced that only one material, his own, caused problems.

But it was not only the material.

The marginal thickness of the windows definitely had more than just some detrimental influence.

Being under pressure by the airlines, or better, due to realistic warranty contracts, material changes were promptly introduced and the situation improved significantly.

With delivery of the first aircraft of a smaller version of this aircraft type, some years later, using the same window material, the situation was reversed: crazing after just a couple of flight hours - but in a different pattern.

What has changed?

To fulfill some excessive optical requirements and to avoid rejections from aircraft manufacturer's quality control, the manufacturer was forced to use

a detrimental buffing process - even there was already a strong suspicion that there will be an adverse effect on service life.

It needed a flight test, expensive warranty claims, high maintenance costs, passenger complaints, long discussions, failed windows in flight, and quite an amount of wasted time, before realistic changes were introduced.

The result was a well designed window, using the best available base material, perfect stretching process, and careful manufacturing.

The result was a window made by the state of the art, which guaranteed at least 15000 flight hours on a short range aircraft, instead of less than 2000 flight hours before.

But it seems to be that somebody was not happy about everyone being satisfied.

Changes were introduced without our knowledge, but clearly realized some years later. More and more windows developed early crazing and deformed after a short time in service - a problem never observed with this type of material before.

But it was no longer the material we assumed to be installed!

Under pressure by aircraft manufacturer's purchasing, the window manufacturer was forced to revise the cost calculation.

The solution was found in the use of two materials instead of one.

One offering a long service life due to low water absorbing capability - the second, being a standard type with high water absorbing characteristics, with the disadvantage of a known short service life, but being cheaper.

Both materials were legal per window specification. Even the affected aircraft manufacturer normally is maintaining the specification very carefully, they disregarded that these materials were not interchangeable due to their different properties and resulting inservice behaviour. The latter material should have been considered as obsolete and should have found no more application for exterior aircraft window glazing.

Because of close and good cooperation this little problem was easily solved technical wise, but the administrative part of the story will definitely last for a long time.

Unfortunately, this situation is not the same with other aircraft manufacturers, making most of the aircraft operated worldwide.

A great deal of conviction is still required until realistic recommendations are to be followed and long overdue changes are implemented.

Window manufacturers show much more interest in close cooperation and recognize the need for necessary changes in the production process.

Because of their dependence of the aircraft manufacturers, having a different conception and interest, nothing is happening - except that the quality of acrylic windows is deteriorating with time passing by.

Before going into detail on this subject, let's have a review of the rest of the crazing history, of that part known as the crazing problem, everyone in airline industry was struck by in the early eighties.

This problem was overlapped by the circumstance that a great number of aircraft windows reached the end of a long and satisfactory service life and needed replacement at the same time the crazing problem became wide spread.

Due to lack of experience and documentation this natural damage was very often misjudged and considered to be part of the growing and headache-causing problem.

Actually, in springtime 1981 - with first indications going back to 1980 - a tremendous increase of craze damage showing a new, unknown craze pattern was realized.

Because crazing never had been a real problem before and a lot of young engineers being in charge, a lack of experience and knowledge was existing at most airlines, influencing the investigation process negatively.

Deicing fluids, being suspected due to the proximity of winter time, were disclosed to have a detrimental effect. This was achieved by extensive laboratory and flight testing.

Second suspicion were material changes.

It was obvious that recently delivered aircraft and windows were more affected than old ones.

The aircraft manufacturers contacted to initiate corrective action, first denied that a real problem existed.

Later we received the confirmation that we were not alone with our suspicion and findings.

The following statements from an aircraft manufacturer were received in September 1981.

Quote.

Although window crazing has been experienced by a number of operators, only one other operator has indicated an apparent increase in the evidence on newer airplanes.

To our knowledge there has been no change in material and/or manufacturing technique. The current production airplanes have the same stretched acrylic windows that were used on the older airplanes

Unquote.

And later.

Quote

Monomer is made on same continuous line. It is the same raw material since 14 years

Unquote.

At the same time this statement was published, one material manufacturer had to acknowledge that changes have been made - but just of minor nature as they explained. The rest of the manufacturers denied any changes.

Even we failed to confirm the changes by cracking the material, we believe that we are now able to prove it.

We are operating 14 long range aircraft of a certain type. These aircraft were delivered between November 1973 and January 1981. 13 aircraft had windows from one source installed. This was the only one for this type of aircraft. Because of lack of a competitive situation, which as you later will see has a great influence on quality, it is assumed that all windows were made under comparable conditions.

But surprisingly their performance was not uniform. Service life dropped from 48000 flight hours on the first aircraft to less than 18000 flight hours on the thirteenth aircraft, delivered in December 1979.

Starting with the 8th delivered aircraft (March 1975), a new defect developed aside of crazing-excessive deformation of the outer pane, requiring premature replacement.

This type of defect was and still is completely unknown on the windows of the first 4 aircraft.

Still unknown, because quite a number of windows were reworked after 43000 flight hours in service, reducing window thickness by about 1.5 mm. These are again in service in excess of 20000 flight hours, without any problems, while all younger windows were scrapped a long time ago, mainly due to deformation and inplane cracking.

Just the oldest windows provided a problem free operation.

This circumstance forced us to check the water absorbing capability of windows from these 13 aircraft.

The result was no surprise:

The oldest windows delivered with the aircraft on November 12, 1973 gained a weight increase of 2.4 % when immersed in water of 60 ° C. Those of the eighth aircraft of 3.9 % and those from the last aircraft of 4.6 % on most of the tested windows, but with 4.9 % as the maximum.

Do the manufacturers still insist that no changes have been introduced? Let's try to come back to a common language. I propose to talk no longer about changes and hope that the manufacturers are able to agree on a common phrase like: "slight material adjustments have been made since 1974". The indications are over whelming.

One of the affected aircraft manufacturers, denying the problem in the past, last year issued the following statement

Quote

The basic raw material was compounded by manufacturers A and B per MIL-P-8184. Subsequently, in 1974/75 because of the energy problems these two compounders had material shortages and made some substitutions which would not have any affect on finished parts, but they did. We had early crazing and other things. While others blamed the effects on an outside influence, we believe it was caused by material substitutions

Unquote

But this is not the whole story as you will see when looking at the fourteenth aircraft of that type.

A dramatic change was observed.

After just 2000 flight hours, no view was possible through the window panes any longer. The first extremly deformed windows had been replaced already after lesser flight hours. What was the difference from the other 13 aircraft?

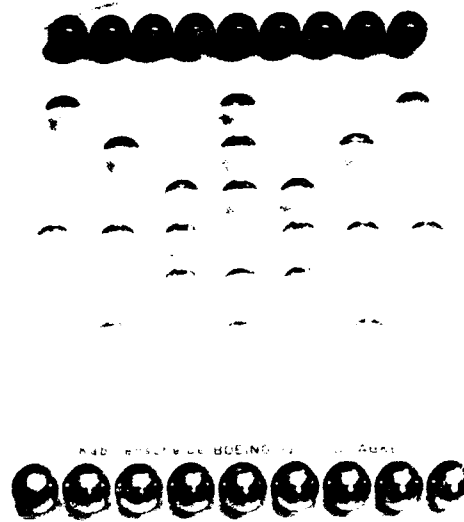
Not only a new manufacturer appeared. Press-stretching was applied for the first time, with all the now known disadvantages. But this effect was increased by crude grinding and buffing processes and two new materials with water absorption capabilities between 5.6 and 8.08 % at 60°C.

The effect of water absorption or better desorption, which is creating high stress loads can be best observed in nature. Just have a look at a drying up mud hole. Comparing this with a crazed acrylic window - not too much difference can be found.

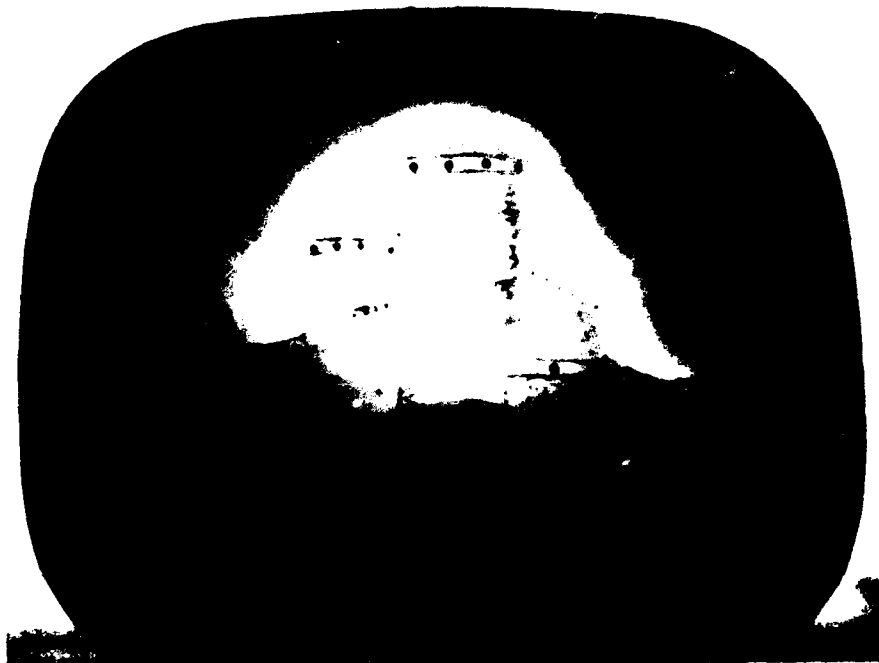


A little earlier, the same problem was observed on windows made from 1980 and on, for all types of aircraft from a third aircraft manufacturer. Because most of our aircraft were from that source, this really hurt us. This time not only the above mentioned manufacturer was creating the problem. Due to some new competitive demands two other manufacturers followed and applied any effort to ruin the windows before they were installed on an aircraft.

Window performance was so lousy that some attempts were made to find other kinds of application instead of installation on an aircraft. We started to make gaming boards



By the way we are able to offer quite a variety now. Others used them for paintings.



Now we are able to offer a more modern kind of application. Two polarizing filters, a light source and an acrylic cabin window framed as a unit , may be sold as modern art.



But back to more serious facts and history.

In 1982 some crazed windows from different sources removed from one aircraft were sent to the aircraft manufacturer and a window manufacturer for investigation. Both got the same type of windows showing the same degree of craze damage.

The comments we received were quite different.

First the aircraft manufacturer:

Quote

Examination of windows concludes that crazing was caused by detrimental chemical contact

Unquote.

You can be assured that this answer created some comments.

So we received a new answer.

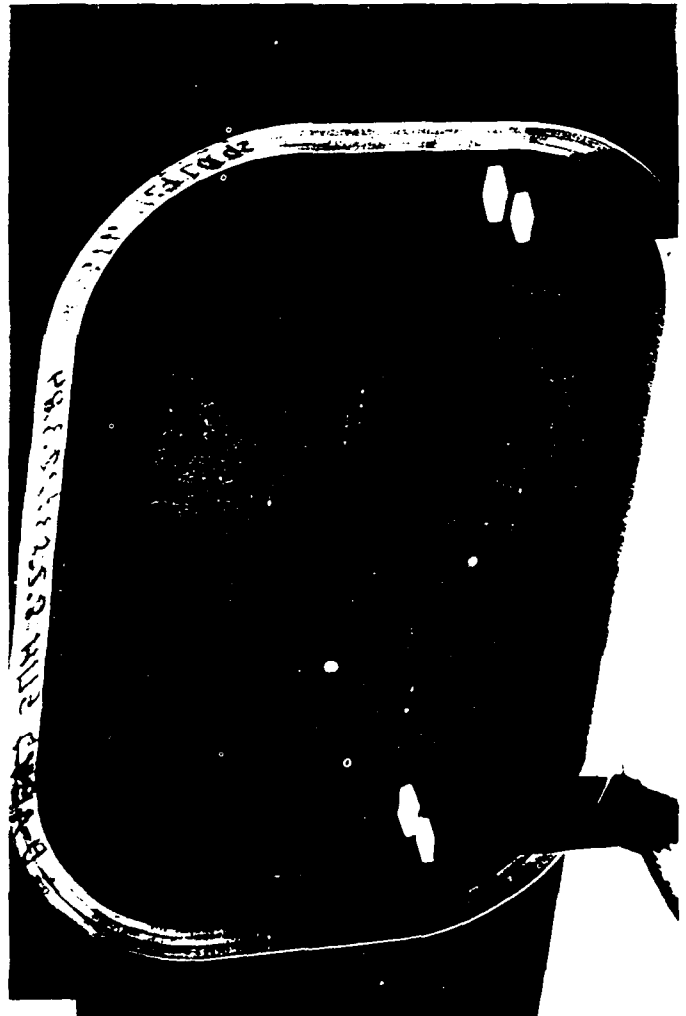
Quote

"We do not feel that further examination of the windows submitted by DLH will be of any value in determining the cause for crazing. A stretched acrylic window will not craze without something to cause it. We have examined the subject windows and determined they exhibit typical crazing as can be achieved by chemical contact

Unquote.

One statement is absolutely correct: a stretched acrylic window will not craze without something to cause it. But it was absolutely for sure - there was absolutely no indication of a chemical attack.

Every window manufacturer developed his own, very typical, unmistakable craze pattern, spreaded absolutely uniform across the whole window pane outer surface, which has to draw suspicion to the manufacturing process.



Much closer to reality was the investigation result of the window manufacturer, even nobody was able to interpretate the result correctly during those days. The answer was as follows:

Quote

Both windows showed an abnormally low craze threshold - 1250 psi as compared to the MIL-Spec standard of greater than 2000 psi (with lacquer thinner). Although this is an ascast test we would expect stretched acrylic to perform better, even up to 4000 psi level.

Unquote.

Today we know that this answer really was quite close to the whole truth, but it needed several years to pass by before that was detected.

Shortly later the major aircraft manufacturers presented the reason for our craze problem: atmospheric pollution of volcanic origin, as are sulfuric acid droplets and silicate particles, were blamed to be the causing factors.

This theory had one great advantage as the inventor clearly stated - this phenomenon was not within their control!

Even the inventor of the theory was never able to present just a tiny bit of evidence for the correctness, the whole industry was and still is so much influenced that even after 5 years the introduction of long overdue corrective action is still hampered. Instead of it, wrong, but very costly approaches to solve the problem or better to cover and hide it were initiated.

Progress is still not visible.

In a report published in August 1983 it was clearly stated that absolutely no evidence for the correctness of the theory was ever found. See page 27 of that report. Nevertheless, nearly the whole industry followed the new demands, even the conclusion on page 35 was exclusively based on an irrelevant assumption on page 2.

Just by looking at a real aircraft in flight it is obvious that something absolutely magic must have been involved, when windows being parallel to the airstream are attacked and leading edges being perpendicular to the airstream are excluded from contact with a detrimental acid.

ATA WINDOW TASK FORCE MEETING
ACRYLIC WINDOW CRAZING PROBLEM
BOEING REVIEW

SEATTLE, WASHINGTON
AUG. 17, 1967

JOHN T. BUCKS

TE 27526



KEY POINTS FROM JULY 10 ATA MEETING

- EPIDEMIC PROPORTIONS FOR MANY AIRLINES
- NO PROBLEM FOR OTHER AIRLINES
- PRIMARILY OCCURRING ON LONG RANGE MODELS
- AFFECTING ALL MANUFACTURERS ACRYLIC WINDOWS
- CRAZING FEATURES OFTEN DIFFERENT THAN NORMAL STRESS OR CHEMICAL CRAZING
- AIRCRAFT MANUFACTURERS, WINDOW MANUFACTURERS AND RAW MATERIAL SUPPLIERS ARE PROVIDING DATA FOR SOLUTION
- CIRCUMSTANTIAL EVIDENCE AND ATMOSPHERIC DATA RELATED TO VOLCANIC ACTIVITY POINTS STRONGLY TO IN-FLIGHT ENCOUNTERS IN NORTHERN LATITUDES WITH VOLCANIC DUST AS CAUSE
- SOME AIRLINES FELT THEY HAD EVIDENCE THAT CONTRADICTED THIS EXPLANATION
- HIGH PRIORITY IS BEING GIVEN TO DEVELOPMENT OF HARD COAT AND GLASS WINDOW DESIGNS
- ATA/ATA TASK FORCE WAS SET UP TO COORDINATE AIRLINE ACTIVITIES WITH AIRCRAFT AND WINDOW MANUFACTURERS

D-10-82
TE 27526



PARTICLE IMPINGEMENT
MATERIAL COLLECTED FROM
737 AIR CONDITIONING COALESCEUR BAGS

- EXAMINATION OF BAGS
- AS PART OF THE WATER SEPARATOR ASSEMBLY OF THE AIR CONDITIONING DUCT TO AIR CONDITIONING, PACK THE COALESCEUR BAGS BEAD AND COLLECT WATER AS WELL AS PARTICULATE WHICH ENTER THE AIR CONDITIONING DUCT
- BAGS EXAMINED FROM
 - 737 PAA N136 PA 1 BAGS NGA
 - 737 NGA N462 1 BAG
 - 737 ALA N136 1 BAG
- FINDINGS
- CARBONIZING MATERIAL AND SILICATE PARTICLES RANGING IN SIZE FROM 0.5 TO 15 MICROMETERS. SILICATES WERE SIMILAR TO DUST FROM VOLCANIC ASH. HOWEVER, DUST DUST HAS SIMILAR COMPOSITION, PH OF ABOUT 5

D-10-82
TE 27518



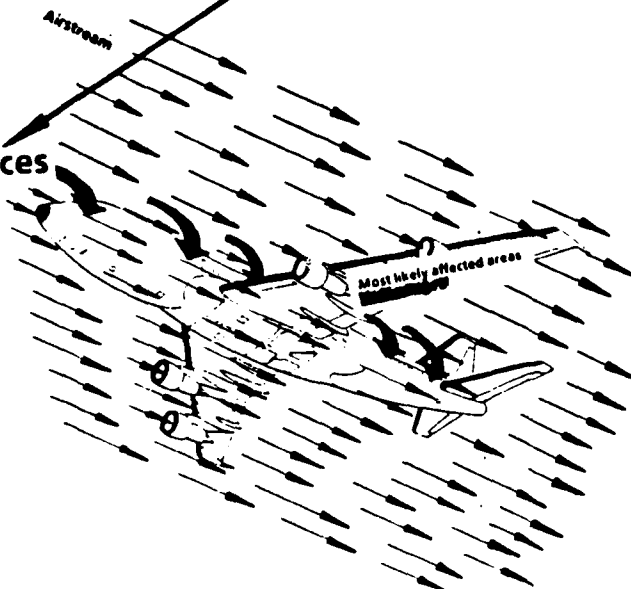
CURRENT BOEING CONCLUSIONS

- EVIDENCE IS OVERWHELMING THAT CURRENT ACRYLIC WINDOW CRAZING PROBLEM IS DUE TO DAMAGE FROM VOLCANIC DUSTS (SULFURIC ACID DROPLETS AND SILICATE PARTICLES) IN THE STRATOSPHERE (PARTICULARLY IN NORTHERN LATITUDES)
- AT BEST THIS ATMOSPHERIC CONDITION WILL EXIST FOR A LONG PERIOD OF TIME AND MAY WORSEN IF MORE VOLCANIC ERUPTIONS OCCUR
- LABORATORY TESTS INDICATE THAT SULFURIC ACID DAMAGES THE SURFACE OF ACRYLIC MATERIAL
- NEW MATERIALS, PROTECTIVE COVERINGS OR HARD COATS MUST RESIST SULFURIC ACID ATTACK IF THEY ARE TO PROVIDE EFFECTIVE RELIEF

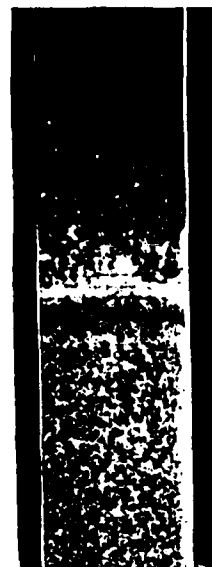
Why?

D-10-82
TE 27527

Magic Forces



Cled aluminum after
5 min of exposure
in 75 % sulfuric acid



The comment given by one aircraft manufacturer a little later sounds much more realistic:

Quote

Realistically, we do not believe that aircraft are being exposed to a 75 percent concentration of sulfuric acid. If this were true, we should experienced greater damage to metallic and painted structures.

Our analysis of star crazed cabin windows forwarded revealed no trace of sulfuric acid residue

Unquote

This statement meets completely our findings. Absolutely no indication of the slightest trace of sulfuric acid was ever found on an aircraft.

But nobody seemed to be able or to be willing to understand this message at the time the comment was made.

The sulfuric acid theory was so strongly implanted that serious attempts were made to include a sulfuric acid craze test in the base material specification.

Furtunately the devious path was recognized before final publication

But lets have a look at the existing specification and it's influence on material development in wrong or right direction.

Manufacturers and airlines should much more be interested in better flight performance than in improved resistance against chemicals, which some involved parties are just trying to proclaim as the most important factor.

We all are more or less able to avoid that chemicals like lacquer thinner come in contact with acrylic windows. If not, it is our own fault that the windows are damaged.

But we can absolutely not avoid that windows absorb moisture from atmospheric surroundings during flight.

Materials as already specified by the existing MIL-P-8184 have due to their crosslinking density high stress to craze values against chemicals as isopropanol, lacquer thinner or tolouence/isobutylacetat, but they develop early crazing under flight conditions because of high water absorption.

The relatively good solvent crazing resistance of high water absorbing materials is achieved by use of relatively high amounts of crosslinking systems containing highly hydrophilic components.

Low water absorbing materials have a better behaviour against moisture and consequently crazing under real flight conditions but less craze resistance against crazing agents used in MIL-P-8184.

Therefore the specification should follow more the real in service demands instead of protecting some manufacturers interests only.

Of course a specification always will be a compromise, but it first should take all "real life" conditions into consideration, before additional requirements for testing are requested, due to what ever reason.

The specification should reflect mainly inservice burdens, which are UV-exposure, temperature variations, and moisture - and not lacquer thinner and other organic solvents .

Materials, intended to be used for exterior aircraft glazing, gaining more than 2.5 % of weight increase when immersed in water at 60 °C, should be considered as obsolete and should be withdrawn from the specification.

The preconditioning procedure required by the specification before testing seems to need some adjustment to real inservice conditions, also. In the present from it protects faulty material more, than helping the user to find a satisfactory material.

In addition, the existing specification does not take the surface quality into consideration as an influence factor for the development of crazing.

This is, as we later will see, of tremendous importance.

A last word regarding sulfuric acid: Sulfuric acid is acting as an extremely efficient desiccant. When applied to acrylic it causes an extreme desorption of water from the surface, resulting in high tensile stresses. As a result, crazing developes. It seems to be just logical, that high water absorbing materials as used today, craze in a matter of seconds at low or no stresses, but all other aircraft structure has to be attacked with the same efficiency.

Therefore everybody should forget this episode as sone as possible, as it has created already enough confusion, errors, superfluous and very costly developments, and is still hampering the introduction of better windows.

These windows are available since a long time.

Most of the window manufacturers, who always had been loyal supporters of the aircraft manufacturers, in bilateral negotiations indicated their readiness to supply windows meeting our demands, but are not able to do so because of lack of interest by some, but most influential aircraft manufacturers.

But another very important factor is hampering the supply of better windows.

Most airlines seem to have not yet noticed that a real problem is existing. In many cases it seems to be that the passenger is buying just the right for a seat on an aircraft, but vision is something that is not included.

As long as airlines continue to act in this way or better continue to sleep, there is just little chance to change the aircraft manufacturers policy, which very often means - a demand for low prices but not for quality. Low prices for themselves, but not for the users - the airlines.

To find an explanation what is actually causing this drop in quality, manufacturers from around the world were asked for samples.

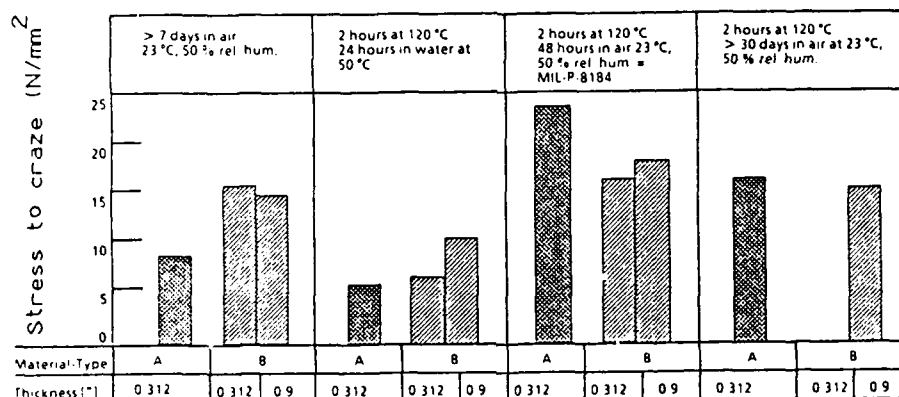
Stretched material - polished and unpolished, demonstrating every surface treatment step having been applied in production.

All samples were checked for surface roughness, craze stress threshold and crazing under high load using IPA as a craze medium.

First we had to realize, that the conditioning procedure described in MIL-Specification, resulted in misleading and not comparable outcome, reflecting reality in no way.

Several different conditioning procedures were tested.

Two suitable methods were found:



Stress to craze on two different acrylic materials from one US-manufacturer (as cast) in dependence of conditioning of specimens before testing

A Water absorption capability about 4.5 % max. service life 3500-7000 fh windows made by material manufacturer

B Water absorption capability about 2.2 % max. service life 12500-15000 fh windows made by material manufacturer

- 1) 7 days in air at 50 % relative humidity and 23 °C, and
- 2) 30 days in water at 23 °C.

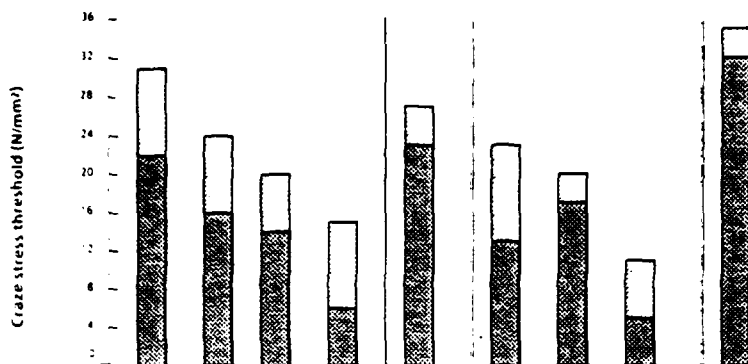
The following chart summarizes how perfect manufacturers are in ruining even the best material.

Conditioning procedure before craze test

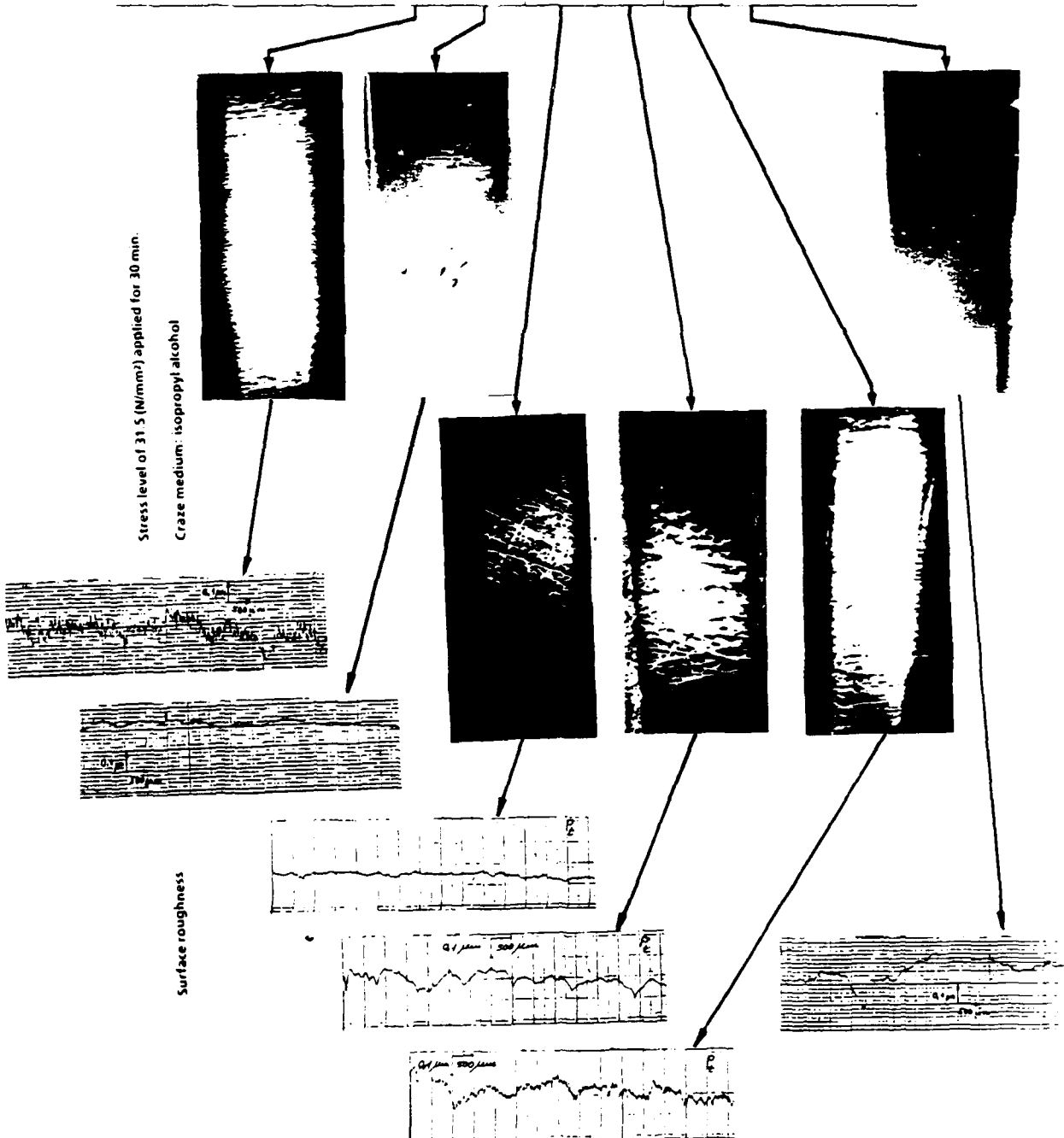
7 days air 23 C 50% rel humidity

30 days in water at 23 C

craze medium: isopropyl alcohol



Material	A, max. water absorption capability 4.5%					B, max. water abs. cap. 2.2%			C, max. water abs. cap. 4.8%	
Window Manufacturer	I					III			IV	
Stretching company	Same as window manufacturer I					Same as window manufacturer III			Same as window manufacturer V	
stretch ratio	75.74	70.74	75.72	77.71	73.74	68.68	67.66	71.66	91.64	
Grinding/polishing step	unpolished	1	2	finished window	finished window	unpolished	1	finished window	finished window	



Let's start with manufacturer III, shown in the center of the chart:

A relatively high craze stress threshold on an unpolished, stretched sample. Under high stress it becomes evident that not too much care is being used during handling of the sheet. Quite severe cracks as a result of a lot of scratches have developed.

As a result of the first grinding step the surface of the acrylic is severely damaged, as clearly to be seen on the surface roughness diagram. Much more severe crazing is the result of such a surface treatment.

But the final step on the window, which is still a detrimental buffing process, is destroying the window completely. This is clearly to be seen on the surface roughness diagram and resulting craze pattern.

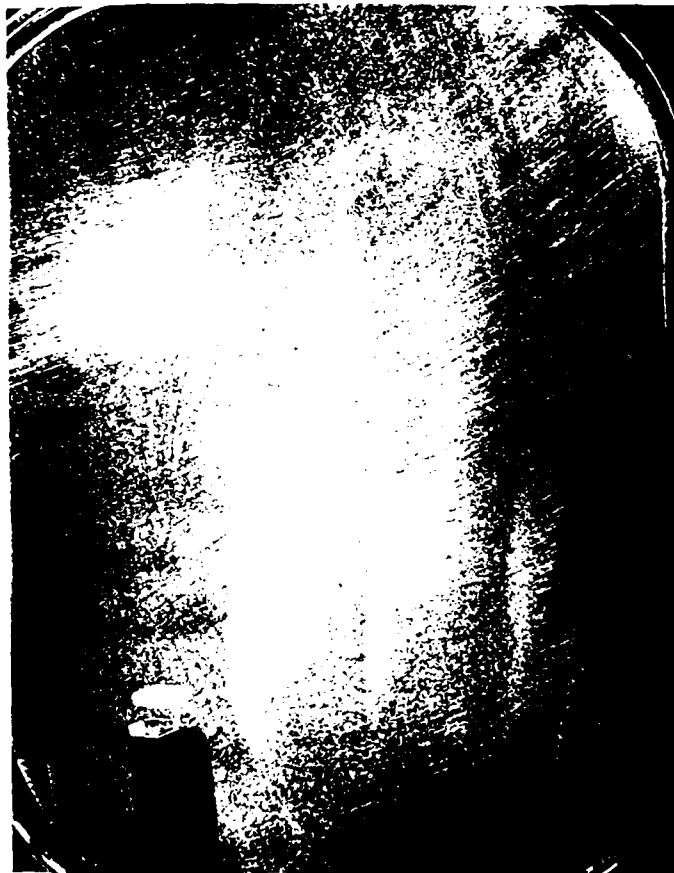
The craze stress threshold is below that of as cast acrylic.

All efforts to increase the craze resistance by stretching have been made superfluous.

In this condition, windows are sold to the airlines under protection of the aircraft manufacturers specification.

As an example, in one case their qualification specification asks for waxing and reinspection afterwards before windows are rejected due to scratches.

The maintenance and/or overhaul manual for rework or repair of acrylic windows recommends a wide variety of repair materials and processes definitely being able to destroy any window, but never restoring it.



So nobody can expect a better quality from new windows.

The first example represented a relatively small manufacturer.

Second example (manufacturer I) is dealing with one of the major manufacturers.

With every surface treatment step the material is more and more destroyed.

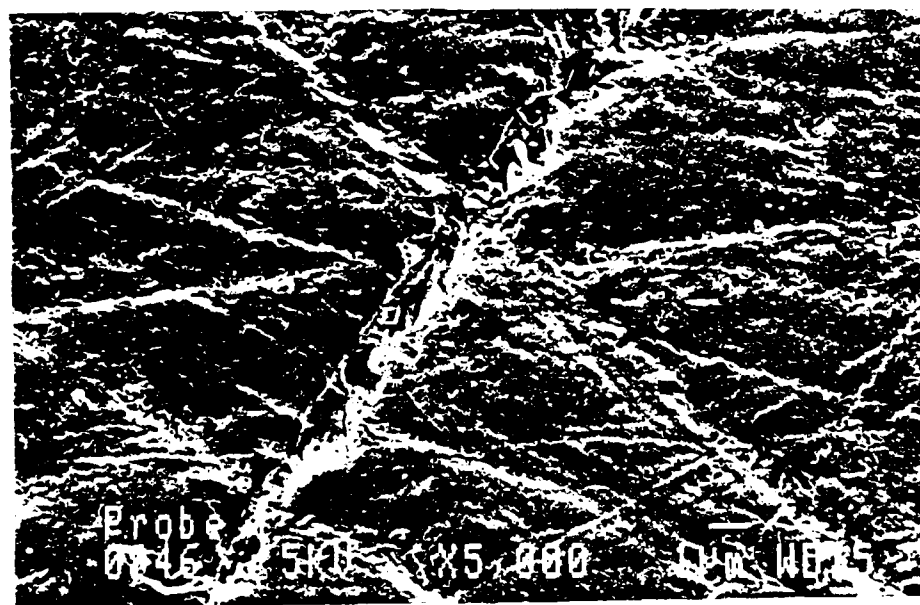
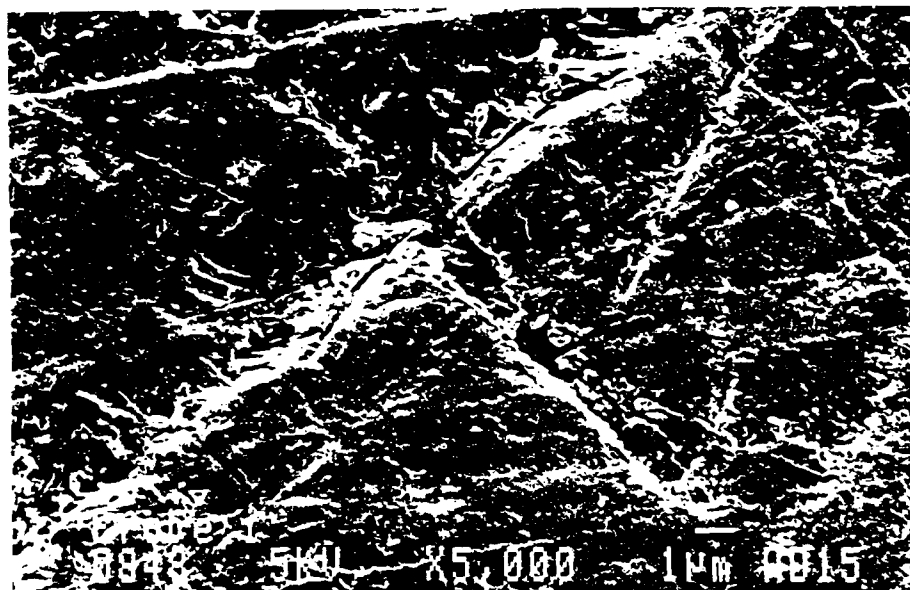
The final window is absolutely not better than the first one.

But don't draw the wrong conclusion from that what you have just heard.

Some manufacturers are even better. They don't need three or more steps.

They destroy the acrylic sheet already completely during the very first grinding step, just after stretching.

The result of just one grinding step is demonstrate on next photo.



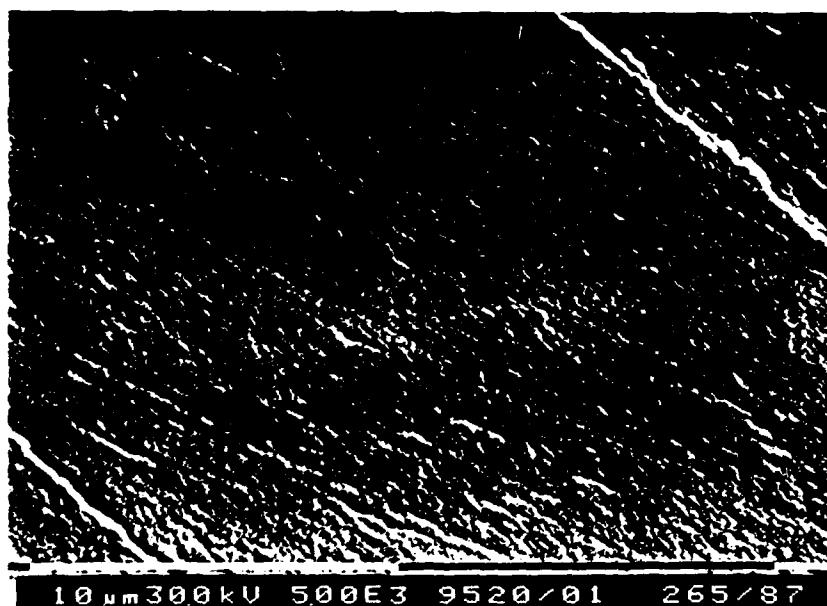
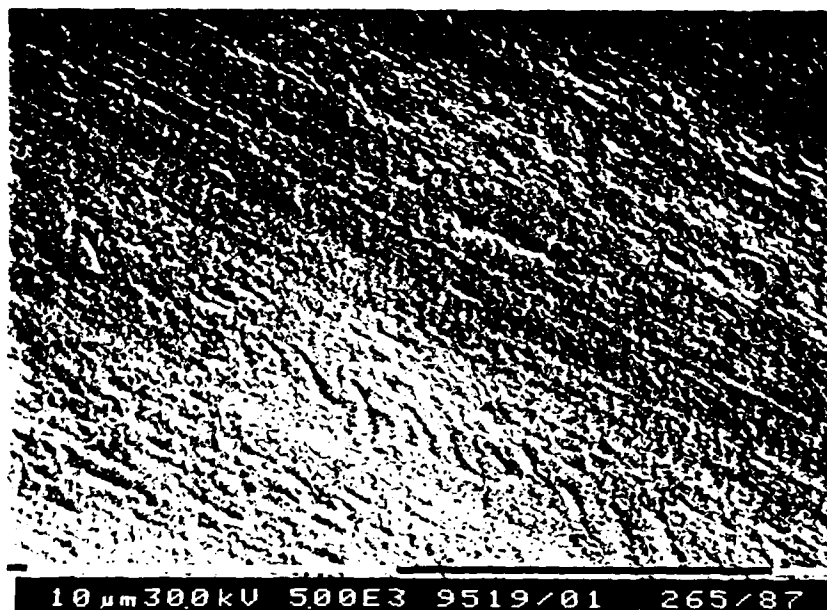
Cracks developed at the bottom of the grinding scratches due to the use of the wrong polishing material. Any further attempt, which is applied to improve the surface quality, has to fail.

Nobody is able to get rid of such a subsurface damage.

Because this adverse influence of polishing and grinding materials was found quite early during our investigations an extensive search for a process not harming the acrylic was initiated.

Milling instead of grinding was found to be the most promising process, but had still a small disadvantage: the cutter traces were always visible, requiring a polishing step to finish the window.

In a joint effort together with machine manufacturers we believe to have found the solution now. A diamond cutting process on a special designed machine seems to offer a surface treatment (rework in our case) in one step, without any additional polishing.



Coming back to our chart on the ability of the manufacturers to ruin even the best acrylic material, it is clearly to be seen, that good windows can be made with the same material, when only some more care is being applied.

Material, with only the first grinding step applied, sold by manufacturer I to manufacturer II, will be converted to a much longer lasting window.

The craze stress threshold on the final window is much higher. Only minor crazing was gained under high load. Being obvious, a fantastic smooth surface is the reason for these good results. As we know from service experience, these windows will last about 100 % longer than manufacturer I's windows.

The last manufacturer -no IV on our chart - gave some real surprise and astonishment.

Normally windows from that source perform just lousy due to material and workmanship.

A fantastic high craze stress thresholds was found. No crazing under high load. A relatively good surface quality.

What was wrong?

When a shrinkback test was carried out, there was no longer doubt why the windows had to have a poor inservice performance, but created good test results.

Just by chance, we have cut our craze test samples in the wrong direction. The material was stretched by 93 % in one, and 58 % in the other direction. Installed on an aircraft, with multiaxial cabin pressure load applied, the low stretch will be the only counting factor and early crazing will be the result.

At this stage of our investigation we started to look for a nondestructive test method, to find such faulty windows before they are installed on an aircraft.

In close cooperation with a German acrylic manufacturer a cheap, but very reliable test was found, which will be used as a 100 % screening test for all windows in the future.

Only a couple of seconds are required to determine whether a window is acceptable or not.

The test which is already mentioned in the MIL-Handbook-17 dated August 14, 1961, gives not only information on the uniformity of stretch, but on the crack propagation resistance of a stretched acrylics, also.

Even the explanation given in MIL-Handbook-17 seems to need some clarification and revision, a clear statement is already been made - material can be immediately rejected, when certain indications are to be observed during the test.

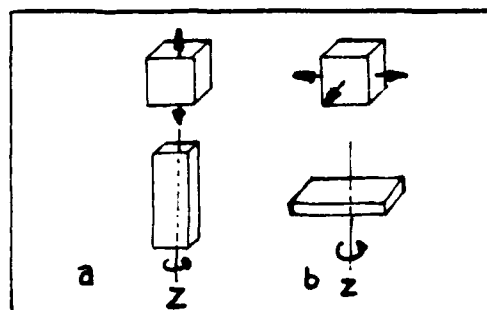


Fig. 1: Deformation of a volume unit during stretching
a = uniaxial stretching b = biaxial stretching
Z = axis of symmetry

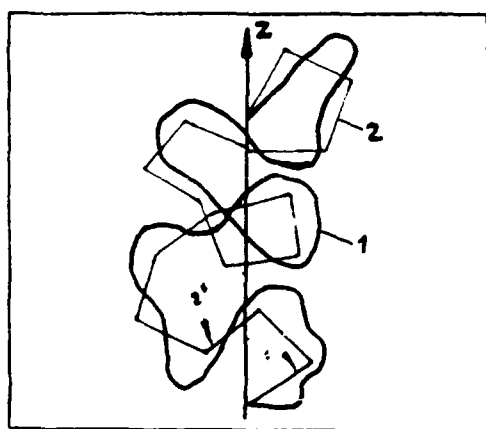


Fig. 2: Segment model
1 = chain molecule j = orientation angle
2 = segment Z = axis of symmetry

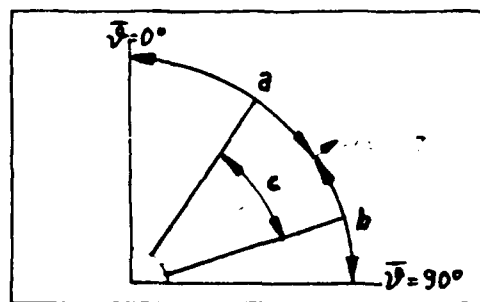


Fig. 3: Mean angle of orientation \bar{j} of the segments during uniaxial and biaxial stretching
a = uniaxial orientation
b = biaxial orientation
c = achievable in practice
 $\bar{j} = 0^\circ$ ideal uniaxial orientation
 $\bar{j} = 54.7^\circ$ isotropy
 $\bar{j} = 90^\circ$ ideal planar orientation

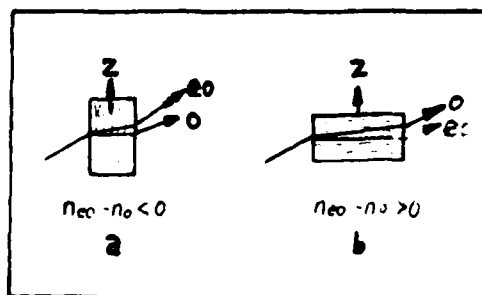


Fig. 4: Birefringence in uniaxially and uniformly biaxially stretched PMMA.

a = uniaxial orientation
molecular orientation
parallel to the optical
axis (axis of symmetry)
b = uniform biaxial orientation
molecular orientation at
right angles to the optical
axis (axis of symmetry)
Z = axis of symmetry = optical axis
o = ordinary ray
eo = extraordinary ray
n = refractive index

Polymethyl methacrylate (PMMA) is an amorphous polymer with long molecular chains forming a tangled coil, in which they are entangled with themselves and neighbour chains.

The highest strength properties of the material are to be found in the chain direction.

By deformation (stretching) of the material in either one direction (uniaxial stretching) or inplane (biaxial stretching) the strength and toughness properties of the material can be improved. This is reached by deformation or better alignment of the molecular chains in one direction, respectively in one plane.

The mechanism can be best explained using a simplified model of the molecular chains, in which straight line segments of equal length approximate the real chain contour.

The segments form certain angles ψ with an initially arbitrary assumed axis of symmetry. The angles ψ are equally represented between 0° and 360° in as cast material condition.

During stretching, all angles ψ and the angle of orientation $\bar{\psi}$ which is the statistical average of all represented angles ψ , become smaller (in case of ideal uniaxial stretching) and approach 0° , while 90° are approached in case of ideal biaxial stretching.

The test takes advantage of some optical properties of the acrylic material which becomes birefringent due to an anisotropy caused by some deviation from ideal stretch.

The birefringence will increase with greater deviation from the ideal case.

Any light ray entering the acrylic material perpendicular to the surface, but consequently not parallel to the symmetry axis of the molecular orientation due to deviation from the ideal case will be split up in two components, named ordinary and extraordinary ray. Both are linearly polarised at right angles to each other. The ordinary ray oscillates perpendicular to, and the extra ordinary ray parallel to the axis of symmetry. Each ray is propagating at a different speed in different directions. The difference in speed results in a path difference between the two component rays which increases proportionally with the path length.

The birefringence is defined by the maximum difference between the two refractive indices when the rays are perpendicular to the optical axis.

In PMMA, the higher speed propagating ray has it's plane of oscillation always coincided with the molecular chain segment orientation.

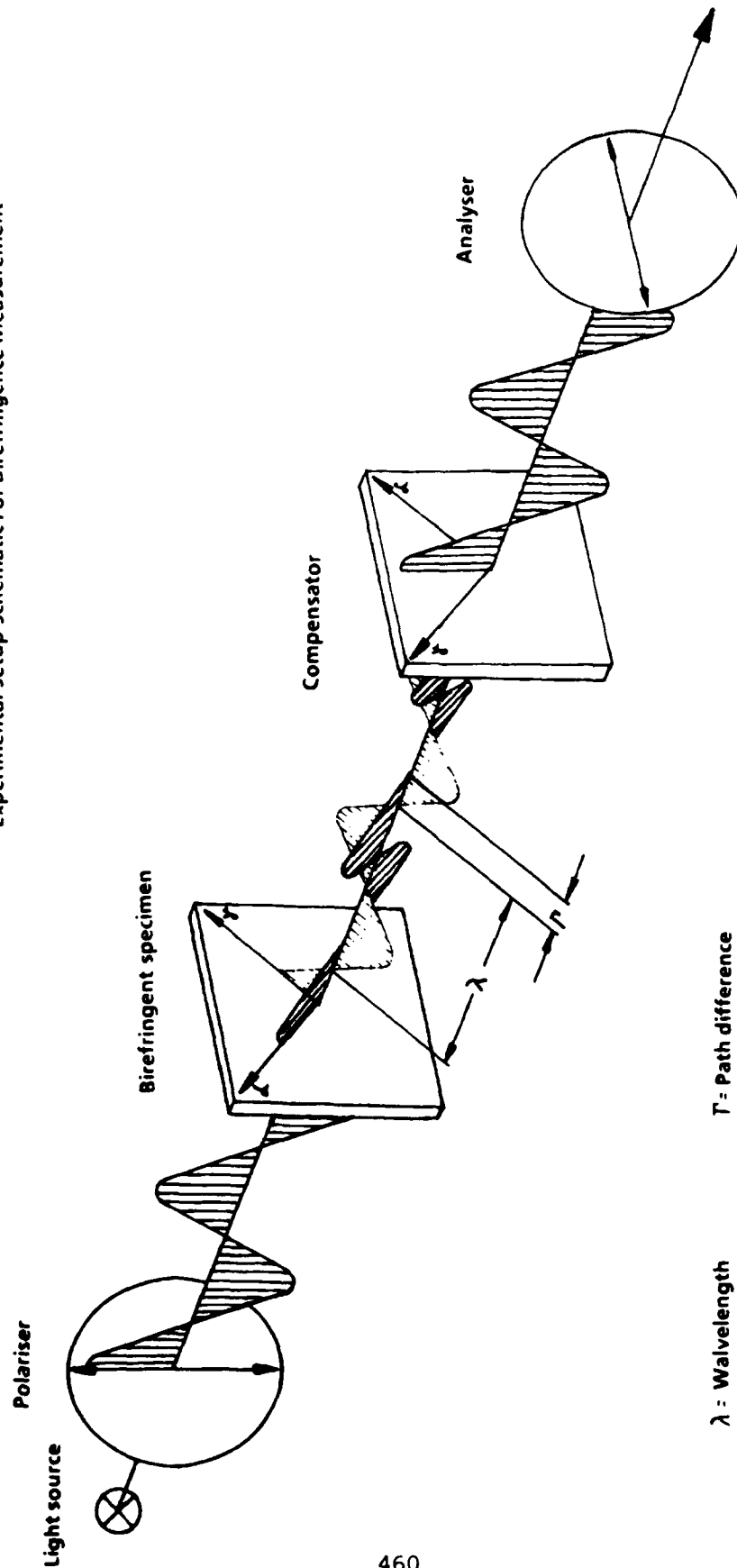
It has the smaller refractive index.

In case of biaxial orientation it is the ordinary ray.

Because the path differences between light waves are measurable, we have a method for the determination of the birefringence.

The schematic representation of the experimental set up used to measure birefringence is shown on the next chart.

Experimental Setup Schematic For Birefringence Measurement



In order to clearly identify the case of a uniform biaxial stretch where the path difference Δ equals 0, the test setup departs from common optical practise and is using polychromatic light instead of monochromatic light.

A dark field behind the analyser is evidence for a path difference Δ equal to 0, where as coloured fields are to be seen in all other cases.

At this point I like to point out that this test has absolutely no relation to stress optics. All samples were treated at 80 °C for 48 hours. So stresses are not be present. The colors are just a matter of molecular chain misorientation due to improper stretch and resulting birefringence.

The knowledge of the relationship between birefringence and orientation function gave us an economical, nondestructive test for the quality of stretched acrylic windows which can be applied in production and as an acceptance test for airlines. It separates those windows, which never should have passed the manufacturer's quality control, because they never fulfilled anyones specification requirements.

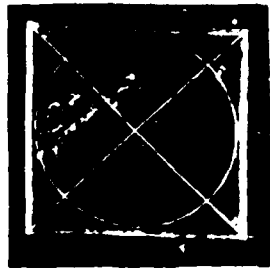
But this test is able to give reliable information on the crack propagation resistance of the acrylic, also.

Extensive material testing has confirmed that *any material showing a path difference of 610 nm or greater should be rejected because of K-factors being smaller than the required value.*

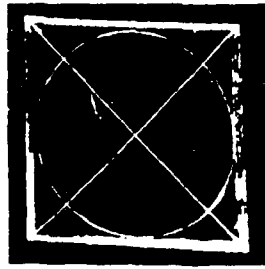
The test is not able to present exact quality values, but is a reliable "go - no go" tool.

rate
[%]

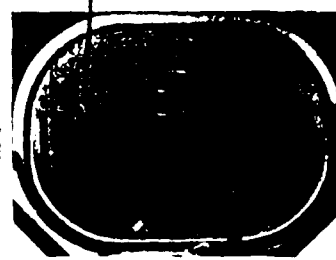
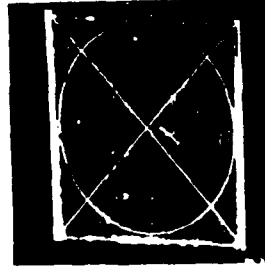
64.74 ± 73.01



62.76 ± 77.81



54.74 ± 83.04



measured
path difference
[nm]

165

168

1625

K factor below
required value

First Order

Second Order

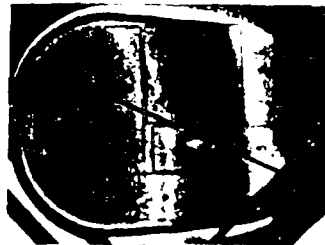
Third Order

Michal Lamy Color Chart



measured
path difference
[nm]

A310



DC10



B747



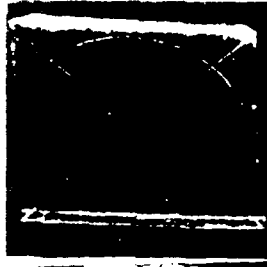
10/10

stretch
ratio
[%]

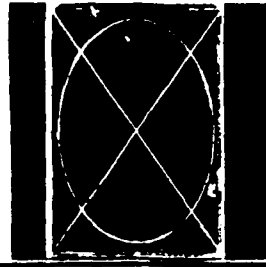
51.03 ± 81.49



48.11 ± 87.1

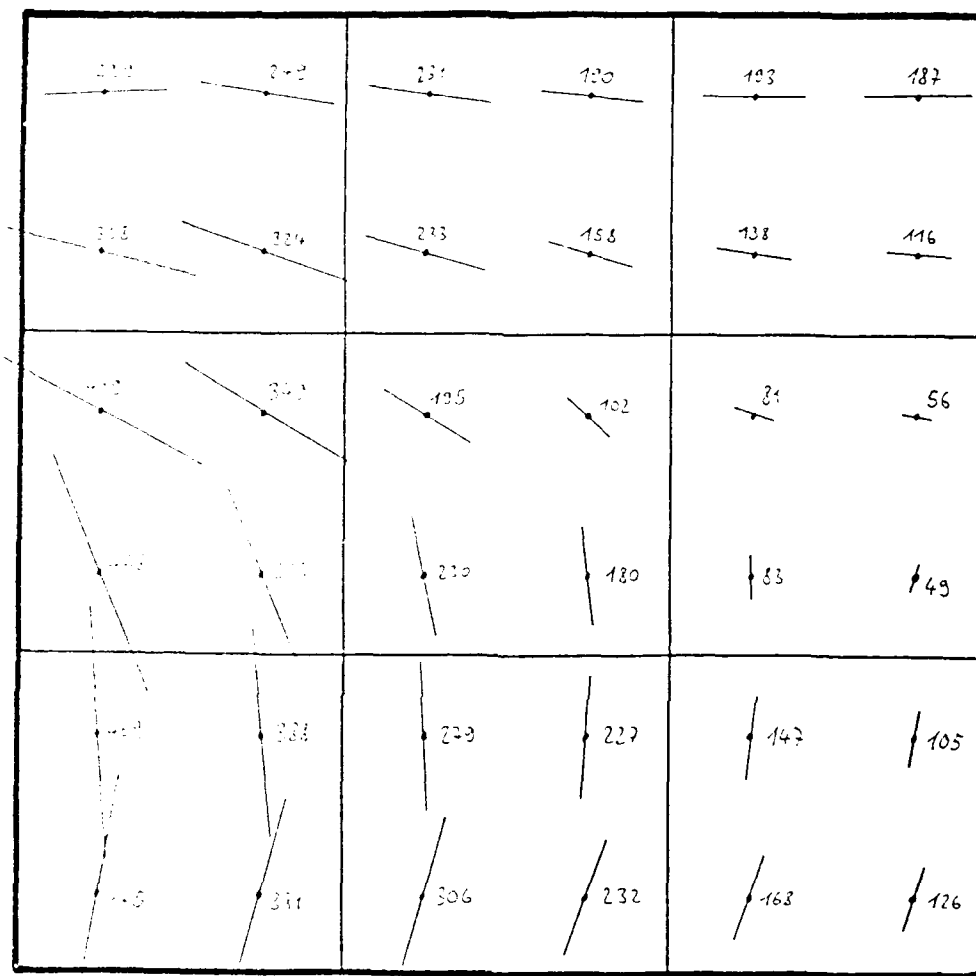


41.06 ± 101.67



Using a polarising microscope with compensator, the exact path differences and their orientation can be determined.

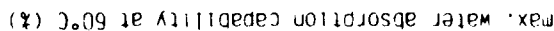
This is giving a clear demonstration of the problems encountered from a press-stretching process, where a uniform material flow seems to be not obtainable



It is no secret, that the bulk of press-stretched windows failed to pass the test requirements, but an amazing high number of tension - stretched windows was found, also.

It seems to be that some manufacturers are trying to improve their business by selling windows made from edge pieces which should have been scrapped due to known disqualification.

A summary of the influence of surface treatment, water absorption capability, and stretching uniformity is demonstrated on the next chart, representing the results of the flight tests on three of our 747's with about 500 windows involved.



Flight tests conducted on short range aircraft, using similar windows, developed comparable results. Due to shorter flights, resulting in less cabin pressure load application time, less UV exposure time, and less water desorption capability, crazing developed at a later term, but created absolutely the same craze pattern.

Therefore, it seems to be permissible to conclude, that development of crazing is independent from aircraft type, installation position, and (at least in our case) the operational environment, as long it is a good mixture of everything. Only in case of a sole operation in a warm, high humidity environment, this may be a larger influence factor.

By the way, all together we have testflown some 800 windows on 7 aircraft of three different types.

The flight tests have proven that existing, high water absorbing materials are not able to provide a longer service life than 10000 flight hours on a 747 in regard to crazing, but may have to be removed earlier due to inplane cracking.

Only the new, low water absorbing types of material promise a longer, satisfactory service life.

It seems to be long overdue, that the aircraft manufacturers stop to hamper the general introduction of low water absorbing materials and declare the high water absorbing materials as obsolete.

But regardless of airline experience worldwide, one major aircraft manufacturer is stating that the benefits gained due to the change do not justify the higher costs for the material.

The general introduction of low water absorbing type of acrylics was therefore rejected.

Regardless of the benefits gained from the material itself, we have to keep in mind, that the surface treatment can negate the improvements offered by low water absorbing type of acrylic. Our flight test experience chart demonstrates this very clearly.

In the row of low water absorbing type of materials we have four different types of windows, actually made from the same batch of material. The first three in the row and the very last one represent these windows.

Half of that material was tension-stretched. The other half press-stretched. Half of the stretched material was used by the stretching companies to

make windows, the remaining half of material from both stretching companies was delivered to a third window manufacturer.

First, the windows made by the tension-stretch company failed due to the use of a wrong polishing material at less than 7000 flight hours, while the windows made by the press-stretch company lasted already 8000 flight hours. Crazing was here initiated by the use of the wrong grinding material, and detrimental grinding/polishing procedures, causing severe subsurface damage

Those windows made by the third manufacturer lasted longest - about 9500 flight hours for the press-stretched material, where the same craze pattern developed as on the windows made by the stretching company. This is a clear indication that most of the damage was already introduced during grinding/polishing of the sheets after stretching and the window manufacturer had no chance to get rid of this subsurface damage.

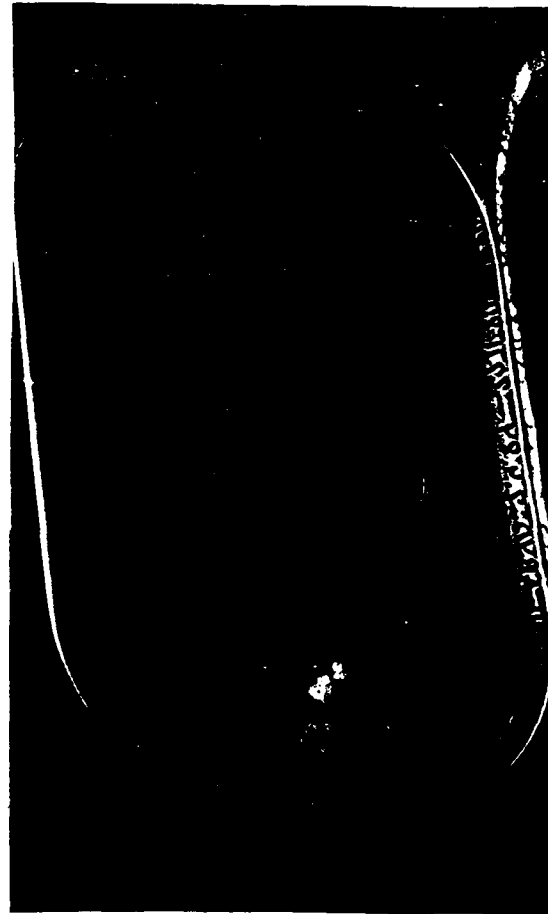
The tension-stretched windows made by the third manufacturer were removed at about 18000 flight hours due to a cabin refurbishment program, but were still good for at least another 4000 flight hours of service.

The difference in performance is demonstrated on the next photo.

Upper left: 7000 flight hours

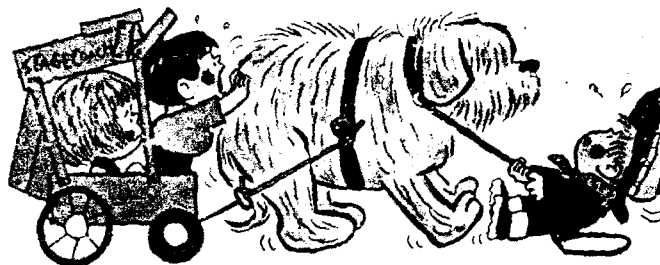
upper right: 8000 flight hours

Lower center: 18000 flight hours

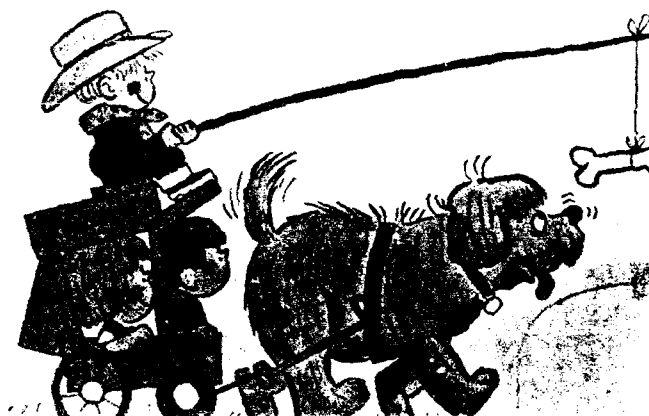


Even all knowledge and experience for the immediate introduction of satisfactory windows is on hand, nothing is happening.

Our proclamation, made in February 1984 for concentration on solving problems instead of fighting them,



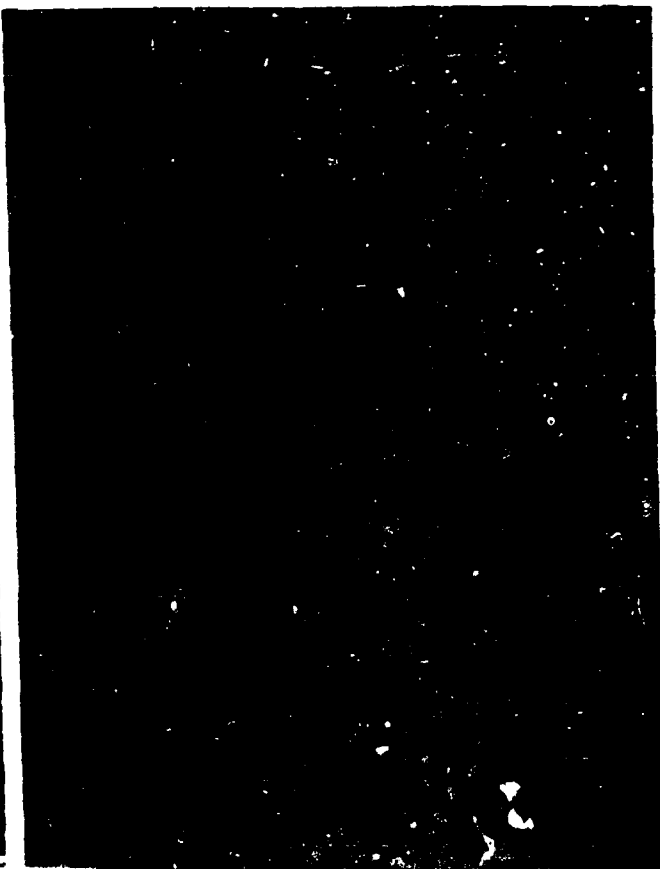
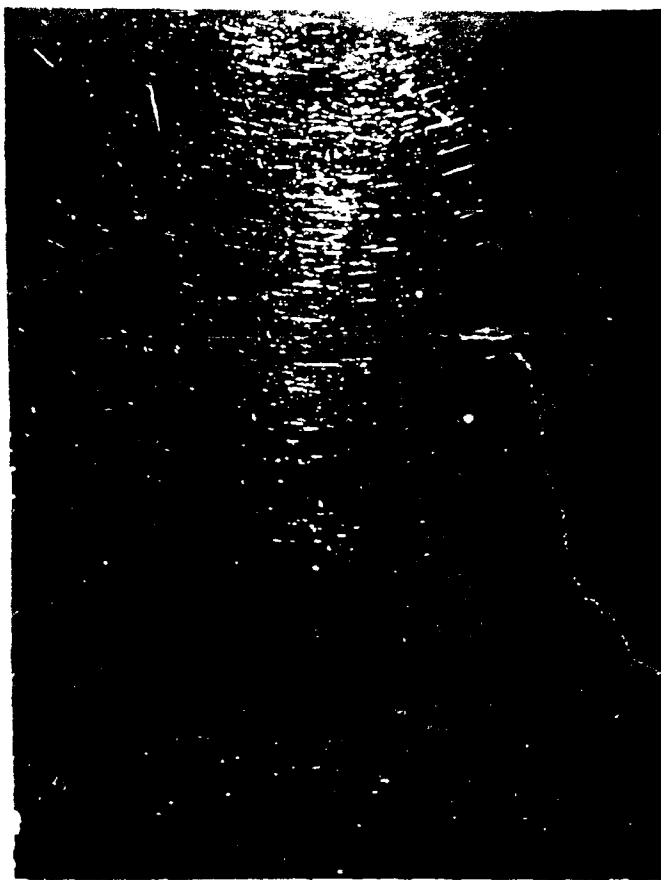
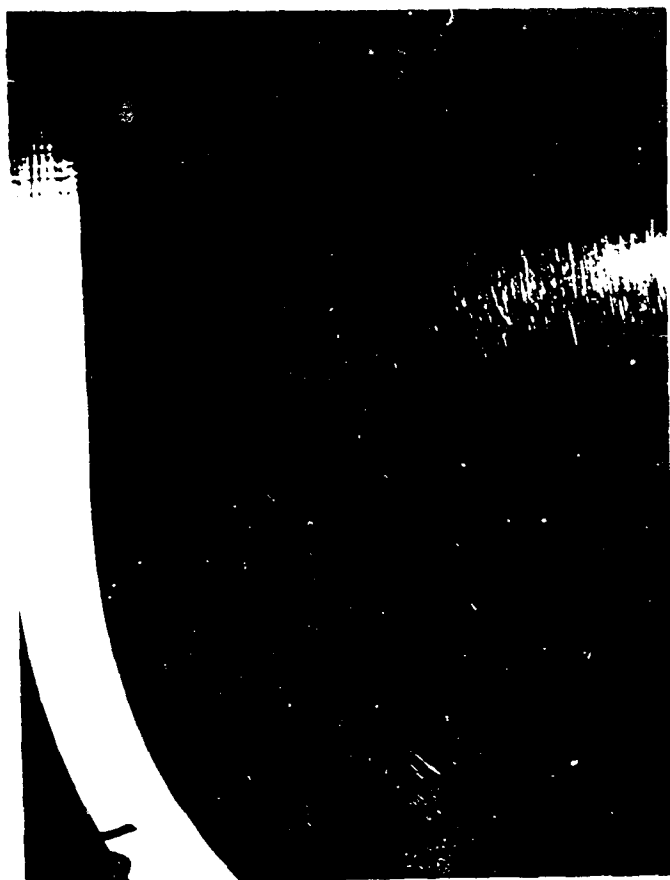
Let's concentrate
on solving problems
not fighting them!



resulted in no visible action, except the window quality is becoming more and more lousy, as you can see on the next photo showing two acrylic cabin windows just after landing from the delivery flight of a brand new aircraft.



Even the aircraft is not
to produce similar
aircraft after the first



The windows have been complained by passengers. Not just the two windows, but all of them installed on the aircraft.

The removed windows are at top, right, and bottom, left position.

The window at top, left position represents the quality of a window taken from the aircraft manufacturers stock, while at bottom, right position the quality of our refurbishment process is demonstrated.

The first reaction of the aircraft manufacturer after receipt of our two windows was absolutely surprising.

Quote

We have evaluated the three passenger windows forwarded. The two windows removed from your airplane do exhibit polishing scratches, the window from DLH stock (which is the refurbished window) did not have polishing scratches.

We are very concerned regarding the quality of our windows and, consequently are initiating a program to determine the optimum method of window surface preparation

Unquote.

This was a real surprise because for the first time the poor window quality was acknowledged and confirmed that action is required.

But this didn't last too long.

Less than three months later everything was back to normal.

The same three windows were now rated completely different.

Quote

We have received and evaluated the three passenger windows forwarded by DLH.

Two windows removed from the airplane had surface scratches which appear to be caused from shipping. Typically, new airplane passenger windows installed at our facility do not have surface scratches of this magnitude

Unquote.

So, again some mystery must have been involved between their facility and our home base.

But the story continues and is becoming more and more unbelievable. Seven months later, this aircraft manufacturer sent us a copy of an engineering report on their polishing scratch evaluation.

The report contains mainly a broad description of scratch patterns, with a clearly noticeable attempt to equalize the quality of all checked windows. To reach that goal, this aircraft manufacturer, having a tremendous and

fantastic resource and laboratory facility even used incredible, but absolutely irrelevant and unscientific test methods.

Small amounts of methyl ethyl ketone (MEK) were allowed to flow across the surface for a few seconds. After the MEK wash a much sharper, more detailed, scratch pattern was revealed. The severity of the scratches was more evident. A similar effect occurs probably on new airplanes after a low number of flight hours, was the suspicion of the aircraft manufacturer.

Instead of using their resources to find answers on all open questions, and finally give recommendations to the window manufacturers to improve the window quality, they seem to use their influence and power to hide everything and to force us - the airlines - to buy more and more disqualified windows from them at a high price level.

They set up the rule, that all windows have to be purchased through them, because they have the responsibility for that major structural part and this is the only way to keep the parts under control.

But the only control they seem to have, is a price control.

Up to now, they always found somebody willing to make windows at a lower price, even that one had absolutely no experience in that business.

Most of the traditional manufacturers had only the choice to produce rubbish at low price or to be out of business.

Just recently, one other aircraft manufacturer issued a letter to all airlines operating their model aircraft, warning them not to use windows from unauthorized sources.

They have not tested such windows and cannot attest to their serviceability and therefore cannot approve the use of such components on aircraft manufactured by them.

They claim to have no knowledge that such components have been subjected to environmental, fail-safe, and fatigue testing as required by the established Federal Aviation Administration procedures and their on design criteria. They hold to this opinion regardless of any FAA Parts Manufacturing Approval or other regulatory agency licensing approval which may have been granted to a vendor.

Things cannot go on like this!

Testing the windows in question and spare windows from that aircraft manufacturer in our facilities, we have to announce that the unapproved windows met all specification requirements, but the windows delivered from the aircraft manufacturer did not.

For quite a period of time a material was used, which I believe, never fulfilled MIL-Spec requirements.

Nearly all windows delivered since about 8 years are believed to have had such an uneven stretch, that the K-factor requirements were never met.

So, I believe it is really time to get together and change the system.

We don't want highly sophisticated windows.

We only like to have windows of the same quality we had some years ago.

Under protection of the aircraft manufacturers, we seem to be unable to receive windows we like to have.

Summarizing the whole fairytale which seems to be more a nightmare, we have to state that, after enforced material adjustment have been made, making the material more susceptible to rough handling and moisture absorption, and the introduction of new materials having the same poor properties, crazing once was created by a legal competitive situation.

Crazing was allowed to spread under the protection of the aircraft manufacturers by non-observance of their own specification requirements and inservice findings.

Or may it have been, that specifications have been adjusted to qualify some poor quality manufacturers?

Today, we have to state that crazing is being caused by some aircraft manufacturers not caring about quality, but dictating so low prices to the window manufacturers, that nobody is able to make a proper window.

But where are the airlines?

Where are their complaints?

Why do they waste so much money?

Why do they keep the existing disqualified system going?

Why don't they show more interest?

What is wrong with them?

Wake up !

I believe that I have done my homework

Now it is time that some others do theirs

Thank you for your attention

Let's get it together



**Failing to communicate
causes mistakes.**

SESSION IV

NEW MATERIALS AND PROCESSES (PART A)

Chairman: W. P. Johnson
Materials Laboratory
Wright-Patterson AFB, Ohio

Co-Chairman: R. J. Skubic
McDonnell Douglas Company
St. Louis, Missouri

Coordinator: R. H. Barrett
General Dynamics Corp.
Fort Worth, Texas

TRANSPARENT COMPOSITE

Raymond J. Skubic

McDonnell Aircraft Company

Transparent Composite
Mr. Raymond J. Skubic
Senior Principal Technical Specialist - Structural Research
McDonnell Aircraft Company, McDonnell Douglas Corporation

Abstract - Progress in developing a method to strengthen transparent materials is presented. The method, for which a patent application has been completed, adds reinforcing glass fibers to the transparency material to create a transparent composite. The research work is being conducted by the University of Missouri (Rolla) Materials Research Center, under MCAIR sponsorship.

The basic theoretical principles relating to a transparent composite are discussed, as are the components which make up the composite, that is, the fibers, interface material and the matrix. Their effects on structural and optical characteristics are addressed. The discussions cover the fiber drawing process, fiber quality and strength as a function of size, the interface and the ability to wet the fiber and form a covalent bond between the fiber and the matrix, and the matrix and its function as a load transfer medium. Test results of bending strength, stiffness and fracture energy at both room temperature and at elevated temperature are presented. The results of optical studies include the effects of fiber size, light incidence angle, and the variation in temperature.

Introduction - Transparency materials with improved structural properties are needed for aircraft applications. Of particular interest for high performance aircraft, are properties which provide bird impact and ballistic resistance and good performance at elevated temperatures. The work described in this paper is directed toward the development of a method to improve the strength of transparency materials. It consists of reinforcing the material through the addition of fibers while retaining its transparent property, that is, forming a transparent composite.

Composite materials are widely used in the aerospace industry because of their structural efficiency. Similar properties can be obtained by reinforcing transparent materials, although retaining optical clarity is an added challenge.

Theoretically, a transparent composite can be developed by using individual constituents which are optically transparent and have a matched index of refraction. In addition, one can use a reinforcing constituent which is very small and visually imperceptible. Ideally it would be smaller than the wavelength of visible light. The small size has an added benefit, in that fiber strength varies inversely with diameter. Therefore smaller diameter fibers are stronger. An optimum composite would have ultrafine reinforcing fibers which match the matrix index of refraction.

This research is funded by MCAIR and is being conducted at the University of Missouri in Rolla (UMR) and at MCAIR. At UMR, the work is under the direction of Dr. Del Day, Director of the Materials Research Center, and Dr. Jim Stoffer, Professor of Polymers and Coatings in the Chemistry Department.

**"EXPORT AUTHORITY
22CFR 125.4(b)(13)"**

A sample specimen is shown in Figure 1. The specimen on the right side of the Figure contains a quantity of fibers equal in volume to the group shown on the left in the figure (20000 fibers of 15 micron diameter). A similar group was chopped and blended into the monomer to produce the specimen in the figure. The chopped fiber amounts to 3.8 percent of the specimen volume.

20,000 Fibers
 $d \approx 15 \mu\text{m}$

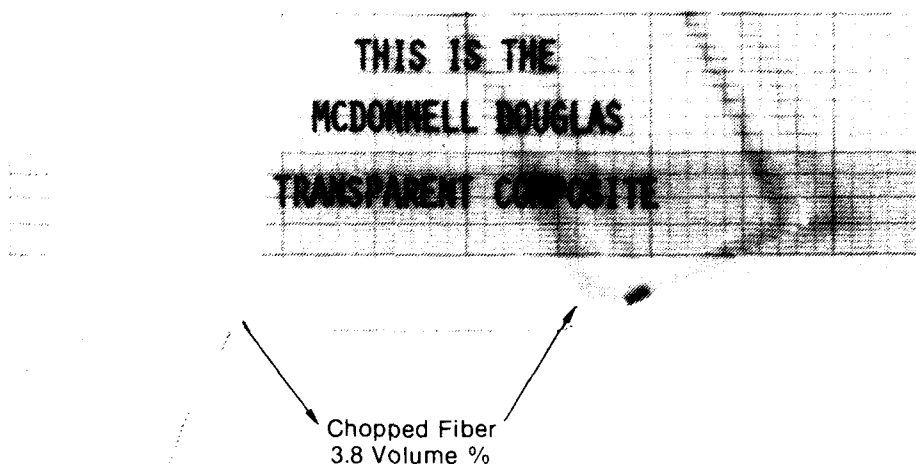


Figure 1. BK-10 Fiber Reinforced Acrylic

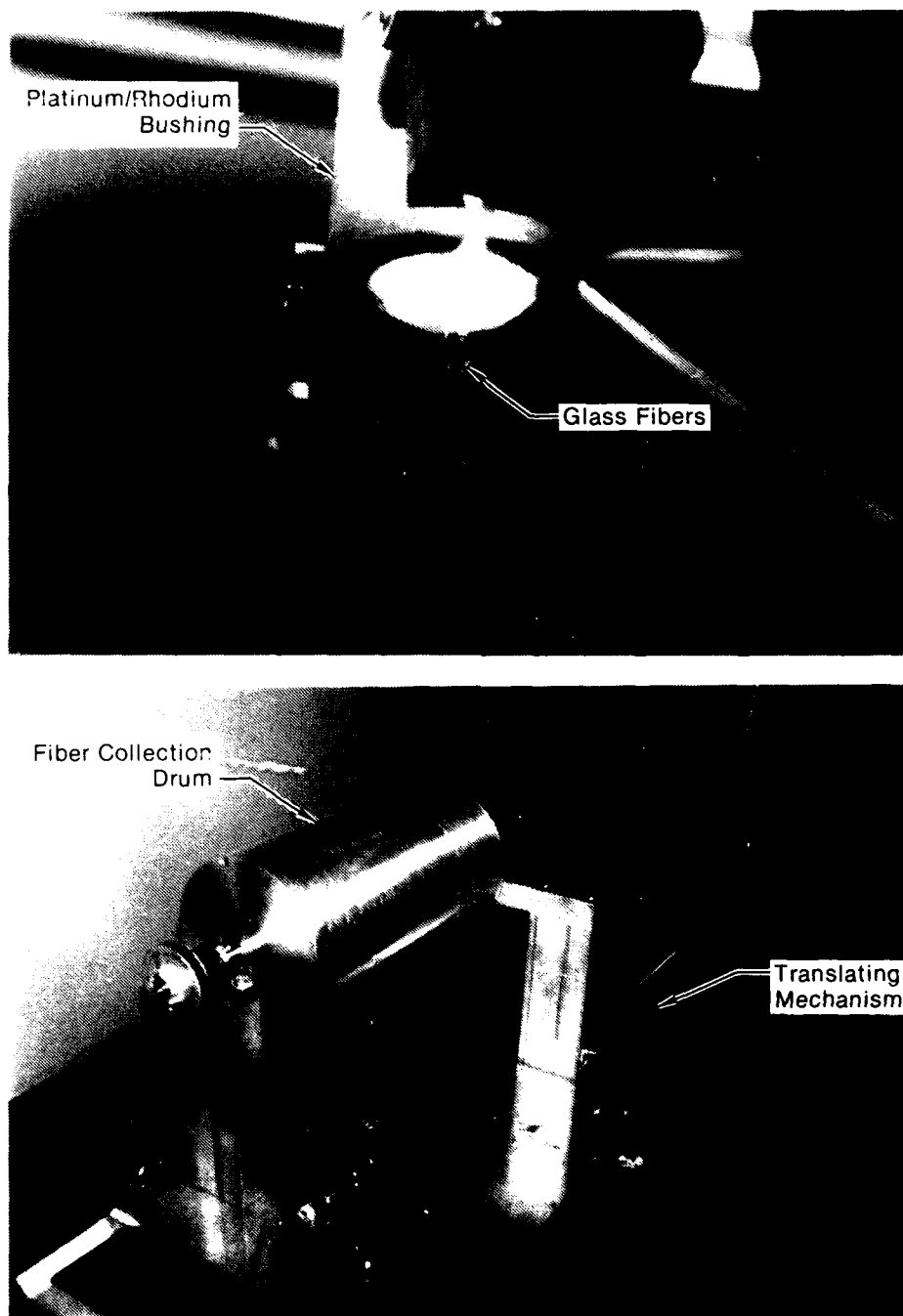
GP83-0450-6

This paper discusses the process used to fabricate the specimens in the laboratory, the constituents of the composite, the results of mechanical property tests at room and elevated temperatures and the results of some optical studies.

Constituents - Three components make up the composite; the fiber, the interface material, and the matrix. Each of these contributes to the mechanical and optical properties of the composite as discussed below.

Fibers - The fibers used in this study are produced from a borosilicate optical glass. Their index of refraction, at one particular temperature, closely matches that of the polymer selected for the matrix. In this work, two types of glass have been studied. Their designation is BK-10 and FK-5. BK-10 glass was used for most of the work. Its index of refraction in bulk form is 1.498 at the sodium D line.

Figure 2 shows the fiber production equipment. It consists of a platinum rhodium bushing, equipment to control the resistive heating of the bushing, and an aluminum drum, 22 cm in diameter, which is used to collect the fibers. Also under evaluation is a coating bath which can be used to coat the fibers.



GP83-0450-7

Figure 2. Fiber Production

To produce the fibers, the glass, which is purchased in 5 pound billets, is fractured into marble sized pieces and placed in the bushing. The bushing material is inert to the glass at elevated temperatures. As shown in Figure 2, it contains five orifices or nozzles through which the glass is extruded into fibers. The glass is initially heated to a temperature above the melting point, about 1320 degrees C. Gas bubbles trapped in the melt, rise to the surface and escape. Once the melt is bubble free and chemically homogeneous, the temperature is reduced so that the melt viscosity is suitable for fiber pulling.

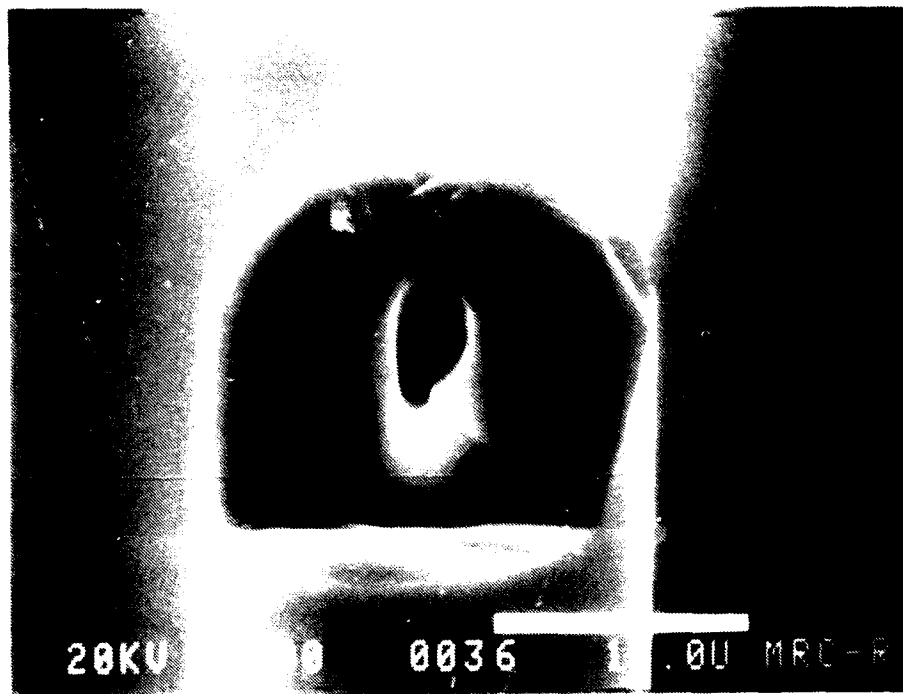
The ends of the fibers are attached to the drum which can be rotated at various speeds and can be translated parallel to its rotational axis. By controlling the drum speed and the temperature of the glass melt, one can control the diameter and, to some extent, the refractive index of the fibers. Fibers with the proper index of refraction were produced with diameters between 10 and 70 microns.

As the drum rotates and collects fibers, it is translated along its rotational axis so that a strip of fibers is produced. When the proper width is obtained, the process is stopped. An epoxy ribbon, about one-half inch wide, is applied at two locations on the fiber strip, about two centimeters apart. The fibers are cut between the two epoxy ribbons and the fiber strip is removed from the drum. In this way a strip of fibers about 65 cm long is produced and held intact by the epoxy ribbons at each end.

Producing a quality fiber is important. Obviously it must have the proper index of refraction, but equally important are its structural properties, since they are the basis of the composite strength. Theoretically, silicate glasses should be very strong. Their chemical bond strength is very high. Various theories predict the interatomic ultimate strength to be between 1,500,000 and 6,500,000 psi. Typically, however, stress concentrations caused by material flaws, significantly reduce the ultimate strength. To optimize the strength, the material must be as flaw free as possible. Producing fibers of very fine diameter, with little surface area, is a means of reducing flaw size and is in fact the basis of current composite material's strength.

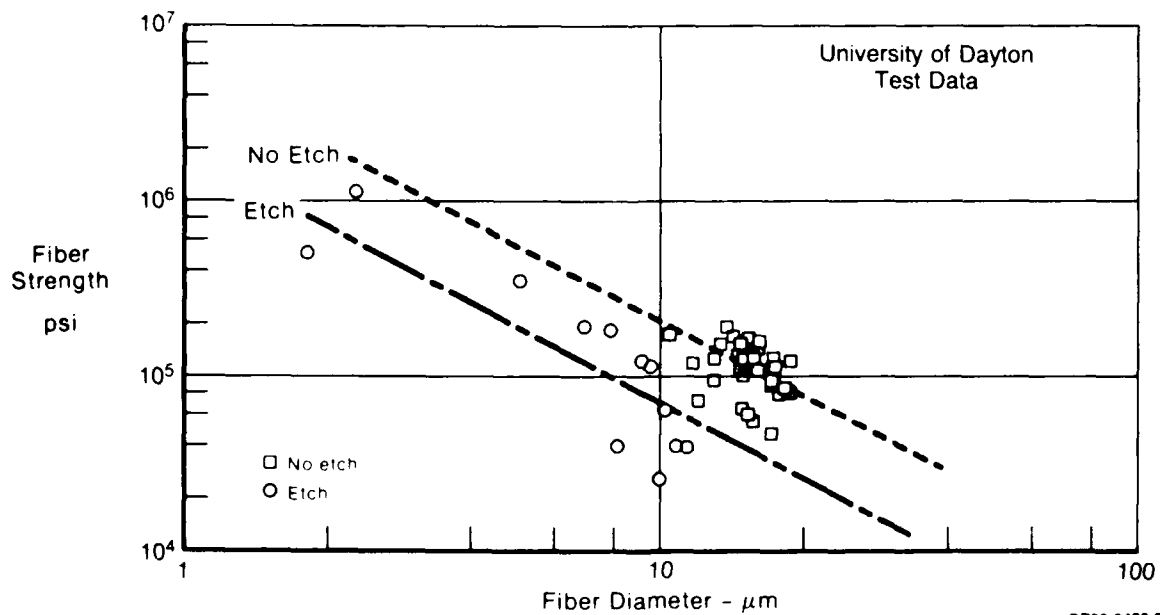
An example of a flawed fiber is shown in Figure 3. A long cylindrical air channel was drawn into the fiber because of an ultrafine bubble in the melt. This condition would reduce fiber strength and optical quality. In particular, the optical quality of the composite which depends on the refractive index match of the components, is affected because trapped air or gas within the fiber has a refractive index much different than the glass.

Fibers produced in our research were evaluated at the University of Dayton Research Institute, at UMR and at MCAIR. The results of structural tests of individual fibers are shown in Figure 4. A definite trend of increased strength with reduced diameter is evident and a similar effect occurs for the elastic modulus. These data represent fibers produced early in our work and more recent specimens appear to be stronger because of better fiber quality.



GP83 0450-5

Figure 3. Flawed Glass Fiber



GP83-0450-21

Figure 4. Fiber Tensile Strength Results

We also studied the effects of coating on the fiber. Protective coatings can reduce flaws created by atmospheric moisture and abrasive handling. Figure 5 compares the strength of coated and uncoated fibers and indicates an increase of more than 100% in fiber strength as a result of two different coatings.

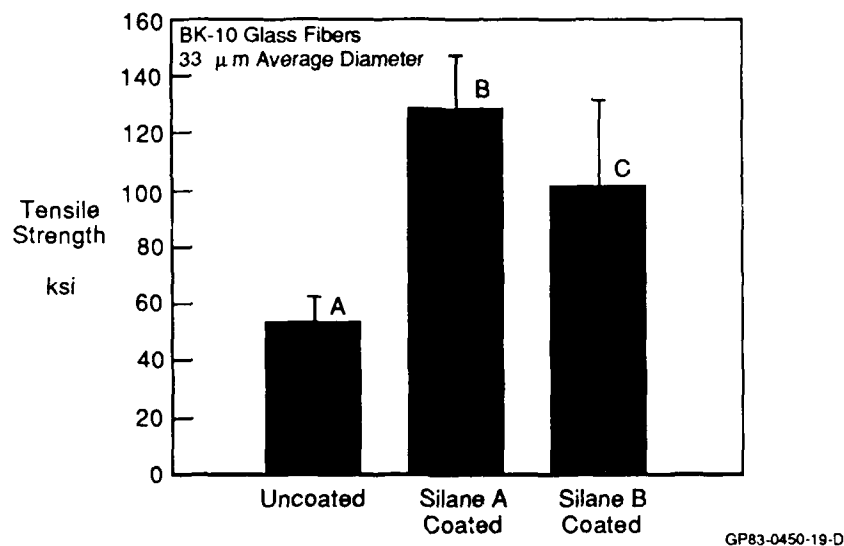


Figure 5. Glass Fiber Tensile Strength With Coatings

Interface Material - The interface material is important for the structural and optical properties of the composite. Both properties rely on the complete wetting of the fiber. An optimum interface material forms a covalent bond between the fiber and the matrix over 100% of the surface of each fiber.

Structurally, the interface serves to transfer load, through shear, between the matrix and the fiber. Obviously adequate shear strain and strength are needed and, to a certain extent, the elasticity of the interface is important. Discontinuities in the interface or complete gaps result in failure initiation sites or complete pullout of the fibers.

Optical properties are affected by the wetting property of the interface and by its thickness. Poor wetting results in trapped air or gas between the fibers and the matrix. Because of the large difference in index of refraction between the trapped air or gas and the other constituents, optical transmission is reduced. If the thickness of the interface is less than the visible wavelength, its index of refraction is less important. Therefore, a monolayer of interface material is the goal.

The exact coating materials are proprietary and continue to be studied. However, we have evaluated several typical silane coupling agents along with other contributing compounds. The effect of the coating was obtained by examining BK-10 fibers in a PMMA matrix with the Scanning Electron Microscope. Figure 6 shows the fracture surface of a fiber reinforced specimen without coating. Poor wetting is indicated by the fiber pullout and the air gaps around the fibers. Figure 7, however, shows excellent wetting using an appropriate coating material. We are continuing to study a variety of methods to apply the coating.

Matrix - The matrix material used in this study is poly(methyl-methacrylate). It is one of the few materials currently used in today's transparency systems and conveniently adaptable to laboratory study. The intent of the research is to develop a concept which is applicable to any polymer system and, for use in high performance aircraft, the preferred system is one with good elevated temperature properties.

The function of the matrix in a composite is to distribute and transfer load into the reinforcing fibers. On the basis of compatible strains, the high strength fibers react the majority of the load. Therefore the shear capability and stiffness of the material is important particularly at temperature extremes.

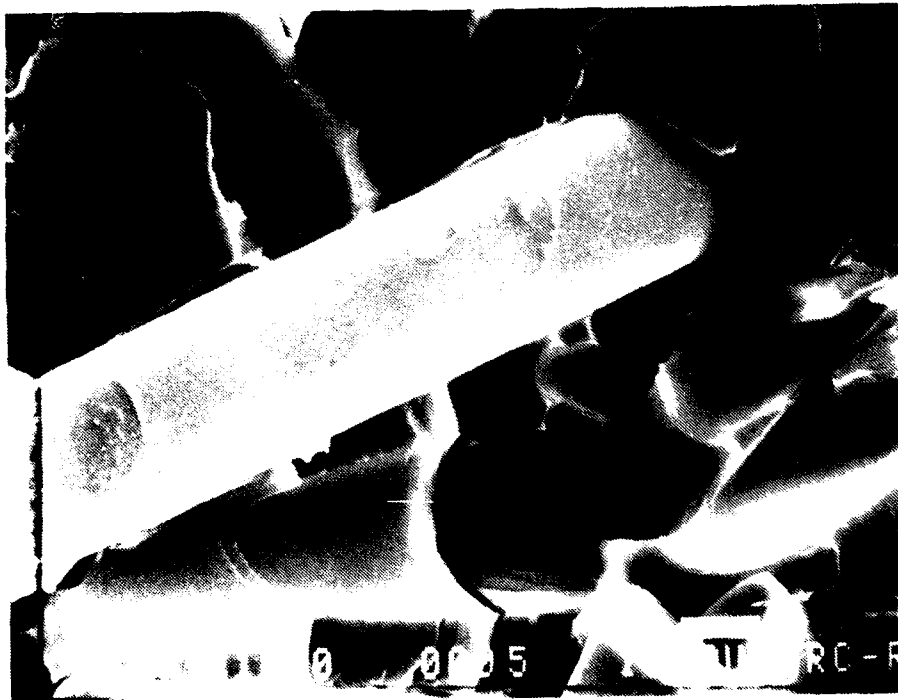
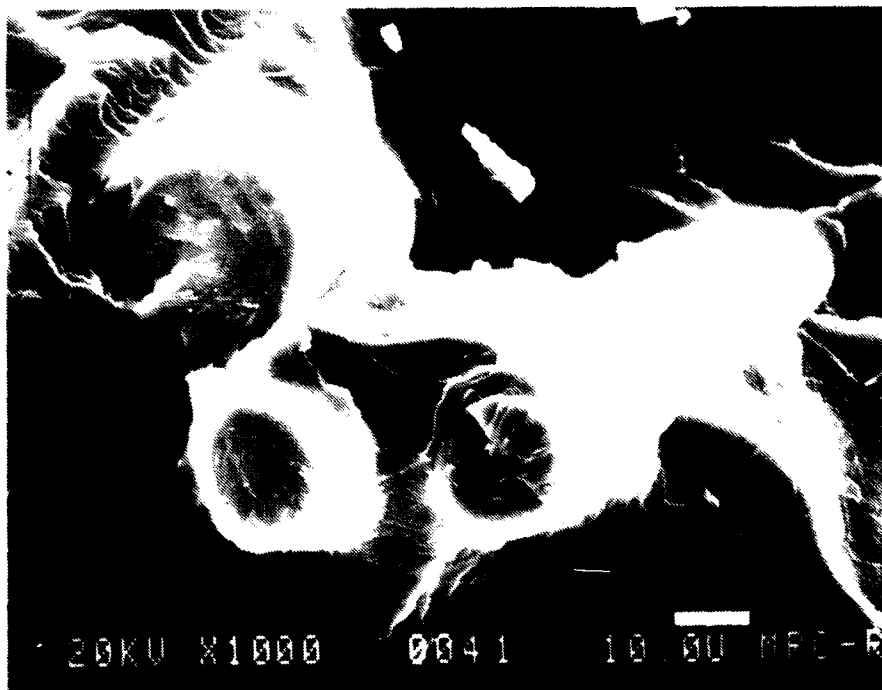


Figure 6. Fracture Surfaces of PMMA Containing Uncoated BK-10 Glass Fibers



GP83-0450-3

Figure 7. Fracture Surfaces of PMMA Containing Coated BK-10 Glass Fibers

The reinforcing material is intended to increase the bending strength and stiffness of the matrix and depending on the failure mode, the damage tolerance as well. Since all polymers contain inherent flaws, the latter property is a major concern, particularly for impact loadings. The fibers should act as crack arrestors or deflectors delaying crack propagation and increasing the work of fracture.

Specimen Preparation - The laboratory specimens are fabricated in a mold which consists of two glass side plates, a plastic bag liner and a clamping system. The glass plates form the sides of the mold and ensure flat and parallel surfaces on the specimens. The bag liner material is heat-sealable and nonreactive with the monomer. It serves as a barrier between the monomer, which contains the coupling agent, and the glass sides of the mold. The clamping system is used to maintain some pressure between the plates to account for shrinkage during the polymerization process and to produce reasonably parallel surfaces.

Various steps are required in the fabrication process. The fiber strips, produced as described previously, are stacked with the desired volume percent and the stack is glued at each end with epoxy. All of the fibers are parallel. The stack is inserted into the plastic bag. PMMA monomer containing initiator and coupling agents is added. The bag is partially sealed, placed in a vacuum desiccator, and degassed at 200 mm Hg for one hour to remove gases dissolved in the monomer and adsorbed on the fibers.

Ultrasonic vibration is used to dislodge gas bubbles which tend to cling to the fibers. After degassing, the bag is sealed and clamped between the glass plates. The entire assembly is suspended vertically in a water bath until polymerization is complete. After polymerizing, the specimens are removed from the mold and given a post cure heat treatment to ensure complete polymerization.

Mechanical Properties Data - Three point bending tests were used to evaluate mechanical properties. Specimen geometry and loading rate were based on recommendations in ASTM standard #D790-86. The specimens were 10 mm wide and 5 mm thick. The span length was 80 mm. All contained unidirectionally oriented continuous fibers.

Figure 8 summarizes the room temperature bending strength as a function of fiber volume percent for various fiber diameters. The data reflect three sample groupings which were fabricated at different times. Line A represents data for 13 micron fibers. Line B represents data which contained 10 or 65 micron fibers. The specimens used for group C contained either 12, 42 or 56 micron fibers. The dashed lines are ± 3 sigma confidence limits for the B group specimens.

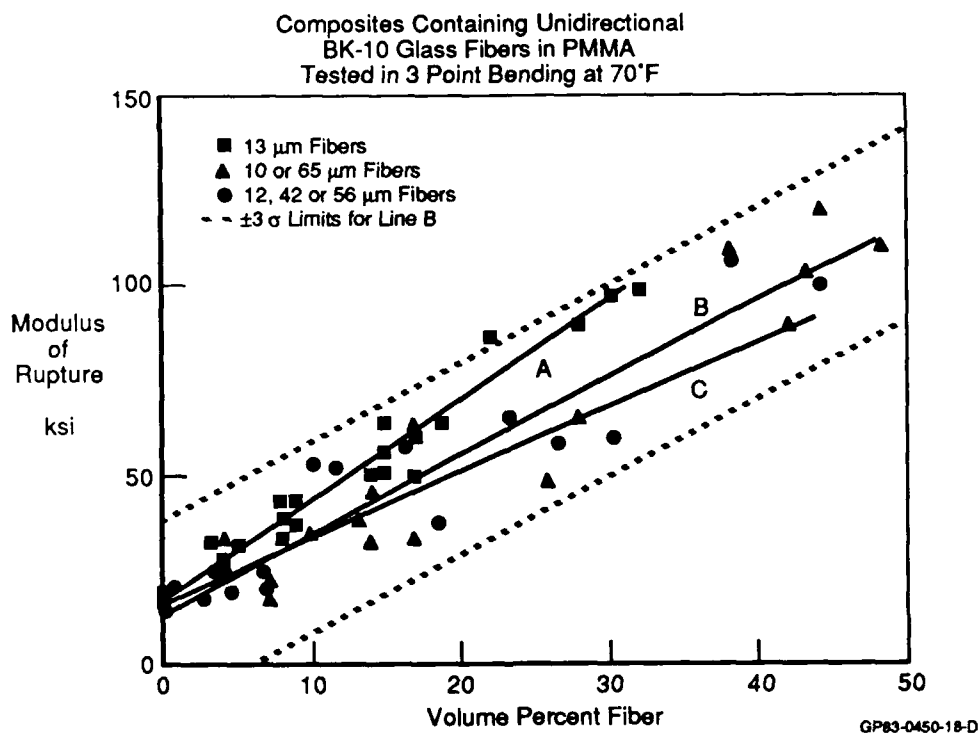
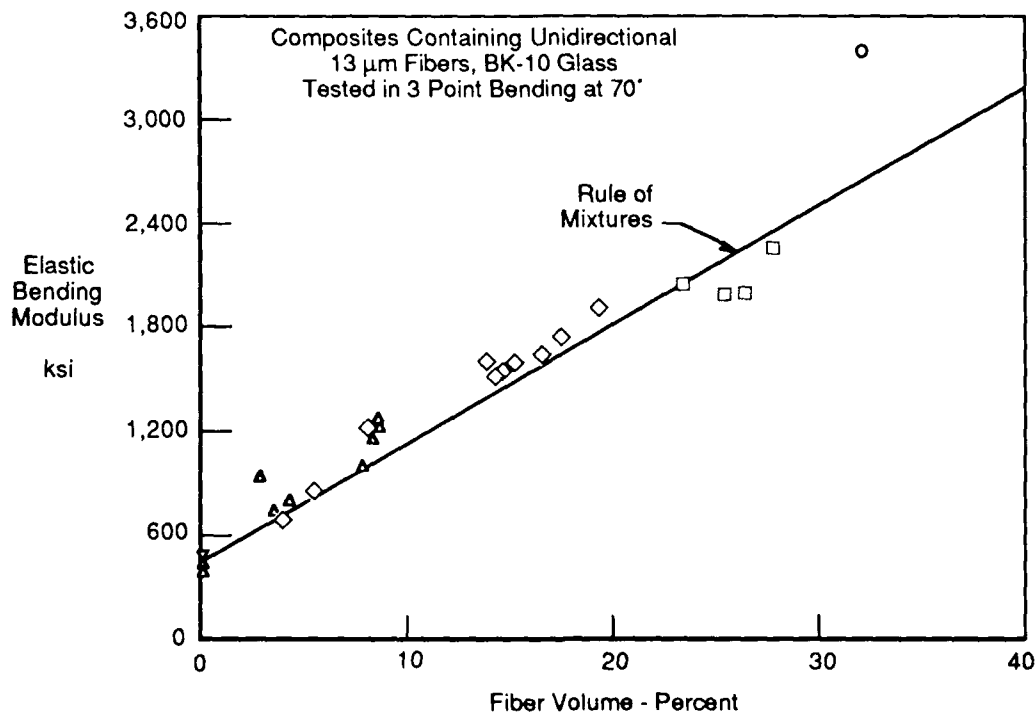


Figure 8. Composite Bending Strength

The results indicate a significant increase in bending strength in the composite relative to the neat resin PMMA. The effects of fiber diameter over this range seem small, because all of the data lies within the B group ± 3 sigma limits. The scatter may be due to fiber or composite specimen quality. Considering the maximum potential strength of the fibers, even greater composite strength is anticipated.

Similar improvement is noted in the bending modulus as shown in Figure 9. These data reflect the 13 micron fiber specimens. Again substantial increase is noted as a function of fiber volume. The modulus data also correlates well with predictions based on the rule of mixtures using a glass modulus of 7,500,000 psi.

Another important property is the work of fracture, particularly at the strain rates related to bird impacts. The work of fracture is defined as the energy used to create a new fracture surface in exchange for stored elastic energy. It is calculated by dividing the area under the load displacement curve by the cross-sectional area of the beam. To date all of our testing has been at low strain rates, but the trend is of interest. Figure 10 shows the variation in work of fracture for specimens containing one of three different fiber diameters. The scatter is fairly large, but the data clearly indicates the expected increasing trend. Work of fracture data at bird impact strain rates would be more useful and these tests will be conducted when larger specimens are fabricated.



GP83-0450-17-D

Figure 9. Composite Bending Modulus

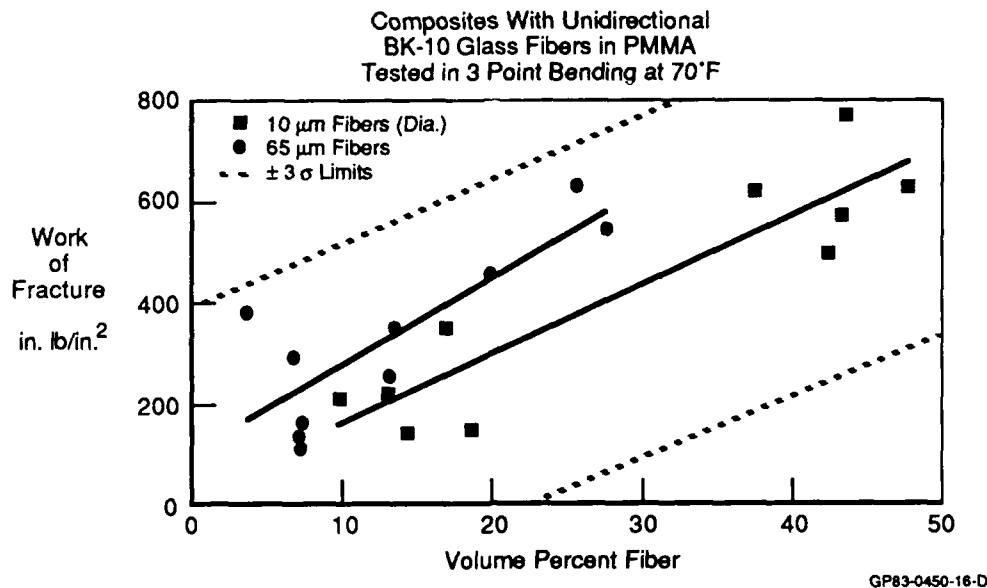


Figure 10. Composite Work of Fracture

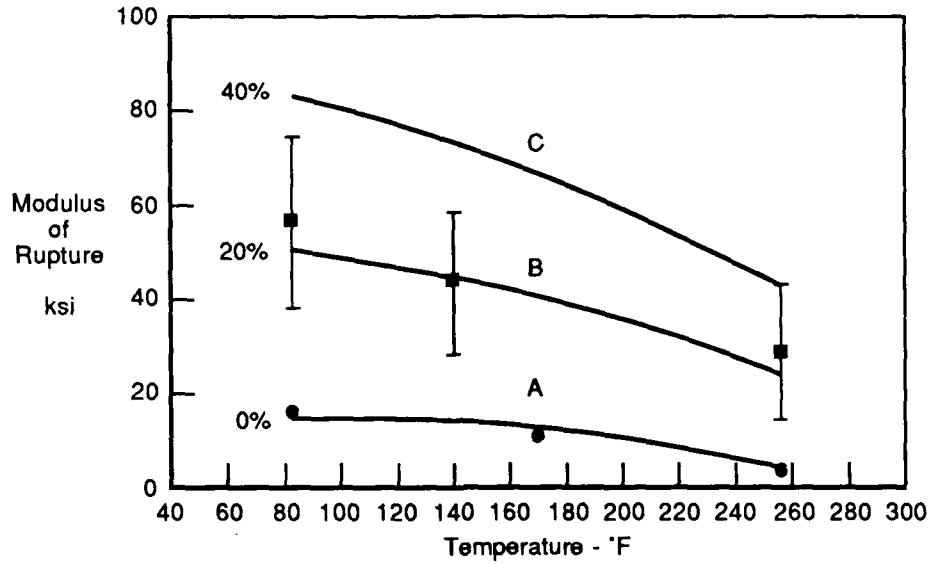
Elevated Temperature Mechanical Properties - To help evaluate the structural behavior of the composite at elevated temperatures, a computer aided experimental design package called ECHIP was used. This package provided a means to determine a relationship between fiber content and mechanical property variations with temperature based on a minimum number of specimens. Specimens were tested at five different temperatures up to 257 degrees F.

Figures 11 and 12 show the variation of bending strength and modulus versus temperature for several fiber volume percentages. The curves reflect a multiple quadratic regression analysis of the test data based on the experimental design package. Line B represents composites with fiber contents between 18 and 22 volume percent. The error bars indicated for the data on line B represent ± 3 sigma limits based on the residual standard deviation of the data with the regression line. Line C is calculated from the expression generated from the regression analysis because specimens were not available for this volume percent.

As expected, the bending strength and modulus decreased with increasing temperature. However, the results in comparison to the unreinforced resin system are encouraging as far as demonstrating the benefit of the process. Even above the glass transition temperature the reinforcement appears beneficial.

Optical Studies - Four parameters are important for the development of an optically transparent composite. These are, the index of refraction of the constituents, the angle of incident light to be transmitted, the quality of the fiber and the interface material. The latter two have already been discussed.

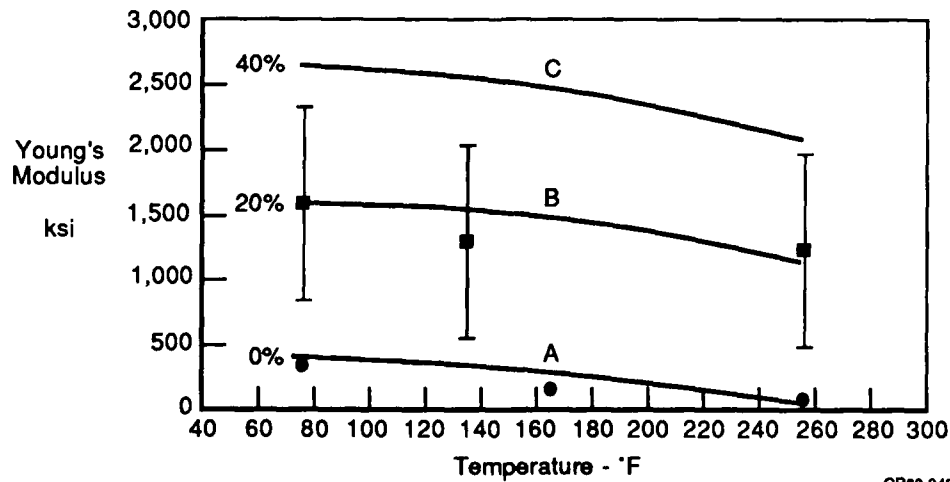
Composites Containing Unidirectional
12, 42 or 56 μ m Diameter
BK-10 Glass Fibers in PMMA
Tested in 3 Point Bending



GP83-0450-15-D

Figure 11. Composite Bending Strength at Temperature

Composites Containing Unidirectional
12, 42 or 56 μ m Diameter
BK-10 Fibers in PMMA
Tested in 3 Point Bending



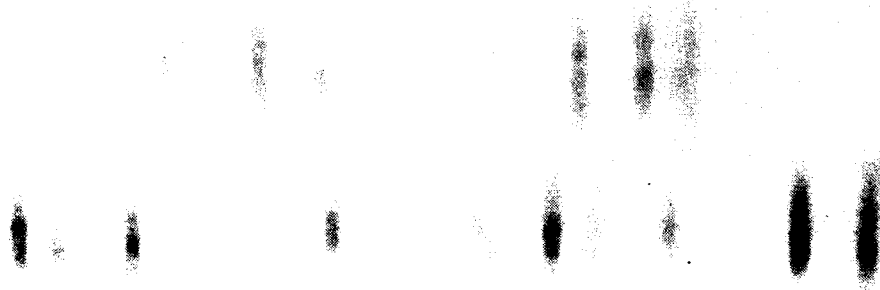
GP83-0450-14-D

Figure 12. Composite Bending Modulus at Temperature

The angle of incident light is important because the fibers have a circular cross section. Therefore light is incident on the surface of the fibers between an angle of zero degrees (where it is normal to the fiber cross section) and 90 degrees (where it is tangent to the fiber cross section). At high angles of incidence, there can be some distortion of the light ray depending on the difference in index of refraction of the fiber and matrix and the degree of fiber wetting. With some mismatch in index of refraction, an image close to the composite is viewed clearly. However, as the image is moved away, it becomes distorted. Figure 13 shows this difference for one of the composite specimens with 25 volume percent of reinforcement and a refractive index mismatch of .005. It should be noted that the specimen in Figure 13 was produced early in our research and the distortion shown in the figure may be due to incomplete fiber wetting or to other interface anomalies as well as to the circular cross section of the fiber. In fact our most recent work indicates as much.

**MCAIR
RESEARCH**

**MCAIR
RESEARCH**



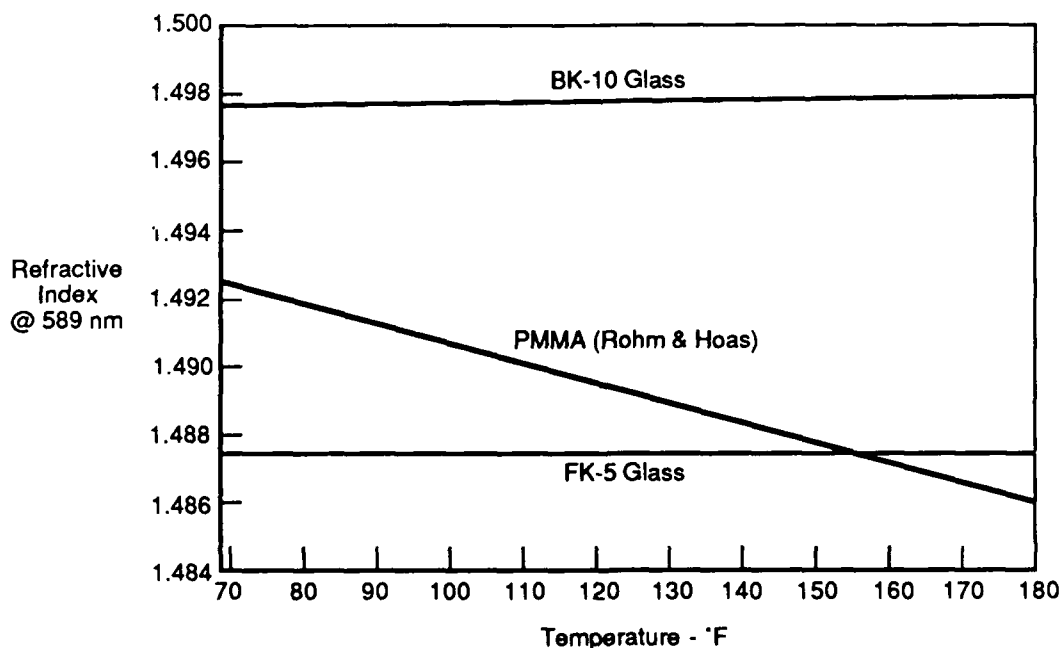
GP83-0450-1

Figure 13. MCAIR Research

The other factor of importance, is the variation of refractive index with temperature. Figure 14 compares this variation for the acrylic matrix and the two glasses used in this study. It shows that the index of refraction for the polymer varies significantly relative to that of the glass, which is insensitive to these temperatures. The mismatch variation is seen to be .0000577 per degree F.

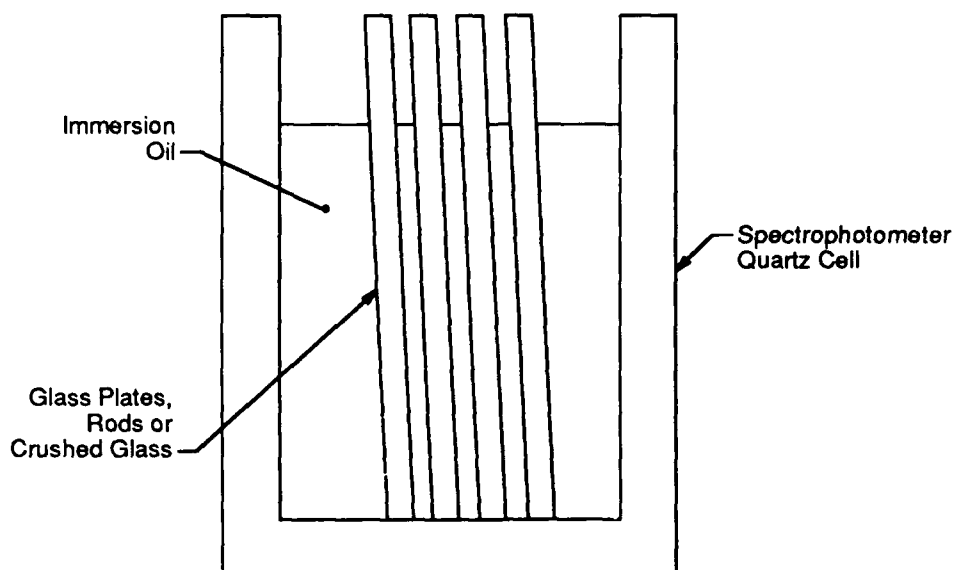
The two glass systems used in this study were selected because they matched the polymer at some point in the temperature range of interest. That range is based on the windshield temperatures of a typical high performance combat aircraft. Depending on the flight profile, the windshield temperatures typically vary over a range of 350 degrees F or ± 175 degrees about an appropriate mean value. Based on the variation shown in Figure 15, the range in index of refraction of interest is $175 \times .0000577$ or about $\pm .01$.

To study the effects of optical transparency in a composite, an experimental model using a spectrophotometer was designed. Through this system the percent of light transmission was measured over the visible spectrum for models of composites. These models contained flat plates, crushed glass and right circular cylinders of a known index of refraction and immersion oils of various refractive index values. The index of refraction of the glass was 1.523 and the values for the five oils used were 1.480, 1.500, 1.523, 1.540 and 1.560. Quartz spectrophotometer cells were used to contain the glass and oil composites. The setup is shown schematically in Figure 15.



GP83-0450-13-D

Figure 14. Refractive Index vs Temperature



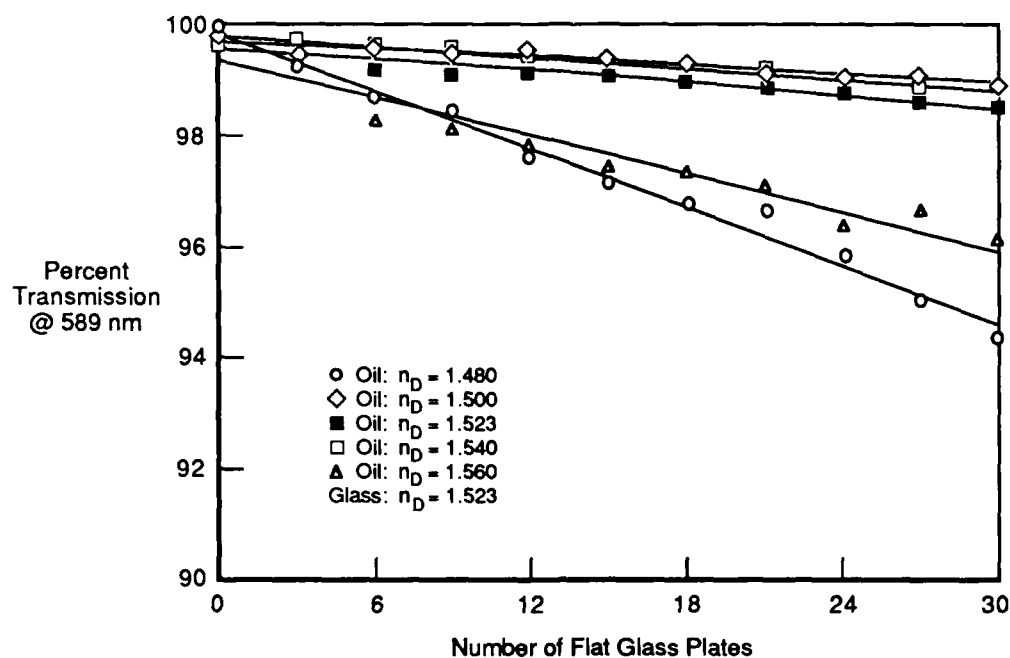
GP83-0450-12-D

Figure 15. Schematic of the Transmission Model

The variation of light transmission at 589 nm (sodium D line) as a function of glass volume for flat plates is shown in Figure 16. In this case the incident light is normal to the surface of the plates. It shows a decrease in transmission as the glass volume and number of surfaces is increased. However, even at the maximum glass volume, which with 30 plates is about 30%, the transmission loss is very small.

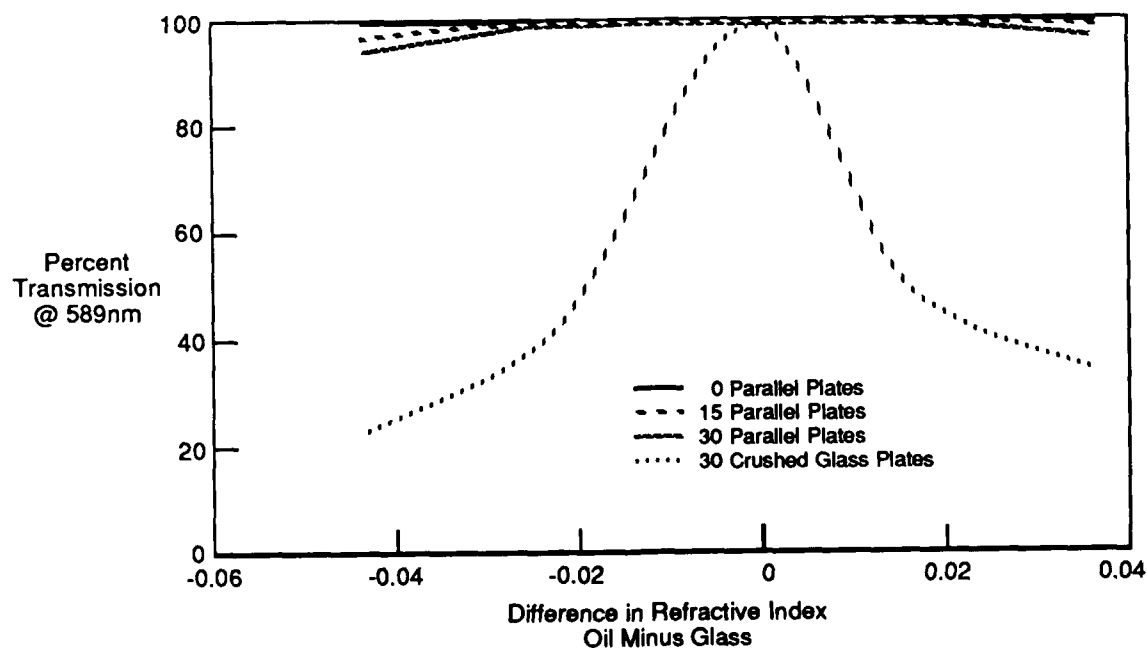
To determine the effect of random incident angles of light, the above procedure was repeated with 30 glass plates crushed and placed in the immersion oils. The result is shown in Figure 17. This data clearly shows several points. The transmission for systems having a matched or nearly matched index of refraction is high regardless of the angle of incident light and is not very sensitive to the volume percent of the glass. However, it decreases dramatically for larger incident angles if the indices are mismatched. Figure 18 provides a visual example of these points.

This experiment was also used to model a system more nearly like the composite specimens, ie, one containing fiber-like shapes, whereby one could determine the effect of the fiber circular shape and size. Long, thin cylindrical rods of two different set of diameters were used for this. As with the glass plates, transmission was measured for the range of mismatch in index of refraction and for various volume percentages of rods.



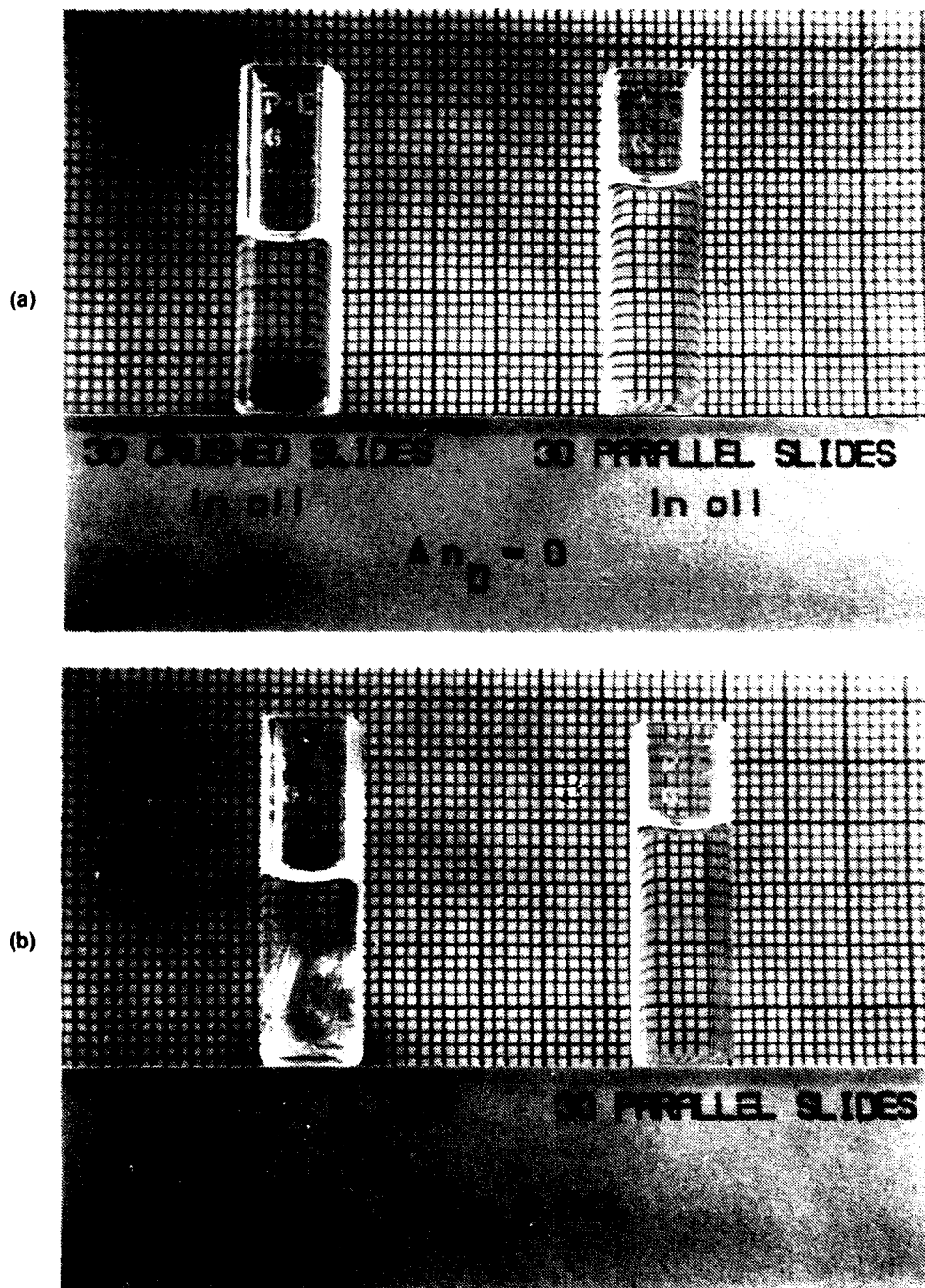
GP83-0450-11-D

Figure 16. Transmission With Zero Degree Incident Light and Refractive Index Mismatch



GP83-0450-10-D

Figure 17. Light Transmission With Random Incidence and Refractive Index Mismatch

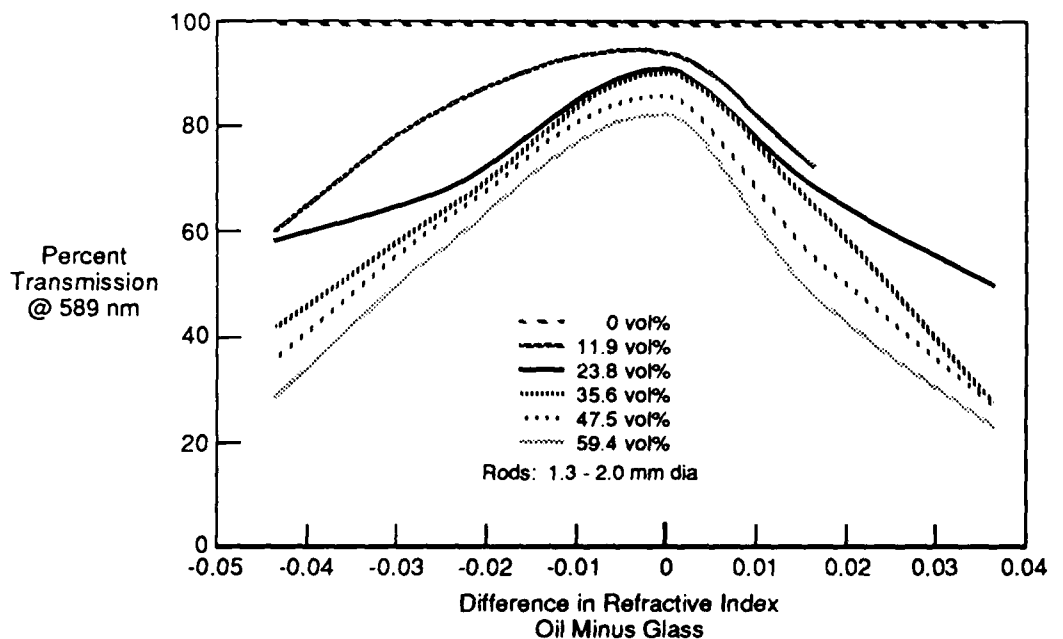


GP83-0450-2

Figure 18. Light Transmission as a Function of Incidence Angle and Refractive Index

Figure 19 shows the results for rods whose diameter averaged about .79mm. This data again shows the benefit of retaining a close match in index of refraction between constituents in a composite. For mismatched values of refractive index between $\pm .01$, and glass volumes up to 35%, the transmission is relatively good. Greater mismatches rapidly degrade the transmission for any significant volume percent. For rods of smaller diameter the effect is more pronounced. The transmission is degraded with smaller rods because many more surfaces are involved for the same volume percent.

The optical transmission of the structural specimens with fine diameter fiber reinforcement further demonstrates the effect of fiber diameter. Figure 20 presents the transmission measurements of some of the structural specimens with fiber diameters of 12, 42 and 56 microns. This is room temperature data using BK-10 fibers whose index of refraction is mismatched with respect to the polymer by .005. At 25 volume percent, the transmission is reduced to 60% for the specimens with the largest diameter fibers. However, it is important to reemphasize that the transmission may be influenced by factors relating to fiber wetting as much as fiber size. If this is the case, and our recent work seems to verify this, optical clarity will improve significantly with better fiber wetting.



GP83-0450-9-D

Figure 19. Light Transmission Through Glass Rods as a Function of Volume Percent and Refractive Index

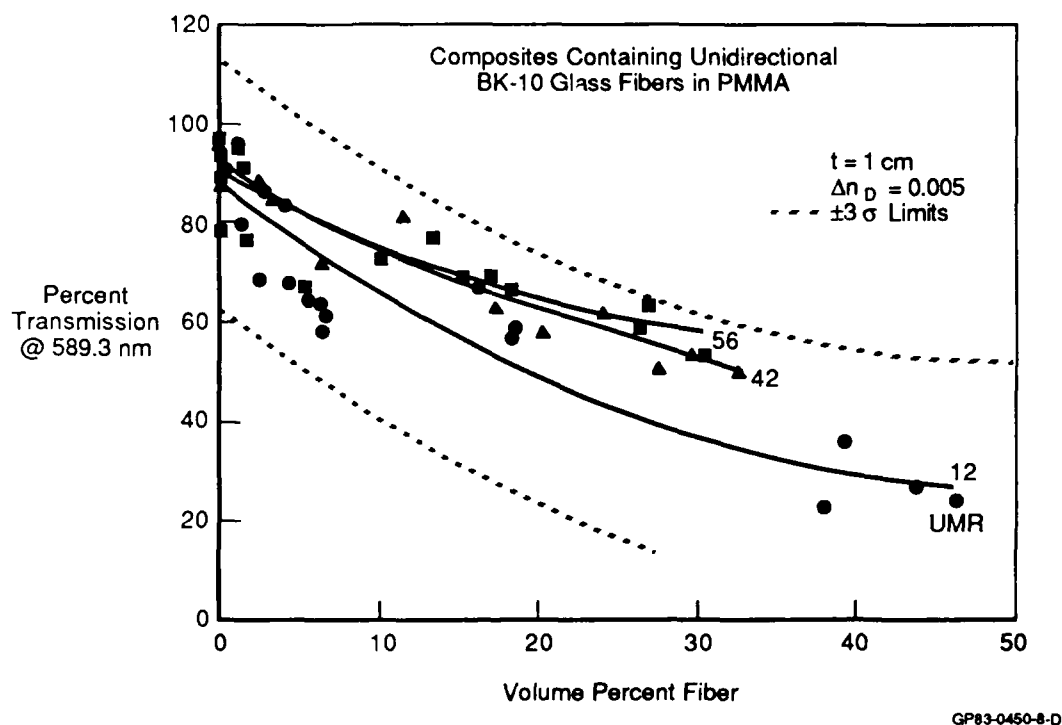


Figure 20. Light Transmission Through Composite Specimens

The effect of fiber size and index of refraction mismatch is summarized in Figure 21 for a glass volume of 25%. The data includes optical transmission results of the model study and the fiber reinforced composites from Figure 21. Also shown is an estimated curve for a refractive index mismatch of .01. These data indicate that using the fine diameter fibers, which provide optimum strength, poor optical quality results, at least for this percentage of fiber volume and the processing used to date.

Summary - The mechanical properties of the transparent composite material were significantly greater than the unreinforced polymer. These properties are enhanced by the interface material in the composite which forms a covalent chemical bond between the fiber and matrix. The increase in properties is evident in both room and elevated temperatures. The properties evaluated in the current work consist of bending strength, bending stiffness and work of fracture.

The optical clarity of the composite system depends on the refractive index values of the constituents and their variation with temperature, the degree of fiber wetting, the homogeneity of the fiber, the fiber geometry and the volume of fiber used to reinforce the matrix material.

Additional work is underway to improve the optical quality while retaining the increase in structural properties. This includes changes in the processing and evaluation of various interface materials. In addition, we are pursuing polymers for this study which have a higher elevated temperature capability than the PMMA.

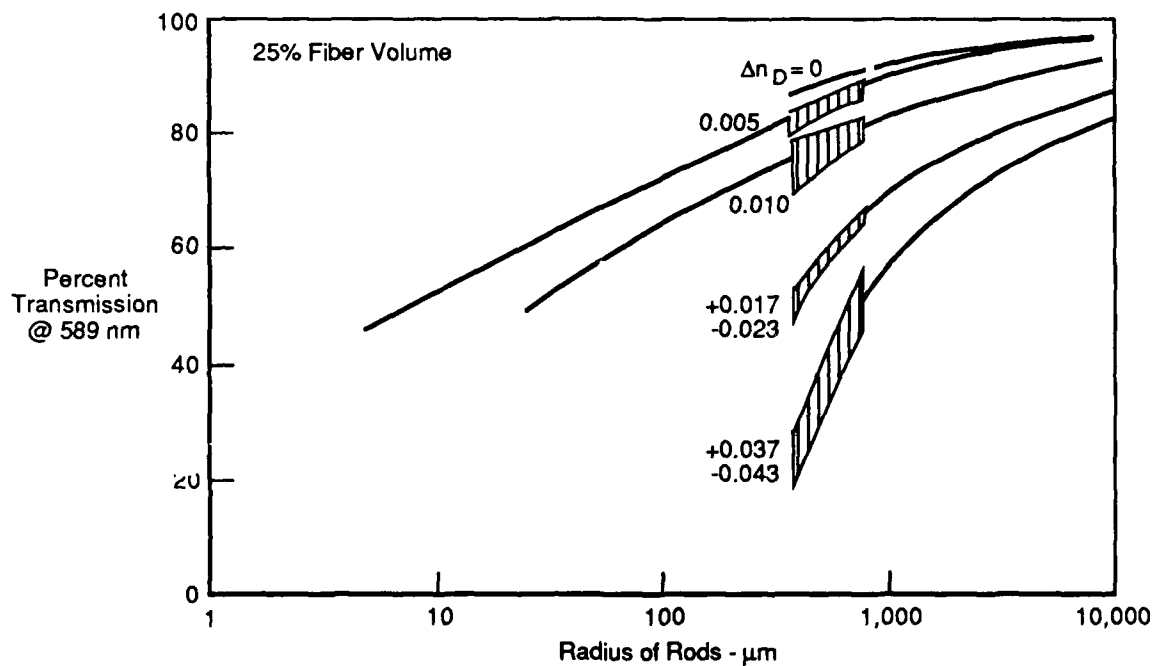


Figure 21. Trends in Light Transmission as a Function of Reinforcement Radius and Refractive Index Mismatch

THE EFFECT OF ION BEAM PROCESSING ON TRANSPARENT PLASTICS

I. H. Loh
P. H. Lu
R. A. Moody
P. Sioshansi
Spire Corporation

T. J. Reinhart
AFWAL/MLSE
Wright-Patterson Air Force
Base

THE EFFECT OF ION BEAM PROCESSING ON TRANSPARENT PLASTICS

I.H. Loh, P.H. Lu, R.A. Moody and P. Sioshansi
Spire Corporation
Patriots Park
Bedford, MA 01730

and
T.J. Reinhart
AFWAL, MLSE
Wright-Patterson Air Force Base, OH 45433

ABSTRACT

Surface chemical and physical modifications of polymers via ion beam processing have shown promise for achieving very desirable increase in chemical and abrasion resistances, with the added potential for achieving the desired surface electrical characteristics by the proper choice of ion beam processing conditions. The resulting properties could be explained by the combined effects of radiation chemistry and chemical replacement reactions.

INTRODUCTION

Ion implantation has been a firmly entrenched technology in the semiconductor industry since the 1970s and over the past decade has been increasingly used as a means of modifying the surface properties of metals. Most notably, improvements in wear and corrosion resistance of ion implanted metals have been observed and documented for many different alloys. Some applications, including Ti alloy orthopedic prostheses and precision aerospace bearings, have now proceeded through trial stages to pilot and full-scale production of ion-implanted parts. Similarly, in the past few years, several research groups have experimented with ion implantation to improve surface properties of polymers via ion implantation. M. Dresslhaus, et al.[1] at MIT, T. Venkatesan, et al.[2] at Bell Laboratories, and D.C. Weber, et al. [3] at the Naval Research Laboratory have pioneered research using ion implantation of polymers primarily to produce electrically conductive material potentially for use in the microelectronics industry. There have been, however, very few investigations of other properties modified by the effects of ion beams on polymeric materials.

In this study, we report our efforts in the area of ion implantation processing of polymer surfaces. Surface chemical and physical modification of polymers via ion beam processing have shown promise for achieving very desirable increases in chemical and abrasion resistance, with the added potential for achieving the desired surface electrical characteristics by the proper choice of ion beam processing conditions.

EXPERIMENTAL

Substrate Materials

Polymer films, such as polyimide (Kapton-H, from DuPont), polyphenylene sulfide (PPS from Phillips), polyethylene terephthalate (Mylar from DuPont), and polycarbonate (Lexan from General Electric), were selected for ion implantation study.

Ion Implantation

The equipment used in ion implantation is based on ion acceleration and mass separation technology. Ion implantation can be divided into three major stages: 1) production of positive ions in a plasma, 2) subsequent acceleration and mass selection of the desired ions, and finally, 3) ion-beam shaping and scanning over the target (see Figure 1).

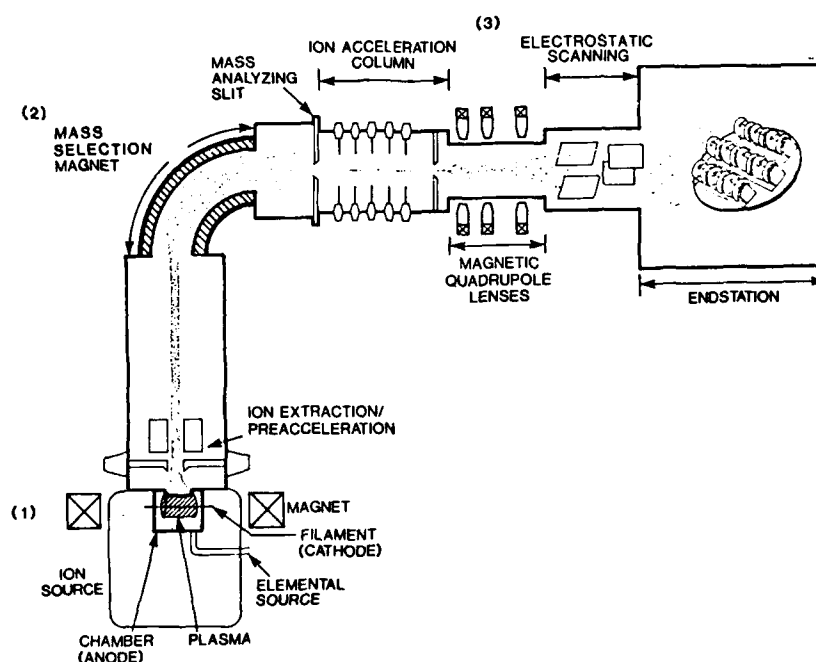


FIGURE 1. SCHEMATIC LAYOUT FOR A TYPICAL ION IMPLANTER

To produce the positive ions, a gas is introduced into an ion source, where it is typically ionized by energetic electrons emitted from a negatively biased hot filament. The positive ions are then extracted from the

ion source by a high voltage electrode and passed through a magnetic analysis system to allow for mass selection of the desired element. The beam is then accelerated to its final energy, typically 25 to 200 keV. Finally, the ion beam is directed toward the substrate material by a series of specialized magnetic lens and electrostatic scanning elements. These components shape and scan the beam and ultimately determine the implant area and implant uniformity at the target plane. The target temperature can also be controlled by affixing the material to thermally-controlled substrate holders.

Test coupons of polymer samples were ion implanted with a variety of different ions at various implantation conditions, such as ion fluence, ion energy, and beam current density. The substrates were mounted in a specially designed endstation which provides sample cooling and Faraday cup collectors for measuring ion dose and beam current density.

Testing

The surface microscopic atomic structure of the ion implanted polymer specimens were evaluated by X-ray Photoelectron Spectroscopy (XPS), Rutherford Backscattering (RBS), and FTIR-ATR. The ion implanted polymer specimens were also subjected to optical transmission, chemical solvent stability, mechanical performance, and electrical conductance tests.

ANALYSIS

The effects of ion beam interactions on polymers can be discussed from four different perspectives: chemical, mechanical, electrical, and optical properties.

Chemical Properties

Chemical changes produced in polymers by implantation include cross-linking of neighboring polymer chains and chain scissions, which break bonds along polymer chains. Cross-linked materials show a significant improvement in resistance to chemical attack. Shown in Figure 2 are the results of implanted polycarbonate materials. An unimplanted polycarbonate sample, shown on the right side of the figure, was completely hazed and visibly dissolved after 30 seconds of submergence in acetone. In contrast, all ion implanted samples showed no such sign of chemical attack after a 30-second immersion. This markedly improved solvent resistance behavior is due to the highly cross-linked structure produced by ion beam bombardment.

Mechanical Properties

Ion beam irradiation of polymers can also produce novel materials with favorable mechanical properties; e.g., Bell Communication Researchers [4] irradiated a silicon-containing (C:Si:H 9:2:14) polymer (dimethylsilane-co-methylphenylsilane), which caused a silicone enrichment (C:Si:H = 6.4:2:0.2). The resultant films were very hard and could not be scratched by steel or quartz scribes (1,300 Knoop hardness) attributed to the formation of silicon-carbide bonds.

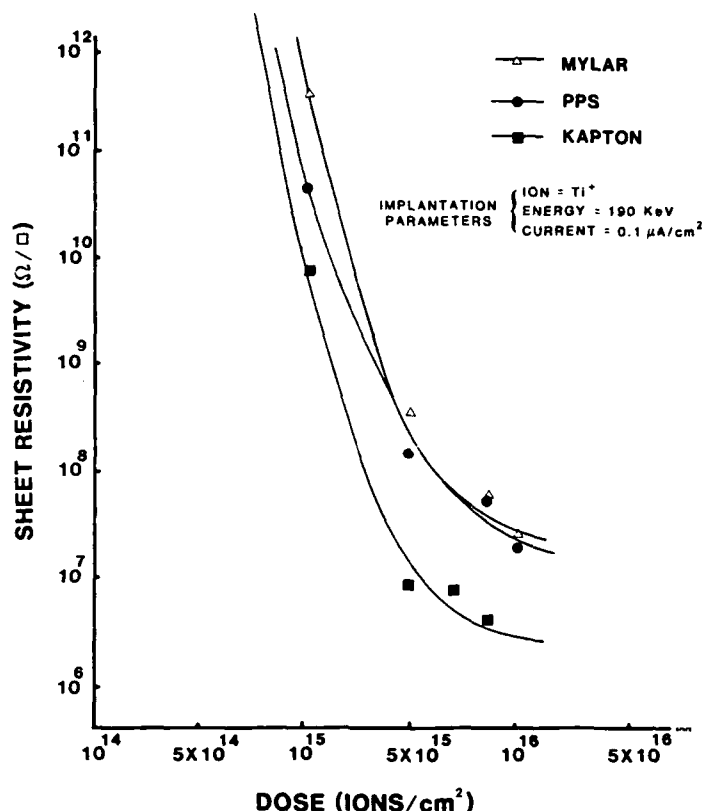


FIGURE 2. ENHANCED SOLVENT RESISTANCE OF ION IMPLANTED POLYCARBONATE.

Several studies performed at Spire also show that ion implantation causes densification of the surface of most common plastics. The implantation of ion species such as H, He, Li, Al, Ti, and Ar into polycarbonate and acrylics has shown a 350% increase in hardness of these substrates and has imparted a significant abrasion resistance on these surfaces. The studies performed in this area are still preliminary in nature and the results limited. However, the potential applications of improvements of this kind are extremely broad, including high value items requiring improved wear protection, such as eye-glass lenses.

Enhanced adhesion is another benefit of ion beam processing. We have previously shown that dramatic improvements in thin film adhesion can be produced by ion beam processing [5]. These results are shown in Figure 3 for Au/Teflon, Cu/Teflon, and Ag/Teflon pairs. The adhesion was enhanced by the promotion of non-equilibrium "interdiffusion" and the creation of nucleation sites at the interfaces by low energy ion bombardment before and during metal deposition onto the polymer substrate.

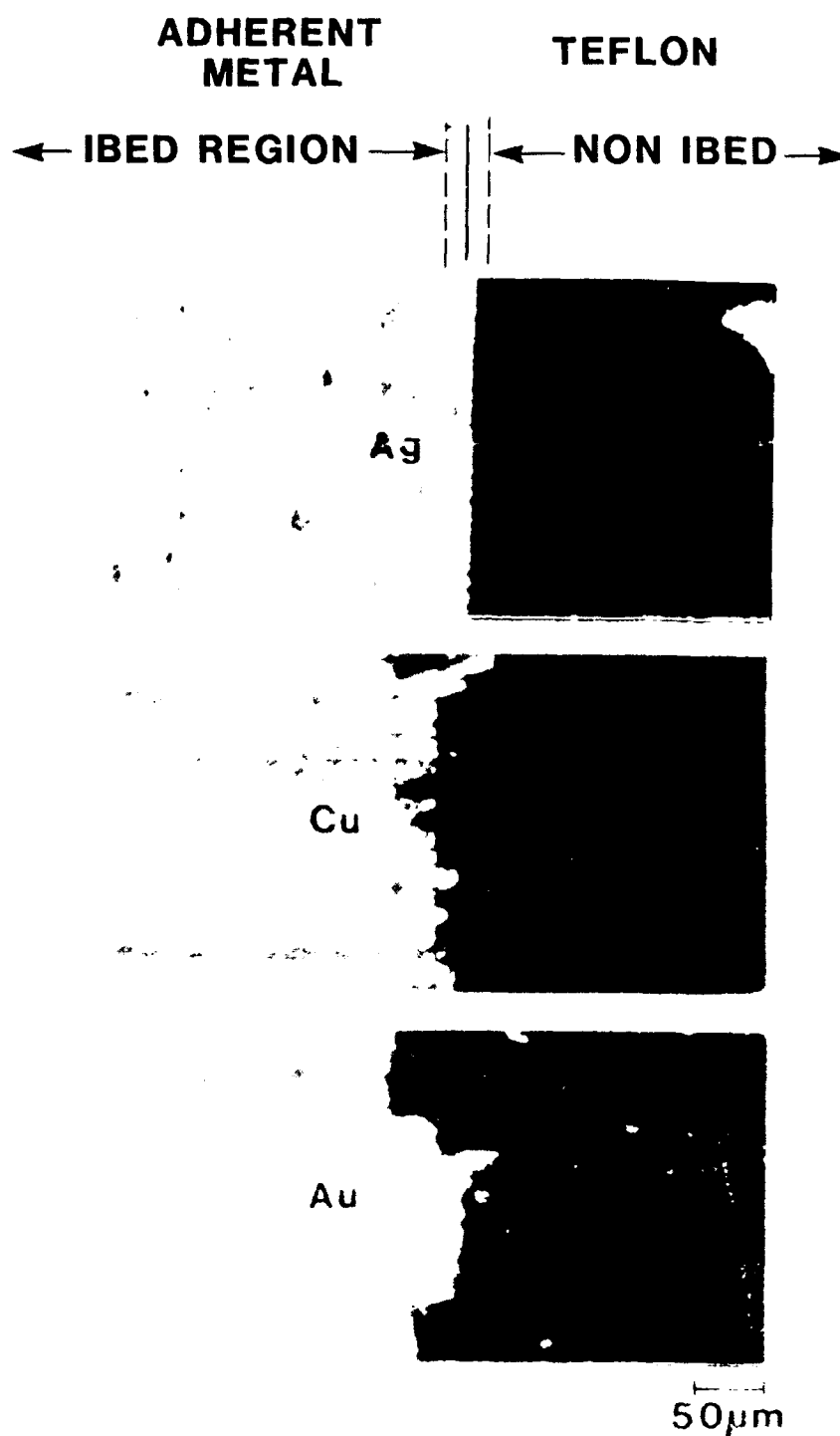


FIGURE 3. OPTICAL MICROGRAPHY OF METAL/TEFLON SPECIMENS AFTER SCOTCH TAPE TEST. (Strongly adherent metal films remain on the left ion beam prepared region.)

Electrical Properties

Ion implantation has been demonstrated to dramatically increase the surface conductivity of non-conducting polymeric materials, including polymethyl methacrylate, polyvinylchloride, polyacrylonitrile, poly(p-phenylene sulfide), and Kapton-H [6]. Figure 4 shows the dose dependence of sheet resistivity at room temperature for Kapton-H, Mylar and PPS films irradiated with Ti ions at an implantation energy of 190 keV. Implantation has produced fourteen orders of magnitude increase in the electrical conductivity of these normally insulating polymers as can be seen in Figure 4.

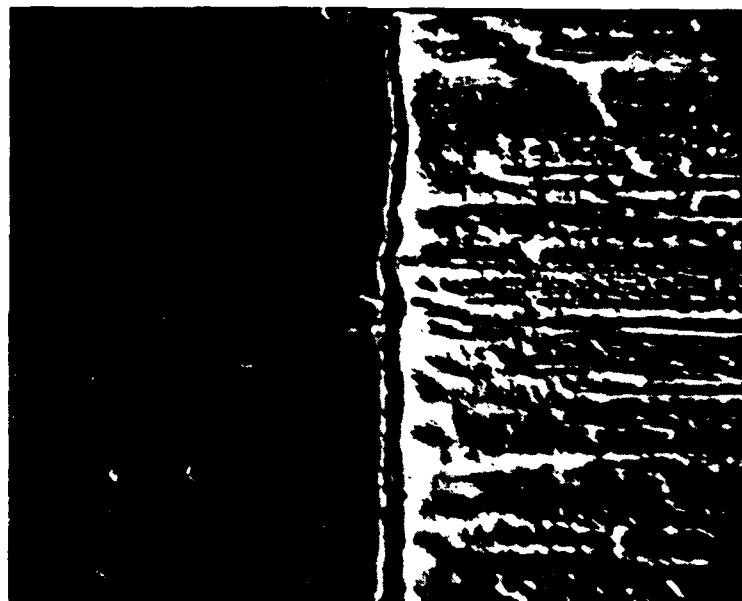


FIGURE 4. SHEET RESISTIVITY OF VARIOUS Ti ION IMPLANTED POLYMER FILMS AT ROOM TEMPERATURE.

The potential applications of an inherent conductive surface on an otherwise good insulator and the ability to selectively tailor the conductivity of the materials should be very useful in a wide variety of industrial products. Among these would be lightweight batteries, microelectronic devices, chemical sensors, antistatic materials, and switchable contact bridges. Implantation also has been investigated as an alternative to chemical intercalation for increasing the conductivity of polyacetylene.

Optical Properties

Refractive index changes resulting from injection of ions into the optical materials have also been observed, which allows one to form optical waveguides in the solid's surface. Oleszkiewicz [7] reported a refractive index increase from $n = 1.49$ to $n = 1.80$ on boron implanted polymethyl methacrylate and related this result to the amorphization and carbonization processes.

We have conducted a preliminary investigation into determining the change in index of refraction of the implanted polycarbonate samples. Using a Rudolph Auto-El III null-seeking ellipsometer which uses an He-Ne laser at 6320 Å wavelength, we can measure the optical quantities n and k (i.e., the real and imaginary parts of the complex index of refraction $N = n - ik$). It is not yet clear if this is a valid method of index determination nor if the results can be explained on the basis of some model. However, the implications regarding potential applications of controlling refractive index in polymers through implantation are great, particularly in the area of optical waveguides. Table 1 lists the index data for the four implants examined thus far.

TABLE 1. REFRACTIVE INDEX DATA.

Sample	Implantation Conditions	Refractive Index
Polycarbonate	control	1.579 ± 0.003
Polycarbonate	Si^+ , 25 keV, 1×10^{15} ions/cm ²	1.867 ± 0.049
Polycarbonate	Si^+ , 25 keV, 5×10^{15} ions/cm ²	1.845 ± 0.013
Polycarbonate	Si^+ , 70 keV, 1×10^{15} ions/cm ²	2.098 ± 0.037
Polycarbonate	Si^+ , 70 keV, 5×10^{15} ions/cm ²	1.861 ± 0.015

Discussion

The fundamental principles of ion-solid interactions were postulated by Lindhard, Scharff, and Schiott [8] (LSS) for the energy loss rates of fast ions incident on amorphous solids. When an energetic ion enters a solid target, it loses energy both by interactions with electrons and the nuclei of the target atoms until it eventually comes to rest. The total energy loss rate of the ion can be represented as the sum of two independent energy loss mechanisms.

$$(dE/dR)_{\text{total}} = (dE/dR)_{\text{electronic}} + (dE/dR)_{\text{nuclear}}$$

The electronic contribution dominates at high energies while the nuclear stopping contribution dominates at low energies,. Energetic charged particles inelastically interact with substrate electrons as they pass through

the solid, analogous to a viscous drag, until their energy (velocity) is decreased to the point where their energy is lost mostly by elastic (nuclear) collisions with the atoms. It is this nuclear stopping mechanism which normally acts to produce many atomic displacements within the substrate lattice and which predominates at the end of the ion range. However in polymer substrates, Kaplan, et al. [9] have indicated that the ion-beam-induced structure changes are primarily a result of secondary electron interactions and not of direct nuclear collision. Hence, it seems that for polymers the electronic contributions to energy loss are as important as nuclear stopping contributions in affecting property changes.

The effects of ion implantation on polymers can also be further delineated as due to heat effecting and effects of the physical bombardment of charged particles on the polymers. Heating effects are determined by the power dissipation rate of target materials and substrate cooling provisions. The power density of the ion beam at the target can be substantial (i.e., watts/cm²). Therefore, precautions must be taken to prevent unwanted temperature excursions of the target in the vacuum environment. This is especially important for polymers, because polymeric materials are very sensitive to temperature changes, and any significant temperature rise will lead to the deformation and/or degradation of the polymer. Parameters such as ion energy, ion beam current, and mainly target cooling provisions during implantation, are the major factors controlling the target temperature.

Although several theoretical models, including LSS,[8] are available for the calculation of the ion concentration profiles in a solid and provide information on both the electronic and nuclear energy loss components, no reported theoretical model has been able to successfully describe the behavior of ion implanted polymers. This is due to the complexity of the polymer structures and the ion interactions of polymers by chain scissions, cross-linking, gas evolution, and chemical reactions. Therefore, further investigations are required to further understand the ion interaction mechanisms in polymer materials in order to permit successful commercial development.

ACKNOWLEDGEMENT:

This work is partially supported by the Department of Air Force under grant F33615-87-C-5220.

REFERENCES

1. M.S. Dresslhaus, B. Wasserman, G.E. Wnek, Mat. Res. Soc. Symp. Proc., 27, 413 (1984).
2. T. Venkatesan, R.C. Dynes, B. Wilkens, A.E. White, J.M. Gibson, and R. Hamm, Mat. Res. Soc. Symp. Proc., 27, 449 (1984).
3. D.C. Weber, P. Brant, C. Carosella, and L.G. Banks, J.C.S. Chem. Comm., 522 (1981).
4. T. Venkatesan, Nucl. Instr. and Methods in Physics Research B7/8, p. 461-467 (1985).

5. I.H. Loh, J.K. Hirvonen, J.R. Martin, P. Revesz, and C. Boyd, Mat. Res. Soc. Symp., 108, 241 (1987).
6. I.H. Loh, P. Sioshansi, and R.W. Oliver, Nucl. Instru. Meth., B34, 337 (1988).
7. E. Oleszkiewicz, Optica Applicata, XV(2), 157 (1985).
8. J. Lindhard, M. Scharff, and H.E. Schiott, Mat. Fys. Medd. Dan. Vid. Selsk, 33, 14 (1963).
9. M.L. Kaplan, S.R. Forrest, P.M. Schmidt, T. Venkatesan, A.Y. Lovinger, J. Electr. Mat., 12, 989 (1983).

FRAMELESS AIRCRAFT TRANSPARENCY TECHNOLOGY DEVELOPMENT

William R. Pinnell

AFWAL/FDER
Wright-Patterson Air Force
Base

FRAMELESS AIRCRAFT TRANSPARENCY
TECHNOLOGY DEVELOPMENT

a paper prepared by

William R. (Bob) Pinnell
Air Force Wright Aeronautical Laboratories
AFWAL/FDER
Wright Patterson Air Force Base, Ohio 45433

for presentation at the

Conference on Aerospace Transparent Materials and Enclosures
16-20 January 1989
Monterey, California

ABSTRACT

This paper introduces the Frameless Transparency concept and addresses concept potentials, technology development, and important progress. Revolutionary changes in the design and manufacture of windshields and canopies for high performance fighter and trainer aircraft will accompany successful implementation of the Frameless Transparency concept. Utilizing toughness inherent in impact resistant transparent plastics and methods for direct forming affords a multitude of potential improvements over current design and manufacturing practices. Elimination of frames from transparency assemblies and single thermal process direct forming permits improvements in durability, performance, and reliability in addition to lower acquisition and maintenance costs.

FRAMELESS AIRCRAFT TRANSPARENCY TECHNOLOGY DEVELOPMENT

BACKGROUND:

Continuing efforts to produce windshields and canopies which satisfy stringent optical, structural, and safety requirements are impeded by current design and manufacturing practices which dictate compromised durability, life cycle cost, and maintenance. The number of materials which have the potential to survive in-flight impacts with birds at high speeds is severely limited. Polycarbonate, currently the principal aircraft transparency structural material, is obtained primarily from two commercial sources in the form of extruded flat sheets. Resin formulations for the material in this form have been controlled by these two sources and influenced by large volume commercial markets other than aircraft transparencies.

Historically, an aircraft transparency has been an assembly of transparent panel, frame, fairings, seals, sealants, fasteners, and hardware necessary for attachment to aircraft structure. The Frameless Transparency concept includes elimination of the frame and all components necessary for attachment of the transparent panel to the frame. This will be achieved by forming the transparency directly from molten resin in a mold which permits tailoring thickness to provide structural stiffness at transparency edges. Molded external shaping will match aircraft mold lines eliminating the need for frame fairings. Aircraft interface hardware will be molded in place when the transparency is formed. Figure 1 is a schematic representation of the frameless transparency sill edge.

Current manufacturing methods for transparencies is characterized in the Figure 2 schematic. Completing the transparency assembly requires many labor intensive and highly specialized tasks which dictate high cost and are generally inconsistent with obtaining maximum material performance potentials. Current methods include the following processes:

Flat sheet extrusion	Pressure polishing
Laminating with inner layers	Bending to shape
Edge trimming	Drilling for fasteners
Panel to frame sealing	Installation into frame
Application of fasteners	Installation of frame fairings
Coating for abrasion resistance	

In transparency designs which feature bonded panel edges, requirements for fasteners and drilling could be minimized.

POTENTIAL ADVANTAGES:

The Frameless transparency concept eliminates the requirement for many of the conventional processes by forming directly (see Figure 3) and forming the transparent panel with thickened edges which replace the frame.

**FRAMELESS TRANSPARENCY
AIRCRAFT INTERFACE APPROACH**

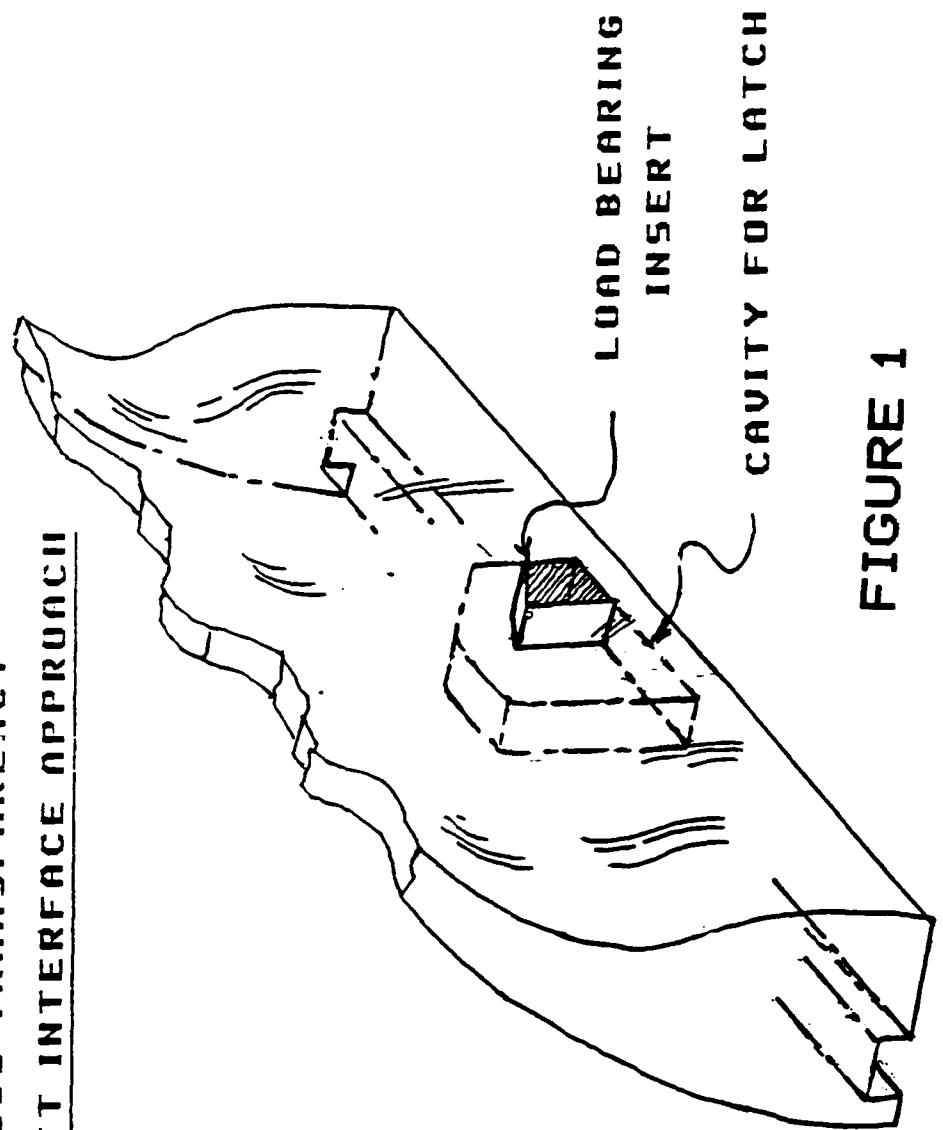


FIGURE 1



CONVENTIONAL AIRCRAFT TRANSPARENCIES

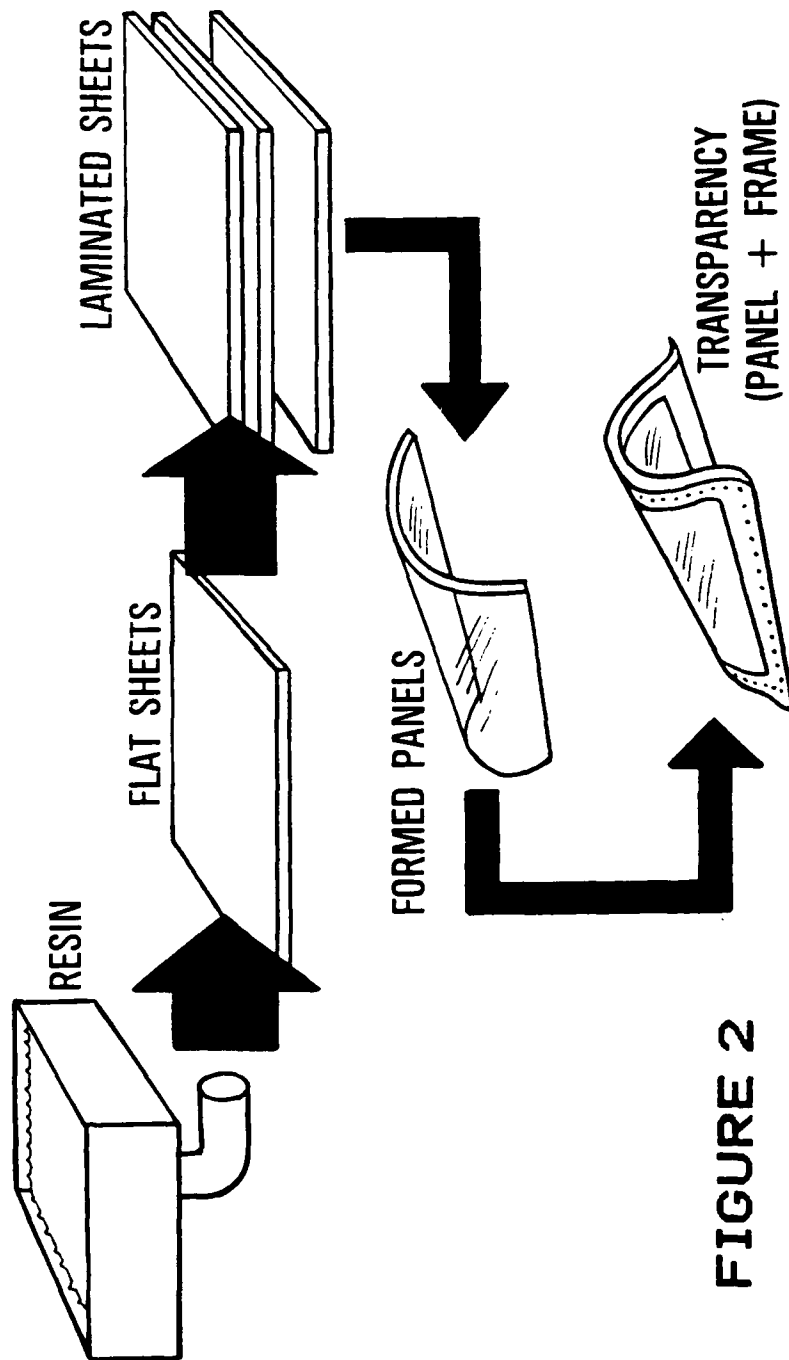


FIGURE 2



FRAMELESS AIRCRAFT TRANSPARENCY

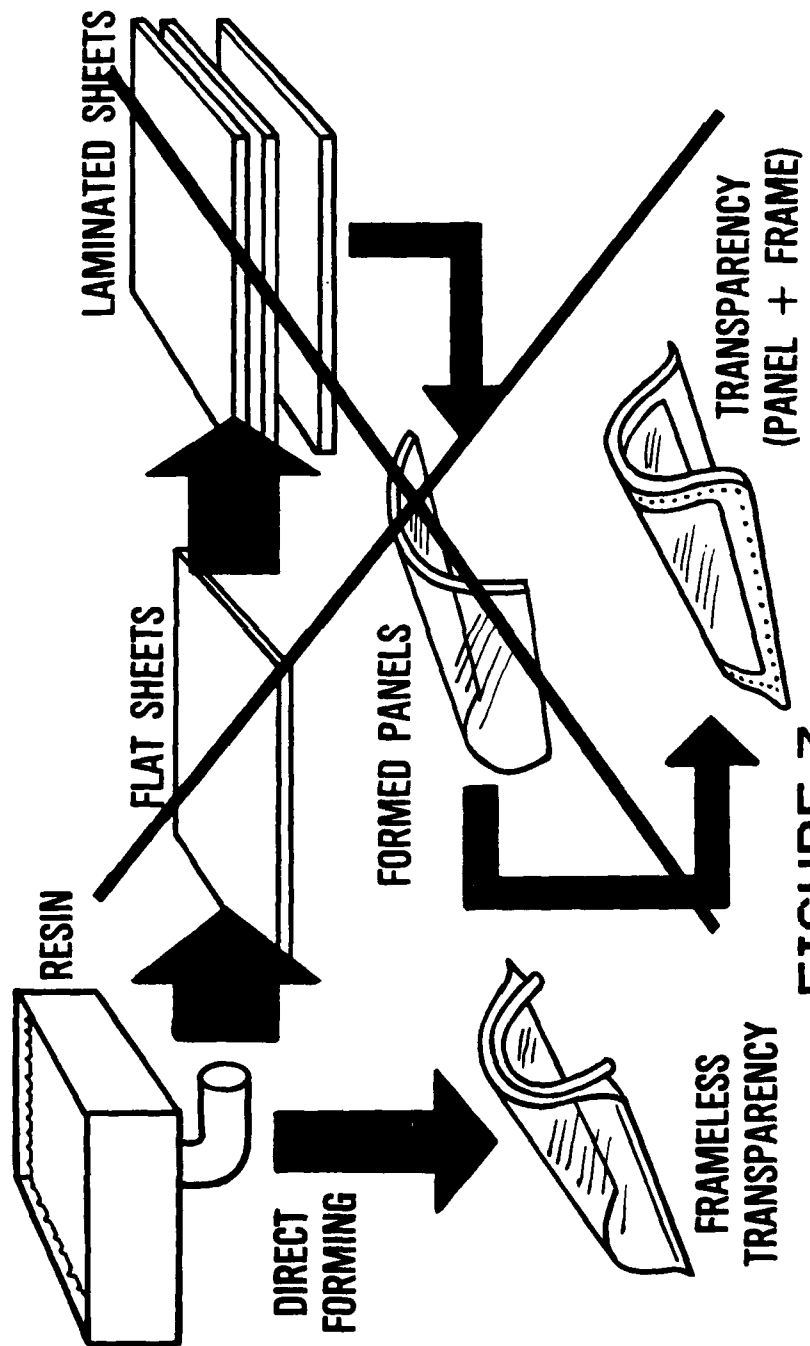


FIGURE 3

Potential advantages of directly formed frameless transparencies relative to transparencies of conventional design and manufacture include those listed and discussed below:

Better Materials Properties - Because temperature, pressure and heatflux can be closely controlled in a mold, polymer chain consistency and materials property reliability can be improved. An example is the reduction in impact resistance and the consistency in impact resistance of extruded Polycarbonate sheet as thickness increases. Direct forming has the potential for reducing or eliminating the requirement for laminating for structural integrity. Thermal processes required to obtain surface uniformity, cure bonding to inner layers, and to bend flat sheet laminations to final shape produces degradation in polymer chains which result in reduced material properties. Direct forming eliminates the need for these thermal processes.

Reduced Residual Stress - Direct forming of the transparency to its final shape precludes the requirement for bending which introduces tensile and compressive strains with associated residual stresses. Residual stress is a major cause of degraded material structural performance and resistance to chemical and mechanical crazing.

Thickness Tailoring - Direct forming permits optimal selection of local thickness for achieving structural, dynamic, optical, or functional requirements. A closely controlled constant thickness (or lenticular corrective shape) necessary for optics can be combined with thickened edges necessary for stiffness required for attachment to the airframe and incorporation of pressure seals. Tailoring of stiffness in nonoptical areas may be desired for controlling deflections associated with in-flight bird impacts, weight savings, or creation of structural load paths.

Forming Process Repeatability - Relative to current forming techniques which include multiple process stages which are labor intensive and difficult to control, injection molding is primarily a one process technique which can be closely controlled and repeated. Transparencies can be produced with less labor and in less time, with less variation in finished transparency material properties.

Elimination of Seal Parts - Currently frames consisting of metal or composite sills, arches, skins, and fairings are attached to transparent panels utilizing fasteners (bolts) and associated nuts, washers, shims, and bushings. The frameless concept eliminates the frame and all components necessary for the frame to transparent panel interface.

Elimination of Pressure Seal - The requirement for a pressure seal between the transparent panel and the windshield frame is eliminated. In addition to reductions in requirements for sealing materials, labor necessary to effect this seal and integrate the frame to the transparent panel is not required. The task of changing aircraft transparencies will not include mounting of the transparency in the frame.

Elimination of Structural Discontinuities - Holes in transparent panels

for frame to panel fasteners will be eliminated. Currently holes are typically closely spaced (1 to 2 inches) around the periphery of the transparent panel, perforating the panel near its edges and creating discontinuities in the material which compromise impact resistance and create stress risers from which cracks and crazing of the transparent material are initiated. Fastener holes in notch sensitive materials like polycarbonate must be carefully machined and often require special bushings to attain even modest durability. Bolts through frames and laminated transparent panels must be carefully torqued to effect required pressure seal without compressing soft interlayer materials.

Thermally Induced Stresses - Differential thermal expansions exist between plastic transparent panel materials and materials included in conventional frames. Thermally induced stresses in transparent panels can compromise impact resistance, create optical distortions, crack plastic structural plies, initiate stress crazing, reduce chemical craze resistance, and promote delamination. Frameless transparencies will utilize the same plastic material for the entire transparency.

Visual Inspection - Currently, transparency frames are opaque and prevent visual observation of cracks and crazing until these failures have progressed beyond the opaque frame edges. Latching mechanisms for canopies are often internal to frames and latching cannot be confirmed by visual observation. The frameless transparency concept includes utilization of transparent material which will permit visual inspection of the transparency and the position of latching devices by maintenance as well as aircrew personnel.

Lower Acquisition Cost - Because the directly formed frameless transparency is much less expensive to produce, eliminates the need for many components, and because the concept has potential for improved service life, dramatic reductions in acquisition costs are possible. Table 1 shows an example of potential cost saving for a 20 year aircraft life and current replacement rate based on F-16 aircraft data and assumptions. For this analysis, service life for frameless transparencies is assumed to be three times longer than the current canopy life. It should be noted that the current F-16 canopy has a very short service life. It should also be noted that the F-16 was not designed for a frameless canopy and that retrofit is the largest single item in the frameless cost for each F-16. For the F-16, Table 1 indicates that the current transparency is over eleven times more expensive than the frameless transparency. Total potential savings for fleet size quantities are quite substantial.

Lower Maintenance Costs - Longer service life due to improved materials properties, minimal residual stress, and reduced structural discontinuities will result in fewer transparency changes. Elimination of the requirement for mounting a transparent panel in a frame reduces the time for changing the transparency dramatically. Properly designed aircraft interface hardware should reduce transparency change time from three or more days to a few hours. These advantages will effect significant reductions in aircraft downtime.

COST ANALYSIS - Frameless Transparency Retrofit to F-16

Per Aircraft (20 yr life)

CURRENT		FRAMELESS	
Transparent Panel (1.75 yr change) (coating included)	11.4 @ \$ 23K	Frameless Canopy (5.3 yr change) Coating	3.81 @ \$ 3K 3.81 @ \$ 2K
Frame	2 @ \$ 32K	Frame Retrofit Hardware	M/A 1 @ \$ 10K
			\$ 29K
			\$ 326.2K

FRAMELESS IS 11.2 TIMES LESS COSTLY

FRAMELESS COST SAVINGS	
NR of A/C	\$
1	297K
1000	297M
2000	594M

TABLE 1

PINNELL
30 JUN 88
COSTP-1B

APPROACH TO TECHNOLOGY DEVELOPMENT:

From concept initiation (late 1983), the approach to developing technology necessary to put frameless transparencies in the field has included a series of three phases; Development of Direct Forming Processes, Development of Analytical Design Capability, and Prototype Demonstration. The product of these efforts will be the analytical design capability confirmed by design, molding, testing and field evaluation of the frameless transparency on operational aircraft. Figure 4 is a schematic for this approach.

PHASE 1:

Development of Direct Forming Processes - A research and development contract was awarded in September 1985 to Loral Defence Systems Division, Litchfield Park AZ (formerly Goodyear Aerospace Corp.) for demonstrating direct forming processes applicable to fabrication of frameless aircraft transparencies. After an extensive study, candidate forming methods were narrowed to injection molding. Since aircraft transparencies are very large parts for injection molding, an injection molding must be accomplished at low pressure to preclude a requirement for very large molding machines. The Loral effort resulted in demonstrating a low pressure injection molding process by molding flat and conical demonstration panels from three candidate transparency materials (see Figures 5 and 6). Molding trials were conducted by EIMCO Molded Products Company, Salt Lake City UT, a Loral subcontractor.

The molded panels were designed to demonstrate the capability to tailor thickness, retain materials properties in molded parts, and to permit evaluation of the effects of variations in molding parameters. Extensive coupon testing has shown that impact resistance and other material properties of injection molded polycarbonate are equivalent to or exceed properties measured for extruded sheets of this material. Simulated bird impact testing indicated large plastic deformation capability in molded panels. Polyphthalate carbonate has also been successfully injection molded and has a potential for higher temperature applications than polycarbonate. This subscale direct forming capability is the basis from which frameless transparency technology necessary for field implementation can be developed. Technical effort under this contract was completed in June 1988. A final report (ref 1) will be published and distributed by the Air Force. Objectives of this effort were accomplished. The demonstrated direct forming capability is the basis for subsequent frameless transparency technology development phases and field implementation of the frameless concept.

Technical details associated with the effort which developed and demonstrated direct forming processes are addressed in a separate paper presented at this conference (ref 2) by Darrel Fuller, Loral Defence Systems Division.

PHASE 2:

Development of Analytical Design Capability - Based on the process



APPROACH

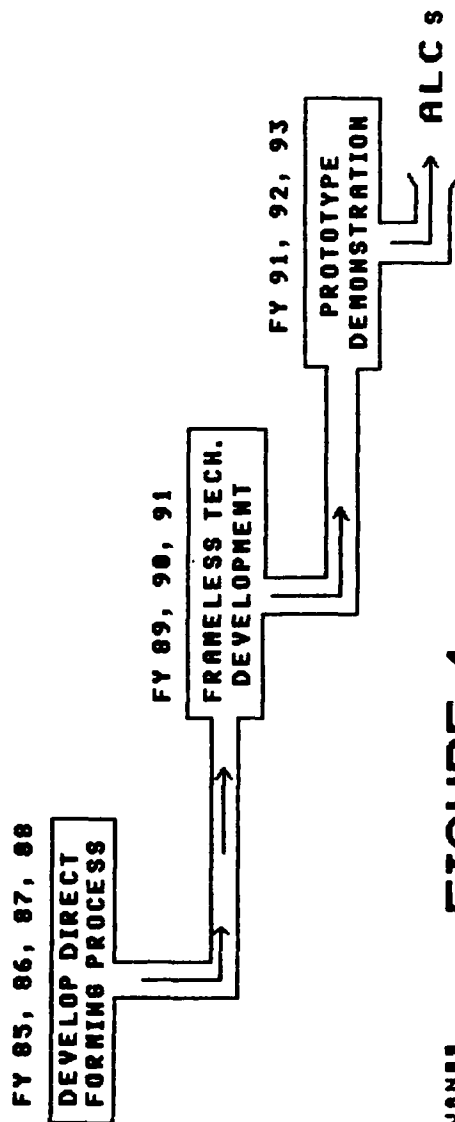
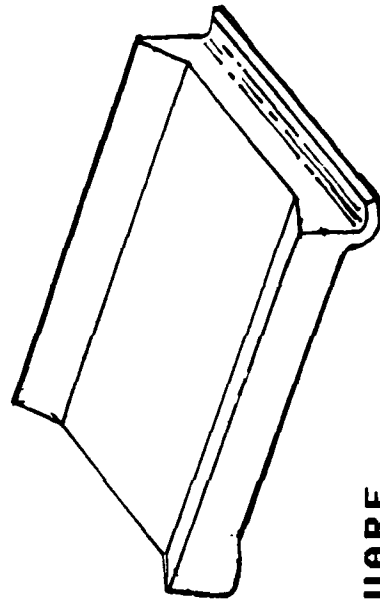


FIGURE 4

10 JAMES
PINNELL
APPROACH

FRAMELESS TRANSPARENCY
INJECTION MOLDED DEMONSTRATION
FLAT PANEL



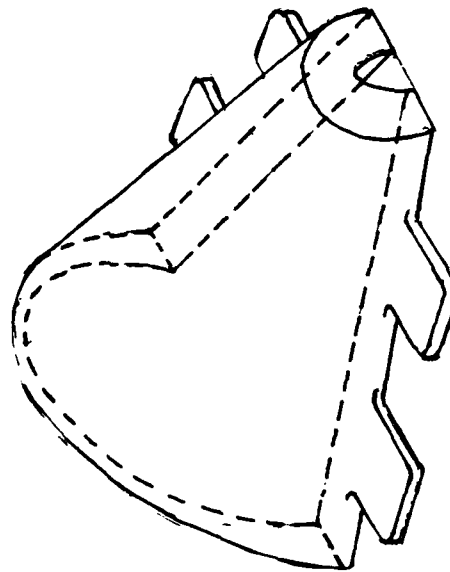
24 INCH SQUARE
THICKNESS TAILORING
1/2 TO 2 INCHES
SIMULATED SILL AND ARCH

IMPACT
RESISTANT
OPTICALLY
CLEAR

DENOVBB
PINNELL
WCPPTXT

FIGURE 5

FRAMELESS TRANSPARENCY
INJECTION MOLDED DEMONSTRATION
CONICAL PANEL



22 IN DIA HALF CONE
THICKNESS TAILORING
1/2 TO 2 INCHES
SIMULATED SILL

IMPACT
RESISTANT
OPTICALLY
CLEAR

DENOU88
PINNELL
HCCPTXT

FIGURE 6

demonstration and the molded materials properties resulting from testing in Phase 1, the objective of Phase 2 is to develop and confirm an integrated design capability for frameless transparencies, aircraft interfaces, and molds. The design capability will be an integration of existing computer analytical design and analysis software packages (see Figure 7). Included in the design capability will be Computer Aided Design (CAD) for overall structural and geometrical design, finite element analysis for investigating structural response to impact loading, thermal analysis, and software for injection mold design and molding process definition. From aircraft transparency requirements and geometry, the design capability will produce a frameless transparency, the aircraft interface, an injection mold, and molding process parameters for selected materials. The design process will be iterative, producing transparency, interface, and mold designs in concert so that high confidence is generated prior to mold fabrication. In this phase of the overall effort, the design capability will be exercised to produce injection molded forward windshield test transparencies complete with interfacing hardware and meeting requirements typical of high performance fighter/trainer type aircraft. These test transparencies will be subjected to tests and evaluations for determining the effectiveness of and to establish confidence in the design capability.

PHASE 3:

Prototype Demonstration: - In addition to molding and extensive testing to establish the design capability developed in phase 2, efforts utilizing the design capability will produce, qualify, and evaluate a frameless transparency prototype through Operational Test and Evaluation (OT&E). To accomplish this the coordinated design methods will be applied to production of prototype transparencies for a chosen aircraft. Technology for abrasion resistance and improved tolerance for high operational thermal environments being developed in parallel efforts outside this project will be integrated into the prototype design. Frameless transparencies with aircraft interfaces will be fabricated in sufficient quantities to support evaluation testing (structural, optical, impact, and fit and function), flight qualification testing, and installation on seven to ten operational aircraft for an OT&E period of one year.

SUMMARY:

A revolutionary approach to design and fabrication of aircraft transparencies (windshields and canopies) is offered by the Frameless Transparency concept. This approach is primarily applicable to high performance fighter and trainer type aircraft although various facets of the technology are applicable to other aircraft types and to components other than transparencies. The concept offers lower cost concurrent with reliability, maintainability, improved performance, and design and fabrication methods which permit greatly broadened capabilities for aircraft transparencies.

REFERENCES:

1. AFWAL-TR-88-3071, Development of Forming Process for Frameless Aircraft

Transparencies, June 1988, Darrel B. Fuller, Barbara L. Penunuri, Theresa A. Taylor

2. Conference Paper, AFWAL Conference on Aerospace Transparent Materials and Enclosures, 16-18 Jan 1989, Monterey CA, "Direct Forming Process for Aircraft Transparencies", Darrel B. Fuller

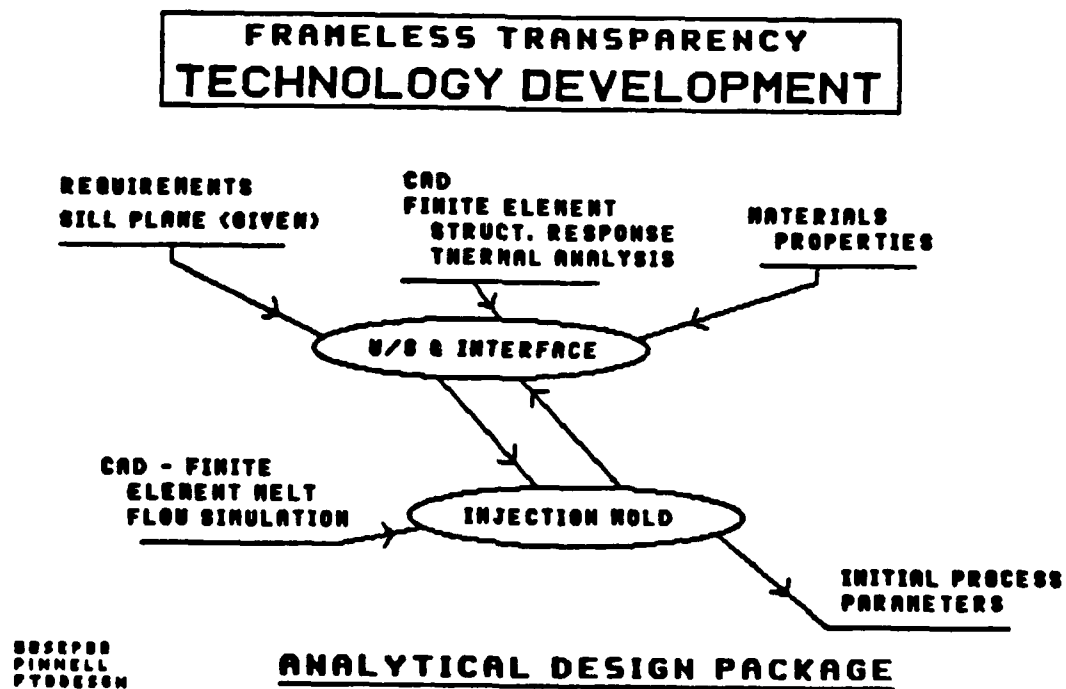


FIGURE 7

DIRECT FORMING PROCESSES FOR AIRCRAFT TRANSPARENCIES

D. B. Fuller

Loral Defense Systems-
Arizona

DIRECT FORMING PROCESSES FOR AIRCRAFT TRANSPARENCIES

D.B. Fuller

Loral Defense Systems-Arizona

Abstract

Current fabrication processes for plastic aircraft transparencies include thermally forming flat sheet stock to the desired contour, followed by trimming, drilling, and other finishing operations. The process is labor intensive and relatively expensive. Direct forming processes have the potential of significantly decreasing fabrication time and costs. Injection molding is particularly promising as a direct forming process.

The Development of Forming Processes for Frameless Aircraft Transparencies program (contract no. F33615-85-C-3402), addresses direct forming processes. The program was performed by Loral for the U.S. Air Force (USAF) from September 1985 to November 1988. Subscale transparent articles, e.g., 24-inches square were successfully injection molded and evaluated for dimensional conformity, optical quality, material properties, environmental durability, and impact strength.

Conformity of the articles to design geometry and the dimensional consistency from article to article was good. Distortion-free articles with good optical quality were attained. Physical properties of injection molded material proved to be comparable to those of extruded polycarbonate in tensile, flexural, compressive, and fatigue tests.

Evaluation of the injection molded articles included bird impact. Finite element modeling was performed (MAGNA) and verified by empirical impact tests with gelatin projectiles.

1. INTRODUCTION

1.1 General

Current fabrication techniques for transparent panels begin with flat sheets such as glass, acrylic, and polycarbonate. Often it is necessary to thermoform the flat sheets to large shapes of compound curvature. To achieve specific properties, such as bird impact resistance, it is often necessary to laminate several plies of acrylic and/or polycarbonate. After forming to the desired shape, the transparent panels are trimmed of excess material. The transparent panels are then installed in a metal frame. The metal frame is then mechanically attached to the airframe. The process is labor intensive, inefficient in material use, and expensive.

1.2 Program Objective

The objectives of this program were to investigate the feasibility of direct forming processes for aircraft transparencies. Such processes would allow direct forming from bulk materials and eliminate several of the current manufacturing operations. Elimination of the frame by incorporating aircraft interfacing hardware directly into transparency edges was also a potential.

1.3 Program Scope

This program constituted only the first phase of the development of direct forming process for aircraft transparencies. The scope of this program included a study of transparency technology and requirements, evolution of forming processes compatible with frameless transparencies and their required performance, evaluation of forming processes, and selection of a process for further development. Injection molding was selected as the preferred fabrication process.

Process evaluation panels, which were smaller than actual aircraft transparencies, were fabricated to develop and validate the direct forming processes under study. The process evaluation test panels were of two shapes specified by the contracting agency. One shape was relatively flat, as shown in Figure 1. The other shape was a half-cone, as shown in Figure 2. Molded panels conforming to the two geometries have been referred to throughout this document as "flat panels" and "conical panels".

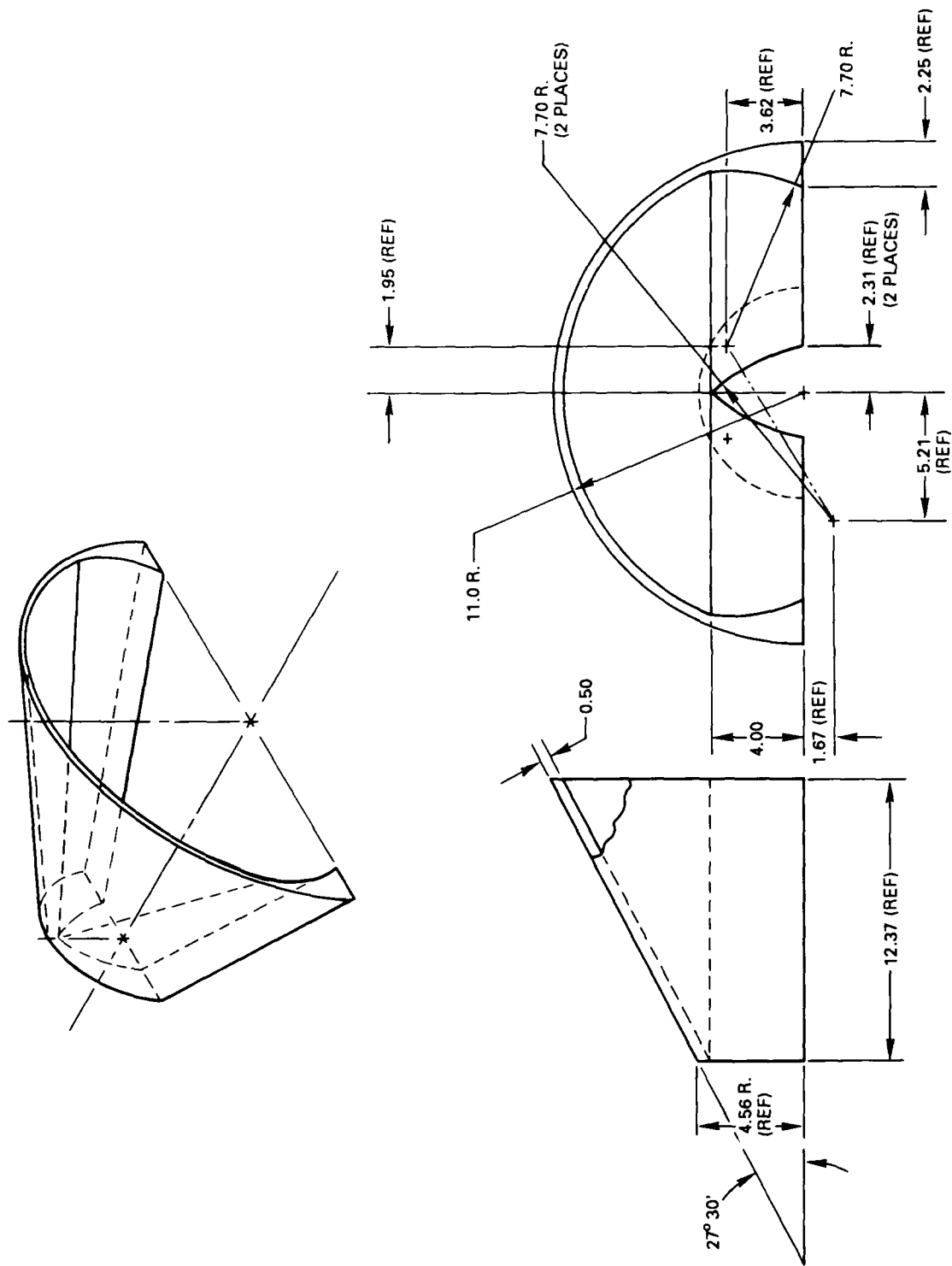
As shown in Figures 1 and 2, both geometries included tapered, thickened edge sections as might be used to eliminate the frame currently used on aircraft transparencies. The geometry of the flat panel included a "nesting feature" which allowed any two flat panels to be fitted together, as might be desired between a windshield and a canopy in the absence of a metal frame or arch.

After fabrication, flat and conical panels were evaluated by extensive optical, static mechanical, dynamic impact, and durability testing. Based on these test results, one material was selected and additional panels were molded of it for delivery to USAF.

2. SELECTION OF A DIRECT FORMING PROCESS

In the initial stages of the program, candidate forming processes were identified and studied. These processes included casting, compression molding, injection molding, reaction injection molding, and injection-compression molding. Of these processes, injection molding was judged to be the best suited to transparent panel fabrication. The other processes were rejected for a variety of reasons, including unavailability of suitable transparent materials compatible with the processes and incompatibility of the processes with complex geometries typical of aircraft transparencies.

84017-1 (84015-1)



NOTE: ALL DIMENSIONS ARE IN INCHES

84017-2 (84015-2)

Figure 2. Conical process evaluation panel, orthographic view.

Conventional injection molding entails heating a solid thermoplastic material to a fluid state. The material is then transferred under pressure (injected) into a closed hollow space (mold cavity), where it cools and solidifies, conforming to the shape of the cavity.

Typically, commercially available injection molding equipment is limited to relatively small plastic parts. Shot sizes of only a few ounces are common. The panels molded in this program are much larger than typical injection molded articles. The flat and conical panels weigh 25 and 15 pounds (lb), respectively, requiring the use of specialized injection molding equipment. The equipment used in this program is depicted in Figure 3.

Resin Dryer - When exposed to ambient conditions, plastic materials absorb moisture from the air. If the moisture is not removed prior to injection molding, it typically causes defects in the molded parts. To mold optically clear parts, it is imperative that the material be dried adequately prior to being molded.

Extruder - After being dried, plastic pellets flow from the dryer into the extruder. As material passes through the extruder, it is heated to a liquid state by electrical heaters as well as mechanical action of the screw.

Accumulator - As material exits the extruder, it enters the accumulator. As the name implies, the accumulator is a reservoir for molten resin. Resin is extruded into the accumulator until a sufficient quantity exists to fill the mold. While residing in the accumulator, the material is maintained at a molten temperature. When a sufficient quantity is accumulated, material is forced under pressure into the closed mold.

Mold - Clamping the mold in a large hydraulic press ensures that the mold remains closed during injection and provides an easy and fast means of opening it afterwards. Upon being injected into the mold, the molten material cools and solidifies under pressure. The mold is then opened and the molded part is removed.

Eimco Molded Products of Salt Lake City, Utah performed all of the injection molding in this program. Eimco's specialized equipment and expertise in molding extremely large articles proved to be a great asset.

3. MATERIAL SELECTION

3.1 General

In the initial stages of the program, concurrent with selection of a forming process, a number of potential transparent materials were identified for direct forming of transparencies. Material types included acrylic, allyl ester, epoxy, polyamide, polycarbonate homopolymer, polycarbonate copolymers, aromatic polyester, polyetherimide, butadienestyrene, polyurethane, styrene-acrylonitrile, and sulfone polymers. Upon choosing injection molding as the process to use in this program, all nonthermoplastic materials were eliminated from further consideration.

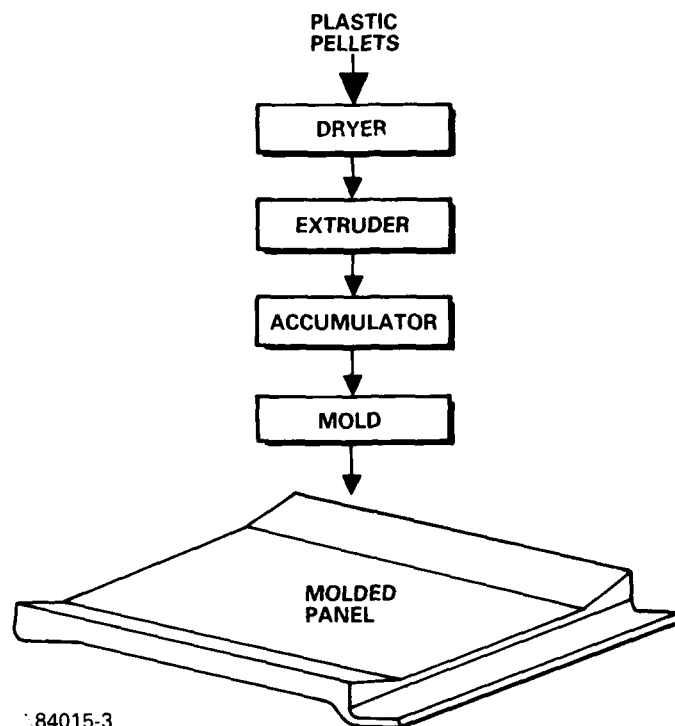


Figure 3. Injection molding equipment components.

After studying all available information, three thermoplastic materials were selected for molding flat and conical panels. Materials were selected primarily on the basis of impact strength, optics, and high temperature tolerance. The materials selected were Calibre 303 , Lexan PPC 4701 , and Durel 400 .

3.2 Calibre 303

Calibre 303 is a bisphenol-A polycarbonate homopolymer manufactured by the Dow Chemical company. Extruded polycarbonate homopolymer sheets are currently used extensively in aircraft transparencies, primarily as structural plies for bird impact resistance.

Bisphenol-A polycarbonate homopolymer has excellent impact strength, good dimensional stability, good resistance to crack propagation, and other favorable physical properties. Monolithic polycarbonate has many deficiencies including poor abrasion resistance, difficult surface refinishing, ultraviolet (UV) radiation degradation, poor chemical resistance, and susceptibility to stress

crazing. However, these deficiencies can be overcome with laminated face plies or abrasion resistant coatings.

Calibre bisphenol-A polycarbonate resin was selected for use in this program over other brands because it was available in grades of specific melt indices. This allowed the choice of a grade which was best suited to the injection molding process and equipment used in this program.

The Calibre 303 material molded in this program contained an internal mold release and a dye, resulting in the molded panels having a light blue tint. The presence of the dye was undesirable because it resulted in a decrease in luminous light transmittance. However, resin without dye was not readily available. Since the molded panels were intended solely for evaluation of the molding process, the presence of dye in the material did not preclude its use.

3.3 Lexan PPC 4701

Lexan PPC 4701 is a polyphthalate carbonate copolymer manufactured by General Electric (GE). It can be processed similar to bisphenol-A polycarbonate homopolymer. Published values for impact strength and other strength and physical properties of the material are similar to bisphenol-A polycarbonate homopolymer. This material is of interest primarily because of its relatively high 325° F heat distortion temperature (HDT), per American Society of Testing and Materials (ASTM) designation D-648.

3.4 Durel 400

Durel 400 is a polyarylate material under development by Hoescht-Celanese. The published HDT for this material (340° F) is very attractive. Manufacturer's literature also suggests good optical clarity, UV stability, reasonably good impact and tensile strengths, and good chemical resistance.

4. MOLD DESIGN

Two molds were fabricated for this program - one each for flat and conical panels. The flat panel mold was a simple two-piece design. The complex shape of the conical panel required a three-piece design including a sliding core.

The program's mold design concentrated on mold material, gate design, and temperature control. Clamping was provided by interfacing the molds with hydraulic press platens, and panel ejection was manual. Recirculating hot oil heating and cooling provisions were used for mold temperature control via a manifold distribution system with channels in each mold.

Each mold was fabricated out of 6061-T6 aluminum. The cavity surfaces were machined to the desired geometry on a numerically controlled machine. The final surface finish was obtained by hand polishing.

Each half of the flat mold was machined from single 6-inch (in.) thick pieces of aluminum which resulted in relatively distortion free molded panels.

Machining each component of the conical mold from single billets of aluminum was also preferred. However, billets of sufficient size were not readily available. As a result, the two major components of the mold were of a laminate construction. Six-in.-thick sections were bolted together to form a block from which the components were machined. This resulted in seams in the optical area of the mold. Prior to final machining operations the seams were welded. However, when the mold cavity was polished, surface irregularities developed at each weld, resulting in severe distortions in molded conical panels.

5. PROCESS EVOLUTION

Many process parameters are associated with the injection molding process used in this program, including material melt temperature, mold temperature, material drying time and temperature, and extruder screw speed. Proper settings for each parameter is essential to molding optically clear panels. Improper settings result in gross defects in the panels such as those seen in Figure 4.

The determination of optimum parameters was an iterative process comprised of defining process parameters, molding panels using the defined parameters, followed by panel evaluation and parameter adjustment. This cycle was repeated until evaluation of the molded panels revealed no appreciable improvement from those evaluated previously. Evaluation of the panels molded during this cycle included visual inspection (normal room light), luminous light transmittance (ASTM D-1003), and falling plummet impact tests. The impact test consisted of dropping from various heights a 20-lb "dart" with a 1.5-in. diameter tip onto a flat 6-in. square sample.

Each material which was molded required a different set of process parameters. This required that the optimization cycle described above be repeated for each one. Panels molded of each material after process parameter optimization are shown in Figure 5.

6. MOLDING OF CALIBRE 303

Initially 71 flat and 29 conical panels were molded of Calibre 303. This included optimization of process parameters and molding of panels for extensive evaluation as described in Sections 9 through 13. Toward the end of the program, approximately one year after Calibre 303 panels were initially molded, an additional 19 flat and 15 conical panels were molded.

As discussed in detail in Sections 9 through 12 Calibre 303 panels were generally of better quality than panels molded with Lexan PPC or Durel 400. Some Calibre 303 panels such as that shown in Figure 6 were exceptional, free of streaks, distortions, and opaque particles.

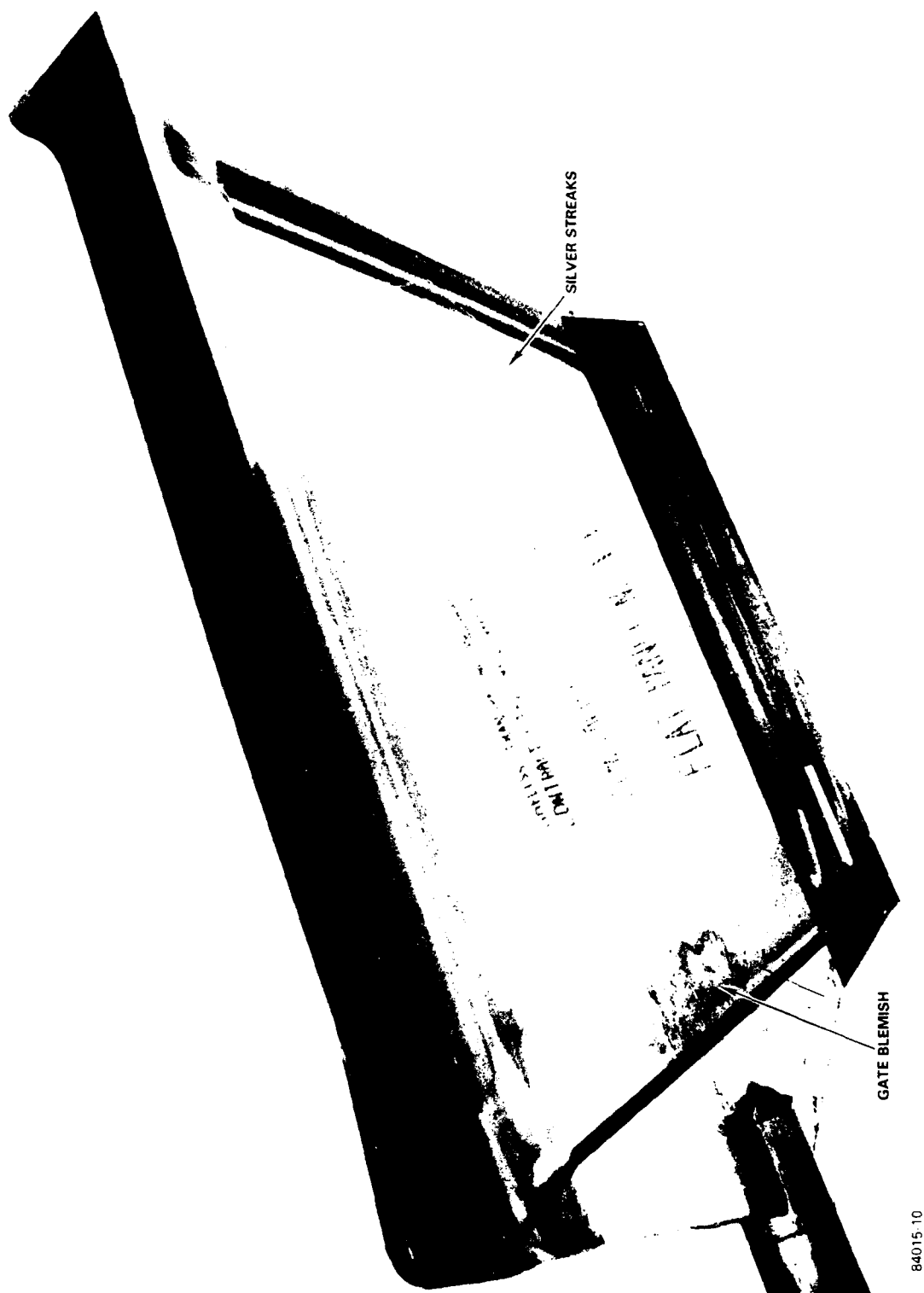
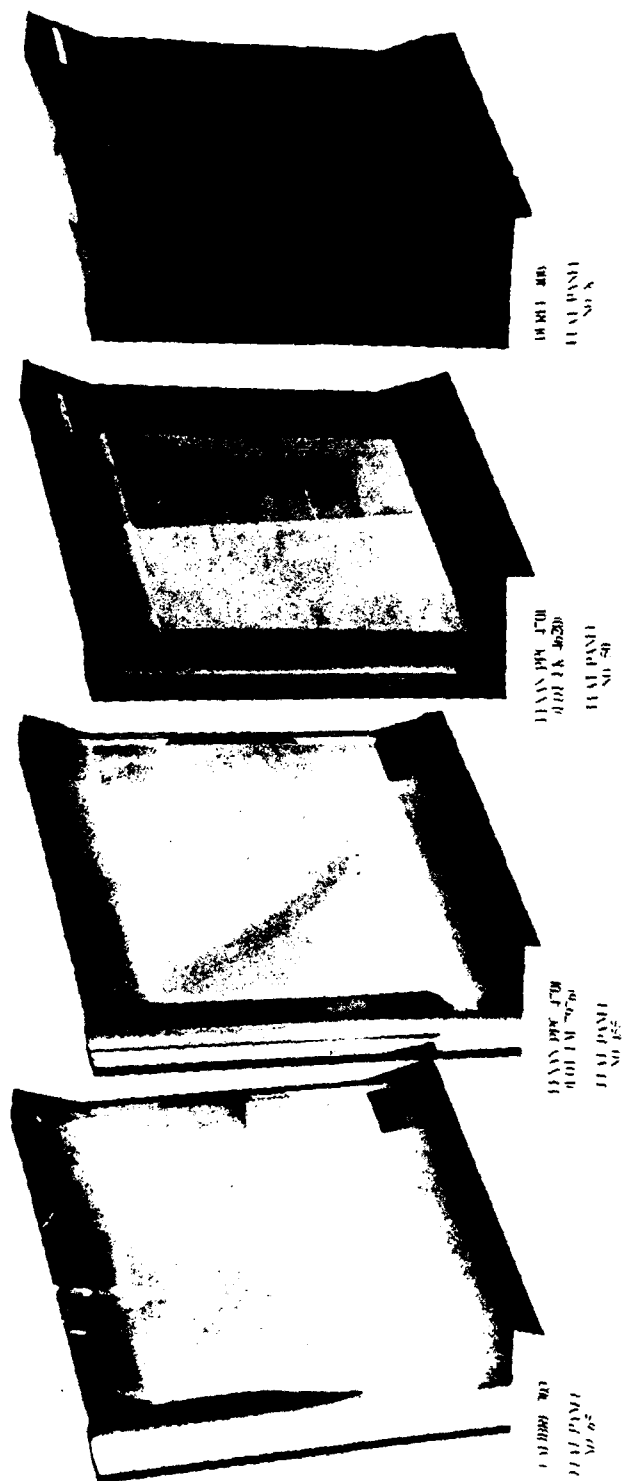


Figure 4. Defects in Calibre 303 flat panel.



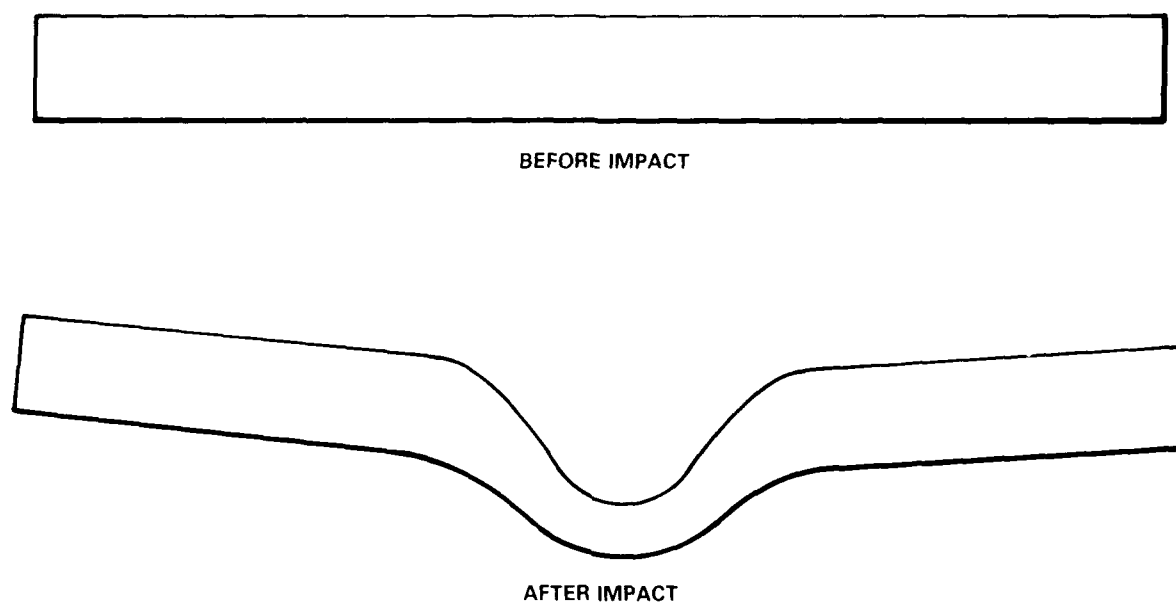
284015-11

Figure 5. Calibre 303, Lexan PPC 4701, and Durel 400 flat panels.



84015 12

Figure 6. Calibre 303 flat panel.



84015-13

Figure 7. Falling plummet test results for Calibre 303.

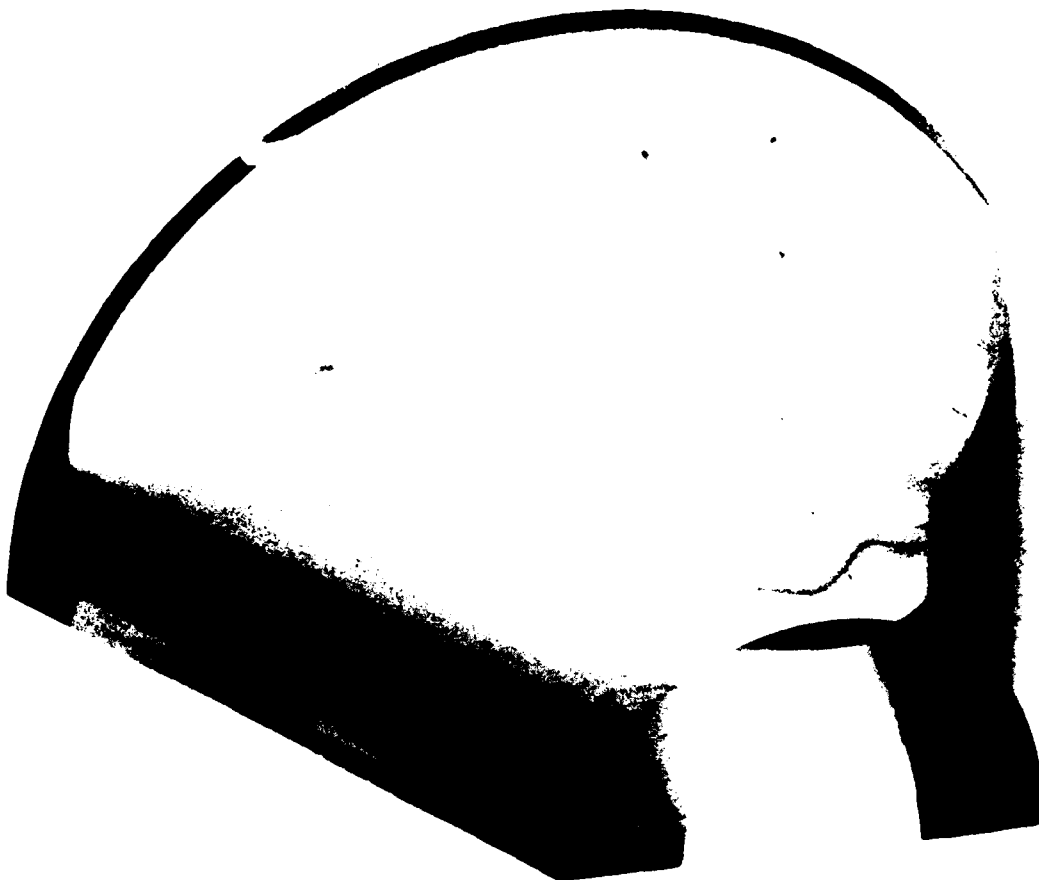
Falling plummet impact tests indicated that many Calibre 303 panels were very impact resistant, as good as, or better than extruded polycarbonate homopolymer sheet. For example, the sample in Figure 7 developed a deep, permanent, ductile bulge but did not fracture when impacted at relatively high energy.

Figure 8 shows a conical panel molded of Calibre 303. As discussed in detail in section 11, the optical quality of the conical panels was generally poorer than the flat panels due to severe distortions at the mold seams.

In general, the Calibre 303 molding process was very promising. It was demonstrated that large transparent articles could be injection molded with good clarity, substantially free of distortions, streaks, and opaque particles.

7. MOLDING OF DUREL 400

Durel 400 was a developmental material supplied by Hoechst-Celanese. The manufacturing lots used in this program were among the first from the semi-works facility established for Durel polyarylates. Durel 400 was supplied for this



FRAMELESS TRANSPARENCY PROGRAM
CONTRACT F3615-85-C-3402

DOW CALIBRE 303
CONICAL PANEL NO. 5

△84015-14

Figure 8. Calibre 303 conical panel.

program with complete disclosure of its development status and acknowledgement that its quality was inadequate for commercialization. Durel 400 was included, despite its immaturity, since its ultimate property goals were very attractive.

Panels molded of Durel 400 were of poor quality. As a result, after molding only eight flat panels, a decision was made to discontinue further molding and evaluation of the material.

All of the Durel 400 panels were dark brown similar to panel eight in Figure 5. Luminous light transmittance of the panels was low, ranging from 25 pct to 31 pct. Each panel also had streaks and other objectionable defects in the optical area. In the falling plummet impact tests, samples proved to have very poor impact strength, experiencing massive brittle failure at relatively low impact energies.

8. MOLDING OF LEXAN PPC 4701

8.1 General

Three manufacturing lots of Lexan PPC 4701 were molded in this program. Each lot provided somewhat different results. Regardless of lot, the panels molded of this material were generally not as good as those molded of Calibre 303.

Lots LK 4620 and LK 9096 were manufactured at a time when large-scale production of the material was just beginning. Material manufactured during this time period was acknowledged by GE to have thermal stability variations. Because of excessive lot variance, Lexan PPC 4701 was reformulated by GE to include a new heat stabilization package. The third lot, LM 7976, contained the new stabilizer package.

8.2 Lexan PPC 4701, Lot LK 4620

Initially, 20 flat panels were molded of lot LK 4620 to optimize process parameters. An additional 36 flat and 21 conical panels were then molded for extensive evaluation as described in sections 9 through 12. Though these panels were not as good as Calibre 303 panels, some were reasonably good in quality.

All panels molded with lot LK 4620 material had a distinct brown color as opposed to the yellow color of other lots. This tint resulted in relatively low luminous transmittance (approximately 55 percent). Lot LK 4620 contained a blue dye, despite the order specification of natural color. The discoloration may have been due to dye or other additive degradation, or degradation of the polymer itself.

Falling plummet impact tests were performed on a number of panels molded of lot LK 4620. Test results were somewhat erratic. Many samples proved to be very impact resistant, developing a deep permanent ductile bulge similar to Figure 7. Other samples experienced brittle failure when impacted.

8.3 Lexan PPC 4701, Lot LK 9096

Only eight flat panels were molded of lot LK 9096 material. The results of molding lot LK 9096 were significantly different from those of lot LK 4620. All panels molded with this lot were light yellow in color, with reasonably good light transmittance (82 to 84 percent). In falling plummet impact tests, the material proved to have poor impact strength.

8.4 Lexan PPC 4701, Lot LM 7976

This third lot of Lexan PPC 4701 was included late in the program to evaluate the reformulated material considered by GE to be typical of current commercial lots. One hundred and five flat panels were molded to optimize process parameters and obtain panels for extensive evaluation as described in sections 9 through 12. Lot LM 7976 had a light yellow tint similar to lot LK 9096. In falling plummet impact tests, impact strength from panel to panel was random. Some samples developed a ductile bulge similar to Figure 7 at high impact energies. Other samples experienced brittle failure at lower impact energies.

In addition to visual inspection, impact strength and light transmittance, gel permeating chromatography (GPC), and thermogravimetric analysis (TGA) were employed while molding lot LM 7976 material. GPC measured the molecular weight distribution of the material and TGA measured volatile content (primarily moisture). GPC data indicated slight thermal degradation of the resin as it progressed through the molding cycle, evidenced by decreases in molecular weight after extrusion, after residing in the accumulator, and after injection. TGA measurement of resin moisture content before molding combined with GPC test data proved that adequate drying is critical. Excessive moisture in the resin resulted in significant molecular degradation (decrease in molecular weight) during the molding process.

9. TESTING OF PANEL GEOMETRY FOR DESIGN CONFORMITY

Molded panels were measured to determine how well they conformed to design geometry. Calibre 303 and Lexan PPC 4701 lot LK 4620 panels were measured. PPC 4701 lot LM 7976 panels were not measured but were believed to be comparable to lot LK 4620.

The lengths, widths, and heights of many of the molded panels were measured with vernier calipers. The amount of panel warpage was determined on a flat granite slab by measuring the gap between the panels and the slab with a feeler gauge.

In general, the dimensional conformity achieved with the injection molding process met or exceeded that of conventional fabrication techniques.

10. OPTICAL EVALUATION OF MOLDED PANELS

10.1 General

The optical evaluation of each panel included visual inspection and measurements of luminous transmittance (T_{LUM}), haze, distortions, and angular deviation. These properties are summarized in Table 1 with the exception of angular deviation which is shown in Table 2. The values of Table 1 resulted from testing 21 flat and 10 conical Calibre 303 panels, 24 flat and 11 conical Lexan PPC 4701 lot LK 4620 panels, and 11 flat Lexan PPC 4701 lot LM 7976 panels.

10.2 Light Transmittance and Haze

Luminous transmittance and haze measurements (ASTM D-1003) on flat and conical panels are included in Table 1. All measurements were from the 0.5-in.-thick optical areas of the panels.

Average luminous transmittance of Calibre 303 flat and conical panels combined was approximately 75 pct. If no dye had been present in the material, values near 85 pct probably would have resulted.

Luminous transmittance of Lexan PPC 4701 lot LK 4620 panels was approximately 56 pct. The low light transmittance was due to the brown discoloration experienced by the material during the molding process. In contrast, average light transmittance of panels molded of lot LM 7976 was 83 percent.

The average haze of Calibre 303 flat and conical panels combined is 5.8 percent. Lexan PPC 4701 panels average 4.5 and 3.8 percent for lots LK 4620 and LM 7976 respectively. These haze values are only slightly higher than the requirements of actual laminated transparencies (e.g., 3 and 4 percent, respectively, for A/T-37 bird impact resistant transparencies, and F-16 uncoated canopies).

10.3 Visual Inspection

Each panel was inspected in normal room light for obvious defects. The following observations were made.

The majority of the flat Calibre 303 panels exhibited no significant defects in the optical areas of the panels such as streaks, opaque particles, or bubbles.

Conical panels molded of Calibre 303 also exhibited few defects in the optical area. However, every panel exhibited an undesirable light brown color.

The appearance of Lexan PPC 4701 panels was generally much poorer than Calibre 303 in that most exhibited objectionable streaks and other defects in the optical areas of the panels. Also, as previously mentioned, lot LK 4620 panels had an undesirable brown color.

TABLE 1. OPTICAL PROPERTIES OF PROCESS EVALUATION PANELS.

Material	Panel Type	T _{LUM} (pct)	Haze (pct)	Maximum Distortion
Calibre 303	Flat	74.3 to 75.4 X = 75.4	4.5 to 6.3 X = 5.0	1/18 to 1/20 X = 0.9
Lexan PPC 4701 Lot LK 4620	Flat	54.1 to 57.0 X = 55.9	3.6 to 6.2 X = 4.3	1/14 to 1/20 X = 1/18.1
Lexan PPC 4701 Lot LM 7976	Flat	82.5 to 83.8 X = 83.3	2.8 to 7.0 X = 3.8	1/3 to 1/20 X = 1/12
Calibre 303	Conical	72.3 to 74.2 X = 73.3	5.8 to 11.4 X = 7.5	
Lexan PPC 4701 Lot LK 4620	Conical	50.5 to 56.9 X = 54.3	4.2 to 6.4 X = 5.0	

X Denotes Average Value

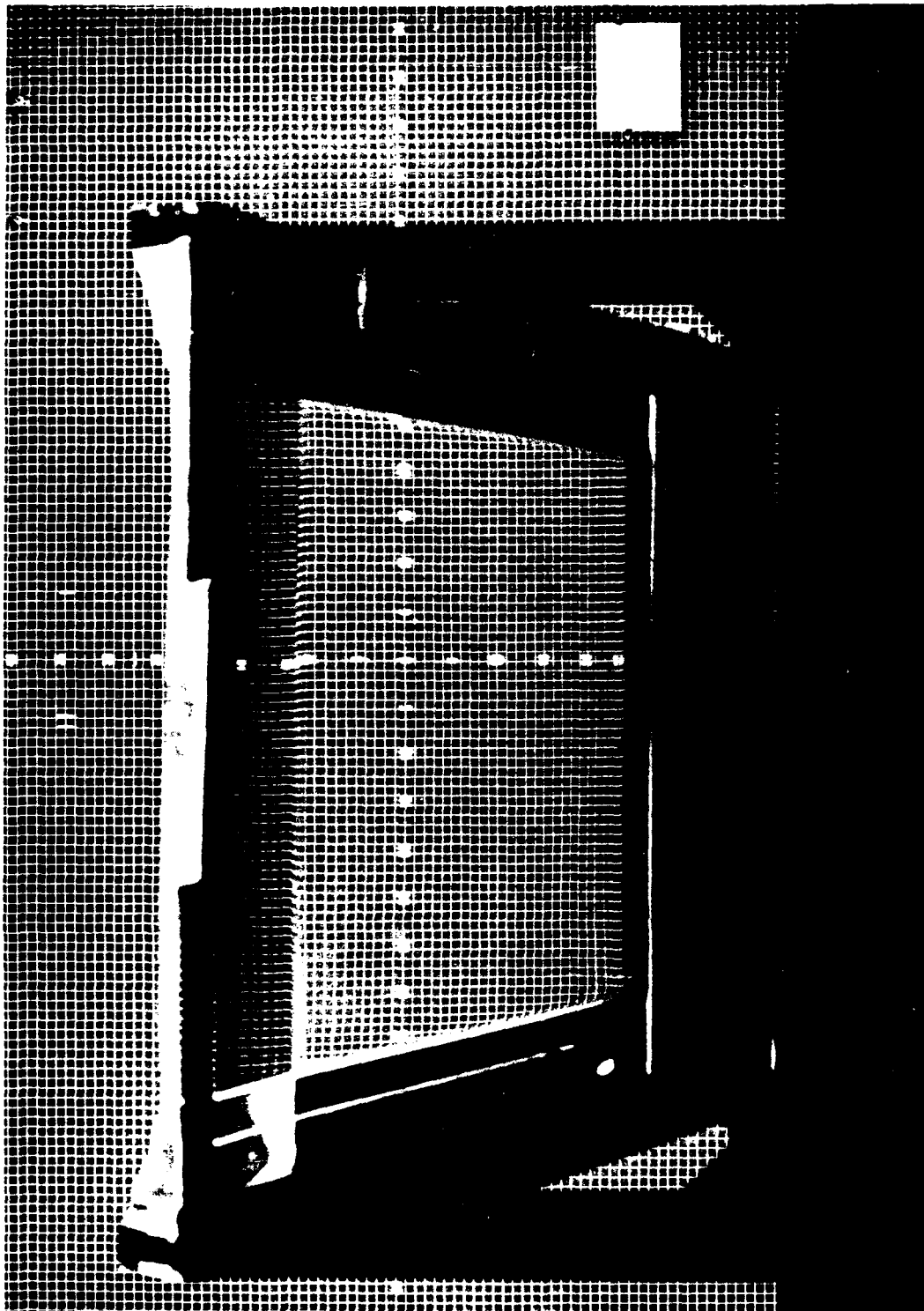
10.4 Optical Distortions

Gridboard photographs were taken per ASTM F-377 to measure optical distortion. The maximum grid slope of flat panels is included in Table 1. The viewing angle for the panels was 30 deg from the optical surface.

Flat panels molded of Calibre 303 and Lexan PPC 4701 lot LK 4620 were relatively distortion free, as typified by Figure 9. The maximum grid slope of Calibre 303 panels was excellent averaging approximately 1/20. Lexan PPC 4701 lot LK 4620 panels also had minimal distortions. Flat panels molded of Lexan PPC 4701 lot LM 7976 had slightly more severe optical distortions than other flat panels, but was still generally good (ref Table 1).

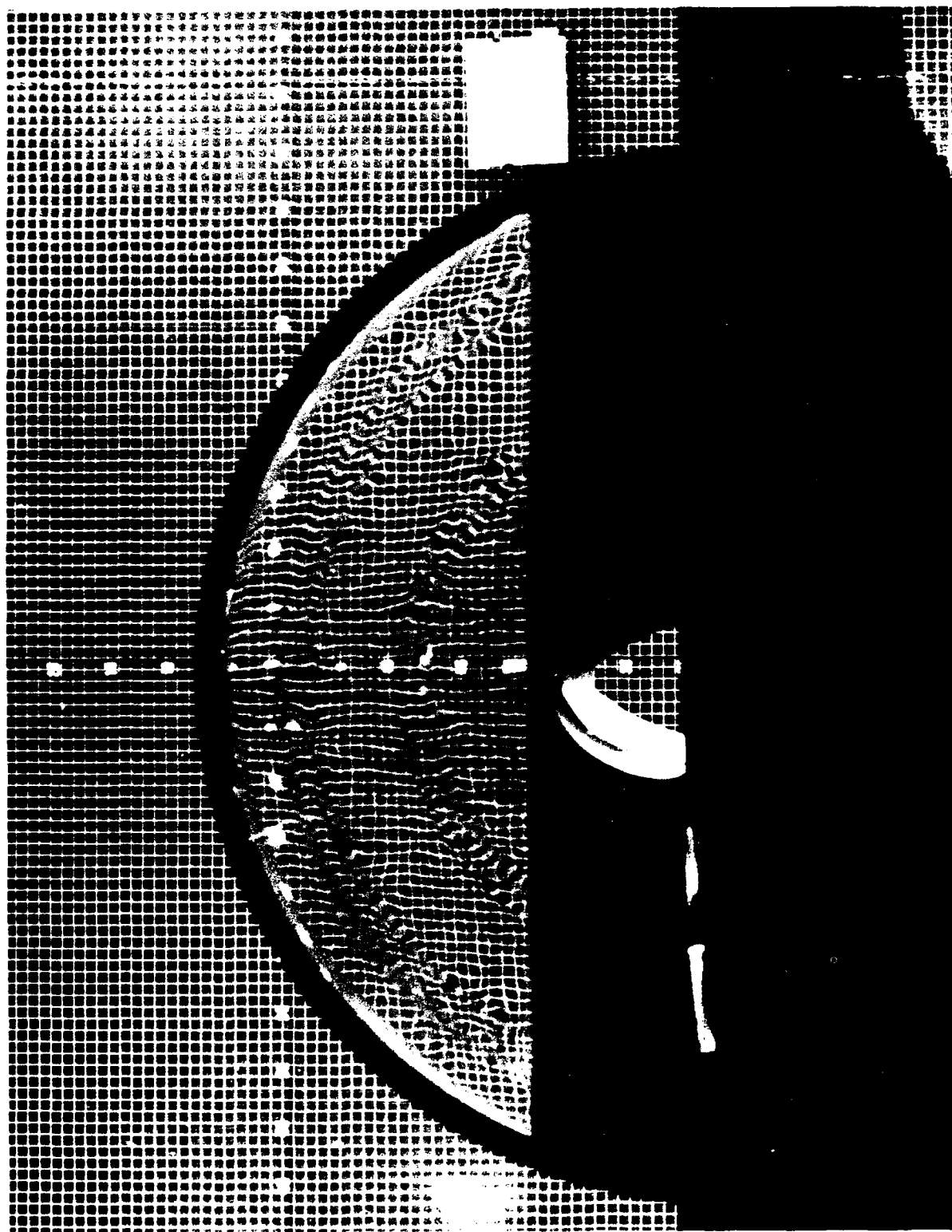
All conical panels, regardless of material type, exhibited severe distortions typified by the gridboard photograph of Figure 10. Because of the extremely poor optical quality of the panels, the maximum grid slope on conical panels was not measured.

The optical distortion in the conical panels was due to the seams in the mold. If the conical mold had been fabricated without seams in the optical area, distortion free panels comparable in quality to the flat panels probably would have resulted.



84015-32 E870109 63

Figure 9. Gridboard photograph of Calibre 303 flat panel.



84015-36 E870109 71

Figure 10. Gridboard photograph of Calibre 303 conical panel (ASTM F-733).

10.5 Angular Deviation

Angular deviation measurements were made per ASTM F-801 on all flat test panels at the five locations shown in Figure 11. Measured milliradian values for Calibre 303 and Lexan PPC 4701 flat panels are listed in Table 2. Angular deviation measurements of molded flat panels were more severe than typically attained with conventional fabrication techniques.

Because angular deviation is normally caused by nonparallel surfaces, thickness variations in the optical areas of several flat panels were measured. Both flat and conical panels exhibited a tendency to be thinner in the center of the panel, increasing in thickness toward the thick edge section and the gate. This thickness variation is believed to be, in essence, a "sink" caused by material shrinkage during solidification in the mold. Additionally, thickness profiles of the molded panels correlated with the flow pattern of molten materials into the molds.

11. PHYSICAL PROPERTIES OF MOLDED MATERIALS

11.1 General

The intent of performing physical properties tests in this program was to provide a comparison between molded material and currently used extruded polycarbonate homopolymer sheet, provide physical property design data, check for panel homogeneity and determine process reproducibility.

Tests were performed on samples cut from flat and conical panels in optical areas as well as the thick edge sections. All extruded polycarbonate control samples were cut from monolithic 0.5-in.-thick commercial grade Lexan sheet.

11.2 Tensile, Flexural and Compressive Properties

Physical properties testing included the following test methods:

- a. Tensile tests, ASTM D-638 (Standard Test Method for Tensile Properties of Plastics); static test with dog-bone shaped test specimen
- b. Flexural Tests (static), ASTM D-790 (Flexural Properties of Unreinforced and Reinforced Plastics and Electrical Insulating Materials); static test method utilizing simply supported three-point bending of rectangular test specimens
- c. High Rate MTS Beam (dynamic flexural) performed by University of Dayton Research Institute; test nearly identical to ASTM D-790 but with much higher strain rates
- d. Compressive tests, ASTM D-695 (Standard Test Method for Compressive Properties of Rigid Plastics).

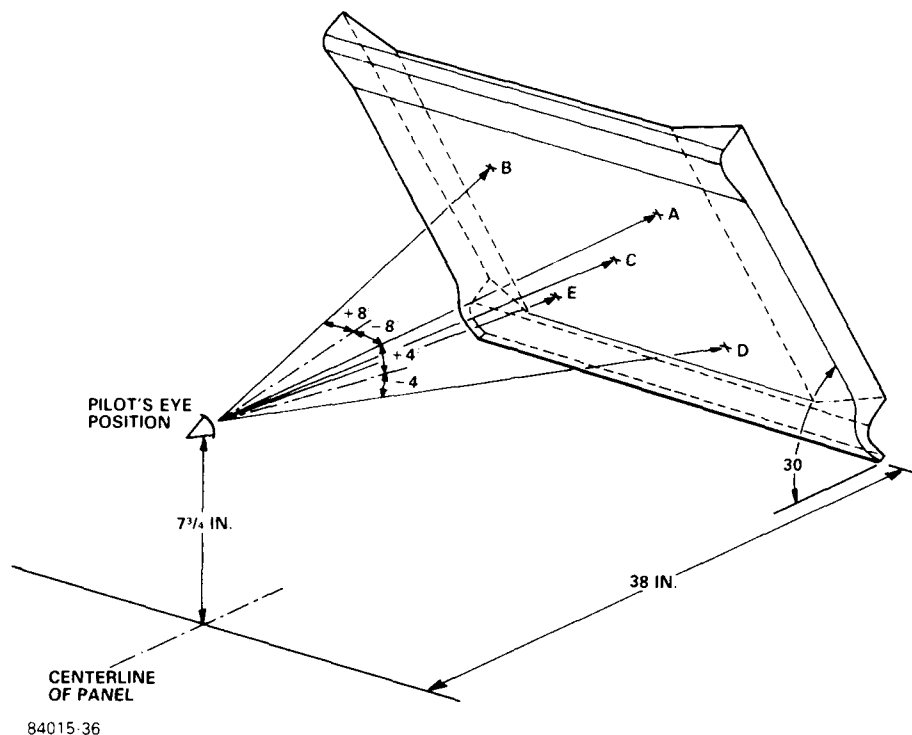


Figure 11. Locations and test geometry for angular deviation measurements.

Because of service temperatures experienced by aircraft transparencies, tensile, static flexural, and compressive tests were performed at -50 , 78 , and 150° F. All samples were allowed to reach thermal equilibrium prior to being tested. Tensile, flexural, and compressive properties of molded Calibre 303 and Lexan PPC 4701 proved to be very similar to extruded polycarbonate sheet.

The normalized tensile test data in Table 3 indicated that tensile properties of molded Calibre 303 and Lexan PPC 4701 were very similar to those of extruded polycarbonate. Flexural and compressive properties of these molded materials also proved to be very similar to extruded polycarbonate sheet. The test data also generally indicated that injection molded material was anisotropic and homogeneous.

Visual inspection of samples after tensile and dynamic flexural testing indicated that Lexan PPC 4701 was less ductile than the other materials. All Calibre 303 and extruded polycarbonate samples exhibited ductile deformation (necking) before fracture. However, from both lots of Lexan PPC 4701, many samples exhibited brittle fracture, particularly at -50° F.

TABLE 2. ANGULAR DEVIATION OF FLAT PANELS.

Material	Panel Location	Maximum Azimuth (mrad)	Minimum Azimuth (mrad)	Mean Azimuth (mrad)	Azimuth Standard Deviation	Maximum Elevation (mrad)	Minimum Elevation (mrad)	Mean Elevation (mrad)	Elevation Standard Deviation
Calibre 303	A	0.7	0.3	0.5	0.1	5.4	3.6	4.4	0.6
	B	-1.3	-0.7	-1.1	0.2	4.7	3.3	4.0	0.4
	C	0.3	-0.3	0.0	0.2	4.6	2.9	3.7	0.5
	D	1.8	1.1	0.8	0.3	2.4	-0.5	0.7	0.8
	E	-1.9	-1.3	-1.7	0.2	2.8	-0.3	0.6	0.7
Lexan PPC 4701 Lot LK 4620	A	1.9	1.2	1.6	0.2	8.9	5.6	6.5	0.7
	B	-2.4	-1.0	-1.9	0.3	7.8	5.8	6.6	0.5
	C	0.8	-0.3	0.2	0.3	6.5	3.6	4.9	0.7
	D	3.6	2.1	2.7	0.4	-2.6	0.6	-0.9	0.8
	E	-3.7	-2.1	-2.8	0.3	-2.0	1.5	-0.5	0.9
Lexan PPC 4701 Lot LM 7976	A	-0.8	-0.3	-0.6	0.1	8.0	5.3	6.3	0.8
	B	-0.3	0.2	-0.1	0.2	6.1	4.4	5.4	0.5
	C	0.6	-0.2	0.1	0.3	6.4	4.9	5.5	0.5
	D	-1.4	-0.6	-1.1	0.3	6.3	3.0	4.4	1.1
	E	1.0	0.2	0.4	0.2	4.7	2.7	3.4	0.5

TABLE 3. MEAN TENSILE PROPERTIES NORMALIZED TO THOSE OF EXTRUDED POLYCARBONATE SHEET AT 78° F WITH PARALLEL ORIENTATION.

Material	Panel Type	Sample and Location Orientation	-50° F				78° F				150° F			
			0.2 pct Offset Yield Stress (psi)	Ultimate Stress (psi)	Young's Modulus (psi)		0.2 pct Offset Yield Stress (psi)	Ultimate Stress (psi)	Young's Modulus (psi)		0.2 pct Offset Yield Stress (psi)	Ultimate Stress (psi)	Young's Modulus (psi)	
Calibre 303	Flat	Optical, parallel	1.34	1.35	1.05		1.01	1.00	1.00		1.04	0.85	0.99	
		Optical, perpendicular	1.33	1.34	1.05		1.01	0.99	0.99		1.13	0.88	0.95	
		Edge					0.98	1.02	1.05					
	Conical	Optical, parallel					1.02	0.97	0.93					
		Edge					1.05	1.00	0.97					
Lexan PPC 4701 (Lot 4620)	Flat	Optical, parallel	1.10	1.27	1.02		1.02	1.10	0.93		1.18	0.99	0.85	
		Optical, perpendicular	1.16	1.37	0.99		1.01	1.10	0.94		1.19	0.98	0.88	
		Edge					1.04	1.11	0.95					
	Conical	Optical, parallel					1.05	1.09	0.90					
		Edge					1.03	1.10	0.98					
Lexan PPC 4701 (Lot 7976)	Flat	Optical, parallel	1.03	1.37	0.86		1.12	1.13	0.93		1.02	0.98	0.90	
		Optical, perpendicular	1.09	1.21	0.90		1.06	1.14	0.96		1.02	0.98	0.95	
		Edge					1.05							
Extruded Polycarbonate Sheet		Parallel	1.20	1.36	1.03		1.00	1.00	1.00		1.15	0.88	0.92	
		Perpendicular	1.02	1.27	1.02		1.01	0.99	1.00		1.10	0.87	0.94	

11.3 Flexural Fatigue

ASTM D-631, entitled "Standard Test Method for Flexural Fatigue of Plastics by Constant-Amplitude-of-Force" was used to measure the ability of materials to resist mechanical degradation as a result of cyclic stress. This test method involved flexing of test specimens held in a cantilever manner.

Test results of molded Calibre 303 and extruded polycarbonate sheet specimens were nearly identical. Lexan PPC 4701 was more likely to fatigue than the other two materials.

11.4 Crack Propagation

Crack propagation tests were conducted per the following test method: "Resistance to Crack Propagation of Stretched Acrylic", sometimes referred to as the "Compact Tension" test. This method varies from the "K Factor" test of MIL-P-25690. The method is not widely used in the aircraft transparency industry but is currently under consideration by ASTM F7.08.

The test procedure involves tensile testing of notched specimens having a specially initiated precrack. The crack propagation factor (K_C) is relative, useful for comparative purposes only. Large values of K_C are indicative of greater crack resistance than lesser values.

As shown in Table 4, the average K_C value for molded Calibre 303 was even better than that for extruded polycarbonate sheet. Lexan PPC 4701 samples exhibited less crack resistance than the other materials.

12. ENVIRONMENTAL DURABILITY

Tests were performed to determine how resistant each of the molded materials were to chemical attack, condensing humidity, accelerated weathering, and abrasion. Extruded polycarbonate sheet was included in environmental tests for comparative purposes. Test specimens from molded panels were all cut from the optical areas of flat panels. The following environmental tests were performed:

- a. Chemical Stress Craze Tests: Flexurally stressed cantilever beam test specimen with solvent contact on tension surface
- b. Exposure to Condensing Humidity: Continuous exposure to 120° F/95 percent relative humidity for up to 1,000 hours
- c. Accelerated Weathering: ASTM E-838 (Standard Practice for Performing Accelerated Outdoor Weathering Using Concentrated Natural Sunlight). Total UV radiation corresponded approximately to the total incident UV radiation of a typical year in Phoenix, Arizona
- d. Abrasion Testing: ASTM F-735 (Standard Practice for Abrasion Resistance of Transparent Plastics and Coatings using Oscillating Sand Method).

TABLE 4. CRACK PROPAGATION TEST RESULTS

Material	Number of Samples	Maximum K_C	Minimum K_C	Average K_C	Standard Deviation
Calibre 303	32	10,704	8,198	9,138	552
Lexan PPC 4701 Lot LK 4620	28	6,798	4,728	5,430	528
Lexan PPC 4701 Lot LM 7976	32	10,337	6,480	7,951	743
Extruded polycarbonate sheet	12	9,235	7,540	8,261	545

In general, injection molded Calibre 303 and Lexan PPC 4701 performed comparably to extruded polycarbonate. The environmental deficiencies of extruded polycarbonate are well known and documented. Injection molded Calibre 303 and Lexan PPC 4701 exhibited the same deficiencies, including extremely poor abrasion resistance. If an actual aircraft transparency were to be injection molded from these materials, abrasion-resistant coatings or abrasion-resistant face plies would be required.

13. BIRD IMPACT ANALYSIS ON MOLDED PANELS

13.1 General

Bird impact of molded flat panels was studied empirically and analytically with finite element numerical methods. Empirical tests were performed with Loral's in-house air cannon, using simulated birds (gelatin cylinders). Finite element modeling of bird impact was performed using Materially and Geometrically Nonlinear Analysis (MAGNA) software. The purpose of this effort was to: (1) study the performance of molded material when subjected to the high strain rates of bird impact, and (2) using MAGNA, predict the dynamic response of molded panels during impact and compare that prediction with empirical results.

13.2 Empirical Tests

All impact tests were performed on Calibre 303 flat panels. A total of 11 shots were made, each on a different panel. Each test included projectile velocity measurements. High-speed photography recorded the dynamic response of each panel.

13.2.1 Test Method

Each impact test was performed identically with exception of the velocity of the projectile which was intentionally varied. Impact location was near the center of the panel at a 30-deg angle as shown in Figure 12. Nominal gelatin projectile weight was 2 lb. Geometry was cylindrical having a 3.5-in. diameter and 5-in. length. The panel support structure was of a heavy-walled steel I-beam construction.

For nine of the impact tests, the panels were supported (clamped) on three sides, with the aft edge unrestrained. For two tests (numbers 1136 and 1137), four sides of the panels were clamped, including the aft edge.

13.2.2 General Test Results

Impact velocities ranged from 175 to 220 knots. With the aft edge unrestrained it appeared that velocities in the range of 180 to 190 knots were required to cause panel failure.

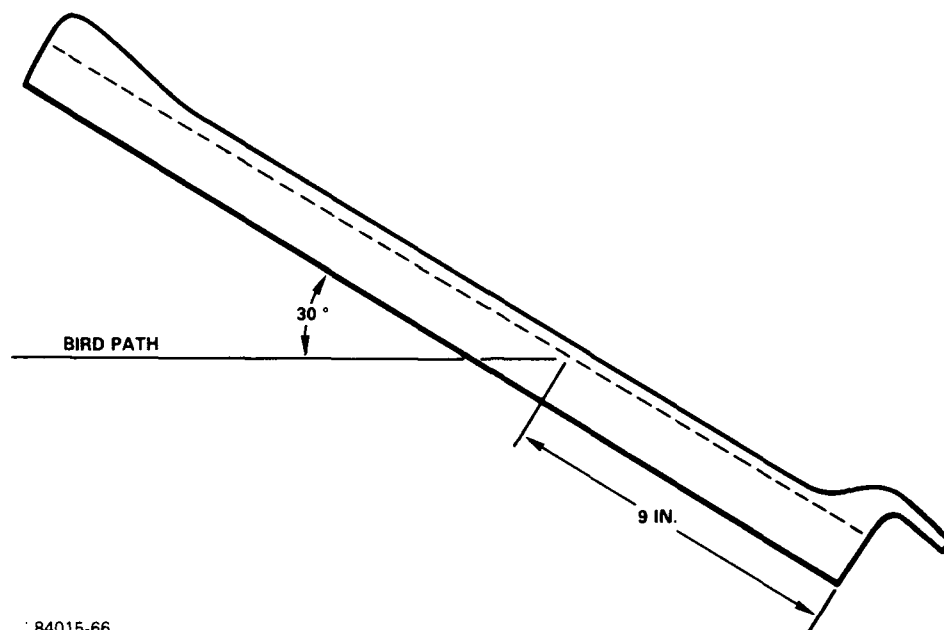
Inspection of panels after impact revealed no plastic deformation. Unfortunately, of panels that fractured, it appeared that material failure occurred in the linear region of the stress strain curve.

Fracture patterns were different on each panel that failed. Tendencies for fracture to occur at specific points on the panels or at knit lines were not evident.

13.2.3 Dynamic Response of Test 1134

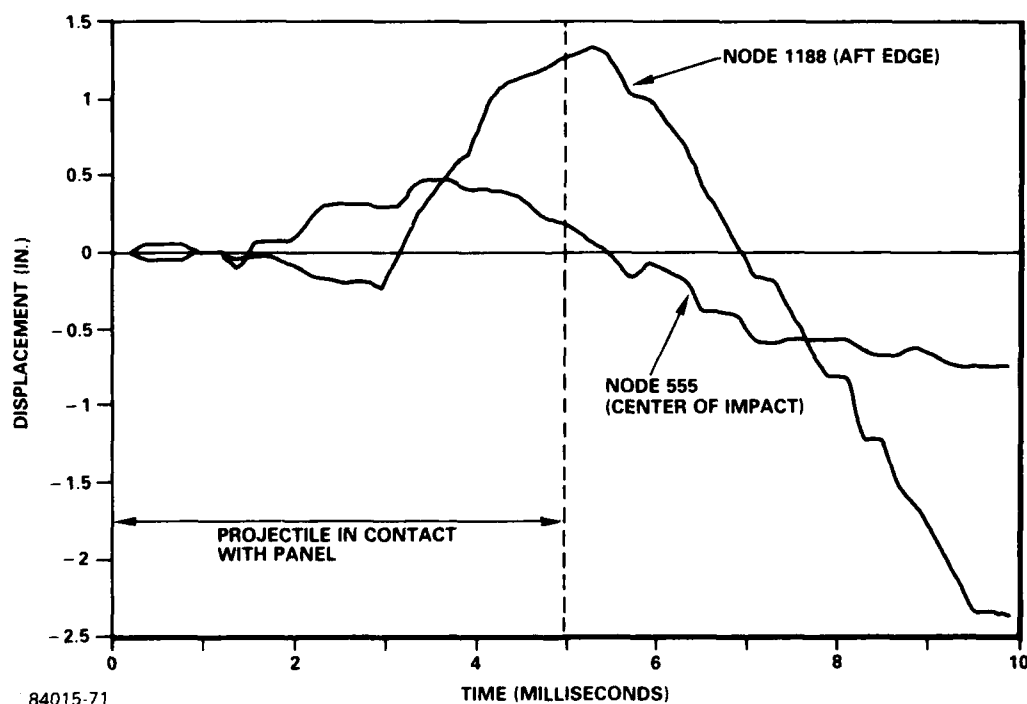
By triangulation, using film footage from two cameras, displacement of several points on the panel surface was calculated for one test. For comparison, the points corresponded with node locations of the MAGNA model.

Displacement normal to the panel surface for two points along the centerline of the panel is shown in Figure 13. Point locations are identified in Figure 14.



84015-66

Figure 12. Orientation of panel for simulated bird impact testing.



84015-71

Figure 13. Deflection normal to panel surface during impact test 1134.

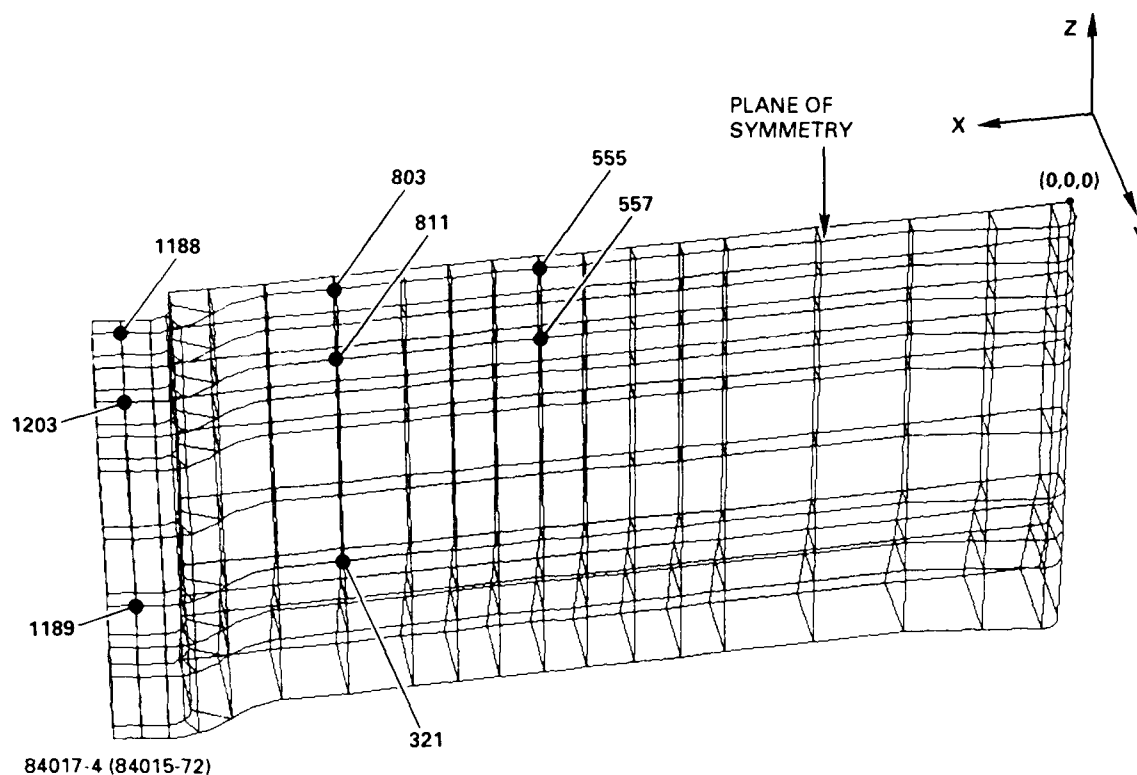


Figure 14. Locations and node numbers of triangulation/displacement measurements.

Typical of such tests, impact results in an oscillatory motion, with the panel rebounding after contact by the projectile. Displacement of the points is quite large, particularly at the aft edge.

For a rigidly supported panel, hysteresis dictates decaying oscillation after impact. Contrary to the expected, more displacement was measured on the rebound than during initial contact by the projectile. For example, node 1188 displacement in Figure 13 peaked at 1.34 in. shortly after the projectile passed. Rebound deflection peaked considerably higher at 2.42 in. Film coverage indicated that this excessive rebound deflection was due to movement of each side clamp relative to the main support structure. This allowed some slippage of the tapered edge sections of the panel in the clamps. This was probably the biggest contributor to the difference between empirical and MAGNA derived displacements.

13.3 MAGNA

13.3.1 Objective

The primary objective of the MAGNA analysis was to predict the dynamic response of a flat panel during impact and the impact velocity required to cause failure of the panel.

Similar to empirical tests, a 2-lb projectile was assumed for the MAGNA model. The impact velocity of test 1134 was used for the model (184 knots). This velocity was near the threshold velocity required to cause failure.

13.3.2 MAGNA Model Description

13.3.2.1 Geometry

The initial geometry of the molded panel for use with MAGNA was supplied to Loral by USAF. This model was refined by Loral, using the MAGNA preprocessor PREP, to obtain the model shown in Figure 14, having 180 elements and 1270 nodes. Only half the panel was modeled due to symmetry in the panel and an impact location along the centerline.

13.3.3 MAGNA Results and Conclusions

MAGNA predicted panel deflection during impact is depicted in Figure 15. MAGNA predicted displacement at each node is generally less than empirically derived displacement. At many nodes such as that shown in Figure 16, agreement is reasonably close up through the initial deflection (5 to 6 milliseconds). Upon rebound of the panel agreement is very poor with empirical displacement being much larger than MAGNA predicted.

The major factor contributing to the discrepancies between empirical and MAGNA predicted displacements was inconsistencies between MAGNA boundary conditions at the tapered edges and those actually observed. Three-dimensional constraints along the edge sections allowed absolutely no movement in the MAGNA model. However, high-speed film coverage revealed that movement occurred. The tapered edge clamps were not as rigid as supposed. Movement was much more pronounced during panel rebound than initial deflection, explaining the large discrepancies between MAGNA predicted and empirical results during that portion of the event.

14. PROGRAM CONCLUSIONS AND RECOMMENDATIONS

Injection molding is a very promising forming process for aircraft transparencies. There is potential for significant cost reduction and improved quality over conventional fabrication processes. The process is applicable to virtually any transparent thermoplastic material, offering the potential of reducing time lags between material development and incorporation into a transparency.

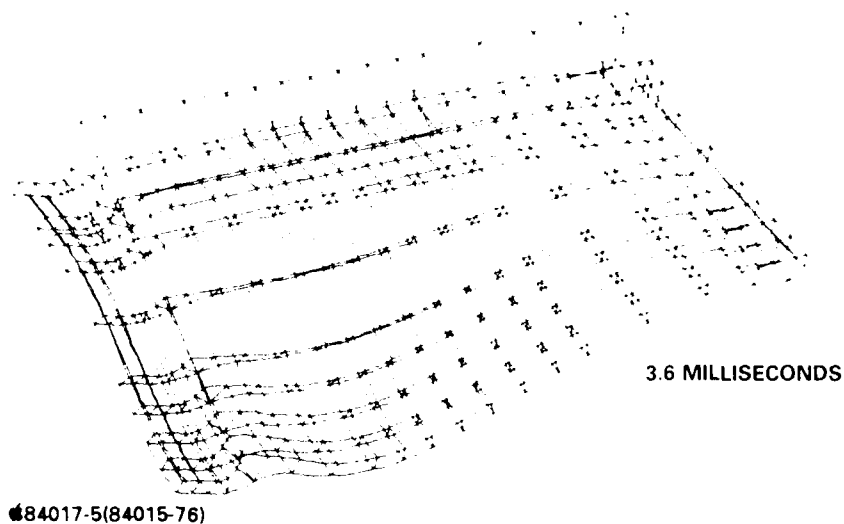


Figure 15. MAGNA-predicted panel deflection 3.6 milliseconds after initial contact by projectile.

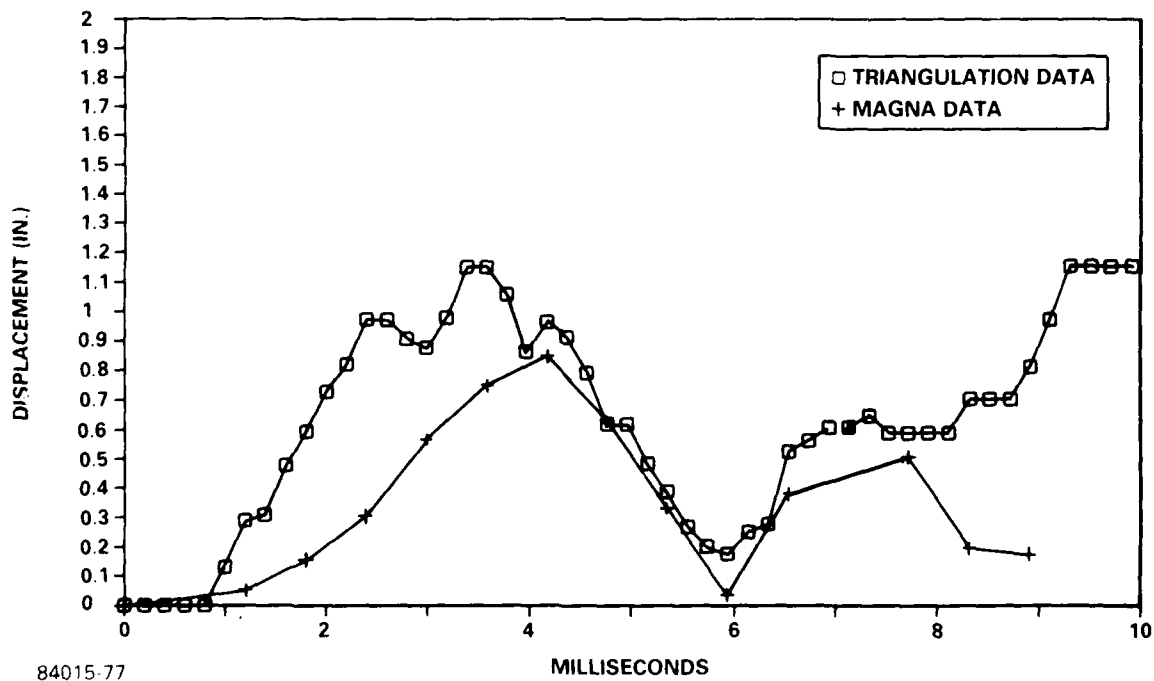


Figure 16. MAGNA-predicted and actual displacements at node 555.

While showing great potential, injection molding of transparencies is in its infancy. Further development is required and recommended, with scale-up to full size articles.

The areas of success in this program as well as those requiring further development in subsequent programs are discussed as follows:

- a. Dimensional Conformance: The panels molded in this program exhibited excellent dimensional consistency, suggesting that close tolerances can be met. Dimensional tolerances of injection molded transparencies can most likely match or exceed those of conventional fabrication processes.
- b. Optical Quality: The optical quality attained with Lexan PPC 4701 was less than desired. The optical quality of Calibre 303 panels was generally good. Panels were molded with acceptable light transmittance and haze, exhibited good clarity, and were virtually free of opaque particles and other objectionable defects. The flat panels demonstrated that distortion-free transparencies can be injection molded.

Angular deviation measured on injection molded panels is significantly higher than typically attained with conventional fabrication processes. For improvement, better thickness uniformity in optical areas is required and should be addressed in subsequent programs.
- c. Physical Properties of Molded Material: Injection molding of material can result in acceptable physical properties for aircraft transparencies. The properties of molded Calibre 303 compare very favorably with those of extruded polycarbonate sheet. Lexan PPC 4701 compares favorably in most aspects but is less ductile.
- d. Environmental Durability: The environmental durability of molded materials is generally comparable to extruded polycarbonate. Abrasion-resistance of each molded material is poor. Abrasion resistant coatings or face plies are required on these materials for transparency use. This should be addressed in subsequent programs.
- e. Bird Impact Test: Bird impact tests were successful in that molded panels withstood significant impact velocities without failure. Panel deflections were quite large. Knit lines molded in the panels did not appear to diminish structural integrity of the panels which fractured. Thickness discontinuities designed into the panel (optical area/edge section transition) were not locations for failure origins.

Material failure in the Hookean region of the stress strain curve, prior to plastic deformation, was unfavorable. MAGNA predicted deflection agreed fairly well with empirical results through the initial deflection of the panel. During panel rebound, agreement was poor, with empirical deflection being much greater than that predicted by MAGNA. Nonrealistic MAGNA boundary conditions accounted for the discrepancy.

- f. Final Article Molding: The Calibre 303 flat and conical panels which were molded for delivery to USAF at the end of the program further demonstrated that injection molding of aircraft transparencies is feasible. The quality of the panels was even better than those molded previously in the program. This group of panels also was indicative of the repeatability of the molding process.

ULTRAVIOLET-CURED PROTECTIVE COATING SYSTEMS FOR
AEROSPACE TRANSPARENT PLASTICS

Alexander Z. Bimanand
J. A. Raffo

Sierracin/Sylmar Corporation

ABSTRACT

ULTRAVIOLET-CURED PROTECTIVE COATING SYSTEMS FOR AEROSPACE TRANSPARENT PLASTICS

by

Alexander Z. Bimanand
J. A. Raffo

Sierracin/Sylmar Corporation

Due to its ductility, stability and good optical and electrical properties, gold coating has emerged as a viable choice for solar coating of advanced aircraft windshields and canopies.

New technology gold solar coating systems for polycarbonate and acrylics have been developed in this work. The organic coatings involved in these systems as base and topcoat are cured by ultraviolet radiation and offer significant improvements over traditional, thermally cured coating systems in adhesion, abrasion resistance, solvent resistance and humidity resistance.

F-16 canopies coated with UV system perform successfully against bird strikes at 350 knots. UV technology also offers processing advantages such as faster turnaround, cleaner coatings, close-to-room-temperature curing and energy and area efficiency.

In the course of this work, a UV robot was developed to cure coatings on production canopies and windshields. The robot is capable of three axes of simultaneous motion; e.g., horizontal, vertical and sweep.

BACKGROUND

Coatings were initially used in Sierracin/Sylmar designs for the thin, transparent heating system (designated S-303 using gold as the conductive metal), which defogged or de-iced commercial aircraft windshields and side panels; they incorporate a thin organic basecoat to accept the metal and a polymer film topcoat to protect the fragile gold conductive layer from processing or environmental damage. The organic coatings also enhanced light transmittance due to reduction of substrate roughness and improved refractive index match with the metal film. These coatings along with the metal film are laminated to the structural plies to form an integral part of the final laminate.

Another utilization of coatings by Sierracin/Sylmar Corporation was introduced in 1969 on the interior surface of the Grumman EA-6B monolithic stretched acrylic forward and aft canopies. This was the first use of a continuous metal 'first surface' film coating system as an energy-reflective coating which protects the cockpit crew from exposure to radiation emitted as part of the aircraft's electronic countermeasure (ECM) mission.

The coating systems used from the early '60's thru the mid-'80's have proven adequate to withstand the field environment on an extensively-used aircraft such as the F-16, but they are not sufficiently abrasion and solvent resistant and have a limited service life when used on exposed surfaces. In answer to these service-life-limiting characteristics, Sierracin has developed, through internal Research and Development funding, a new class of first-surface coating systems for aircraft windshields.

INTRODUCTION

Traditional coating technology has required the use of film-forming polymer systems to thoroughly wet and cover relatively rough substrates, promoting adequate adhesion and coverage through a combination of physical and chemical interaction. These systems very easily resisted the chemical attack of aggressive solvents and acquired abrasion resistance by incorporating thermosetting characteristics brought about during thermal cure of crosslinking chemical groups or, in the case of thermoplastic (or lacquer) systems, by the thermal evaporation of carrier solvents from relatively high molecular weight polymers.

These heat-curing systems often require extensive time at high temperature to effect chemical cure or evaporation and thus the range of coatings useful for application on finished aircraft windshield

laminates or components is limited to the maximum temperature to which the part can be exposed. Usually, compromises in the curing temperature must be made to maintain part contour through prolonged heat exposure.

These departures from an ideal cure may reduce ultimate coating properties. For this reason, effective coating systems which cure at or near room temperature have long been desired by transparency chemists and engineers.

Sierracin/Sylmar Corporation has developed a family of such coating systems for use on polycarbonate and acrylic aircraft windshield substrates which, in conjunction with gold or other metal films, can perform the traditional coating roles of substrate protection, heating/de-ice/defogging and ECM/RCS/solar reflection. These coating systems are able to perform at the maximum of their capabilities without extensive thermal curing through the utilization of ultraviolet light (UV) curing chemistry which causes extensive crosslinking reactions to occur at room temperature. This technology has been developed and scaled-up to production processing on the interior polycarbonate surface of all Sierracin F-16 aft and forward canopies under the designation S-373.

This paper describes the attributes and production process characteristics of the S-373 UV coating system and compares them to a Sierracin and a competitor's older technology coating system designated P-1 and P-2, respectively. An analogous UV technology system for acrylic carries the S-383 nomenclature.

RESULTS AND DISCUSSION

Advantages and Benefits of Radiation Curing

Radiation-curable coatings have several advantages over conventional thermal cure systems. Some of the benefits are listed below.

1. Fast cure: Application and curing of S-373 system on canopies takes minutes instead of hours for heat-cured systems.
2. Reduced energy consumption: The means of producing the energy is electrical, which could save 60-90% in energy over thermal curing.
3. Smaller floor area requirement: The parts can be coated and cured in the same coating room. No need for bulky ovens.
4. Ability to coat heat-sensitive parts: The risk for loss of contour and delamination of canopies and windshields due to heat is eliminated since the curing is done near room temperature. No need for expensive oven fixtures.

5. Cleaner coating: Because both application and curing are done in the same clean room, the UV coatings are generally cleaner than the conventional coatings that remain tacky after the air-drying period.
6. Versatility in chemistry: It is possible to obtain coatings with a wide range of physical properties using acrylated resins and monomers.

Formulations

The UV curable coating compositions used in this work can contain mono-, di-, and multi-functional acrylate monomers, acrylated urethane and epoxy oligomers, acrylated acrylic, polyester and cellulosic polymers, photoinitiators, flow control agents, antioxidants and solvents. The coatings are applied to the parts and, after the air-drying period, are exposed to ultraviolet radiation to initiate polymerization and crosslinking by free radical mechanism. Table 1 shows a typical recipe for a UV curable acrylate composition with a solids content of about 50%. Wide variations in cured properties can be achieved by varying the ratios of ingredients in the composition.

In a complex formulation such as a UV curable coating, each component contributes to the overall performance.¹ For example, urethane acrylates enhance extensibility and flexibility properties. Multi-functional monomers have two or more reactive sites per molecule. Because of this, they are generally useful for increasing the cure speed and crosslink density of the cured film. This latter property is important for developing solvent and abrasion resistance. Mono-functional monomers are primarily incorporated into formulations to reduce viscosity and, in some cases, to promote adhesion.²

The choice of a photoinitiator package could have a major effect on surface cure and through-cure characteristics of a clear film.³ The cure speed and adhesion are also affected by the photoinitiators. The stabilizers must be selected so as to adequately prevent the system from curing prematurely, yet not significantly inhibit the cure upon exposure to UV light. Other additives are added to counteract oxygen inhibition during UV curing in air, and to modify viscosity and surface flow properties of the liquid coatings.

The film integrity, appearance and application are significantly affected by the nature of the solvent mixture even though solvents are not a permanent component of these compositions. After flow-coating on the substrate, the film viscosity increases as the solvents evaporate. A solvent must evaporate relatively quickly during initial drying to prevent excessive flow, but it must evaporate slowly enough to give sufficient leveling and adhesion. If the solvent composition changes adversely during evaporation, precipitation of the resin can occur, and the film will have no mechanical integrity.

Flow-coatable coatings free from surface defects such as cratering, fish-eyes, haze, orange-peel, sagging, etc. have been formulated by proper choice of monomers and oligomers, adjusting viscosity and surface tension, and balancing the solvency and evaporation rate of the solvents. We have investigated several hundred compositions and the culmination of these studies gave several preferred UV-curable formulations to be used as base and topcoat in S-373 and S-383 systems.

Coating Application

Because of the large size of some canopies such as F-16, it was quickly decided to make all liquid applied coatings compatible with Sierracin's standard flow-coating technology. This has been used for many years for application of basecoats, topcoats, hardcoats, etc. on a large number of aircraft windshields and canopies. The coatings are applied to the substrate and the solvents evaporated, leaving a layer of deposited solids which is then exposed to ultraviolet radiation to initiate curing without retaining any solvents after the air-drying period.

Production UV Curing Equipment/Facility

A programmable position-controlled gantry robot, shown in Figure 1, has been designed and constructed by Sierracin to cure the coatings uniformly at desired energy levels on compound-curved canopies of different shapes and sizes.

The robot moves the UV lamp through three axes of motion, singly or simultaneously, to cure coatings on canopies up to 10 feet long. The motions are horizontal, vertical and sweep (270°) with resolution of 1×10^{-2} inches. The robot also has a 4th axis which enables it to cure coatings on large flat or curved panels up to 6 x 78 feet.

The controller system includes an indexer, driver, motor power supply, related switches, relays, etc. for each motor. The indexer has non-volatile (EEPROM) program storage with limited capacity, but can be accessed by a computer through its RS-232C interface.

The clean room doors are equipped with safety interlock switches to turn off the UV lamps if the room doors are opened during an automatic cure cycle. Also, an explosive atmosphere detector, with its sensor in the room, can override the controller to shut down all electrical systems if a dangerous concentration of explosive vapor is detected in the cell.

Basecoat

The basecoat is a vital part and is the foundation of the assembly of layers which comprise the metal coating system, as shown in Figure 2.

It serves to promote and assure adhesion between the thermally-deposited gold layer and polycarbonate substrate. The basecoat must not only adhere tenaciously to the polycarbonate substrate but must have the metal adhere similarly to it. It has been shown that some coatings, even as thin as a few microns, can very significantly reduce the impact resistance of the substrate. The important impact resistant properties of polycarbonate must not be affected by the basecoat. The basecoat should also not have undesirable functional groups which may render the metal layer optically unacceptable. Additionally, surface defects on the polycarbonate (or acrylic) should be effectively covered by the basecoat. It should be hydrolytically stable to remain intact during humidity exposure and have relatively good solvent and abrasion resistance to withstand washing and handling procedures encountered in production.

Gold Coating

The gold is thermally evaporated onto basecoated parts in high vacuum chambers. The following parameters have been optimized in order to maximize the gold adhesion in the S-373 and S-383 solar coating systems.

- Initial pumpdown pressure.
- Type of gas used as glow discharge (GD) medium.
- Pressure in the chamber during GD.
- Duration of GD.
- Period of time between GD and gold deposition.
- Pressure in chamber during gold deposition.

Topcoat

The function of the topcoat is to protect the underlying layers, in particular the gold, from the severe environmental exposures to which the solar coating system is subject. Clearly then, not only must the crosslinkable UV topcoat adhere well to the gold layer, but it must not deteriorate gold-basecoat adhesion. The topcoat must also have no adverse effect on impact resistance of polycarbonate; it must have good optics free from cosmetic defects, good hydrolytic stability to offer good humidity resistance, and good solvent and abrasion resistance.

Adhesion

To determine the adhesion of each coating, 100 uniform squares were scribed into each cured film using a scribe with 11 equally spaced (1 mm) parallel blades. 3M's #600 pressure-sensitive tape was then applied to the scribed area and rapidly pulled away from the substrate. The tape pull was repeated 5 times using a fresh tape for each pull. The adhesion was recorded as the approximate percentage of squares remaining after tape removal from the surface. This method is similar to one described in ASTM D 3359-87.

Abrasion Resistance

Sierracin uses two methods to screen and characterize the abrasion resistance of plastic surfaces.

Bayer Abrasion

The Bayer abrader test (ASTM F-735) has been used to evaluate the ability of a surface to resist scratching and rubbing erosion. The test has been adopted by ASTM as a standard abrasion test method for abrasion resistance of transparent plastics used in aircraft glazing. The test consists of quartz silica sand oscillating over the test specimen surface. The amount of surface haze induced in the panel is a measure of abrasion resistance. The comparative data for P-1 and P-2, S-373 and S-383 solar coating systems, as well as polycarbonate, acrylic II and stretched acrylic is presented in Table 2 and Figures 3 and 4.

According to these results, the Bayer abrasion resistance of S-373 and S-383 is markedly superior to the other production systems.

Taber Abrasion

The Taber abrader test (ASTM D-1044-73) is a widely-used method for plastics. This test consists of two grit-filled rubber wheels to which a predetermined weight is applied. The wheels abrade the substrate surface as it rotates on a table. Increase in haze is used as the criteria for measuring the severity of abrasion. The test results after 100 cycles using CS-10F wheels, 500 g load, are provided in Table 2 and Figure 5. The data indicates that S-373 and S-383 systems have excellent Taber abrasion resistance.

Solvent and Chemical Resistance

The solar coating systems, P-1, P-2, S-373 and S-383 were exposed to solvents and chemicals for a period of 30 minutes and then inspected for haze, blistering, crazing, swelling and any other defects. The resistance of S-373 and S-383 to chemicals normally encountered by aircraft transparencies is shown in Table 3. For other chemicals and solvents, the comparative results are given in Table 4.

The P-1 and P-2 systems have limited solvent resistance. Even non-aggressive solvents such as methanol and isopropyl alcohol readily swell and soften these systems. On the other hand, S-373 and S-383 offer outstanding resistance to a wide range of aggressive chemicals and solvents including alcohols, ketones, acetates, aromatics, chlorinated hydrocarbons, and acids and bases.

Temperature/Humidity Exposure

Coupons of S-373 solar coating on F-16 laminates and S-383 on stretched acrylic were exposed to condensing humidity (100% RH) at 106°F for 1000 hours. After exposure, the specimens were inspected for evidence of degradation, adhesion loss and change in light transmittance or haze. Results for S-373 are listed in Table 5. After the test, there was no evidence of deterioration, loss of crosshatch adhesion or crazing by 30-minute exposure to methyl ethyl ketone, isopropyl alcohol, and ethylene glycol. The initial light transmittance and haze did not change significantly after exposure. Similar results were obtained for S-383 and P-1. However, after only 72 hours of humidity exposure, P-2 mottled and blistered, with loss of adhesion. This data shows that despite the superior solvent and abrasion resistance, no compromise is made in the humidity resistance of S-373 and S-383.

Luminous Reflectance and Transmittance of S-373

Samples of F-16 laminates were coated with S-373 at various metal densities and measured for luminous reflectance and transmittance using a Sierracin-developed Model 20 Photometer. Reflectance was measured from the conductive-coated side. Reflectance standards were a Pyrex disc at 7.1% and air at 100%. Sheet resistance was measured using a contact probe and a non-electrical contact Sheet Resistance Monitor also developed at S/SC. Similar resistivities were measured using both techniques. Table 6 shows the average resistance of each coupon with corresponding light transmittance and reflectance. The reflectance of S-373 as a function of resistivity on F-16 laminates is shown in Figure 6.

Bird Impact Test

An F-16 'C' forward canopy coated with S-373 successfully passed the impact of a 4-pound bird at 350 knots.

Dart Impact Test

Dart Impact tests were performed at General Research Corporation in Santa Barbara, California. This test provides a record of the load and energy absorption that the sample experiences as fracture occurs. Brittle versus ductile failures are differentiated by the computerized loading profile. The Dynatup Model 810 equipment assures that each impact sample will be exposed to an adequate amount of energy necessary to cause failure reproducibly. The total energies absorbed by F-16 laminates (with S-111 urethane interlayer) at 72°F coated with various solar coating systems is presented in Table 7. The specimens were impacted at 8 ft/sec. by a hemispherical (1" dia.) indenter, made from hardened steel, on the opposite side of the solar coatings (reverse impact). The new technology solar coatings, S-373 and S-383, do not

change the impact strength of the laminate. Coupons coated with S-373 system were exposed to QUV (112 hours) and humidity (96% RH, 120°F, 96 hours) before they were subjected to the impact test. The data shows no significant deterioration in impact strength.

In general, the dart impact test is a good tool for screening the basic impact characteristics of new materials. Since the strain rates involved in the bird test are very high, it is difficult to establish any sort of correlation between dart impact test and bird test. The material response is expected to be drastically different in these tests.

Mandrel Bend Test

Using series of Sierracin-made cylindrical mandrels of different diameters (Figure 7), the elongation of S-373 system on polycarbonate substrate was found to be 2.5%. This test method to determine the elongation of cured films is similar to that outlined in ASTM D 522-85.

Other Tests

The following tests were performed on F-16 laminates coated with the S-373 system.

- Sunshine: Done in accordance with Mil-Std-810, Method 501, Procedure 1. The test is to verify if the transparency is able to withstand prolonged exposure to sunshine.
- Thermal Cycling: 400 cycles in the range of -65° and +203°F to verify if the transparency can withstand the temperatures experienced during ground storage and runway exposure.
- Cyclic Humidity/Temperature: Done in accordance with Mil-Std-810, Method 507, Procedure I. This is a 10-day cyclic humidity test where the temperature varies between ambient and 149°F and the humidity between 85% and 95%.
- Salt Atmosphere: Performed in accordance with Mil-Std-810, Method 509, Procedure I to verify the resistance of the transparency to corrosive effects of salt spray.

At the conclusion of the exposures, there was no significant change in luminous transmittance, haze, chemical resistance, and crosshatch adhesion.

CONCLUSIONS

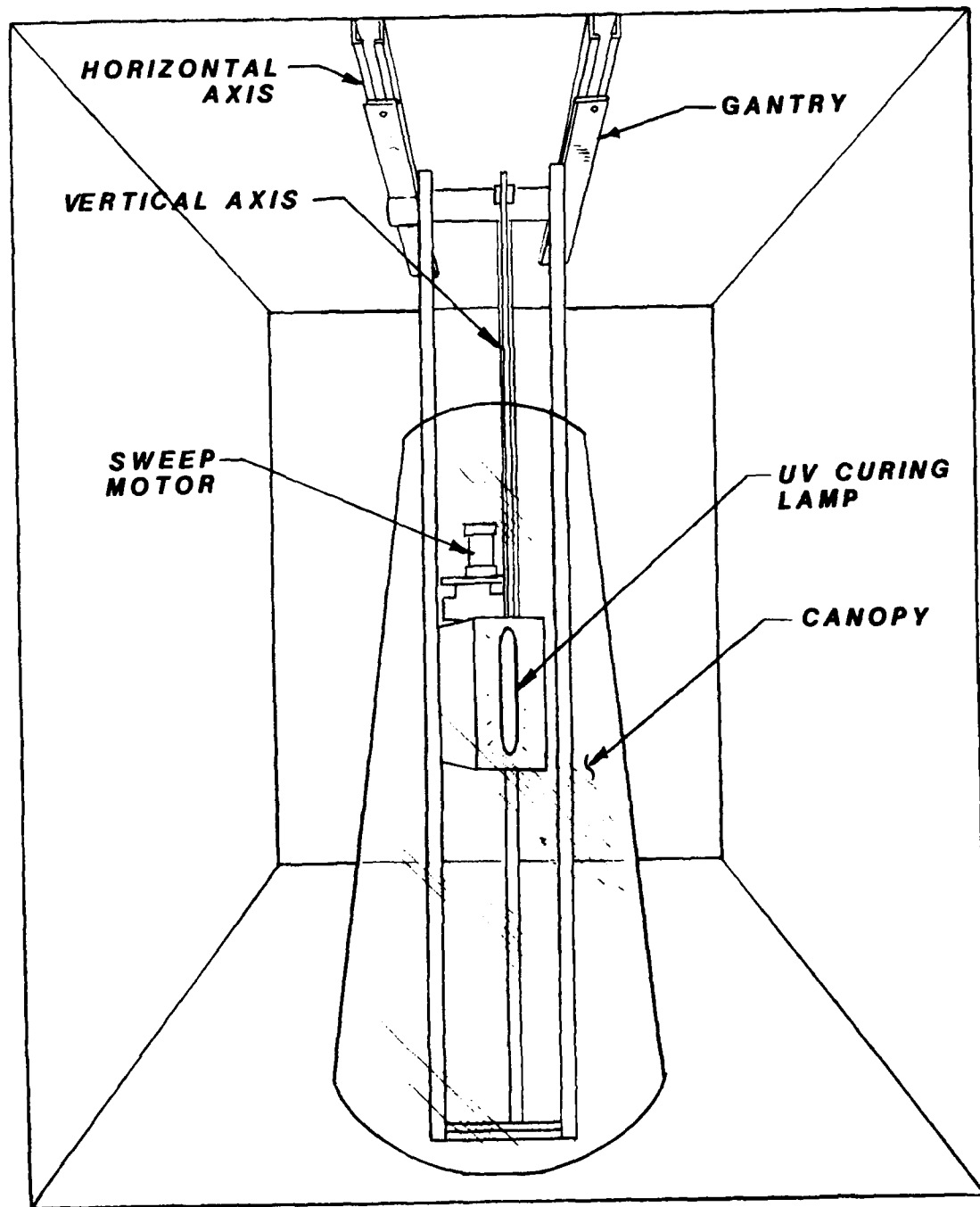
Sierracin/Sylmar Corporation has developed new technology, first-surface S-373 and S-383 solar coating systems for polycarbonate and acrylic substrates. The UV curable coating compositions developed in this work are cured in air with high speed and minimum oxygen inhibition to form adherent, flexible coatings. These compositions are used as base and topcoat for the metal layer whose vacuum deposition parameters are also optimized for maximum adhesion to the basecoat. In addition to outstanding abrasion resistance, S-373 and S-383 systems also demonstrate excellent chemical and solvent resistance, as well as excellent humidity exposure stability. These systems are expected to extend the service life of solar-coated canopies and windshields.

ACKNOWLEDGMENTS

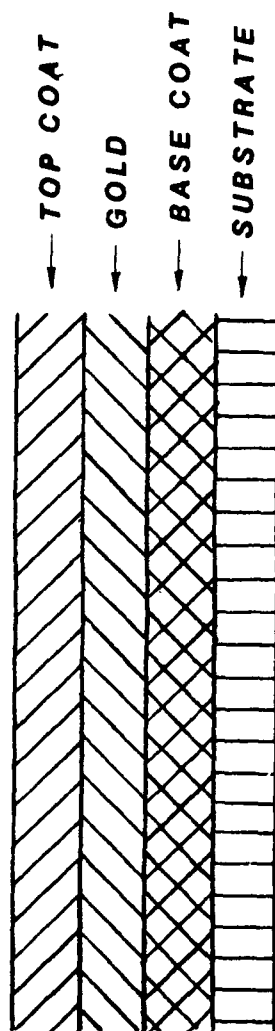
The authors wish to acknowledge the efforts of Greg Dancy, who performed most of the lab testing and formulations, and Dennis Jacques for programming and electronic assembly of the robot.

REFERENCES

1. B. K. Christmas and E. G. Zey, "Radcure 86: Conference Proceedings," Baltimore, Maryland, 1986: Association for Finishing Processes, p. 4-57.
2. Z. W. Wicks, Jr. and L. W. Hill, UV Curing: Science and Technology, S. P. Pappas, Ed., Vol. II, Chapter 3, p. 77, Technology Marketing Corp., Norwalk, CT, 1985.
3. S. P. Pappas, UV Curing: Science and Technology, S. P. Pappas, Ed., Vol. I, Chapter 1, p. 11, Technology Marketing Corp., Norwalk, CT, 1980.



PRODUCTION UV COATING FIXTURE
FIGURE 1



THE GOLD COATING SYSTEM

FIGURE 2

BAYER ABRASION RESISTANCE

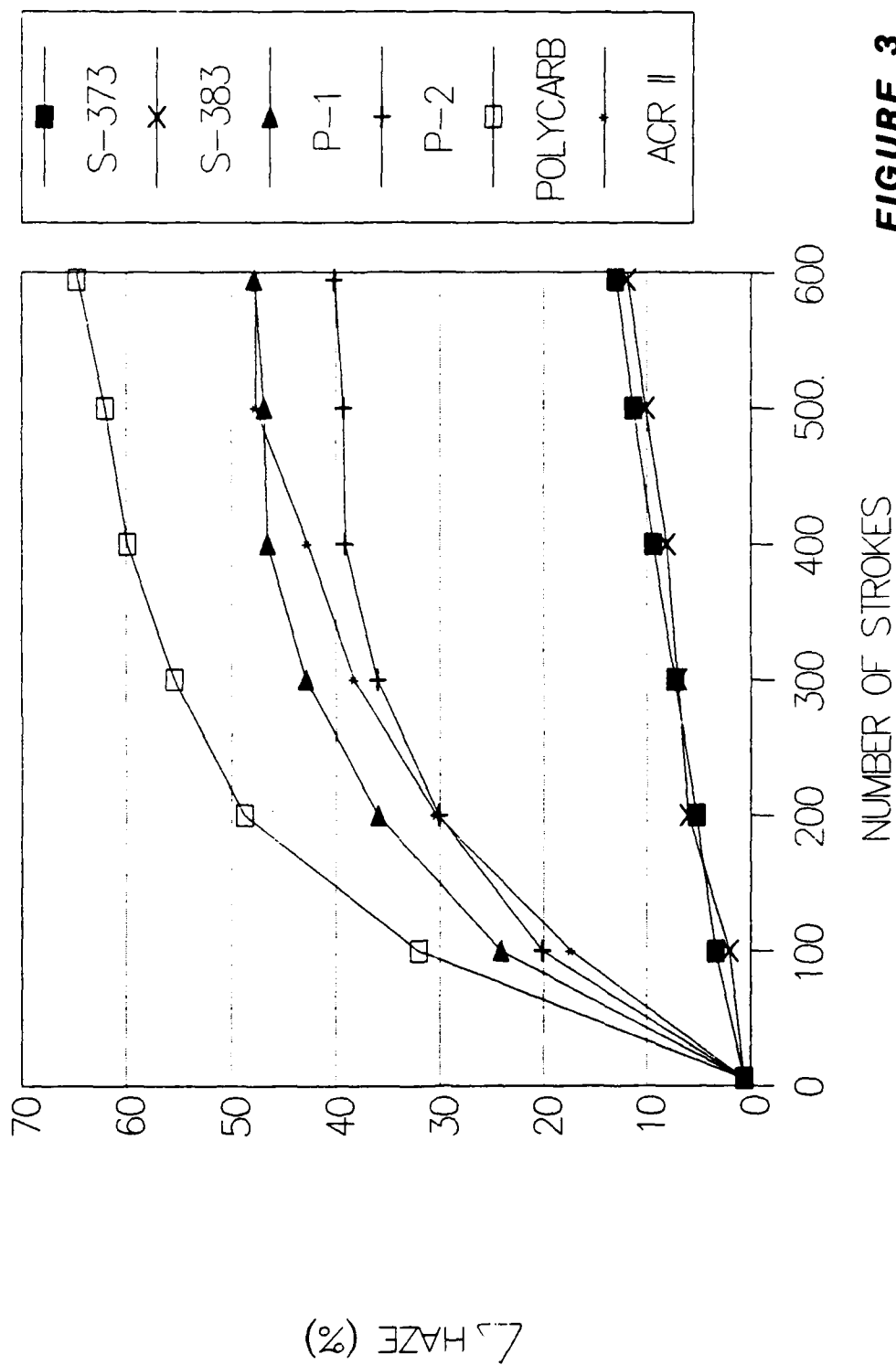


FIGURE 3

BAYER ABRASION RESISTANCE

AT 600 STROKES

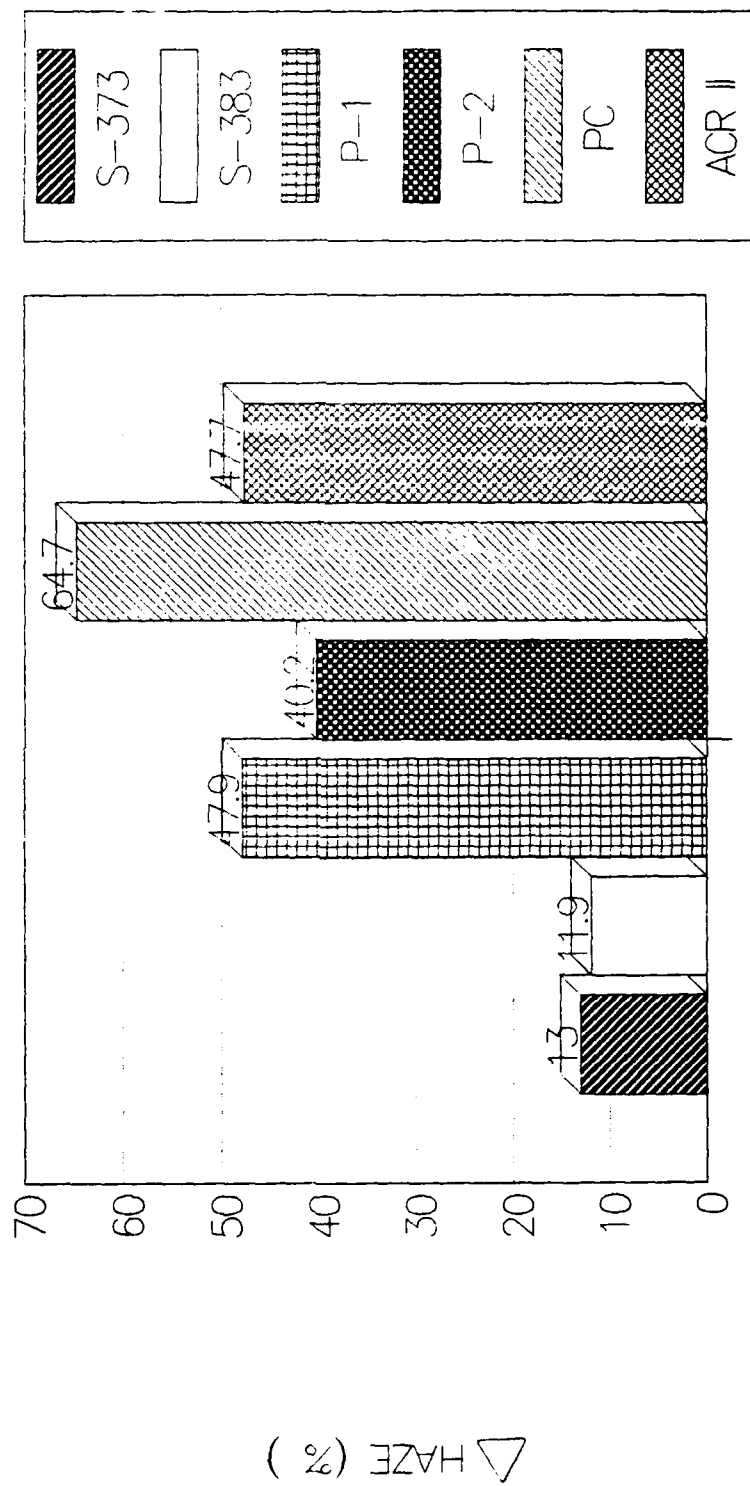


FIGURE 4

TABER ABRASION RESISTANCE

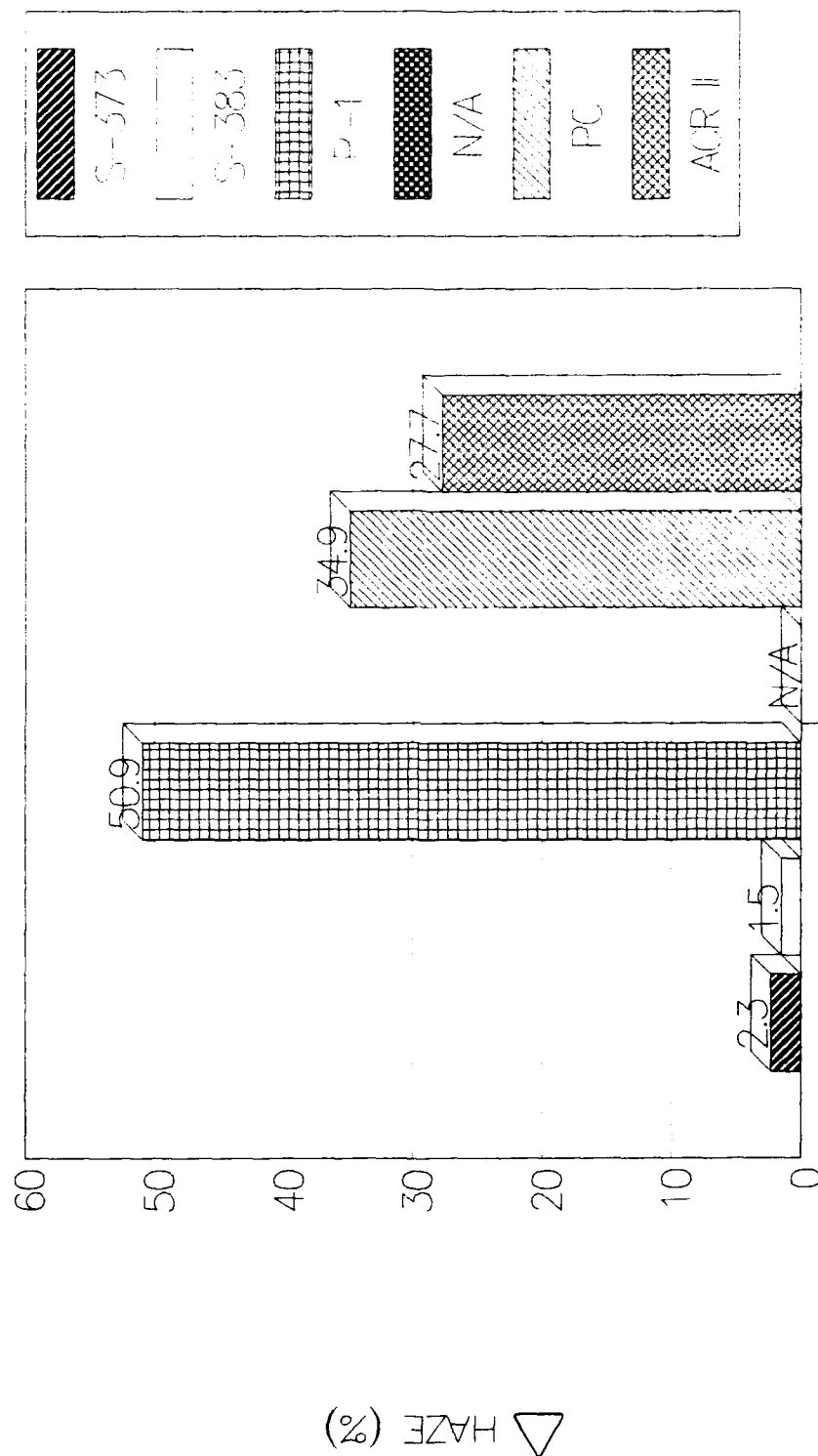


FIGURE 5

S-373 REFLECTANCE AS A FUNCTION OF COATING RESISTIVITY

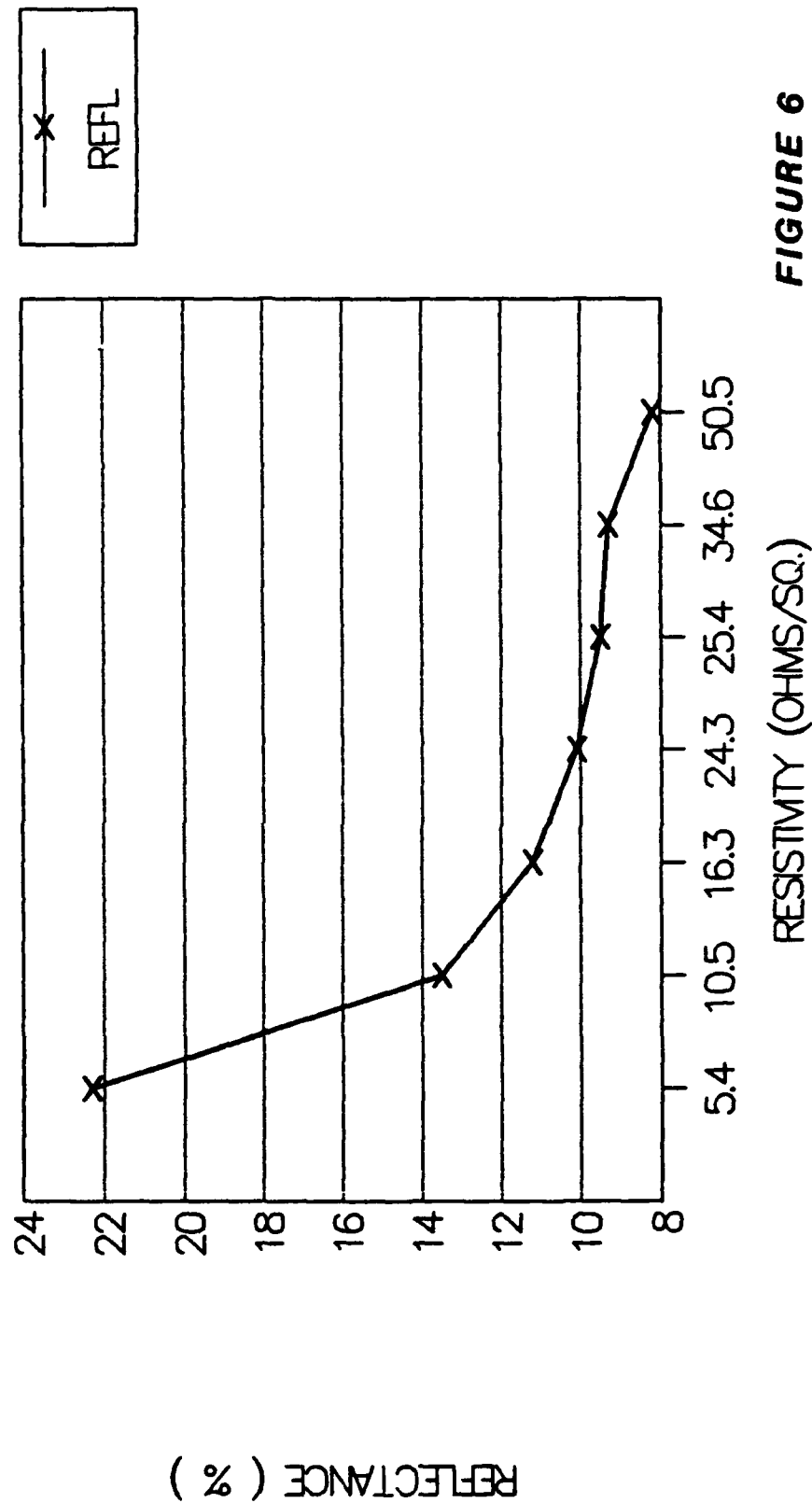
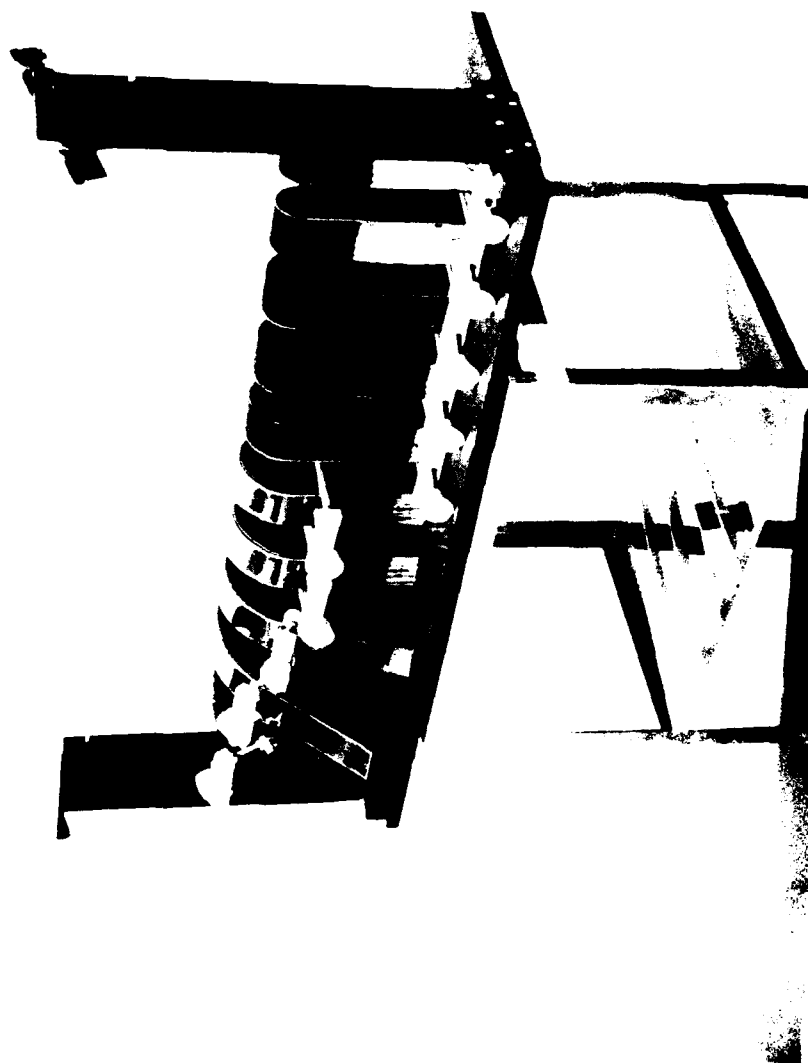


FIGURE 6



MANDREL TEST APPARATUS

FIGURE 7

TYPICAL UV CURABLE COMPOSITION

COMPONENT	AMOUNT BY WEIGHT (%)
OLIGOMERIC OR POLYMERIC ACRYLATE	50 SOLIDS
TRIFUNCTIONAL ACRYLATE	
MONOFUNCTIONAL ACRYLATE	
PHOTOINITIATOR	
SURFACTANT	50 SOLVENTS
SOLVENT MIXTURE	

TABLE 1

ABRASION RESISTANCE OF SOLAR COATINGS AND PLASTICS

NUMBER OF STROKES	0	100	200	300	400	500	600	TABER HAZE (%)
COATING\SUBSTRATE								
S-373/PC	0	3.4	5.2	7.3	9.4	11.3	13.0	2.3
S-383/STR. ACR.	0	2.0	6.0	7.0	8.1	10.1	11.9	1.5
P-1	0	24.1	35.9	42.9	46.6	46.9	47.9	50.9
P-2	0	20.1	30.1	36.0	39.1	39.3	40.2	N/A
POLYCARBONATE (PC)	0	32.0	48.8	55.4	59.9	62.0	64.7	34.9
ACRYLIC II (MIL-5425)	0	17.3	30.3	38.2	42.7	47.7	47.7	27.7
STR. ACR. (MIL-25690)	0	22.6	29.3	46.1	52.6	56.1	59.5	25.7

TABLE 2

BAYER DATA TAKEN PER ASTM F-735

TABER DATA TAKEN PER ASTM D-1044-73

N/A DATA NOT AVAILABLE

RESISTANCE OF S-373/S-383 SYSTEMS TO CHEMICALS

CHEMICAL	S-373	S-383
MILD SOAP AND WATER	NO EFFECT	NO EFFECT
AIRPLANE WASH CLEANER (MIL-C-08514)	NO EFFECT	NO EFFECT
PHOSPHORIC ACID CLEANER (MIL-C-08514)	NO EFFECT	NO EFFECT
ALODINE 1200 (MIL-S-5541)	NO EFFECT	NO EFFECT
BUG REMOVER FLUID (MIL-P-6009)	NO EFFECT	NO EFFECT
RAIN REPELLANT (REPCON)	NO EFFECT	NO EFFECT
NAPHTHA	NO EFFECT	NO EFFECT
JET FUEL (JP-4)	NO EFFECT	NO EFFECT
ISOPROPYL ALCOHOL (IPA)	NO EFFECT	NO EFFECT
DE-ICING FLUID (ETHYLENE GLYCOL)	NO EFFECT	NO EFFECT
HOT DI-ICING FLUID (180 DEG. F)	NO EFFECT	NO EFFECT

TABLE 3

COMPARATIVE RESISTANCE TO CHEMICALS AND SOLVENTS

CHEMICAL\COATING	S-373	S-383	P-1	P-2
ACETONE	GOOD	GOOD	ATK	ATK
METHYL ETHYL KETONE	GOOD	GOOD	ATK	ATK
BUTYL ACETATE	GOOD	GOOD	ATK	ATK
TOLUENE	GOOD	GOOD	ATK	ATK
TRICHLORO ETHYLENE	GOOD	GOOD	ATK	ATK
METHANOL	GOOD	GOOD	ATK	SWL
ACETIC ACID	GOOD	GOOD	ATK	ATK
SULFURIC ACID, 20 %	GOOD	GOOD	GOOD	SWL
SULFURIC ACID, 50 %	GOOD	GOOD	GOOD	ATK
SODIUM HYDROXIDE, 20 %	GOOD	GOOD	GOOD	SWL
SODIUM HYDROXIDE, 50 %	GOOD	GOOD	GOOD	SWL

GOOD= NO EFFECT,
SWL= COATING SWELLS AND SOFTENS,
ATK= COATING IS ATTACKED OR DISSOLVED

TABLE 4

HUMIDITY RESISTANCE OF S-373 SYSTEM

COUPON NUMBER	LUMINOUS TRANSMITTANCE (%)	HAZE (%)	SOLVENT EXPOSURE	ADHESION CROSSHATCH
PRE-TEST RESULTS				
1	71.3	1.1	NO EFFECT	100 %
2	71.0	1.3	NO EFFECT	100 %
3	71.6	0.9	NO EFFECT	100 %
POST-TEST RESULTS				
1	70.0	1.4	NO EFFECT	100 %
2	70.7	1.4	NO EFFECT	100 %
3	70.7	1.0	NO EFFECT	100 %

TABLE 5

1000 HR. EXPOSURE TO 100 % HUMIDITY AT 106F

S-373 REFLECTANCE AND TRANSMITTANCE AS A FUNCTION OF RESISTIVITY

COUPON NO.	RESISTIVITY (OHMS/SQ.)	LUMINOUS TRANSMITTANCE (%)	LUMINOUS REFLECTANCE (%)
1	5.4	51.7	22.3
2	10.5	70.1	13.5
3	16.3	72.3	11.2
4	24.3	72.2	10.1
5	25.4	72.7	9.5
6	34.6	72.1	9.3
7	50.5	69.5	8.2

DATA TAKEN ON SAMPLES OF FULL F-16 CROSS-SECTION

TABLE 6

DART IMPACT DATA FOR SOLAR COATED F-16 LAMINATES

COATING	EXPOSURE	IMPACT ENERGY (FT.-LBS.)
NONE	AS PROCESSED	1285
S-383	AS PROCESSED	1352
S-373	AS PROCESSED	1476
P-1	AS PROCESSED	1294
S-373	QUV	1306
S-373	HUMIDITY	1320
S-373	350 KT. BIRD TEST	PASSED

TABLE 7

SESSION IV

NEW MATERIALS AND PROCESSES (PART B)

Chairman: R. J. Skubic
McDonnell Douglas Company
St. Louis, Missouri

Co-Chairman: W. P. Johnson
Materials Laboratory
Wright-Patterson AFB, Ohio

Coordinator: R. H. Barrett
General Dynamics Corp.
Fort Worth, Texas

GAC-590 AN ADVANCED TRANSPARENCY MATERIAL

J. Uram, Jr.
Loral Defense Systems

S. Sandlin
Swedlow, Incorporated

SWEDLOW, INC.

Member of the Pilkington Group
Aircraft Transparencies

LORAL

Defense Systems – Arizona

Transparent Products

GAC-590 AN ADVANCED TRANSPARENCY MATERIAL

**Joint Paper presented at the
Conference on Aerospace Transparent Materials and Enclosures
16 to 20 January 1989**

**Hyatt Regency Monterey Resort
and Conference Center
Monterey, California**

GAC-590 AN ADVANCED TRANSPARENCY MATERIAL

Prepared by

**Loral Defense Systems — Arizona
P.O. Box 85
Litchfield Park, AZ 85340-0085**

and

**Swedlow, Inc.
12122 Western Ave.
Garden Grove, CA 92641**

January 1989

Data furnished are based on information believed to be reliable. They are offered in good faith, but without guarantee. The prospective user should determine the suitability of the materials before adopting them. No warranty is made that any material is fit for any particular purpose.

GAC-590 AN ADVANCED TRANSPARENCY MATERIAL

Mr. John Uram, Jr.
Loral Defense Systems, Arizona

Mr. Stephen Sandlin
Swedlow, Inc.

ABSTRACT

GAC-590 is the code name for a family of developmental water-white, thermoset polyurethanes which exhibit a unique combination of desirable physical properties including: high luminous transmittance, low haze, high heat distortion temperature, good abrasion resistance, good chemical agent resistance, and excellent weatherability. Based on its physical properties, GAC-590 may be used as an external face ply for aircraft transparency composites.

The following items will be discussed: comparative wind tunnel performance, optical, thermal, and mechanical properties, abrasion and chemical agent resistance, accelerated and outdoor weathering tests, and thin film coating results. GAC-590 processing/manufacturing experience will also be discussed, including sheet casting and compound forming of monolithic and composite laminates.

1. INTRODUCTION

Many aircraft transparencies are constructed from multilayer composites. The composite constructions are used because no single state-of-the-art material possesses all of the necessary properties needed to satisfy the transparency requirements. This is often the case when bird strike resistance is a factor. Of particular importance to the success of each composite is the durability of the external face ply. The face ply must be capable of withstanding the hostile flight environment of the aircraft. Thermal stability, chemical resistance, abrasion resistance, and weatherability to both humidity and ultraviolet radiation are all property requirements of a face ply material.

The list of materials currently used for exterior face ply transparency applications is quite limited. This is true not because the materials that do exist perform exceptionally well, but instead because the requirements are so difficult that few materials can satisfy them, even partially. The few materials which are used have significant limitations which must be recognized. Acrylic is limited by an upper service temperature of approximately 250 deg F. Its lack of toughness and crack propagation resistance, however, can often be overcome in a composite with impact resistant structural layers. Polycarbonate, even though it can withstand temperatures as high as 300 deg F for short periods and has outstanding impact strength, is not suitable for face ply applications. Polycarbonate is limited by poor weatherability and abrasion resistance as well as chemical-stress cracking and thermal embrittlement. Tempered glass, although frequently used for windshields, is limited by weight, brittleness, and formability to compound shapes.

To complicate the situation, the demands currently being placed on aircraft transparency face ply materials are becoming even more extreme. The development of high speed advanced aircraft is resulting in additional high temperature requirements. Also, the outer ply in many applications must now function as a substrate for the deposition of transparent conductive coatings. In addition, the increasing importance of "hardness" to new threats, including chemical agents and lasers, must be recognized.

Clearly, the development of additional materials for face ply transparency applications is needed. A limited number of material research programs has been completed. For example, the polyester-carbonates and fluoro-acrylics appear to be quite promising.^{a1,2,3} However, these materials are not commercially available in the size, quantity, and optical quality needed for transparency applications. Also, their eventual commercial development, by one of the large industrial chemical supply companies, for example, will

^aSuperior numbers in the text refer to items in List of References

depend on the development of additional markets outside the aircraft transparency industry in order to provide a sufficient driving force for commercialization. Therefore, commercialization should not be assumed.

GAC-590*, a water-clear thermoset polyurethane, should be added to the list of new advanced transparency face ply materials. It possesses many of the required properties, including optical transparency, heat resistance, abrasion resistance, and weatherability. Although GAC-590 does not possess high impact strength, it is suitable for nonstructural applications in much the same way as as-cast acrylic is currently utilized. Many of the "next generation" material property requirements, including substrate suitability for coating deposition and chemical agent resistance appear to be improved relative to state-of-the-art materials.

GAC-590 was developed specifically for aircraft transparency applications from within the transparency manufacturers' community and is patented. Driven by currently funded programs, sheet production as well as composite manufacturing processes are being scaled to the sizes needed for aircraft transparencies.

2. GAC-590 CHEMISTRY

GAC-590 is a transparent polyurethane made from at least one very low equivalent weight, multifunctional hydroxyl-containing intermediate and an aliphatic isocyanate. The resulting prepolymer is crosslinked further with a multifunctional low equivalent weight polyol. Physical properties may be varied within a reasonable range by varying the equivalent weights of the hydroxyl-functional intermediates. In this context, GAC-590 refers to a family of formulated polyurethanes. Figure 1 illustrates the basic chemistry involved.

3. GAC-590 BACKGROUND

Figure 2 illustrates the development of the GAC-590 technology base.

GAC-590 was initially developed in the early 1970's by Goodyear Aerospace (now Loral Defense Systems-Arizona). By 1975, heat resistance, weather resistance, and abrasion resistance were already well known attributes. However, since there were not any aircraft in inventory at the time

*The term "GAC-590" will be used throughout the paper. GAC-590 is a trade mark of Loral Defense Systems-Arizona. In products sold by Swedlow, the material designation will be Acrivue 590.

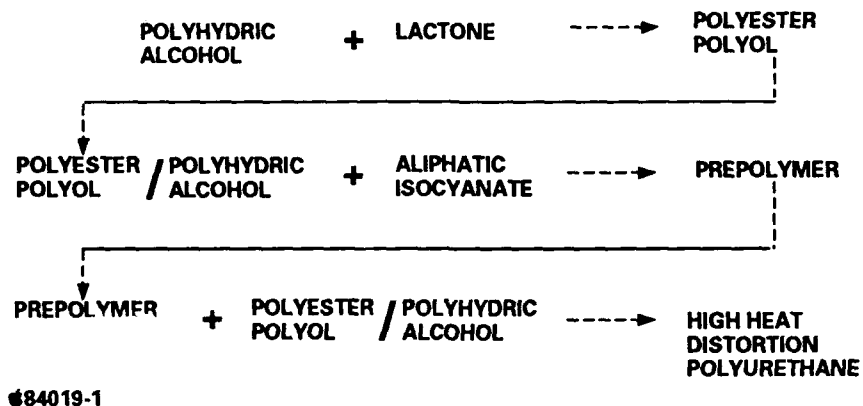


Figure 1. GAC-590 Chemistry

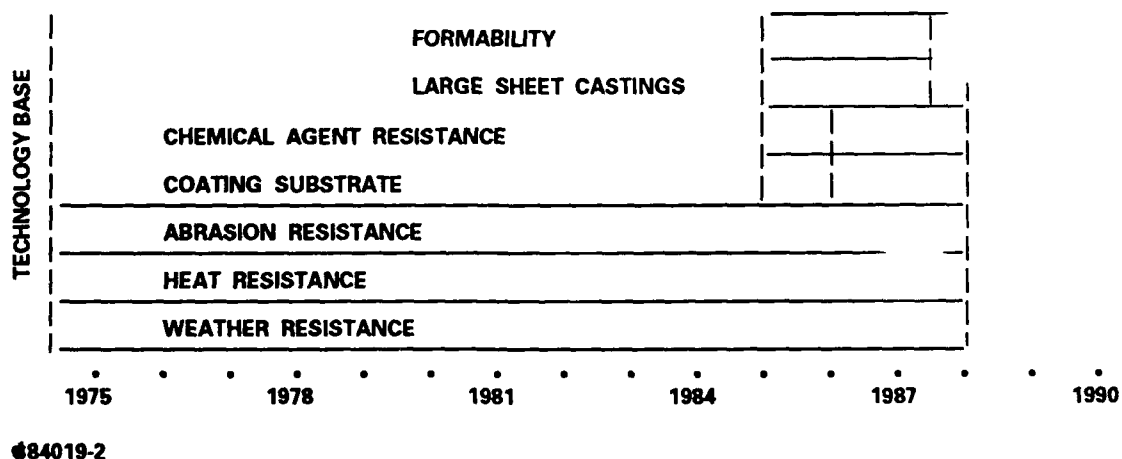


Figure 2. GAC-590 Technology Base

which required a transparency which could address aerodynamically-induced heating up in the 350 - 400 deg F region, GAC-590 did not have a home. Although strong interest existed, scale-up development did not take place due to the lack of a market.

In 1977, wind tunnel tests⁴ were conducted to determine the comparative performance of various transparency materials in simulated supersonic flight environments. Two different formulations of GAC-590 were included in the test series. The performance of GAC-590 was quite impressive; the panels exhibited the smallest change in haze, the lowest permanent optical distortion, the best resistance to pitting, and no structural failure. Results are summarized in Table 1. Again, there was significant interest but limited funding.

In 1981, there were indications that GAC-590 undergoes thermal decomposition by a mode different from that of traditional aircraft canopy transparent materials. This observation was confirmed in 1986 and is being explored further to ascertain the advantages or disadvantages of GAC-590's mode of decomposition for an advanced transparency material.




In 1985, the evaluation of GAC-590 as a substrate for optical coatings was initiated. Since then, it has been determined that GAC-590 functions as an excellent substrate for the deposition of transparent conductive metal and metal oxide coatings. High temperature durability has been demonstrated on one proprietary coating system.

In 1985, the use of GAC-590 as a chemical agent resistant material was proposed. Currently, studies are being conducted by several different companies and agencies. While most of the data is proprietary or classified and is not available for public disclosure, the overall performance of GAC-590 is excellent.

In 1985, compound curvature formability as well as sheet casting scale-up issues were addressed for the first time. Monolithic and composite dome-blowing trials were initiated. The concept of forming compound shapes by using partially cured or "B-staged" sheets of GAC-590 was also evaluated (to be discussed later in the paper).

Problems associated with cast sheet thickness tolerance, release agents, bubble-free casting techniques and casting cell design were identified and studied. In 1988, the full-scale development of sheet casting and composite forming processes was initiated.

Table 1. COMPARATIVE WIND TUNNEL PERFORMANCE OF
HIGH-PERFORMANCE AIRCRAFT CANOPIES

MATERIAL/ CONSTRUCTION	CHANGE IN LIGHT TRANSMISSION	CHANGE IN HAZE (PERCENT)	PERMANENT OPTICAL DISTORTION	PHYSICAL CHANGE
AS-CAST ACRYLIC-CLAD POLYCARBONATE	 SLIGHT CHANGE	+9.6	LOW	SOFTENING OF ACRYLIC
COATED POLYCARBONATE		+4.0	MODERATE	DISTORTED
STRETCHED ACRYLIC		+6.7	HIGH	THERMAL RELAXATION, PITTING
GLASS/POLYCARBONATE LAMINATE		—	—	GLASS FAILURE
GLASS/POLYCARBONATE LAMINATE		—	—	GLASS FAILURE
AS-CAST ACRYLIC/ POLYCARBONATE LAMINATE		—	—	SOFTENING OF ACRYLIC
GAC-590-55 URETHANE/ POLYCARBONATE LAMINATE		 <3.0	MODERATE	 BEST RESISTANCE TO PITTING
GAC-590-65 URETHANE/ POLYCARBONATE LAMINATE			LOW	
GAC-590-55 URETHANE/ POLYCARBONATE LAMINATE			MODERATE	

NOTES: — NO TEST PERFORMED
DATA ABSTRACTED FROM: "EVALUATION OF WINDSHIELD MATERIALS SUBJECTED TO SIMULATED
SUPERSONIC FLIGHT ENVIRONMENTS," J.B. HOFFMAN (DOUGLAS A/C CO.), AFFDL-TR-77-92, SEPT 1977.

484019-16

4. OPTICAL, THERMAL AND MECHANICAL PROPERTIES

Typical physical property data is presented in Table 2. GAC-590 is water clear, with a typical yellowness index of 1.2 - 1.6. Heat deflection temperature (HDT) can be varied over a relatively broad range from 266 to 315 deg F. This HDT tailoring is accomplished by fine tuning the cross-link density. The performance of GAC-590 at high temperature can be attributed to the fact that it is thermoset. Unlike thermoplastics, which lose most of their physical properties at or beyond their HDT, GAC-590 performs very well above its HDT without significant degradation in physical properties. Tensile strength,⁵ tensile modulus, tensile elongation, flexural modulus, and flexural strength all exhibit significant property values at temperatures 20 deg F higher than its HDT. As previously stated, GAC-590 does not exhibit good impact resistance properties. Values for coefficient of linear expansion and specific gravity are also listed in Table 2.

5. ABRASION RESISTANCE

Several different types of abrasion resistance tests have been conducted. Results from an oscillating sand abrasion test (ASTM F735-81) are illustrated in Figure 3. With a HDT of approximately 266 deg F, GAC-590-65/65 (one of the softest formulations), performed as well as as-cast acrylic. With an increase in HDT to approximately 280 deg F, the abrasion performance of formulation GAC-590-65/55 is improved relative to as-cast acrylic. A further increase in HDT to approximately 300 deg F will result in further improvement in abrasion resistance.

Comparative Taber abrasion (ASTM D1044) results for GAC-590, acrylic, polycarbonate, and polyarylate are presented in Figure 4. GAC-590 exhibited superior performance.

6. CHEMICAL, AND CHEMICAL AGENT RESISTANCE

Test data on GAC-590 in the area of chemical agent resistance is somewhat limited. Figure 5 illustrates data that was generated when GAC-590 was exposed to agent HD (mustard). Exposure to saturated HD vapor for three hours resulted in a weight gain of only 0.05 percent. The weight gain did not increase even after exposure for an additional seven days. Light transmittance and haze did not change significantly during the exposure.

In a separate study,⁶ it was concluded that "GAC-590 showed good chemical resistance and should be considered for further evaluation and possible use in future Army systems". The statement was based on preliminary immersion tests which demonstrated excellent chemical resistance to DS2 (a

TABLE 2. GAC-590 PHYSICAL PROPERTY DATA

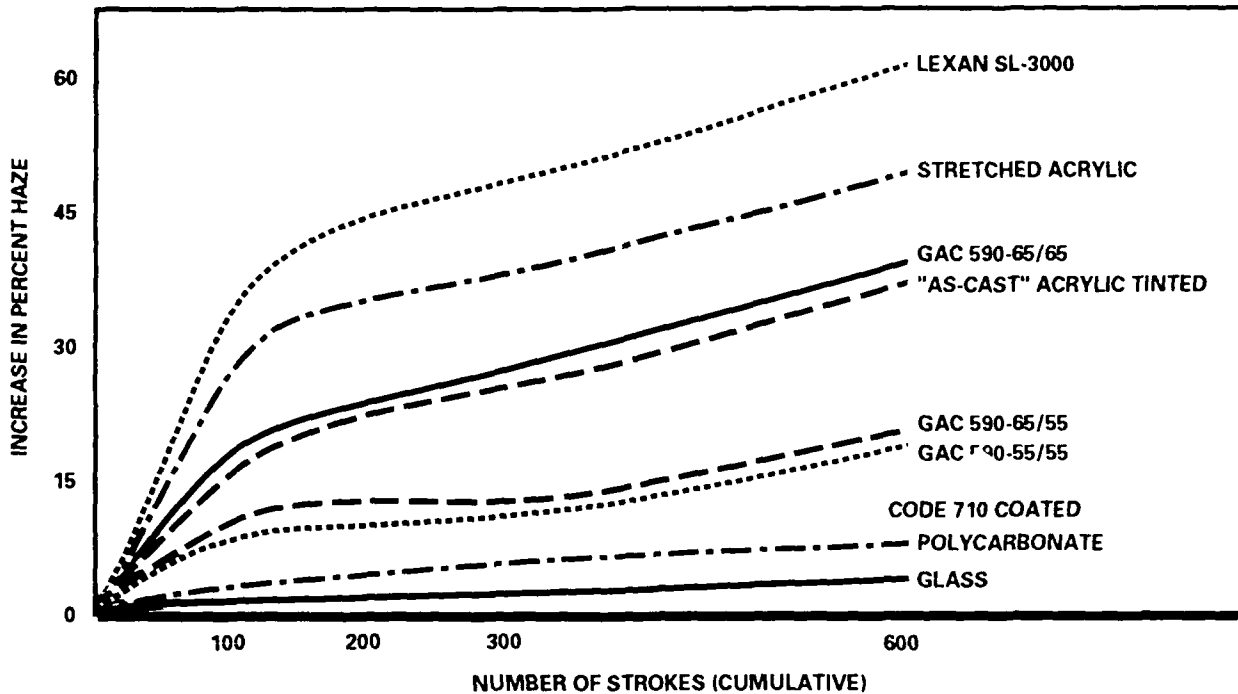
TEST	TEST TEMPERATURE	RESULTS
LIGHT TRANSMISSION		90.8 PERCENT
HAZE		2.0 PERCENT
COLOR		WATER WHITE
HARDNESS (SHORE D)	-65 DEG F RT +300 DEG F	88 87 77
HEAT DEFLECTION TEMPERATURE (264 PSI)	DEG F	280 TO 315*
TENSILE STRENGTH, ULTIMATE, PSI	-65 DEG F RT +300 DEG F	12,400 12,450 2,900
TENSILE MODULUS, PSI	-65 DEG F RT +300 DEG F	700,200 403,000 156,000
TENSILE ELONGATION, PERCENT	-65 DEG F RT +300 DEG F	2 PERCENT 5 PERCENT 15 PERCENT
FLEXURAL STRENGTH, ULTIMATE, PSI	-65 DEG F RT +300 DEG F	22,490 21,250 3,750
FLEXURAL MODULUS, PSI	-65 DEG F RT +300 DEG F	520,000 299,000 124,000
IMPACT STRENGTH 0.100-IN. THICK (6 POUND FALLING PLUMMET) 0.225-IN. THICK	RT RT	5 IN. (SHATTERED) 12 IN. (SHATTERED)
COEFFICIENT OF LINEAR EXPANSION (IN./IN./DEG C)		8.05×10^{-5}
SPECIFIC GRAVITY		1.13

NOTES: *DEPENDS ON SPECIFIC FORMULATION.

RT = ROOM TEMPERATURE.

TYPICAL VALUES OBTAINED WITH 0.125 TO 0.250-INCH-THICK TEST SPECIMENS,
EXCEPT AS NOTED.

84019-8



84019-4

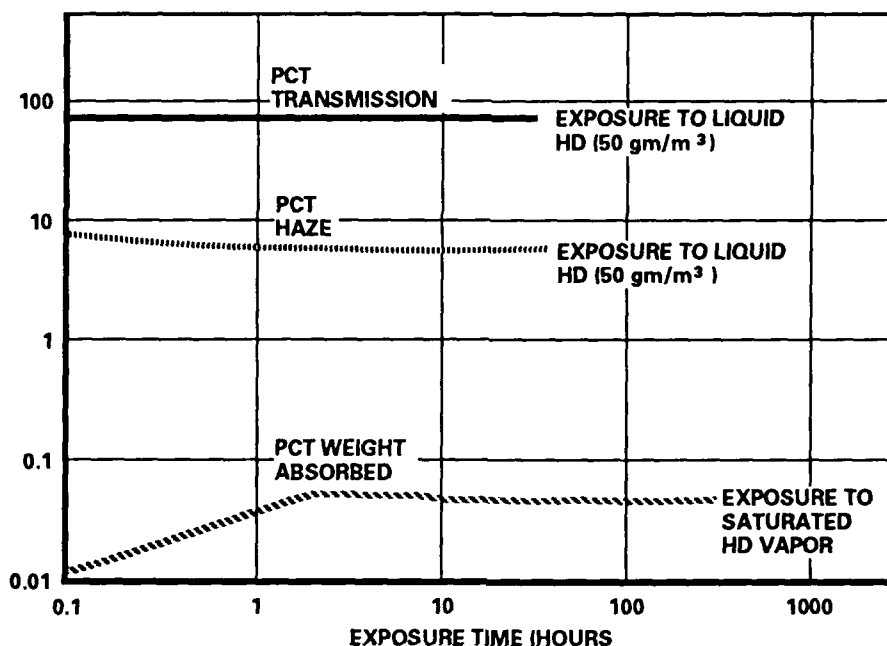
Figure 3. Oscillating Sand Abrasion Resistance (ASTM F 735-81)

MATERIAL	Δ HAZE ²
GAC-590	3.0
ACRIVUE 350 ³	34.6
POLYCARBONATE ⁴	36.7
POLYARYLATE	25.7

1. ASTM D-1044. 100 REVOLUTIONS, 500 G LOAD
2. ASTM D-1003, CHANGE IN PERCENT HAZE
3. MIL-P-8184 ACRYLIC
4. MIL-P-83310

84019-10

Figure 4. Taber Abrasion Resistance¹



84019-23

Figure 5. GAC-590 Chemical Agent Resistance Data

universal decontaminant which consists of 70 percent diethylene triamine, 28 percent methyl cellosolve, and 2 percent sodium hydroxide by weight), DIMP (diisopropyl methylphosphonate, a simulant for GD), and DCP (1,5-dichloropentane, a simulant for HD).

Comparative test results for craze resistance when exposed to isopropanol and lacquer thinner for GAC-590, acrylic and polycarbonate are presented in Figure 6.

7. STRESS OPTICAL COEFFICIENT

Birefringence or "rainbowing" can be observed in transparencies when certain viewing conditions exist. It is especially prevalent in polycarbonate transparencies at certain altitudes where there is a relatively large percentage of polarized light. Birefringence is the result of the directional dependence of refractive index in an anisotropic material. The anisotropic state may result in amorphous plastics because of residual stresses.

MATERIAL	STRESS TO CRAZE (PSI) ¹	
	ISOPROPYL ALCOHOL	LACQUER THINNER
GAC-590-65	5,000	4,800
ACRIVUE 350 ²	3,500	2,500
ACRIVUE 350S ³	6,000	4,000
POLYCARBONATE ⁴	4,000	200

1. TESTED PER PROCEDURE IN MIL-P-8184 EXCEPT APPLIED LOAD VARIED TO DETERMINE MINIMUM STRESS TO CRAZE.

2. MIL-P-8184 ACRYLIC

3. MIL-P-25690 STRETCHED ACRYLIC

4. MIL-P-83310

484019-9

Figure 6. Craze Resistance

To quantify the tendency for a material to exhibit birefringence, the stress optical coefficient can be used to compare it with other relevant materials. The stress optical coefficient was measured for GAC-590, acrylic, and polycarbonate in uniaxial tension applied by a Universal Tensile Tester (Table 3). A plane polariscope was used with a "tint of passage" isochromatic fringe-order counting method. The coefficient for GAC-590 is less than that for polycarbonate but more than that for acrylic. However, this should be evaluated in the context that residual stress levels are expected to be higher for GAC-590 because of its high cross-link density.

8. ACCELERATED WEATHERING AND OUTDOOR WEATHERING

A number of accelerated weathering tests have been conducted on GAC-590. Light transmission, haze, yellowness index, and tensile strength were evaluated after exposure to various periods of time at 160 deg F/100 percent relative humidity and Q-UV (ultraviolet radiation) exposure (Table 4). No significant changes were observed. Also, no significant change occurred in light transmission, haze, and yellowness index, after 1000, 2000, and 3000 hours of Weather-O-Meter exposure (Table 5).

In addition to accelerated weathering tests, GAC-590 was also exposed to outdoor weathering in both monolithic and composite constructions. For monolithic panels, changes in color, light transmission, haze, hardness, and

TABLE 3. STRESS OPTICAL COEFFICIENT

MATERIAL	MEASURED VALUE ¹ (IN ² /lb)	PUBLISHED VALUE ² (IN ² /lb)
GAC-590-65	1.8×10^{-7}	—
ACRIVUE 350 ³	0.5×10^{-7}	0.31×10^{-7}
POLYCARBONATE ⁴	4.8×10^{-7}	5.5×10^{-7}

1. MEASURED METHOD DERIVED FROM BUDYNAS,
ADVANCED STRENGTH AND APPLIED STRESS ANALYSIS
2. KUSKE, ROBERTSON, PHOTOELASTIC STRESS ANALYSIS, PG 153.
3. MIL-P-8184 ACRYLIC
4. MIL-P-83310

484019-7

TABLE 4. ACCELERATED WEATHERING

PROPERTY	UNEXPOSED CONTROL	TEMPERATURE-HUMIDITY ¹			ULTRAVIOLET RADIATION ²		
		24 HR	48 HR	100 HR	24 HR	48 HR	100 HR
LIGHT TRANSMISSION ³ (PERCENT)	92.2	92.5	92.2	92.2	92.1	91.9	91.9
HAZE ³ (PERCENT)	1.2	1.8	1.5	1.6	1.3	2.3	2.0
YELLOWNESS INDEX ⁴	1.6	1.6	1.7	1.6	1.6	1.8	1.8
TENSILE STRENGTH ⁵ (PSI)	12,013	—	—	11,110	—	—	12,131

1. 160 DEG F, 100 PCT RELATIVE HUMIDITY
2. Q-UV
3. ASTM D-1003
4. ASTM D-1925
5. ASTM D-638

494019-11

TABLE 5. ACCELERATED WEATHERING¹

PROPERTY	UNEXPOSED CONTROL	1000 HR	2,000 HR	3,000 HR
LIGHT TRANSMISSION ² (PERCENT)	92.4	91.7	91.8	90.8
HAZE ² (PERCENT)	1.5	2.3	2.0	2.9
YELLOWNESS INDEX ³	1.3	1.3	1.3	1.6

1. WEATHER-O-METER, XENON LAMP

2. ASTM D1003

3. ASTM D1925

484019-5

tensile strength, were determined after 3, 6, and 9 months of outdoor exposure (45 deg south-Arizona). Results are presented in Table 6.

Figure 7 illustrates a composite construction which was fabricated with a GAC-590 face ply. The face ply was laminated to a structural element with a silicone interlayer. No edge-sealer was used. After outdoor exposure (45 deg south-Arizona) for three years, a significant increase in haze was noted. The increase was attributed to moisture absorption by both the polycarbonate structural ply and the silicone interlayer. All of the urethane bondlines along with the GAC-590 face ply were relatively haze-free (Figure 8). During the three year exposure, the panel did not experience any bubble formation or delamination.

9. SUBSTRATE FOR THIN FILM COATINGS

GAC-590 functions as an excellent substrate for the deposition of transparent conductive metal and metal oxide coatings. When fully cured, GAC-590 can tolerate significantly higher deposition temperatures than the current plastics which are used in aircraft transparencies. Higher temperature deposition often results in desirable thin film properties which may be unachievable at lower temperatures.

TABLE 6. GAC-590-65 OUTDOOR TEST RESULTS
45 DEGREE SOUTH - ARIZONA

PROPERTY	UNEXPOSED CONTROL	3 MONTHS EXPOSURE	6 MONTHS EXPOSURE	9 MONTHS EXPOSURE
COLOR (GARDNER)	1	1	1	1
LIGHT TRANSMISSION (PERCENT)	89.5	89.9	89.9	90.3
HAZE (PERCENT)	2.3	2.2	2.8	3.4
HARDNESS (SHORE D)	86	—	89	89
TENSILE STRENGTH (PSI)	12,172	13,002	13,133	12,905

NOTES: — NOT TESTED
TEST TERMINATED AFTER 9 MONTHS EXPOSURE.

84019-14



84019-17 G870521 28

Figure 7. Outdoor Weathering Test Specimen
(After 3-Year Exposure)

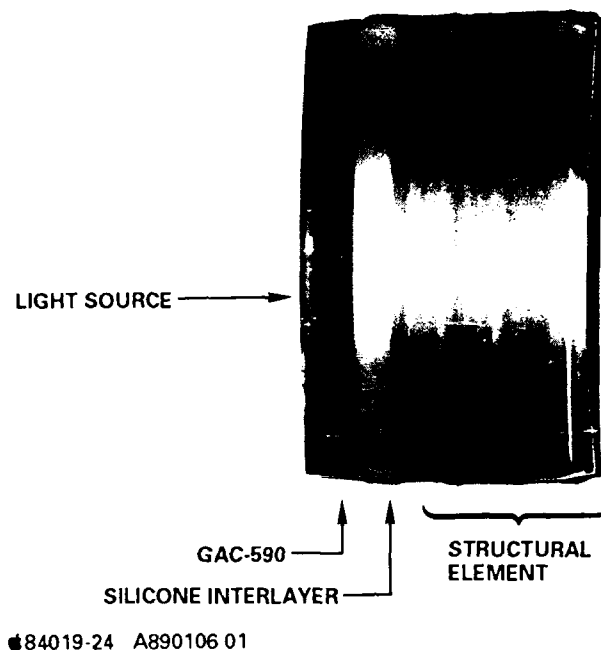


Figure 8. Outdoor Weathering Test Specimen (Cross-Sectional View)

High temperature durability has been demonstrated on one proprietary coating system to 375 deg F (Table 7). No evidence of degradation (micro-cracking, adhesion loss, etc.) was observed in the low resistance coating after the high temperature exposures.

10. GAC-590 PROCESSING/MANUFACTURING

GAC-590 flat sheet stock is manufactured using process technology very similar to that used for acrylic. First, a prepolymer is prereacted in an independent process step. Next, the prepolymer and the appropriate amount of curative is charged into a continuous stir tank reactor. The mix is polymerized to a specified degree of polymerization and then pumped as a liquid into a casting cell. The cell is then thermally cured and parted to obtain the sheet. Presented in Figure 9 is a photograph of an 82 in. x 72 in. x 0.125 in. cast sheet of GAC-590.

Composites constructed from GAC-590 and formed to single-degree curvature can be produced using standard transparency manufacturing processes. However, when GAC-590 is cast into completely cured flat sheet (i.e., the reaction is taken to completion in the casting process such that full development of mechanical and thermal properties is obtained) and laminated with

TABLE 7. THIN FILM¹ COATED GAC-590

SAMPLE EXPOSURE TEMP (F)/ TIME (HRS)	INITIAL			POST EXPOSURE		
	LT (PCT) T ²	HZ (PCT) ²	ADH (PCT) ³	LT (PCT) T ²	HZ (PCT) ²	ADH (PCT) ³
275/12	72.4	2.3	100	72.9	2.3	100
300/12	72.9	2.6	100	73.4	2.5	100
325/12	73.5	2.1	100	73.8	2.4	100
340/12	74.9	2.8	100	74.4	3.4	100
375/12	74.9	3.6	100	73.6	3.1	100

1. PROPRIETARY SWEDLOW TRANSPARENT CONDUCTIVE COATING
2. ASTM D1003
3. TAPE PULL (3M600)

84019-6

84019-27

Figure 9. GAC-590 Sheet, 82 in. x 72 in. x 0.125 in.

polycarbonate, then composites formed to the degree of compound curvature needed for some aircraft canopies can not be obtained. The cross-link density inherent to "fully-cured" GAC-590 is such that the extensibility is too low to form highly compound shapes.

However, this apparent limitation can be overcome by using innovative manufacturing techniques. First, GAC-590 is cast to a "B-staged" state of partial cure such that the desired forming operation can be completed. Next, the composite is constructed with the B-staged sheet using standard manufacturing techniques. Forming to the desired compound curvature is then accomplished, followed by a post-cure to obtain the ultimate GAC-590 physical properties. The manufacturing process just described is currently in the full-scale development stage.

Examples of formed GAC-590 domes are presented in Figures 10 and 11. All of the domes were formed from B-staged sheets. The 10 inch diameter monolithic GAC-590 dome was formed to 16 percent biaxial elongation. The 40 inch diameter monolithic GAC-590 dome in Figure 11 was formed to 29 percent biaxial elongation.

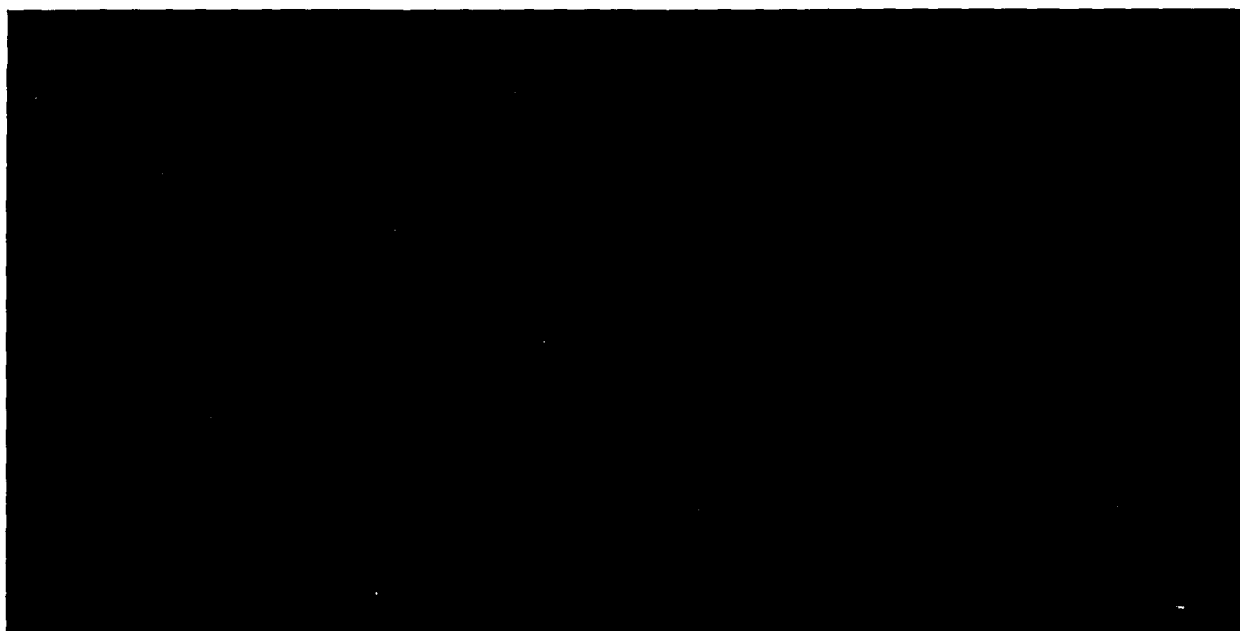
Both fully-cured and B-staged GAC-590 can be laminated using either castable cure-in-place (CIP) or sheet (thermoplastic and B-staged thermoset) interlayers. Good adhesion can be obtained to both silicone and polyurethane interlayers with the appropriate primers.

GAC-590 can be ground and polished to obtain the level of optical quality required for aircraft transparencies. The standard techniques commonly used within the industry are effective. Polishing is labor intensive, however. For comparison, the time required is similar to that needed for polycarbonate.

11. SUMMARY

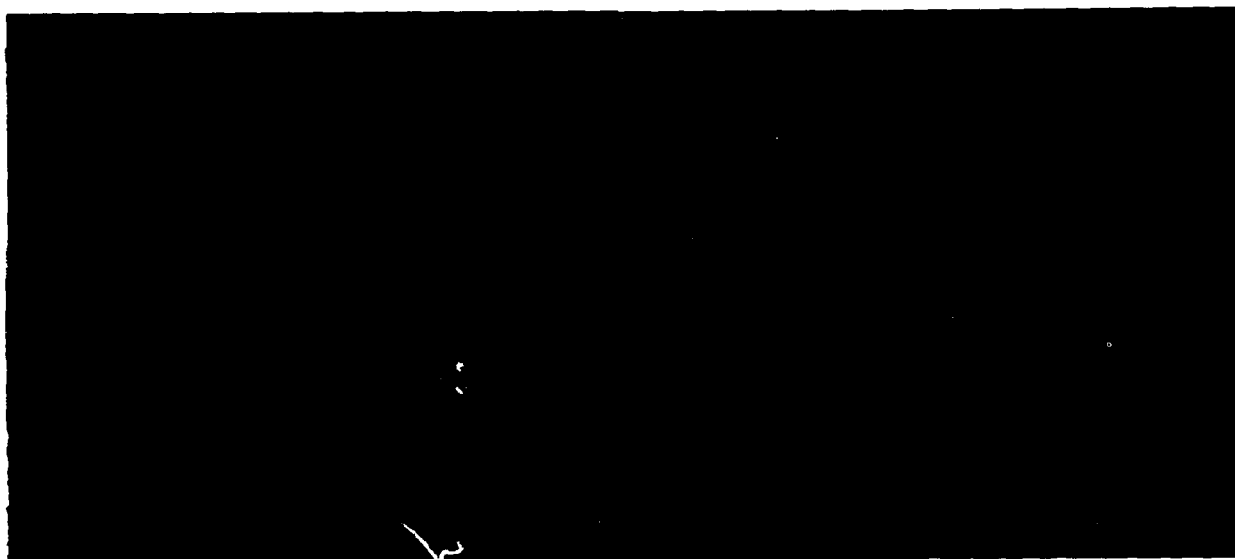
GAC-590 (Acrivue 590) is the code name for a family of formulated water-clear, cross-linked, aliphatic polyurethanes. GAC-590 exhibits many of the basic material property requirements needed for aircraft transparency applications. It may be used as an external face ply, based on its mechanical, thermal, and optical properties, along with its chemical and abrasion resistance and weatherability. Its relatively low impact resistance precludes its use as a structural material.

GAC-590 offers a lightweight alternative to tempered glass as well as a higher upper service temperature than acrylic. GAC-590 offers significant advantages with respect to its use as a high temperature substrate for transparent conductive coating deposition. GAC-590 also offers chemical agent resistance.



84019-25

Figure 10. Ten-inch Diameter Monolithic GAC-590 Dome
Formed to 16 Percent Biaxial Elongation



84019-26

Figure 11. 40-inch Diameter Monolithic GAC-590 Dome
Formed to 29 Percent Biaxial Elongation

Loral Defense Systems-Arizona and Swedlow, Incorporated have established a teaming arrangement to develop GAC-590 for use in the aircraft transparency industry. A Technical Assistance, Co-Development and Co-Production License Agreement was formalized between the two companies in the Spring of 1988. Currently, the development of full-scale sheet production processes and composite manufacturing processes are taking place.

REFERENCES

1. DeBona, B.T., Prevorsek, D.C., "New High Performance Windshield/Canopy Materials", AFWAL-TR-83-4154, December, 1983, pp. 340-381.
2. Reinhart, T.J., "Heat Resistant Copolyester-Carbonate Transparent Plastics", AFWAL-TR-83-4154, December, 1983, pp. 469-495.
3. Griffith, J.R., "Fluoroepoxy and Fluoroacrylic Transparencies", AFWAL-TR-83-4154, December, 1983, pp. 408-414.
4. Hoffman, J.B., "Evaluation of Windshield Materials Subjected to Simulated Supersonic Flight Environments", AFFDL-TR-77-92, September, 1977.
5. Uram Jr., J., "GAC-590, Advanced Transparency Material", AZB-9717, 3 July, 1987, Loral Defense Systems-Arizona.
6. Hsieh, A.J., Vanselow, J.J., "Evaluation of Transparent Polymers for Chemically Hardened Army Systems", MTL-TR-88-24, July, 1988, pp. 16.

FLUOROACRYLATE POLYMERS FOR WATER RESISTANT TRANSPARENCIES

R. L. Soulen
J. R. Giffith

Naval Research Laboratory

FLUOROACRYLATE POLYMERS FOR
WATER RESISTANT TRANSPARENCIES

R. L. Soulen and J. R. Griffith
Naval Research Laboratory
Washington, DC 20375-5000

ABSTRACT

The absorption of water into glassy transparent materials, e.g., poly(methyl methacrylate), has been shown to produce a number of serious deleterious effects. An acrylic polymer saturated with water shows a significant drop in fatigue performance and may undergo as much as 0.7% linear dimensional change. Polymer samples under these conditions will craze with isopropyl alcohol at zero stress loading. Transparency failure due to crazing is a significant and costly problem to commercial and military aircraft.

Fluoroacrylates, especially those which contain one or more trifluoromethyl groups per monomer unit, have been shown to produce materials with non-wetting surfaces. This highly desirable property is frequently off-set by low T_g values and limit their application to coatings for textiles and bulk materials. It has been assumed that polymer materials with non-wetting surface will absorb less water into the bulk polymer although there is little data to support this conclusion.

In this study we report on the preparation of copolymers based on methyl methacrylate with either hexafluoro-2-propyl methacrylate or hexafluoro-2-phenyl-2-propyl acrylate. Mixtures of the monomers containing up to 50 weight percent of the fluoroacrylate and 0.02 weight percent AIBN were polymerized by a temperature program starting at 50 C. and ending at 90 C. The copolymer samples possessed T_g values 98 C. or better and significantly decreased water absorption with increasing fluoroacrylate concentration. Polymer samples containing 50 weight percent hexafluoro-2-phenyl-2-propyl acrylate in 120 F. water absorbed one third as much water as poly(methyl methacrylate). Desorption of water from the fluoroacrylate copolymers was up to 70 percent faster than PMMA.

INTRODUCTION

The basic premise of this work is that water-induced damage to aircraft transparencies should be reduced in severity if water can be partially precluded from ingress into the molecular structure of the plastic materials. A means to such an end is to alter the chemistry of the plastics to include hydrophobic components within the molecules, and fluorocarbon components are the most hydrophobic known to organic chemistry. Here we have synthesized a series of fluorinated acrylic copolymers and studied some aspects of the response to water exposure.

DISCUSSION

The well-established instability of completely perfluorinated alcohols has precluded their use in the synthesis of perfluoroalkyl esters of acrylic and methacrylic acids [1]. Alternative structures which have successfully overcome this problem of instability are the 1,1-dihydro and 1,1,2,2-tetrahydroperfluoroalcohols. These alcohols are rugged starting materials and have a greatly reduced tendency to spontaneously split out hydrogen fluoride. Dihydro and tetrahydroperfluoroalkyl acrylate and methacrylate esters are currently available from several commercial sources, where, in general, the perfluoroalkyl portion of the monomers is a blend of the straight chain C_4 through C_{20} homologous series. However, the principal portion of the fluoroalkyl groups is found in the C_6 , C_8 , C_{10} fraction. Two major disadvantages of the long chain perfluoroalkyl acrylates are their low glass transition temperature (T_g) and their incompatibility with nonfluorinated acrylate and methacrylate monomers. These problems have limited their uses to surface applications to provide soil stain, water and oil repellency to fabric apparel and non-woven fibers.

It is important here to recall the pioneering work of Zisman [2], who established that the lowest energy surface, i.e., the least wettable surface, is the theoretical surface composed of well-packed trifluoromethyl groups. The CF_2 and CH_2 groups increase surface energy above this minimum and provide less protection compared to the ideal close packed array of trifluoromethyl groups. With this basic principle in mind, we have prepared a variety of stable fluoroalcohols containing two up to eight trifluoromethyl groups and no CF_2 or CH_2 groups. Acrylate and methacrylate esters of the polytrifluoromethyl alcohols appear to form compatible copolymers with methyl methacrylate up to about 30 weight percent of the fluoroacrylate. The major drawback of these copolymers was the lowering of the glass transition temperature as the percent of methyl methacrylate fell below 90 percent. A similar situation was noted by Roitman and Pittman who prepared homo and copolymers of perfluoro-*t*-butyl acrylates [3]. They

ascribed the lower glass transition temperatures, absence of crystallinity and increasing surface energy values to the inability of the polymer backbone to orient the bulky perfluoro-t-butyl group to the interface.

Our initial experiments with copolymers of methyl methacrylate and 2[3,5-bis(trifluoromethyl)phenyl] hexafluoropropyl acrylate and methacrylate indicated that a bulky fluoroaryl group suffered similar restrictions to free rotation. Copolymer samples were frequently brittle and showed significantly lower glass transition temperatures even at low concentration of the fluoroaryl monomer. By contrast, 2-phenylhexafluoropropyl and hexafluoropropyl groups appear to have less restriction to their orientation around the polymer backbone and did not show as dramatic a fall in the glass transition temperature. For example, the glass transition temperature values for 10/90 mixtures of 2[3,5-bis(trifluoromethyl)phenyl]hexafluoropropyl acrylate (BTPHFPA), phenylhexafluoropropyl acrylate (PHFPA) and hexafluoropropyl methacrylate (HFPMA) in methyl methacrylate were 105.2°C, 115.1°C, and 113.3°C, respectively. Structures for the fluoroacrylate monomers and their abbreviations may be found in the appendix of this report.

In this study, we selected the latter two monomers for copolymerization with methyl methacrylate as physical properties of the polymer samples were superior. Table I presents the compositions of the copolymers with glass transition temperatures and density data. The inverse relationship of density to glass transition temperature is obviously a function of the amount of the fluoroacrylate in the copolymer. However, within a given composition slight variations in polymer density were often reflected in the glass transition temperature and the rate of water absorption. For two samples with similar weight percent fluoroacrylate, the higher density sample usually absorbed less water within a given time period and had a slightly higher glass transition temperature. The principal factor which led to variations in the polymer density was the temperature profile for the polymerization process. It was observed that polymer samples prepared at a higher initiation temperature were lower density than those prepared at lower initiation temperature. The polymerization temperature profile used in this study may be found in the experimental section. Graph 5 shows a plot of copolymer composition (percent hexafluoro-2-propyl methacrylate in methyl methacrylate) versus polymer density. The polymer samples with ten percent fluoroacrylate demonstrate this observation. The higher density sample had a glass transition temperature of 113°C and absorbed 0.78 percent water after 21 days. The lower density sample had a glass transition temperature of 111°C and absorbed 1.15 percent water after 21 days in a 120°F water bath.

Water absorption studies were carried out in two separate test runs. The first test run was conducted for 28 days in 120 F distilled water. This information is found in Graph 1. The second test run was conducted for 21 days under identical conditions. These results are found in Graph 2.

The first test data shows that except for the 50 percent HFPMA, the samples had not reached saturation in the 120°F water. The 50 percent HFPMA sample increased only 0.017 percent during the 1st week of the test. By contrast, two pure MMA samples increased during the last week of the test by 0.123 percent and 0.131 percent. One can estimate from the graphs that these samples would not reach saturation until 6 to 8 months.

Another feature of the water repellency displayed by these samples is the apparent threshold value necessary to achieve significant lowering of the water saturation percent. In Graph 1, a pronounced change in the rate of water absorption occurs between 10 and 15 percent. In Graph 2, it can be seen that PHFPA affords less protection at lower concentrations and the apparent threshold concentration lies somewhere between 25 and 30 percent PHFPA. It is interesting to note, however, that at the 50 percent concentration level the PHFPA affords better protection than HFPMA. The presence of the phenyl group in the fluorocarbon portion of the PHFPA may restrict rotation in polymer backbone structure and prevent an ideal orientation of the trifluoromethyl groups to the interface. Thus, the higher concentration of the fluoroacrylate is necessary to saturate the bulk polymer in a nonideal conformation.

In Graph 3, a plot of the copolymer composition (MMA and HFPMA) versus percent water absorption shows a reasonably smooth correlation. Given a desired water absorption maxima one can add sufficient HFPMA to achieve the result needed.

In Graph 4, selected samples from the 28 day water absorption test run were allowed to dry at room temperature in air, average 70 F and 35 percent relative humidity. The 50 percent HFPMA sample lost water approximately 50 percent faster than the pure MMA samples. When the samples were placed in a 122°F oven, the 50 percent HFPMA sample again lost absorbed water about 50 percent faster than the pure MMA samples.

Additional studies are now being carried out with thinner samples where water saturation can be achieved in a much shorter time period. Other studies on the hydrolytic stability of acetates of the fluoroalcohols used in this report are nearly completed.

EXPERIMENTAL

The fluoroalcohols used in this study were prepared and purified to greater than 99% prior to their conversion to the fluoroacrylate. The 2-phenylhexafluoro-2-propanol was prepared using a previously reported procedure which was modified through the use of a large excess of benzene [4]. The principal impurity (1.0%) in the alcohol was the diol 1,3-bis(hexafluoro-2-hydroxy-2-propyl)benzene which had a great propensity to codistill with the alcohol. The other alcohol, hexafluoro-2-propanol, was purchased from commercial sources, dried, and then distilled using a center fraction which was better than 99.6% pure.

The acrylate and methacrylates were prepared by the reaction of the alcohol and acid chloride in the presence of an excess of tertiary amine using a solvent mixture of Freon-113 and ether [5]. Purification of the monomers to greater than 99% purity was achieved by fractional distillation at reduced pressure and column chromatography through charcoal and neutral activated alumina. The fluoroacrylates used in this study were not stabilized by free radical inhibitors and remained stable for over two years in a refrigerator.

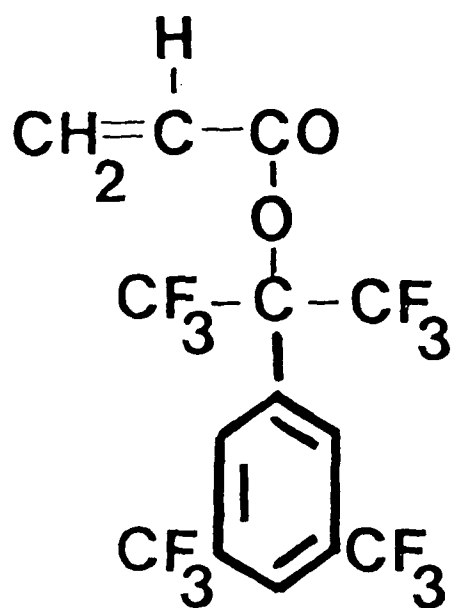
Copolymer samples of the methyl methacrylate and the fluoroacrylates (see Table I) were prepared by mixing the monomers in the desired ratio at room temperature with azobis isobutyronitrile (AIBN) (monomer/AIBN ratio = 5000/1) for 10 minutes. The monomer-catalyst mixture was transferred to 8 mL vials (17 x 16 mm) by syringe and sealed.

Polymerization was carried out by heating the mixture at 50°C (96 hours) then 70°C (24 hours) and finally 90°C (24 hours). The glass vials were broken to give molded samples which were cut on one end to form a cylinder ca. 25 mm long by 14.6 mm diameter. The cut end was sanded with emory paper to give a smooth finish. Each sample was dried at 50°C (48 hours) then cooled in a dessicator and weighed to 0.01 mg accuracy. The samples were immersed in 120°F water bath, removed periodically and cooled to room temperature in a plastic bag. Each sample was quickly towel-dried and again weighed to within 0.01 mg accuracy. The data for copolymers samples exposed to 120°F water for 28 days appear in Graph 1. The data for a 21 day exposure test appear in Graph 2.

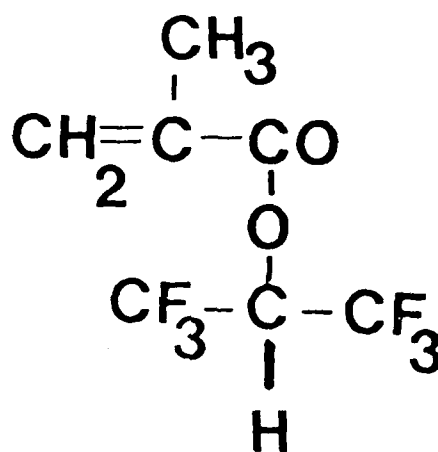
Polymer sample densities were determined by the ASTM D792, method A-1 procedure. These data appear in Table I.

REFERENCES

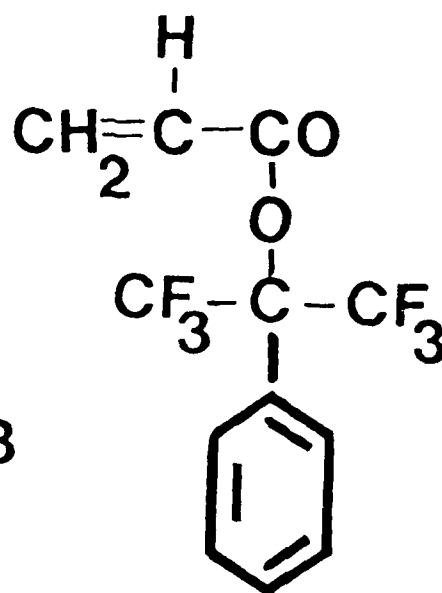
1. A. M. Lovelace, D. A. Rausch and W. Postelnek, Aliphatic Fluorine Compounds, Reinhold, New York, 1958, pg 137.
2. E. F. Hare, E. G. Shafrin, and W. A. Zisman, J. Phys. Chem., 58, 236 (1954).
3. J. N. Roitman and A. G. Pittman, J. Polymer Sci. B 10, 499 (1972).
4. J. Sepiol and R. L. Soulen, J. Fluorine Chem., 24 (1985) 61.
5. J. R. Griffith and J. G. O'Rear, "Biomedical and Dental Applications of Polymers", ACS Polymer Science and Technology, Vol. 14, Plenum Press, New York, pg 373-377 (1980).



BTPHFPA



HFPMA



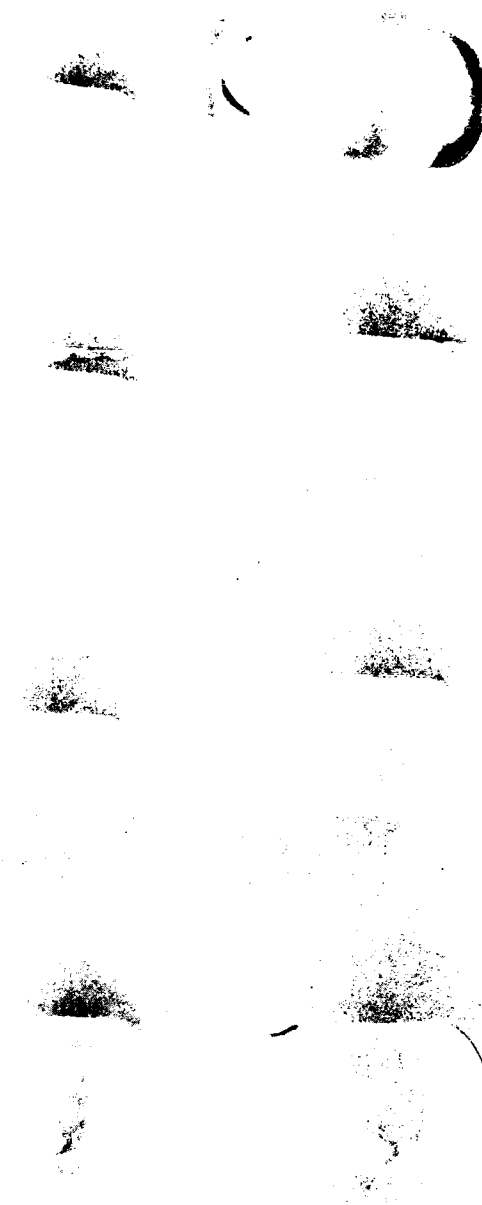
PHFPA

FIGURE 1 FLUOROACRYLATE STRUCTURES

COPOLYMERS OF HFPMA-MMA WATER ABSORPTION STUDIES

AFTER 28 DAYS
IMMERSION IN
120 F WATER

DRY SAMPLES



0 10 25 50
PERCENT HFPMA

FIGURE 2

COPOLYMERS OF PHFPA MMA WATER ABSORPTION STUDIES

AFTER 21 DAYS
IMMERSION IN
120 F WATER

DRY SAMPLES

0 25 50

PERCENT PHFPA

FIGURE 3

TABLE - 1
FLUOROACRYLATE PROPERTIES

Polymer Composition*	Density	Tg C
1.) 100% MMA	1.18	119
2.) 10% BTPHFPA	1.19	105
3.) 5% HFPMA	1.18	106
4.) 10% HFPMA	1.20	111
5.) 10% HFPMA	1.25	113
6.) 15% HFPMA	1.22	110
7.) 25% HFPMA	1.26	99
8.) 50% HFPMA	1.35	99
9.) 10% PHFPA	1.24	115
10.) 25% PHFPA	1.22	111
11.) 50% PHFPA	1.33	103

KEY: MMA = Methyl methacrylate

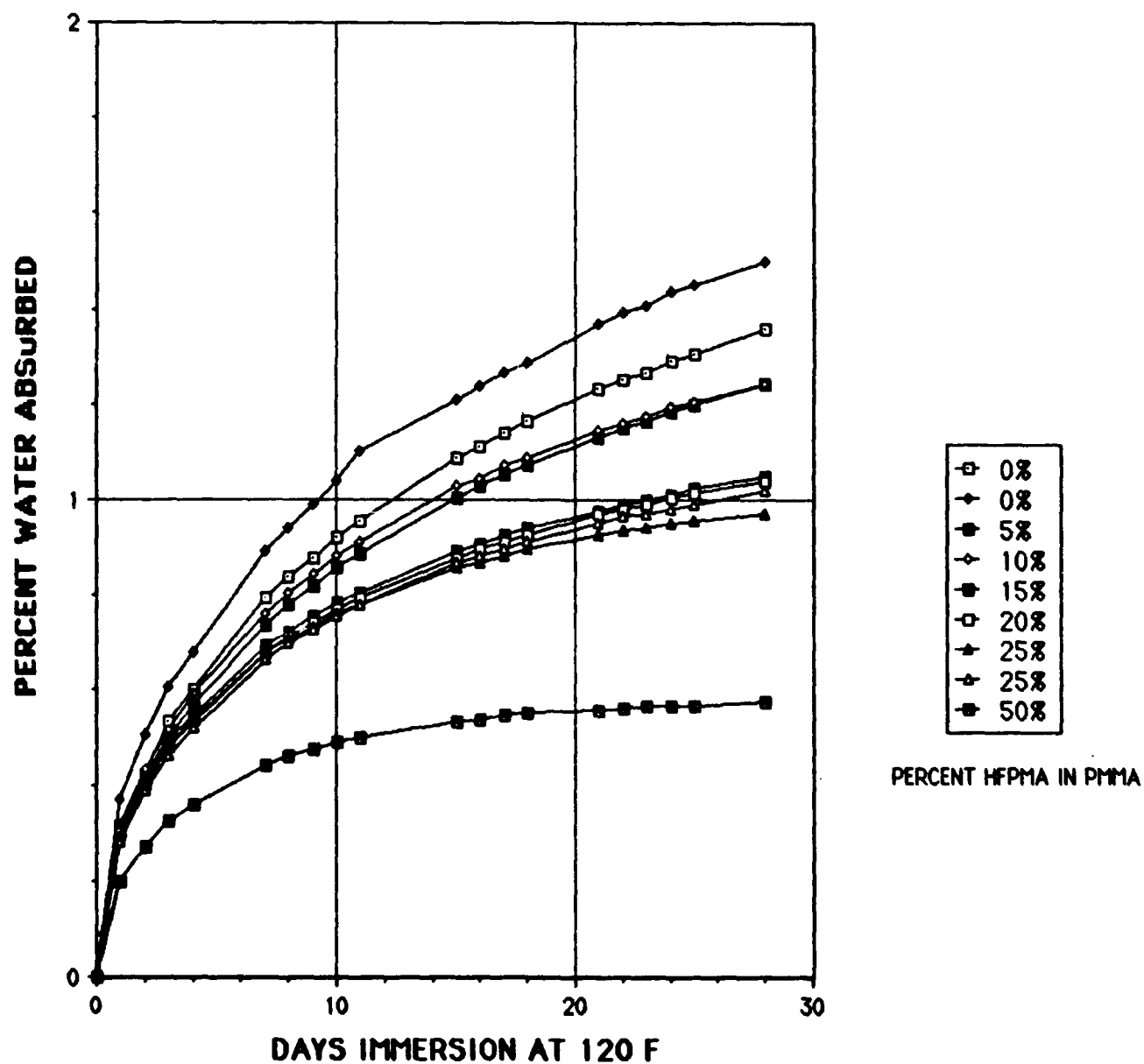
HFPMA = hexafluoro-2-propyl methacrylate

BTPHFPA = 2(3,5-bis(trifluoromethyl)phenyl)hexafluoro-2-propyl acrylate

PHFPA = 2-phenylhexafluoro-2-propyl acrylate

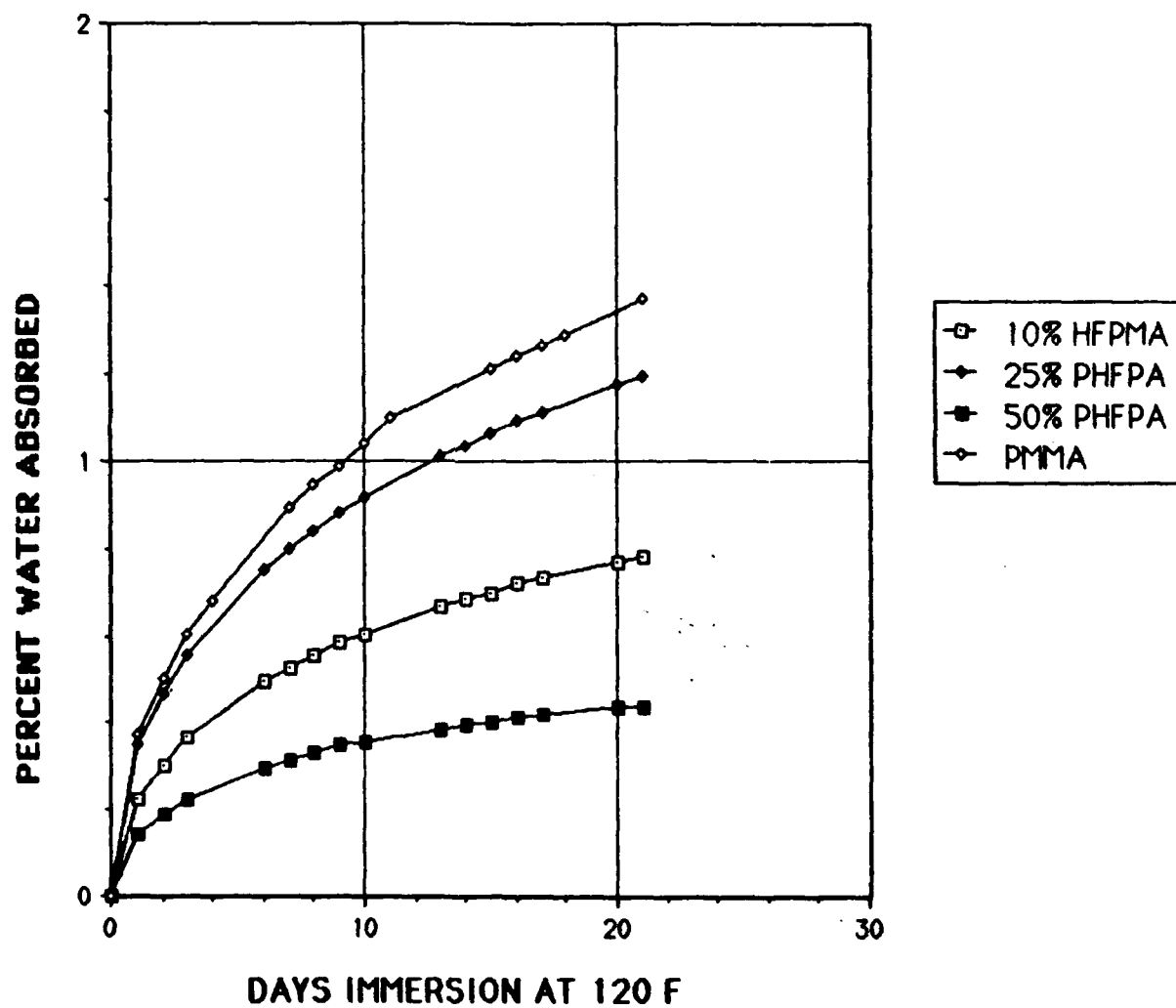
GRAPH-1

WATER ABSORPTION IN FLUOROACRYLATES



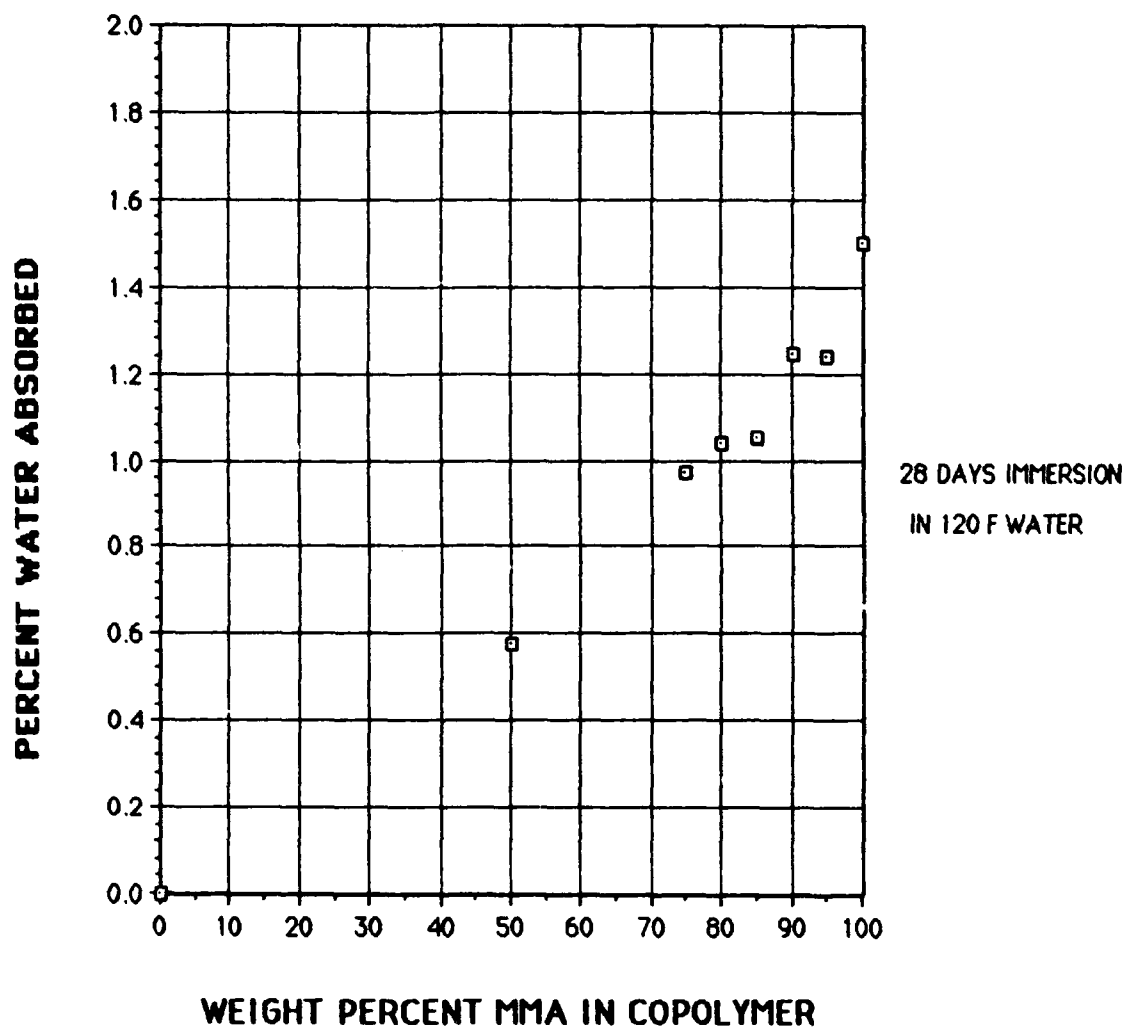
GRAPH-2

WATER ABSORPTION IN FLUOROACRYLATES



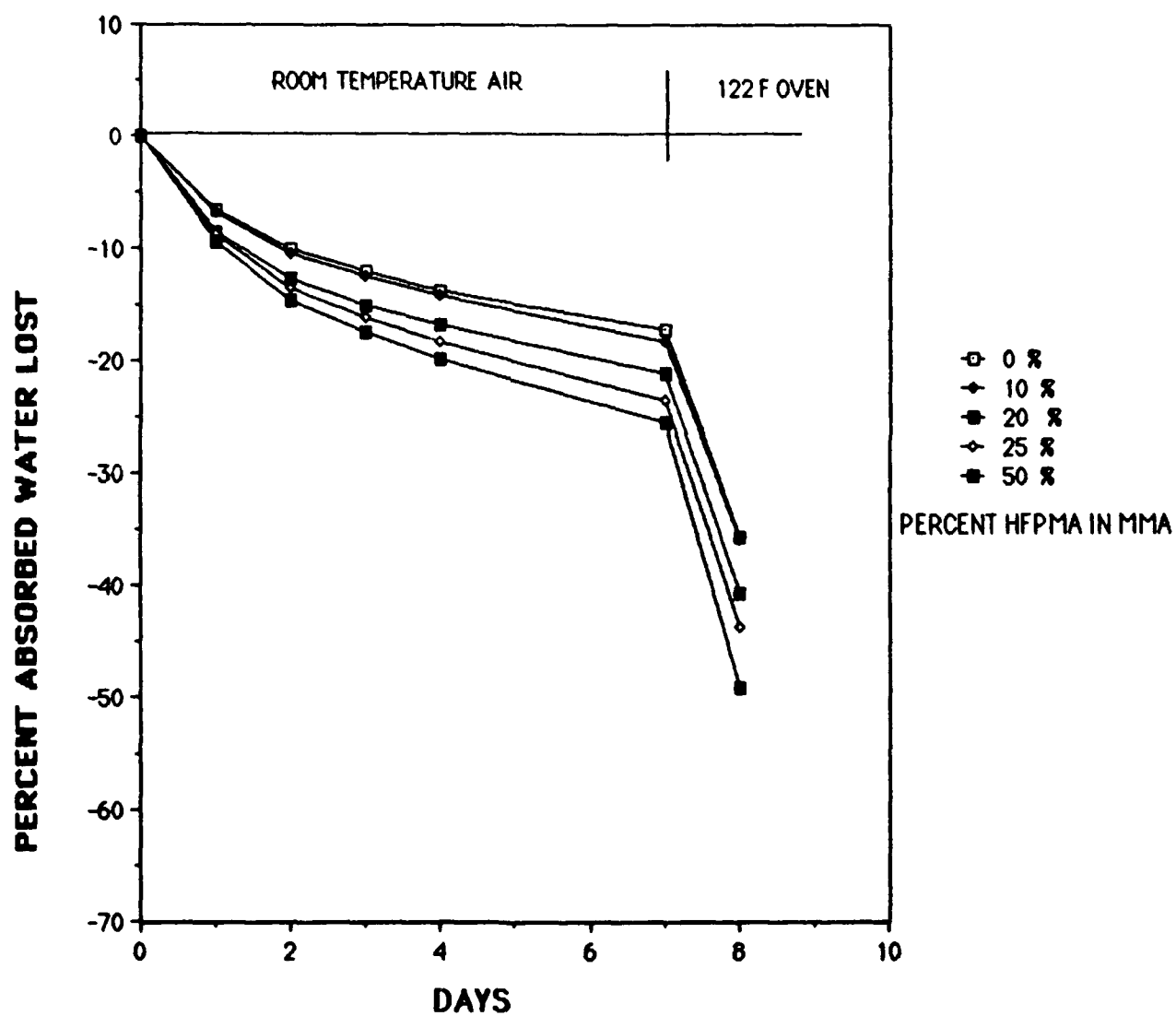
GRAPH-3

WATER ABSORPTION VERSUS COMPOSITION



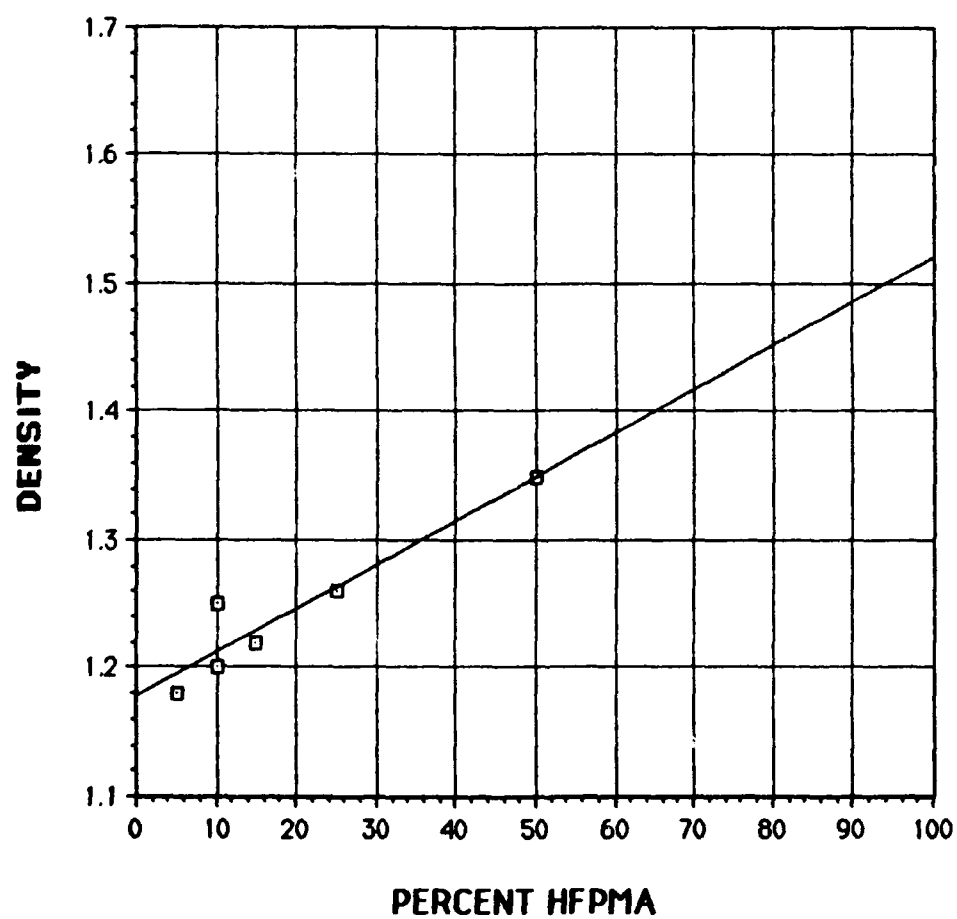
GRAPH-4

WATER DESORPTION FROM FLUOROACRYLATES



GRAPH-5

POLYMER COMPOSITION-DENSITY



NEW TRANSPARENCY MATERIALS

Stephen E. Bales

Dow Chemical Company

NEW TRANSPARENCY MATERIALS

Stephen E. Bales
Central Research
The Dow Chemical Company

This paper describes Dow's development of new polycarbonates for aerospace transparencies. Compared to currently used bisphenol A polycarbonate and acrylics, these new aromatic ester carbonate copolymers provide higher glass transition temperatures, improved toughness, and superior resistance to thermal embrittlement (physical aging), fatigue, crack propagation, solvent attack, UV radiation, and abrasion. Performance profiles, based on our internal studies and joint development programs with canopy OEMs, are used to detail the structure-property relations and advantages of these new polycarbonates, with an emphasis on comparisons to the transparency materials of today's aircraft.

INTRODUCTION

The development of a new aircraft transparency material must take into consideration the increasingly severe effects of weather, impact and temperature at higher Mach numbers. The required property improvements must be accompanied by long term property retention under the predicted operational stresses imposed on the transparency. Moderate processing conditions are required to permit ready fabrication of large area, complex curvature, wrap-around windshield/canopy assemblies. Further, the raw materials used should be commercially available and low in cost. Required synthesis techniques should insure reproducible and predictable properties in the final product.

The objective of this paper is to provide an introduction to Dow's new family of aromatic ester carbonate (AEC) copolymers.¹⁻⁴ Compared to acrylics and bisphenol A polycarbonate (PC), the AEC copolymers provide significant improvements in a variety of properties key to aerospace transparencies. This paper will discuss the level of AEC performance enhancement and will indicate how the canopy operating envelope can be expanded to meet the continuing increase in both natural hazards and combat threats.

DISCUSSION

AEC Synthesis

The AEC copolymers are prepared by the condensation polymerization reaction of a diol with a mixture of phosgene and a diacid chloride, as summarized in Figure 1. Dow's first generation AEC copolymers are prepared using bisphenol A and a mixture of phthaloyl chlorides. These are the compositions described in this paper. For a given set of monomers, copolymer properties will be determined by the ratio of ester to carbonate, molecular weight and dispersity ratio, and the degree of functional group alternation in the copolymer backbone. By taking advantage of these compositional factors, the copolymer may be tailored to meet specific requirements of aircraft transparencies.

Thermal Resistance

Figure 2 shows the increase in thermal resistance for AEC as a function of increasing ester content. Values are included for Vicat heat distortion (ASTM D-1525), deflection temperature under load (DTUL, ASTM D-648, 264 psi), and glass transition temperature (T_g) as determined by differential scanning calorimetry. Values for PC are shown on the Y-axis at zero ester content. The highest ester content AEC that has been evaluated for canopies has a T_g of approximately 365°F, compared to 300°F for PC and 220°F for acrylic.

Impact Resistance

Toughness values as determined by the notched Izod (ASTM D-256) procedure are presented for AEC (0.125 inch thick) in Figure 3 at two different notch tip radii. Room temperature impact strength, using a standard 10 mil notch radius, decreases with increasing ester content from 16 ft-lb/in (PC) to 6 ft-lb/in (high ester AEC). When tested using a sharper 5 mil notch radius, PC shows a dramatic drop to a level of about 2

ft-lb/in. However, the AEC copolymers do not exhibit this notch sensitivity; values observed at a 5 mil radius are approximately 90% of the 10 mil values.

Figure 4 shows the effect of low temperature on notched Izod values. At -22°F, PC is quite brittle, showing a dramatic reduction from the room temperature values. As with changes in notch radius, this drop in temperature has little effect on the AEC copolymers. Again, the values of Izod at -22°F are 90% of those at room temperature.

A similar improvement in Izod resistance is observed for AEC using thicker specimens. The 16 ft-lb/in value of PC measured at 0.125 inch falls to about 2 ft-lb/in when 0.250 inch thickness is tested. However, AEC does not exhibit this thickness sensitivity; high ester AEC with a notched Izod of 6 ft-lb/in at 0.125 inch thickness only drops to 5 ft-lb/in at 0.250 inch thickness. Because of the very low standard Izod values obtained for acrylics, in the range of 0.3 to 0.5 ft-lb/in, these materials have not been evaluated at sharper notch or low temperature.

Another procedure we have employed for toughness evaluation is instrumented 90° incidence angle drop-dart impact using a Dynatup 8000 apparatus.⁵ In this equipment the impacting tup (0.625 inch diameter) attached to a 138 lb hammer is released from a 12 inch drop height. Tup velocity at impact is in the range of 94 to 96 inch/second. Toughness evaluations using this procedure are based on the maximum force during the impact event and the energy to break the specimen. Dynatup values are shown in Table 1 at different thicknesses for PC, high ester AEC, and MIL spec samples of cast (MIL P-8184) and stretched (MIL P-25690) acrylic supplied by a canopy OEM. These results demonstrate the significant improvement in toughness for PC and AEC versus the acrylics. Further, the comparable impact resistance of AEC and PC using this procedure enhances the confidence factor for PC replacement by AEC.

Thermal Aging Resistance

One of the most important advantages of AEC compared to PC is superior resistance to thermal embrittlement, or physical aging. The loss of toughness and ductility as a function of elevated temperature exposure is of obvious concern for military aircraft canopies exposed to aerothermal heating during supersonic flight. Physical aging is manifested as an increase in density (a decrease in free volume) and a shift in molecular conformations from those favoring ductile deformation to those favoring brittle deformation. Because of its importance, the process of physical aging has been extensively studied, and the molecular basis for this phenomena in PC and AEC has been reported.⁶⁻⁸

One procedure for evaluating the susceptibility of a polymer to aging is to monitor notched Izod resistance as a function of exposure to elevated temperature below T_g. Results of this type of evaluation for PC and AEC copolymers are shown in Figure 5. The Izod test was performed at room temperature after different periods of 250°F exposure. A standard 10 mil notch radius was used. PC exhibits a dramatic embrittlement after 4 days aging, whereas the AEC copolymers show only minimal loss of impact strength, even after 64 days of aging.

Solvent Stress Cracking

Solvent resistance has been evaluated by determining the time to failure (fracture) of specimens exposed to various liquids at different applied loads. Solvent exposure is via

gasketed cylinders containing the liquid that are placed on the central portion of the sample. Tensile loading is employed. Results for exposure to a simulated gasoline mixture of isooctane/toluene (3/1 volume ratio) are shown in Figure 6. The AEC copolymers provide significant improvement in fracture time compared to PC. Note also the increased stress crack resistance with increasing ester content.

Hydrolytic Stability

This property has also been evaluated in terms of a stress cracking phenomenon. In this case the liquid is water at 175°F. Results for fracture time versus applied load are shown in Figure 7. For comparison, results for Udel® polysulfone (PSO) are also shown. Again, the AEC copolymers provide significant improvement over PC, and the high ester AEC approaches the performance of PSO, a material well known for excellent hydrolytic stability.

Hydrolytic stability has also been evaluated, in conjunction with physical aging, by measuring notched Izod impact and optical properties after steam autoclaving at 250°F and 21 psi.⁴ Using this procedure, the AEC copolymers exhibited improved performance compared to both PC and PSO.

Fatigue Resistance

Another key property for an aerospace transparency material is resistance to cyclic stress, as in the pressurization-depressurization cycles of canopies during flight. Results for tensile fatigue are shown in Figure 8. These results, presented as peak stress versus cycles to failure, were obtained at 73°F, 1 hertz frequency, and using 0.125 inch thick specimens. Figure 8 demonstrates the dramatic improvement for high ester AEC compared to PC. At a peak stress of 3,000 psi, PC fails after about 70,000 cycles. At this stress level AEC approaches one million cycles prior to failure. Although not shown, fatigue resistance increases with increasing ester content.

Biaxial fatigue measurements have been conducted according to the procedure of Takemori.⁹ Key results from this test are shown in Table 2, including crack band width, cycles to failure, and endurance limit (the loading level where no failure occurs after one million cycles). As with the tensile experiment, these biaxial results again show the dramatic enhancement in fatigue resistance for AEC compared to PC.

Tensile Properties

Tensile properties measured according to ASTM D-638 at 73°F using 0.125 inch thick specimens are given in Table 3. The acrylic specimens were MIL spec samples as described previously. A crosshead speed of 0.2 inch/minute was employed. Results are listed for tensile strength at yield (Ty), elongation at yield (Ey) and break (Eb), post-yield stress drop (PYSD),⁶ and tensile modulus (TM).

Tensile strength at break (Tb) measured at various temperatures is shown in Figure 9, which indicates the level of improvement for AEC compared to PC and acrylic.

Other Properties

Typical optical properties obtained for injection molded or extruded sheet samples of high ester AEC are typically 88 to 90% transmission, 1 to 2% haze, and 3 to 4 yellowness index (ASTM D-1003, D-1925, 0.125 inch thickness). High ester AEC has a refractive index of 1.60 and a specific gravity of 1.20. These values are essentially the same as for PC.

Abrasion resistance using the Taber procedure was performed by measuring weight loss following 1,000 cycles at 1 Kg loading using CS-17 wheels. AEC lost 9 mg, compared to 17 mg for PC, 14 mg for stretched acrylic, and 13 mg for cast acrylic.

The critical strain for crazing in isopropanol was determined by the procedure of Wyzgoski¹⁰ using an exposure period of 30 minutes. Values obtained were 2.0% for high ester AEC, 1.0% for PC and stretched acrylic, and 0.3% for cast acrylic.

SUMMARY

Compared to currently used thermoplastics, the Dow AEC copolymer family provides an opportunity to significantly improve the performance of aircraft transparencies. Extruded sheet samples of high ester AEC have been extensively sampled to canopy OEMs, aircraft primes, and the Air Force Wright Aeronautical Laboratories. Initial feedback from these external to Dow evaluations has been very positive regarding AEC performance in such areas as high strain rate impact, polishability and repairability, solvent resistance, and optical properties after abrasion. These samples have provided experience regarding such fabrication procedures as press polishing, fusion bonding, lamination, and complex shape formation.

This cooperative effort will continue to ensure that the composition and property profiles of the AEC copolymers are properly tailored to most closely match the mission profiles of current and future military aircraft.

ACKNOWLEDGEMENTS

Mark W. Roll, Market Development Manager in the Dow Plastics Group, has been an invaluable partner in our transparency development program. Other Dow personnel that have made significant contributions to the results described in this paper include R. A. Bubeck, T. A. Dodds, H. J. Marton, D. R. Near, and V. I. Stuart.

REFERENCES

1. S. E. Bales, U.S. Patent 4,330,662 (1982).
2. H. J. Marton *et al.*, Soc. Plast. Eng., Tech. Pap., 32 (1986).
3. H. J. Marton *et al.*, Plast. Eng., 42, 49 (1986).
4. H. J. Marton and H. Farah, "Emerging Applications for New Polycarbonate Copolymers," Ryder Conference on Performance Plastics and Markets (Feb. 1987).
5. J. K. Rieke, In "Physical Testing of Plastics Correlation with End-Use Performance," ASTM STP 736, R. E. Evans, Ed., American Society for Testing and Materials, 1981.
6. R. A. Bubeck, S. E. Bales, and H. D. Lee, Polym. Eng. Sci., 24, 1142 (1984).
7. R. A. Bubeck, P. B. Smith, and S. E. Bales, In "Order in the Amorphous State of Polymers," S. E. Keinath and J. K. Rieke, Ed., Plenum, 1986.
8. P. B. Smith, R. A. Bubeck, and S. E. Bales, Macromolecules, 21, 2058 (1988).
9. M. T. Takemori, J. Mat. Sci., 17, 164 (1982).
10. M. G. Wyzgoski, General Motors Research Publication GMR-3779 (1981).

TABLE 1
DYNATUP IMPACT RESISTANCE

<u>Sample</u>	<u>Max. Force (lb)</u>		<u>Energy to Break (ft-lb)</u>	
	<u>0.125"</u>	<u>0.250"</u>	<u>0.125"</u>	<u>0.250"</u>
Acrylic-Cast	150		0.3	
Acrylic-Stretched	315		0.8	
PC	1,890	3,390	55	110
AEC-High Ester	1,910	4,200	42	115

TABLE 2
BIAXIAL FATIGUE RESISTANCE

<u>Sample</u>	<u>Discontinuous Crack Growth Band Width (μm)</u>	<u>Cycles to Failure at 9,000 psi</u>	<u>Endurance Limit (psi)</u>
PC	1 - 3	8,000	2,700
AEC-High Ester	60	65,000	4,400

TABLE 3
TENSILE PROPERTIES

Sample	Ty (psi)	Ey (%)	Eb (%)	PYSD (%)	TM (10 ⁵ psi)
Acrylic-Cast	9,600 ^a	- -	3	--b	5.0
Acrylic-Stretched	11,600	6.8	11	--b	4.5
PC	9,000	6.0	>100	23	3.3
AEC-High Ester	9,400	8.3	>40	11	3.3

^a Value at break, did not yield.

^b Eb too low to measure.

FIGURE 1
AEC SYNTHESIS

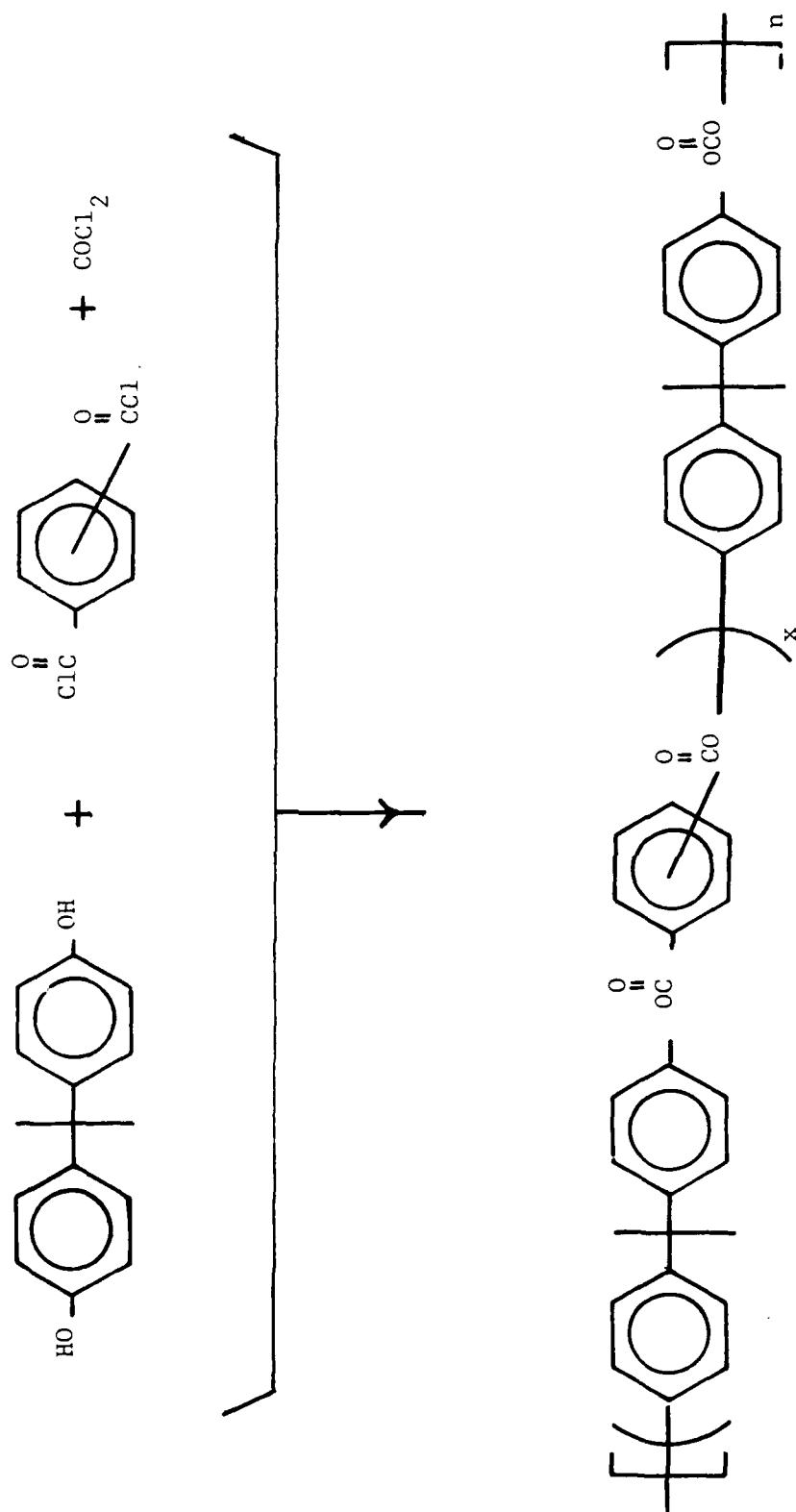


FIGURE 2
AEC THERMAL RESISTANCE

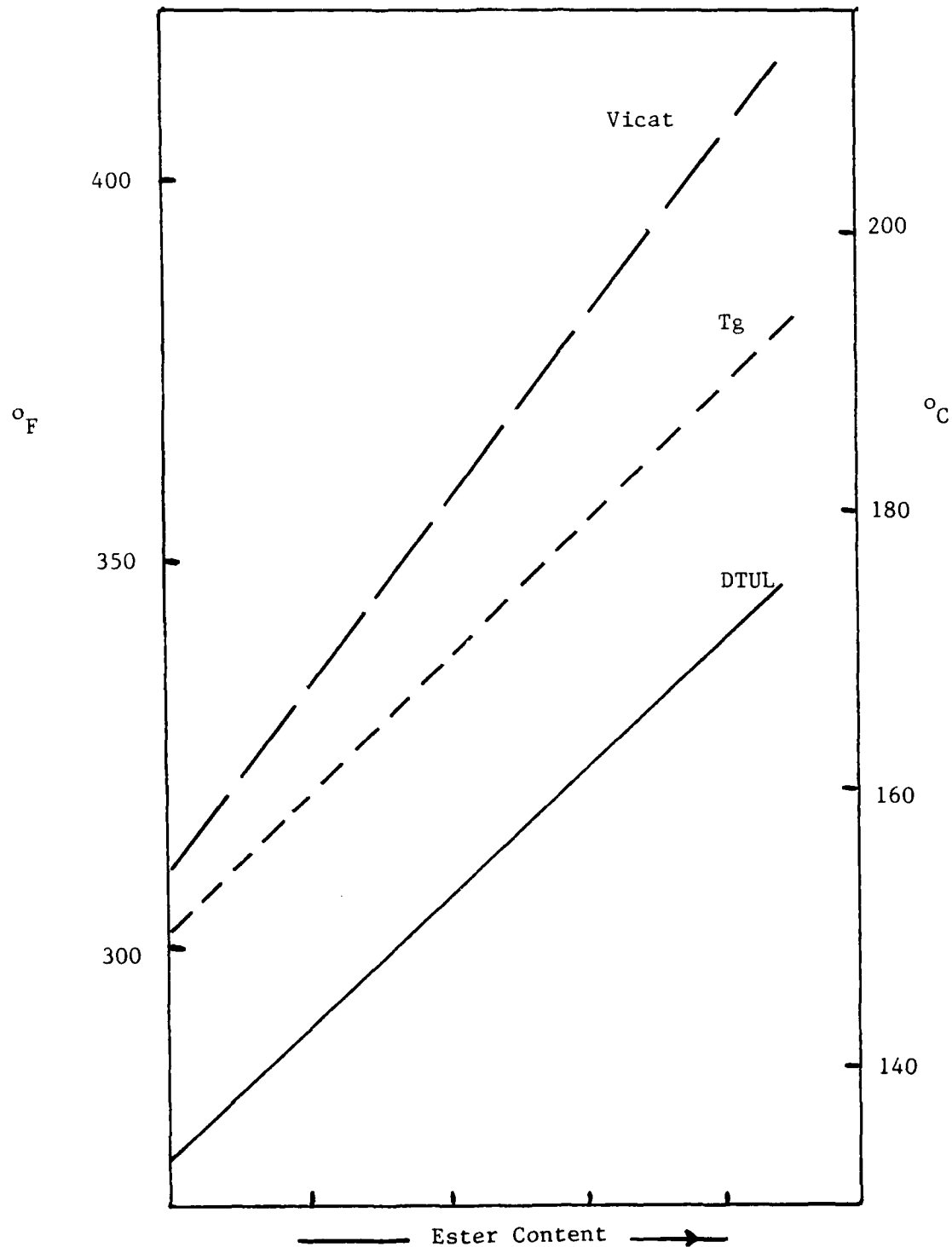


FIGURE 3
NOTCHED IZOD: EFFECT OF NOTCH RADIUS

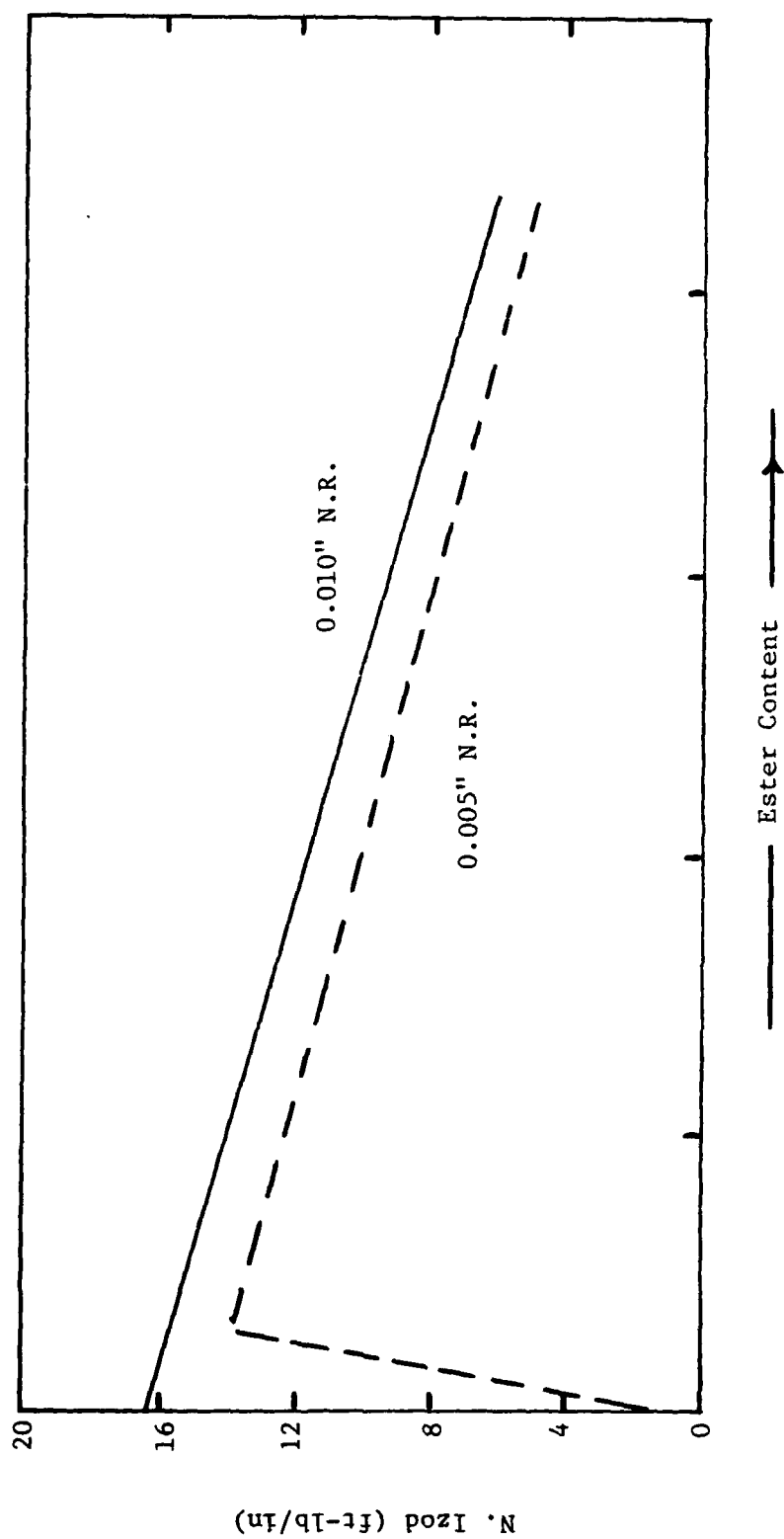


FIGURE 4
NOTCHED IZOD: EFFECT OF TEMPERATURE

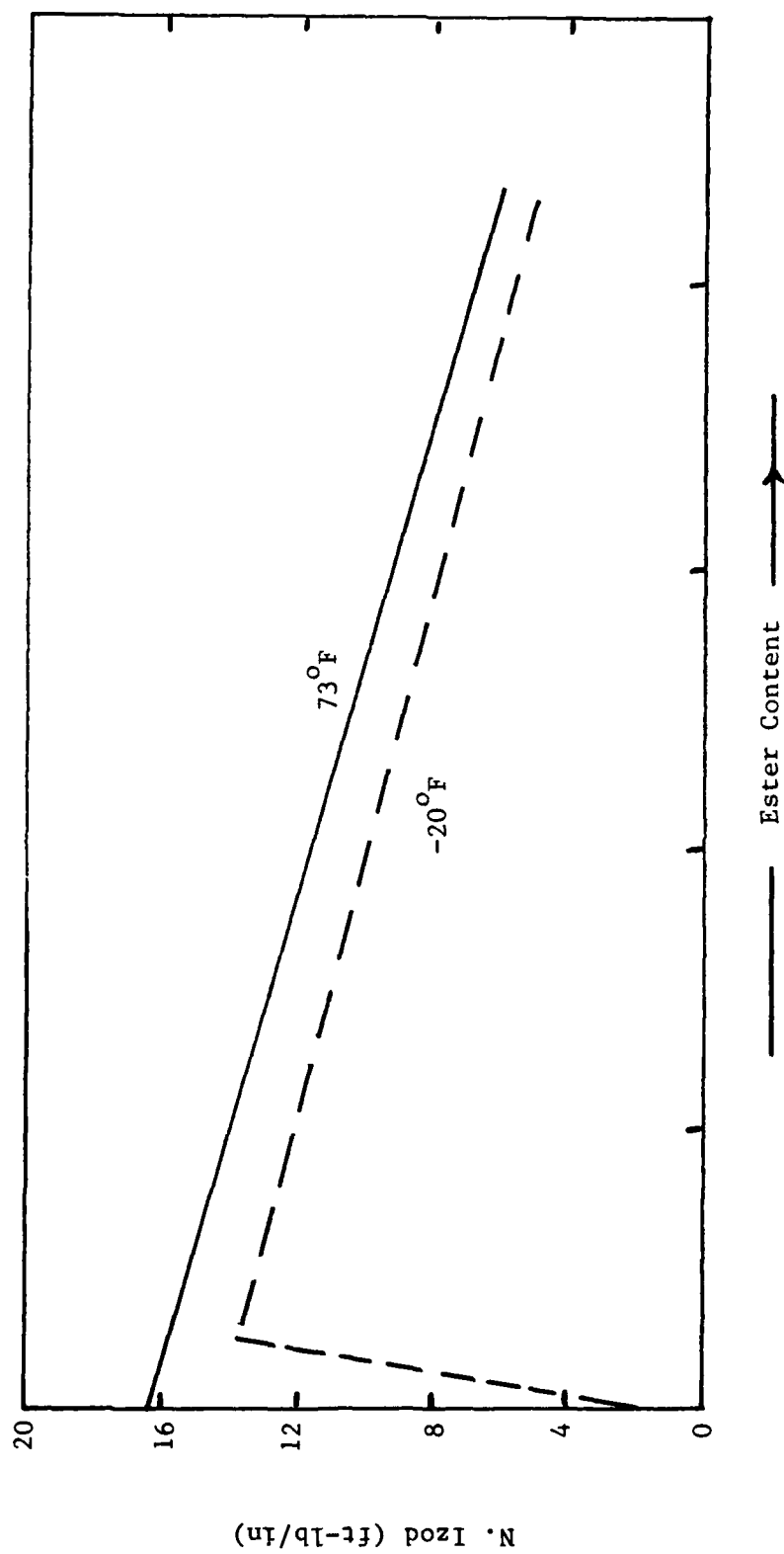


FIGURE 5
RESISTANCE TO PHYSICAL AGING

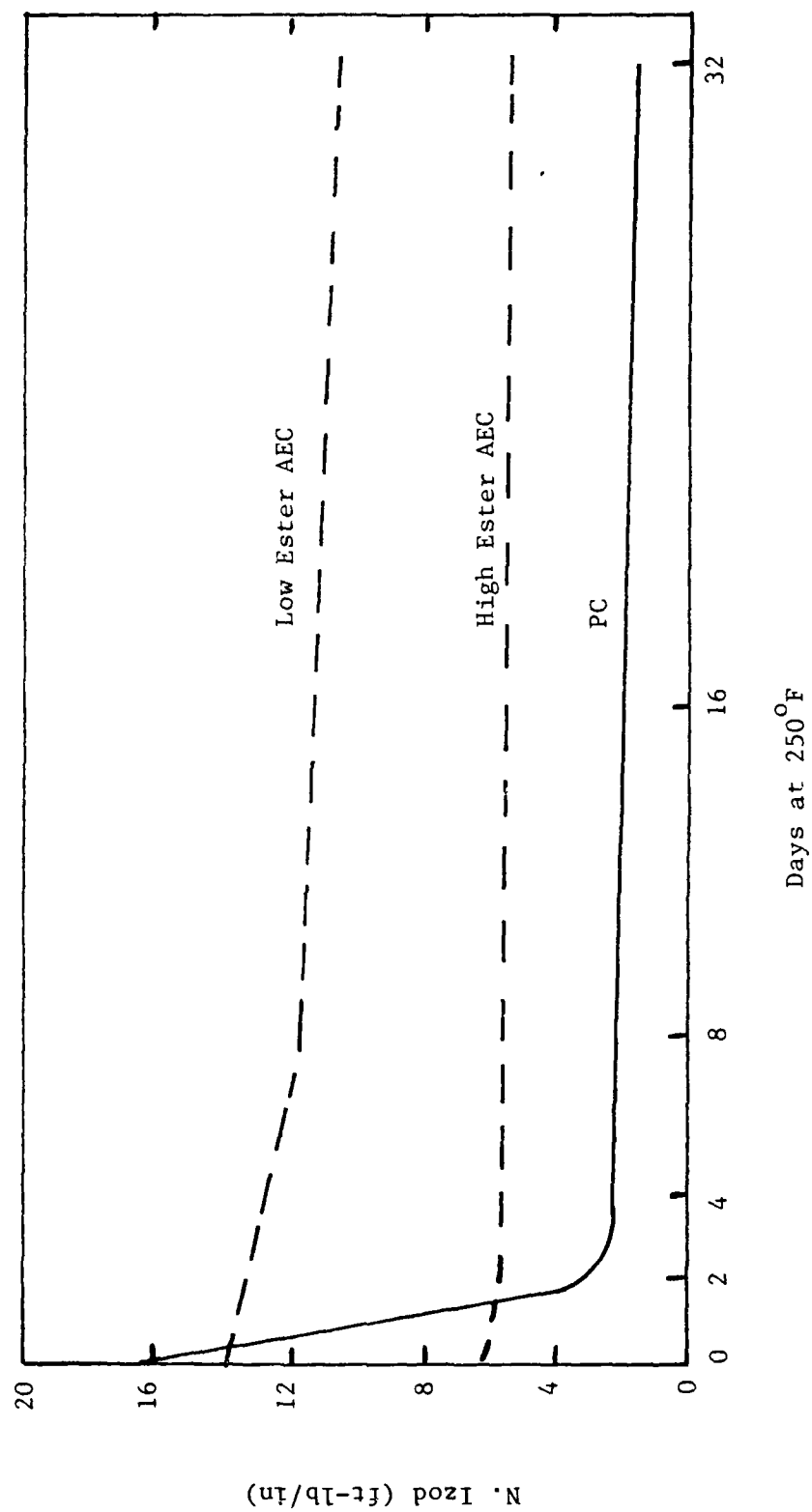


FIGURE 6
SOLVENT STRESS CRACKING: GASOLINE RESISTANCE

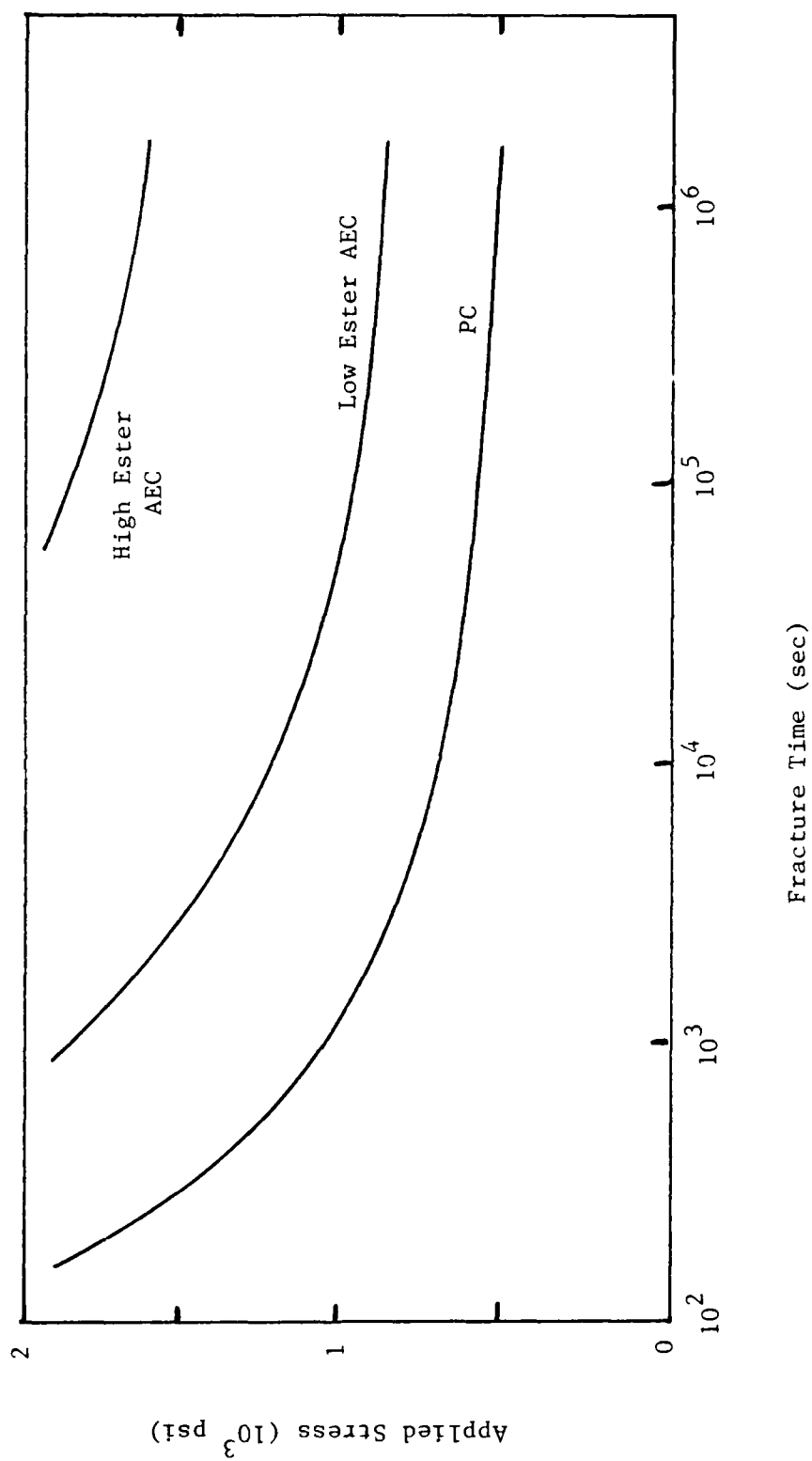


FIGURE 7
HYDROLYTIC STABILITY

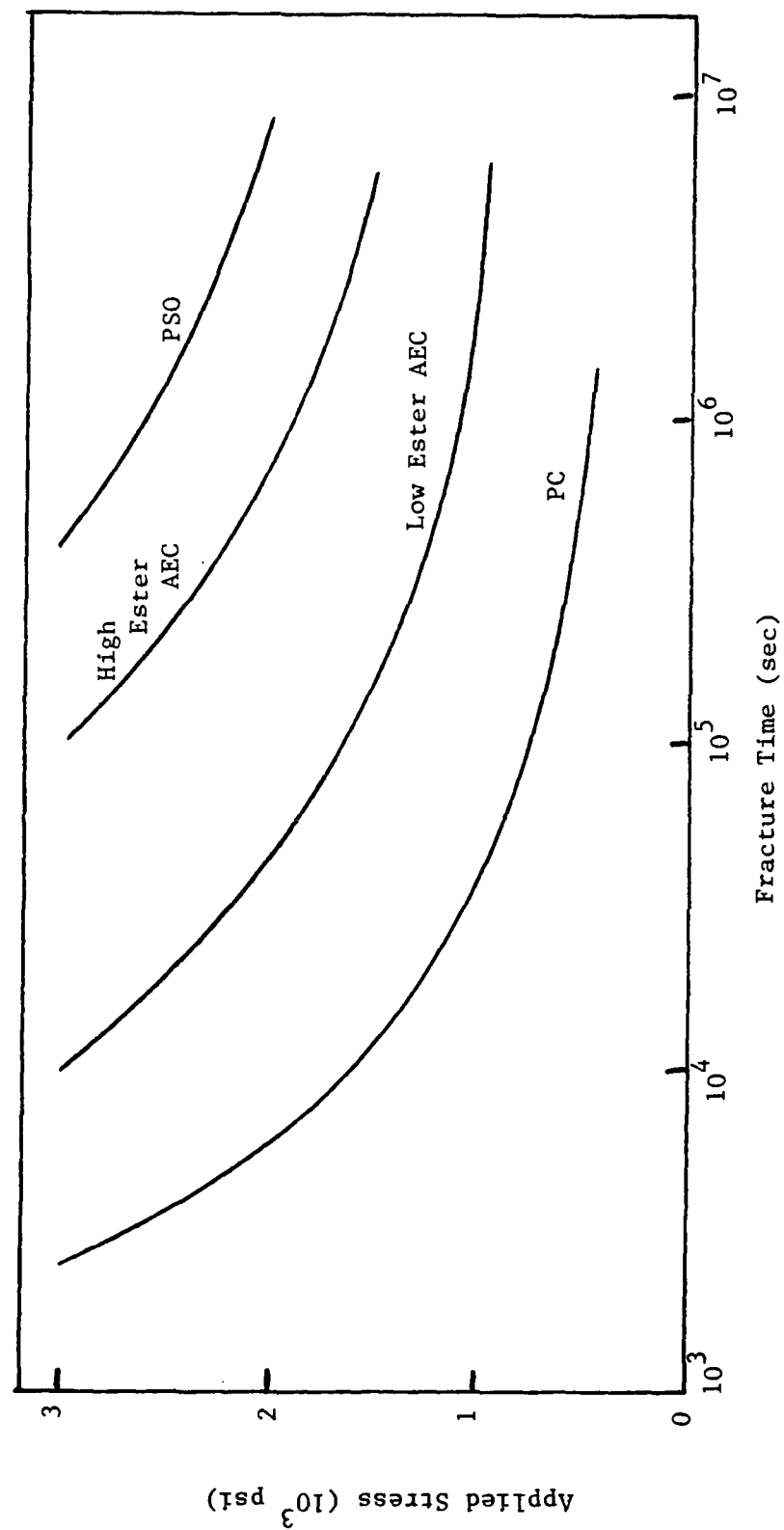


FIGURE 8
TENSILE FATIGUE RESISTANCE

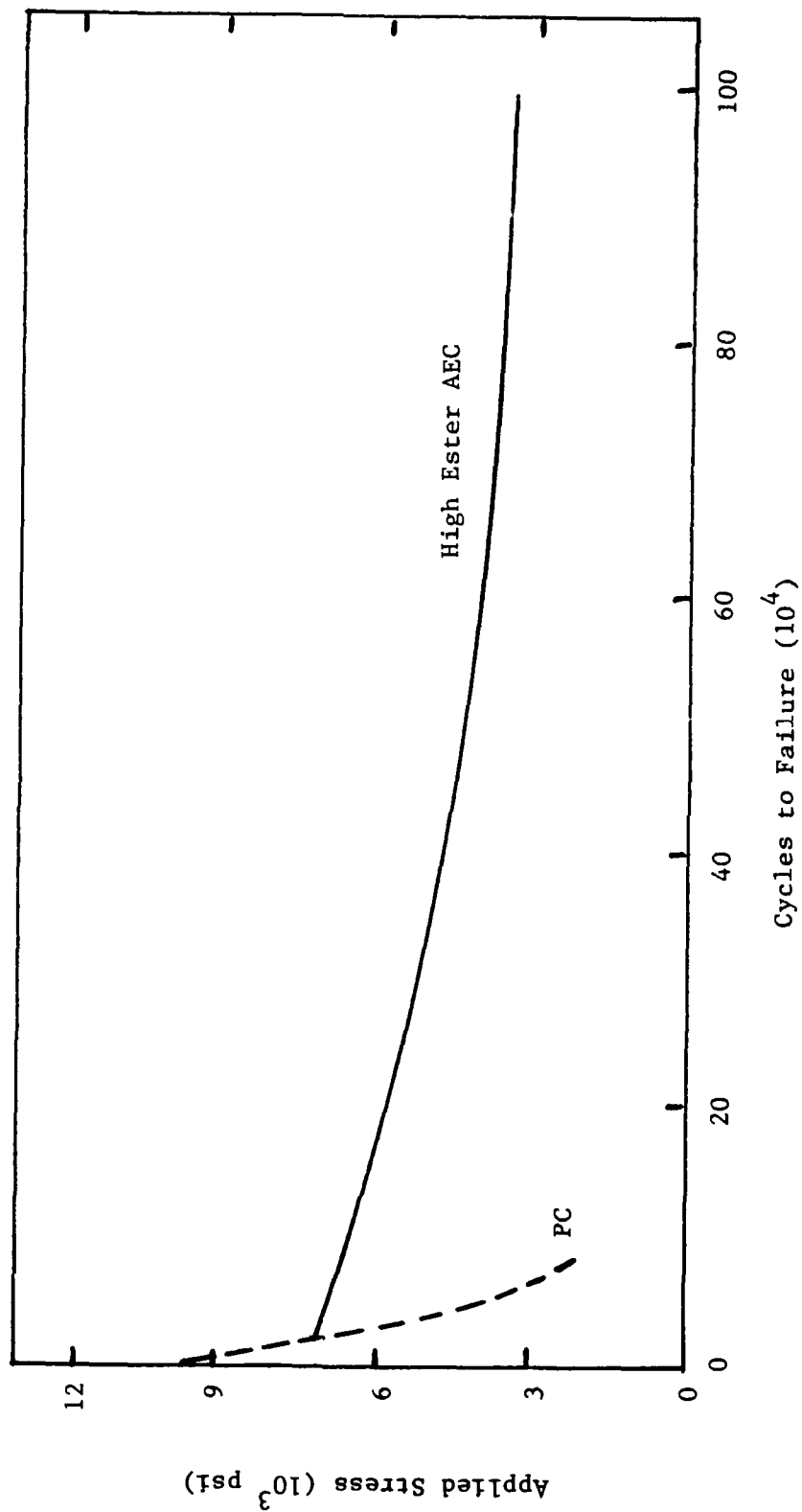
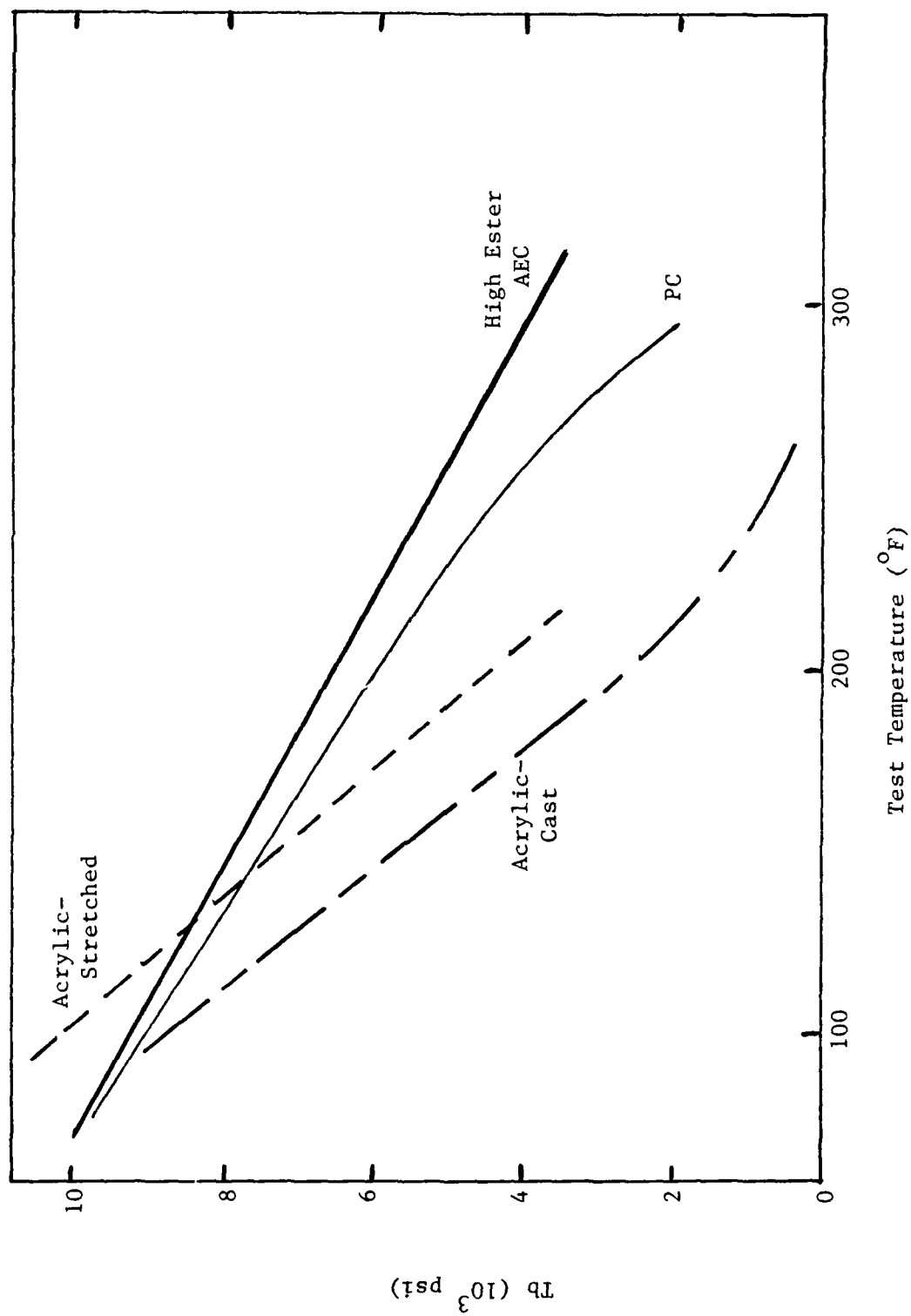


FIGURE 9
TENSILE STRENGTH AT BREAK VS. TEMPERATURE



A VACUUM COATER FOR THE APPLICATION OF ITO TO
PLASTIC CANOPIES

Paul E. Schumacher

Sierracin/A.P.G.

A VACUUM COATER FOR THE APPLICATION OF
ITO TO PLASTIC CANOPIES

Paul E. Schumacher
Sierracin/A.P.G.

ABSTRACT

A large vacuum coater has been designed, fabricated, and placed in service by Sierracin, for depositing ITO on plastic, fighter aircraft canopies. The deposition process is reactive sputtering. Typical ITO characteristics achieved are 500 microhm-cm resistivity and 250 cm^{-1} mid-visible absorption coefficient. The coating has proved durable when subjected to a range of environmental stresses.

This coater has been used to apply ITO to the interior of both polycarbonate and stretched acrylic canopies. It has also been adapted and used to coat both the external and internal surfaces of large, singly curved transparencies, both polycarbonate and glass. Currently a further adaptation to allow coating the exterior of large canopies is being completed.

INTRODUCTION

There is an ever increasing demand for transparent conductive coatings on fighter aircraft windshields and canopies. Evaporated gold coatings typically have been used to meet this demand. Objections to the gold coatings have been raised based on their high luminous reflectance (resulting in low transmittance) and color, particularly for low sheet resistance coatings.

An alternate transparent material, the semiconductor indium-tin oxide (ITO), has less intrinsic color and may offer as much as 10 percentage points higher luminous transmittance in the 10 to 15 ohm per square range as shown in Figure 1.

ITO has long been used on glass substrates where it provides a very durable conductive layer. When applied to plastics such as those used for aircraft canopies, the durability of ITO is somewhat reduced. This stems primarily from the large disparity in material properties of coating and substrate. Nevertheless, properly applied ITO on plastic is reasonably rugged and retains its optical advantages over gold.

COATING PROCESS

ITO coatings are usually applied using vacuum coating processes, most often sputtering. The process used in the coater described here is reactive sputtering from a metallic (indium-tin alloy) target. A magnetically enhanced cathode is used as a glow-discharge source of ions. These ions are attracted to the target and cause its atoms to be sputtered. The metal atoms are deposited on the substrate (canopy) where they are oxidized to form ITO. The oxygen concentration in the chamber is carefully controlled to provide the desired deviation from stoichiometry in the growing film. This is necessary because much of the electrical conductivity of ITO is derived from a deficiency of oxygen in the oxide.

COATING EQUIPMENT

The coater was originally designed for the application of ITO to canopy interiors. Two alternate configurations - to coat nearly flat transparencies and canopy exteriors - have since been implemented. These will be discussed briefly later. The coater geometry selected for interior coatings is circularly cylindrical. That is, a post cathode, the canopy, a heater array and the vacuum chamber are concentric as illustrated in the schematic shown in Figure 2.

Vacuum Chamber

The horizontal chamber is 8 feet in diameter and 16 feet long. Each end of the chamber is closed by an end bell. These add another 2 feet of length along the axis. Each end bell can be moved away from the chamber on floor rails in order to access coater interior components.

Pumping

The chamber is evacuated by a pair of identical, 4-stage pumping stacks operating in parallel. A schematic of one of these stacks is shown in Figure 3. Each of the stacks is coupled to the chamber by a 42 inch diameter high vacuum duct which incorporates a variable conductance valve. The latter is used to control pumping speed during sputtering operations. Figure 4 is a view of these ducts.

An overview of the pumping stacks and their relationship to the coating chamber is shown in Figure 5. The vacuum lines are connected high on the chamber to eliminate the need for pits to house the diffusion pumps. The equipment mounted on the platform supporting the near end bell supplies the necessary utilities to the cathode.

Heater

Substrate heating is used to optimize the characteristics of the conductive coating. While ITO can be deposited at room temperature, both its electrical conductivity and optical absorption can be reduced at elevated temperatures. Residual coating stress can also be influenced.

The concentric, radiative heater is comprised of a number of hairpin-shaped heating elements connected in a series/parallel arrangement. These elements are surrounded by a series of radiation shields to minimize power requirements. The innermost element of the heater is a muffle which serves to lower the temperature and increase the temperature uniformity of the heater as seen by the canopy.

Cathode

The post cathode is 28 inches long and 6 inches in diameter. Its outer surface (the target) is an indium-tin alloy which supplies the metallic component of the ITO coatings. A negative d.c. potential is applied to the cathode to generate the glow discharge.

The cathode is of the type commonly designated as a rotatable magnetron. That is, a magnetic field at the surface of the target and parallel to it increases the ionization efficiency of the secondary electrons generated at that surface. This allows the establishment of the glow discharge at lower voltages than otherwise possible. The magnetic enhancement also enables sputtering at lower operating pressures and higher film deposition rates. Substrate heating from secondary electrons is also reduced.

The magnetic field is generated by an array of permanent magnets. In the conventional rotatable magnetron, the magnet array is fixed and the outer cylinder of the cathode, together with its attached target material, rotates. The post cathode used in this coater reverses that arrangement; i.e., the outer cylinder is fixed and the (internal) magnet structure rotates. In this way, the distribution of sputtered material emanating from the target is uniform in azimuth as well as along its length. Figure 6 is a photograph of the cathode during sputtering operation. All light is from the luminous portion of the glow discharge which is confined to the region of high magnetic field. Anode rods surround the cathode; they, in turn, are surrounded by a canopy.

Robot

In order to deposit a uniform ITO coating over the interior of a canopy, it is necessary to provide for relative motion of the cathode and canopy. The approach chosen is to hold the canopy stationary and to move the cathode. That motion is obtained by mounting the cathode on a robot which provides 3 degrees of (motion) freedom. These are axial, vertical and pitch. The combination allows the cathode to be moved along a path which maintains approximately equal distance to the canopy surface. In addition, the axis of the cathode is kept parallel to the tangent of the canopy surface (along its top) at all points.

Robot motion is computer controlled using a trajectory which is individually tailored to each canopy. Coating parameters can be varied as a function of cathode position in order to adjust coating characteristics. These parameters include cathode speed, cathode current, sputter gas flow rate and mixture ratio.

Figure 7 is a three quarter view of the post cathode, surrounded by anode rods, mounted on the robot. The end-on view of Figure 8 shows a larger portion of the robot. The axial motion is provided by moving the entire robot assembly on a pair of rails which, in turn, move with the end bell. The utilities-sputtering gases, electrical power and cooling water-are supplied to the cathode by means of flexible conduits and tubing which are paid out in a cable coiler of the type seen in Figure 9.

The utility supply to the movable end bells of the chamber is handled in the same manner.

Process Control Instrumentation

As mentioned earlier, the conductivity of the ITO coatings derives in large measure from oxygen deficiency in the coating. Excess deficiency causes the coating to become highly absorbing and, ultimately, metallic. To obtain the proper degree of oxygen deficiency, close control of the sputtering gases is required. To achieve this control, the growing ITO film is monitored both as to electrical and optical properties. Witness plates with the same exposure as the canopy are used for this purpose. Sierracin proprietary-instrumentation is used to measure those properties.

The information obtained from this ITO monitoring is used to control the process, primarily through adjustment of the reactive/inert gas mixture ratio.

The control console for the ITO coater is shown in Figure 10. The cathode-end bell of the coater with its utility supply is in the background. The several coating parameters are displayed on meters. Chart recordings of the critical parameters are also made to aid the operator in evaluating trends as the coating proceeds.

COATING RESULTS

The vacuum coater described here has been used to deposit ITO coatings on the interior of several types of canopies for the F-16 and other aircraft. An F-16 D-Forward canopy is shown in Figure 11. It is mounted in place on rails which are attached to the moveable end bell at the substrate end of the coater.

Characteristics of the resultant ITO coatings have been measured. Typical values obtained are listed here. Electrical resistivity is 500 microhm-cm. The mid-visible absorption coefficient is 250 cm^{-1} and the index of refraction in that region is slightly under 2.

For purposes of maximizing the durability of the ITO, auxilliary coatings are used in conjunction with the conductive layer. In the case of the above canopies, these additional coatings are thermally cured, solvent-borne layers applied using Sierracin's standard flow coating techniques. Such coatings include: An adhesion promoting layer between the canopy and the ITO (base coat) and a protective cover layer atop the ITO (top coat).

ITO coatings incorporating such base coats and top coats have been exposed to a wide range of environments to assess their suitability for use in fighter aircraft canopies. Environments included temperature cycling, humidity, salt atmosphere, solvents, abrasion, etc. The ITO coatings have successfully survived these exposures.

COATER MODIFICATION

The coater as described is configured to apply ITO to canopy interiors. As such it is not suitable for coating (nearly) flat windshields and nor for coating canopy exteriors. To accommodate the need to coat windshields, a different version of the cathode, robot and heater have been implemented. A planar, magnetically enhanced cathode was fabricated and installed on a robot modified to accept it and provide a fourth degree of freedom. Flat heaters were also incorporated.

This modified version of the ITO coater has been used to coat a large number of aircraft windshields. This modified coating arrangement was designed so that the coater can be reconverted readily to the previously described post cathode arrangement.

Yet another modification of the coater has been designed and fabricated. It will be installed in the coater shortly. This modification will be used to ITO coat the exterior of a canopy. A schematic illustration of this version is shown in Figure 12. It too has been designed so that the coater can be reconverted readily to either the canopy interior or windshield coating configuration.

CONCLUSIONS

A large vacuum coater for the application of ITO to plastic aircraft canopies and windshields has been put into operation at Sierracin. It exists in 3 versions: One for coating canopy interiors; one for coating (nearly) flat windows; and one for coating canopy exteriors. The first two versions have been used successfully for the production coating of numerous aircraft transparencies. The third version is soon to be implemented.

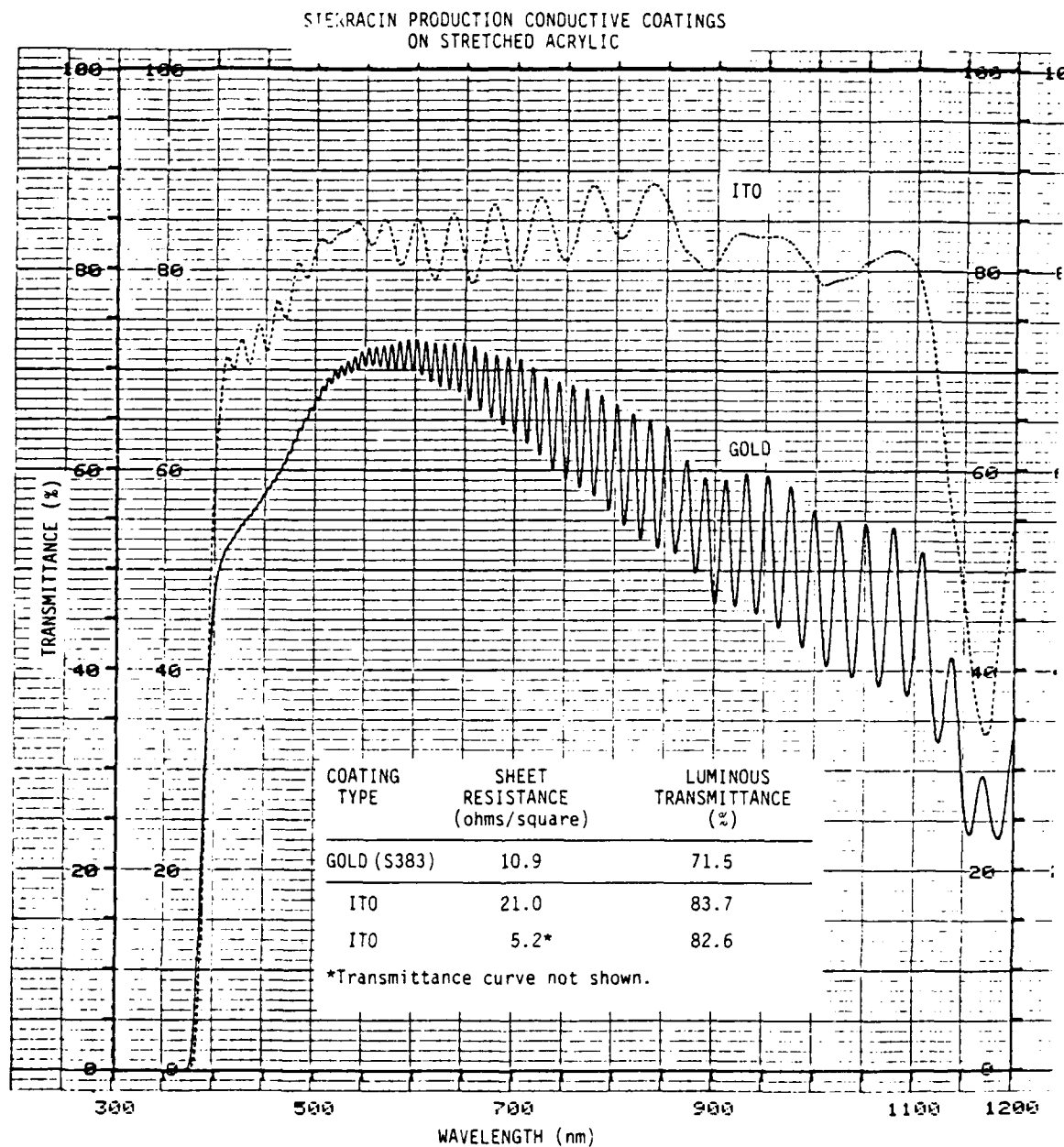


FIGURE 1
TYPICAL TRANSMITTANCE DATA FOR SIERRACIN CONDUCTIVE COATINGS

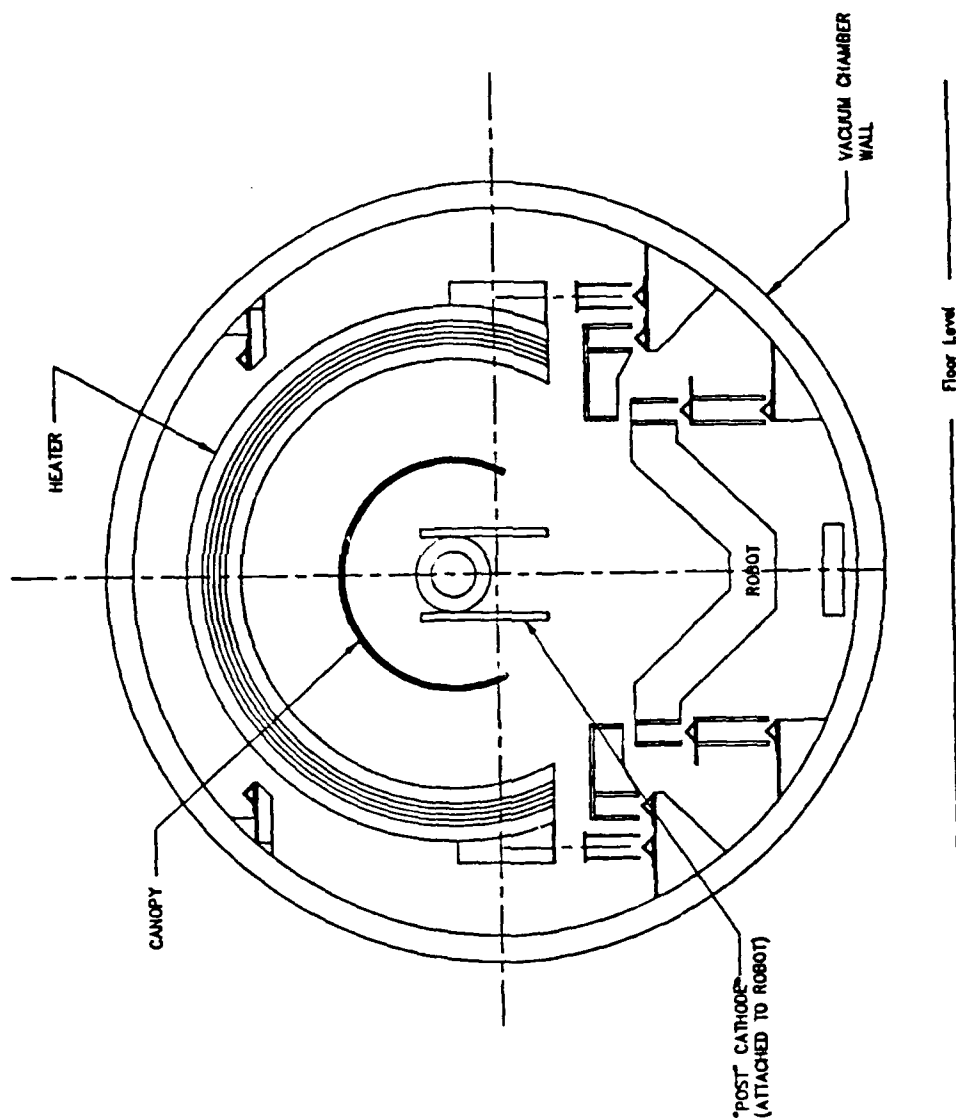


FIGURE 2

COATER CONFIGURATION FOR ITO COATING CANOPY INTERIORS

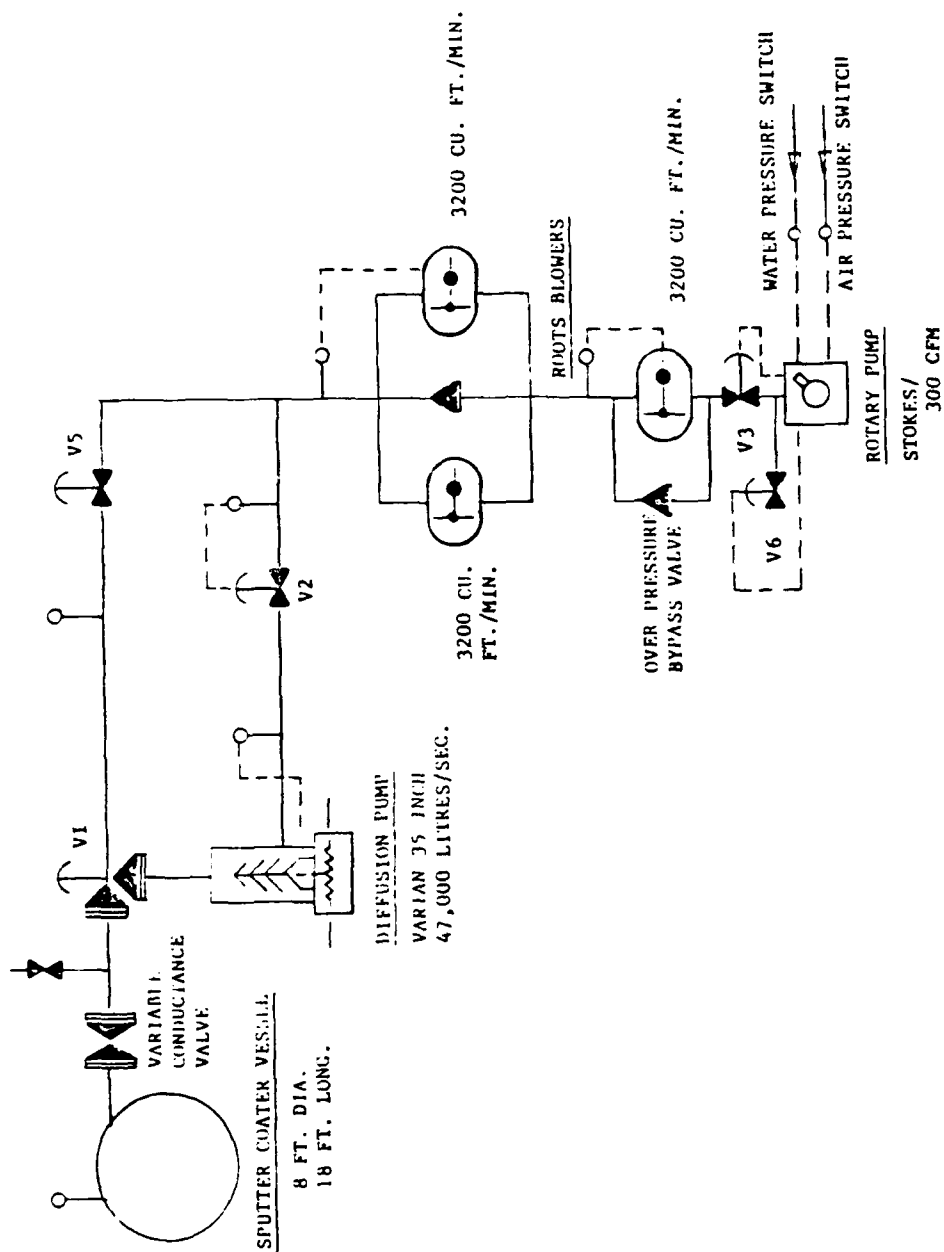


FIGURE 3
VACUUM PUMPING STATION



FIGURE 4
HIGH VACUUM LINE TO COATER

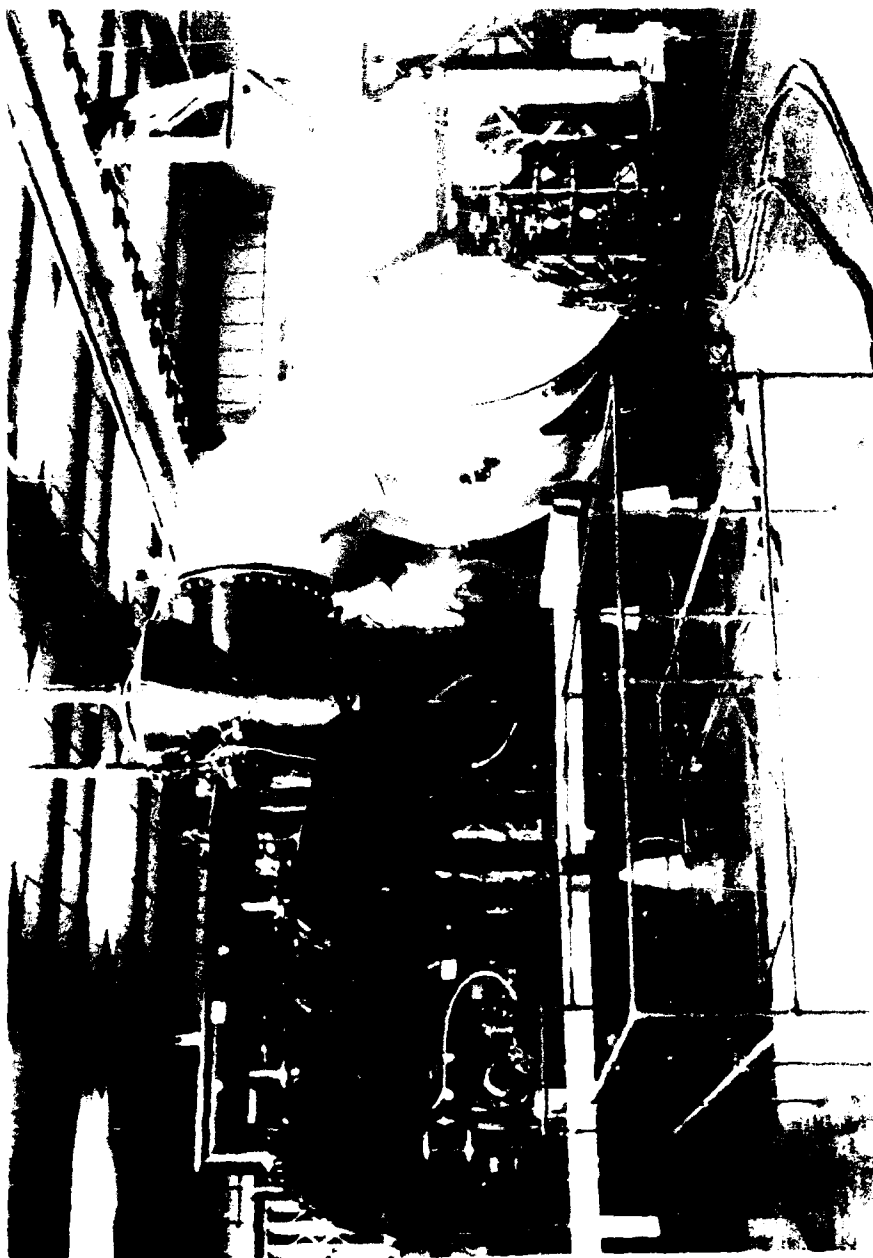


FIGURE 5
PHOTOGRAPH OF THE COATER AND ITS PUMPING STATION

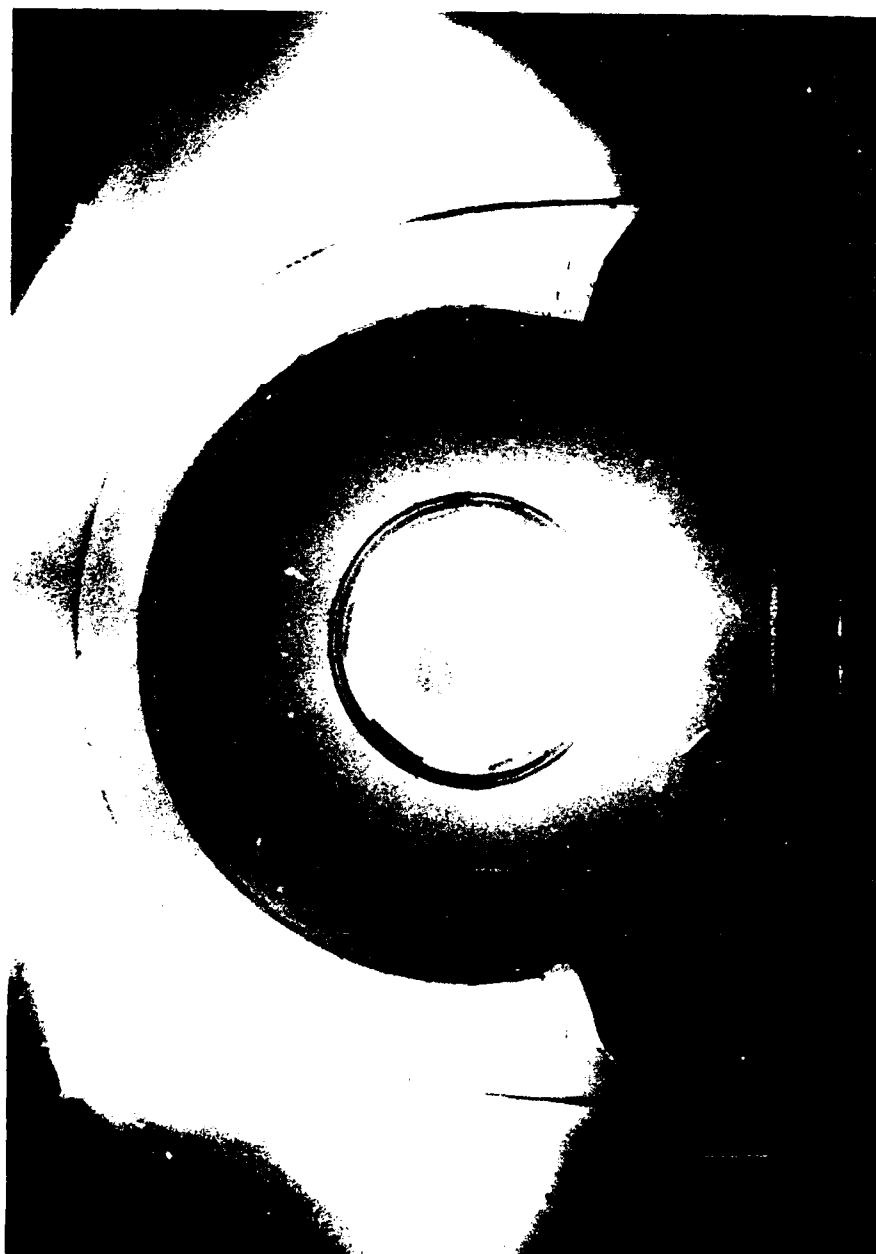


FIGURE 6
POST CATHODE DURING ITO SPUTTERING, SELF ILLUMINATED



FIGURE 7
POST CATHODE (AND ANODE) MOUNTED ON THE "ROBOT"

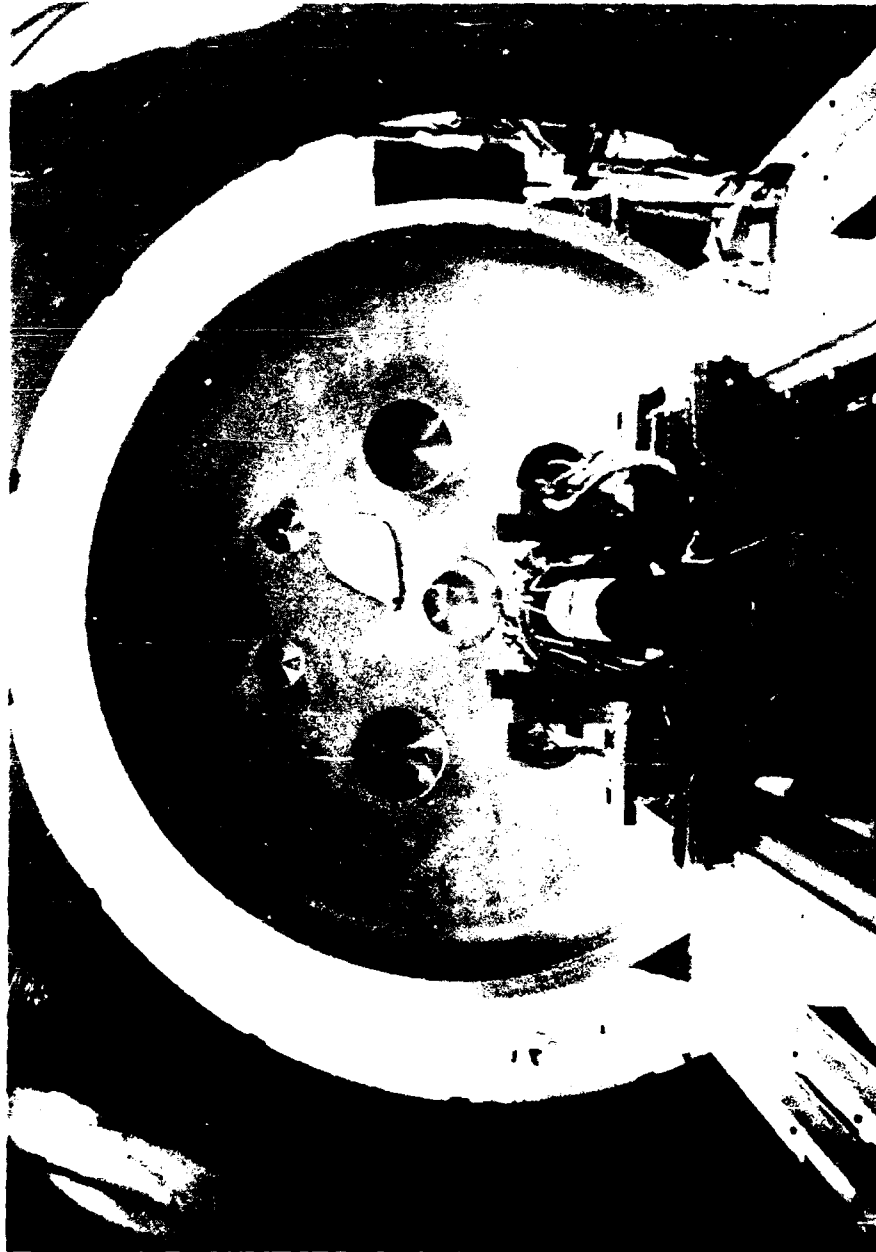


FIGURE 8
END VIEW OF POST CATHODE AND "ROBOT"



FIGURE 9
CABLE COILER FOR ITO COATER UTILITY SUPPLY

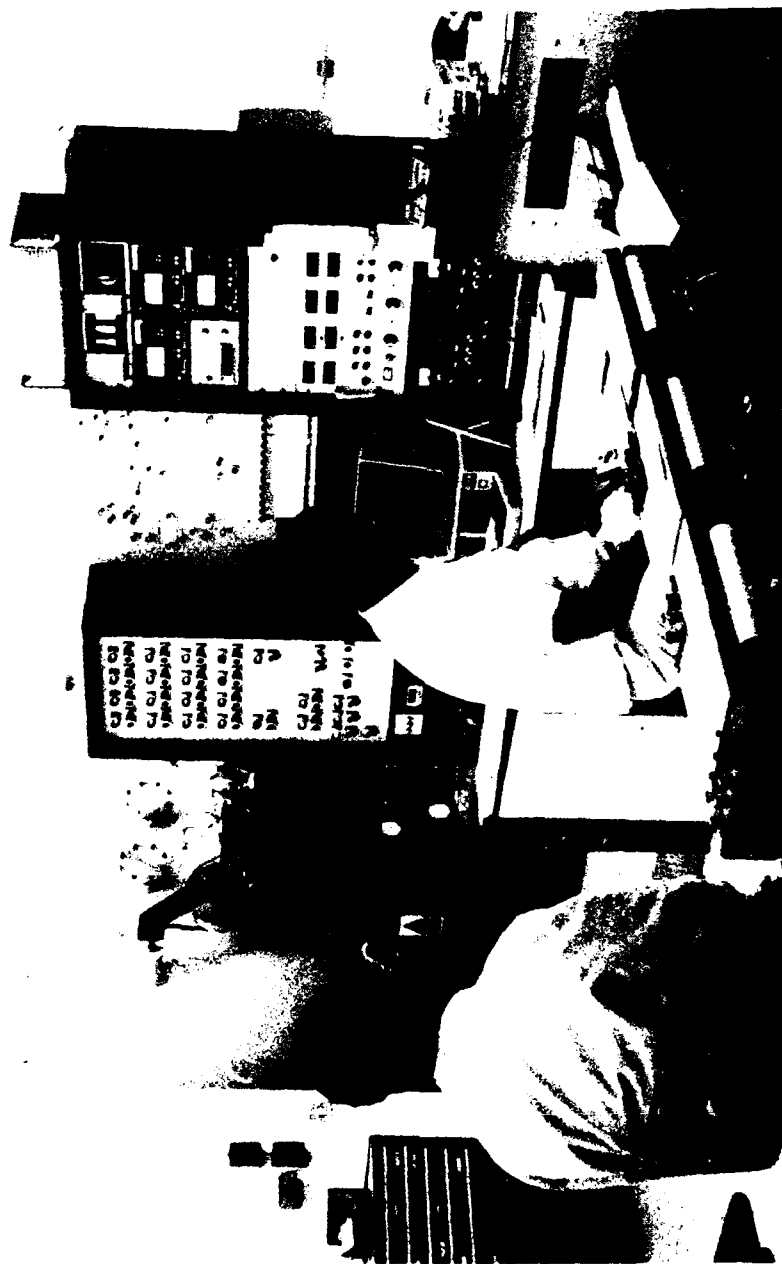


FIGURE 10
CONTROL CONSOLE OF THE ITO COATER

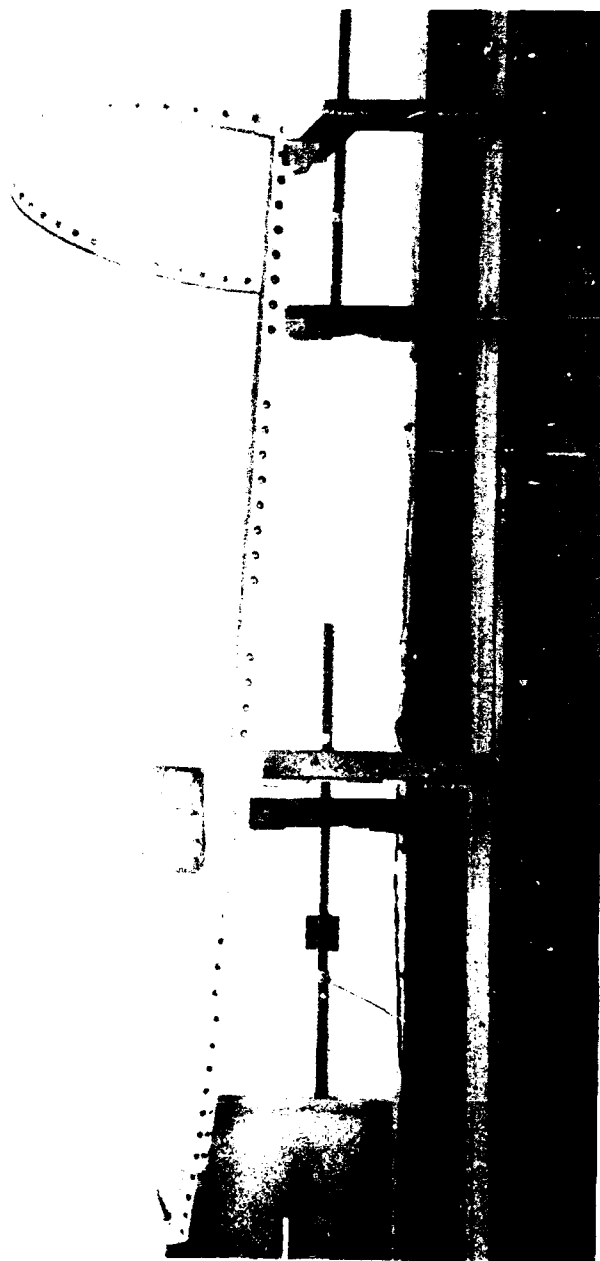


FIGURE 11

F-16 D FORWARD CANOPY MOUNTED IN PLACE IN THE ITO VACUUM COATER

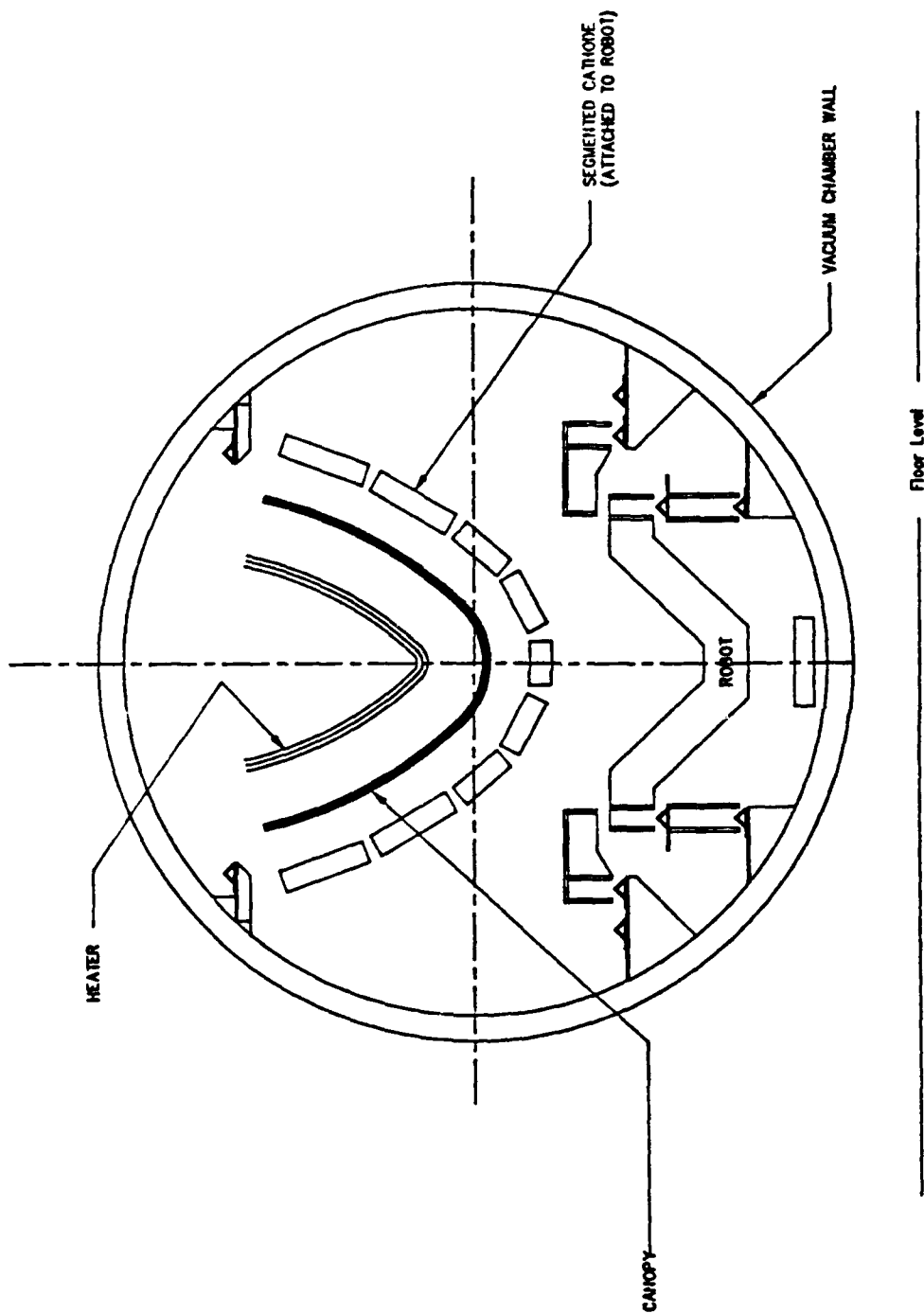


FIGURE 12
COATER CONFIGURATION FOR ITO COATING CANOPY EXTERIORS

SESSION V

TESTING TECHNOLOGY (PART A)

Chairman: K. I. Clayton
University of Dayton
Dayton, Ohio

Co-Chairman: J. W. Kozmata
Rockwell International
Los Angeles, California

Coordinator: R. E. Urzi
Flight Dynamics Laboratory
Wright-Patterson AFB, Ohio

AIRCRAFT TRANSPARENT MATERIALS CHARACTERIZATION

Richard A. Smith
AFWAL/FDER

Blaine S. West
Robert A. Brockman
University of Dayton

AIRCRAFT TRANSPARENT MATERIALS CHARACTERIZATION

by

Richard A. Smith

Air Force Wright Aeronautical Laboratories (AFWAL/FIER)

Wright-Patterson Air Force Base, OH 45433 USA

and

Blaine S. West and Robert A. Brockman

University of Dayton Research Institute

Dayton, OH 45469 USA

Prepared for:

Conference on Aerospace Transparent Materials and Enclosures

Monterey, California

January 1989

AIRCRAFT TRANSPARENT MATERIALS CHARACTERIZATION

Richard A. Smith
Air Force Wright Aeronautical Laboratories (AFWAL/FIER)
Wright-Patterson Air Force Base, OH 45433 USA

Blaine S. West and Robert A. Brockman
University of Dayton Research Institute
Dayton, OH 45469 USA

ABSTRACT

The requirements imposed on aircraft transparencies and supporting structure have been increasing and are becoming more stringent. The expense in time and money to optimize any number of these requirements using the fabricate, test, evaluate, and redesign method is prohibitive. An alternate approach, using state-of-the-art computer codes followed by validation/qualification testing, is preferred for developing an optimized system. However, the accuracy of any computer analysis is limited by the material model used and the amount of data available on the material physical properties. Early computer codes for aircraft transparency and support structure design analysis used relatively simplistic material models, and a limited material properties database sufficed. Computer codes are now available that use more detailed material models and can take advantage of a much more extensive database. The problem then becomes: What data are required? Are test methods and equipment available for obtaining this data? How do we generate the required data? This paper critiques the existing transparency material properties database and presents Air Force recommendations for filling material property data voids.

INTRODUCTION

MIL-HDBK-17A, Part II, Transparent Glazing Materials [1], has served the transparency design community well as a source of material properties data. This handbook was last updated in 1977 to reflect major changes in material utilization to comply with evolving birdstrike design requirements.

Since that time, economic and time constraints have dictated transition from a "build and test" philosophy to a more rigorous design/analysis approach coupled closely with carefully planned and instrumented developmental/qualification testing. This change has been accomplished in conjunction with the development and implementation of sophisticated computer-aided analysis tools. In addition, current and future mission oriented requirements are far more complex and demanding than those of the recent past. Advanced technologies are emerging in the areas of natural hazards, combat hazards, man-machine interface, fuselage integration and supportability. These more stringent requirements have led, and continued to

lead, to the development of new materials, new design concepts, and new manufacturing processes.

New materials, new design and fabrication concepts, and the emergence of analytical techniques as tools for improved design all contribute to the evolution of our requirements for material behavior characterization. This paper reviews current needs in transparency materials characterization in the light of transparency design objectives and current analytical methods. Suggestions are made for exploratory efforts in several critical areas.

TRANSPARENCY DESIGN CONSIDERATIONS

Highly sophisticated transparency systems of various configurations are operational today on high performance military aircraft; monolithic stretched acrylic being used on the F-15, coated monolithic polycarbonate on the F-16, acrylic faced laminates on the F-111 and F-16, and glass faced laminates on the B-1. The transparency shape and cross-section for each of these examples is shown in Figure 1 to illustrate the significant advances that have been achieved in material usage, design concept, and fabrication procedures. Significant changes include elimination of the once-traditional three-piece windshield with a flat glass center panel. This improves overall pilot visibility but introduces curvature and reduces optical quality in critical optical regions of the transparency. The F-16 bubble canopy maximizes pilot visibility at the expense of a more complex double curvature shape which increases fabrication difficulties. The deep drawn forming results in material thinning at the canopy crown and the shape generates a critical traveling deflection wave during bird impact. Interior and exterior surface abrasion resistant coatings can minimize weight, cost, and complexity, but may result in decreased durability. Laminates offer advantages for birdstrike protection but tend to increase complexity, reduce optical quality, and may be susceptible to delamination.

Glass has many qualities that make it a desirable material for use as an aircraft windscreen or canopy (i.e., good optics, hardness, resistance to chemicals, good thermal stability, etc.). However, it is a brittle material with a low toughness; therefore, it is not suitable as the structural ply for light weight bird impact resistant transparencies.

Acrylic, particularly stretched acrylic, offers a significant improvement in elongation to failure and toughness. It has been utilized with some success in the development of improved bird impact resistance for a number of high performance aircraft (i.e., F-15, F-18, T-38, F-4, etc.). Disadvantages are susceptibility to crazing and scratching, notch sensitivity, and instability at temperatures above 220°F.

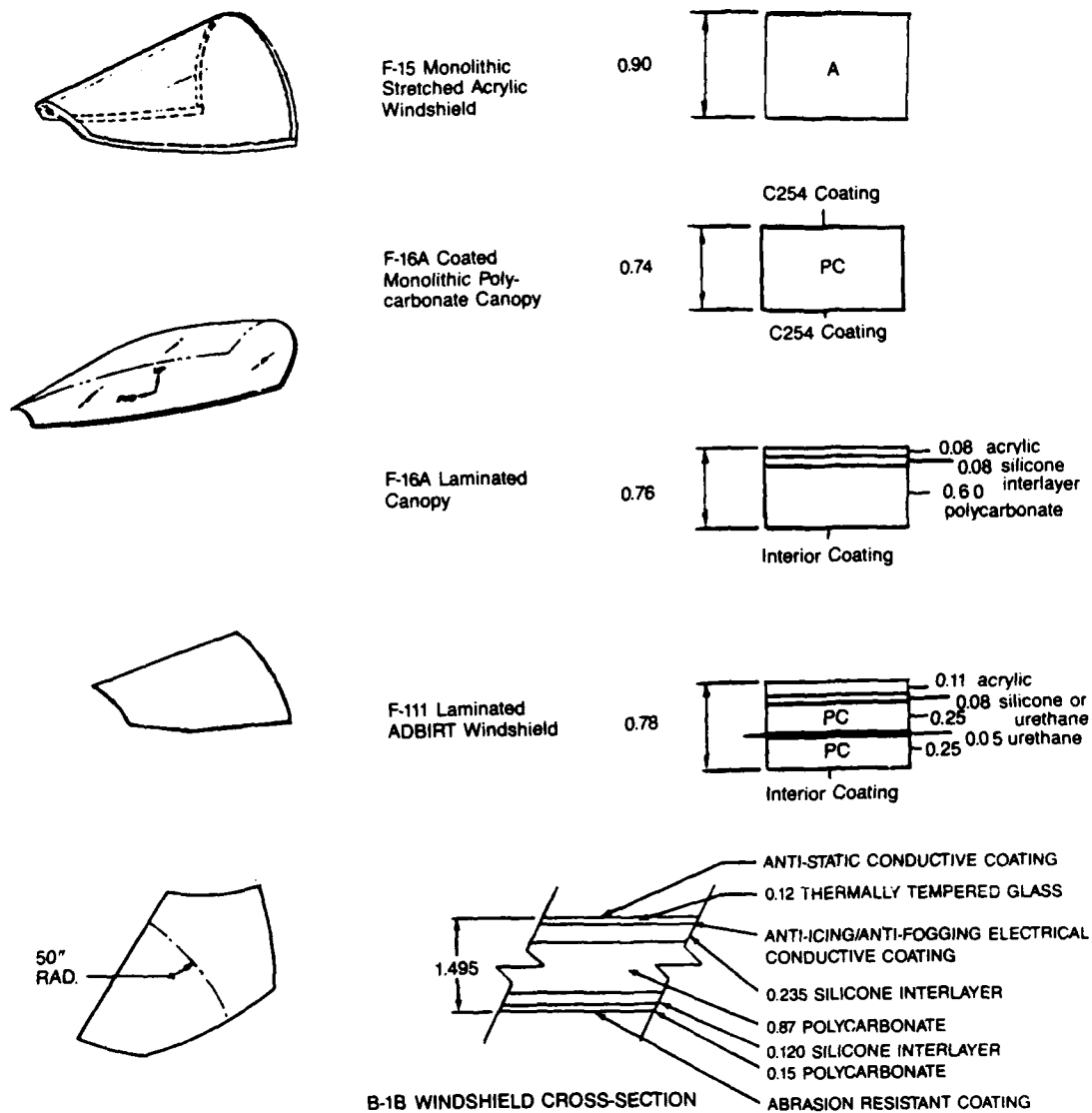


Figure 1. Operational Transparency Shapes and Cross-Sections.

Polycarbonate sheet offers excellent toughness/impact resistance as illustrated in Figure 2. Thus, it has emerged as the most used structural ply material for providing a high level of bird impact protection for high performance aircraft. However, polycarbonate is extremely sensitive to surface condition. In service it must be protected from abrasion, chemical solvents, and environmental degradation. This has been accomplished through the use of interior and exterior surface coatings and/or the use of acrylic or glass surface plies.

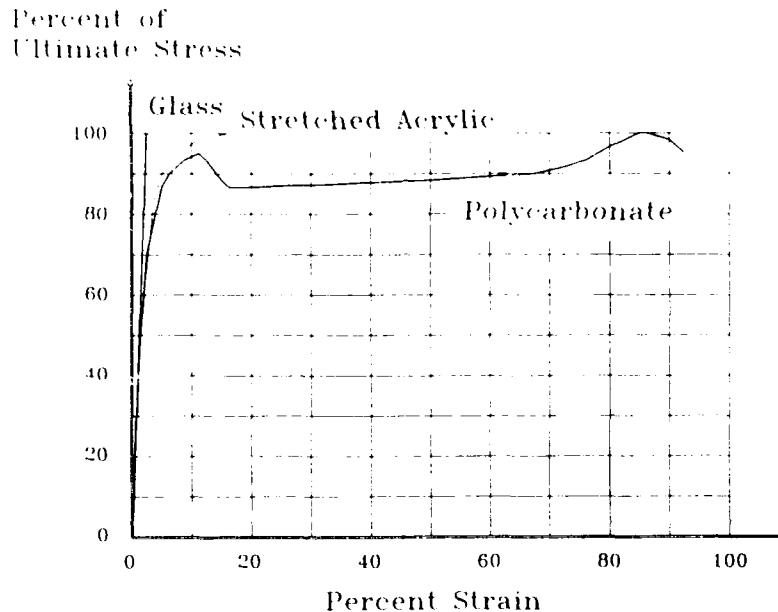


Figure 2. Stress-Strain Curves for Transparent Materials.

Another approach is the use of state-of-the-art production techniques to manufacture laminated windshield/canopy assemblies having properties superior to those of the acrylic and polycarbonate constituents. Liquid cast-in-place or sheet interlayers of silicone, urethane, or PVB can be used to join acrylic or glass outer plies to multiple polycarbonate structural plies to provide an optimum design configuration.

The design drivers for the transparency systems shown in Figure 1 were birdstrike resistance, optics, and durability. Additional mission oriented requirements for next generation (1995) air vehicle systems are more complex than any that have been successfully addressed to date. The information required to design a mission integrated aircraft transparency system (MITS) can be divided into five general technology areas. To successfully meet the requirements posed by each of these areas will require compromises and trade-offs within the framework of a balanced emphasis, as illustrated in Figure 3. Technological advances in every one of the five technology areas will be required to meet future mission requirements. The development of new materials and an expanded material database for new and exist-

ing materials will be a key to successfully meeting these design objectives. Specific design requirements that will place demands on material development, characterization, and utilization include:

- ☐ A more severe thermal environment associated with sustained flight at higher Mach numbers.
- ☐ Improved durability to increase service life and reduce life cycle costs.
- ☐ Wide field-of-view HUD with helmet mounted display and sighting capability combined with night and all-weather operation.
- ☐ Radar cross-section (RCS), infrared signature (IR), and visual signature reduction.
- ☐ Hardening against nuclear weapons, chemical/biological agents, and lasers.
- ☐ Bird impact and ballistic impact.
- ☐ Geometric, structural, and electrical fuselage integration.

ANALYSIS METHODS AND PROPERTY REQUIREMENTS

This section reviews material characterization requirements in the context of analytical techniques, where material properties and behavioral models play a pivotal role. In many disciplines which are important to transparency system design, one of two situations exists:

- ☐ a lack of adequate material property data limits the sophistication (and accuracy) of the simulation; or
- ☐ adequate models do not exist for some phenomena of interest, so that essential data are missing from the analytical results.

Additional materials data are needed to attain good accuracy with the current generation of modeling tools, and to formulate new material models where gaps exist.

Aerothermodynamic Analysis

Aerodynamic heating and the absorption of solar radiation are primary concerns in the optimization of transparency designs for increasingly demanding mission requirements. Improved concepts for active cooling are needed in particular, since applications already envisioned for the 1990's far exceed the capabilities of current transparency materials. Likewise, improved predictive capabilities are required for use in the timely development of new designs.

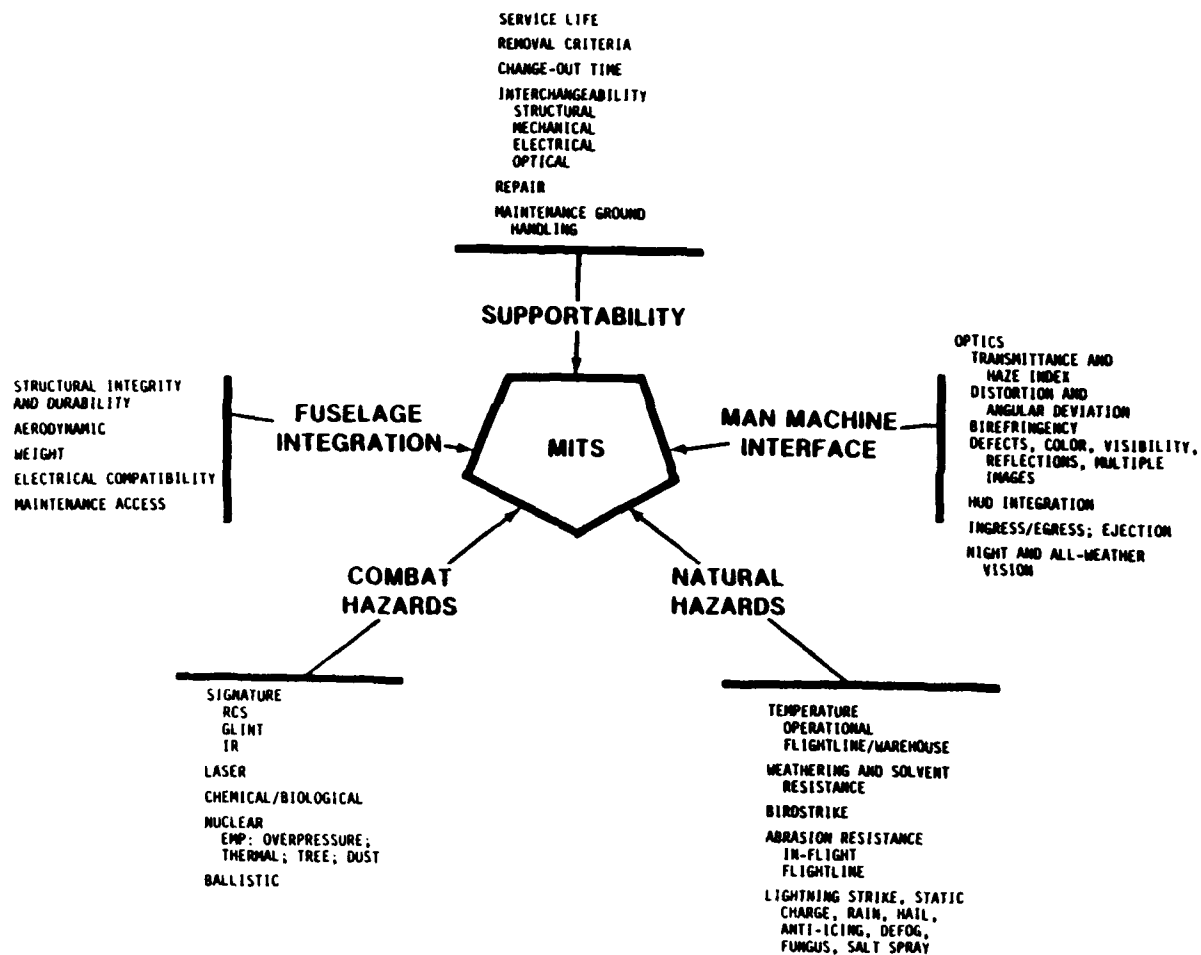


Figure 3. MITs Technology Areas.

The most advanced analytical methods for aerothermodynamic prediction and design for aircraft transparency structures are embodied in the STAPAT software package [2], developed by Sverdrup Technology under contract to the Air Force. STAPAT allows engineers to perform simulations of aerodynamic heating, solar radiation, and heat transfer for complex transparency structures subjected to realistic mission profiles. The effects of support structure, air gaps, and active cooling systems can be included in the analysis. Current development efforts in this area are concerned with refinements such as improved fluid dynamic analysis.

At face value, material characterization needs for aerothermodynamic analysis seem limited: the bulk thermal properties are known for most materials of interest, and these exhibit only mild variation with processing and fabrication variables. The real limitations which exist lie in the lack of adequate models for the effects of irradiation, cyclic heating, and environmental exposure on material response and integrity. Simulating the thermal response for a prescribed mission profile presents no fundamental difficulties; however, crucial information is missing from the results. How, for instance, do irradiation and thermal cycling affect mechanical properties such as yield strength, rate sensitivity, ductility, and fracture toughness? While the effects mentioned above influence the mechanical behavior of the material, the thermal analysis (which must consider the mission profile in detail) is a natural setting for evaluating the results of heating and environmental exposure.

The preferred approach to this class of problems is to develop, where possible, chemical structure-property relationships which reflect the influence of key variables on property degradation. Such models exist for some properties of polymeric materials, but these are used chiefly to estimate the property changes which might result from modifying processing variables. Existing predictive models normally deal with basic mechanical properties, such as moduli and loss characteristics; both theoretical developments and experimental efforts are needed to establish the necessary models for failure properties of typical transparency materials. Mechanical characteristics of interest include bulk and shear moduli, quasistatic yield strength, strain rate sensitivity, ductility and fracture toughness.

Some important factors are not likely to yield to the type of modeling suggested above. The effects of ageing, in particular, are poorly understood and are likely to remain so. Even the development of phenomenological models presents significant obstacles, since methods of accelerated testing for environmental effects are still controversial. Exploratory development in this area is highly desirable.

Structural Analysis

The role of structural analysis in transparency design and evaluation encompasses the prediction of mechanical responses to internal pressurization and thermal inputs, as well as bird impact response and ballistic resistance. Analytic techniques may be used to assess the effects of parameter changes, such as mechanical properties, impact velocity, laminate thickness and layup, or panel dimensions, without reformulating materials or modifying laboratory fixtures.

Computerized analyses prove useful not only for predicting cases which have not been evaluated experimentally, but also for clarifying the meaning of experimental data. Used in conjunction with test data, a simulation may be useful in determining what happened in the test, and in estimating data which are difficult to measure.

Studies described by McCarty, Smith and co-workers [3-5], performed using the MAGNA finite element code [6], are representative of transparency structural analysis capabilities at present. While the more complex analyses (of birdstrikes, for instance) consume large resources for modeling and computation, they are much less expensive than full-scale experiments, and provide results in a relatively short time.

Thus far, transparency structural analysis efforts have employed relatively simple material models (linear elastic or elastic-plastic behavior), for which existing data are adequate but which fail to capture many phenomena of interest:

- strain-rate dependence, before and after yielding;
- nonlinear pressure-volume behavior, particularly in nearly-incompressible interlayer materials; and
- ductile and brittle material failure.

Constitutive models which include these effects are well-known, and are being implemented in the next generation of transparency structural analysis tools [7]. These improved predictive techniques will be limited in accuracy by a lack of appropriate data for nonlinear pressure-volume behavior, rate dependence, and failure characteristics.

The discussion below describes some basic concerns in transparency material modeling. We address the modeling of glass components, for which methods and data in common use are quite good, and polymeric structural and interlayer materials, for which more detailed models are under development.

Material Models for Structural Analysis

Structural plies made of glass can be described adequately by existing models for mechanical behavior, including brittle failure based on point stress criteria. Modeling of the stiffness properties of a glass ply is straightforward since the force-deformation relationship is linear to failure for the temperatures of interest. For tempered and semi-tempered glasses, initial stresses may be added to those obtained from the elastic stress-strain relation for use in a failure model.

For polymeric transparency materials, including soft interlayers, the current generation of shear (deviatoric) material models can simulate simple linear viscoelastic response without failure, linear elastic or elastic-plastic response with failure, or nonlinear elastic response without failure. The pressure-volume relationships available to complete the idealization are quite general: most of the popular bulk models use a polynomial equation of state, whose coefficients in tension and compression may be different.

It is useful to cite an example of such a material model to demonstrate the important role of material properties data. A rudimentary viscoplastic model, appropriate for describing the response of a polymeric structural ply during impact analysis, might consist of the following relations:

$\sigma = \sigma' - pI$	Total stress divided into shear (deviatoric) & pressure parts
$p = \begin{cases} -K_1\eta & (\eta < 0) \\ -K_1\eta - K_2\eta^2 - K_3\eta^3 & (\eta \geq 0) \end{cases}$	Pressure-volume relation
$\eta = \frac{\rho - \rho_0}{\rho_0}$	Compression ratio
$\dot{\sigma}' = 2G (\dot{\epsilon}' - \dot{\epsilon}'_p)$	Elastic stress relation
$\dot{\epsilon}'_p = \begin{cases} 0, & \text{if } \sigma_e \leq \sigma_y \\ \phi N, & \text{otherwise} \end{cases}$	Inelastic strain rate
$\sigma_e = \left[\frac{3}{2} \sigma' : \sigma' \right]^{1/2}$	Effective stress
$\sigma_y = \sigma_y^0 \left[1 + \left(\frac{\dot{\epsilon}}{D} \right)^{(1/p)} \right] + H \epsilon_p$	Dynamic yield stress
$\dot{\epsilon} = \dot{\epsilon}' $	Nominal strain rate
$\epsilon_p = \epsilon'_p $	Effective plastic strain

The first equation divides the stress into hydrostatic (pressure) and shear contributions. The next two relations define the elastic bulk (pressure-volume) characteristics of the material. The remaining equations describe the rate-dependent elastic-plastic response of the material, which (in this case) is independent of the pressure. Besides the initial density ρ_0 , the constitutive model above requires eight material properties:

- ☐ bulk moduli K_1, K_2, K_3 ;
- ☐ shear modulus G ;
- ☐ quasistatic yield stress σ_y^0 ;
- ☐ work hardening slope H ; and
- ☐ rate sensitivity parameters $D, 1/p$.

Most of these parameters vary with temperature; the temperature dependence of the moduli is quite strong for some materials in common use. Although it is practical to apply material models of this complexity in numerical simulations, there is seldom sufficient data. Strain rate sensitivity, a dominant property of most polymeric materials, has received very little attention for materials such as polycarbonate, acrylic, silicon, polyurethane, and PVB. Nonlinear bulk response is a key characteristic of soft interlayer materials. However, the data necessary for accurate material modeling often are buried in the results of tension tests, which by themselves are insufficient to define both the bulk and shear properties of the material.

The division of the material model into bulk (pressure-volume) and deviatoric (shear) components, as suggested above, is typical both in the theoretical development of constitutive equations, and in their numerical implementation. However, the measurement of these properties as distinct entities is relatively rare, since it is so convenient to perform a simple tension test. This is unfortunate since the results of the tension test may obscure characteristics which are otherwise simple to interpret. For example, many polymeric materials exhibit nonlinear bulk behavior due to their near-incompressibility, while the shear behavior is predominantly linear. The information obtained from the tension test indicates only that strong nonlinearity is present, and provides little insight into the reasons for the observed behavior [8,9]. Similar observations can be made about viscous effects such as damping and strain rate sensitivity, which may be minimal for the hydrostatic response.

Typically, polymeric materials used in structural applications are subjected only to a limited amount of mechanical properties testing (e.g., quasistatic, room-temperature tension tests, or the determination of master compliance curves). Furthermore, tests sometimes are not repeated when processing variables are changed, though the mechanical characteristics may change markedly. This philosophy is appropriate in the sense that chemical and optical properties of the compound are more relevant to the routine use of the product. However, in impact situations the structural performance of the polymer assumes a central importance, and an accurate mechanical characterization of the polymer is necessary. The needed materials data for analyzing exceptional events such as impact, and for describing the more unusual aspects of material behavior (nonlinearities, rate dependence) rarely are available.

Among the unusual characteristics of common transparency materials which require further experimental evaluation we can cite:

- ☐ near incompressibility (stiff pressure-volume response);
- ☐ strong temperature dependence of some properties [1,10];
- ☐ nonlinear elastic behavior which is rate-dependent and exhibits a Mullins effect (softening during the first several cycles of stretching); and
- ☐ strain hardening, also rate-dependent, whose origins are poorly understood [11];

We wish to re-emphasize that, given sufficient data for the materials of interest, most of the phenomena mentioned above can be described accurately using existing constitutive models. Lack of adequate data presents very real limitations in the application of current modeling techniques.

Failure Models for Structural Analysis

Unlike the mechanical model, a failure model may play two different roles in a structural analysis study. For steady-state conditions such as cockpit pressurization and convective heating, the failure model provides the criterion for severity of the loading condition, which is applied to the final results of the analysis. The specific criteria and failure modes depend upon the material in question and mission requirements. In other circumstances, such as a birdstrike or ejection analysis, structural failure at a point influences the subsequent response at least in the neighborhood of the failure zone. Analyses of this type are considerably more difficult, since the criterion for point failure may involve strain-rate (or other) dependencies which are hard to determine.

Point failure in a glass can be characterized in relatively simple terms as well. For untempered glass, the critical quantities are maximum principal surface tensile stress for cracking, and the hydrostatic pressure for compressive failure. In tempered glasses, in which surface flaw sensitivity is not a critical factor, a pressure-dependent yield criterion, which reflects the differing strengths in tension and compression, is appropriate. One can increase the nominal strength of the glass by an approximate factor which depends upon the amount of temper [12] or include the estimated residual stress field in the stress values used in the failure criterion.

Suitable models for unstable crack growth in glass are still an area of research. A rudimentary approach is to rely upon the point failure criterion to determine when and where fracture occurs. This level of detail seems most appropriate for use with present-day simulation tools, since it captures the effect of local failure upon structural stiffness and dynamic load paths. Specialized methods of tracing cracking patterns are available but often provide relatively little useful information at a substantial expense in modeling complexity. The use of a detailed cracking model may be justified if a very accurate prediction of crack propagation patterns (as opposed to laminate impact resistance) is required.

Failure modeling for polymeric materials is relatively uncharted territory. The failure models implemented in the current generation of finite element structural analysis codes are quite simple, and are limited to criteria which apply to common metals. However, it may be feasible to formulate approximate failure models for polymeric materials using either durability (time dependence of strength) concepts [13] or the principles of continuum damage mechanics [14]. Experimental work is needed to provide points of reference for the development of suitable approximate failure models.

Optical Analysis

An optical ray trace computer code, OPTRAN, currently is being developed to predict the optical quality of high performance multilayered aircraft transparencies as designed and when subjected to operational loads. The optical analysis will accept temperature, deformation, and stress data obtained from STAPAT and MAGNA. The finite element pre- and postprocessing system PATRAN is being used as the common interface among the thermal, stress, and optics software.

The optical performance analysis involves tracking rays of various wavelengths through the transparency to evaluate distortion effects, and to compute focus and astigmatism for selected regions of the transparency. Deformed geometry from the stress analysis will be used in determining angles of reflection and refraction at layer boundaries. The ray tracing algorithm computes birefringent indices of refraction within each material as functions of temperature and stress state.

Material properties needed to support transparency optical analysis include indices of refraction as functions of temperature and (ideally) stress level, transmissivity and reflectivity versus angle of incidence, and surface and volume absorption characteristics for various light frequencies.

The influence of residual stresses on optical performance (and upon our ability to predict optical quality) is an open issue at present. Some investigation of optical property variations resulting from forming and installation stresses is appropriate, if only to determine the effective optical characteristics of actual hardware components. For example, an optically uniform material subjected to (unknown) residual stresses may appear to be naturally birefringent, with orthotropic (direction-dependent) indices of refraction.

MATERIALS CHARACTERIZATION NEEDS

Additional work in transparency materials characterization is needed to keep pace with new design requirements and concepts, and to support the proper use of tools for analysis and simulation. Some of the more critical concerns are summarized below.

Environmental Hazards

The weathering and ageing of modern transparency materials influences their characteristics in a dramatic way, affecting durability, toughness, and impact resistance, and other properties of central interest in design. Important research and testing needs include:

- ☐ Identify reliable methods for accelerated-time testing
- ☐ Develop and verify phenomenological models for effects of environmental exposure on mechanical properties
- ☐ Collect data to better characterize current materials

This aspect of transparent materials behavior is far-reaching in the context of computer-aided transparency design. Without reliable information on environmental hazards, the meaning of design analysis results is vague and our ability to assess service life, structural integrity and safety is limited.

Mechanical Properties

The trend in mission requirements toward lower altitudes, higher speeds, and higher temperature conditions, together with the emergence of birdstrike resistance as a key factor in design, call for a more thorough approach to transparency materials characterization. New data are sorely needed on the nonlinear response (yielding and plastic flow), strain rate sensitivity, and temperature dependence of most common transparency materials. Likewise, with the increasing use of laminated transparency designs the role of soft interlayer materials, which exhibit significant nonlinear and viscous (damping) behavior, assumes a greater importance.

For structural materials such as acrylics and polycarbonate, mechanical characteristics of primary interest include:

- ☐ pressure-volume relationships, including temperature dependence;
- ☐ shear and tensile moduli versus strain rate and temperature;
- ☐ yield point and work hardening moduli versus temperature and strain rate; and
- ☐ effects of fabrication residual stresses on mechanical properties.

In some instances mentioned above, test methods development is needed. For the stiffer structural materials, the difficulty lies chiefly in obtaining unambiguous data for rate-dependent properties, particularly in shear.

Interlayer materials present other problems. Priorities for materials data collection include:

- ☐ nonlinear pressure-volume relations;
- ☐ shear moduli versus temperature and strain rate;
- ☐ damping characteristics versus rate and temperature.

Test methods development is required both for bulk properties measurement [15] and rate-dependent shear modulus.

Failure Properties

Failure prediction in glass plies based upon a point stress criterion is within the scope of existing analytical methods. The collection of additional properties data is desirable to define the thermal limits of specific materials, and to assess quantitatively the effect of chemical strengthening.

The prediction of failure in structural transparent materials such as polycarbonate and acrylic is an undeveloped area, and exploratory efforts are needed. Experimental work is needed to provide parametric data which can be used in developing phenomenological models; priorities include:

- ☐ defining the relative influence of key variables such as peak stress, peak strain, temperature, strain rate, and residual stress;
- ☐ collecting parametric data for a reasonable cross-section of conditions for use in mathematical modeling; and
- ☐ performing experiments with simple components (such as monolithic and laminated beams) to validate failure predictions in a controlled setting.

Failure modeling of typical interlayer materials is an interesting subject, but is less of a priority than for structural ply materials. In general, materials which are useful as interlayers are capable of executing fairly large strains and have relatively small stiffness. The interlayer carries high loads only during impact, and then only in hydrostatic compression. Collection of failure-related data for interlayer materials is desirable primarily to define thermal limits, and to establish criteria for debonding from structural layers.

Additional Considerations

Materials characterization to meet design objectives relative to fuelage integration and combat hazards (Figure 3) is also a serious need. The effect of these requirements on material usage, optics, and structural integrity represents a critical design issue. However, since the threats/requirements and the corresponding materials and responses are classified they cannot be addressed here.

CONCLUSIONS

The current transparency materials database is inadequate to support the aircraft crew enclosure designer in meeting current and future requirements. An update to MIL-HDBK-17A, Part II, is needed to incorporate data for new materials and to provide additional data for existing materials to support emerging requirements, advanced design concepts, computer-aided analysis tools, failure prediction models, and improved durability/supportability. Several areas have been identified in which data collection, model development, and exploratory efforts are required to support existing and planned transparency applications into the mid-1990's.

REFERENCES

1. _____, MIL-HDBK-17A, Military Standardization Handbook: Plastics for Aerospace Vehicles. Part II. Transparent Glazing Materials, (1977).
2. M. O. Varner and C. A. Babish, "Status of New Aerothermodynamic Analysis Tool for High-Temperature-Resistant Transparencies," in S. A. Morolo (ed.), Conference on Aerospace Transparent Materials and Enclosures, AFWAL-TR-83-4154, Air Force Wright Aeronautical Laboratories, Wright-Patterson Air Force Base, Ohio (1983).
3. R. E. McCarty, "Finite Element Analysis of F-16 Aircraft Canopy Dynamic Response to Bird Impact Loading," Proceedings of the 21st AIAA/ASME/ASCE/AHS Structures, Structural Dynamics, and Materials Conference, Seattle, Wash. (1980)
4. R. E. McCarty, "MAGNA Computer Simulation of Bird Impact on the TF-15 Aircraft Canopy," in S. A. Morolo (ed.), Conference on Aerospace Transparent Materials and Enclosures, AFWAL-TR-83-4154, Air Force Wright Aeronautical Laboratories, Wright-Patterson Air Force Base, Ohio (1983).
5. R. E. McCarty and R. A. Smith, "Simulation of T-38 Aircraft Student Canopy Response to Cockpit Pressure and Thermal Loads using MAGNA," in S. A. Morolo (ed.), Conference on Aerospace Transparent Materials and Enclosures, AFWAL-TR-83-4154, Air Force Wright Aeronautical Laboratories, Wright-Patterson Air Force Base, Ohio (1983).
6. R. A. Brockman, "MAGNA: A Finite Element System for Three-Dimensional Nonlinear Static and Dynamic Structural Analysis," Comp. Struc. **13**, 415-423 (1981).
7. T. W. Held and R. A. Brockman, "Explicit Finite Element Techniques for Transparency Impact Analysis," Conference on Aerospace Transparent Materials and Enclosures, Monterey, California (1989).
8. L. R. G. Treloar, "The Elasticity and Related Properties of Rubbers," Rubber Chem. Tech. **47**, 625-696 (1974).
9. R. W. Ogden, "Recent Advances in the Phenomenological Theory of Rubber Elasticity," Rubber Chem. Tech. **59**(3), 361-383 (1986).
10. G. Bickford, "Interlayer Needs for Subsonic Windshields," in R. E. Wittman (ed.), Conference on Transparent Aircraft Enclosures, AFML-TR-73-126, Wright-Patterson AFB, Ohio (1973).
11. H. F. Brinson and A. DasGupta, "The Strain Rate Behavior of Ductile Polymers," Experimental Mechanics **12**, 458-463 (1975).

12. E. B. Shand, Glass Engineering Handbook, McGraw-Hill Co. (1958).
13. G. M. Bartenev and Yu. S. Zuyev, Strength and Failure of Visco-elastic Materials, Pergamon Press, New York (1968).
14. J. Lemaitre, "Coupled Elasto-plasticity and Damage Constitutive Equations," Comp. Meths. Appl. Mech. Engng. **51**, 31-49 (1985).
15. R. W. Warfield, J. E. Cuevas, and F. R. Barnett, "Single Specimen Determination of Young's and Bulk Moduli," J. Appl. Polymer Sci. **12**, 1147-1149 (1968).

AIRCRAFT TRANSPARENCY LIFE CYCLE DURABILITY FACILITY

Russ Urzi
AFWAL/FDER

Capt. John Anselmo
AFWAL/FDST

Abstract

AIRCRAFT TRANSPARENCY LIFE CYCLE DURABILITY FACILITY

Aircraft windshields are flight safety components and as such a need exists for predicting life cycle durability. As a transparency increases in its complexity to meet emerging mission requirements, so does its procurement cost. Many high performance aircraft are experiencing short service lives of their windshield systems. The Structures and Vehicle Subsystems Divisions of the Flight Dynamics Laboratory sponsor a joint program to assess the durability of aircraft transparencies. Overall program management is conducted by the Vehicle Subsystems Division (FDER). Transparency testing is conducted by the Structures Division (FDST).

Durability testing involves subjecting the transparency system to flight typical temperature gradients, net pressure loadings, and flight line cleaning solutions. Testing conducted by FDST can subject a transparency system to 1200 flight hours in approximately four months of test time. The durability facility plays an instrumental role in screening out poor transparency designs as well as assuring compliance with minimum service life requirements.

Aircraft windshields are flight safety components and as such, a need exists for predicting life cycle durability. As a transparency increases in its complexity to meet emerging mission requirements, so does its procurement cost. Many high performance aircraft are experiencing short service lives of their windshield systems. The Structures and Vehicle Subsystems Divisions of the Flight Dynamics Laboratory (AFWAL/FDE & AFWAL/FDS) sponsor a joint program to assess the durability of aircraft transparencies. Overall program management is provided by the Aircraft Windshield Systems Program Office (AFWAL/FDER). Full-scale transparency durability testing is conducted by the Structures Test Branch (AFWAL/FDST).

The Convection Heat Test Facility is just part of an effort to establish a methodology for assessing the durability of aircraft transparencies. Currently, there is an effort to validate full-scale durability testing as well as several different coupon-scale tests. The main goal is to gain control of transparency durability at the point of acquisition rather than through belated correction of field problems. This can be accomplished by applying validated durability test methods to enforce the required product quality.

The Structures Test Branch (AFWAL/FDST) began research into test methods for evaluating the durability of aircraft transparencies around 1974. Durability is defined as the ability of the transparency to withstand the actual service environment. The service environment includes thermal and pressure loading, along with chemical, humidity and ultraviolet exposure. Early testing subjected aircraft transparencies to flight typical temperature and pressure cycles. Testing used a reflective shroud supporting radiant quartz lamps which heated the outer surface of the transparencies. Temperature distributions were applied by dividing the lamps into different control zones. Transparencies were mounted in an actual aircraft fuselage so the proper end conditions could be obtained. The aircraft cockpit was pressurized or evacuated to simulate the net pressure loading on the transparencies. Testing utilizing radiant heat worked well for monolithic silicon glass transparencies; however, problems developed during testing of laminated transparencies. Radiantly heated laminated transparencies would become prematurely unbonded at the lamina interfaces. Each layer of the transparency was absorbing radiant energy directly from the lamps. The natural mode of heat transfer is primarily conduction from the outer surface

through the transparency thickness. In 1982 the Structures Test Branch began developing a test method to duplicate the thermal input into the surface of the transparencies in a more natural manner: convective heating.

Full-scale checkout of the Convection Heat Test Facility began in January, 1985. The facility subjects the transparencies to flight typical temperatures by passing heated or cooled air through the test section. The test section contains the transparencies mounted in a fuselage section which has a sealed cockpit and a shroud to cover the cockpit and form a closed loop system. The shroud design is unique for each aircraft tested to yield the correct temperature distribution over the surface of the transparencies. The area enclosed by the shroud is varied throughout the test section to force a temperature gradient across the transparencies. The cockpit temperature is controlled so that the transparencies experience the correct thermal distribution through the thickness. The transparencies are subjected to a net pressure loading based on the dynamic pressure for the flight condition minus the cockpit pressurization. The pressure loading is applied by evacuating or pressurizing the cockpit as needed. Flight line cleaning solutions are periodically used on the transparencies to determine what affect, if any, they have on the service life. The "Facility Control Console" manages all the functions of the Convection Heat Test Facility.

The Facility Control Console integrates the actions of eight separate facility subsystems. Six of the subsystems interact through the facility safety circuitry and the redundant parameter datalogger recorders. The "Hot Loop" and "Cold Loop" temperature controllers are both independent subsystems. The cockpit pressure is a separate control function as is the cockpit temperature. The two largest and most important subsystems are the airflow mixing valve actuator control subsystem and the data acquisition and flight profile control computer.

The data acquisition and flight profile control computer directs the facility and test article parameters for each of the separate controllers. The computer can record a maximum of 115 channels of data at a rate of 1 sample per channel per second. Forty of the channels are reserved for facility parameters. The computer also supplies voltage signals corresponding to flight temperatures and pressures for each mission profile. See Figure 1 for a picture of the test control console. The mission profiles are analytically determined by applying a three dimensional finite element code to the various Mach number and altitude versus time trajectories provided by the aircraft user. Thermocouples are attached to the exterior and interior surface

of the transparencies to monitor the temperature distribution. Thermocouples are also suspended inside the cockpit for monitoring the cockpit air temperature.

Air flows in the facility through three separate duct loops. The facility ducting is 24 inch diameter, 10 gauge, 316 stainless steel. Air flow is provided by two custom designed variable speed, low pressure centrifugal fans. Each fan provides continuously variable airflow from 12,000 to 24,000 cubic feet per minute at the extreme continuous service temperature for each loop. The fans are driven by variable speed motors with frequency control. Air flows through two primary closed loops before mixing into the test section loop. See Figures 2 & 3 for a picture of the facility ducting layout.

The "Hot Loop" circulates air at temperatures to 1000° Fahrenheit (F) continuously. The air is heated by six 30 kilowatt (Kw) resistance type duct heaters. The heaters are controlled by two 300 amp, 480 volt SCR controllers. The driving voltage for the SCR's is generated by an analog setpoint controller. Feedback to the controller is provided by averaging three thermocouple probes inserted into the ducting. The setpoint for the Hot Loop is approximately 20-40% higher than the maximum surface temperature required, depending upon the maximum temperature rise rate for the series of tests.

The "Cold Loop" circulates air at down to -100° F continuously. Liquid nitrogen is injected into the airflow immediately downstream of the Cold Loop fan outlet for cooling the loop. A two inch cryogenic flow control valve is operated by an analog setpoint controller for maintaining the loop temperature. Four thermocouple probes are averaged for Cold Loop control feedback. The setpoint for the Cold Loop is approximately 20-50° F lower than the minimum surface temperature required, depending upon the maximum temperature drop rate for the test series.

Airflow in the facility is regulated by mixing valves in the ducting. Air from each of the above two loops is mixed into the "Working Loop." There are six airflow mixing valves: three in the Hot Loop and three in the Cold Loop. The valves are 316 stainless steel opposed louvers. The Working Loop directs air over the test section which contains the transparencies mounted in the fuselage. One or more of the thermocouples on the exterior surface of the transparencies controls the mixing valves. Control program voltage feeds an analog controller and is compared to the actual temperature measured on the transparencies. The error signal generated drives the airflow mixing valve actuator controller. The controller calculates the motor driving signal based upon programmed velocity and

acceleration curves. A DC voltage driving signal is then sent to the electric direct drive actuator package to reposition the valve. The primary valve in each loop is the valve that lets air directly into the Working Loop. The primary valve is controlled directly and the other two valves in each loop are electronically slaved to the primary. The valves modulate to any position between full open and full closed to minimize the error. The system repositions the actuators every 10 milliseconds (ms) based on a temperature profile updated every 30 ms throughout the test.

The cockpit interior temperature is also controlled. Interior temperature is an independent control loop. The cockpit is maintained at 75° F so that the correct temperature distribution through the thickness of the transparencies is obtained. The cockpit is sealed and fans are installed for airflow. The air circulates over a conventional air conditioning coil and a 6 Kw resistance duct heater. One of the four thermocouples suspended in the cockpit is used for temperature control. The temperature can be maintained $\pm 5^{\circ}$ F at pressure ranges from -12 psi (vacuum) to +15 psi while the exterior temperature varies throughout the test.

Cockpit interior pressure is also controlled to simulate the net pressure that the aircraft experiences during flight. Cockpit pressurization or evacuation is directed by an analog servovalve controller. The controller modulates the input from two one inch diameter feed lines: one from a 140 psi pressure source, and one from a vacuum pump. A two inch return line is also controlled. A pressure voltage is provided to the controller by the control computer. The controller maintains the pressure to $\pm 5\%$ over the complete range.

The Facility Control Console houses all the above analog controllers, and the data acquisition and control computer. The console also contains the safety circuitry which can take action on the facility based upon alarm signals from any of the controllers. There are also two 32 channel dataloggers tied into the safety circuitry. One of the data loggers acts as a redundant checker for the facility parameters. The other datalogger provides the same function for the test articles. The dataloggers have relays which can activate the Facility Control Console safety circuitry.

The facility safety circuitry has three modes: alarm only, fail safe mode, and facility shutdown. Conditions which might indicate the lower bounds of an error band will signal an audible alarm only. Conditions which could possibly jeopardize the integrity of the test or test article, or which might be an indication of a facility component failure, cause a fail safe or

standby condition. The fail safe action causes the control program to hold at the current time increment and forces the primary valves to the closed position. Airflow over the test section is halted. The test operator must take action at this point to clear the faults before the test can be continued. The final mode can be initiated by three occurrences. If the fail safe condition begins, but fails to get confirmed by switches on the valves within 20 seconds, or by test operator action, the facility shuts down automatically. Certain facility or test article conditions which might cause personnel harm or facility damage cause a shutdown. A power disruption to a major component also causes a shutdown. The operator may manually initiate the fail safe or shutdown actions.

The original facility checkout was conducted on F-111 transparencies. The four mission profiles provided a temperature range of 25° to 355° F and a pressure range of -0.5 psi to +10 psi. The control system maintained the temperatures within 10% of the program signal on ramps and within 5% on plateaus. The pressure controller kept the pressure within 5% at all times. All the facility safety and redundant circuitry was checked and verified. The facility was moved beginning in January 1988 to a new location roughly 500 feet from the original location. The primary reason for the move was to upgrade several key facility components which had become unreliable such as the Hot Loop Fan and original butterfly valves. The extra space provided in Building 68 allowed a slight redesign of the facility duct layout to provide a larger test section and smoother airflow into the test section. No primary control circuitry was modified. Checkout of the new facility will use the same F-111 transparencies as before and excellent correlation is expected.

The original facility was used to test three competing designs for F-111 transparencies. Durability testing involved four mission spectrums. Two of the profiles were training missions (MH & LH) with surface temperatures ranging from 25° to 120° F. One of the profiles was taken from the Red Flag war games (RF) and subjected the transparencies to temperatures varying from 45° to 210° F. The remaining profile was a "Functional Check Flight" (FCF) which had a temperature range of 70° to 355° F. See Figures 4 & 5 for plots of the temperature and pressure profiles for the four missions. Testing began in August 1985 and ran through September 1987. Testing on each set of transparencies was to evaluate the durability of the design for 1200 simulated flight hours (four years of service).

Testing was completed in September 1987. Some generalized comments concerning the test results of all three vendors can be made. The predominate failure mode was delamination between the

acrylic and polycarbonate plies. After each high speed mission, the delamination bubbles tended to grow. Other failures were the edge seals/weather seals splitting away. Some crazing was also noticed primarily on the canopies, but was by no means the major failure mode.

The first round of testing was completed in July 1986. Two of vendor A's windshields (one clear and the other coated) and two of vendor B's canopies were evaluated. After 8.62 flight hours, it was noticed that the urethane interlayer began to creep out the edges of the canopies after the FCF mission. Both windshields were unaffected. After 54.57 flight hours, small bubbles were observed on the canopies along the forward edge. After 104.69 hours, small bubbles on the canopies tended to grow and the urethane seepage caused the edges to dip in slightly (see Figure 6). At 117.44 flight hours, both windshields showed no damage. At 138.74 flight hours, small bubbles were observed to form along the sides of both canopies. The bubbles grew after each FCF mission. At 380.20 flight hours, the canopies began to delaminate and the weather strip began to separate. At 392.95 flight hours, very small bubbles were observed on the forward edges of the windshields. At 691.46 hours, the damage to the canopies worsened slightly, and at 703.99 hours, there was no additional damage to the windshields. At 850.11 hours, light crazing was observed on the left canopy. After 1157.74 hours, the delamination of the canopies worsened and after 1170.27 hours the clear windshield began to delaminate near the forward beam. Also, the leading edge of both windshields began to split (see Figure 7 & 8). After four years of simulated service, the canopies were delaminated, showed some light crazing, and their edge seals were split away. The coated left windshield showed no damage while the right clear windshield had a small delamination. Both forward edge seals had split away from the outer ply.

The second round of testing began in December 1986. Two of vendor C's windshields (both coated) and one each of vendor B and C's canopies (both coated) were tested. Some initial defects were noted prior to testing (except for vendor B's canopy). Extensive damage was observed on all of vendor C's parts after 13.88 flight hours. However, this damage would not normally cause removal of the parts. At 184.17 hours, the delaminations grew to 2" x 1/4" and were observed along the forward edge of both windshields. The edge seal separation of the right canopy continued to grow. By 308.03 hours, the delaminations continued to worsen, getting as large as 7" x 3" on the right canopy. Eventually this delamination got even larger, causing the outer acrylic ply to break off during flight. During testing at 300° F, this outer ply could be seen lifting off the surface 10-15 inches. Testing was completed

after 847.19 hours. Both windshields were severely delaminated and were considered failures. The right canopy only had 30% of its face ply left intact while the left canopy delaminated all the way around its perimeter. Total service life of these parts were estimated to be 2.79 years. See Figures 9 through 12 for pictures of the transparencies after testing.

The third round of testing was completed in September 1987. All the parts were supplied by vendor B. After 18.34 hours, a large 8" x 5" delamination was observed on the right windshield and several small delaminations on the left windshield. At 164.21 hours, the canopies showed some light crazing and small delaminations. The test was halted when a significant amount of damage on the windshields was accumulated. Total hours for the canopies was 219.63 hours and for the windshields 73.76 hours. The left windshield was an improved version and showed much less significant damage than the right (unimproved) windshield. Estimated service life for the windshields was 1/4 year and for the canopies 3/4 year. See Figures 13 & 14 for pictures of the windshields after testing.

The testing produced results which were substantiated with flight evaluations. A limited quantity of vendor B's parts were installed and flown in Upper Heyford and Lakenheath, England. During a field inspection, two of these parts were found to be installed. One had been in service for only five weeks and was defect free. The other windshield had less than 100 flight hours and exhibited the same delamination characteristics observed on the transparencies durability tested in the laboratory. The aircraft's crew chief indicated that he first noticed the delaminations upon the aircraft's return from a high-speed mission.

The Convection Heat Test Facility will be used in the comparative evaluations of the durability of several new transparency designs for the B-1B and F-16 aircraft. In conjunction with these evaluations, the process of validating the facility will be accomplished. This will be done by testing production transparencies using mission profiles reflecting the actual flight trajectories currently being flown by those aircraft and comparing the test results with field performance data. This would also serve as a baseline test in which the prototype windshields could be compared to.

Production F-111 windshields and canopies will be tested using the same mission profiles previously mentioned. An extensive database has already been established so that a comparison with the test results could be made. The resulting correlation results in a time factor which could be used to

predict the service life of future F-111 transparencies.

B-1B durability testing will follow F-111 production testing. Five alternative designs will be evaluated as well as the current design. As for the F-111, a baseline test will determine a correlation factor with field performance. The B-1B testing will take one year to complete.

Following the B-1B tests, the comparative evaluation of several new F-16 designs is tentatively scheduled. The main thrust is again to evaluate the durability of each candidate design as well as to establish a baseline figure using current production parts. The F-16 also has an extensive field performance database with which results can be correlated.

AFWAL's Convection Heat Test Facility is the only full-scale transparency durability test facility in the United States. Once validation is completed, AFWAL intends to establish a set of durability requirements to be used in the design of future transparency systems. The requirements will include methods for establishing standardized flight profiles for design and testing, as well as specifying the test methods to be used for qualification. A technical report will be published detailing the design and operation of the facility so that the test methods developed can be transitioned to industry. AFWAL is working jointly with the Logistics Command to sponsor a joint System's Command -- Logistics Command program for controlling the life cycle costs of modern aircraft transparencies.

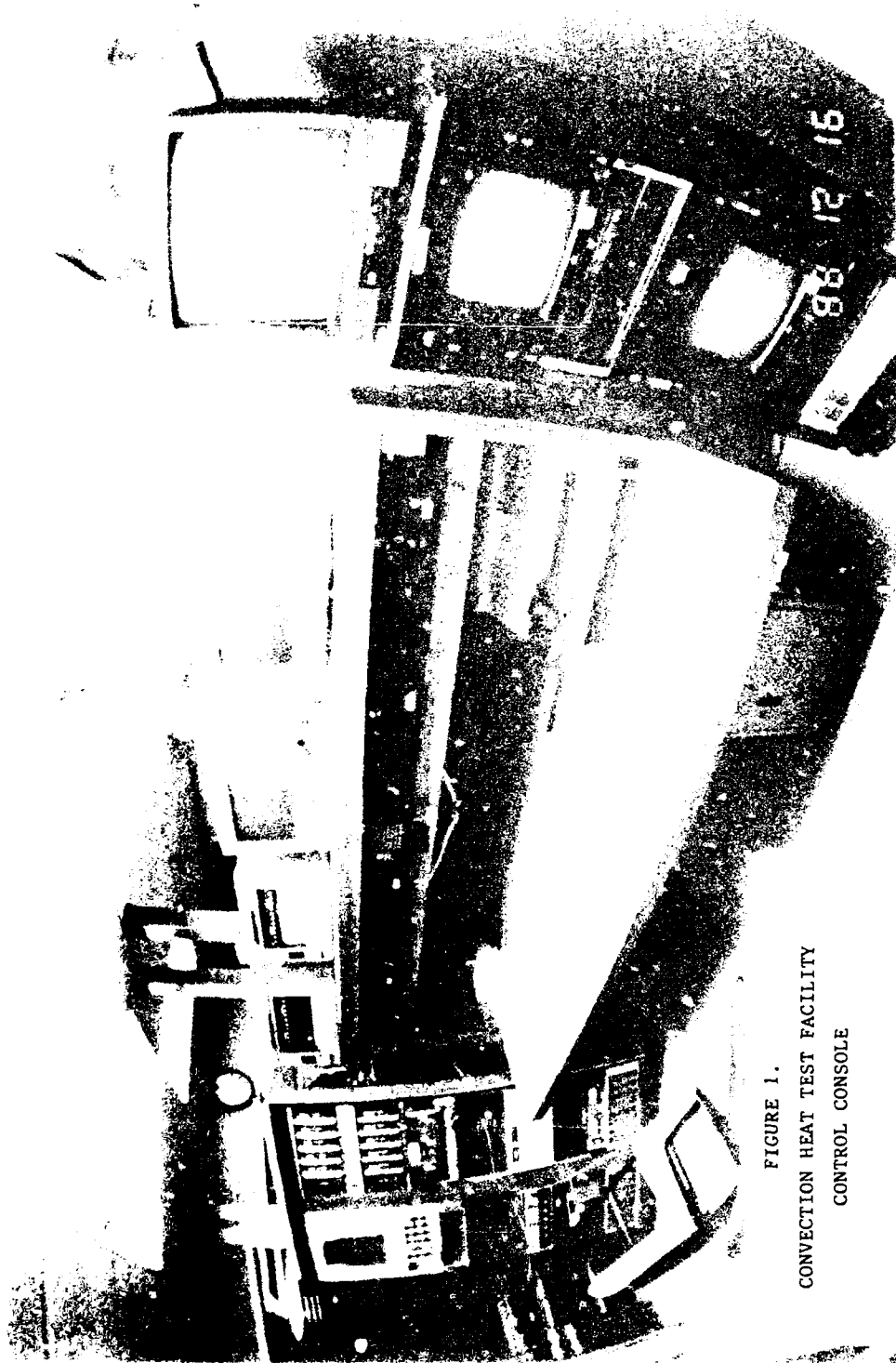


FIGURE 1.
CONVECTION HEAT TEST FACILITY
CONTROL CONSOLE

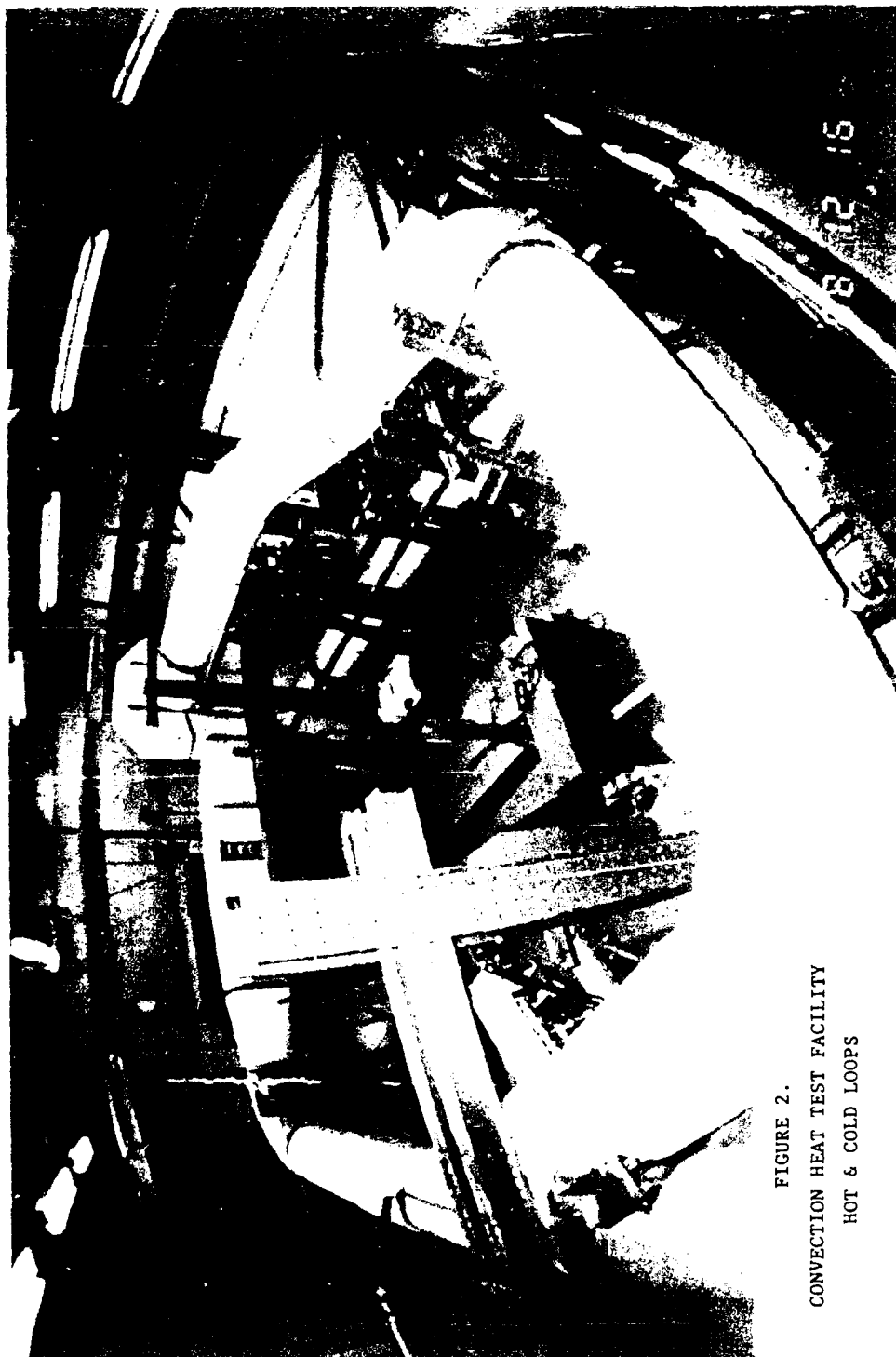


FIGURE 2.
CONVECTION HEAT TEST FACILITY
HOT & COLD LOOPS

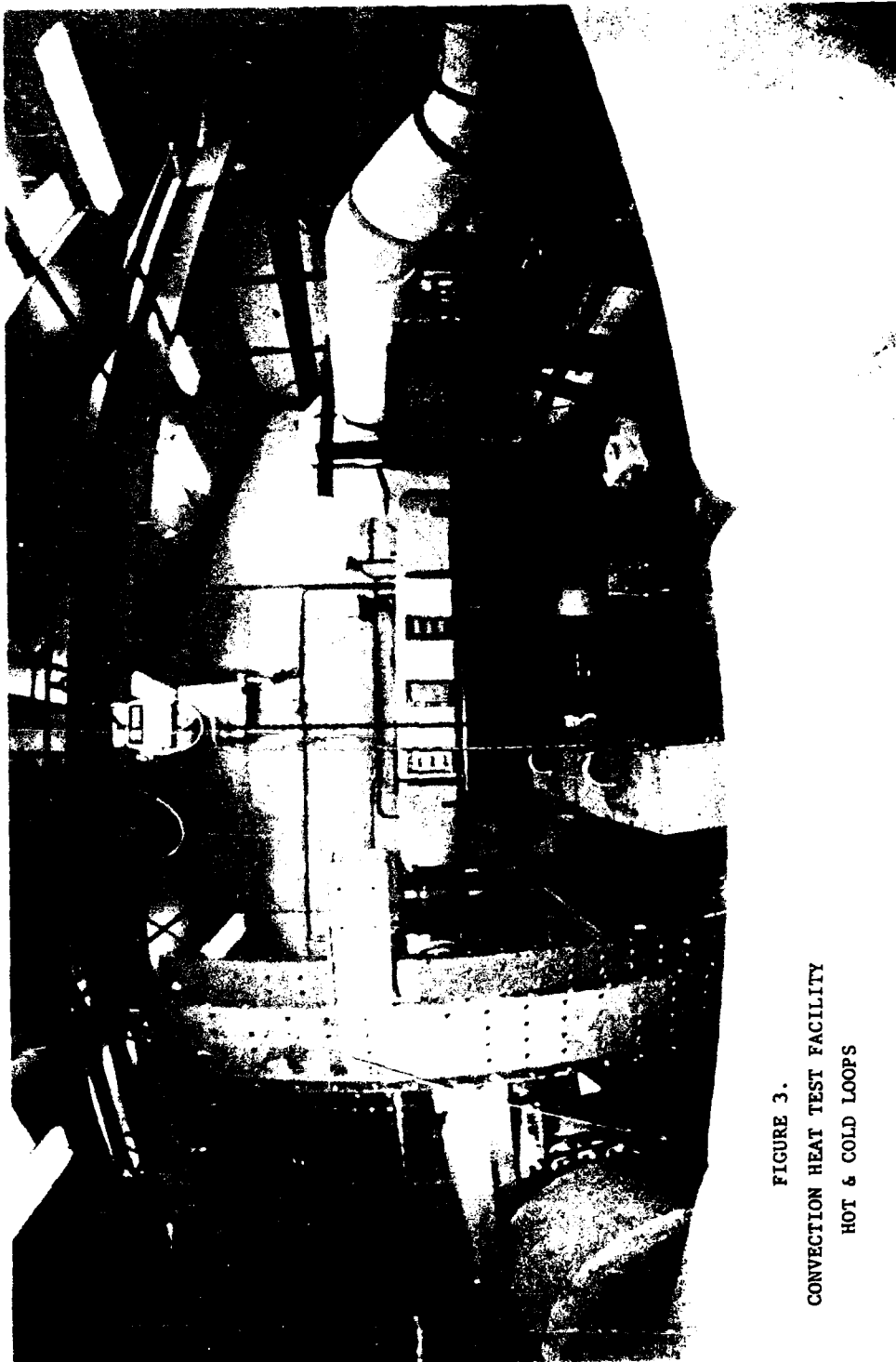


FIGURE 3.
CONVECTION HEAT TEST FACILITY
HOT & COLD LOOPS

F-111 TRANSPARENCY DURABILITY TEST TEMPERATURE FLIGHT PROFILES

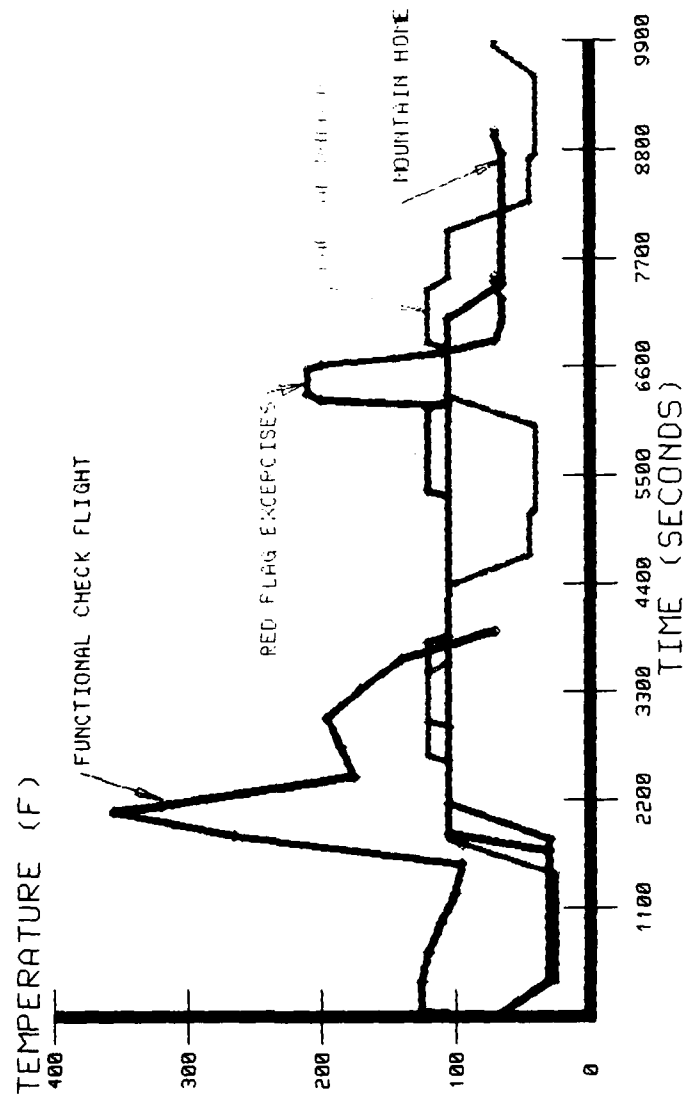


FIGURE 4.
F-111 TRANSPARENCY TEST
TEMPERATURE PROFILES

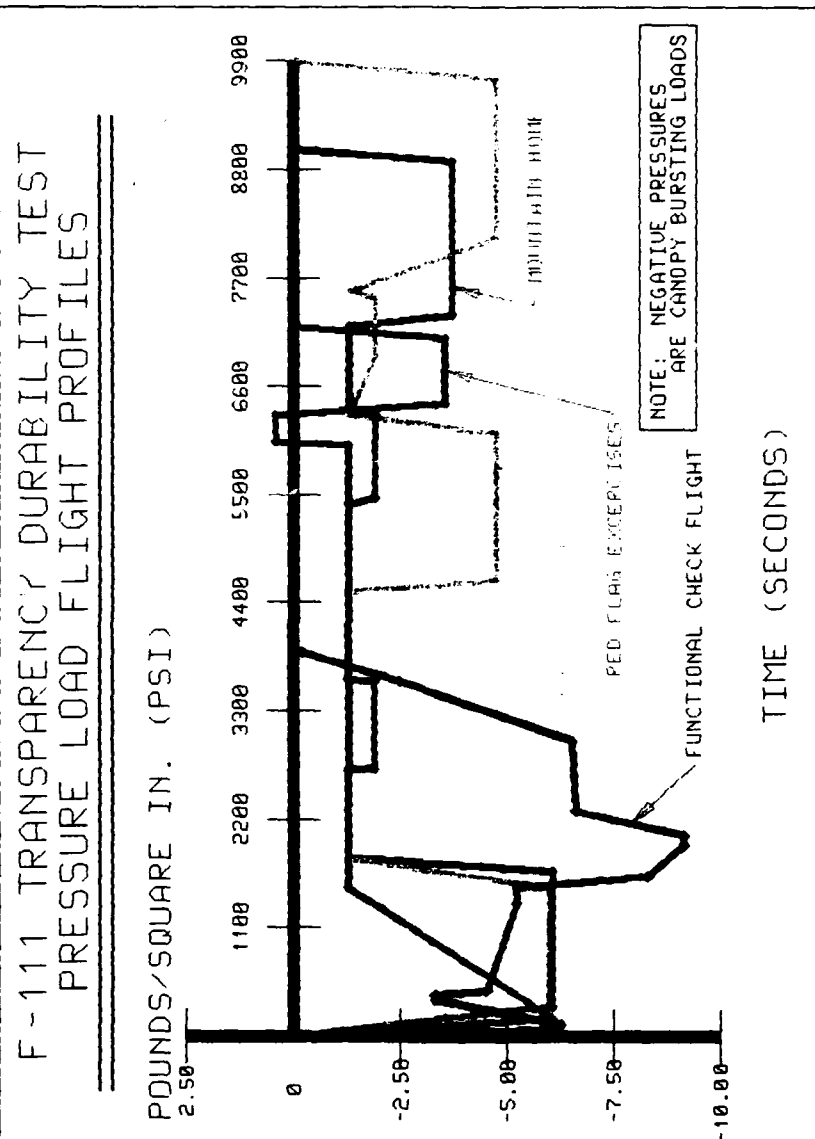


FIGURE 5.
F-111 TRANSPARENCY TEST
PRESSURE PROFILES

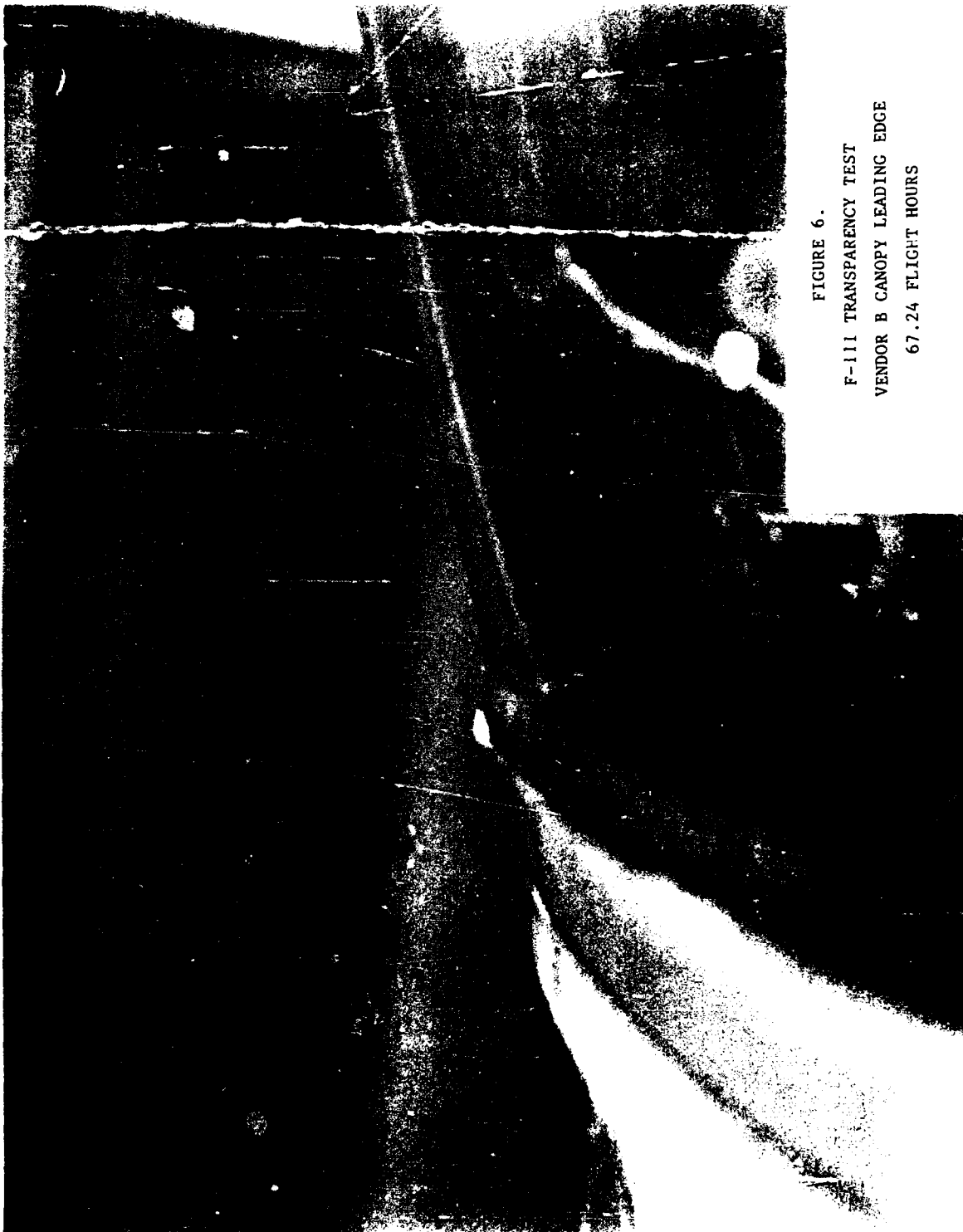


FIGURE 6.
F-111 TRANSPARENCY TEST
VENDOR B CANOPY LEADING EDGE
67.24 FLIGHT HOURS

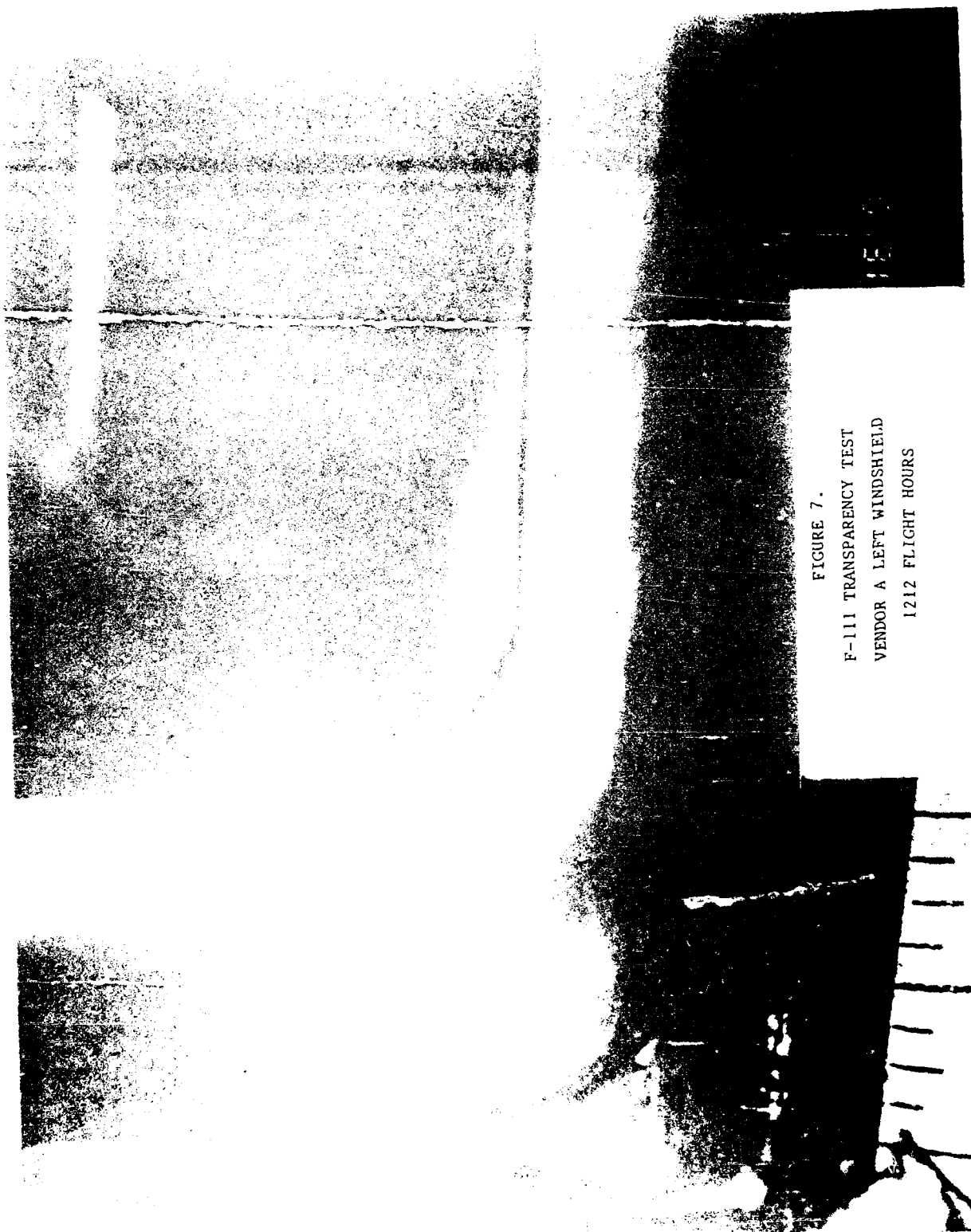


FIGURE 7.
F-111 TRANSPARENCY TEST
VENDOR A LEFT WINDSHIELD
1212 FLIGHT HOURS



FIGURE 8.
F-111 TRANSPARENCY TEST
VENDOR A RIGHT WINDSHIELD
1212 FLIGHT HOURS



FIGURE 1
 TRANSPARENT TEST
 VENTOR C LEFT WINDSHIELD
 200 FLIGHT HOURS

FIGURE 10.
F-111 TRANSPARENCY TEST
VENDOR C RIGHT WING/REAR
7:50 FLIGHT HOUR



FIGURE 11.
F-111 TRANSPARENCY TEST
VENDOR B CANOPY
800 FLIGHT HOURS



FIGURE 12.
F-111 TRANSPARENCY TEST
VENDOR C CANOPY
225 FLIGHT HOURS

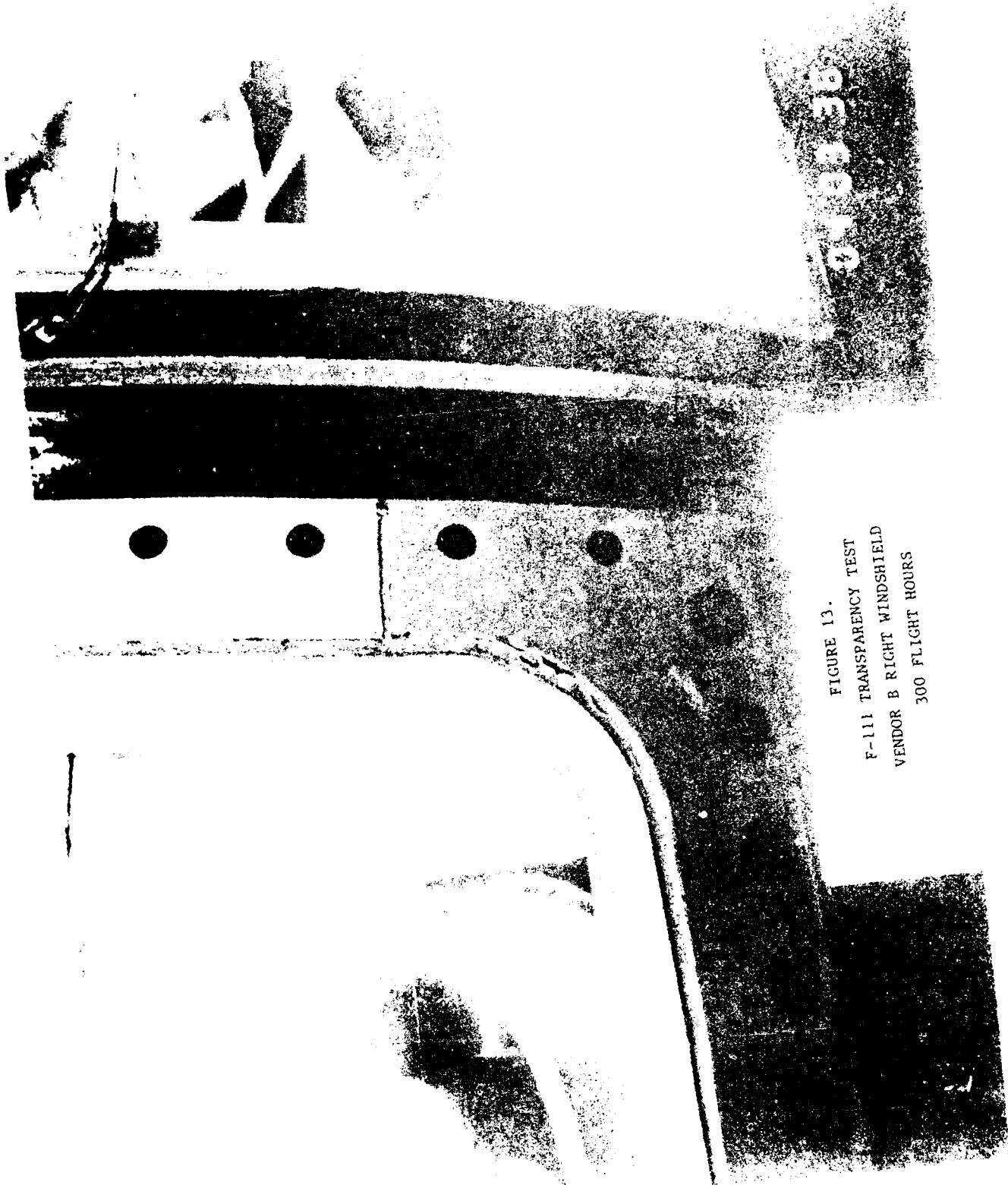


FIGURE 13.
F-111 TRANSPARENCY TEST
VENDOR B RIGHT WINDSHIELD
300 FLIGHT HOURS



AN EXPERIMENTAL EVALUATION OF THE AIR CANNON TECHNIQUE
FOR USE IN IMPACT RESISTANCE SCREENING OF POLYCARBONATE

Lt. Paul J. Kolodziejcki
AFWAL/FDER

Michael P. Bouchard
University of Dayton

AN EXPERIMENTAL EVALUATION OF THE AIR CANNON
TECHNIQUE FOR USE IN IMPACT RESISTANCE
SCREENING OF POLYCARBONATE

Lt Paul J. Kolodziejski
Air Force Wright Aeronautical Laboratories

Michael P. Bouchard
University of Dayton Research Institute

Abstract

Several test techniques exist for evaluating the impact resistance of polycarbonate, including the falling weight, notched Izod, notched Charpy, high rate flexure, high rate tension, and air cannon techniques. The air cannon technique is the subject of the present paper. A projectile is propelled by a compressed gas or powder charge through a gun barrel into the specimen. One potential advantage of the air cannon technique is that specimen strain rates typical of birdstrike can be achieved (100-450 in/in/sec).

An evaluation of the air cannon test technique for impact resistance screening of polycarbonate is presented. Tests are described for plate specimens of various spans and thicknesses impacted by projectiles of various diameters, masses, and velocities. Results consist of strain rate, failure energy, failure mode, and percent thickness reduction. For comparison, falling weight tests and results are discussed.

The air cannon failure energy is found to depend nonlinearly on the projectile velocity. A relationship between the ratio of projectile diameter-to-plate thickness and failure mode is noted. The air cannon strain rates are higher than the falling weight strain rates (300-3000 in/in/sec versus 40-100 in/in/sec) yet both techniques show the same trends in the failure energy-versus-geometric parameter and in failure mode as the falling weight results.

INTRODUCTION

BACKGROUND: High performance United States Air Force Aircraft are being fitted with transparencies utilizing polycarbonate (MIL-P-83310) material as the structural ply. Polycarbonate offers many advantages as a structural transparency material, having excellent impact (e.g., birdstrike) resistance as well as acceptable optical and thermal properties. Polycarbonate impact resistance is influenced by a variety of parameters including thickness, temperature, ply configuration, processing procedures, surface finish, aging, and environmental exposure. In order to optimize the impact resistance of a candidate transparency design, the transparency designer must be able to evaluate the effect of these parameters.

Several test techniques exist for evaluating the impact resistance of polycarbonate, including the falling weight, notched Izod, notched Charpy, high rate flexure, high rate tension, and air cannon techniques.

This presentation will focus on the air cannon technique and will compare air cannon test results with the accepted ASTM F736-81 falling weight technique.

A potential advantage of the air cannon technique is that high specimen strain rates can be achieved. The University of Dayton Research Institute has computed peak strain rates of 100-450 in/in/sec from birdstrike tests on the T-38 and F-111 windshields. Tensile testing of polycarbonate has demonstrated that the polycarbonate material properties are strain rate dependent. Therefore, a potential exists for performing impact screening of polycarbonate specimens at strain rates characteristic of bird impact events.

OBJECTIVES: The objectives of this test program were to: (1) collect data to show the effects of various test parameters on air cannon test results, and (2) compare air cannon test results and trends with falling weight test results and trends.

APPROACH: The air cannon tests were performed while varying the test parameters (plate span/thickness, boundary conditions and projectile diameter/mass/velocity) one at a time. The following test results were recorded and then correlated with changes in the test parameters: strain rate, failure energy, percent reduction in plate thickness, and failure mode. Finally, air cannon test results and trends were correlated with falling weight test results and trends.

TEST PROGRAM

Figure 1 shows the air cannon test set up. A six-foot long 1.5 inch bore, thick walled steel tube, supported on a heavy I-beam, served as the gun barrel.

Seven different types of projectiles were used for the tests as shown in Figure 2. The projectiles were designed to test the effects of varying nose diameter, holding mass constant; and of varying mass, holding nose diameter constant. All projectiles had hemispherically shaped noses.

AIR CANNON TEST PROCEDURE. Twenty-three sets of seven tests each, were performed for a total of 161 tests. Several test parameters were varied to determine their effects on the results. These parameters included plate thickness and span; specimen edge fixity; and projectile diameter and mass.

The results recorded for each test were specimen failure mode, absorbed energy to failure, and percent reduction in specimen thickness. To obtain specimen failure mode, the impact site of the tested specimen was observed, noting whether the specimen tended to fail in bending, shear, or tension.

Failure energy was defined as the minimum energy absorbed by the specimen that produced a visible, open crack. Failure energy was computed from $E = mv^2/2$ where E =failure energy (ft-lb), m =projectile mass (lb-sec²/ft), v =projectile velocity (ft/sec). (1)

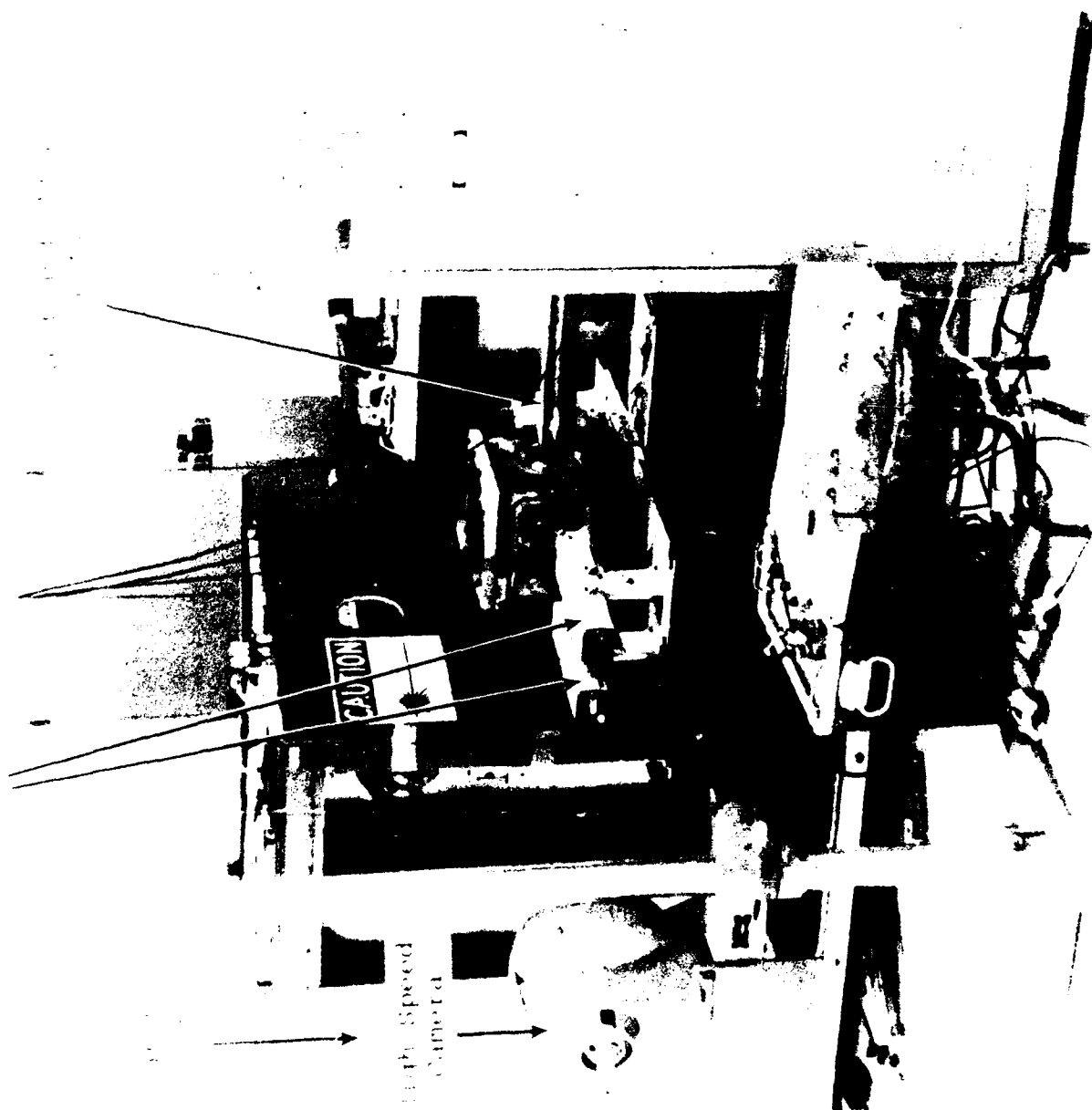


Figure 1. Air Cannon Test Setup.

TYPE 1



TYPE 2



TYPE 3



TYPE 4



TYPE 5



TYPE 6



TYPE 7



Figure 2. Air Cannon Projectiles.

Percent reduction in specimen thickness was recorded to provide a measure of ductility. It was computed from $\%R = \frac{t - t_0}{t_0} \times 100\%$, where (2)

t_0 = specimen thickness before impact
 t = specimen thickness after impact

Measurement of post-test thickness was performed with a micrometer, generally at the center of impact.

TEST RESULTS

The test results are discussed in terms of failure mode versus geometry, energy versus geometry, energy versus projectile velocity, and finally percent thickness reduction. Three types of failure modes were observed as shown in Figures 3-5.

CORRELATION OF FAILURE MODE WITH GEOMETRY. Plate span did not influence the failure mode. However, the results showed that the ratio of projectile diameter to plate thickness (D/T) did determine the failure mode. This is summarized as follows:

$D/T < \frac{1}{2}$	plugging (shear) failure
$1 \leq D/T \leq 4$	petalling (bending) failure
$D/T > 4$	cupping (tensile) failure

The same trends were observed for both the air cannon and falling weight tests.

ENERGY VERSUS GEOMETRY. For both the air cannon and falling weight tests failure energy increases with: increasing plate span, increasing plate thickness, and increasing projectile diameter. Plate thickness appeared to have the greatest effect on failure energy of the three geometric parameters (that is, doubling the thickness changed failure energy more than doubling span or projectile diameter). The air cannon failure energies were consistently greater than or equal to the falling weight failure energies, for a given plate geometry and projectile diameter.

ENERGY VERSUS PROJECTILE VELOCITY. Figure 6 shows a plot of energy versus projectile velocity for 0.5 inch thick plates and 1.0 inch diameter impactors for various plate spans. Included in the plot are falling weight results, which represent low velocity impacts.

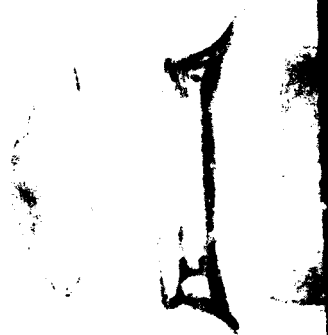
The plot indicates that for the relatively thick (0.5 inch) specimens the failure energy changed with velocity. For the five-inch span results, the energy increased continually and non-linearly with velocity. For the eight-inch and ten-inch span results, the energy increased non-linearly with increasing velocity to a peak value, after which it decreased non-linearly with increasing velocity. The non-linearities of the energy versus velocity curves may have been due to strain rate dependent stiffening of the polycarbonate, specimen inertia (energy is required to accelerate the portions of the specimen being deformed; the significance may decrease as velocity increases because deformation



MULTIPLE PETAL
FAILURE
(SPECIMEN M-5)

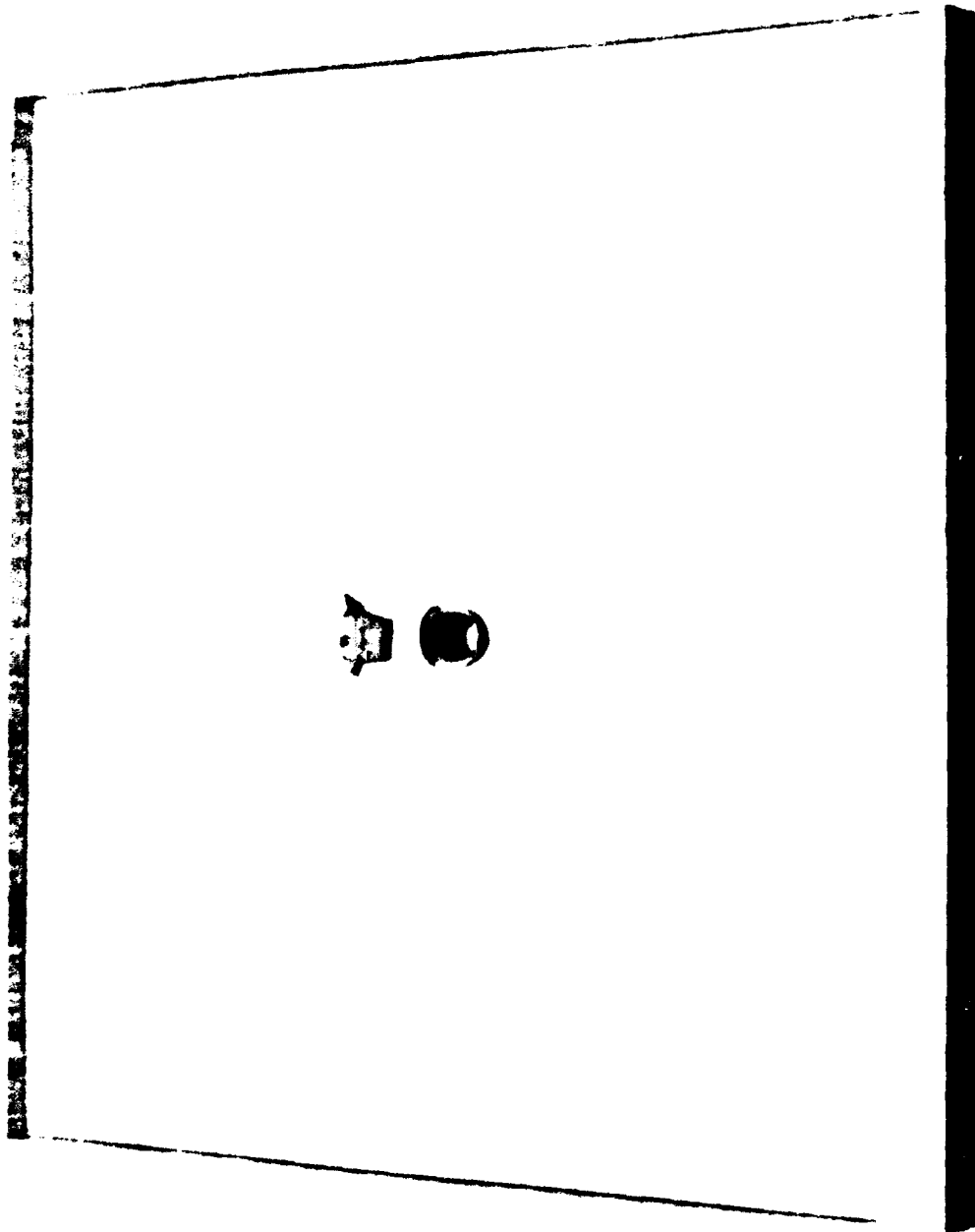
TWO-PETAL
FAILURE
(SPECIMEN CC-6)

Figure 3. Petalling Failure.



SPECIMEN FC-7

Figure 4. Cupping Failure.



SPECIMEN
FE-1

Figure 5. Plugging Failure.

ALL PLATES 0.5" THICK
ALL PROJECTILES 1" DIA.

M_p = mass of projectile

F.W. = Falling weight data

- Span = 5", clamped
- Span = 8", clamped
- △ Span = 10", clamped
- ⬡ Span = 10", simply supported

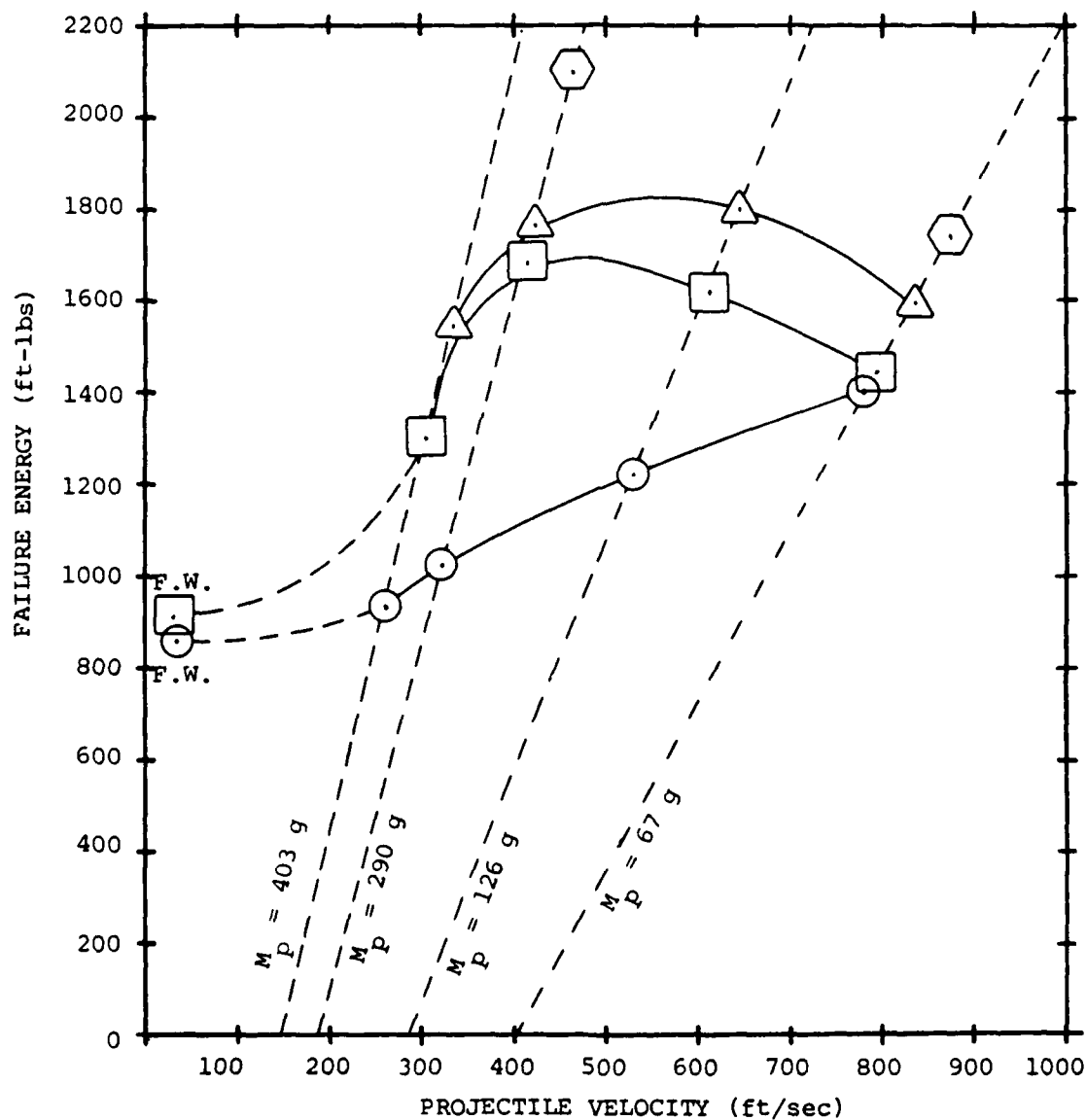


Figure 6. Failure Energy Versus Projectile Velocity.

becomes more localized), and vibration effects (overall plate bending modes and elastic wave propagation).

In summary, for the tests performed, the air cannon and falling weight failure energies showed similar trends. That is, failure energy increased with increasing plate span, plate thickness, and projectile diameter, and decreasing edge fixity. Plate thickness appeared to have the greatest effect on failure energy of the three geometric parameters (that is, doubling the thickness changed failure energy more than doubling span or projectile diameter).

PERCENT REDUCTION IN THICKNESS. The air cannon test data indicated that percent thickness reduction increases with decreasing plate thickness and decreasing velocity. The falling weight data did not show any such dependencies on plate thickness, velocity nor the other geometric parameters. This indicates that the falling weight test is a flexible means of comparing specimens of differing geometries using percent thickness reduction measurements. The dependency of the air cannon test on plate thickness and projectile velocity limits the flexibility of using this technique when comparing percent thickness reduction of various specimens.

SUMMARY

The following conclusions were reached as a result of this investigation.

1. The air cannon strain rates were generally higher than those typical of birdstrike. However, strain rates in the range typical of birdstrike were achieved for both thin (0.125 inch) and thick (0.5 inch) plates. The data indicates that it may be possible to achieve strain rates characteristic of birdstrike for a given plate geometry by varying projectile mass and diameter.
2. The falling weight strain rates were generally lower than those typical of birdstrike. Strain rates coinciding with the low end of the birdstrike range were only achieved for thin (0.125 inch) plates.
3. The energy versus geometric parameter trends for the air cannon tests were the same as those for the falling weight tests; that is, failure energy increased with increasing plate span, plate thickness, and projectile diameter.
4. The air cannon test technique achieved the required failure energy for all geometries of specimens. The falling weight test achieved the required failure energy for all but very thick (0.75 inch) plates, for which drop height and impactor weight maximum limits were insufficient to cause failure.

RECOMMENDATIONS

The following are recommended as a result of this investigation.

1. Based on the test data reported herein, the air cannon test technique should be used for impact resistance screening of polycarbonate sheet whenever obtaining strain rates characteristic of birdstrike is deemed critical (and specimen thicknesses exceed 0.125 inch). The falling weight test method should be used for polycarbonate impact resistance screening whenever strain rate is considered to be of lesser importance, since good qualitative results can be obtained and test and maintenance costs are low compared to the air cannon technique to screen very thick (0.75 inch) specimens if failure cannot be achieved by the falling weight technique.
2. If air cannon testing is to become a requirement, then it is recommended that an ASTM standard test method be developed. Such a test method would provide testing guidelines which would properly account for velocity-dependent behavior so that meaningful test results are ensured.

METHODS FOR THE DETERMINATION OF THE
DEGRADATION OF POLYCARBONATE

Lance Teten
Texstar, Inc.

METHODS FOR THE DETERMINATION OF THE
DEGRADATION OF POLYCARBONATE

by

Lance Teten
Director of Research and Development

Texstar, Inc.
802 Avenue J. East
P.O. Box 534036
Grand Prairie, Texas 75053-4036

METHODS FOR THE DETERMINATION OF THE DEGRADATION OF POLYCARBONATE

Abstract

Field service exposure of polycarbonate components has shown some degradation and potential failure due to this degradation.

This degradation has possibly been caused by chemical attack from aggressive cleaning agents, paint solvents or improperly labeled transparency cleaning materials. Polycarbonate can also be degraded by improper processing, such as excess temperature or processing with excess moisture present within the material.

This paper outlines three methods for the evaluation of this degradation. The first method utilizes a melt flow technique per ASTM D 1238. Each polycarbonate resin lot is manufactured to meet a specific range of melt flow. Once the material is extruded and processed, the melt flow rate should not change by more than a given amount.

A second method used for polycarbonate is intrinsic viscosity testing per ASTM D 2857. This method uses a solvent that dissolves the polymer completely, without chemical reaction or degradation.

Again, the resin materials are evaluated before and after processing. The intrinsic viscosity should not change more than a small percentage.

The third method involves the use of HPLC. This method uses a set of columns to separate the polymer by size exclusion. This type of equipment can give the molecular weight and intrinsic viscosity, while comparing materials as manufactured to materials after processing. Prior to testing, the material is normally calibrated to a known set of polystyrene standards.

The polycarbonate materials used for transparencies generally fall into a certain range of values for each of the above test.

Utilizing these evaluation techniques, field serviced or degraded parts can easily be evaluated and compared to the original values or retained materials which have not had environmental exposure. Testing has shown that degraded polycarbonate is less crack or craze resistant and may have lower physicals, resulting in a less than structural part.

INTRODUCTION

Polycarbonate materials can be degraded in a number of ways. Polycarbonate can be degraded by improper processing, such as excess temperature or excess moisture during temperature processing. The polycarbonate can be degraded by exposure to solvent or environmental exposure. Some lots of polycarbonate have shown to degrade at a faster rate than others. This appears to be the results of poor hydrolytic stability of the polycarbonate due to a poor stabilizer system.

This paper outlines three methods which can be used to evaluate the degradation that might take place.

TEST METHODS

The first method utilizes a Melt Flow technique per ASTM D-1238. Each polycarbonate resin manufactured will exhibit a melt flow rate based on the particular molecular weight of the polymer and additives. The viscosity of the resin used to manufacture aircraft transparencies is normally a medium viscosity, that is, a 4 to 10 grams/10 minutes melt flow rate. It becomes very important that any processing, such as extrusion, polishing, or forming not significantly change this melt flow rate. The processing should not change the melt flow rate by more than 2 grams/10 minutes. A significant increase of more than 2 gram/10 minutes indicates the polycarbonate is being degraded by the process or environmental exposure and may result in the polycarbonate having different properties. Factors that become affected are lower mechanical properties, less chemical resistance, lower impact, and less environmental resistance. This change is an indication of a lower molecular weight polymer. This test uses six (6) grams of material for each test. Three to five tests are normally performed.

A second method, for polycarbonate, is Intrinsic Viscosity per ASTM D-2857. This method uses a solvent system of methylene chloride to dissolve the polymers completely without chemical reaction or degradation. The polycarbonate solution is tested for viscosity in capillary viscometers. This test uses .2 grams polycarbonate, and three tests are normally averaged for the comparison. A degradation is indicated by a reduction of the intrinsic viscosity of more than 12%. The intrinsic viscosity for polycarbonate materials used for transparencies fall into the range of .45 to .58 depending on the lot of material. However, we feel

that the intrinsic viscosity should not be below .45 for any polycarbonate in a transparency.

The third method involves the use of HPLC, per ASTM D-3593, which yields a variety of data. From this type of equipment, a molecular weight and viscosity can be developed. This equipment is first standardized, using a set of polystyrene standards of known molecular weight. Thus, all the data is based on this standardization. The polycarbonate is dissolved in THF, then injected in a known concentration thru a set of micro-styragel columns, which separate the polymers by the molecular size of the polymer. The resultant chart and data indicates the polycarbonate molecular weight distribution, as well as the additives, such as stabilizers. This is the most expensive test, but yields the most data. At best, two separate tests are performed and the data is compared for evaluation.

MATERIAL TEST

A comparison chart (Figure 1) shows how the intrinsic viscosity and melt flow compare to each other. Several lots of polycarbonate sheet materials supplied by General Electric and Rohm & Haas (Mobay) are shown.

A second chart (Figure 2), is the comparison of molecular weight and intrinsic viscosity.

Three canopies, which and previously seen field service, were evaluated for polycarbonate degradation, using the test systems described earlier.

Figure 3 shows the comparison of retained, in house materials and material taken from two canopies after service.

Canopy S/N 500 (in Figure 3) shows a very slight increase in the melt flow rate and a slight decrease in intrinsic viscosity when comparing the original retained samples of polycarbonate to a sample after being exposed to service. This canopy was manufactured in March, 1981.

Canopy S/N 189 shows some increase in the melt flow rate and a small increase in intrinsic viscosity, also before and after exposure. This canopy was manufactured in December 1979.

These units have performed per specification in service and show no major polycarbonate degradations. The physical properties of these transparencies should not be degraded,

as indicated by these tests, after several years of field exposure.

Canopy 047 was returned from field service for evaluation of cracks along the longeron. As the photograph shows, the canopy had severe damage resulting from chemical exposure. A review was undertaken to evaluate the material. The evaluation shows that the materials had degraded since the original manufacture in 1978.

Figure 4 shows the melt flow change on the original sheet of 6.4 grams/10 minutes to the current 17 grams/10 minutes and the melt flow on the canopy after in flight and environmental exposure of 57 grams/10 minutes. There has been a significant change in the retained material and the transparency.

Figure 5 is a comparison of the retained sheet and canopy using the melt flow rate and intrinsic viscosity.

The molecular weight of the canopy, as tested per the method outlined above, indicates the molecular weight to be from 23,000 to 33,000 depending on the area of sample removal from the transparency. This is a significant change from the normal 40,000 to 50,000 values obtained in other materials.

CONCLUSION

These test systems provide a means of evaluation of polycarbonate degradation. These methods can be used to evaluate the material produced to the Mil-P-83310 specification, as well as evaluate the processing parameters utilized in the production of transparencies. Not all polycarbonate materials are the same and some characterization of the polymers is necessary. As the data shows, some of the polymers do degrade for various reasons. As shown above, the materials may even degrade without environmental exposure due to the polycarbonate additives.

These test methods will allow a better evaluation of polycarbonate and should provide the data necessary to produce better transparencies. They can serve as control for material procurement or process control in the fabrication process and historically to determine the degradation degree after field exposure. Texstar, Inc. has and continues to test each lot of polycarbonate used in processing transparencies. From these records, comparative values can be assessed as this report outlines. This certainly gives the user a better understanding of what takes place in the real world of transparency use.

FIGURE 1

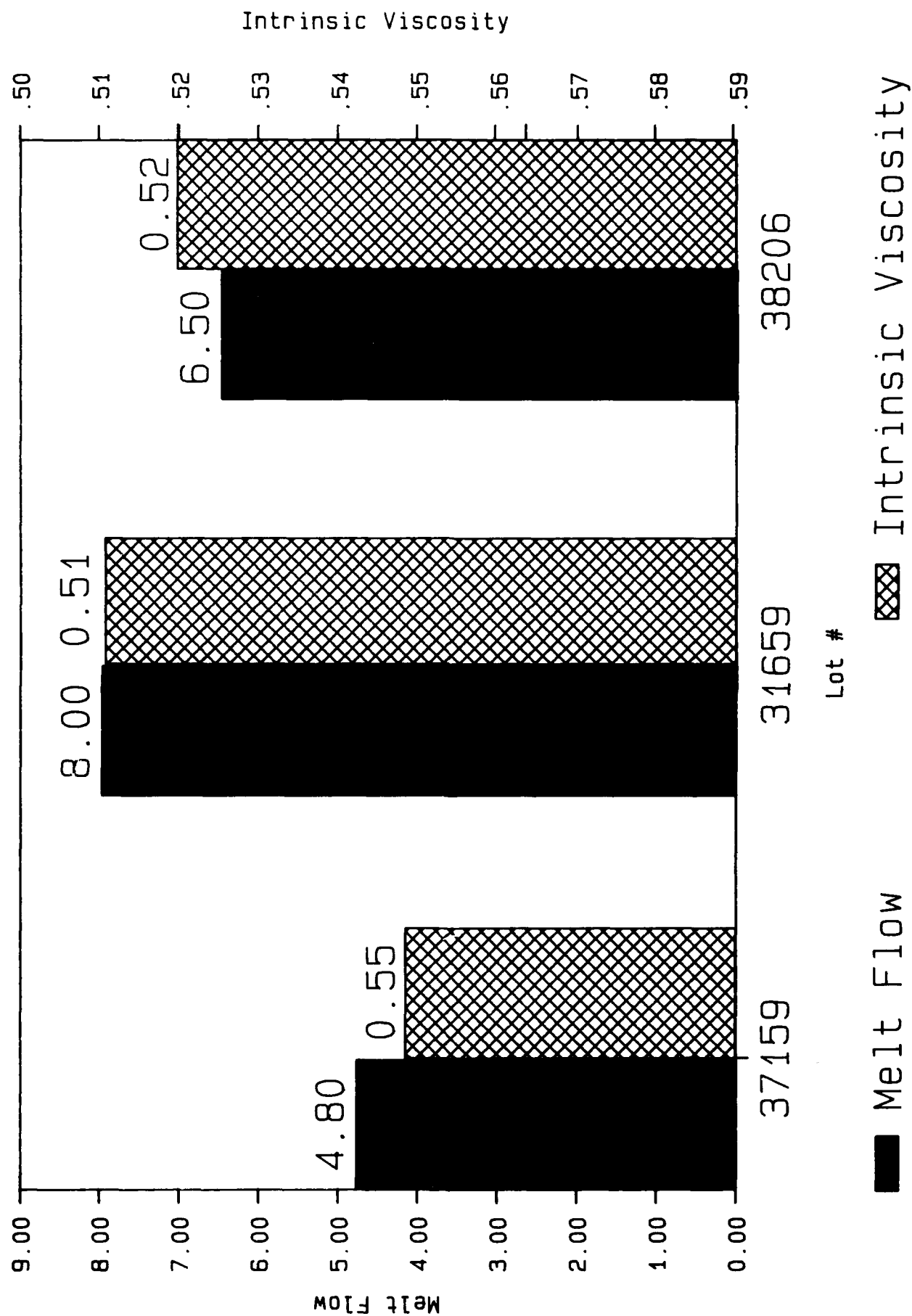
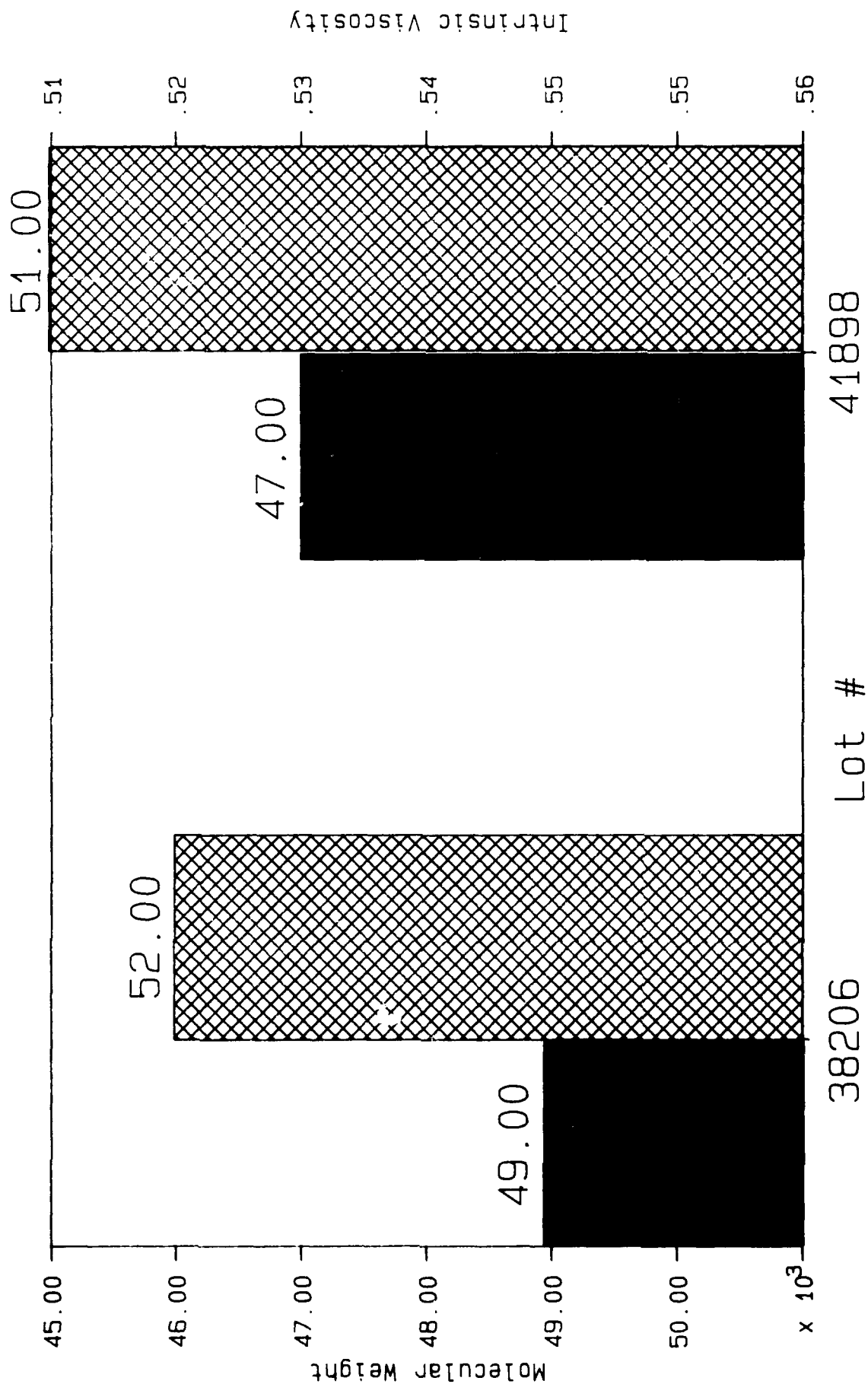


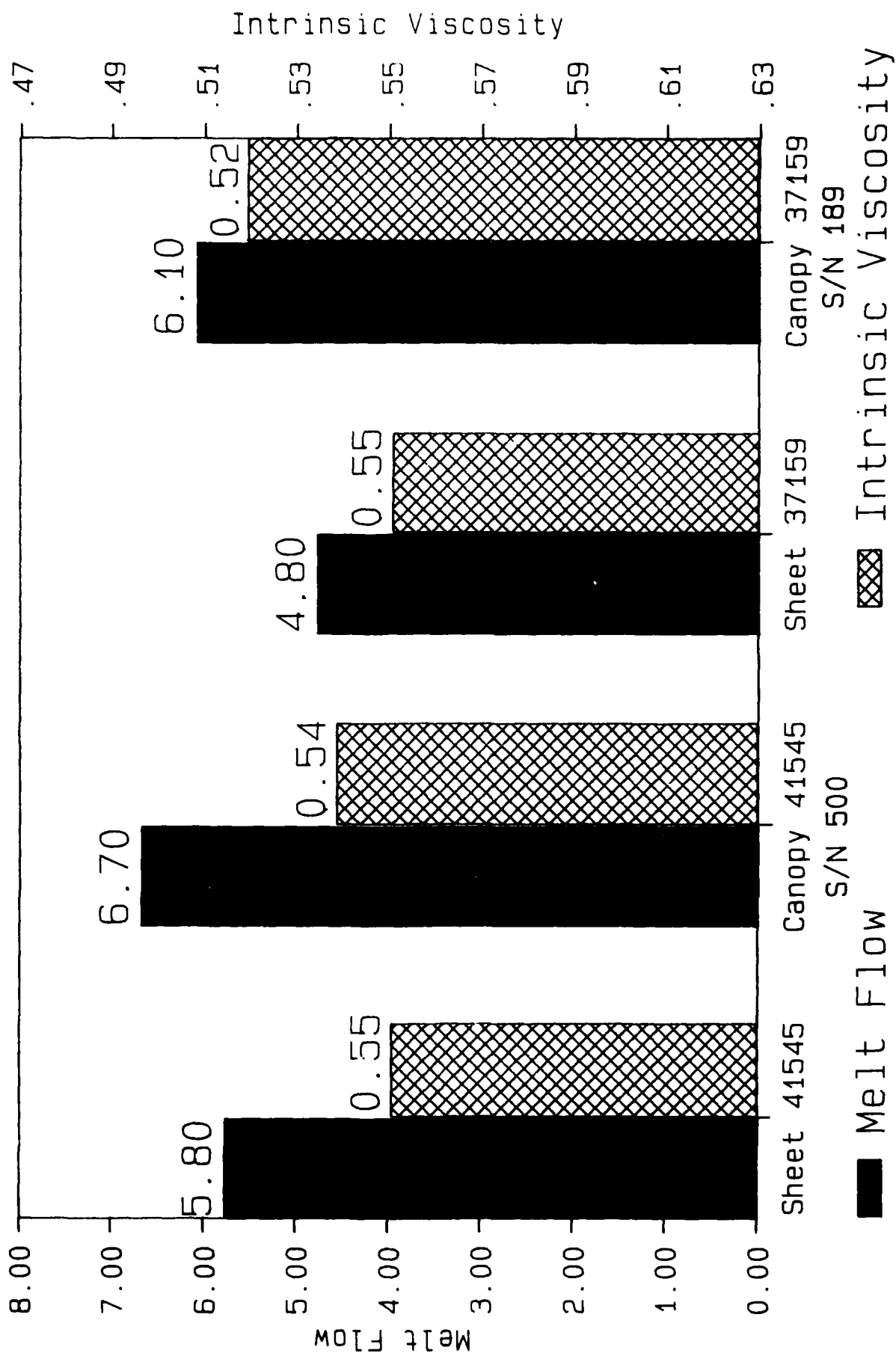
FIGURE 2



■ Molecular Weight

▨ Intrinsic Viscosity

FIGURE 3



Canoo 047

↑ Cracked Longer on ↑

Figure 3.

FIGURE 4

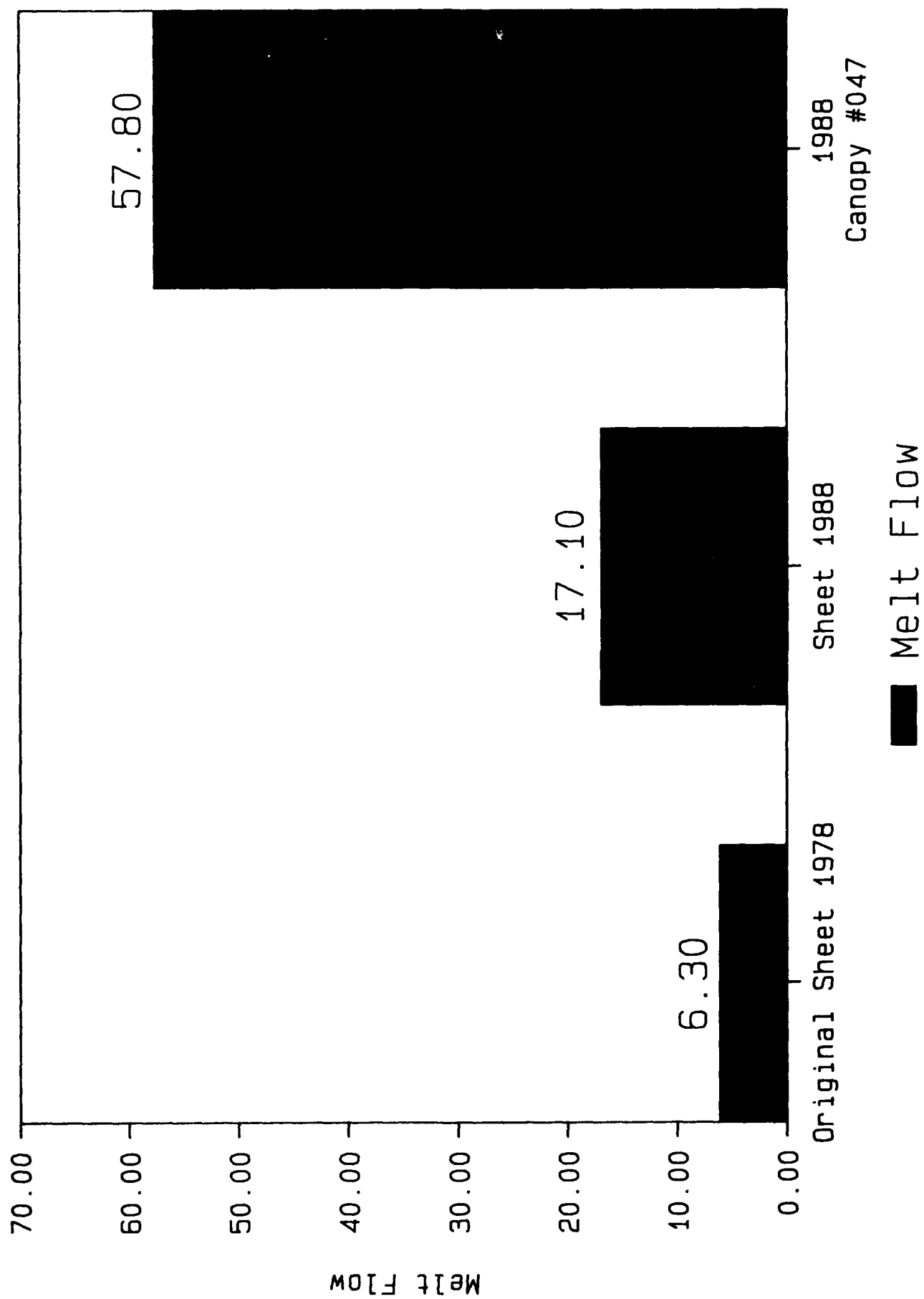
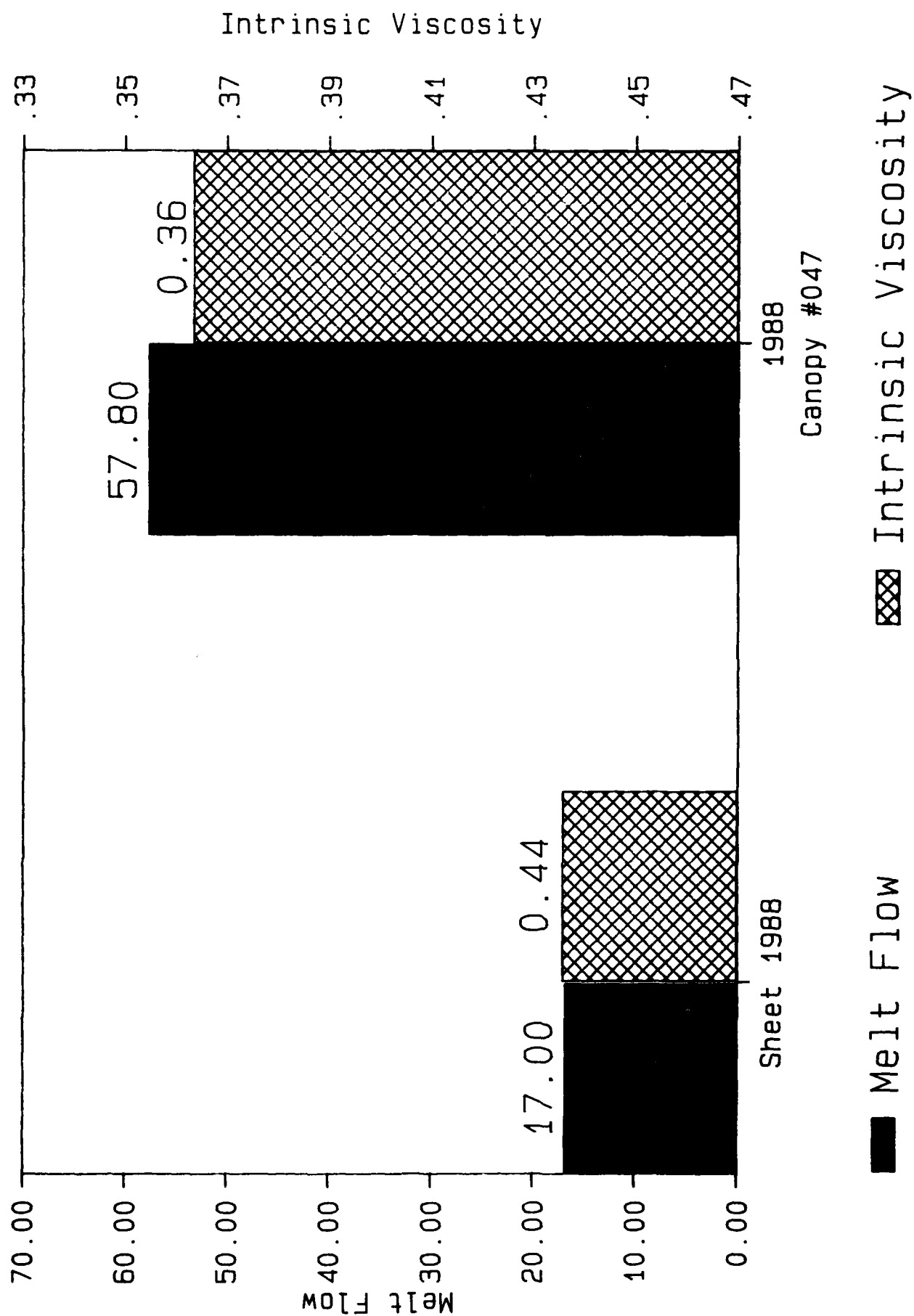


FIGURE 5



SESSION V

TESTING TECHNOLOGY (PART B)

Chairman: J. W. Kozmata
Rockwell International
Los Angeles, California

Co-Chairman: K. I. Clayton
University of Dayton
Dayton, Ohio

Coordinator: R. E. Urzi
Flight Dynamics Laboratory
Wright-Patterson AFB, Ohio

EVALUATION OF AIRCRAFT TRANSPARENCY DURABILITY
TEST METHODOLOGY

K. I. Clayton
University of Dayton

Malcolm Kelley
AFWAL/FDER

EVALUATION OF AIRCRAFT TRANSPARENCY DURABILITY TEST METHODOLOGY

K. I. Clayton
University of Dayton Research Institute

Malcolm Kelley
AFWAL/FDER

ABSTRACT

A survey of developmental testing and in-service durability of F-15, F-16, and F-111 transparencies provided valuable insight into the primary types of in-service failure. Crazing, scratching, and haze were associated with monolithic stretched acrylic; protective surface coating adhesion, abrasion resistance, and embrittlement were associated with monolithic coated polycarbonate; and delamination was associated with acrylic-faced/polycarbonate laminated construction; optical degradation being the single greatest cause for removal and replacement.

Subsequently, a methodology and criteria for testing and evaluating the durability of high performance aircraft transparencies was defined, using simulated in-service environmental conditions in conjunction with a minimum amount of coupon, subscale, and full-scale testing in order to provide a maximum amount of reliable data in a timely manner. Based on this methodology, laboratory generated data has been produced from tests performed on coupon-type specimens cut from the following full-scale production transparency designs:

- F-16A coated monolithic polycarbonate with the original production coating;
- F-16A laminated canopy;
- F-15 monolithic stretched acrylic windshield;
- F-15 monolithic stretched acrylic canopy; and
- F-111 ADBIRT windshield.

Various simulated environmental conditions were combined with the following test parameters: surface/chemical craze, haze/transmittance, impact, coating adhesion, interlaminar bond integrity, thermal shock, in-flight abrasion, and flightline abrasion. The degree of validity of the existing durability test methodology has been assessed when compared to available in-service failure data.

Introduction

The U.S. Air Force, recognizing that high performance aircraft transparencies are a high cost item, is committed to achieving lower cost-of-ownership for aircraft transparencies. A

means of achieving this goal would be to incorporate a realistic laboratory test methodology which adequately addresses and simulates all applicable in-service mission environmental factors, either sequentially or in combination as appropriate, into the acquisition cycle of any transparency system.

During 1981, a survey of developmental testing and in-service durability of F-15, F-16, and F-111 transparencies was conducted for AFWAL/FDER.^[1] Visits to six Air Force bases, two prime aircraft manufacturers, and five transparency suppliers provided valuable insight into the primary types of in-service failures such as crazing, scratching, and haze associated with monolithic stretched acrylic; protective surface coating adhesion, abrasion resistance, and embrittlement associated with monolithic coated polycarbonate; and delamination and optical deterioration associated with acrylic faced/polycarbonate laminated construction.

Subsequently, during 1982 a methodology and criteria for testing and evaluating the durability of high performance aircraft transparencies was defined for AFWAL/FDER using simulated in-service environmental conditioning.^[2] It was designed to provide the maximum amount of reliable data, in a timely manner, using a minimum amount of coupon, subscale, and full-scale testing. Candidate test/exposure methods, simulation techniques, operational environments, and existing standards were screened and evaluated, considering their relative value in predicting the durability of transparency material systems.

Many qualification tests of developmental USAF aircraft transparency designs have been, and continue to be, conducted using new unexposed material. Sufficient data has now been generated to make it evident that environmental conditioning must be experienced by these test specimens prior to test. Figure 1 shows the degradation in energy absorption for aged impact beams versus new baseline beams. It remains extremely difficult to predict the durability of a new transparency design when subjected to the operational environment. Deficiencies exist in the present state of the art for (a) simulating environmental conditioning with laboratory methods, and (b) translating results into accurate durability predictions. It is the assessment of the validity of the coupon test portion of the resultant transparency durability test methodology that forms the basis for this paper.

Technical Approach

Test samples were fabricated, environmentally conditioned, and tested in accordance with a comprehensive test plan based on a test matrix of 364 coupon type specimens.^[3] The experimental test phase was primarily based on the previously developed and documented aircraft transparency testing methodology for

durability evaluation. Tests were performed on specimens cut from the following full-scale production transparency designs:

- F-16A coated monolithic polycarbonate with the original production coating;
- F-16A laminated canopy;
- F-15 monolithic stretched acrylic windshield;
- F-15 monolithic stretched acrylic canopy; and
- F-111 ADBIRT windshield.

Various simulated environmental conditions were combined with the following test parameters: surface/chemical craze, haze/transmittance, high-rate impact, falling weight impact, coating adhesion (rain erosion), flatwise tension, torsional shear, wedge peel, thermal shock, in-flight abrasion, flightline abrasion, and edge attachment. All specimens were identified using the code shown in Figure 2.

The durability evaluation of monolithic stretched acrylic, coated monolithic polycarbonate, and acrylic faced/polycarbonate laminated transparencies is highly dependent on a realistic accelerated weathering exposure. During this program, accelerated weathering was simulated using QUV, 120°F, 7 hour UV/5 hour condensation cycles with 168 hours run time equaling one equivalent year of in-service experience (reference: Figure 3). Several tests used this accelerated weathering condition in combination with other parameters such as salt blast abrasion, induced stress, and normal cleaning cycles.

Test Results

After subjecting all material types to three equivalent years of the specified accelerated weathering, surface craze and haze were extreme; degradation being far in excess of proposed acceptance criteria (reference Figures 4 and 5). However, after introducing cleaning cycles into the accelerated weathering exposure condition to simulate flightline abrasion, no haze readings exceeded four percent after three equivalent years, as shown in Figure 6. The accelerated weathering exposure alone appears too severe; the accelerated weathering exposure combined with normal cleaning cycles appears to be representative of in-service usage.

Salt blast abrasion is extremely severe to transparent plastics unless the specified cycles are held to the recommended minimum. Figure 7 presents in-flight abrasion test results. Thermal shock and impact requirements appear to be satisfactory as defined. Figure 8 presents impact beam test results. The interlaminar bond integrity tests for laminated transparencies, namely flatwise tension, torsional shear, and wedge peel, require a more comprehensive design allowables database for determining acceptance or rejection. Coating adhesion was evaluated using the rain erosion rotating arm apparatus at Wright-Patterson Air Force Base; test results being presented as Figure 9. Edge

attachments are unique to each specific design and must be evaluated as such.

In addition to coupon tests, it is recommended that subscale air cannon impact tests be conducted on unexposed and aged 12-inch-square plates. It is also recommended that full-scale transparencies be installed in the airframe support structure and be birdstrike tested unexposed; following flight/flightline testing at Wright-Patterson AFB; and from in-service at yearly intervals.

The integration of accelerated flight line environmental exposure with actual flight cycle pressure-temperature simulation at Building 65 Wright-Patterson AFB Test Facility is demonstrating the practicality of more realistic developmental and qualification testing.

REFERENCES

1. West, Blaine S., Clayton, Kenneth I., and Giessler, F. Joseph, Survey of Developmental Testing and In-Service Durability of F-15, F-16, and F-111 Transparencies, AFWAL-TR-81-3151, January 1982.
2. Clayton, Kenneth I. and West, Blaine S., Aircraft Transparency Testing Methodology and Evaluation Criteria, AFWAL-TR-83-3045, Part I and II, April 1983.
3. Clayton, K. I., West, B. S., and Bowman, D. R., Aircraft Transparency Test Methodology, AFWAL-TR-85-3125, March 1986.

Acknowledgement

The work described herein was performed under Contract F33615-84-C-3409 with the Air Force Wright Aeronautical Laboratories (AFWAL/FIER), Wright-Patterson Air Force Base, Ohio.

TYPICAL LOAD vs. DISPLACEMENT PLOTS **MTS BEAM (2000 IN/MIN)**

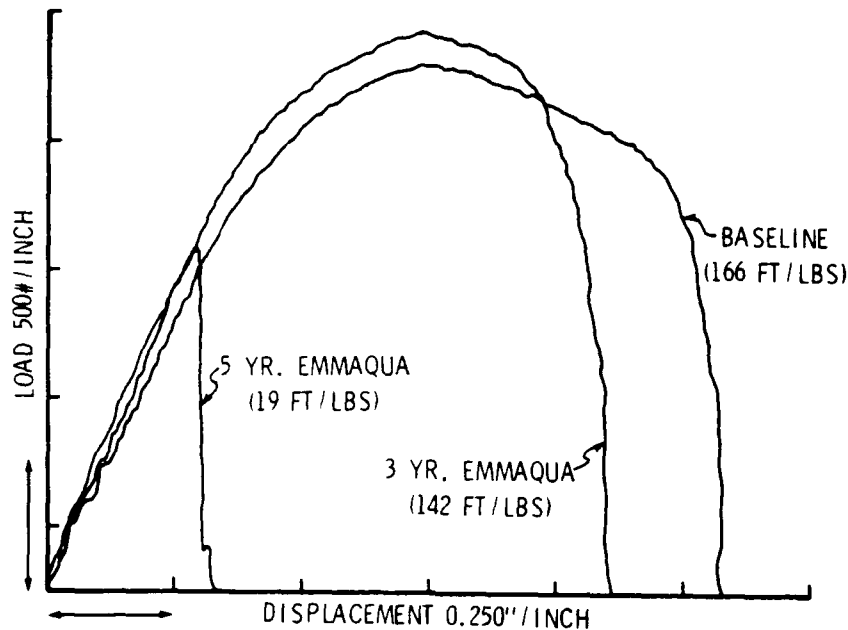


Figure 1. Degradation of Energy Absorption in Aged Impact Beams

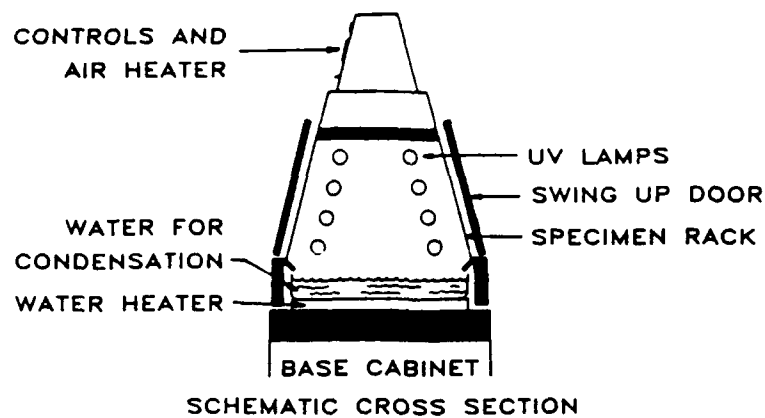
TRANSPARENCY DESIGN:

- A = F-15 MONOLITHIC STRETCHED ACRYLIC WINDSHIELD
- B = F-15 MONOLITHIC STRETCHED ACRYLIC CANOPY
- C = F-16A COATED MONOLITHIC POLYCARBONATE CANOPY
- D = F-16A LAMINATED CANOPY
- E = F-111 LAMINATED ADBIRT WINDSHIELD

TEST PARAMETER:

- O = SURFACE/CHEMICAL CRAZE
- P = HAZE/TRANSMITTANCE
- Q = IMPACT - MTS BEAM
- R = IMPACT - FALLING WEIGHT
- S = COATING ADHESION
- T = FLATWISE TENSION
- U = TORSIONAL SHEAR
- V = WEDGE PEEL
- W = THERMAL SHOCK
- X = IN-FLIGHT ABRASION
- Y = FLIGHTLINE ABRASION
- Z = EDGE ATTACHMENT

Figure 2. Specimen Identification Code



QUV ACCELERATED WEATHERING TESTER

USING UVB-313 LAMPS, 120 F TEMPERATURE, AND ALTERNATING CYCLES OF 7 HRS UV FOLLOWED BY 5 HRS CONDENSATION: 168 HRS RUN TIME SIMULATES 1 YR OF NATURAL WEATHERING

Figure 3. QUV Accelerated Weathering Exposure

ACCEPTANCE CRITERIA

NO CRAZING FROM ISOPROPYL ALCOHOL OR ETHYLENE GLYCOL AT AN OUTER FIBER STRESS OF 2000 PSI AFTER 3 EQUIVALENT YEARS OF ACCELERATED WEATHERING EXPOSURE

TEST DATA

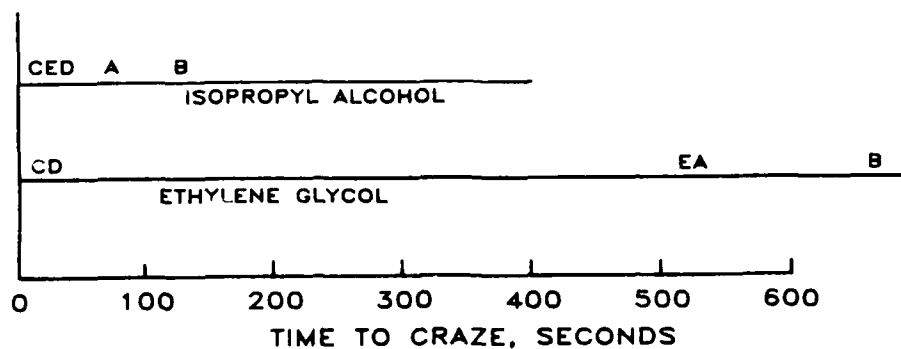


Figure 4. Surface/Chemical Craze Test Results

ACCEPTANCE CRITERIA

AFTER 3 EQUIVALENT YEARS OF ACCELERATED WEATHERING EXPOSURE, HAZE SHALL NOT EXCEED 4% AND TRANSMITTANCE SHALL BE WITHIN 2% OF UNEXPOSED BASELINE VALUE

TEST DATA

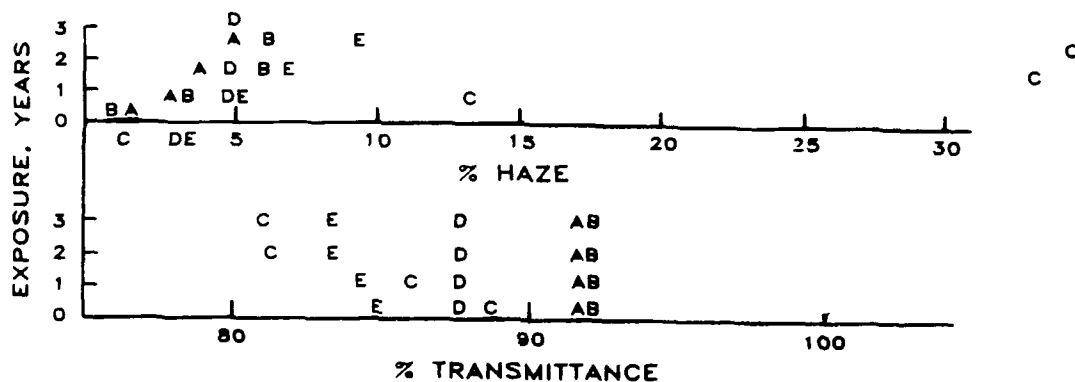


Figure 5. Haze/Transmittance Test Results

ACCEPTANCE CRITERIA

NO VISIBLE DAMAGE; RESULTANT HAZE NOT TO EXCEED 4%. AFTER 1, 2, AND 3 EQUIVALENT YEARS OF ACCELERATED WEATHERING EXPOSURE PLUS 50 CLEANING AT 33-HR INTERVALS

TEST DATA

	HAZE	TRANSMITTANCE
A	1.6-2.5	91
B	1.7-1.9	92
C	2.2-3.6	87
D	2.9-3.4	87
E	3.3-3.6	86

Figure 6. Flightline Abrasion Test Results

ACCEPTANCE CRITERIA

PERCENT HAZE SHALL NOT EXCEED 4%, 5%, AND 6% AFTER
1, 2, AND 3 EQUIVALENT YEARS OF EXPOSURE (WEATHERING
PLUS ABRASION)

TEST DATA

YEARS EXPOSURE	NO. OF SALT BLASTS	TRANSPARENCY				
		A	B	C	D	E
1	2	2.4	2.5	4.3	3.6	4.6
	4	2.9	3.7	3.5	4.0	3.9
	8	4.8	3.3	4.0	4.2	4.8
2	2	2.4	2.9	7.0	3.5	4.1
	4	3.0	3.6	6.7	3.8	3.8
	8	4.9	4.0	5.7	4.3	4.4
3	2	2.8	3.5	17.8	3.3	4.2
	4	3.5	4.0	16.9	4.8	4.3
	8	4.6	4.6	20.3	4.6	4.6

Figure 7. In-Flight Abrasion Test Results

ACCEPTANCE CRITERIA

AFTER 3 EQUIVALENT YEARS OF ACCELERATED WEATHERING
PLUS STRESS (1,000 PSI), Δ THRESHOLD-OF-FAILURE ENERGY
SHALL NOT EXCEED 15% OF UNEXPOSED BASELINE VALUE

TEST DATA

MTS BEAMS

	ENERGY, FT-LBS		
	BASELINE	EXPOSED	% CHANGE
A	71.9	64.5	-10
B	2.1	1.6	-24
C	180.9	291.8	+61
D	202.2	223.2	+10
E	244.4	147.5	-40
<u>FALLING WEIGHT</u>			
B	4.13	4.56	+10
C	171.00	330.00	+93
D	229.00	238.00	+4

Figure 8. Impact Beam Test Results

COATING ADHESION ("C" ONLY)

ACCEPTANCE CRITERIA

AFTER 5 MINUTES OF RAIN IMPINGEMENT TESTING, NO SUBSTANTIAL
AMOUNT OF COATING REMOVAL

TEST DATA

SPEED: 500 mph, RAINFALL: 1 in/hr

EXPOSURE: 3 EQUIVALENT YEARS OF ACCELERATED WEATHERING
PLUS STRESS (1,000 PSI)

SPECIMEN NO.	COATING REMOVAL, PERCENT		
	TEST TIME, MINUTES		
	1	2	5
CS-1	5	30	64
CS-2	1	5	33
CS-3	5	25	85
CS-5	3	20	91
CS-6	2	10	69
CS-7	10	30	84
CS-8	2	25	68
CS-9	2	20	76
CS-10	1	10	30
CS-11	1	10	70

Figure 9. Coating Adhesion Test Results

SCREENING TESTS FOR HARDENED TRANSPARENCY MATERIALS

Ken Clayton
University of Dayton

SCREENING TESTS FOR HARDENED TRANSPARENCY MATERIALS

Ken Clayton
University of Dayton Research Institute

Abstract

Highly sophisticated transparency systems of various configurations are operational today on high performance military aircraft. Transparencies for next generation air vehicle systems must possess the capability to provide protection against evolving combat hazards in addition to current performance requirements. It is this area where conflicts between requirements arise, creating a need to consider design trade-offs. An overview of complex mission-oriented requirements is presented relevant to new or derivative aircraft and to retrofits of current inventory aircraft operating in a 1995 combat environment.

Several samples of candidate near-term producible hardened transparency materials were procured for evaluation in order to assess if such materials are or are not in compliance with next generation transparency requirements. Test procedures are discussed for screening tests and/or exposures as follows: thickened analog agents to determine resistance to chemical threats; irradiation to a representative heat flux combined with aerodynamic flow to determine resistance to nuclear flash; irradiation to continuous wave laser; salt blast to determine the effect of in-flight abrasives and airborne particulates such as nuclear dust; rain erosion to evaluate coating adhesion; thermal shock to determine the effect of operational temperature extremes; transmittance/haze to evaluate the optical effects of coatings and degradation from accelerated weathering; and interlaminar bond integrity tests to determine resistance to delamination.

Introduction

Highly sophisticated transparency systems of various configurations are operational today on high performance military aircraft. Monolithic stretched acrylic is being used on the F-15; coated monolithic polycarbonate on the F-16; acrylic-faced laminates on the F-111 and F-16; and glass-faced laminates on the B-1B.

General performance parameters used to develop such state-of-the-art transparencies are itemized in the following section for the major technology areas of natural hazards, man-machine interface, supportability, and fuselage integration; each needing to be further defined and/or expanded on specific vehicle design requirements and operational mission requirements.

State-of-the-Art Performance Parameters

Natural hazards are those condition which occur without regard to the influence of either the pilot or an outside antagonist. Included are operational and flightline temperatures, weathering and solvent resistance, birdstrike, abrasion resistance, and general environmental conditions such as lightning strike, rain, hail, static charge, fungus, salt spray, anti-icing, and defog.

The area of man-machine interface technology encompasses optical quality, integration of heads-up display (HUD) capability, ingress and egress, along with night and all-weather operation.

The transparent cockpit enclosure is now considered primary aircraft structure and, as such, must maintain structural integrity as an integral part of the forward fuselage. Structural, dimensional, and aerodynamic compatibility must be achieved during the design process. Supportability issues of service life, mean time between failure (MTBF), changeout time, interchangeability, repair, and maintenance must be addressed.

Combat Hazards and Advanced Requirements

The projected threats to the transparency systems for "black" aircraft development, derivative aircraft, and operational aircraft retrofit (B-1B, F-16) as a result of next generation combat engagements are most severe and will require the highest order of protection. It is when these requirements are superimposed over the previously listed performance parameters that conflicts arise in the design optimization. "Must" and "Want" categories, depending on the design mission, will have to be established for the additional needs in order to guide compromises resulting from unavoidable tradeoffs of incompatible requirements.

Combat hazards will dictate requirements for signature, laser hardening, nuclear hardening, and protection against chemical/biological agents. In addition, higher temperatures will influence the extension of polymeric materials into new material systems, including face plies, structural plies, interlayers, and sealants. Longer service life, higher MTBF, and rapid battle damage repair can also be added to the "wish" list.

Screening Test Program

The basic assumption made in order to define a coupon-type laboratory screening test program was that the candidate materials would be laminated construction incorporating coatings. For the first iteration, new material samples without preconditioning are being tested, since all-encompassing protection appears to be premature; major efforts being under way in all areas.

Although emphasis is being placed on protection from combat hazards, laminates are also being evaluated for

interlaminar bond integrity, transmittance, thermal shock, abrasion resistance, and coating adhesion using standard test methods. Transmittance is being measured in accordance with ASTM D1003; thermal shock per ASTM F520; flatwise tension using ASTM D952 or F521 as guidelines; torsional shear using ASTM D229 as guideline; wedge peel using ASTM D3762 as guideline; abrasion resistance per ASTM F1128; and coating adhesion using the rain erosion rotating arm apparatus at Wright-Patterson Air Force Base.

Three replicates, each 1-1/2" x 1-1/2" x t, of each candidate material system are being exposed to the chemical/biological warfare agents: thickened soman (TGD), thickened mustard (THD), and agent VX. One sample of each material is being contaminated with four droplets of one of the agents. Haze and transmittance measurements are being made before and after exposure; this testing being conducted by Battelle-Columbus Division.

Three replicates, each 2" x 2" x t, of each candidate material system are being exposed to laser irradiation at the Laser Hardened Materials Evaluation Laboratory (LHME), Wright-Patterson AFB. Samples are being subjected to different power levels and times using a continuous wave (CW) carbon dioxide (CO₂) laser having a flat-top beam profile to determine the severity of resultant frosting.

Three replicates, each 4" x 4-1/2" x t, of each candidate material system are being exposed to the heat flux needed to simulate nuclear flash. These tests are being conducted at the Tri-Service Thermal Radiation Test Facility established by the Defense Nuclear Agency at Wright-Patterson AFB. Thermal radiation is provided by tungsten filament quartz lamps mounted to one wall of a wind tunnel. The opposite wind tunnel test section wall holds the test sample which is mounted flush with the wind tunnel wall (reference Figure 1). A flux level of 55 cal/cm²-sec for a duration of 3 seconds is being used; a gold coated reflector directing most of the radiant energy to the test specimen. Aerodynamic flow over the specimens corresponds to a Mach number of 0.6. The rapid rise and accurately controlled pulse shown in Figure 2 is obtained with a pneumatically actuated shutter. Visual inspection after exposure is proving adequate to subjectively determine comparative material degradation and/or pass/fail criteria.

Acknowledgement

The work described herein is being performed under Contract F33615-84-C-3404 with the Air Force Wright Aeronautical Laboratories (AFWAL/FDER), Wright-Patterson AFB, Ohio.

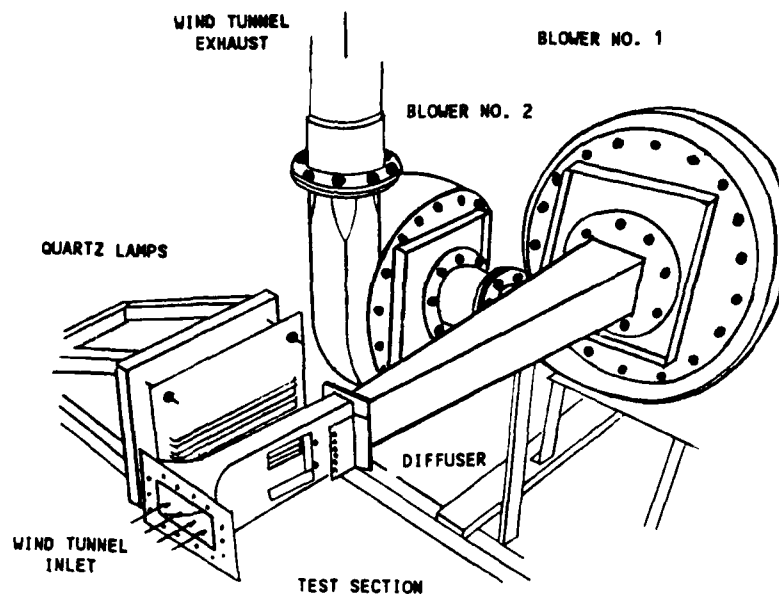


Figure 1. Wind Tunnel at Tri-Service Thermal Radiation Test Facility.

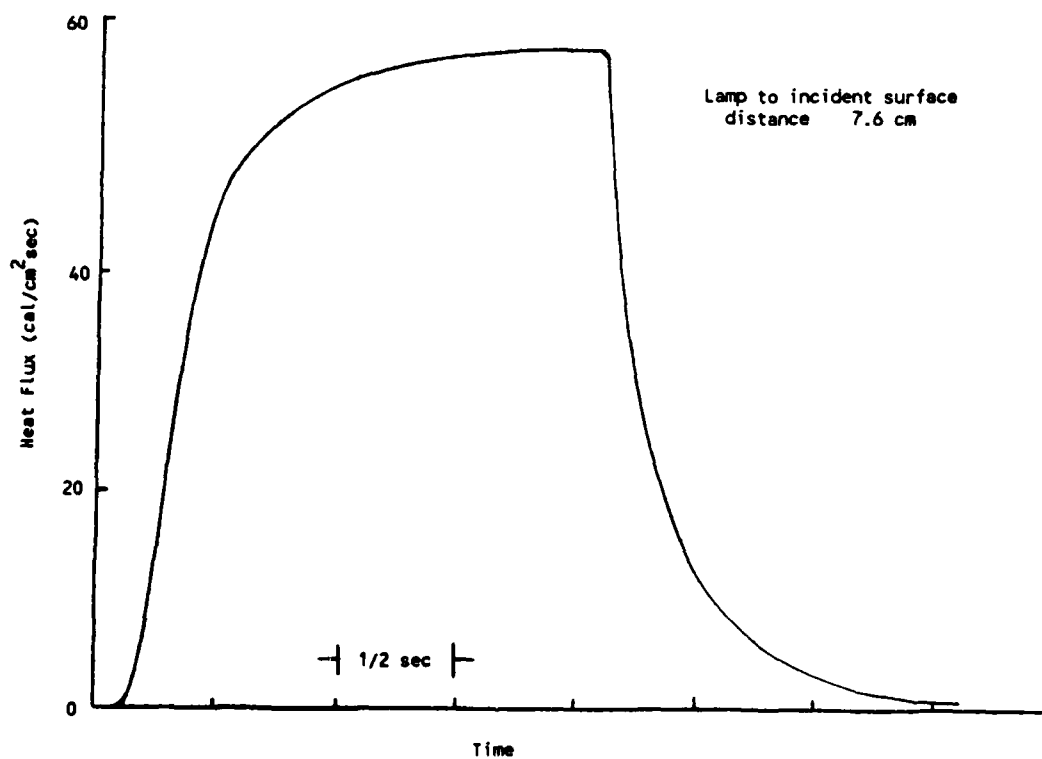


Figure 2. High Density Lamp Bank Radiation Heating Profile (Full Lamp Voltage).

VIDEO THERMOGRAPHY, A TRANSPARENT(CY) APPLICATION

Don Chapin
Sierracin/Sylmar Corp.

VIDEO THERMOGRAPHY
A TRANSPARENT(CY) APPLICATION

by

Don Chapin
Sierracin/Sylmar Corporation

ABSTRACT

A brief description of the origin, development, present features and future potential of an automated, dynamic test capability designed to determine thermal uniformity of electrically-heated anti-ice and defog systems.

Presented at the
Conference on Aerospace Transparent
Materials and Enclosures

16-20 January 1989

What is Video Thermography?

Without becoming involved in the physics of the phenomena, Video Thermography (VT) is simply a means to translate energy output from the infrared region (IR) of the electromagnetic spectrum to the visual spectrum. This particular application accomplishes this electronically so that the translated IR image can be viewed on a normal cathode ray tube (ref. Figure 1).

Electronic thermography normally uses a super-cooled detector (to approximately -190°C) to provide a temperature reference, but for applications such as this, for real-time temperature tracking and instantaneous data acquisition, we also need an A/D converter and a built-in microcomputer to handle image digitization (ref. Figure 2).

Why Video Thermography?

Most aircraft require some form of anti-ice and/or defog systems for their transparencies in order to maintain some degree of visibility under various environmental conditions. The generally-accepted method of accomplishing this is to use electrical heating circuits laminated within the transparency. The design and application of these circuits must meet certain Quality Assurance criteria in order to maintain a degree the desired degree of heating uniformity and power availability. Some of the most popular criteria are detailed in AFWAL TR-80-3003, and shown in Figure 3.

Through the years, the evaluation techniques used to determine whether a particular part might be in compliance with these criteria have been:

- **melted wax** - where paraffin is melted onto a heating zone and data is acquired from the various times/areas where the wax is remelted. This test is normally performed in a cold-box while powering the window;
- **thermocouples** - where a number of thermocouples are placed on the panel and temperature readings are taken at these discrete points during a heating cycle;
- **blue paint** - which, philosophically, is an updated version of the melted-wax technique, in that a special temperature-sensitive paint is used to determine when a particular heating zone achieves a certain temperature;
- **IR gun** - again, a philosophical update of the thermocouple technique, in which an infrared spot-meter provides a temperature reading at discrete positions.

All of these techniques suffer from relatively long setup and data-gathering times, sometimes subjective interpretations of relative heating times/zones, and data acquisition at different times in the same heating cycle. The advantage of the VT technique is quite obvious by comparison. As an example, the test times involved for the techniques used by Sierracin demonstrate a decided advantage for the VT Technique.

<u>Test Method</u>	<u>Average MH/Part</u>
Thermocouple	1.1
Blue Paint	1.0
IR Spot Meter	0.8
Video Thermography	0.25

Background

In the 1983/84 time frame, when this project was first envisioned, proposed to and approved by General Dynamics and the USAF as an Industrial Technology Modernization Program, there were only two VT systems known to have the capabilities of real-time tracking, pictorial digitization and external computer control. One was AgaVision, used in Europe, and the other was the Hughes Probeye Thermal Video System. Systems comparisons showed a strong financial and technical support advantage for the Hughes system, which was acquired at the end of 1984.

The goals for this system, in order to be fully incorporated into the production system, were:

- **full** computer control, fast data capture and reduction;
- **foolproof** part evaluation (pass/fail, eliminates human judgement);
- **simple** operation with **minimum** operator involvement;
- applicable to **any** heated part;
- **small** data storage volume;
- **traceable** source code for maintainability;
- temperature and power-related **K-factors** (later revised to temperature only related K-factors);
- maximum **information reduction** from the raw data.

The Phase I portion of this effort was completed in approximately April 1986, while the Phase II portion was thought to have been completed in October 1987, but has had to be extended because of hardware/software compatibility problems. The Phase III Production Implementation Program is now (still) in progress.

Description of Present Test Station - Hardware

General

The VT Test Station hardware that has evolved from the original design goals encompasses the Hughes 4100 system, controlled through a Hughes IEEE-488 Interconnect Box, an extra color monitor that can be driven from either the Hughes TVS or from the computer, an ultrasonic distance measurement device (UDM) operated from its own board in the computer, a digital voltmeter (DVM) with a IEEE-488 interface to the computer, and a Sierracin-designed and developed 0-210 volt AC power supply operated from a Metrabyte DDA06 board in the computer through interconnect and relay boxes (ref. Figure 4). The computer used for this test station is a Datacat, a ruggedized PC-compatible running at 4.77 MHz, with 512K of RAM and a math co-processor. In addition, a universal holding fixture was also developed and built for this test station that will accommodate every heated transparency which Sierracin has ever manufactured.

Probeye Lens

The test station normally uses a 45 x 22.5° field-of-view (FOV) lens on the Probeye camera which allows for a relatively short focal length (parts can be brought closer to the lens) which in turn permits a smaller overall test facility floor plan. With the built-in zoom capability for a 2 x 2 picture enlargement of the 4100, this gives four different lens-viewing capabilities to cover a wide variety of test conditions. Each condition is appropriately covered with a curve-fit, test-part-area-per-pixel equation in the software. This FOV lens does introduce a constant, small error (approximately 3-4°F) into the measured temperatures, but this is correctable by using a Hughes Programmed ROM table.

Monitors

The additional color monitor, also acquired from Hughes, provides good operator-viewability of the test part heating pattern from the TVS, a source of Polaroid pictures for data comparison during development, and a method of alerting the operator if a warning notice for some missed communication attempt is required. The small screen of the PC-compatible Datacat computer, being monochromatic, does not have the command presence of the larger RGB screen and provides questionable attention-getting capability for a warning. The test station is designed so that if a warning to the operator is necessary, the RGB screen will be temporarily slaved to the computer rather than the TVS.

Digital Voltmeter

The DVM utilizes the IEEE-488 board so that the computer can read the test part's resistance and the setup voltages from within the power supply as well as the fluctuating voltage going to the test part -- the DVM cannot integrate over the duty cycle imposed by the activated SSR. This DVM is not 488-programmable, so the operator must switch from the ohms to the AC volts modes at the appropriate program prompts. The computer program, however, does check on the DVM mode to ensure that such mode changes have taken place.

Power Supply

The on-board power supply utilizes both a 120 VAC and a 240 VAC input. The lower voltage powers the 24-volt relays, while the higher input voltage is stepped down to the appropriate range through a transformer and five secondary-tap relays to provide discrete AC voltage ranges of 0-12, 12-28, 28-60, 60-120 and 120-210. All of the relays are turned on and off through digital signals from the DDA06 board in the computer. A safety switch in the form of a 3-relay system also governs the input side of the transformer. Originally, only one relay was used for this protection circuit until it was discovered that the DDA06 board used to activate these relays, went to an automatic FULL-ON when the computer was turned on and proceeded to 'cook' all the relays in the power supply! Another problem was discovered at a relatively late stage in the power supply checkout in that absolutely NO electrical commonality could exist between any of the 5-volt data or signal circuits and any of the 9, 12 or 24-volt circuits! Low voltage power lines were then extracted from data-carrying cables and opto-isolators were inserted between any 5-volt signal connections and any points that carried 24-volt power.

Power variations within each of the output voltage ranges is provided by a proportioned 5-volt DC signal output through the DDA06 board to a solid-state relay (SSR). The SSR then provides an ON/OFF duty cycle that effectively provides appropriate power to the test part. In this way, the mechanical relays are never activated with a power load on them since the SSR is always shut down at the time. The only variation of this philosophy is in the event of an external emergency requiring an immediate power-off situation, such as an operator stepping on a safety mat at the wrong time in the power-on cycle. The operation of the power supply is intended for repetitive cycling during a given test, duplicating the on/off action of a bang-bang controller. A future software modification could easily be made to duplicate the action of a proportional controller through the SSR, but such a capability is probably not necessary unless cold-box testing is to be accomplished.

Additional features of this power supply board include the capability to switch both the DVM and the RGB monitor inputs to different circuits.

A list of the major pieces of hardware used in the test station is included in Appendix I.

Description of Present Test Station - Software

The software to operate this test station was developed using Turbo Pascal, Version 3.01, since the Basic language drivers that were available at the time were perceived to be somewhat slow for a repetitive test sequence and the significant amount of data-reduction expected. Even though there were some very trying times in blazing a new trail through the different syntax structure for the Hughes TVS, it looks as if the effort was well worth it at this point. Using the Universal Test Fixture, a part can be positioned in approximately three minutes, a 1-cycle test run for either a monolithic or a simple laminate panel can be accomplished in 6-7 minutes, while the data-reduction would take another two minutes, including approximately 25 seconds for the statistical reduction of over 4200 data points!

For each piece of hardware (range-finder, DVM, VTS and power supply), a separate computer program was developed to ensure operation of that hardware and of code syntax before incorporation into the main program of VIDEO. With the exception of the DVM, which operates from the same GPIB computer control board as the TVS, nothing was willing to cooperate from within the VIDEO program as when controlled from its own dedicated program!

The data acquisition and reduction programs have been compiled into a set of three programs, generating disk files read by succeeding programs and tied together by a DOS batch file called VT. This batch file also calls another program, DDA06-0, before and after the power supply is activated, to ensure that all signals issuing from the appropriate power supply computer ports have been zeroed out.

In developing the data reduction software for the program CHECK, the original goal was to incorporate both temperature and power-related K-factors for maximum flexibility. The equations were developed and sample data entered for reduction when it became obvious that there were considerable differences between the theoretical world of equation development and the real world of daily QC operations and measurements. In order to incorporate the power-related K-factors, several additional pieces of information were required; i.e., heat transfer coefficients (non-linear for plastics), local ply thicknesses (often slightly variable for plastics), time measurements between data points (assuming a room temperature start and a computer-tracked time difference), and the local heat transfer coefficients for each surface. As a result, although the equations and capabilities were initially built into the software for the power-related K-factors, this capability was removed in favor of the more-explicitly defined temperature-related K-factors.

because the set of data acquisition and reduction programs require very explicit data files for each part number or configuration, a menu-driven data file generation/modification program was written, called VIDINPUT. One of the task-selection options within this program is a capability to run a modified version of CHECK to accomplish the data reduction on any picture file for which there is a data file available; i.e., this program is not limited to data reduction for only the last test cycle of a given test, as is required for CHECK.

A synopsis of the Source Code Files/Program Description is included in Appendix II.

System Operation

The first program that is activated for the test run is VID POSN, a routine that obtains 1) operator inputs for P/N and S/N, 2) ensures that an appropriate data file exists for that P/N, 3) ensures proper part positioning, 4) gets the correct test date and test start time from the computer clock for the data file, and 5) activates the UDM to obtain a distance measurement. This distance measurement is used to ensure that the heated area will fit into the Probeye lens viewing area, and to translate each display pixel into physical dimensions on the part.

Once the main data acquisition program, VIDEO, is started, the TVS and DVM are initiated, the TVS is set to the appropriate test parameters for temperature and emissivity, and the operator is prompted to place a small light bulb (also powered from the test station power supply) on the test part. For a monolithic ply (before sensor installation) the bulb is to be placed in the center of the allowable sensor location area. For a laminated assembly, the bulb is located first on the over-temp sensor (OT), then on the control sensor (CS). In either case, the computer program, through the TVS, then establishes the exact screen coordinates of the bulb location, by detecting the highest temperatures on the screen and moving the cursor to that point. The last bulb location is used to dynamically monitor the power-on temperature changes.

The light bulb is then removed by the operator and the automatic power-on and data-gathering cycles are initiated, following the requirements established in the respective P/N data files. At the peak of the allowable temperature, the TVS Screen is 'frozen,' the power shut off and the screen data transferred to the computer. For a monolithic test part, the allowable sensor area is searched for a warmer area than the presently-tracked position and that location and temperature, if of sufficient size, is recorded. The OT sensor location and temperature is calculated from the remaining (assumedly cooler) sensor area. All of this information is then stored on disk in a picture file (including the test requirement data) which requires less than 16K bytes of disk storage space, allowing over 20 picture files per 360K byte diskette.

VIDEO then monitors the TVS cursor temperature to a pre-determined value and, emulating a voltage controller's function, repeats the heatup/data-gathering cycle for as many times as the P/N data file requires. For a monolithic part, after the last cycle Power On/Off, if there is a large enough hot area within the sensor zone, so that the sensor could be affected by this relatively hot area, the operator is instructed where to best place the control sensor by placing the TVS cursors at that point.

Once the data-gathering mode has been completed, the data-reduction program CHECK is called and the latest picture data file is read for data-reduction and output. The heart of this program is a STATS procedure that rapidly reduces the large quantity of picture data to key figures (it takes 25 seconds to reduce approximately 4200 data points). The results are then printed out in a one-page format as shown in Figure 4, for a total reduction/printout time of less than two minutes. An optional output routine, that is primarily useful for engineering evaluation also provides a detailed pixel-by-pixel temperature chart including sensor location and sensor zone limits and center. Full-color plot or isotherm chart drivers can be developed in the future from the optional detailed output format.

Synopsis of VT Test Capabilities

- | | |
|-----------|---|
| VID_POSN: | 1) Reads the data file for an operator-input P/N. |
| | 2) Tracks start date/time. |
| | 3) Electronically measures distance to test part. |
| VIDEO: | 4) Reads DVM for part resistance and power-on voltage steps. |
| | 5) Reads operator input for sensor zone center or existing sensor location. |
| | 6) Controls the TVS for |
| | a) video screen parameters of date, time, legend, emissivity, scale, low temperature, and sensitivity; |
| | b) 'hot' area detection; |
| | c) cursor movements; |
| | d) freeze-frame action; |
| | e) data acquisition. |
| | 7) Controls the Sierracin-developed power supply for a near- infinite voltage selection from 0-240 volts. |
| | 8) Controls DVM monitoring point on power supply as a safety precaution. |
| | 9) Controls external monitor display between TVS picture and the operator prompts/warnings. |
| | 10) Constantly monitors the progress of the test and either prompts the operator for an action (or to confirm that a step has been taken) or a malfunction/warning. |

- 11) On monolithic plies, the operator is told where to place the control sensor.
 - 12) Checks to see how far the sensor is from the nearest hot area.
 - 13) Stores the picture test data by S/N and P/N with the test requirement parameters and
 - a) test time to each power-off cycle;
 - b) time to end-of-test (not incl. data red'n).
- CHECK:
- 14) Reduces the data to usable parameters.
 - 15) Data output
 - a) P/N, S/N, Test date, total test time;
 - b) heater resistance and comparison to allowables;
 - c) sensor locations;
 - d) sensor distance from closest 'hot' pixel;
 - e) data for hi, low, sensor, and at sensor temperature;
 - f) four K-factors and comparison to allowables;
 - g) stats for mean, variance, deviation, skew, kurtosis;
 - h) total heated area;
 - i) number of pixel points at each data point and that percentage of total.
 - 16) Optionally produces a printout of part heated area, showing temp @ each data point, exact sensor zone and location of control sensor.

Present Video Thermography Systems

Today, even as we are finally evolving the Hughes 4100 into a production evaluation tool, the technology is opening up with additional Hughes 3000 machines which are in the same price/performance range as the 4100; as well as the Hughes 7X00 series systems, and the Mikron Thermo Tracer 6T61. Both of these latter units possess higher screen resolution than the 4100, can be used in real-time or near real-time, and are computer-interfaceable. Both are in a higher price range, but the Mikron has lower software cost. The Hughes 7000 series system also gets away from dependence on an external gas supply by using a thermal, electrically-cooled detector and virtually eliminates periodic recalibration by incorporating a self-calibration capability.

While the 7100 series system could not produce the appropriate color resolution in the temperature range our industry needs, the newer 7300 systems apparently can. These systems also do not need an external gas supply for cooling or a temperature reference, nor do they require an annual inspection/calibration. Repair costs, however, at least for the detector systems, are considerably higher.

With these newer systems, the software drivers all seem to be going to the systems-oriented C-language, and away from the applications-oriented Basic language. The Basic language usage for the Hughes 4100 was one of the reasons we had decided to develop our own program, using Pascal, which can be either systems- or applications-oriented. One serendipitous effect of choosing Pascal is that its syntax and structure is somewhat similar to C, so that downstream systems upgrades or adaptations should not be overly difficult.

The Hughes 7000 series also seems to be setting another trend which we would strongly agree with -- that of going to a more reliable communications interface such as the RS-232 to RS-170 interface standard. In our experience, we have found the IEEE-488 interface to have problems which have resulted in many hours of additional programming time to resolve.

Possible Future Upgrades

- 1) Addition of color plotter, color printer or isotherm output.
- 2) Maintenance/trouble-reporting capability that will provide a disk-stored trace.
- 3) Development of an automatic TVS-reset program to be inserted as a call from VT.bat in the event of an emergency bailout from the VIDEO program.
- 4) Incorporation of DMA from TVS to computer, if needed.
- 5) Possibly use a more focused Polaroid range-detector.
- 6) Release drawings, schematics and computer source code for data file generation and test operation, including Config.sys, Autoexec.bat and VT.bat files, but excluding any commercially-available code for which a release is not obtainable.

Conclusions

Keeping in mind the original goals of this test station, as listed earlier:

- **full** computer control, fast data capture and reduction;
- **foolproof** part evaluation (pass/fail, eliminates human judgment);
- **simple** operation with **minimum** operator involvement;
- applicable to **any** heated part;
- **small** data storage volume;
- **traceable** source code for maintainability;
- temperature-related **K-factors**
- maximum **information reduction** from the raw data;

it would certainly appear that we have attained all of the original goals!

APPENDIX I
12-8-88

- Probeye 4100 Thermal Video System consisting of:
 - Infrared Imager Unit
 - Processor/Display Unit
 - IEEE-488 Computer Interface Unit
 - External Color (RGB) Monitor

Hughes Aircraft Company
Probeye Marketing
Industrial Products Division
6155 El Camino Real
Calsbad CA 92008
619 931-3000
- Datacat (ruggedized PC-compatible) Computer (any PC/AT compatible should be acceptable) including: 512K RAM, math co-processor, (1) 360K 5-1/4" disk, (1) 20 MB HD.

Datacraft Inc.
13714 S. Normandie Ave.
Gardena CA 90249-2696
- Keithley Model 1753 (includes IEEE-488 Interface)

Keithley Instruments Inc.
28775 Aurora Rd.
Cleveland OH 44139
216 248-0400
- GPIB, IEEE-488 Instrumentation Interface Board: Scientific Solutions (PN 020030) (Tecmar) Personal Computer Products Div., 6225 Cochran Road, Solon OH 44139, 216 349-0600.
- DDA06 Analog/Digital I/O Expansion Board
- ERA-01 Relay Box
- STA-01 Interconnect Box

Metrabyte Corp.
440 Miles Standish Blvd.
Taunton MA 02780
617 880-3000
- UDM-PC Ultrasonic Distance Measurement System

Contaq Technologies Corp.
15 Main St.
Bristol VT 55443
802 453-3332

APPENDIX II

EXPLANATION OF VIDEO THERMOGRAPHY PROGRAMS/FILES 12-8-88

VIDINPUT.COM OR PAS by Sierracin.

The part number-oriented data file generator designed to initiate data files for VIDEO or update them at the operator's option. Any changes to a data file automatically records the date of the latest file version. Option #3 in the menu uses a version of CHECK.PAS for independent data analysis or simple picture-file recovery, in deliverable source code.

VID_POSN.COM or .PAS (General) by Sierracin for Test Part Positioning.

Setup program for establishing start date, start time, test part rotation and distance from the Probeye lens (distance measured by a distance-measurement board and transducer assembled by Contaq Technologies Corp. No software copyright by Contaq).

- Assembly language *.COM files, from source, provided by Contaq Technologies, but integrated into a Pascal program in an unusual programming manner to alleviate interface problems:
 - a. U_INIT.COM - called as an external file.
 - b. RANGE_ST.COM - "
 - c. POLL_UDM.COM - "

This UDM operation has been found to work only by placing the *.COM external files low on the stack, hence a separate preprocessing program.

VIDEO.COM or .PAS (General) by Sierracin for device control and data retrieval/storage.

Sub-file Attributes and Relationships

All *.INC and *.COM files listed below are needed with VIDEO.PAS for proper compilation.

All *.COM files listed below are needed with VIDEO.COM for proper operation.

Files for VTS Operation by Sierracin, controlling the VTS and DVM through the GPIB board:

Route 488.COM - by Scientific Solutions, used as a device interface from Autoexec.bat.

GPIBERR.INC - include file using function check error.
VTSOPER.INC - include file using several procedures and functions translated from Hughes manual; also controls DVM read operations.

For power control/digital voltmeter and monitor switching - by Sierracin
POWER.INC - include file to control test voltages and switch monitor/DVM application, by Sierracin.

- Heavily-expanded code using control routines from Quinn-Curtis, 49 Highland Ave., Needham, MA 02194 for operation of the DDA06 interface board. Quinn-Curtis copyright release on DDA06 routines in letter of Sept. 21, 1987.

For data acquisition and control - by Sierracin
TESTING.INC - include file using procedures begin_test and complete-test...test procedures.

For sensor zone calculations - by Robometrics, modified by Sierracin
SENSCALC.INC - include file called from TESTING.INC to calculate hot areas of sensor zone.

For cyclic power application - by Sierracin
WAITTEMP.INC - for tracking TVS cursor temperature and periodically applying power.

For large (>64K size) file generation using Turbo Pascal Version 3.X, TURBO EXTENDER by TurboPower Software, Scotts Valley CA can be used. Also, TURBO PASCAL Versions 4.0 or 5.0 can be used.

CHECK.COM or .PAS by Sierracin

Program for data file retrieval, statistical data reduction and results presentation. A version of this file is also included as option 3 in VIDINPUT, the part number data file generator (not to be included in released source code.)

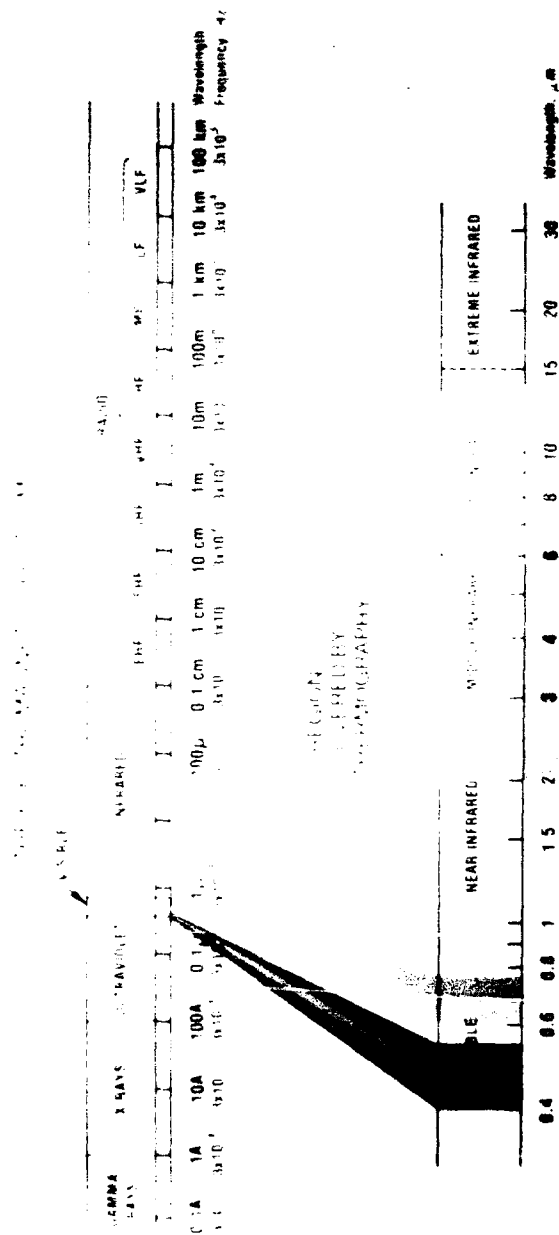


FIGURE 1

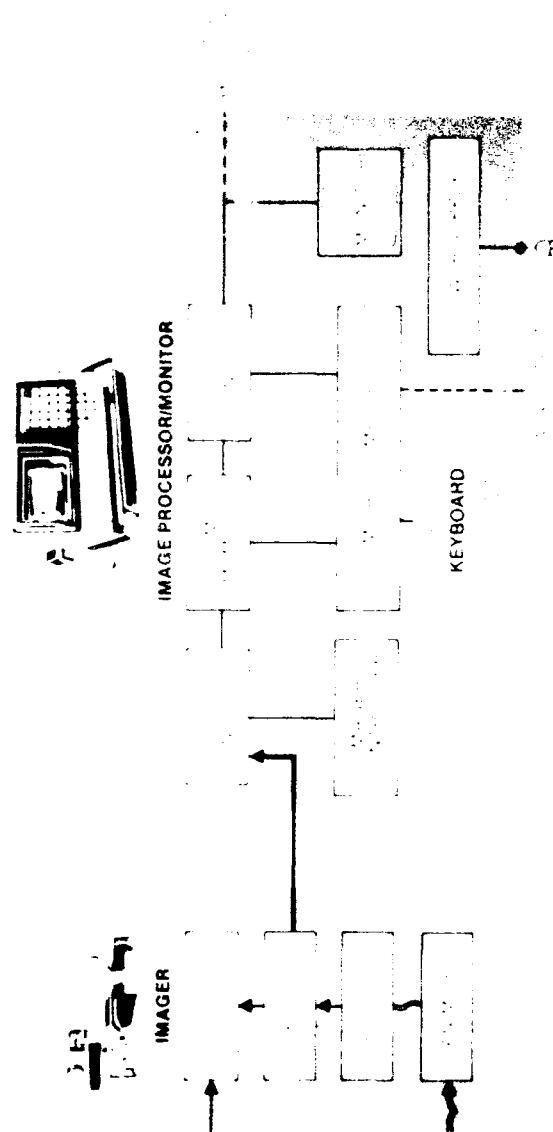


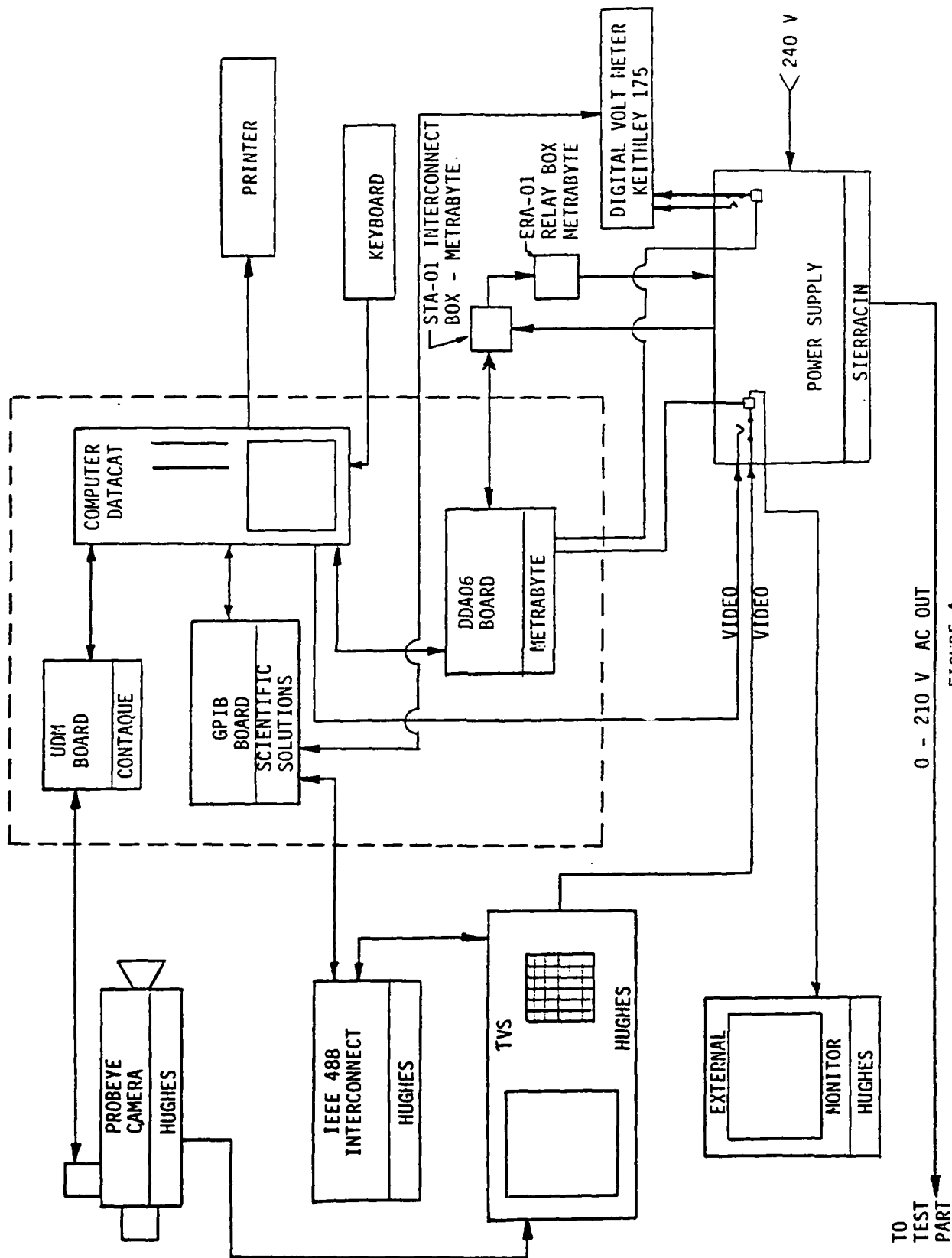
FIGURE 2

POWER UNIFORMITY "K" FACTORS (from AFWAL-TR-80-3003)

- $K_h = \frac{\text{Power @ Hot Spot}}{\text{Power @ Control Pt}} \leq 1.4$
- $K_a = \frac{\text{Average Power}}{\text{Power @ Control Pt}} \geq 0.7$
- $K_m = \frac{\text{Average Power}}{\text{Power @ Hot Spot}} \geq 0.5$
- $K_c = \frac{\text{Power @ Cold Spot}}{\text{Power @ Control Pt}} \geq 0.55$
-
- $K_o = \frac{\text{Power @ OverTemp Sens}}{\text{Power @ Control Pt}} 0.9-1.1$

Sierracin Function :

FIGURE 3.



Data results for P/N 153700, S/N comstt, TESTED 08/14/1987
for cycle 3 of 3 cycles.
total test accomplished in 10.0073 minutes.

Heater Resistance =18.47 ohms, with 3 power-on cycles
with Rmin =15.75 and Rmax =19.25

X-direction Control sensor distance from Zone-Center =1.14 inches.
Y-direction Control sensor distance from Zone-Center =0.98 inches.

Control sensor distance from hot area is 0.00 inches.

Highest Panel Temp. = 121.0
Lowest Panel Temp. = 93.0
Average Panel Temp. = 107.12
Panel Temp. Variance = 47.68
Temp. at Sensor = 121.00
Temp. at OT Sensor = 114.51

K-factor	Value	Required Min.	Max.	Ratio Description
Ka	0.89	0.75	1.00	average / control sensor
Km	0.89	0.10	1.00	average / hot
Kh	1.00	0.75	1.00	hot / control sensor
Ko	0.95	0.90	1.10	OT sens / control sens

Standard Deviation, Temp. = 6.91 with allowed dev'n =8.00

Skew = -0.5613 with a 'perfect distribution' value of zero (0.0).
this data shows a right-leaning curve.

Kurtosis = 2.2192 with a 'perfect distribution' value of three (3.0),
this data shows a relatively 'flat' curve.

Total Panel Heated Area is 592.005 inches² ; Area expected =636.700

This data has been calculated from a data base of 4246 picture elements,
over a total of 15 temperature ranges, at a distance of 72.82 inches.

Temperature population table :

At a temperature of 93.0 there are	197 data points,	for 4.64 %.
At a temperature of 95.0 there are	247 data points,	for 5.82 %.
At a temperature of 97.0 there are	189 data points,	for 4.45 %.
At a temperature of 99.0 there are	212 data points,	for 4.99 %.
At a temperature of 101.0 there are	225 data points,	for 5.30 %.
At a temperature of 103.0 there are	230 data points,	for 5.42 %.
At a temperature of 105.0 there are	301 data points,	for 7.09 %.
At a temperature of 107.0 there are	318 data points,	for 7.49 %.
At a temperature of 109.0 there are	371 data points,	for 8.74 %.
At a temperature of 111.0 there are	632 data points,	for 14.88 %.
At a temperature of 113.0 there are	808 data points,	for 19.03 %.
At a temperature of 115.0 there are	371 data points,	for 8.74 %.
At a temperature of 117.0 there are	82 data points,	for 1.93 %.
At a temperature of 119.0 there are	41 data points,	for 0.97 %.
At a temperature of 121.0 there are	22 data points,	for 0.52 %.

FIGURE 5.